Caracterització de l'efecte de compostos naturals en models *in vitro* i *in vivo* de càncer de còlon

Susana Sánchez Tena

UNIVERSITAT DE BARCELONA

Departament de Bioquímica i Biologia Molecular

Facultat de Biologia

Caracterització de l'efecte de compostos naturals en models *in vitro* i *in vivo* de càncer de còlon

Susana Sánchez Tena

2012

UNIVERSITAT DE BARCELONA

Departament de Bioquímica i Biologia Molecular

Facultat de Biologia

Programa de Doctorat de Biomedicina de la Universitat de Barcelona

Caracterització de l'efecte de compostos naturals en models *in vitro* i *in vivo* de càncer de còlon

Memòria presentada per **Susana Sánchez Tena**, llicenciada en Biologia per la Universitat de Barcelona, per optar al grau de **Doctora per la Universitat de Barcelona**.

Tesi realitzada sota la direcció de la Dra. **Marta Cascante Serratosa**, el Dr. **Josep Lluís Torres Simón** i el Dr. **Pedro Vizán Carralcázar**.

Dra. Marta Cascante **Dr. Josep Lluís Torres** **Dr. Pedro Vizán**

Susana Sánchez Tena

Sólo una cosa convierte en imposible un sueño: el miedo a fracasar

Paulo Coelho

CONTINGUT

INTRODUCCIÓ GENERAL

1. EL CÀNCER

El càncer és un conjunt de malalties que s'origina a partir d'una proliferació accelerada, desordenada i descontrolada de les cèl·lules d'un teixit que envaeixen, desplacen i destrueixen, localment i a distancia, altres teixits sans de l'organisme. El càncer, també denominat neoplàsia o tumor maligne, és un terme molt ampli que engloba més de dos-cents tipus de tumors malignes. Cadascun d'ells posseeix unes característiques particulars, que en alguns casos són completament diferents a la resta de càncers, podent-se considerar malalties independents, amb les seves causes, evolució i tractament específics (www.aecc.es).

Segons estimacions de l'Organització Mundial de la Salut (OMS), el càncer és una de les principals causes de mort a escala mundial (http://www.who.int/es/). Concretament, 7,6 milions de defuncions (aproximadament el 13% del total) produïdes en tot el món l'any 2008 es van atribuir a aquesta malaltia. A més, les morts degudes a neoplàsies segueixen augmentant any rere any, ocupant el primer lloc les produïdes com a conseqüència del càncer de pulmó, seguides de prop per les d'estómac, fetge, còlon i mama.

El procés pel qual les cèl·lules normals es transformen en canceroses i adquireixen la capacitat de multiplicar-se descontroladament i d'envair teixits i altres òrgans s'anomena carcinogènesi. La carcinogènesi es dóna per un procés anàleg a l'evolució Darwiniana, en el qual es produeixen canvis genètics successius, que confereixen avantatges de proliferació, portant a la conversió progressiva de les cèl·lules normals en cèl·lules tumorals (Foulds, 1954; Nowel *et al.*, 1976). Aquest procés pot produir-se per alteracions genètiques espontànies, heretades o bé per l'acció d'agents carcinògens externs: els carcinògens físics (llum ultraviolada o radiacions ionitzants), els carcinògens químics (components del fum del tabac o contaminants en aliments) i els carcinògens biològics (infeccions víriques, bacterianes o parasitàries). La carcinogènesi pot durar anys i es desenvolupa en tres fases diferents: iniciació, promoció i progressió (Ziech *et al.*, 2011). La iniciació consisteix en una lesió irreversible a l'àcid desoxiribonucleic (ADN) d'una cèl·lula que li confereix la capacitat de proliferar descontroladament respecte a la resta de cèl·lules que l'envolten. La cèl·lula iniciada pot donar lloc a cèl·lules filles portadores de la mateixa alteració al material genètic. En les cèl·lules iniciades, la multiplicació cel·lular comença a ser més ràpida i la probabilitat de que es produeixin noves mutacions augmenta. Aquesta és la fase de promoció. Finalment, les cèl·lules pateixen noves mutacions i cada vegada es fan més anòmales pel que respecta al seu creixement i comportament. Aquestes cèl·lules adquireixen la capacitat d'invasió, tant a nivell local com a distància, originant les metàstasis. Aquesta és la fase de progressió.

Com a norma general s'ha de tenir en compte que una única mutació no és suficient per provocar la transformació d'una cèl·lula normal (Hahn *et al.*, 2002). Les mutacions s'han d'acumular i afectar diferents gens involucrats directa o indirectament en el control del creixement cel·lular com els protooncogens o els gens supressors de tumors. Els protooncogens es troben en les cèl·lules normals exercint funcions relacionades amb el control de la proliferació cel·lular. Aquests codifiquen per a factors de transcripció, proteïnes de transducció de senyal que estimulen la divisió i factors reguladors del cicle cel·lular i l'apoptosi. Quan un protooncogen sofreix una mutació de guany de funció, és a dir, una alteració que fa que es mantingui actiu en situacions en què no hauria d'estar-ho, es converteix en un oncogen i provoca un increment en la taxa de proliferació cel·lular. D'una altra banda, els gens supressors de tumors són gens la funció dels quals consisteix a limitar el creixement tumoral constituint una defensa per a l'organisme enfront de la formació de tumors. Per tant, quan una mutació afecta a un gen supressor de tumors i l'inactiva, es dóna un efecte complementari a l'observat quan s'activa un oncogen. Per altra banda, els factors epigenètics també juguen un paper fonamental en la progressió tumoral, ja que exerceixen una important funció reguladora de l'expressió gènica. Els canvis epigenètics són heretables i, a diferència dels factors genètics, marquen la cadena d'ADN sense modificar la seqüència de nucleòtids en si mateixa (Wong *et al.*, 2007). Fins al moment s'han caracteritzat tres esdeveniments epigenètics associats al càncer: la hipometilació global de l'ADN, la hipermetilació de les illes CpG (regions amb elevada concentració de citosina i guanina) i la desregulació de les modificacions de les histones. Mentre que la hipometilació de l'ADN sol portar a l'activació de certs gens que haurien d'estar silenciats, la hipermetilació de les illes CpG que formen part de regions promotores és un mecanisme pel qual s'inactiva l'expressió de gens supressors de tumors en cèl·lules tumorals. Per la seva banda, les principals modificacions que poden sofrir les histones són la metilació i l'acetilació. Les histones són proteïnes sobre les quals s'empaqueta l'ADN. Quan aquestes no presenten les modificacions mencionades, la cromatina es troba empaquetada i es restringeix l'expressió gènica. En canvi, quan les histones es troben acetilades o metilades, la cromatina es desempaqueta, de tal manera que els gens queden exposats a la maquinària transcripcional i s'activa l'expressió.

1.1. Característiques tumorals

L'any 2000, Douglas Hanahan i Robert Weinberg van publicar una coneguda revisió on s'establien les sis propietats distintives que caracteritzen les cèl·lules tumorals (Hanahan *et al.*, 2000). Aquestes característiques comuns necessàries per a la malignància tumoral són:

senyalització sostinguda de la proliferació independent de factors de creixement, insensibilitat a senyals inhibidores del creixement com són la densitat cel·lular i l'adherència cèl·lula-matriu i cèl·lula-cèl·lula, una capacitat proliferativa il·limitada, la capacitat d'evadir la mort cel·lular programada o apoptosi i la capacitat d'invasió, angiogènesi i metàstasi. Tot i això, recentment s'ha demostrat que aquests sis fenotips no representen la totalitat dels trets distintius de les cèl·lules cancerígenes, sinó que aquestes també presenten inestabilitat genòmica, adaptacions metabòliques específiques, la capacitat d' evadir la resposta immunitària i es veuen promogudes per l'inflamació (Hanahan *et al.*, 2011) (Figure 1).

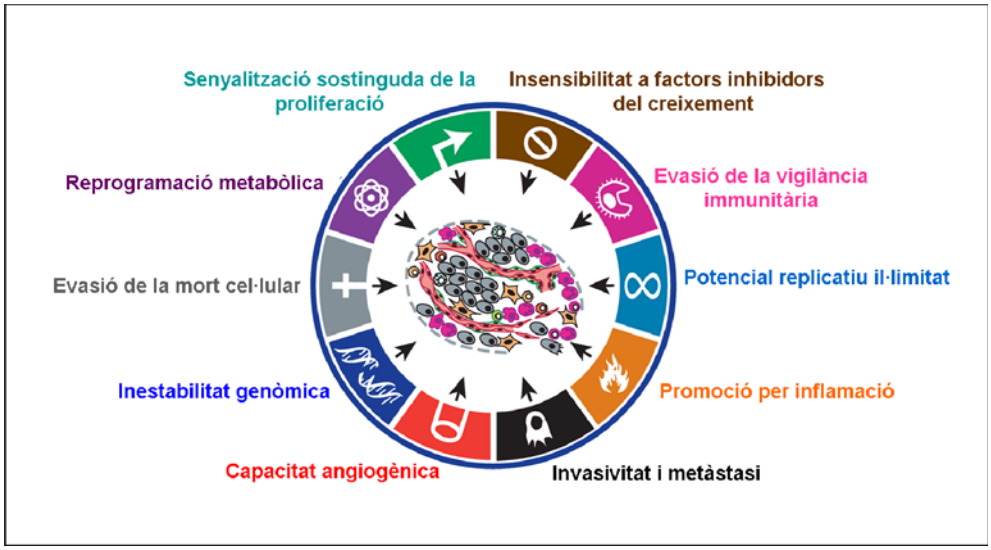

Figura 1. Propietats de les cèl·lules tumorals (adaptada de Hanahan i Weinberg, 2011)

La primera de les característiques destacades per Hanahan i Weinberg és l'autosuficiència de senyals de creixement. Per comprendre el funcionament del procés s'ha de tenir en compte que existeix un conjunt ordenat de successos que condueixen al creixement i la divisió de la cèl·lula. Aquest procés s'anomena cicle cel·lular i serà detallat més endavant (punt 1.3.). Per dividir-se, les cèl·lules normals necessiten d'una sèrie d'estímuls proliferatius regulats per factors de creixement. Algunes cèl·lules tumorals són capaces de sintetitzar i alliberar factors de creixement als quals elles mateixes responen. A més, sovint es produeix una sobreexpressió dels receptors de factors de creixement en les cèl·lules tumorals, amb el que aquestes es tornen hipersensibles als lligants presents al seu entorn. També existeixen casos en què les cèl·lules tumorals tenen alterat el tipus de receptors que expressen a la seva superfície, de tal manera que incrementen la proporció d'aquells que generen estímuls promitòtics (Hagedorn *et al.*, 2001). Per últim, les cèl·lules tumorals poden reduir la seva dependència de les senyals de creixement

externes degut a que diversos oncogens tenen la capacitat de mimetitzar aquestes senyals sense necessitat de rebre senyals externes. Per exemple, una de les vies més importants en aquest sentit, és la formada per la família de proteïnes senyalitzadores Ras, les quals presenten mutacions puntuals en els gens que les codifiquen donant lloc a espècies constitutivament actives en un gran nombre de tumors humans (Gulhati *et al.*, 2012).

A part de l'estimulació per factors de creixement, per entrar en divisió les cèl·lules normals requereixen també la desactivació dels senyals antiproliferatius que bloquegen el creixement. La majoria de proteïnes que controlen aquestes senyals inhibidores del creixement estan codificades per gens supressors de tumors (Poznic, 2009; Al-Ejeh *et al.*, 2010).

El fet que aquest potencial replicatiu sigui il·limitat és un altre factor imprescindible per garantir el creixement d'un tumor. Les cèl·lules normals, després d'un nombre de cicles de creixement i divisió determinat, entren en un procés de senescència mitjançant el qual són eliminades de manera natural evitant així que pugui donar-se una acumulació excessiva de mutacions o alteracions que puguin afectar la seva funció. Aquest control es realitza gràcies als telòmers, seqüències repetitives i no codificants, riques en timina i guanina, que es troben als extrems dels cromosomes i que s'escurcen en cada divisió cel·lular funcionant així com un rellotge biològic. Les cèl·lules tumorals presenten alteracions en els mecanismes que exerceixen aquest control, de manera que poden continuar dividint-se indefinidament adquirint la immortalitat que les caracteritza. En aquest fenomen l'enzim telomerasa exerceix un paper clau (Shay *et al.*, 2012). Aquesta ADN polimerasa, que està especialitzada en allargar els telòmers, és pràcticament inexistent en cèl·lules no immortalitzades, mentre que s'expressa a nivells més alts en cèl·lules immortalitzades com són les tumorals.

A part de l'increment en la proliferació, l'augment en el nombre de cèl·lules que s'observa en els tumors s'explica també per un descens acusat en la mort cel·lular. En aquest sentit, juguen un paper clau el procés d'apoptosi, el qual s'explicarà en detall a l'apartat 1.4; la senescència (Ohtani *et al.*, 2012) i l'autofàgia (White *et al.*, 2009). Aquests processos es desencadenen en resposta a nombrosos factors tals com el dany a l'ADN, la falta de nutrients, l'estrès oxidatiu, la hipòxia o la manca de factors inductors de la supervivència. Les cèl·lules tumorals, però, evolucionen per evitar aquests processos.

En formar-se una gran quantitat de noves cèl·lules, aquestes comencen a créixer allunyades dels vasos sanguinis que irrigaven el teixit inicialment. Aquest distanciament fa que les cèl·lules tumorals sofreixin restriccions en l'aportació d'oxigen i nutrients, dos elements imprescindibles per a la seva funció i supervivència. En aquest punt juga un paper important la capacitat angiogènica de les cèl·lules tumorals, que afavoreix la formació de nous vasos

sanguinis que irriguen el tumor i permeten l'aportació de nutrients i d'oxigen que les cèl·lules necessiten (Shojaei, 2012). Aquest procés serà detallat a l'apartat 1.5.

Les característiques esmentades anteriorment expliquen la formació d'un tumor primari. Tanmateix, la formació d'un tumor secundari requereix la capacitat d'envair teixits i formar metàstasi. La metàstasi és un procés estructurat en diverses etapes successives que requereixen unes especificitats cel·lulars molt concretes en cadascuna d'elles (Chaffer *et al.*, 2011). Inicialment, les cèl·lules han de ser capaces de degradar la matriu extracel·lular que les manté unides a la resta del tumor i al teixit al que pertanyen per tal d'alliberar-se'n. Aquest desarrelament permet l'entrada de les cèl·lules als vasos sanguinis que irriguen el teixit i el seu transport fins a zones distants de l'organisme. Durant aquest trànsit, les cèl·lules tumorals circulants han de presentar resistència al sistema immunitari per a no ser eliminades de l'organisme. A continuació, les cèl·lules malignes han de ser capaces d'extravasar, d'integrar-se en una nova regió i de reprendre la proliferació per així formar un tumor secundari o metàstasi.

Pel que fa a la nova generació de característiques tumorals, la primera propietat destacada per Hanahan i Weinberg l'any 2011 fou l'acumulació d'alteracions a nivell genòmic. Com s'ha comentat anteriorment, les cèl·lules tumorals presenten sovint unes taxes de mutació majors que les cèl·lules no tumorals. Aquest fet s'ha associat a alteracions en gens que s'encarreguen de controlar la integritat del genoma detectant danys a nivell de l'ADN i activant la maquinària de reparació, reparant directament aquests danys o interceptant i/o inactivant possibles mutàgens (Negrini *et al.*, 2010).

Recentment, nombroses evidències revelen que les cèl·lules tumorals mostren una reprogramació metabòlica característica que els permet abastir l'alta demanda energètica i biosintètica necessàries per mantenir el seu creixement accelerat (Samudio *et al.*, 2009; Jozwiak *et al.*, 2012). A més, s'ha demostrat que l'adaptació metabòlica tumoral actua activament en la progressió tumoral, facilitant, per exemple, la invasió (Vizán *et al.*, 2008; Kamarajugadda *et al.*, 2012). El metabolisme tumoral serà detallat a l'apartat 1.6.

Durant els últims anys s'ha descrit que els processos d'inflamació juguen un paper important en la formació de tumors. Malgrat que el procés inflamatori és un mecanisme del sistema immune destinat a protegir l'organisme contra agressions externes i a afavorir la recuperació de lesions, durant la progressió tumoral aquest procés pot promoure l'adquisició de diverses característiques tumorals. La resposta inflamatòria permet proveir les cèl·lules tumorals de factors de creixement que activen la proliferació, de factors de supervivència que protegeixen contra la mort cel·lular, de factors angiogènics i d'enzims que modifiquen la matriu extracel·lular (Grivennikov *et al.*, 2010a).

Amb relació a l'última propietat tumoral, l'evasió de la vigilància immunitària s'ha descrit com un mecanisme per protegir les cèl·lules tumorals de la destrucció pel sistema immune, evitant així l'eliminació del tumor d'una banda i, tal com s'ha comentat anteriorment, afavorint la formació de metàstasi (Grivennikov *et al.*, 2010b).

1.2. Càncer de còlon

El còlon o intestí gruixut és l'últim tram del tub digestiu i s'estén des del final de l'intestí prim fins a l'anus. El còlon té aproximadament una longitud de 135 cm en humans i de 4-5 cm en ratolí. L'arquitectura del còlon es caracteritza per criptes d'aproximadament 50 cèl·lules de profunditat anomenades criptes colòniques o de Lieberkühn. Les parets intestinals del còlon estan compostes per diverses capes de teixit: la més interna, en contacte amb el lumen intestinal, és la mucosa, que es troba envoltada per la submucosa. Més externament es situa la capa muscular que al seu torn està recoberta per la serosa (Figura 2). A la mucosa colònica existeixen glàndules secretores on es produeixen amb major freqüència els tumors malignes. En aquest cas, parlem d'adenocarcinomes.

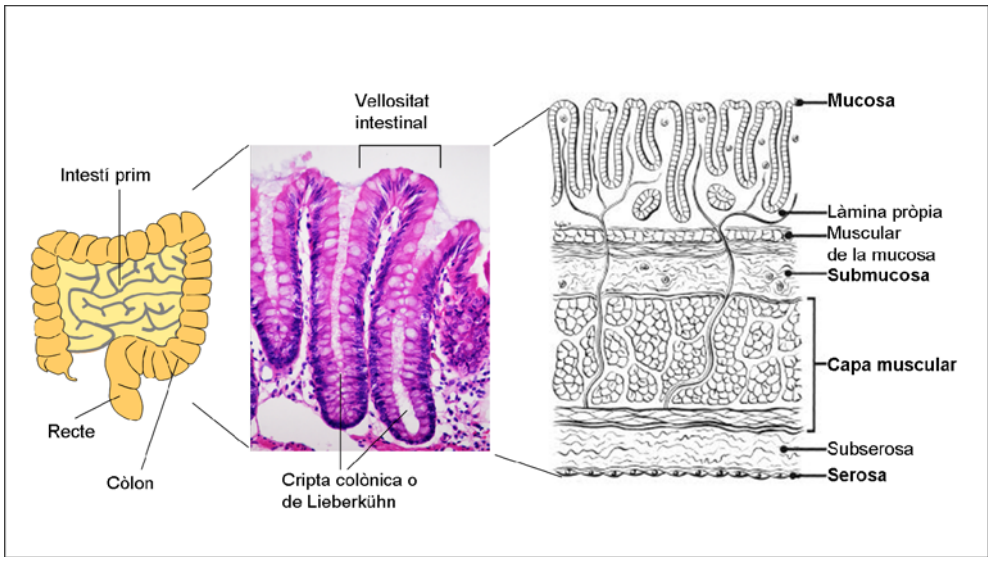

Figura 2. Estructura del còlon (Adaptada de http://sosbiologiacelularytisular.html).

Les funcions principals del còlon són emmagatzemar residus, mantenir l'equilibri d'hidratació mitjançant l'absorció d'aigua i electròlits i absorbir algunes vitamines com la vitamina K.

Es important destacar que el càncer de còlon és el tercer en freqüència després del càncer de pulmó i pròstata en l'home, i el segon darrere del de mama en la dona. Si es tenen en compte els dos sexes a la vegada, el de còlon és el tipus de càncer més freqüent, amb casi 28.000 nous casos a l'any (www.aecc.es). A més, el càncer de còlon està augmentant en incidència any rere any als països desenvolupats. Així, malgrat que en els últims anys s'ha produït un augment en la supervivència dels pacients amb càncer de còlon gràcies al major coneixement sobre les causes d'aparició i evolució, a millores en el tractament i a les campanyes de detecció precoç, entre d'altres (Jemal *et al.*, 2010); el càncer de còlon encara és una de les malignitats més freqüents i és essencialment incurable quan assoleix una etapa avançada. Per aquesta raó, es precisen noves estratègies més eficients que les actuals per augmentar la supervivència dels pacients amb càncer de colon.

1.2.1. Genètica de la carcinogènesi colònica

El càncer colorectal s'ha classificat en base a la seva forma de transmissió i origen, coneixent-se com hereditari i esporàdic. La forma esporàdica és la més comuna, amb aproximadament el 75% dels casos, i la resta està representada pel càncer colorectal hereditari (Rustgi, 2007). Entre els càncers colorectals d'origen hereditari cal destacar la poliposi adenomatosa familiar (FAP - *Familial Adenomatous Polyposis*), que és una malaltia autosòmica dominant en la qual es desenvolupen múltiples pòlips adenomatosos al còlon durant la segona o tercera dècada de vida. D'altra banda, el càncer colorectal hereditari no polipoide (HNPCC - *Hereditary Non-Polyposis Colorectal Cancer*), conegut també com a síndrome de Lynch, es descriu com una malaltia autosòmica dominant relacionada sobretot amb mutacions en els gens de reparació de l'ADN que moltes vegades va acompanyada del desenvolupament de càncer d'endometri, estómac, pàncrees, ronyó o tracte urinari.

Es distingeixen dos vies moleculars en la carcinogènesi colorectal: la via del fenotip supressor o via d'inestabilitat cromosòmica (CIN - *Chromosomal Instability*) i la via del fenotip mutador o via d'inestabilitat de microsatèl·lits (MSI - *Microsatellite instability*) (Li *et al.*, 2009). La via supressora o CIN agrupa el 85% dels casos esporàdics i els hereditaris de FAP. L'inestabilitat cromosòmica es manifesta en el desenvolupament de tumors amb alteracions en el nombre de cromosomes (aneuploïdia) i pèrdues d'heterozigositat (LOH - *Loss Of Heterozygosity*), així com mutacions que activen oncògens i bloquegen gens supressors de tumors. Aquestes últimes alteracions segueixen el model proposat per Fearon i Vogelstein l'any 1990, el qual explica com les diferents etapes clíniques definides en el càncer de colon van associades a successius canvis genètics (Fearon *et al.*, 1990) (Figura 3). El procés s'inicia quan

una cèl·lula adquireix una mutació que desregula la via de senyalització Wnt, la qual es detalla més endavant. Mutacions que constitutivament activen les vies BRaf/kRas i la pèrdua del control associat a la via del TGF/Smad s'associen amb el creixement d'un petit adenoma fins a una mida clínicament significativa. Mutacions subsegüents en el gen *Tp53* i delecions al cromosoma 18 on es troba el gen *Dcc (Deleted in Colorectal Cancer)* són responsables de la transició d'un tumor benigne a un tumor maligne. Aquesta seqüència adenoma-carcinoma és acceptada actualment, no obstant, s'han identificat canvis addicionals en aquest model. Per exemple, s'ha demostrat que mutacions en els gens de NF-kappaB, AP-1 i PIK3CA també estan implicades en el pas d'adenoma a carcinoma (Vaiopoulos *et al.*, 2010; Ogino *et al.*, 2011).

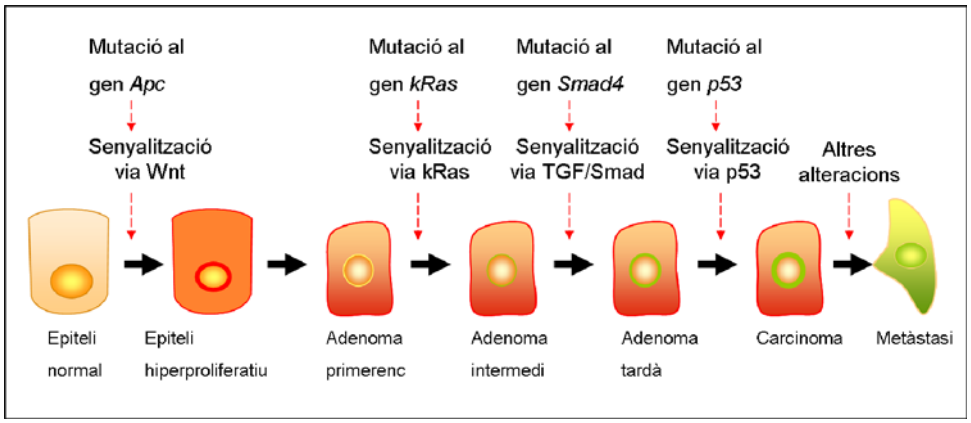

Figura 3. Esquema dels canvis genètics clau en la tumorigènesi colorectal.

D'una altra banda, la via del fenotip mutador o MSI es troba present en HNPCC i en un 15% dels tumors esporàdics. Aquests tumors són diploides i generalment mostren una absència de mutacions en els gens que habitualment estan alterats en tumors generats per la via supressora. En canvi, aquests tumors presenten un augment en mutacions en gens relacionats amb la maquinària de reparació de l' ADN com són MLH1 i MSH2 (Gatalica *et al.*, 2008).

1.3. El cicle cel·lular

Les cèl·lules es divideixen a través d'una sèrie ordenada de passos denominats cicle cel·lular; durant el qual la cèl·lula augmenta la seva grandària, el nombre de components intracel·lulars, duplica el seu material genètic i finalment es divideix.

Encara que en realitat el cicle cel·lular està compost per una sèrie continua d'esdeveniments, per conveniència s'ha dividit en dues etapes: divisió i interfase (Figura 4).

- Divisió: En aquesta etapa, cada cèl·lula es divideix en dues cèl·lules filles. La divisió també es coneix generalment com a Mitosi (M), tot i que consta de dos processos fonamentals: mitosi i citocinesi.

  - La mitosi consisteix en el repartiment equitatiu del material genètic per formar els nuclis de les cèl·lules filles.
  - La citocinesi és la separació física del citoplasma en dos cèl·lules filles.

- Interfase: Es denomina així al període que es dóna entre dos divisions successives. La interfase es composa de vàries fases:

  - Fase G1: és el període de temps comprès entre el final de la divisió anterior i la síntesi d'ADN. Si una cèl·lula es manté en estat de repòs i no es divideix, aquesta fase es denomina G0.
  - Fase S: etapa en que té lloc la duplicació de l'ADN.
  - Fase G2: la darrera etapa de preparació per a la divisió cel·lular. Al final d'aquesta etapa, l'ADN comença a condensar-se i els cromosomes es fan visibles.

Així, les cèl·lules a la fase G1 del cicle cel·lular contenen un contingut 2n d'ADN (on "n" es el nombre de cromosomes que han aportat cada un dels progenitors), mentre que les cèl·lules en la fase G2 el tenen de 4n. Les cèl·lules a la fase S es troben duplicant activament el seu material genètic, i per tant, el seu contingut d'ADN es situa entre 2n i 4n.

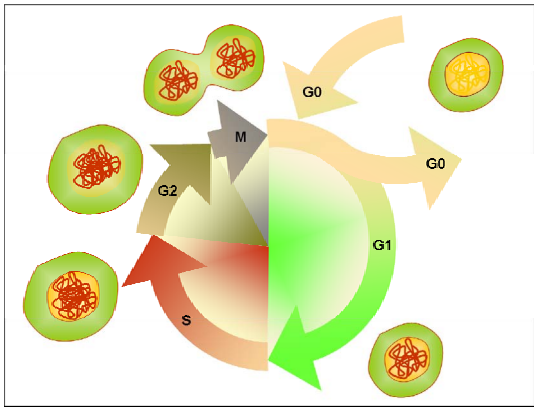

Figura 4. Esquema simplificat del cicle cel·lular i les seves fases.

El conjunt de processos que ocorren durant el cicle cel·lular porten un ordre i supervisió estrictes gràcies a senyals provinents del medi extracel·lular i controladors intracel·lulars. Els

principals efectors de la regulació intracel·lular son uns complexos composts per dos tipus de proteïnes, les cinases depenents de ciclina (CDK - *Cyclin-Dependent Kinases*) i les ciclines. Es coneixen diferents combinacions de CDK-ciclina que actuen en temps específics durant el cicle. D'altra banda, les famílies de proteïnes CIP/KIP i INK4 són inhibidors dels complexos CDK-ciclina. A més d'aquesta regulació intracel·lular, existeix un control extracel·lular del cicle cel·lular mitjançant factors de creixement.

Els mecanismes que controlen el cicle cel·lular són una diana freqüent en càncer, ja que la desregulació del mateix pot provocar una excessiva i inadequada divisió cel·lular. En conseqüència, s'han desenvolupat nombrosos estudis basats principalment en la inhibició de la maquinària que fa possible la progressió del cicle cel·lular com a estratègia antitumoral (Canavese *et al.*, 2012; Roberts *et al.*, 2012).

1.3.1. Diferenciació cel·lular

La diferenciació cel·lular es defineix com el procés durant el qual cèl·lules immadures adopten certes característiques i aconsegueixen la seva forma i funció especialitzades. Com s'ha mencionat anteriorment, les cèl·lules poden sortir reversiblement del cicle cel·lular i entrar en un estat de repòs (fase G0) on hi poden estar fins i tot anys. La sortida del cicle es pot donar també de forma quasi irreversible, com succeeix durant la senescència o durant la diferenciació terminal (Deshpande *et al.*, 2005; Coller *et al.*, 2006).

Les cèl·lules tumorals tenen una morfologia alterada. La diferenciació cel·lular d'un tumor és el grau en el que les cèl·lules tumorals s'assemblen a les cèl·lules normals de les que procedeixen, tant morfològica com funcionalment. Generalment els tumors benignes estan ben diferenciats i els càncers varien des de ben diferenciats a indiferenciats. Generalment quant més desdiferenciat és un càncer més alta és la seva velocitat de creixement i pitjor la prognosi.

1.3.1.1. El butirat com agent diferenciador

Com s'ha comentat anteriorment, l'acetilació de les histones és un mecanisme mitjançant el qual es regula l'expressió gènica. Existeixen diversos grups de compostos amb diferents propietats químiques que són inhibidors d'histones deacetilases (HDACs) (Carafa *et al.*, 2011), enzims encarregats de deacetilar les histones i modificar l'expressió gènica. Entre aquests productes es troben els àcids grassos de cadena curta (SCFA – *Short-Chain Fatty Acids*), els àcids hidroxoàmics i les benzamides. En el primer d'aquests grups es troba el butirat, un àcid gras de quatre àtoms de carboni que s'ha descrit que indueix diferenciació en diverses línies

cel·lulars derivades de tumors de còlon (Zhu *et al.*, 2003; Dashwood *et al.*, 2007). El butirat es troba de forma natural en el còlon, produint-se a partir de la fermentació de la fibra que duu a terme la microflora intestinal (Waldecker *et al.*, 2008) i es utilitzat pels colonòcits com a font d'energia (Ahmad *et al.*, 2000). El butirat realitza la seva acció induint apoptosi i un arrest en la fase G1 del cicle cel·lular (Shen *et al.*, 2008; Andriamihaja *et al.*, 2009). D'una altra banda, s'ha mostrat que el butirat actua també reorganitzant la xarxa metabòlica tumoral (Boren *et al.*, 2003; Alcarraz-Vizan *et al.*, 2010).

1.3.1.2. Diferenciació de les cèl·lules intestinals: via de transducció Wnt

El procés de diferenciació cel·lular està altament regulat al tracte intestinal. Com s'ha mencionat anteriorment, el còlon està organitzat en compartiments de cèl·lules que constitueixen les denominades criptes colòniques. La progènie de cèl·lules mare, localitzades a la base de les criptes, migra a través de les criptes i continua dividint-se fins arribar a la zona medial. En aquest moment, les cèl·lules paren de dividir-se i comencen a diferenciar-se en cèl·lules madures (Medema *et al.*, 2011). Quan les cèl·lules diferenciades arriben a la part apical de la cripta sofreixen un procés de mort per apoptosi i són llavors eliminades per cèl·lules estromals o es desprenen cap al lumen intestinal. Aquest viatge des de la base de la cripta fins al àpex dura al voltant de 3-6 dies.

La fina regulació de la diferenciació intestinal esta bàsicament controlada per la via de transducció Wnt detallada a la figura 5. A les cèl·lules diferenciades de l'epiteli intestinal, no existeix senyalització per Wnt i el complex multi-proteic format per Axina, APC, Glicogen sintasa cinasa 3-beta (GSK3-β) i CKIα participa en la degradació de β-catenina via proteasoma en facilitar la seva fosforilació per GSK3-β i CKIα i el posterior reconeixement per ubiquitina ligases. En presència de senyals Wnt, aquests lligants s'uneixen als receptors Frizzled. Una vegada activat el receptor, la proteïna Dishevelled (Dsh) es fosforilada per CKIε i interacciona amb el complex Axina/APC/GSK3-β/CKIα inhibint la fosforilació i posterior degradació de la β-catenina. Conseqüentment, la β-catenina s'acumula al citoplasma, facilitant-se la seva translocació al nucli, on s'uneix als factors de transcripció T cell factor/lymphoid enhancer factor (TCF / LEF) i actua com coactivador transcripcional de l'expressió de gens implicats en mantenir el fenotip indiferenciat de les cèl·lules, com són *Myc* i *Ciclina D1* (Phelps *et al.*, 2009).

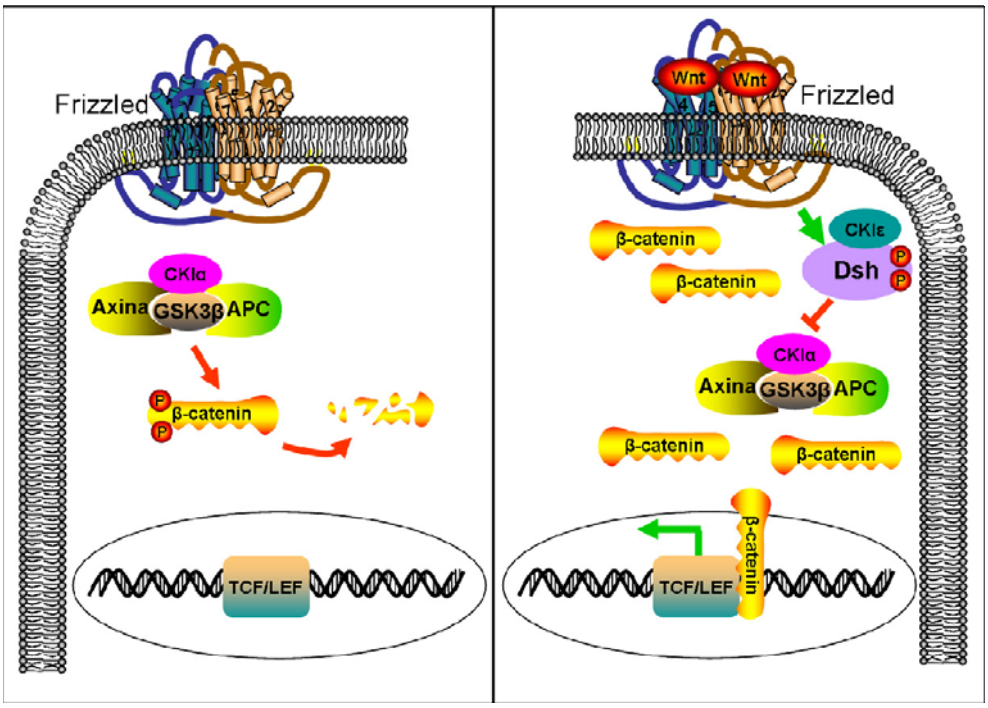

Figura 5. Descripció esquemàtica de la via de senyalització *Wnt*.

1.3.1.2.1. Exemple d'errors en la via Wnt: ratolins Apc$^{Min/+}$

Mutacions que promouen l'activació constitutiva de la via de transducció Wnt condueixen a una taxa de producció de cèl·lules colòniques superior a la taxa de pèrdua, originant així un procés neoplàsic. Un dels exemples més conegut és el model animal de ratolins Apc$^{Min/+}$. Aquest model de ratolí es àmpliament utilitzat per estudiar els efectes d'agents dietètics i farmacèutics sobre el càncer de còlon. El ratolí Apc$^{Min/+}$ conté una mutació autosòmica dominant en heterozigosi al codó 850 del gen *Apc*, homòloga a mutacions presents en càncers de còlon humans. Aquesta mutació causa una proteïna APC defectuosa que promou l'activació aberrant de la senyalització Wnt i predisposa els ratolins a espontàniament desenvolupar pòlips intestinals (McCart *et al.*, 2008).

1.4. L'apoptosi

L'apoptosi és un mecanisme cel·lular clau que consisteix en eliminar de l'organisme aquelles cèl·lules que es troben en excés, danyades o que poden representar un perill per a l'organisme. Aquest procés, que també rep el nom de mort cel·lular programada, finalitza amb el desmantellament complet de les principals estructures cel·lulars de forma controlada, de manera que l'eliminació cel·lular no produeix efectes nocius o inflamatoris a teixits contigus. En aquest

aspecte es diferencia de la necrosi, un procés que es desencadena com a resposta a una agressió més dràstica i que es caracteritza per una dissolució dels orgànuls i pèrdua del control de la permeabilitat de la membrana amb la conseqüent entrada de fluids que causen edema cel·lular, vesiculació i finalment expulsió del contingut intracel·lular per la ruptura de la membrana, alliberant hidrolases que afecten als teixits contigus i generen inflamació. Morfològicament, l'apoptosi presenta una sèrie de característiques ben definides que inclouen la condensació de la cromatina, canvis en els orgànuls i alteracions de la membrana cel·lular, produint eventualment els anomenats cossos apoptòtics. Aquests estan constituïts per restes de components citoplasmàtics i nuclears envoltats de membrana cel·lular i són eliminats de l'entorn extracel·lular per fagòcits, evitant així la lesió i inflamació dels teixits circumdants. La maquinària intracel·lular d'apoptosi depèn d'una família de proteases específiques anomenades caspases. Les caspasas es troben a les cèl·lules en forma inactiva (procaspases) i són activades per proteòlisi. Aquestes al seu torn activen altres procaspases en una cascada d'amplificació (Ghavami *et al.*, 2009). Les caspases activen proteïnes clau com per exemple la laminina que degrada l'embolcall nuclear.

Els senyals de mort poden originar-se a dos nivells (Figura 6):

- La via extrínseca, lligada a receptors de mort (Fas), s'inicia quan l'activació d'un d'aquests receptors recluta molècules adaptadores que subseqüentment activen la procaspasa 8, la qual cosa resulta suficient per processar la caspasa 3 i iniciar la cascada proteolítica.

- La via intrínseca, també anomenada mitocondrial, en la qual la permeabilització d'aquest orgànul condueix a l'alliberament de proteïnes proapoptòtiques com el citocrom c, causant la formació d'un complex anomenat apoptosoma que és capaç de desencadenar la cascada proteolítica apoptòtica.

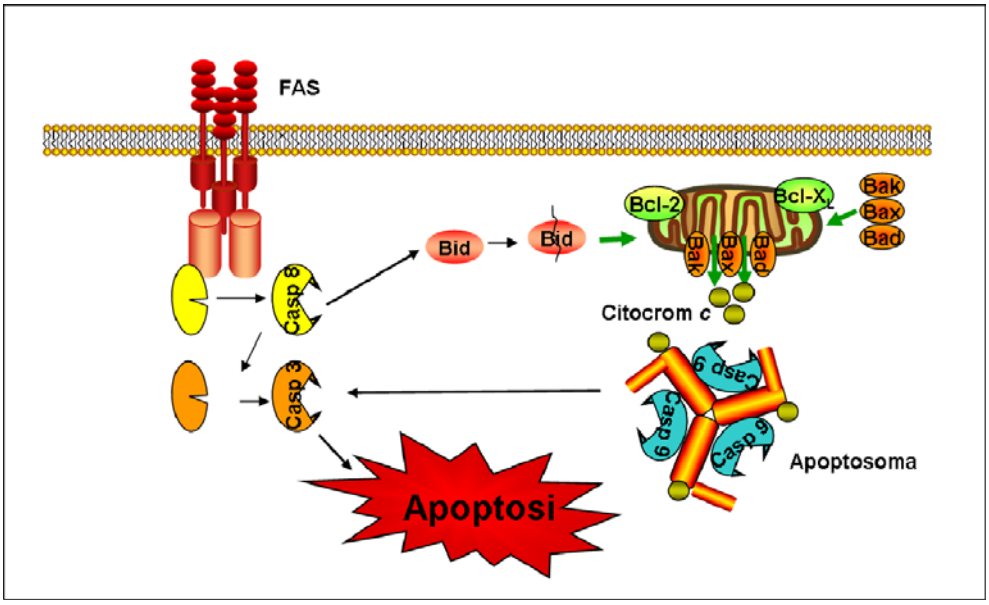

Figura 6. Mecanismes moleculars d'apoptosi a través de la via intrínseca o extrínseca.

El procés d'apoptosi està altament controlat per una complexa xarxa de mediadors intracel·lulars i extracel·lulars. Destaquen els membres de la família Bcl-2, dins de la qual existeixen membres que promouen l' apoptosi mitjançant l'alliberació de proteïnes mitocondrials apoptogèniques (com Bak, Bax o Bad) i també membres antiapoptòtics com Bcl-2 o Bcl-XL, que ajuden a mantenir l' integritat de la membrana mitocondrial. A més, també existeixen proteïnes com Bid que poden connectar els mecanismes extrínsec i intrínsec (Adams *et al.*, 1998).

Com s'ha comentat anteriorment, la capacitat de resistència a l' apoptosi es considera una de les principals característiques de la progressió tumoral. Els defectes en la maquinària apoptòtica ocasionen sovint fenòmens de resistència als fàrmacs antitumorals que actuen induint l'apoptosi de les cèl·lules malignes (MacKenzie *et al.*, 2010; Veldhoen *et al.*, 2012).

1.5. L'angiogènesi tumoral

L'angiogènesi és un procés fisiològic que consisteix en la formació de nous vasos sanguinis a partir de vasos preexistents. En humans, l'angiogènesi és un fenomen normal que es produeix durant el desenvolupament embrionari i la cicatrització de ferides. No obstant això, també és un procés fonamental en la progressió tumoral maligna. En aquest últim cas, es parla d'angiogènesi tumoral. Com s'ha esmentat anteriorment, les cèl·lules tumorals activen el procés angiogènic per tal d'assegurar l'aportació d'oxigen i nutrients essencials per al creixement del tumor.

L'activació angiogènica és fruit d'un desequilibri entre senyals inductores i senyals inhibidores de l'angiogènesi a favor de les primeres. Entre les senyals que regulen l'angiogènesi hi ha factors solubles com el factor de creixement endotelial vascular (VEGF - *Vascular Endothelial Growth Factor*) o el factor de creixement de fibroblasts (FGF - *Fibroblast Growth Factor*), angioestatines i citoquines. Entre aquests factors, cal destacar el VEGF com un factor crucial durant l'angiogènesi tumoral (Shojaei, 2012). L'any 2003, es va aprovar el Bevacizumab (Avastin®, Genetech Inc.), un anticòs neutralitzador del VEGF, com a primer agent anti-angiogènic pel tractament del càncer colorectal metastàtic (Sato *et al.*, 2012). Des de llavors, diferents inhibidors angiogènics s'estan utilitzant com fàrmacs antitumorals. Tot i això, recentment s'han descrit diferents inconvenients per a la teràpia anti-angiogènica existent, incloent l'aparició de resistències i la inducció de l'invasivitat i la metàstasi tumoral (Paez-Ribes *et al.*, 2009). Per tant, es requereixen nous estudis per aconseguir una teràpia més eficient, basada en l'atac d'altres dianes angiogèniques o en la combinació de fàrmacs anti-angiogènics.

1.6. El metabolisme tumoral

El gran potencial maligne de la cèl·lula tumoral no es manifesta mentre que no es produeixin en ella alteracions metabòliques que li permetin abastir l'alta demanda energètica i biosintètica necessàries per mantenir l'elevada taxa de proliferació tumoral (Kroemer *et al.*, 2008; Samudio *et al.*, 2009; Samudio *et al.*). Per tant, per adquirir un fenotip tumoral complert les cèl·lules canceroses han de reprogramar el seu metabolisme. L'adaptació metabòlica tumoral es caracteritza per, entre d'altres, una elevada glicòlisi, fins i tot en presència d'oxigen (característica també coneguda com efecte Warburg), l'activació de vies biosintètiques i un elevat consum de glutamina (Figura 7). Aquestes característiques metabòliques tumorals no només representen el punt final de diverses cascades de transducció cel·lular, sinó que també actuen activament conferint a les cèl·lules la capacitat per sobreviure, proliferar i envair (Vizán *et al.*, 2008). Per tant, el metabolisme tumoral ofereix la possibilitat de dissenyar noves estratègies terapèutiques basades en revertir o bloquejar específicament les adaptacions metabòliques adquirides (Vizan *et al.*, 2009a).

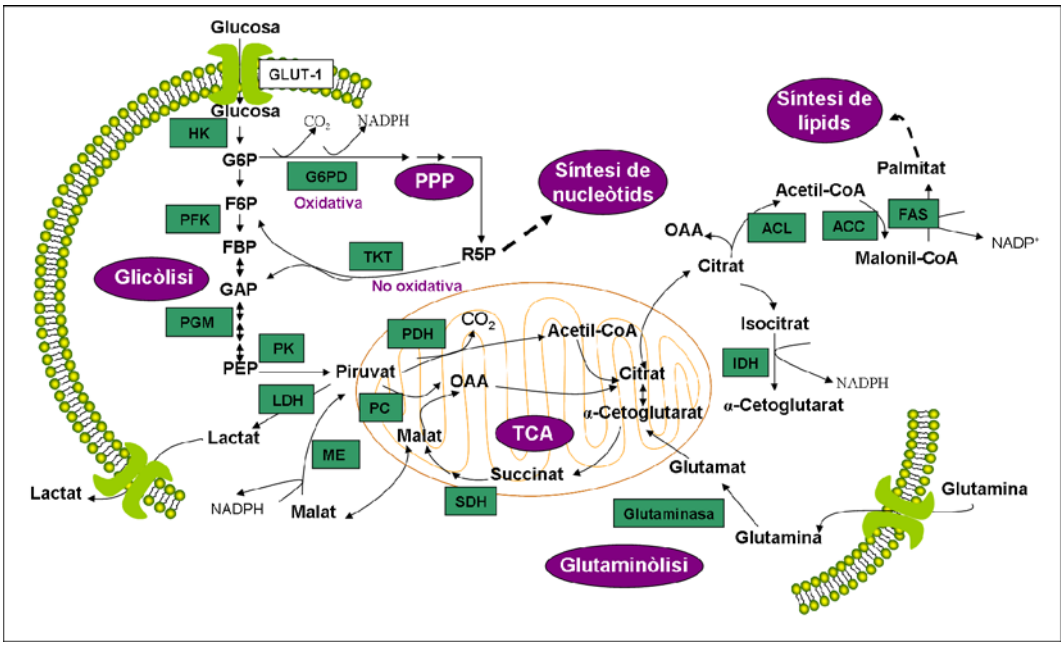

Figura 7. Representació de les vies metabòliques més afectades en càncer. GLUT-1, transportador de glucosa; HK, hexokinasa; PFK, fosfofructocinasa; PGM, fosfoglicerat mutasa; PK, Piruvat cinasa; LDH, lactat deshidrogenasa; ME, enzim màlic; PDH, piruvat deshidrogenasa; PC, Piruvat carboxilasa; SDH, succinat deshidrogenasa; IDH, isocitrat deshidrogenasa; ACL, ATP-citrat liasa; ACC, acetil-CoA carboxilasa; FAS, àcid gras sintasa; TKT, transcetolasa; G6PD, glucosa-6-fosfat deshidrogenasa; G6P, glucosa-6-fosfat; F6P, fructosa-6-fosfat; FBP, fructosa-1,6-bisfosfat; GAP, gliceraldehid-3-fosfat; PEP, fosfoenolpiruvat; OAA, oxaloacetat; R5P, ribosa-5-fosfat; TCA, cicle dels àcids tricarboxílics; PPP, via de les pentoses fosfat.

1.6.1. Glicòlisi

Les cèl·lules tendeixen a degradar la glucosa per via glicolítica fins a formar piruvat. En condicions aeròbiques, aquest piruvat entra a la mitocòndria on continua la seva metabolització a través del cicle dels àcids tricarboxílics (TCA - *Tricarboxylic Acid*) o cicle de Krebs. Aquest procés genera una gran quantitat de poder reductor capaç de donar electrons a la cadena de transport d'electrons o cadena respiratòria per generar energia en forma de d'adenosina trifosfat (ATP - *Adenosine TriPhosphate*) en el procés conegut com fosforilació oxidativa. Per mitjà d'aquest procés metabòlic, la cèl·lula consumeix glucosa i oxigen i genera com a productes finals diòxid de carboni (CO_2) i aigua. En condicions anaeròbiques, les cèl·lules normals poden sobreviure transformant el piruvat en lactat. Aquest mecanisme, conegut com a glicòlisi anaeròbica, és molt ineficient a l'hora d'obtenir energia ja que únicament genera 2 molècules d'ATP per molècula de glucosa, enfront als 36 que produeix la fosforilació oxidativa. A més, d'aquesta manera es genera lactat, que a concentracions elevades és tòxic per a les cèl·lules.

La primera característica distintiva a nivell metabòlic per a les cèl·lules tumorals, ja descrita per Otto Warburg l'any 1924, és la seva elevada taxa de transformació de glucosa a lactat fins i tot en condicions aeròbiques (Govardhan *et al.*, 2011). A aquest mecanisme, a més de com a efecte Warburg, també se'l coneix com a glicòlisi aeròbica en contraposició a la glicòlisi anaeròbica pròpia de les cèl·lules normals. Encara que les causes de la glicòlisi aeròbica i la seva relació amb el desenvolupament del càncer són polèmiques, una glicòlisi elevada ha estat observada sistemàticament en moltes cèl·lules tumorals de diferents teixits d'orígens diversos, suggerint que aquesta alteració metabòlica és comú en el càncer. Durant molts anys es va creure que la disminució en l'oxidació del piruvat en cèl·lules tumorals era deguda a defectes en la cadena respiratòria o en el mateix mitocondri, de manera que la cèl·lula no tenia més alternativa que aconseguir l'energia necessària per a proliferar mitjançant la conversió de piruvat a lactat. Per contra, s'ha demostrat que aquests defectes no són comuns en tots els tumors i que la inhibició de la cadena respiratòria no causa una elevada taxa glicolítica (Lunt *et al.*, 2011). En aquest sentit, un treball de Fantin i col·laboradors demostra que algunes cèl·lules tumorals encara mantenen la capacitat de produir ATP per fosforilació oxidativa però que tot i això "decideixen" promoure la glicòlisi anaeròbica (Fantin *et al.*, 2006).

Els avantatges que la glicòlisi aeròbica ofereix a les cèl·lules tumorals són diversos. En primer lloc, cal tenir en compte que la constant proliferació en què es troben les cèl·lules canceroses exigeix d'una banda, obtenir energia de manera ràpida i per una altra, generar biomassa en gran quantitat i a gran velocitat. En aquesta situació, s'ha demostrat que l'efecte Warburg és un procés que permet obtenir energia de manera molt més ràpida que la fosforilació oxidativa, i a més, s'ha proposat que podria ser un mètode molt efectiu per augmentar les taxes biosintètiques (Grivennikov *et al.*, 2010b). El problema de la baixa eficiència metabòlica en les cèl·lules tumorals es pot solucionar gràcies a la sobreexpressió de transportadors com GLUT1 que permetin elevar el consum de glucosa (Ortega *et al.*, 2009). Cal destacar que aquest fenomen ha estat explotat en la clínica per a la detecció de neoplàsies mitjançant tomografia d'emissió de positrons (PET - *Positron Emission Tomography*). Aquesta tècnica de diagnòstic consisteix en subministrar als pacients 18F-fluorodeoxiglucosa, un anàleg de la glucosa que, malgrat no ser metabolitzable, és reconegut pels transportadors i introduït en les cèl·lules on pot ser detectat. D'aquesta manera, les cèl·lules tumorals, que incorporen més glucosa, també incorporaran una major quantitat de 18F-fluorodeoxiglucosa, revelant l'existència i localització dels tumors (Ozhan *et al.*, 2012).

Una altra possible explicació a la glicòlisi anaeròbica observada en tumors podria ser una reducció selectiva en l'ús de la mitocòndria per evitar l'apoptosi, ja que la cadena respiratòria és

la principal generadora d'espècies reactives d'oxigen (ROS – *Reactive Oxigen Species*) que poden portar a la mort cel·lular programada.

A més a més, la producció de lactat provocada per la glicòlisi aeròbica implica grans avantatges per a les cèl·lules tumorals i propicia l'adquisició d'algunes de les seves característiques malignes. D'una banda, l'acidificació del medi peritumoral indueix la mort de les cèl·lules normals que envolten el tumor, reduint la inhibició de la proliferació per contacte i facilitant el creixement del tumor (Gillies *et al.*, 2008). D'altra banda, existeix un fenomen de secreció induïda per acidosi que activa l'angiogènesi (Shi *et al.*, 2001). A més, l'acidosi provoca que fibroblasts i macròfags de l'entorn tumoral alliberin enzims proteolítics que indueixen la degradació de la matriu extracel·lular i afavoreixen la invasivitat i la metàstasi (Walenta *et al.*, 2004). Finalment, l'acidosi també inhibeix la resposta immunitària (Mendler *et al.*, 2011).

1.6.2. La glutaminòlisi

L'elevat consum de glucosa que presenten les cèl·lules tumorals és una de les característiques més estudiades del metabolisme tumoral (Sottnik *et al.*, 2011). No obstant això, la glucosa no és l'única font de carboni i energia en la que aquestes cèl·lules basen la seva adaptació metabòlica. Les cèl·lules tumorals poden catabolitzar substrats alternatius com la glutamina per generar ATP i lactat. Aquest procés es coneix com glutaminòlisi. Les dades sobre quin és el paper concret del catabolisme de la glutamina en el metabolisme tumoral són dispars. Mentre que diverses publicacions demostren que hi ha cèl·lules tumorals que desenvolupen una dependència total del catabolisme de la glutamina per mantenir la seva taxa de proliferació (Gao *et al.*, 2009; Meng *et al.*, 2010), existeixen altres treballs que defensen tot el contrari (Sandulache *et al.*, 2011). A més, també hi ha divergències en el destí metabòlic de la glutamina consumida per les cèl·lules tumorals. Una línia de resultats defensa que gran part de la glutamina consumida es deriva a lactat o alanina per formar, via enzim màlic, grans quantitats de nicotinamida adenina dinucleòtid fosfat (NADPH - *Nicotinamide Adenine DiNucleotide Phosphate*) que permetin proveir processos anabòlics com la síntesi d'àcids grassos o de nucleòtids (Wise *et al.*, 2008). Aquests treballs donen un paper secundari a l'ús de l'esquelet carbonat de la glutamina per emplenar anapleròticament el TCA i sintetitzar lípids o generar aminoàcids no essencials que es destinin a la síntesi proteica. Altres línies de resultats mantenen que la funció principal de la glutaminòlisi és la formació d'ATP i la conservació de l'homeòstasi redox cel·lular (Gao *et al.*, 2009). D'una altra banda, hi ha estudis que defensen el paper de la glutaminòlisi com a font de nitrogen necessari per a la síntesi d'aminoàcids no essencials i proteïnes (Meng *et al.*, 2010; Sandulache *et al.*, 2011). Probablement totes les funcions

proposades juguen un paper important en el metabolisme cel·lular depenent del tipus cel·lular i de l'estat fisiològic. Independentment dels dubtes que encara existeixen sobre la destinació de la glutamina consumida i la seva implicació en les cèl·lules tumorals, el que és evident és que aquesta via metabòlica es troba sobreactivada en molts tipus de tumors (DeBerardinis *et al.*, 2007). A més a més, s'ha demostrat que la inhibició de la glutaminòlisi disminueix la proliferació de cèl·lules tumorals i es correlaciona amb la diferenciació fenotípica i funcional d'aquestes cèl·lules (Sun *et al.*, 2011b).

1.6.3. L'activació de rutes biosintètiques

L'elevada proliferació pròpia de les cèl·lules tumorals implica una sobreactivació important de totes les rutes biosintètiques. Concretament, la formació de dues cèl·lules filles que continguin la mateixa dotació genètica ve lligada a una duplicació de l'ADN cel·lular. Així mateix, la divisió cel·lular requereix d'una gran quantitat de fosfolípids de nova síntesi que permetin formar les noves membranes cel·lulars. Per això, podem destacar dos grups de molècules la biosíntesi de les quals és fonamental: els àcids nucleics i els lípids.

L'activació de la via de les pentoses fosfat, que genera ribosa-5-fosfat, és necessària per a la biosíntesi de nucleòtids i per a generar poder reductor en forma de NADPH, necessari per a la síntesi lipídica i el manteniment de la capacitat reductora cel·lular (Tong *et al.*, 2009). La ribosa-5-fosfat pot ser sintetitzada a partir de glucosa-6-fosfat a través de la branca oxidativa de la ruta de les pentoses fosfat, així com a partir de fructosa-6-fosfat i gliceraldehid-3-fosfat per la branca no oxidativa. La branca oxidativa està catalitzada per la glucosa-6-fosfat deshidrogenasa (G6PD - *Glucose-6-Phosphate Dehydrogenase*) i la 6-fosfat-gluconat deshidrogenasa mentre que la branca no oxidativa d'aquesta via està catalitzada per la transcetolasa (TKT - *Transketolase*) i la transaldolasa. Cal ressaltar que s'ha demostrat la importància de la via de les pentoses fosfat en diverses línies tumorals (Boros *et al.*, 2000; Boren *et al.*, 2006), i s'han identificat els dos enzims clau de la via, la G6PD i la TKT com a possibles dianes en la teràpia antitumoral (Ramos-Montoya *et al.*, 2006; Vizan *et al.*, 2009a). A més, s'ha descrit que durant l'activació angiogènica augmenta l'activitat de la via de les pentoses fosfat (Vizan *et al.*, 2009b).

La lipogènesi, o síntesi *de novo* d'àcids grassos, és una altra ruta biosintètica clau per al desenvolupament tumoral (Mashima *et al.*, 2009). En aquest sentit, s'ha observat que diverses cèl·lules tumorals expressen alts nivells dels enzims lipogènics ATP citrat liasa (ACL), acetil-CoA carboxilasa (ACC) i àcid gras sintasa (FAS – *Fatty Acid Synthase*) (Swinnen *et al.*, 2006).

2. APLICACIÓ DE PRODUCTES NATURALS COM ANTITUMORALS

Des de fa segles s'han utilitzat els productes naturals com a fàrmacs per tractar innombrables malalties. D'acord amb l'OMS (http://www.who.int/es/), en alguns països asiàtics i africans el 80% de la població depèn de la medicina tradicional. A més, en molts països desenvolupats, del 70% al 80% de la població ha acudit alguna vegada a aquesta medicina alternativa.

L'estudi de l'efecte biològic i de les estructures químiques dels principis actius dels productes naturals ha resultat útil per a la formulació i síntesi de nous fàrmacs. Així, moltes medicines modernes procedeixen de plantes que ja s'utilitzaven en la medicina tradicional.

Certament, nombrosos estudis han relacionat una dieta rica en fruites i verdures i el consum de suplements nutritius naturals amb un menor risc de càncer colorectal (Forte *et al.*, 2008). A més, evidències tant experimentals com epidemiològiques indiquen que l'estil de vida occidental, caracteritzat per una dieta altament calòrica, rica en greix, carbohidrats processats i proteïna animal i, a la vegada, pobra en fibra, fruites i verdures, combinada amb baixa activitat física, augmenta el risc de patir càncer colorectal (Ballinger *et al.*, 2007). Molts d'aquests estudis coincideixen en indicar que el que promou els efectes beneficiosos d'aquests productes és el seu alt contingut en polifenols, triterpenoids i fibra, que arriben al colon en concentracions elevades (Davis *et al.*, 2009).

Les propietats beneficioses dels polifenols s'han relacionat generalment amb la seva activitat antioxidant. Els principals mecanismes d'aquesta activitat són la neutralització directa de les ROS, la quelació d'ions metàl·lics de transició i el manteniment dels sistemes antioxidants endògens com el glutatió (Tourino *et al.*, 2008). D'una altra banda, els polifenols també mostren efectes prooxidants. Així, s'ha descrit que aquests també poden exercir un efecte citoprotector a partir d'un estímul oxidatiu suau que estimula els mecanismes de defensa antioxidant endògenes i els sistemes del metabolisme de xenobiòtics (Halliwell, 2008). Els efectes redox dels polifenols es deuen bàsicament a la seva estructura química que facilita una elevada mobilitat dels electrons en els anells benzènics. L'activitat dual antioxidant/prooxidant s'explica pel balanç entre la forma reduïda del polifenol, la qual actua com antioxidant, i la seva forma oxidada, la qual actua com prooxidant (Galati *et al.*, 2004). A més, s'ha observat que la capacitat redox dels compostos polifenòlics està també relacionada amb la concentració a la qual s'utilitzen. En concret, s'ha suggerit que els polifenols presenten activitat antioxidant a concentracions baixes, podent arribar a ser prooxidants a concentracions elevades (Raza *et al.*, 2005; Tian *et al.*, 2007). A més a més, s'ha proposat que probablement el mecanisme antioxidant/prooxidant depèn del tipus de càncer i de l'entorn cel·lular (Forester *et al.*, 2011). A

part de la seva participació en reaccions redox, els polifenols també poden modificar funcions cel·lulars per interaccions amb biomolècules. La semblança de l'estructura dels polifenols amb la d'altres biomolècules explicaria la capacitat que presenten per inhibir enzims, proteïnes de transducció, factors de transcripció, receptors i la formació de fibres amiloides (Porat *et al.*, 2006; Amakura *et al.*, 2008; Bastianetto *et al.*, 2009; Trzeciakiewicz *et al.*, 2009).

D'una altra banda, la fibra dietètica és també considerada un component clau de la dieta amb potencials beneficis per a la salut. La fibra produeix canvis en la massa i contingut fecal i estimula selectivament el creixement de la microbiota intestinal sana (Lizarraga *et al.*, 2011). A més, diversos estudis han mostrat una relació inversa entre el consum de fibra dietètica i el risc de càncer colorectal. Per exemple, un estudi en rates ha mostrat que alguns components de la fibra poden reduir el desenvolupament de lesions preneoplàsiques. A part de les activitats biològiques esmentades anteriorment, l'acció antitumoral de la fibra s'explica per les propietats beneficioses dels SCFA, com el butirat i el propionat, alliberats per la fermentació de la fibra (Hu *et al.*, 2011).

Finalment, cal destacar la gran varietat d'activitats biològiques produïda pels triterpenoids. Dins d'aquest grup, els triterpens pentacíclics han estat identificats com els principals components de plantes medicinals utilitzades de forma tradicional i han mostrat, entre altres, efectes analgèsics, hepatoprotectors, anti-tumorals, anti-virals, anti-inflamatoris, antioxidants i moduladors del sistema immune (Dzubak *et al.*, 2006).

2.1. *Hamamelis virginiana*

L'avellaner de bruixa (*Hamamelis virginiana*) és un arbust nord-americà que ha estat històricament explotat en la medicina tradicional. Aquesta planta és una font rica en polifenols. D'una banda, conté molts tanins condensats o proantocianidines i de l'altra, conté tanins hidrolitzables com són l'hamamelitanin (HT) i la pentagaloilglucosa (PGG) (Vennat *et al.*, 1988) (Figura 8).

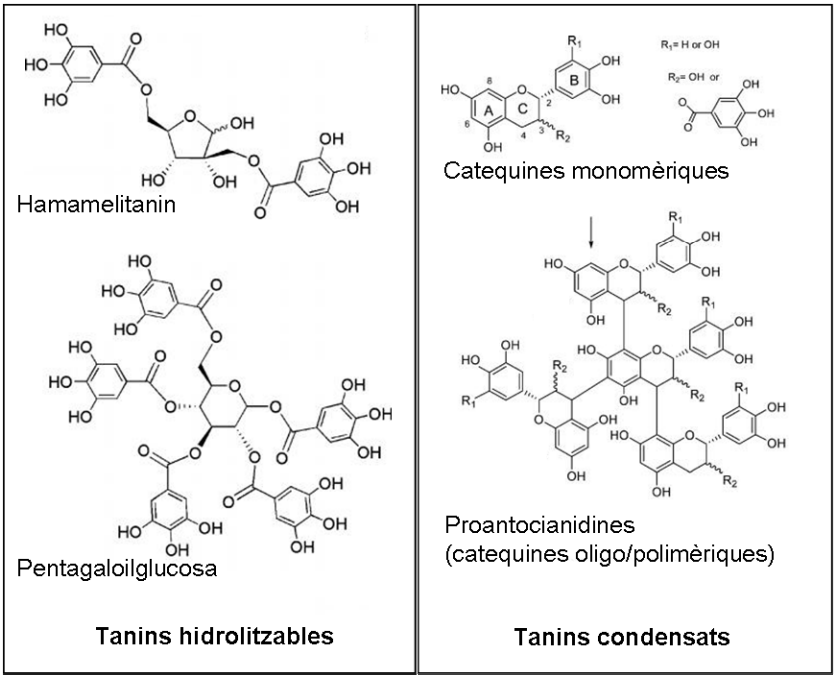

Figura 8. Estructura dels tanins condensats i hidrolitzables presents en *Hamamelis virginiana.*

Diversos estudis han analitzat l'activitat redox i la citotoxicitat dels compostos polifenòlics presents en *H. virginiana*. Un treball de Touriño i col·laboradors (Tourino *et al.*, 2008) descriu que diferents fraccions polifenòliques extretes de l'escorça d' *H. virginiana* són altament actives com neutralitzadors de radicals lliures com són 2,2′-azinobis(3-etilbenzotiazolina-6-sulfonic àcid) (ABTS), 1,1-difenil-2-picrilhidrazil (DPPH) i tris(2,4,6-tricloro-3,5-dinitrofenil)metil (HNTTM). A més, també redueixen el radical tris(2,3,5,6-tetracloro-4-nitrofenil)metil (TNPTM), el qual indica que contenen grups hidroxi altament reactius. D'acord amb això, aquestes fraccions protegeixen uns glòbuls vermells de l'hemòlisi produïda per radicals lliures. A banda d'això, algunes fraccions extretes de l'escorça d'*H. virginiana* han mostrat capacitat per inhibir la proliferació d'una línia cel·lular de melanoma (SK-Mel 28) (Tourino *et al.*, 2008) i també de cèl·lules d'adenocarcinoma de colon HT29. En aquest últim cas, les fraccions d' *H. virginiana* produeixen un arrest en la fase S del cicle cel·lular i indueixen apoptosi (Lizarraga *et al.*, 2008).

Pel que fa als tanins condensats, nombroses evidències indiquen que aquestes proantocianidines extretes de diverses fonts poden inhibir el càncer de còlon (Mutanen *et al.*, 2008; Chung *et al.*, 2009). Per exemple, un estudi *in vitro* ha demostrat que un extracte de llavor de raïm ric en proantocianidines es capaç d'inhibir la viabilitat i augmentar l'apoptosi en

cèl·lules Caco-2 de càncer de còlon. A més, de manera interessant, aquest extracte no afecta la viabilitat d'una línia de colonòcits normals (NCM460) (Engelbrecht *et al.*, 2007).

D'una altra banda, molts estudis *in vitro* i *in vivo* han mostrat que els tanins hidrolitzables d' *H. virginiana* presenten múltiples activitats biològiques, les quals es poden relacionar amb un efecte preventiu o terapèutic contra el càncer. En el cas de la PGG, diversos estudis *in vivo* han demostrat inhibició en càncer de pròstata (Kuo *et al.*, 2009), pulmó (Huh *et al.*, 2005) i sarcoma (Miyamoto *et al.*, 1987). Estudis *in vitro* han mostrat inhibició de càncer de pit, fetge, leucèmia i melanoma (Oh *et al.*, 2001; Ho *et al.*, 2002; Chen *et al.*, 2003; Chen *et al.*, 2004). Aquesta capacitat antitumoral s'ha relacionat amb la seva activitat antioxidant, antiinflamatòria, antiproliferativa, antiangiogènica i amb la seva capacitat per induir apoptosi i arrest del cicle cel·lular. Concretament; p53, Stat3, Cox-2, VEGFR1, AP-1, SP-1, Nrf-2, i MMP-9 s'han descrit com algunes de les dianes de la PGG. En canvi, els efectes antitumorals de l'HT no s'han examinat en profunditat. Tot i això, algunes propietats de l'HT es podrien relacionar amb un efecte protector contra el cáncer. En primer lloc, s'ha descrit que aquest taní hidrolitzable exerceix una activitat antigenotòxica en cèl·lules HepG2 d'hepatoma humà (Dauer *et al.*, 2003). A més, l'HT ha mostrat una activitat inhibidora del factor de necrosi tumoral (TNF) (Habtemariam, 2002) i de la lipooxigenasa (LOX) (Hartisch *et al.*, 1997), els quals han estat implicats en la transformació maligna.

2.2. Té verd

El té (*Camellia sinensis*) és la segona beguda més consumida del món i representa una font particularment important de polifenols coneguts com catequines. Les catequines més importants del te verd són (-)-epigal.locatequin gal.lat (EGCG), (-)-epicatequin gal.lat (ECG), (-)-epigal.locatequina (EGC) i (-)-epicatequina (EC) (Figura 9). Aquests polifenols han estat àmpliament descrits com quimiopreventius en càncer. Les seves activitats antitumorals principals són l'inducció d'apoptosi i arrest de cicle cel·lular. A més, la capacitat antioxidant, l'inhibició d'enzims relacionats amb la promoció tumoral com la ciclooxigenasa (COX) i la LOX, l'inhibició de l'angiogènesi, l'inhibició de l'invasió i la metàstasi, entre altres, també han estat suggerits com potencials mecanismes antitumorals (Siddiqui *et al.*, 2008; Kanwar *et al.*, 2012). Els mecanismes moleculars implicats en aquestes accions són la modulació de la transducció de senyals cel·lulars incloent les cinases activades per mitògens (MAPK), les CDK, les metaloproteinases de matriu (MMP), proteasomes, etc (Yang *et al.*, 2011). Més recentment, s'ha descrit que les catequines del té verd modulen també l'activitat de diferents receptors i transportadors cel·lulars mitjançant l'alteració d'unes regions de la membrana cel·lular

anomenades lípid *rafts* (Patra *et al.*, 2008). Malgrat que l'activitat antitumoral del té verd ha estat estudiada en molts treballs tant *in vitro* com *in vivo*, la capacitat quimiopreventiva dels polifenols del té no ha estat coherentment demostrada en tots els estudis, incloent-hi els assaigs clínics (Yang *et al.*, 2010). Per consegüent, es requereixen estudis addicionals sobre el potencial efecte antitumoral de les catequines del té verd.

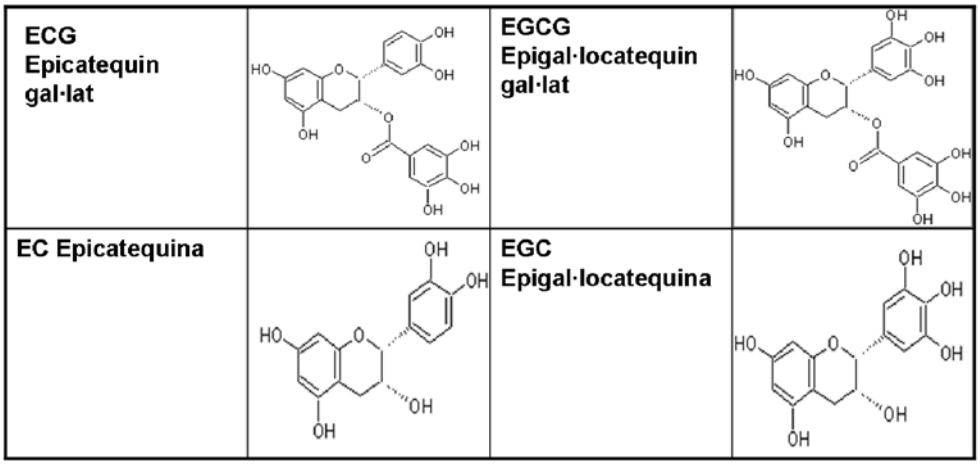

Figura 9. Estructura de les catequines majoritàries en té verd.

2.3. Raïm

Els compostos polifenòlics de raïm (*Vitis vinifera*), principalment oligòmers d'epicatequina i epicatequin gal.lat (proantocianidines), han estat àmpliament descrits com antitumorals. Concretament en càncer de còlon, el tractament de diferents línies cel·lulars amb extractes de raïm ha mostrat una inhibició en la proliferació i una inducció d'apoptosi i arrest del cicle cel·lular en la fase G1 (Lizarraga *et al.*, 2007; Hsu *et al.*, 2009). A més, l'extracte de llavor de raïm s'ha descrit que redueix el creixement de cèl·lules d'adenocarcinoma colorectal HT29 implantades en ratolins atímics (Kaur *et al.*, 2006), la formació de criptes aberrants activada per azoximetà en rates (Velmurugan *et al.*, 2010a) i la formació de pòlips intestinals en ratolins $Apc^{Min/+}$ (Velmurugan *et al.*, 2010b).

2.3.1. Fibra dietètica antioxidant de raïm

La fibra dietètica antioxidant de raïm (GADF - *Grape Antioxidant Dietary Fiber*) és un producte particularment interessant degut al seu alt contingut en proantocianidines polimèriques insolubles. Aquests polímers formen part de la fracció de fibra dietètica juntament amb lignines

i polisacàrids. Durant el seu transit al llarg del tracte intestinal, els polifenols senzills solubles continguts a la fibra són absorbits per les cèl·lules intestinals i les proantocianidines alliberen progressivament unitats d'(epi)catequina que són llavors absorbides. Les proantocianidines polimèriques restants són metabolitzades per la microbiota intestinal en espècies més senzilles com els àcids fenòlics, els quals són finalment absorbits (Tourino *et al.*, 2011). Estudis anteriors en rates Wistar han mostrat que la GADF exerceix un efecte protector de la mucosa colònica el qual ha estat atribuït a la modulació del sistema redox del glutatió i d'enzims antioxidants endògens (Lopez-Oliva *et al.*, 2010). Més recentment, Lizárraga i col·laboradors han descrit que la inclusió de la GADF a la dieta de ratolins C57BL/6J protegeix el teixit colònic del desenvolupament tumoral mitjançant la modulació de gens supressors de tumors, d'oncògens, d'enzims pertanyents al sistema de detoxificació de xenobiòtics i també dels sistemes de defensa antioxidants endògens (Lizarraga *et al.*, 2011).

2.4. Àcid maslínic

L'àcid maslínic (MA – *Maslinic Acid*) (Figura 10) és un triterpè pentacíclic d'origen natural que es especialment abundant a la cera que recobreix les olives (*Olea europaea*) (Li *et al.*, 2010). S'ha descrit que aquest compost exerceix potents activitats antioxidants (Sultana *et al.*, 2007), antiinflamatòries (Marquez-Martin *et al.*, 2006), antivirals (Xu *et al.*, 1996), parasitostàtiques (Moneriz *et al.*, 2011) i antidiabetogèniques (Fernandez-Navarro *et al.*, 2008). Més recentment, alguns estudis han mostrat que l'MA també posseeix capacitat antitumoral en diferents tipus cel·lulars com són les cèl·lules de melanoma (Parra *et al.*, 2011), les cèl·lules de càncer de fetge (Lin *et al.*, 2011), les cèl·lules de càncer del pit (Allouche *et al.*, 2011) i les cèl·lules de càncer del còlon. Amb referència a les malignitats de còlon, s'ha demostrat que l'MA es capaç de reduir la proliferació i d'induir apoptosi, arrest a la fase G1/G0 del cicle cel·lular i diferenciació en cèl·lules de càncer de còlon, sense alterar el comportament de cèl·lules intestinals normals (Reyes *et al.*, 2006). L'estudi dels mecanismes moleculars en aquests estudis *in vitro*, mostra que el MA inhibeix l'expressió de la ciclina D1 (Yap *et al.*, 2012) i de la proteïna antiapoptòtica Bcl-2 (Reyes-Zurita *et al.*, 2009). L' inducció d' apoptosi per l'MA també s'ha relacionat amb la seva capacitat per activar la proteïna JNK (Reyes-Zurita *et al.*). A més, aquest compost també ha estat mostrat com un potent inhibidor dels factors de transcripció nuclear factor κB (NF-κB) i AP-1 i també de COX-2 (Hsum *et al.*, 2011; Huang *et al.*, 2011).

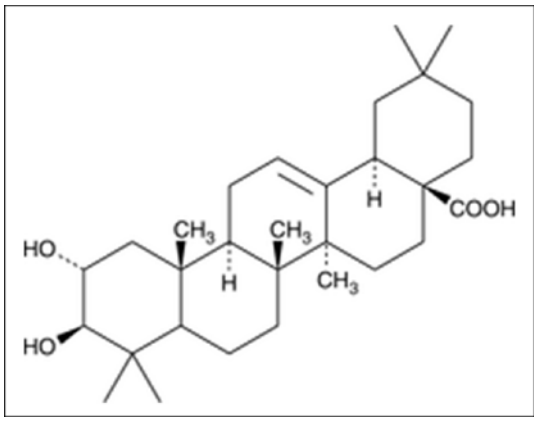

Figura 10. Estructura de l'àcid maslínic.

3. BIOLOGIA DE SISTEMES

Tradicionalment, el mètode científic més habitual per aproximar-se a un sistema biològic complex ha estat el del reduccionisme, per tal d'intentar descompondre'l en les seves parts components, més senzilles de comprendre o modelar. No obstant això, aquest nivell de coneixement biològic resulta molt limitat si no es coneixen les interaccions entre els diferents elements i la manera en què cooperen en cada procés o alteren el funcionament de les altres parts. Un sistema viu, des del microorganisme més primitiu a l'ésser humà, és molt més que la suma de les seves parts components. Es per això que en l'actualitat està àmpliament acceptat que per comprendre el funcionament d'un organisme complet es requereix una aproximació sistèmica que permeti entendre la funció de gens, proteïnes i metabòlits com part d'una xarxa complexa i no tan sols com entitats aïllades. En aquest sentit, la Biologia de Sistemes es defineix com un camp d'investigació interdisciplinària que busca la integració de les dades biològiques per entendre com funcionen els sistemes biològics (Sobie *et al.*, 2011; Brown *et al.*, 2012). La Biologia de Sistemes s'ha convertit actualment en una de les àrees més actives de la Biomedicina, ja que es beneficia no només dels avanços en la descripció molecular, sinó també en la possibilitat d'elaborar càlculs matemàtics de gran complexitat i generar models informàtics gràcies als avanços en les ciències de computació i anàlisi (Ghosh *et al.*, 2011). La visió global dels processos biològics es veu reflectida en el desenvolupament del que es denomina "L'era òmica". El sufix "-oma" té origen llatí i significa "conjunt de". Per tant, l'addició d'aquest sufix a diferents estudis en biologia, cobreix les noves aproximacions massives en les quals s'està enfocant la biologia recentment. El concepte de ciències òmiques recull aquelles disciplines com la genòmica, la transcriptòmica, la proteòmica, la citòmica i la metabolòmica. Totes elles

tenen en comú que es basen en l'anàlisi d'un gran volum de dades, per la qual cosa es valen de la bioinformàtica i de tècniques ràpides i automatitzades d'alt rendiment.

3.1. La transcriptòmica

La transcriptòmica estudia i compara transcriptomes, és a dir, els conjunts d'àcid ribonucleic (ARN) missatgers o transcripts presents en una cèl·lula, teixit o organisme. Els transcriptomes són molt variables, ja que mostren quins gens s'estan expressant en un moment donat. La transcriptòmica es basa principalment en l'ús dels *microarrays* i de la bioinformàtica (Bates, 2011).

3.1.1. Tècnica de *Microarrays*

El terme *microarray* es coneix també com *gene chip*, *DNA chip*, *biochip, array* d'oligonucleòtids o simplement *array*. Gràcies a aquesta tècnica es poden analitzar simultàniament milers de gens en una mateixa mostra d'ARN. El fonament de la tècnica de *microarrays* és la complementarietat de sondes d'ADN. D'una banda, oligonucleòtids o fragments d'ADN específics s'immobilitzen ordenadament sobre el suport del *microarray*. Els suports usats són membranes de niló, nitrocel·lulosa o làmines de vidre. De l'altra, s'aïlla l'ARN de la mostra i es verifica que aquest sigui d'elevada qualitat. Tot seguit, s'inicia el procés d'amplificació i incorporació simultània del marcatge mitjançant la transcripció reversa de l'ARN a cADN. El marcatge es realitza amb fluorescència, agents com la biotina o radioactivitat. A continuació, es procedeix a la hibridació de la mostra amb l'ADN del *microarray*. L'aparellament de les sondes fixades a l'*array* i l'àcid nuclèic procedent de la mostra a avaluar es regeix per la llei de complementarietat de bases nitrogenades: Guanina-Citosina i Adenina-Timina. Posteriorment, després de diversos rentats per evitar interferències i falsos positius, els *microarrays* es sotmeten a un escaneig. D'aquí s'obté la intensitat d'expressió de milers de gens, la qual és proporcional a la quantitat de transcript de la mostra unit a les seves sondes complementàries al *microarray*. L'etapa més important en aquesta tècnica és el processament de la imatge, l'anàlisi de dades mitjançant diferents programes especialitzats i la posterior interpretació d'aquest gran volum d'informació (Figura 11).

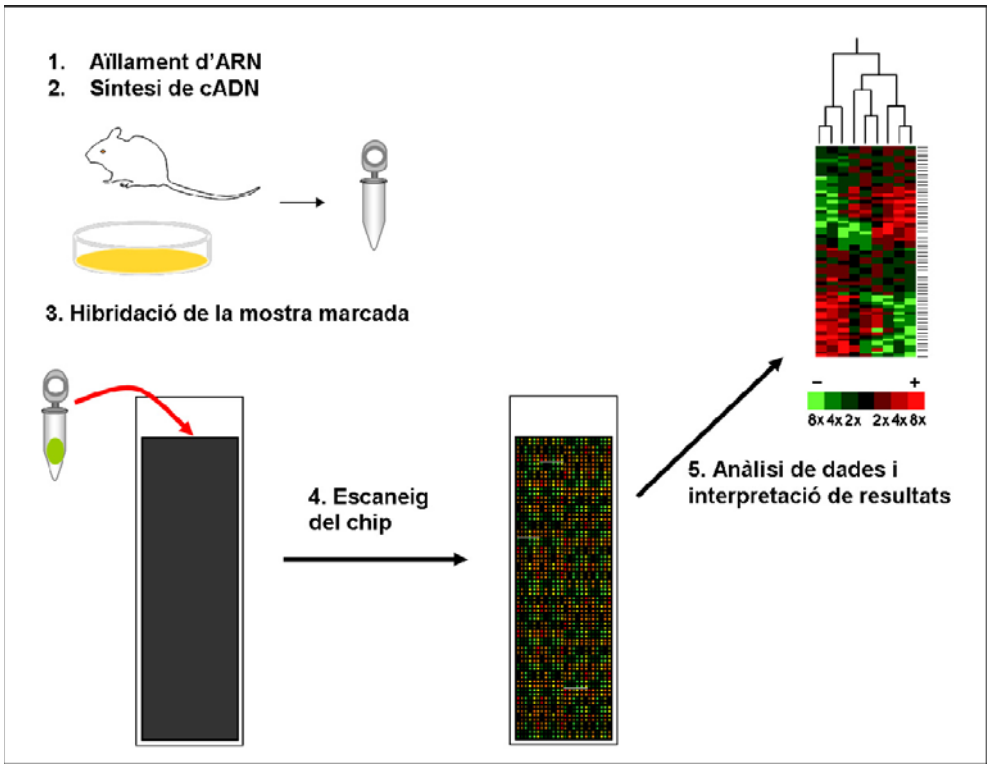

Figura 11. Diagrama simplificat de la metodologia seguida en la tècnica de cADN *microarrays*.

3.1.2. Tècnica de PCR a temps real (RT-PCR o qPCR)

La reacció en cadena de la polimerasa (PCR – *Polymerase Chain Reaction*) a temps real (RT-PCR) és una tècnica utilitzada freqüentment per l'anàlisi de l'expressió gènica.

Al contrari que la tècnica de *microarrays*, la RT-PCR, també denominada PCR quantitativa (qPCR), només permet analitzar un nombre reduït de gens en un petit nombre de mostres (Abruzzo et al., 2007). Usualment, la tècnica de qPCR s'utilitza per quantificar els nivells d'ARN missatger (mARN) d'alguns gens i així validar els perfils d'expressió obtinguts amb la tècnica de *microarrays* (Wang *et al.*, 2012). Normalment s'utilitzen gens control com la β2-microglobulina (B2M) com a referència en el procés de normalització de l'expressió gènica. A més, la quantificació dels canvis d'expressió produïts per un tractament o situació experimental es normalitza sempre respecte un grup control.

3.2. La proteòmica

La proteòmica estudia i compara qualitativa i quantitativament el perfil de proteïnes (proteoma) presents en un conjunt de cèl·lules, teixit o organisme en un moment o condició

particular. No només es limita a analitzar el resultat de l'expressió gènica, sinó que també estudia les modificacions post-traduccionals que poden experimentar les proteïnes, així com la interacció entre elles (Kamath *et al.*, 2011). Les tècniques emprades són, principalment, electroforesi en gel, immunohistoquímica, immunofluorescència, enzimoimmunoassaig (ELISA) i espectrometria de masses. A més d'ajudar a entendre la complexitat dels processos cel·lulars i les respostes fisiològiques de les cèl·lules i organismes al seu entorn, la proteòmica també és crucial per al desenvolupament de millors mètodes de diagnòstic i tractament (marcadors tumorals) (Sun *et al.*, 2011a).

3.3. La citòmica

La citòmica és una disciplina que integra els coneixements de la genòmica i la proteòmica amb la funció dinàmica dels sistemes cel·lulars complexos, és a dir, dels citomes, mitjançant l'anàlisi de cèl·lules individuals. La citòmica té com a objectiu definir exhaustivament el fenotip molecular i constitueix un nexe d'unió entre la biologia molecular i la cel·lular (Valet, 2005). El desenvolupament d'aquesta disciplina s'ha fet possible gràcies a les noves i potents tecnologies d'anàlisi basades en la cèl·lula individual, especialment la citometria de flux i la microscòpia confocal i la seva integració mitjançant anàlisi bioinformàtic. La citòmica representa una eina potent, ja que permet separar eficientment subpoblacions cel·lulars.

L'estudi de l'apoptosi i el cicle cel·lular mitjançant citometria de flux es pot englobar dins de la citòmica. En el cas del cicle cel·lular, la combinació dels mètodes de marcatge amb fluorescència i l'anàlisi mitjançant citometria de flux del contingut d'ADN ha estat una de les estratègies més ràpides i aconsellables per obtenir les distribucions de freqüència del cicle cel·lular de poblacions cel·lulars. S'utilitza iodur de propidi (PI), el qual s'intercala en la doble cadena de molècules d'àcids nucleics, com a marcador de l'ADN i s'aprofita el diferent contingut d'ADN en les diferents fases del cicle cel·lular per diferenciar les subpoblacions de cèl·lules corresponents a cada fase. Amb la finalitat d'identificar cèl·lules en procés apoptòtic, s'utilitza Anexina V conjuntament amb PI. L'Anexina V és una proteïna que té una alta afinitat pels fosfolípids carregats negativament, tals com la fosfatidilserina. Aquests lípids es troben habitualment a la capa interna de la bicapa lipídica i només es desplacen a l'exterior en situació d' apoptosi. Les cèl·lules s'incuben amb Anexina V conjugada amb un fluorocrom que ens indicarà les cèl·lules apoptòtiques. Quan s'addiciona PI es poden classificar les cèl·lules segons hagin perdut totalment la integritat de la membrana (es tenyeixen amb PI) o l'hagin mantingut (no es tenyeixen amb PI). Així, d'acord amb l'explicació dels processos d'apoptosi i necrosi anterior, les cèl·lules Anexina+/PI- són considerades cèl·lules en procés d'apoptosi primerenca.

En canvi, les cèl·lules Anexina+/PI+ i Anexina-/PI+ s'agrupen en un mateix grup d'apoptosi tardana/necrosi degut a que aquest mètode no permet diferenciar aquestes dos subpoblacions cel·lulars.

3.4. La metabolòmica

La metabolòmica és l'estudi i comparació dels metabolomes, és a dir, el conjunt de tots els compostos de baix pes molecular presents en una cèl·lula, teixit o organisme en un moment donat (Oliver *et al.*, 1998). El seu objectiu és identificar i quantificar tots els metabòlits sintetitzats endògenament (Fiehn, 2002). Aquest objectiu tan ambiciós presenta moltes limitacions degut a la gran heterogeneïtat dels metabòlits presents en un organisme, les diferències entre les seves concentracions relatives i la variabilitat en les seves propietats físico-químiques (polaritat, hidrofobicitat, pes molecular o estabilitat química). Malgrat això, s'estan realitzant avenços en el desenvolupament d'eines i tècniques que permetin aconseguir, de manera simultània, la quantificació del major nombre de metabòlits presents en una mostra biològica concreta. Per exemple, l'ús de plataformes analítiques com la cromatografia de gasos o de líquids acoblada a l'espectrometria de masses (GC/MS - *Gas Chromatography Coupled to Mass Spectrometry* i LC/MS - Liquid *Chromatography Coupled to Mass Spectrometry*) i la ressonància magnètica nuclear (NMR – *Nuclear Magnetic Resonance*) ha ajudat a obtenir un millor coneixement del metabolisme cel·lular (Vizan *et al.*, 2007). Una aproximació particularment útil consisteix en l'ús de la GCMS i de molècules marcades amb un isòtop estable i no radioactiu (^{13}C) com a font de carboni. Concretament, l'ús de [1,2-$^{13}C_2$]-glucosa com a traçador permet revelar la contribució de les principals rutes del metabolisme del carboni com són la ruta de les pentoses fosfat, la glicòlisi, el TCA i la síntesi de lípids, a partir de l'anàlisi del patró de distribució del ^{13}C en els intermediaris metabòlics (Marin *et al.*, 2003) (Figura 12). Aquest anàlisi del patró de marcatge dels metabòlits, que es coneix com anàlisi de la distribució isotopomèrica de massa (MIDA - *Mass Isotopomer Distribution Analysis*) o com metabolòmica obtinguda a partir de l'ús de traçadors (*tracer-based metabolomics*), ha permès caracteritzar les adaptacions metabòliques de les cèl·lules en diferents estats i en resposta a malalties com el càncer. Els resultats obtinguts mitjançant aquestes tècniques també han contribuït a identificar noves dianes antitumorals i al disseny de noves teràpies (Boros *et al.*, 2002).

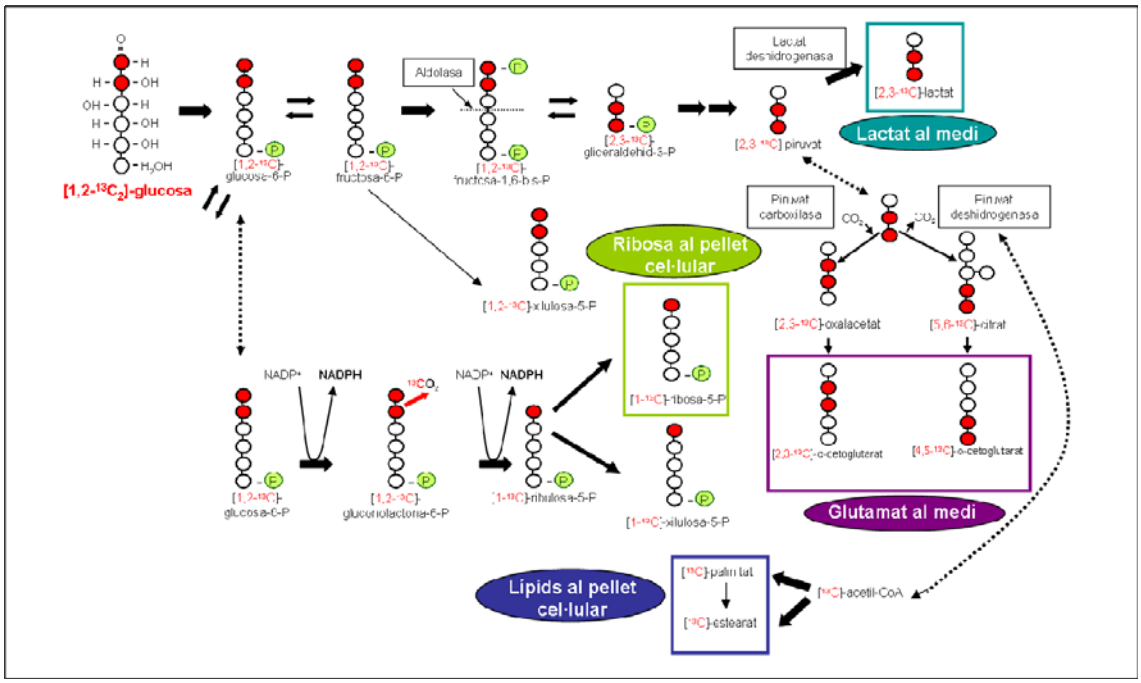

Figura 12. La metabolització de la [1,2-$^{13}C_2$]-glucosa per part de les cèl·lules resulta en un patró característic d'incorporació de ^{13}C en els intermediaris metabòlics que permet caracteritzar l'activitat de les principals vies metabòliques, incloent la glicòlisi, el cicle dels àcids tricarboxílics i la síntesi de lípids i d'àcids nucleics.

OBJECTIUS

L'objectiu general d'aquesta Tesi Doctoral consisteix en la caracterització de l'efecte de diferents productes d'origen natural potencialment antitumorals sobre models de càncer de colon *in vitro* i *in vivo*. Es pretén profunditzar en el mecanisme d'acció d'aquests compostos a fi d'explotar-los com suplements nutritius i preventius en individus amb elevada predisposició a patir càncer, o bé com agents terapèutics en pacients amb càncers ja establerts. A més, es volen determinar noves dianes anti-angiogèniques. D'acord amb aquest objectiu global, aquesta Tesi Doctoral s'estructura en diferents objectius concrets que corresponen als capítols que conformen la present memòria:

1. Caracteritzar uns tanins provinents de l'escorça d'*Hamamelis virginiana* com agents antitumorals amb activitat antiradicalària i capacitat per inhibir específicament la proliferació cel·lular tumoral, per induir arrest en el cicle cel·lular i per provocar mort cel·lular per apoptosi en una línea cel·lular d'adenocarcinoma de colon humà HT29.

2. Analitzar l'efecte de dos catequines majoritàries en té verd sobre la diferenciació de cèl·lules HT29 induïda per butirat.

3. Caracteritzar l'adaptació metabòlica produïda en la línia cel·lular HT29 després del tractament amb epicatequin galat, present en té verd i raïm.

4. Analitzar els mecanismes moleculars d'acció associats a la inhibició de la poliposi intestinal en ratolins $Apc^{Min/+}$ tractats amb una fibra rica en polifenols de raïm.

5. Avaluar l'efecte de l'àcid maslínic, present principalment a la pell de l'oliva, com a inhibidor del desenvolupament de la poliposi intestinal en ratolins $Apc^{Min/+}$.

6. Caracteritzar l'adaptació metabòlica associada a l'activació angiogènica.

INFORME DEL DIRECTOR

Marta Cascante Serratosa, catedràtica del Departament de Bioquímica i Biologia Molecular de la Universitat de Barcelona, Josep Lluís Torres, professor d'investigació de l'Institut de Química avançada de Catalunya (IQAC-CSIC) i Pedro Vizán Carralcázar, investigador postdoctoral del *Cancer Research UK*, com a directors de la Tesi Doctoral titulada "Caracterització de l'efecte de compostos naturals en models *in vitro* i *in vivo* de càncer de còlon" que presenta Susana Sánchez Tena, fan constar que: Aquesta Tesi Doctoral es presenta com a "Compendi de Publicacions", vertebrant-se en sis capítols, dels quals la doctoranda és primera autora en els cinc primers i coautora en el sisè. Els resultats presentats en el capítol 1 han estat publicats a la revista *Journal of Natural Products* amb un índex d'impacte de 2,872 (annex 1). Els resultats del capítol 2 volen ser publicats a la revista *Cancer Research* amb un factor d'impacte 8,243. D'una altra banda, els resultats del capítol 3 volen ser publicats a la revista *European Journal of Nutrition* amb un índex d'impacte 3,343. Amb relació al capítol 4, els resultats volen ser publicats a *Journal of Nutritional Biochemistry* amb un factor d'impacte de 4,538, després de que es resolgui la sol·licitud de protecció sota patent que està essent tramitada per l'Agència de valorització i comercialització dels resultats de la investigació (AVCRI). Els resultats presentats en el capítol 5 volen ser publicats a la revista *American Journal of Clinical Nutrition* amb un índex d'impacte 6,606. Finalment, els resultats mostrats al capítol 6 han estat publicats a la revista *Carcinogenesis* amb un índex d'impacte de 5,402 (annex 2). Pel que respecta a la contribució de la doctoranda a cadascun dels capítols, Susana Sánchez Tena va ser l'encarregada de portar el gruix de la investigació, des de la planificació i desenvolupament dels experiments, fins a l'anàlisi dels resultats i la posterior escriptura dels articles en els cinc primers capítols. En el capítol 1, la purificació química dels compostos i la determinació de l'activitat antiradicalària va esser realitzada a l'Institut de Química avançada de Catalunya (IQAC-CSIC) en col·laboració amb el Dr. Josep Lluís Torres Simón. En el capítol 2, alguns dels estudis d'expressió del transportador MCT1 es van dur a terme en col·laboració amb el Dr. Pradeep K. Dudeja de la *Universitiy of Illinois at Chicago.* D'una altra banda, els experiments amb ratolins $Apc^{Min/+}$ dels capítols 4 i 5 van ser realitzats en col·laboració amb la Dra. Maria Pilar Vinardell Martínez-Hidalgo del Departament de Fisiologia de la Facultat de Farmàcia de la Universitat de Barcelona i la Dra. Daneida Lizárraga investigadora del Departament de Toxicologia de la *Maastricht University.* Els resultats referents al contatge de pòlips del capítol 4, van ser inclosos en la Tesi Doctoral de la Dra. Daneida Lizárraga (segona autora del treball). L'anàlisi per ressonància magnètica nuclear inclòs en el capítol 5 es va dur a terme en col·laboració amb el Dr. Ulrich Günther de la *University of Birmingham*. Pel que fa al capítol 6, la doctoranda va col·laborar en la planificació i desenvolupament dels experiments i

en la posterior escriptura de l'article. Part dels resultats presentats en aquest capítol es van utilitzar per a l'elaboració de la Tesi Doctoral del Dr. Pedro Vizán (primer autor del treball).

D'una altra banda, aquesta Tesi Doctoral conté com annex dos articles més realitzats en coautoria. L'annex 3 correspon a una publicació a la revista *Journal of Agricultural and Food Chemistry* amb un factor d'impacte 2,816. Els resultats de l'annex 4 també han estat publicats en aquesta última revista científica. Pel que fa a la participació de la doctoranda en aquests treballs, Susana Sánchez Tena va col·laborar en la planificació i desenvolupament dels experiments en l'annex 4 i va col·laborar en l'escriptura en l'annex 3. Aquests treballs corresponents als annexos 3 i 4 s'han inclòs en Tesis Doctorals anteriors presentades per la Dra. Cecilia Matito i per la Dra. Anna Carreras, respectivament.

Els directors de la tesi:

Dra. Marta Cascante **Dr. Josep Lluís Torres** **Dr. Pedro Vizán**

RESUM GLOBAL

RESULTATS

La present Tesi Doctoral es centra en l'estudi de l'efecte a nivell transcriptòmic, proteòmic, citòmic i metabolòmic induït per diversos compostos d'origen natural en diferents sistemes biològics relacionats amb el càncer de còlon. Tanmateix, la principal finalitat d'aquest treball és donar valor afegit a aquests productes naturals procedents de fruits i plantes o bé obtinguts de residus de la indústria del vi i de l'oli utilitzant-los per a la prevenció o tractament del càncer de còlon. A més, es realitza un estudi de l'angiogènesi, un dels processos necessari per la progressió tumoral.

Aquesta Tesi Doctoral s'ha estructurat en dues parts: la primera *in vitro* basada en estudis amb cèl·lules en cultiu d'origen colorectal, on s'han avaluat la pentagaloilglucosa (PGG), l'hamamelitanin (HT) i la fracció polifenòlica F800H4 provinents de la planta *Hamamelis virginiana* (Capítol 1) i l'epicatequina (EC), l'epigal·locatequin gal·lat (EGCG) (Capítol 2) i l'epicatequin gal·lat (ECG) (Capítol 3) presents en té verd i raïm. D'una altra banda, s'ha estudiat *in vivo* (en un model murí de càncer de còlon conegut com ratolí $Apc^{Min/+}$) la resposta a la fibra dietètica antioxidant de raïm (GADF - *Grape Antioxidant Dietary Fiber*) (Capítol 4) i a l'àcid maslínic (MA - *Maslinic Acid*) (Capítol 5), provinent de l'oliva. Finalment, l'últim capítol s'ha basat en la determinació de noves dianes anti-angiogèniques a nivell metabòlic.

A continuació, s'exposen de forma resumida els resultats obtinguts en cadascun dels capítols que conformen aquesta Tesi Doctoral i després es procedeix a la discussió general dels mateixos i a l'enumeració de les conclusions aconseguides.

Capítol 1. L'hamamelitanin d'*Hamamelis virginiana* mostra citotoxicitat específica contra cèl·lules de càncer de còlon

L'objectiu d'aquest estudi va ser l'avaluació de diferents tanins d'*Hamamelis virginiana,* també conegut com avellaner de bruixa, com agents anticancerígens en càncer de còlon. Per a cobrir la diversitat estructural dels tanins d'*H. virginiana*, els tanins hidrolitzables hamamelitanin (HT) i pentagaloilglucosa (PGG), i una fracció rica en proantocianidines o tanins condensats (F800H4) van ser inclosos a l'estudi. Mentre que l'HT es troba disponible comercialment, la PGG i la fracció F800H4 es van obtenir mitjançant mètodes químics a partir de l'escorça d'*H. Virginiana* en col·laboració amb el Dr. Josep Lluís Torres del Institut de Química Avançada de Catalunya (IQAC-CSIC). En primer lloc, es va avaluar la capacitat dels compostos de l'avellaner de bruixa per neutralitzar radicals lliures com el 1,1-difenil-2-picrilhidrazil (DPPH), el tris(2,4,6-tricloro-3,5-dinitrofenil)metil (HNTTM) i el tris-(2,3,5,6-

tetracloro-4-nitrofenil)metil (TNPTM). Els resultats van mostrar que la capacitat antiradicalària de la PGG i la fracció F800H4 era similar en tots els casos: van ser capaços de reaccionar amb el DPPH i el HNTTM però no amb el TNPTM. En canvi, l'HT, a més de neutralitzar els radicals DPPH i HNTTM d'una manera similar, també va ser capaç de neutralitzar el radical TNPTM. Això vol dir que l'HT conté algun grup hidroxil més reactiu que el dels altres tanins. A continuació, es va estudiar l'activitat biològica de la PGG, l'HT i la fracció F800H4 en cèl·lules d'adenocarcinoma de còlon humà HT29. Primerament, es va determinar la concentració de producte necessària per inhibir el 50% de la viabilitat cel·lular respecte el control (IC_{50}) i aleshores, aquesta concentració es va utilitzar pels estudis de cicle cel·lular i apoptosi mitjançant citometria. L'HT va mostrar la major inhibició de la viabilitat de les cèl·lules HT29 amb una IC_{50} de 20±4.5 μg/ml, la major inducció d'apoptosi i necrosi (26% i 14% respecte les cèl·lules control, respectivament) i també el major arrest del cicle cel·lular en la fase S, amb un augment del 16% en la població de cèl·lules en aquesta fase respecte el control. En segon lloc, el tractament amb PGG va reduir la viabilitat cel·lular amb un valor de IC_{50} de 28±8.8 μg/ml i va induir un 11% d'apoptosi, un 5% de necrosi i un arrest en la fase S del cicle cel·lular amb un augment del 8% en la població de cèl·lules en aquesta fase. La fracció rica en proantocianidines F800H4 va ser la menys eficaç inhibint la viabilitat cel·lular amb una IC_{50} de 38±4.4 μg/ml i també induint apoptosi (9%) i necrosi (6%). A més, F800H4 no va modificar significativament la distribució del cicle cel·lular normal. En la cerca de nous compostos antitumorals és molt important l'especificitat, és a dir, que els productes siguin capaços d'inhibir el creixement de les cèl·lules tumorals sense danyar les cèl·lules normals. Així doncs, es va determinar la capacitat antiproliferativa de la PGG, l'HT, i la F800H4 en colonòcits humans no tumorigènics NCM460. Els resultats van mostrar que les concentracions d'HT i F800H4 capaces d'induir la mort en cèl·lules HT29 no tenien cap efecte nociu per a les cèl·lules NCM460 (IC_{50} superior a 100 μg/ml). En canvi, la PGG va inhibir la viabilitat de les línies cel·lulars cancerosa i normal d'una manera similar (IC_{50} en HT29 = 28±8.8 μg/ml / IC_{50} en NCM460 23±2.4 μg/ml). Finalment, donat que s'ha descrit una modulació artefactual de la citotoxicitat atribuïda a la formació d'espècies reactives d'oxigen (ROS – *Reactive Oxygen Species*) en el medi de cultiu durant la incubació amb polifenols (Chai *et al.*, 2003), es va determinar la generació de radicals al medi de cultiu i l'efecte antiproliferatiu dels diferents productes en presència de catalasa, capaç de degradar-los. Tots els productes estudiats van mostrar una producció dosi-depenent del radical peròxid d'hidrogen (H_2O_2) en el medi de cultiu. Com s'esperava, quan aquest medi es va suplementar amb catalasa, aquesta gairebé va produir una descomposició completa del H_2O_2 generat en tots els casos. Amb referència a la determinació de la capacitat antiproliferativa dels compostos d'*H. virginiana*, la suplementació

amb catalasa pràcticament no va afectar la citotoxicitat en les cèl·lules HT29 incubades amb tanins hidrolitzables (IC_{50} en medi = 28±8.8 μg/ml / IC_{50} en medi amb catalasa = 34±1.2 μg/ml per la PGG i IC_{50} en medi = 20±4.5 μg/ml / IC_{50} en medi amb catalasa =13±4.6 μg/ml per l'HT), mentre que la citotoxicitat observada per a la fracció F800H4 va resultar ser artefactual (IC_{50} en medi = 38±4.4 μg/ml / IC_{50} en medi amb catalasa = 95±8.7 μg/ml). Conseqüentment, la diferència entre la citotoxicitat de la F800H4 en cèl·lules HT29 i NCM460 no es tan diferent com s'havia observat anteriorment.

Capítol 2. Els polifenols majoritaris en té verd inhibeixen la diferenciació induïda per butirat mitjançant interacció amb el Transportador Monocarboxílic 1 (MCT1)

L'efecte protector de molts productes bioactius presents en aliments com la fibra o els vegetals s'ha relacionat amb l'activitat de la microbiota intestinal. En aquest sentit, el consum de polifenols naturals s'ha descrit que augmenta la concentració intestinal de productes derivats de la fermentació microbiana de la fibra com és el butirat (Juskiewicz *et al.*, 2011; Kosmala *et al.*, 2011; Juskiewicz *et al.*, 2012), un inhibidor de les histones deacetilases (HDACs) que indueix diferenciació en cèl·lules de càncer de còlon (Boren *et al.*, 2003). Tanmateix, el mecanisme pel qual el butirat i els polifenols interaccionen a nivell cel·lular intestinal no ha estat investigat.

En aquest treball es va avaluar l'efecte de dos catequines majoritàries en té verd, l'epicatequina (EC) i l'epigal·locatequin gal·lat (EGCG), en la diferenciació de la línea cel·lular d'adenocarcinoma de colon humà HT29 induïda per butirat. En primer lloc, amb la finalitat de determinar la concentració efectiva dels diferents polifenols que s'utilitzaria en estudis posteriors, es van realitzar assajos de viabilitat en la línia cel·lular HT29. En aquests es va observar que les concentracions de producte necessàries per inhibir el 20% de la viabilitat respecte el control (IC_{20}) corresponien a 100 μM i 20 μM per a l'EC i l'EGCG, respectivament. A continuació, es van incubar les cèl·lules amb aquestes concentracions d'EC o d'EGCG conjuntament amb el butirat amb l'objectiu d'analitzar si els polifenols modificaven d'alguna manera l'efecte diferenciador descrit per aquest àcid gras de cadena curta. Sorprenentment, encara que els polifenols per si sols no produïen cap efecte, es va observar que ambdós polifenols disminuïen l'activitat fosfatasa alcalina (AP) (marcador de diferenciació en cèl·lules intestinals) induïda per butirat. Es va voler aprofundir en el mecanisme d'aquesta interacció entre els polifenols i el butirat. Primer es va voler esclarir si es tractava d'una interferència a nivell de l'enzim AP, a una interferència a nivell del procés de diferenciació cel·lular o bé a una interacció entre el butirat i els polifenols. Es va mesurar l'activitat d'un marcador de

diferenciació intestinal diferent a l'AP, l'aminopeptidasa N. En aquest estudi es van obtenir els mateixos resultats que amb l'AP, eliminant una interacció a aquest nivell. Llavors, es va estudiar si la interacció es donava a nivell dels enzims histona deacetilasa (HDAC), ja que es coneix que el butirat actua inhibint aquests enzims i activant així l'expressió de diferents proteïnes implicades en la diferenciació cel·lular (Humphreys *et al.*, 2012). La mesura de l'activitat HDAC en extractes nuclears de cèl·lules HT29 tractats amb butirat o polifenols va corroborar l'activitat inhibidora d'HDAC del butirat i va demostrar que els polifenols no afectaven l'activitat total HDAC en extractes nuclears de cèl·lules HT29. Quan els extractes cel·lulars es tractaven amb butirat i polifenols simultàniament, s'observava que els polifenols no produïen canvis significatius en la inhibició de l'activitat HDAC produïda pel butirat. Addicionalment, es va mesurar la diferenciació cel·lular induïda per un altre agent diferenciador que actua inhibint les HDACs, la Tricostatina A (TSA), i es va demostrar que els polifenols no afectaven la diferenciació induïda per aquest compost, eliminant així finalment la possibilitat de que l'efecte dels polifenols es produís a través de les HDACs. Per estudiar el mecanisme d'interferència entre butirat i polifenols, les cèl·lules HT29 es van incubar durant 48 h amb butirat sol o bé amb butirat i polifenols conjuntament i posteriorment es va fer un estudi de l'entrada de butirat marcat amb ^{14}C. El tractament amb butirat, tal com estava descrit (Borthakur *et al.*, 2008), va activar el seu propi transport. En canvi, els polifenols combinats amb butirat van produir una disminució significativa de l'entrada de butirat marcat induïda per aquest. Tot seguit, considerant que els resultats mostraven una clara interferència entre butirat i polifenols, es va decidir estudiar el transportador intestinal de butirat anomenat Transportador Monocarboxílic 1 (MCT1 – *Monocarboxylate Transporter 1*) (Saksena *et al.*, 2009). Es va examinar l'efecte dels polifenols sobre el MCT1 mitjançant transfecció d'una construcció que contenia el seu promotor amb el gen luciferasa i també per *Western blot*. Mentre que el tractament amb butirat va augmentar significativament l'activitat del promotor del MCT1, els polifenols no van produir cap canvi. Altrament, l'anàlisi per *Western blot* del MCT1 va mostrar que no hi havia diferències a nivell proteic en cap dels tractaments. Tot plegat, aquests resultats suggerien una regulació del MCT1 a nivells diferents. Recentment, s'ha descrit que la funció d'alguns transportadors i receptors de membrana depèn de la seva associació amb certes regions de membrana anomenades *rafts* lipídics (Chen *et al.*, 2011). Aquestes regions són microdominis de membrana rics en colesterol, esfingolípids i proteïnes, que són insolubles en detergents i que es poden separar fàcilment del material més dens per flotació en un gradient de densitat. Curiosament, alguns polifenols s'han descrit com moduladors de *rafts* lipídics (Annaba *et al.*, 2010). Per consegüent, el següent pas va ser investigar si l'EC i l'EGCG causaven alteracions en l'associació del MCT1 amb els *rafts* lipídics. En aquest cas, es va utilitzar un gradient de

densitat d'OptiPrep per separar aquests microdominis de membrana. Després de la centrifugació, les fraccions obtingudes es van analitzar per electroforesi i *Western blot*. La detecció del MCT1 i la flotilina (marcador de *rafts* lipídics) va mostrar que en les cèl·lules control el MCT1 es trobava majoritàriament a les fraccions no corresponents a *rafts*. Per contra, el tractament amb butirat augmentava la presència de MCT1 en aquestes fraccions. Quan el butirat es combinava amb polifenols, el MCT1 es redistribuïa a totes les fraccions, antagonitzant la localització del MCT1 en lípid *rafts* induïda per butirat.

Capítol 3. L'epicatequin gal·lat interfereix amb la productivitat metabòlica en cèl·lules de càncer de còlon

Les cèl·lules tumorals presenten un metabolisme extremadament actiu i distintiu que els confereix l'habilitat de sobreviure, proliferar i envair (Mathupala *et al.*, 2010; Dang, 2012). Per aquesta raó, la inhibició de l'adaptació metabòlica tumoral ha estat proposada com una aproximació terapèutica potent. En aquest capítol, es va caracteritzar el perfil metabòlic de les cèl·lules d'adenocarcinoma de còlon humà HT29 després del tractament amb epicatequin gal·lat (ECG), un producte present en té verd i raïm amb demostrada capacitat antitumoral (Ravindranath *et al.*, 2006) a fi de determinar les dianes metabòliques d'aquest compost. En combinar l'estudi bioquímic clàssic de mesura d'intermediaris metabòlics i d'anàlisi enzimàtic utilitzant tècniques espectrofotomètriques, amb l'ús de l'isotopòmer estable de la glucosa [1,2-$^{13}C_2$]-glucosa com a font de carboni i les tècniques de cromatografia de gasos acoblada a espectrometria de masses (GC/MS – *Gas Chromatography Coupled to Mass Spectrometry*), es va poder comparar la utilització de les principals vies del metabolisme central del carboni en les cèl·lules HT29 tractades o no amb ECG. En primer lloc, es va determinar la capacitat antiproliferativa de l'ECG en cèl·lules HT29. Segons els resultats, dues dosis d'ECG van ser escollides: una concentració de 70 μM, la qual va produir una reducció de la viabilitat de 18±4 i una concentració més alta de 140 μM, la qual va causar una reducció més important en la viabilitat de les cèl·lules HT29 de 70±11. La quantificació per espectrofotometria dels metabòlits més importants per a les cèl·lules tumorals va mostrar que el consum de glutamina i glucosa i la producció de lactat només es veien reduïts després de la incubació amb 140 μM ECG. L'ús del cicle de Krebs o cicle dels àcids tricarboxílics (TCA - *Tricarboxylic Acid*) va ser estudiat a partir de l'anàlisi isotopomèric del glutamat. L'enriquiment en ^{13}C en aquest metabòlit va mostrar que les cèl·lules tractades amb ambdues concentracions d'ECG presentaven una activitat del TCA més baixa comparada amb les cèl·lules control. A més, pel que fa a l'entrada de piruvat al TCA, els resultats van mostrar que el tractament amb 140 μM ECG augmentava la

contribució de la piruvat carboxilasa (PC) al TCA i en canvi, disminuïa la utilització de glucosa a través de la piruvat deshidrogenasa (PDH). Donat que una inhibició en el TCA podria estar relacionada amb una inhibició de les vies biosintètiques, es va decidir estudiar la incorporació de marca als àcids grassos palmitat (C16) i estearat (C18). Es va estimar la contribució de la glucosa marcada a la síntesi d'aquests àcids grassos i també la fracció de nova síntesi (FNS) la qual indica la quantitat relativa d'àcid gras sintetitzada *de novo* respecte al total d'àcids grassos sintetitzats de nou. Els resultats van mostrar que l'ECG 70 μM va ser capaç de reduir la contribució de la glucosa a la síntesi d'estearat. D'una altra banda, l'ECG 140 μM va disminuir la contribució de la glucosa a la síntesi dels dos àcids grassos estudiats. A més, el tractament de les cèl·lules HT29 amb 140 μM ECG va reduir la FNS tant pel palmitat com per l'estearat. Amb relació a l'anàlisi de la incorporació de marca en la ribosa provinent de l'àcid ribonucleic (ARN), els resultats van posar de manifest que mentre que el tractament amb 70 μM ECG no produïa diferències significatives, 140 μM ECG disminuïa la síntesi *de novo* de ribosa i causava un canvi significatiu en l'equilibri entre les vies oxidativa i no oxidativa (ràtio ox:no-ox) de la ruta de les pentoses fosfat (PPP - *Pentose Phosphate Pathway*) a favor de la via oxidativa. Per analitzar en més profunditat a que es devia aquest desequilibri, es van analitzar les activitats dels enzims claus de la PPP: glucosa-6-fosfat deshidrogenasa (G6PD - *Glucose-6-phosphate dehydrogenase*) i transcetolasa (TKT - *Transketolase*). Els resultats van mostrar que les activitats enzimàtiques eren inhibides un 15% i un 35%, respectivament, per l'ECG 140 μM.

Capítol 4. La fibra dietètica antioxidant de raïm inhibeix la poliposi intestinal en ratolins Apc$^{Min/+}$El gen *Apc* (*Adenomatous polyposis coli*) està directament implicat en el desenvolupament del càncer de colon humà. El ratolí Apc$^{Min/+}$ conté una mutació en el codó 850 del gen *Apc*, homòloga a les mutacions en humans. Així dons, atès que aquest model animal desenvolupa espontàniament adenomes com a resultat de la inactivació del mateix gen involucrat en la patogènesi de la majoria de càncers de còlon humans, els experiments amb aquest model animal són pertinents per a l'estudi d'agents quimioterapèutics per al càncer colorectal humà. L'objectiu d'aquest treball fou l'estudi de l'efecte de la fibra dietètica antioxidant de raïm (GADF - *Grape Antioxidant Dietary Fiber*) sobre la carcinogènesi colònica en ratolins Apc$^{Min/+}$. Aquests estudis es van plantejar a partir d'estudis previs en el nostre grup que demostraven que l'administració de GADF a ratolins C57BL/6J induïa un perfil d'expressió i un perfil metabòlic que implicaven un efecte protector enfront la carcinogènesi intestinal (Lizárraga *et al.*, 2011). Els ratolins Apc$^{Min/+}$ es van obtenir amb quatre setmanes d'edat i després d'una setmana d'aclimatació a l'estabulari, es van iniciar els tractaments. Els animals es van dividir en dos grups: control negatiu (pinso normal) i GADF (pinso complementat amb 1% de

GADF (pes/pes)). Cada grup es va subdividir en dues gàbies, cadascuna amb sis ratolins, en el cas dels controls, o bé cinc ratolins, en el cas dels tractats. Durant les sis setmanes que va durar l'experiment els ratolins es van alimentar amb les dietes corresponents i es va portar a terme un control setmanal del pes dels ratolins i del consum d'aigua i pinso. Després del sacrifici dels animals, es van recollir mostres per analitzar-les posteriorment. En primer lloc, es va separar l'intestí prim dels ratolins, el qual es va dividir en tres parts (proximal, medial i distal) i cadascuna es va col·locar sobre una cartolina que es va conservar en formaldehid al 4%. A continuació, es van contar i classificar segons el diàmetre els pòlips trobats en cada segment de l'intestí utilitzant una lupa binocular. Les observacions van mostrar que els ratolins del grup control presentaven 16 pòlips de mitja al llarg de l'intestí prim, mentre que els ratolins tractats amb GADF mostraven una inhibició en la formació de pòlips del 76% (3.9 pòlips totals). A més, es va observar una inhibició significativa en pòlips menors a 1.0 mm (5.5±1.2 *versus* 1.9±0.4) i majors a 2.0 mm de diàmetre (7.7±2.2 *versus* 1.0±0.3). Els pòlips de grandària intermèdia també van mostrar una tendència a disminuir (3.0±1.1 *versus* 1.0±0.3) encara que no de manera significativa. En la classificació per seccions intestinals, es va observar una reducció en el nombre de pòlips en la zona proximal, medial i distal del 76% (4.6±0.9 *versus* 1.1±0.3), 81% (4.3±1.0 *versus* 0.8±0.3) i 73% (7.3±2.4 *versus* 2.0±0.4) respectivament. Cal destacar que aquests resultats referents al contatge de pòlips es van incloure en una Tesi Doctoral anterior presentada per la Dra. Daneida Lizárraga. Posteriorment, per completar aquests estudis i determinar els mecanismes moleculars pels quals es donava l'efecte quimiopreventiu de la GADF, es va realitzar una comparació dels perfils d'expressió dels ratolins tractats i no tractats. El dia del sacrifici dels animals, es va recollir la mucosa del còlon dels ratolins i es va conservar en trizol. Després, es va procedir a l'aïllament de l'ARN i a l'anàlisi de l'expressió gènica mitjançant *microarrays*. Aquest anàlisi va revelar la modulació de l'expressió de 183 gens en els ratolins tractats amb GADF (amb un canvi d'1.5 o més respecte el control i un p-valor <0.05). El posterior estudi funcional mitjançant diferents eines bioinformàtiques (*Kyoto Encyclopedia of Genes and Genomes* (KEGG) *Mapper*, *Metacore* i *Gene set analysis*) va mostrar que molts dels gens modulats estaven implicats en la progressió tumoral, incloent *Ccnd1*, *Gadd45a*, *Tgfb1*, *Plk3*, *kitl*, *Csnk1e*, *Lfng*. Destaca entre aquests la infraregulació de la ciclina D (*Ccnd1*), la qual és un membre clau del control de la progressió del cicle cel·lular a través de la fase G1. Els gens *Pold1* i *Rfc1*, implicats en la replicació de l'ADN també van ser infraregulats per GADF. A més, la suplementació amb GADF va disminuir l'expressió de gens relacionats amb inflamació i resposta immune.

Capítol 5. Efecte quimiopreventiu de l'àcid maslínic contra la tumorigenesi intestinal en ratolins Apc$^{Min/+}$

En aquest capítol de la tesi es va utilitzar el model de ratolí Apc$^{Min/+}$ esmentat anteriorment amb l'objectiu d'avaluar l'efecte de l'àcid maslínic (MA - *Maslinic Acid*) en el desenvolupament de la poliposi intestinal. Es va seguir el mateix protocol que en el cas anterior: després d'una setmana d'aclimatació a l'estabulari, els animals es van dividir aleatòriament en els grups d'estudi. Per un costat, els animals control alimentats amb pinso normal i per l'altre els animals del grup MA, alimentats amb el pinso normal contenint 100 mg d'MA/ Kg pinso. Després de sis setmanes de tractament, es van recollir diferents mostres per analitzar. En primer lloc, es va separar l'intestí prim per realitzar el contatge de pòlips. Es va observar una disminució significativa del 45% en el nombre total de pòlips trobats en els intestins dels ratolins tractats amb MA respecte als ratolins control (16±3.9 *versus* 9±2.9). En la classificació depenent del segment de l'intestí, la inhibició de pòlips més important es va observar en els pòlips proximals (69%) (4.6±0.9 *versus* 1.4±0.4), seguida pels de la zona medial (48%) (4.3±1.0 *versus* 2.2±0.7) i distal (28%) (7.3±2.4 *versus* 5.3±2.0). Respecte a l'anàlisi per mida de pòlip, l'MA va inhibir el desenvolupament de pòlips <1 mm de diàmetre amb un 44% (5.5±1.2 *versus* 3.1±1.0), de pòlips entre 1 i 2 mm amb un 33% (3.0±1.1 *versus* 2.0±0.7) i de pòlips >2 mm amb un 50% (7.7±2.2 *versus* 3.8±1.4). Tot seguit, per elucidar els mecanismes pels quals l'MA inhibia la tumorigenesis intestinal en ratolins Apc$^{Min/+}$, es va comparar el perfil transcripcional de la mucosa colònica de ratolins Apc$^{Min/+}$ tractats o no amb MA mitjançant *microarrays*. La suplementació amb MA va canviar significativament l'expressió de 2375 gens (amb un canvi d'1.5 o més respecte el control i un p-valor <0.05). L'anàlisi d'aquesta llista de gens diferencialment expressats va mostrar que l'MA produïa principalment modificacions en vies relacionades amb la progressió tumoral. Concretament en càncer de còlon, l'MA va infraregular la glicogen sintasa cinasa 3β (*Gsk3b*), la ciclina D (*Ccnd1*), la proteïna cinasa B o AKT (*Akt1*) i el DIP13α (*Appl1*) mentre que va sobreregular el gen *deleted in colorectal carcinoma* (*Dcc*). Aquesta modulació podria explicar la disminució el creixement tumoral en els ratolins Apc$^{Min/+}$ tractats amb MA. A més, la determinació del perfil d'expressió en els ratolins Apc$^{Min/+}$, va suggerir que l'MA era capaç d'induir apoptosi mitjançant la infraregulació de les proteïnes anti-apotòtiques Bcl-2 (*Bcl2*) i Bcl-XL (*Bcl2l1*). Aquesta inhibició de proteïnes anti-apoptòtiques va anar acompanyada de la modulació d'altres proteïnes relacionades amb el procés d'apoptosi com són el factor de creixement tumoral (*Tgfb1*) i el seu receptor (*Tgfb1r1*), P53 (*Tpr53*), SHC (*Shc1*), GRB (*Grb2*) i SOS (*Sos1*), entre altres. D'una altra banda, l'acció quimiopreventiva de l'MA es va relacionar també amb la inducció d'arrest del cicle cel·lular en la fase G1 mitjançant la infraregulació de gens implicats en la transició a través d'aquesta fase com són la Ciclina D

(*Ccnd1*), *Cdk4*, *Cdk6*, *Btrc*, *Junb* i *Ppp2r4*. Addicionalment, l'MA va produir canvis en l'expressió de gens que codifiquen per proteïnes implicades en la regulació del citosquelet d'actina, de l'adhesió, de la inflamació i del sistema immune. En el sacrifici dels ratolins es va extreure sang a partir de la qual es va obtenir sèrum utilitzat per portar a terme l'anàlisi metabòlic mitjançant ressonància magnètica nuclear (NMR – *Nuclear Magnetic Resonance*) en col·laboració amb el Dr. Ulrich Günther de la Universitat de Birmingham. La comparació dels espectres de NMR dels sèrums control i MA va demostrar que la suplementació amb MA produïa un augment en els nivells de cossos cetònics i una disminució en els nivells de glucosa. De manera interessant, algunes de les modulacions transcripcionals induïdes per l'MA podien explicar aquest perfil metabòlic. La disminució de la concentració de glucosa en el sèrum dels ratolins tractats amb MA podia ser una conseqüència de la sobreregulació de la proteïna CAP (*Sorbs1*). A més, aquests baixos nivells de glucosa podien ser conseqüència d'una acumulació de glicogen provocada pel tractament amb MA el qual regula a nivell transcripcional proteïnes relacionades amb aquest procés com són la GSK3 i la PHK (*Phka1*). D'una altra banda, l'augment en cossos cetònics, el qual requereix una elevada oxidació d'àcids grassos, es va veure controlat per la sobreregulació de l'expressió del gen *Cpt1* el qual codifica per la carnitina palmitoiltransferasa I encarregada de l'entrada d'àcids grassos a la matriu mitocondrial on es dóna l'oxidació d'aquests.

Capítol 6. Caracterització dels canvis metabòlics associats a l'activació angiogènica: identificació de potencials dianes terapèutiques

L'elevada taxa de proliferació de les cèl·lules tumorals deriva en la formació d'una massa cel·lular en la qual es produeix un ambient hipòxic i pobre en nutrients. Així doncs, la capacitat d'un tumor per estimular la creació de nous vasos sanguinis, procés conegut com angiogènesi, li assegura els elements necessaris per seguir progressant. Donat que es coneix molt poc sobre l'adaptació metabòlica que pateixen les cèl·lules endotelials durant aquesta transformació, en aquest treball es van estimular les cèl·lules endotelials umbilicals humanes (HUVEC – *Human Umbilical Vascular Endothelial Cells*) mitjançant l'addició del factor de creixement vascular endotelial (VEGF - *Vascular Endothelial Growth Factor*) o del factor de creixement de fibroblasts (FGF – *Fibroblast Growth Factor*) i es va procedir a un estudi de les vies metabòliques principals d'utilització de la glucosa, utilitzant tècniques anàlogues a les descrites pel capítol 3, amb la finalitat de caracteritzar l'adaptació metabòlica associada a l'estimulació angiogènica. Es va observar que els canvis metabòlics que acompanyaven l'activació angiogènica mitjançada per VEGF i FGF eren molt similars. En primer lloc, la taxa glicolítica,

determinada mitjançant la distribució isotopomèrica del lactat excretat al medi, es mantenia pràcticament idèntica. En tots dos casos es van trobar quantitats importants de glicogen intracel·lular. Un estudi més profund de la glucosa provinent d'aquest glicogen, va mostrar que part del ^{13}C provinent de la [1,2-$^{13}C_2$]-glucosa s'acumulava a les reserves de glicogen, la qual cosa indicava un metabolisme actiu de síntesi i degradació de glicogen en aquestes cèl·lules. A més, es va observar que la síntesi de ribosa per part de la ruta de les pentoses fosfat (PPP – *Pentose Phosphate Pathway*) es donava de manera molt similar amb els dos tipus d'activació endotelial. La utilització de 5-diarilurea-oxi-benzimidazol, un inhibidor del receptor 2 del factor de creixement endotelial vascular (VEGFR - *Vascular Endothelial Growth Factor Receptor 2*), ens va permetre investigar si aquest patró metabòlic característic era essencial per a l'activació de les cèl·lules HUVEC. L'inhibidor va causar aproximadament un 30% d'inhibició de la proliferació en les cèl·lules HUVEC activades amb VEGF i, inesperadament, un 20% d'inhibició de la proliferació quan les cèl·lules s'activaven amb FGF. Contràriament, l'ús de l'inhibidor no va afectar la xarxa metabòlica quan l'activació de les cèl·lules HUVEC es donava mitjançant FGF i si que ho va fer quan s'activaven mitjançant VEGF. En aquest últim cas, l'addició de l'inhibidor va provocar una disminució en la síntesi *de novo* de ribosa, especialment a través de la via oxidativa de la PPP, i en la síntesi de glicogen. A més, un estudi més profund d'aquest glicogen va revelar que les cèl·lules activades amb VEGF i tractades amb l'inhibidor acumulaven més quantitat de glicogen intracel·lular. Els resultats esmentats fins al moment es van incloure a la Tesi Doctoral del Dr. Pedro Vizán. Posteriorment, es va investigar el comportament del glicogen en ambients hipòxics i hipoglucèmics. Mentre que les reserves de glicogen es consumien dràsticament quan s'incubaven les cèl·lules HUVEC en un medi de cultiu sense glucosa, aquestes augmentaven en condicions d'hipòxia. Finalment, les cèl·lules HUVEC es van tractar amb un inhibidor de la glicogen fosforilasa (CP-320626), enzim clau per a la degradació del glicogen i també amb un inhibidor de la glucosa-6-fosfat deshidrogenasa (G6PD - *Glucose-6-Phosphate Dehydrogenase*) (G5) i un inhibidor de la transcetolasa (TKT – *Transketolase*) (O1), enzims clau de la PPP, com s'ha esmentat anteriorment. El tractament amb aquests inhibidors metabòlics va disminuir la viabilitat cel·lular i la capacitat de migració de les cèl·lules HUVEC.

DISCUSSIÓ

Als països desenvolupats, el càncer és la segona causa de mortalitat després de les malalties cardiovasculars. En el cas concret del càncer colorectal, aquest ocupa el quart lloc en mortalitat a nivell mundial segons l'Organització Mundial de la Salut (OMS) (http://www.who.int). A part

de diferents factors de risc per al càncer colorectal que no podem canviar, com són l'edat o els antecedents hereditaris, també existeixen altres factors de risc relacionats amb l'estil de vida. Tanmateix, la relació entre l'alimentació, la inactivitat física i l'obesitat amb el risc de càncer colorectal és una de les més fortes entre tots els tipus de càncer. Amb referència a l'alimentació, s'ha descrit que un consum elevat de carn vermella, de sucres processats i d'alguns tipus de greix poden augmentar el risc de càncer colorectal. Per contra, una alimentació rica en vegetals ha estat associada amb un menor risc de càncer colorectal. D'aquí el creixent interès de la comunitat científica en l'obtenció de substàncies d'origen natural encaminades a la prevenció i el tractament del càncer. Amb tot i això, els mecanismes pels quals aquests compostos antiproliferatius d'origen natural exerceixen la seva acció encara no han estat del tot esclarits. Per tant, amb l'objectiu d'aprofundir en el coneixement d'aquests mecanismes d'acció, en aquesta Tesi Doctoral hem plantejat tot un seguit d'estudis dirigits a caracteritzar l'efecte de diferents compostos polifenòlics i d'una fibra alimentària rica en polifenols sobre models de càncer de còlon *in vitro* i *in vivo*. Finalment, s'han investigat noves dianes anti-angiogèniques amb la finalitat d'identificar potents teràpies combinades que ataquin a la vegada el creixement del tumor i l'angiogènesi estimulada per ell. Per aconseguir aquests objectius, s'han utilitzat diferents disciplines englobades per la Biologia de Sistemes, com la transcriptòmica, la proteòmica, la citòmica i la metabolòmica, les quals ens han permès aprofundir en el coneixement de les dianes moleculars dels diferents productes estudiats. D'aquesta manera, per realitzar el capítol 1 es van utilitzar tècniques pertanyents a la citòmica com són ara l'estudi del cicle cel·lular i de l'apoptosi per citometria de flux. Aquest capítol va avaluar dos tanins hidrolitzables, l'hamamelitanin (HT) i la pentagaloilglucosa (PGG), i una fracció rica en tanins condensats (F800H4) procedents d'*H. virginiana* com possibles agents antitumorals. Estudis previs en el nostre laboratori ja havien avaluat l'efecte de diferents fraccions polifenòliques extretes de l'escorça d'aquest arbust en cèl·lules d'adenocarcinoma de còlon humà HT29 i havien descrit una inhibició important del creixement d'aquesta línia cel·lular (Lizárraga *et al.*, 2008). A diferència del nostre estudi, les fraccions analitzades eren barreges heterogènies que contenien tant tanins hidrolitzables com condensats. En el nostre cas, es va treballar amb productes purificats (puresa del 98% o més), en el cas de l'HT i la PGG i amb un fracció enriquida (83.9%) en tanins condensats. Els nostres resultats van mostrar que els polifenols d'*H. virginiana* actuaven induint apoptosi i necrosi, a més d'un arrest en la fase S del cicle cel·lular en cèl·lules HT29. Aquesta informació és coherent amb la obtinguda a l'estudi amb extractes polifenòlics i indica que els compostos bioactius continguts en les fraccions corresponen molt probablement als tanins estudiats. A més, el nostre estudi va aportar informació addicional molt interessant pel que fa a l'especificitat dels tanins extrets de l'avellaner de bruixa. D'una banda,

es va observar que la PGG inhibia de la mateixa manera el creixement de les cèl·lules canceroses i dels colonòcits normals. De l'altra, la citotoxicitat produïda per la fracció F800H4, rica en tanins condensats, va resultar ser un efecte artefactual causat per la generació de ROS al medi de cultiu. Contràriament, l'HT es va mostrar com un taní amb una prometedora activitat antitumoral gràcies a la seva elevada bioeficàcia i especificitat. Aquests efectes tant diferents produïts pels tanins d'*H. virginiana* probablement es deuen a la seva diferent capacitat redox. Segons l'estructura química, l'activitat biològica de l'HT i la PGG hauria de ser semblant, en canvi, l'HT va resultar molt més activa biològicament. Això es podria explicar per l'elevada capacitat de transferència electrònica de l'HT, demostrada per la seva capacitat per reaccionar amb el radical TNPTM. La posició activada podria ser l'hidroxil geminal a l'éster de gal·lat, el qual podria formar un pont d'hidrogen amb el grup carbonil del gal·lat com a part d'un anell de sis membres estèricament favorable. Aquest pont d'hidrogen podria afavorir la ionització de l'hidroxil. Altrament, l'efecte artefactual produït per la fracció F800H4 probablement es deu al seu alt contingut en grups pirogal·lol altament reactius (Touriño *et al.*, 2008). Així doncs, aquests resultats juntament amb investigacions anteriors (Lizárraga *et al.*, 2007; Singh *et al.*, 2011) ressalten la importància dels grups gal·lat i pirogal·lol per a l'activitat biològica. Això ens van portar a estudiar els polifenols del té verd i raïm epicatequina (EC), epigal·locatequin gal·lat (EGCG) i epicatequin gal·lat (ECG). Mentre que aquesta última catequina que conté un grup gal·lat i que es troba en quantitats elevades en extractes de raïm es va utilitzar en el capítol 3, en el capítol 2 es van utilitzar els dos compostos estructuralment més diferents i presents majoritàriament en té verd. Per un cantó l'EGCG, el qual conté un grup gal·lat i un grup pirogal·lol, i per l'altre, l'EC que no conté cap d'aquests grups. Aquestes diferents característiques químiques s'han relacionat amb l'eficàcia biològica de les catequines (Yang *et al.*, 2009). Concretament, el producte que s'ha descrit com més bioactiu és l'EGCG, seguit de prop per l'ECG i en últim lloc l'EC (Ingolfsson *et al.*, 2011). Curiosament, aquesta tendència es va observar en els nostres de capacitat antiproliferativa en la línia cel·lular HT29, de manera que el producte amb més capacitat antiproliferativa va ser l'EGCG, seguit per l'ECG i finalment, l'EC.

En el capítol 2, es van utilitzar diferents tècniques proteòmiques per determinar l'efecte de l'EC i l'EGCG sobre la diferenciació de les cèl·lules HT29 induïda per butirat. Sorprenentment, tot i que el tractament amb l'EC i l'EGCG sols no va modificar la diferenciació de les cèl·lules HT29, aquests polifenols van reduir la diferenciació induïda per butirat. El mecanisme d'acció d'aquest àcid gras de cadena curta (SCFA – *Short Chain Fatty Acids*) es basa principalment en la seva inhibició de les histones deacetilases (HDAC) (Humphreys *et al.*, 2012), dada que es va confirmar en la detecció de l'activitat HDAC en extractes nuclears de cèl·lules HT29. Per

contra, no es va detectar modificació significativa de l'activitat HDAC per part dels polifenols. Aquest últim resultat coincideix amb estudis anteriors, també en HT29, que revelen que no hi havia canvis en l'activitat HDAC de fraccions citoplasmàtiques o nuclears després del tractament amb sulforafà i EGCG (Nair *et al.*, 2008). El posterior estudi de l'entrada cel·lular de butirat va mostrar que el butirat és capaç d'activar la seva pròpia entrada a la cèl·lula i també que els polifenols disminueixen aquesta entrada. Aquest últim resultat ens va portar a estudiar el transportador monocarboxílic 1 (MCT1), el qual juga una funció important en el transport intestinal de butirat (Saksena *et al.*, 2009). El MCT1 es localitza a la membrana apical del tracte intestinal, on està implicat en l'absorció de SCFA com és el butirat. Aquests àcids grassos també poden entrar a les cèl·lules intestinals ràpidament per lliure difusió, no obstant això el seu transport és fortament facilitat pel MCT1 (Halestrap, 2012). Per tant, considerant que el butirat ha estat descrit com un producte antitumoral en càncer colorectal, el seu transportador MCT1 es considerat un gen supressor de tumors. L'anàlisi del control transcripcional del MCT1 va mostrar que mentre que els polifenols no produïen canvis, el butirat activava l'activitat del promotor del gen MCT1. Això ja s'havia demostrat anteriorment en cèl·lules AA/C1 (Cuff *et al.*, 2002) i Caco-2 (Borthakur *et al.*, 2008) de càncer de còlon humà. Tot seguit, considerant que aquests canvis en regulació transcripcional no es reflectien en canvis a nivell proteic, es va buscar un altre mecanisme per explicar els efectes dels polifenols en la diferenciació induïda pel butirat. Com s'ha comentat, diferents evidències suggereixen que la funció òptima d'alguns transportadors i receptors depèn de la seva localització en microdominis de membrana anomenats *rafts* lipídics (Annaba *et al.*, 2010; Chen *et al.*, 2011). A més, de manera interessant, els polifenols del té s'han descrit com reguladors d'aquestes regions de membrana (Patra *et al.*, 2008; Duhon *et al.*, 2010). Es va estudiar el comportament dels *rafts* lipídics en resposta als diferents tractaments en HT29 i es va observar que mentre que el butirat activava el posicionament del MCT1 en *rafts* lipídics, les catequines del té verd produïen una redistribució d'aquest transportador en zones de la membrana no corresponents a *rafts*. D'aquesta manera, els polifenols inhibien l'entrada de butirat i la posterior inducció de la diferenciació de les cèl·lules HT29. Així, aquests sorprenents resultats suggereixen que, tot i que tant el butirat com els polifenols del té verd posseeixen efectes beneficiosos per la salut humana, han de ser utilitzats separadament per mantenir les seves activitats. Pel que fa als estudis esmentats anteriorment sobre l'augment de la concentració intestinal de SCFA pels polifenols, l'augment en butirat intestinal podria compensar *in vivo* la inhibició de l'entrada cel·lular de butirat descrita aquí, en el cas que l'augment de butirat es degui a un canvi en l'activitat de la microbiota produït pel polifenols. A més, l'augment en la concentració intestinal de butirat també podria ser explicat per l'acció inhibitòria dels polifenols en l'entrada de butirat. Aquest nou coneixement sobre la

interferència de prebiotics és de gran interès per al futur disseny racional d'intervencions preventives o terapèutiques contra el càncer colorectal..

En el capítol 3, es va caracteritzar l'ECG com potencial inhibidor del metabolisme tumoral. Com s'ha esmentat abans, l'adaptació metabòlica tumoral és necessària per suportar el creixement accelerat propi de les cèl·lules tumorals i a la vegada, els aporta avantatges per sobreviure i envair nous teixits (Vizán *et al.*, 2008; Dang, 2012). Així, la xarxa metabòlica tumoral es presenta com una prometedora diana per inhibir el càncer. Es van monitoritzar les principals vies del metabolisme central del carboni, entre les quals destaquen la glicòlisi, el cicle dels àcids tricarboxílics (TCA – *Tricarboxylic Acid*), la síntesi de lípids i la ruta de les pentoses fosfat (PPP – *Pentose Phosphate Pathway*). D'aquesta manera es va descriure el perfil metabòlic de les cèl·lules HT29 tractades amb ECG i, per tant, es van poder determinar les dianes a nivell metabòlic d'aquesta catequina natural. Primerament, els resultats obtinguts van demostrar que les cèl·lules HT29 tractades amb 140 μM ECG consumien menys glucosa i produïen menys lactat. Com ja s'ha comentat a la introducció, una de les principals característiques metabòliques associades a la progressió tumoral és la degradació accelerada de glucosa a lactat inclús en presència d'oxigen. Així doncs, no és d'estranyar que un producte considerat antitumoral disminueixi l'elevada entrada de glucosa i conseqüentment la producció de lactat. A més, el tractament amb 140 μM ECG va disminuir també el consum de glutamina, fet que es podria deure a la coneguda capacitat de l'ECG per inhibir la glutamat deshidrogenasa mitocondrial (Li *et al.*, 2006). Donat que la glutamina, igual que la glucosa, és un substrat crucial per garantir l'elevada taxa proliferativa característica de les cèl·lules tumorals, la inhibició de la seva entrada també és de gran interès per al tractament del càncer (Meng *et al.*, 2010). Respecte a l'estudi de la distribució isotopomèrica en glutamat, cal destacar que aquesta ens va permetre detectar una inhibició del TCA, la qual, a la vegada, es podria deure, almenys en part, a la inhibició en l'entrada de substrats metabòlics esmentada. Ja que en alguns estudis l'activació del TCA es mostra com una adaptació metabòlica per augmentar la síntesi de precursors anabòlics (Chen *et al.*, 2007; Weinberg *et al.*, 2010), aquesta inhibició del TCA per l'ECG pot actuar reduint aquests precursors metabòlics necessaris per la biosíntesi de proteïnes, àcids nucleics i lípids. En aquest sentit, l'anàlisi isotopomèric en els àcids grassos palmitat i estearat va mostrar que l'ECG redueix també la lipogènesi en cèl·lules HT29. Aquesta dada resulta interessant degut al fet que la síntesi d'àcids grassos ha estat proposada com diana antitumoral (Menendez, 2010). En referència a l'anàlisi isotopomèric en ribosa, es va mostrar que mentre que el tractament amb 70 μM ECG no va produir canvis, 140 μM ECG va ser capaç de reduir la síntesi *de novo* de ribosa. Tanmateix, cal subratllar que aquesta inhibició en la síntesi d'àcids nucleics s'ha mostrat com una aproximació potent en quimioteràpia (Nakamura *et*

al., 2011; Senanayake *et al.*, 2011). A més, l'anàlisi en ribosa també va mostrar un augment significatiu en la proporció d'utilització de la branca oxidativa respecte la no oxidativa de la PPP després del tractament amb 140 μM ECG. El posterior anàlisi de l'activitat dels enzims que controlen aquestes vies, glucosa-6-fosfat deshidrogenasa (G6PD - *Glucose-6-Phosphate Dehydrogenase*) i transcetolasa (TKT - *Transketolase*), respectivament, va mostrar una inhibició d'ambdós enzims per l'ECG 140 μM, encara que la inhibició observada en la TKT va ser més important. S'ha descrit que els coeficients de control sobre el creixement tumoral per la G6PD i la TKT són 0.41 i 0.9, respectivament (Boren *et al.*, 2002). Per tant, ambdues inhibicions de l'activitat enzimàtica poden implicar una reducció important de la progressió tumoral, encara que l'efecte de la TKT juga un paper més important. A més, en diverses línies tumorals la branca no oxidativa de la PPP, controlada per la TKT, ha estat descrita com la font principal de ribosa-5-fosfat (Cascante *et al.*, 2000), així que la importància d'aquesta inhibició per a la inhibició tumoral es veu reforçada. Tot i això, la inhibició de la G6PD per l'ECG també pot jugar un rol important en la inhibició tumoral, ja que la branca oxidativa de la PPP no només s'utilitza per sintetitzar ribosa, sinó que també serveix per sintetitzar poder reductor en forma de NADPH necessari per a la síntesi lipídica.

En el capítol 4 diferents tècniques pertanyents a la transcriptòmica ens van permetre determinar els patrons d'expressió associats a l'efecte quimiopreventiu de la GADF. Aquest compost va aconseguir reduir la formació de pòlips a l'intestí prim dels ratolins $Apc^{Min/+}$ en un 76% respecte el control. Cal recalcar que aquests resultats són millors que altres observats en estudis anteriors realitzats en condicions semblants en ratolins $Apc^{Min/+}$ tractats amb fibra o altres compostos polifenòlics. Per exemple, l'administració de dibenzoilmetà al 1% va reduir el nombre total de tumors intestinals en un 50% (Shen *et al.*, 2007) i un extracte polifenòlic de poma va ser capaç de disminuir també aquest nombre en un 35% i un 42% en ratolins $Apc^{Min/+}$ alimentats amb una dieta equilibrada o una dieta occidental, respectivament (Fini *et al.*, 2011). Els millors resultats obtinguts per a la fibra han estat una reducció del 25% en tumors intestinals després de l'administració de segó de sègol al 10% (Mutanen *et al.*, 2000) i una disminució del 51% amb 30% de segó d'arròs (Verschoyle *et al.*, 2007). L'anàlisi de pòlips per mida va revelar que la GADF va inhibir els pòlips de totes les mides d'una manera similar, indicant que actua inhibint tant l'aparició com el desenvolupament dels pòlips. D'una altra banda, l'anàlisi per zones intestinals va mostrar un efecte anti-tumoral molt homogeni que podria estar relacionat amb la composició de la GADF: Aquesta conté una mescla complexa de polifenols associats a la fibra dietètica els quals són gradualment alliberats i absorbits per les cèl·lules intestinals. Pel que fa a l'estudi dels mecanismes moleculars associats a la inhibició de la carcinogènesi intestinal per la GADF, l'anàlisi d'expressió per *microarrays* va suggerir que la GADF es basa

principalment en la inducció d'un arrest del cicle cel·lular en la fase G1 per disminuir el creixement tumoral. La GADF va modular diferents gens crucials per a la progressió d'aquesta fase com són la Ciclina D (*Ccnd1*) i GADD45 (*Gadd45a*). Aquests resultats són coherents amb estudis anteriors on es va observar en immunohistoquímiques de teixit intestinal que el tractament de ratolins $Apc^{Min/+}$ amb un extracte de llavor de raïm produïa una infraregulació de la Ciclina D i una sobreregulació de la proteïna Cip1/p21 (Velmurugan *et al.*, 2010). A més, un altre estudi va coincidir en descriure que l'extracte de llavor de raïm sobreregula p21 i conseqüentment indueix un arrest del cicle cel·lular en la fase G1 (Kaur *et al.*, 2011). L'estudi de la via de senyalització Wnt, defectuosa en els ratolins $Apc^{Min/+}$, i altres vies relacionades com és ara la via Notch, va mostrar que GADF inhibeix també el creixement polipoide a través de la inhibició simultània d'aquestes rutes intracel·lulars. Sorprenentment, l'anàlisi d'expressió també va revelar una inhibició de molts gens relacionats amb el sistema immune i la inflamació. Històricament, la funció d'aquests processos s'ha conegut com protectora enfront de les cèl·lules tumorals, en canvi, més recentment s'ha descrit que, quan la inflamació esdevé crònica, es capaç de promoure el creixement maligne. De manera paral·lela, els polifenols del raïm han estat implicats en ambdues funcions en diferents treballs, enfortint la funció immune (Katiyar, 2007) o bé actuant com antiinflamatoris i atenuadors del sistema immune (Misikangas *et al.*, 2007). Atès que en els ratolins $Apc^{Min/+}$ la tumorigenesi intestinal es conduïda per una inflamació continuada i una senyalització immune excessiva (Saleh *et al.*, 2011), la inhibició de la resposta immune podria reduir la progressió dels pòlips. A més, considerant que recentment s'ha demostrat que el consum de fibra està inversament associat a la presència d'un perfil de citoquines pro-inflamatòries (Chuang *et al.*, 2011), l'efecte atenuador de la resposta immune podria ser causat sinèrgicament pels components polifenòlics i la fibra. A més, aquesta efecte sinèrgic es podria estendre a la resta de modulacions transcripcionals. En el cas dels polifenols, probablement la modulació de l'expressió gènica es dóna directament (Yun *et al.*, 2010), mentre que l'acció de la fibra es mitjançada pels SCFA alliberats durant la fermentació colònica (Hu *et al.*, 2011).

En el capítol 5, l'ús de la biologia de sistemes, integrant dades basades en la transcriptòmica i la metabolòmica ens van permetre identificar un efecte protector de l'àcid maslinic enfront la poliposi intestinal espontània en ratolins $Apc^{Min/+}$. El tractament amb MA va reduir el nombre total de pòlips un 45 % en comparació amb el grup control. L'MA va mostrar una eficàcia inhibitòria diferent depenent del segment d'intestí analitzat. Això es podria deure a canvis en el pH, el patró d'expressió d'enzims, la microbiota i la concentració a causa del contingut intestinal al llarg del tracte intestinal, que podrien modificar l'estructura química i la biodisponibilitat de l'MA. Per exemple, s'ha descrit que el resveratrol es gairebé completament conjugat quan

s'administra oralment i els seus glucoronats i sulfats són realment els metabòlits bioactius (Tessitore *et al.*, 2000; Iwuchukwu *et al.*, 2008). Igual que en el cas de la GADF, la inhibició de pòlips classificats per mida va ser homogènia, suggerint que l'MA inhibia tant l'aparició com el desenvolupament dels pòlips intestinals en els ratolins $Apc^{Min/+}$. La determinació del perfil transcripcional en ratolins $Apc^{Min/+}$ tractats amb MA va mostrar principalment modificacions en vies relacionades amb el càncer, com són el cicle cel·lular o l'apoptosi. A tall d'exemple, l'MA va infraregular l'expressió de JunB, un component de la *activating protein-1* (AP-1) implicat en el control del cicle cel·lular, la diferenciació, la inflamació i la transformació preneoplàsica. Aquest resultat concorda amb un estudi anterior que mostrava que l'efecte quimiopreventiu de l'MA en limfòcits Raji depenia, en part, de la inhibició d'AP-1 (Hsum *et al.*, 2011). Amb relació a l'apoptosi, l'MA va disminuir l'expressió de les proteïnes anti-apoptòtiques Bcl-2 i Bcl-XL. En concret, la infraregulació de la Bcl-2 ja havia estat observada per *Western blot* després del tractament de cèl·lules HT29 amb MA (Reyes-Zurita *et al.*, 2011). A més, l'MA va modular diferents vies de transducció de senyal relacionades amb supervivència. Com a exemple, l'MA va infraregular l'expressió de diferents subunitats de la proteïna PKA. En aquest sentit, cal destacar que el tractament dels ratolins $Apc^{Min/+}$ amb un antagonista de la PKA va ser capaç de reduir la progressió tumoral (Brudvik *et al.*, 2011). En aquest cas, igual que es va observar amb la GADF, l'MA també va infraregular gens relacionats amb la inflamació i el sistema immune. D'acord amb això, l'MA ja havia estat prèviament implicat en activitats anti-inflamatòries i atenuadores del sistema immune a través de la inhibició de NFkB (Huang *et al.*, 2011). Addicionalment, la comparació dels espectres de NMR dels sèrums control i MA va revelar un augment en els nivells de cossos cetònics i una reducció dels nivells de glucosa en els ratolins tractats. A part de la modulació transcripcional implicada, la disminució en els nivells de glucosa podria ser una conseqüència de l'acumulació de glicogen promoguda directament per aquest compost, ja que l'MA s'ha descrit com un potent inhibidor de la glicogen fosforilasa (Guan *et al.*, 2011). D'una altra banda, la mateixa disminució en els nivells de glucosa en sèrum podria contribuir a l'augment en cossos cetònics, ja que la formació de cossos cetònics s'activa quan hi ha poca disponibilitat de glucosa.

Finalment, en el capítol 6, mitjançant tècniques corresponents a la metabòlomica ja esmentades en el capítol 3, es va determinar la modulació de la xarxa metabòlica requerida per donar suport al procés angiogènic. Els resultats van mostrar un patró metabòlic comú característic de l'activació angiogènica quan les cèl·lules endotelials umbilicals humanes (HUVEC – *Human Umbilical Vascular Endothelial Cells*) eren activades amb el factor de creixement vascular endotelial (VEGF - *Vascular Endothelial Growth Factor*) o el factor de creixement de fibroblasts (FGF – *Fibroblast Growth Factor*). Per tal de comprovar si el patró

metabòlic detectat era realment una conseqüència de l'activació angiogènica, es va analitzar l'efecte d'un inhibidor del receptor 2 del factor de creixement endotelial vascular (VEGFR - *Vascular Endothelial Growth Factor Receptor 2*), 5-diarilurea-oxi-benzimidazol, en la xarxa metabòlica de les cèl·lules HUVEC. Aquest inhibidor actua a la part intracel·lular del VEGFR-2 i impedeix la seva fosforilació, causant una disminució en la cascada de senyalització activada per VEGF. La distribució isotopomèrica en lactat no va canviar significativament quan es va afegir l'inhibidor, suggerint que el flux glicolític no depèn de la senyal del VEGF. Tanmateix, el tractament amb l'inhibidor en cèl·lules HUVEC activades amb VEGF va produir una disminució en el flux de la PPP. Curiosament, diversos estudis anteriors han demostrat que la inhibició d'aquesta via redueix la capacitat de migració de cèl·lules endotelials d'aorta bovines (Ascher *et al*., 2001; Leopold *et al*., 2003). A més, els resultats van mostrar que la utilització del inhibidor també disminuïa l'enriquiment en ^{13}C en les reserves de glicogen. Això és va veure confirmat per l'acumulació de reservoris de glicogen en presència de l'inhibidor. La importància fisiològica d'aquests reservoris de glicogen es podria deure a les necessitats de les cèl·lules endotelials durant la formació dels nous vasos, després del reclutament per tumors sòlids, en condicions d'hipòxia i hipoglicèmia. Així, forçant les condicions d'hipoglucèmia fisiològiques, es va observar un catabolisme total dels reservoris de glicogen. Aquesta disminució dramàtica del contingut de glicogen en un medi sense glucosa ja s'havia observat anteriorment en una altra línia de cèl·lules endotelials humanes (Artwohl *et al*., 2007). Al contrari, la hipòxia no va produir l'ús d'aquests reservoris, sinó que va causar un augment en el contingut de glicogen cel·lular. En condicions d'hipòxia, la taxa glicolítica augmenta, fet que pot provocar un augment en la concentració intracel·lular d'intermediaris glicolítics. Per això, s'hipotetitza que l'augment observat en el contingut de glicogen en condicions d'hipòxia es podria explicar per un equilibri metabòlic entre els intermediaris glicolítics i les reserves de glicogen. Així, els nostres resultats mostren la PPP i el metabolisme glicogen com noves dianes terapèutiques contra l'angiogènesi. A més, la importància d'aquestes característiques metabòliques es va veure reforçada quan la inhibició dels enzims clau del metabolisme del glicogen i la PPP va inhibir la viabilitat i la capacitat de migració de les cèl·lules HUVEC. Curiosament, tant la PPP, com s'ha comentat anteriorment, com el metabolisme de glicogen s'han descrit com dianes antitumorals (Lee *et al.*, 2004; Nakamura *et al.*, 2011; Senanayake *et al.*, 2011). Per tant, la inhibició d'aquestes vies metabòliques confereix una nova i potent aproximació terapèutica que ataca simultàniament el creixement tumoral i l'angiogènesi.

A manera de resum, els resultats obtinguts en aquesta Tesi Doctoral donen a conèixer nous mecanismes d'acció i noves dianes terapèutiques associats a l'efecte dels productes naturals en càncer de còlon. A més, les dades obtingudes aporten llum al coneixement sobre

algunes interferències entre diferents productes prebiòtics les quals s'han de tenir en compte en futures intervencions quimiopreventives. Finalment, es mostra una adaptació metabòlica característica de les cèl·lules endotelials activades que pot esser explotada per al tractament efectiu del càncer.

CONCLUSIONS

1. El taní hidrolitzable pentagaloilglucosa i la fracció F800H4 rica en tanins condensats extrets d'*H. virginiana* inhibeixen de manera semblant el creixement de les cèl·lules d'adenocarcinoma de còlon humà HT29 i dels colonòcits normals NCM460. En canvi, el taní hidrolitzable hamamelitanin actua específicament contra les cèl·lules tumorals HT29 induint apoptosi i produint un arrest en la fase S del cicle cel·lular. Els efectes de l'hamamelitanin possiblement es deuen a la presència d'una posició fenòlica altament reactiva capaç de reaccionar amb el radical estable TNPTM.

2. Els polifenols majoritaris en té verd, (-)-epicatequina (EC) i (-)-epigal·locatequin gal·lat (EGCG), inhibeixen l'entrada de butirat a les cèl·lules HT29 i la subsegüent diferenciació induïda per aquest. Aquest efecte no es deu a la modulació de les histones deacetilases ni a canvis en l'expressió del Transportador Monocarboxílic 1 (MCT1) encarregat del transport intestinal de butirat. Tanmateix, l'EC i l'EGCG disminueixen l'activitat del MCT1 mitjançant el seu posicionament en zones de la membrana plasmàtica no corresponents a *rafts* lipídics.

3. El tractament de les cèl·lules HT29 amb epicatequin gal·lat (ECG), present en té verd i raïm, redueix l'entrada de diferents substrats metabòlics com són la glucosa i la glutamina. Conseqüentment, produeix també una disminució en la producció de lactat en les cèl·lules tractades. A més, l'ECG disminueix l'ús del cicle dels àcids tricarboxílics, la síntesi de lípids i la via de les pentoses fosfat. La reducció en aquesta última via es deu a la inhibició de l'activitat dels seus enzims clau glucosa-6-fosfat deshidrogenasa i transcetolasa.

4. El tractament dels ratolins $Apc^{Min/+}$ amb una fibra antioxidant de raïm (GADF - *Grape Antioxidant Dietary Fiber*) va disminuir significativament la poliposi intestinal

espontània produïda en aquest ratolins genèticament predisposats. Aquest efecte quimiopreventiu de la GADF es deu principalment a la modulació de l'expressió gènica relacionada amb un arrest del cicle cel·lular en la fase G1. Així mateix, GADF també infraregula gens relacionats amb la resposta immune i la inflamació, la qual cosa contraresta la inflamació crònica present en ratolins $Apc^{Min/+}$.

5. L'àcid maslínic (MA - *Maslinic Acid*), procedent de l'oliva, inhibeix la poliposi intestinal en ratolins $Apc^{Min/+}$. El mecanisme pel qual es dona aquesta inhibició és la inducció d'apoptosi i d'arrest en la fase G1 del cicle cel·lular. A més a més, el tractament amb MA produeix un perfil metabòlic protector caracteritzat per una disminució en els nivells sèrics de glucosa i un augment en els nivells de cossos cetònics.

6. L'activació angiogènica de cèl·lules endotelials umbilicals humanes HUVEC comporta una adaptació metabòlica, independent del factor de creixement que la produeixi, que es caracteritza per una activació de la ruta de les pentoses fosfat i del metabolisme del glicogen. Els reservoris de glicogen intracel·lulars són exhaurits en un ambient hipoglucèmic i, en canvi, augmentats en condicions d'hipòxia. La inhibició de la via de les pentoses fosfat i del metabolisme del glicogen produeix una reducció en la viabilitat i la migració de les cèl·lules endotelials.

BIBLIOGRAFIA

Adams, J.M. i Cory, S. (1998). The Bcl-2 protein family: arbiters of cell survival. *Science* 281(5381): 1322-6.

Ahmad, M.S., Krishnan, S., Ramakrishna, B.S., Mathan, M., Pulimood, A.B. i Murthy, S.N. (2000). Butyrate and glucose metabolism by colonocytes in experimental colitis in mice. *Gut* 46(4): 493-9.

Al-Ejeh, F., Kumar, R., Wiegmans, A., Lakhani, S.R., Brown, M.P. i Khanna, K.K. (2010). Harnessing the complexity of DNA-damage response pathways to improve cancer treatment outcomes. *Oncogene* 29(46): 6085-98.

Alcarraz-Vizan, G., Boren, J., Lee, W.N. i Cascante, M. (2010). Histone deacetylase inhibition results in a common metabolic profile associated with HT29 differentiation. *Metabolomics* 6(2): 229-237.

Allouche, Y., Warleta, F., Campos, M., Sanchez-Quesada, C., Uceda, M., Beltran, G. i Gaforio, J.J. (2011). Antioxidant, antiproliferative, and pro-apoptotic capacities of pentacyclic triterpenes found in the skin of olives on MCF-7 human breast cancer cells and their effects on DNA damage. *J Agric Food Chem* 59(1): 121-30.

Amakura, Y., Tsutsumi, T., Sasaki, K., Nakamura, M., Yoshida, T. i Maitani, T. (2008). Influence of food polyphenols on aryl hydrocarbon receptor-signaling pathway estimated by in vitro bioassay. *Phytochemistry* 69(18): 3117-30.

Andriamihaja, M., Chaumontet, C., Tome, D. i Blachier, F. (2009). Butyrate metabolism in human colon carcinoma cells: implications concerning its growth-inhibitory effect. *J Cell Physiol* 218(1): 58-65.

Annaba, F., Kumar, P., Dudeja, A.K., Saksena, S., Gill, R.K. i Alrefai, W.A. (2010). Green tea catechin EGCG inhibits ileal apical sodium bile acid transporter ASBT. *Am J Physiol Gastrointest Liver Physiol* 298(3): G467-73.

Ballinger, A.B. i Anggiansah, C. (2007). Colorectal cancer. *Bmj* 335(7622): 715-8.

Bastianetto, S., Dumont, Y., Han, Y. i Quirion, R. (2009). Comparative neuroprotective properties of stilbene and catechin analogs: action via a plasma membrane receptor site? *CNS Neurosci Ther* 15(1): 76-83.

Bates, S. (2011). The role of gene expression profiling in drug discovery. *Curr Opin Pharmacol* 11(5): 549-56.

Boren, J., Lee, W.N., Bassilian, S., Centelles, J.J., Lim, S., Ahmed, S., Boros, L.G. i Cascante, M. (2003). The stable isotope-based dynamic metabolic profile of butyrate-induced HT29 cell differentiation. *J Biol Chem* 278(31): 28395-402.

Boren, J., Montoya, A.R., de Atauri, P., Comin-Anduix, B., Cortes, A., Centelles, J.J., Frederiks, W.M., Van Noorden, C.J. i Cascante, M. (2002). Metabolic control analysis aimed at the ribose

synthesis pathways of tumor cells: a new strategy for antitumor drug development. *Mol Biol Rep* 29(1-2): 7-12.

Boren, J., Ramos-Montoya, A., Bosch, K.S., Vreeling, H., Jonker, A., Centelles, J.J., Cascante, M. i Frederiks, W.M. (2006). In situ localization of transketolase activity in epithelial cells of different rat tissues and subcellularly in liver parenchymal cells. *J Histochem Cytochem* 54(2): 191-9.

Boros, L.G., Cascante, M. i Paul Lee, W.-N. (2002). Metabolic profiling of cell growth and death in cancer: applications in drug discovery. *Drug Discovery Today* 7(6): 364-372.

Boros, L.G., Torday, J.S., Lim, S., Bassilian, S., Cascante, M. i Lee, W.N. (2000). Transforming growth factor beta2 promotes glucose carbon incorporation into nucleic acid ribose through the nonoxidative pentose cycle in lung epithelial carcinoma cells. *Cancer Res* 60(5): 1183-5.

Borthakur, A., Saksena, S., Gill, R.K., Alrefai, W.A., Ramaswamy, K. i Dudeja, P.K. (2008). Regulation of monocarboxylate transporter 1 (MCT1) promoter by butyrate in human intestinal epithelial cells: involvement of NF-kappaB pathway. *J Cell Biochem* 103(5): 1452-63.

Brown, J.B. i Okuno, Y. (2012). Systems biology and systems chemistry: new directions for drug discovery. *Chem Biol* 19(1): 23-8.

Brudvik, K.W., Paulsen, J.E., Aandahl, E.M., Roald, B. i Tasken, K. (2011). Protein kinase A antagonist inhibits beta-catenin nuclear translocation, c-Myc and COX-2 expression and tumor promotion in ApcMin/+ mice. *Mol Cancer* 10: 149.

Canavese, M., Santo, L. i Raje, N. (2012). Cyclin dependent kinases in cancer: Potential for therapeutic intervention. *Cancer Biol Ther* 13(7).

Carafa, V., Nebbioso, A. i Altucci, L. (2011). Histone deacetylase inhibitors: recent insights from basic to clinical knowledge & patenting of anti-cancer actions. *Recent Pat Anticancer Drug Discov* 6(1): 131-45.

Cascante, M., Centelles, J.J., Veech, R.L., Lee, W.N. i Boros, L.G. (2000). Role of thiamin (vitamin B-1) and transketolase in tumor cell proliferation. *Nutr Cancer* 36(2): 150-4.

Coller, H.A., Sang, L. i Roberts, J.M. (2006). A new description of cellular quiescence. *PLoS Biol* 4(3): e83.

Cuff, M.A., Lambert, D.W. i Shirazi-Beechey, S.P. (2002). Substrate-induced regulation of the human colonic monocarboxylate transporter, MCT1. *J Physiol* 539(Pt 2): 361-71.

Chaffer, C.L. i Weinberg, R.A. (2011). A perspective on cancer cell metastasis. *Science* 331(6024): 1559-64.

Chai, P.C., Long, L.H. i Halliwell, B. (2003). Contribution of hydrogen peroxide to the cytotoxicity of green tea and red wines. *Biochem Biophys Res Commun* 304(4): 650-4.

Chen, E.I., Hewel, J., Krueger, J.S., Tiraby, C., Weber, M.R., Kralli, A., Becker, K., Yates, J.R., 3rd i Felding-Habermann, B. (2007). Adaptation of energy metabolism in breast cancer brain metastases. *Cancer Res* 67(4): 1472-86.

Chen, G., Howe, A.G., Xu, G., Frohlich, O., Klein, J.D. i Sands, J.M. (2011). Mature N-linked glycans facilitate UT-A1 urea transporter lipid raft compartmentalization. *Faseb J* 25(12): 4531-9.

Chen, W.J., Chang, C.Y. i Lin, J.K. (2003). Induction of G1 phase arrest in MCF human breast cancer cells by pentagalloylglucose through the down-regulation of CDK4 and CDK2 activities and up-regulation of the CDK inhibitors p27(Kip) and p21(Cip). *Biochem Pharmacol* 65(11): 1777-85.

Chen, W.J. i Lin, J.K. (2004). Induction of G1 arrest and apoptosis in human jurkat T cells by pentagalloylglucose through inhibiting proteasome activity and elevating p27Kip1, p21Cip1/WAF1, and Bax proteins. *J Biol Chem* 279(14): 13496-505.

Chuang, S.C., Vermeulen, R., Sharabiani, M.T., Sacerdote, C., Fatemeh, S.H., Berrino, F., Krogh, V., Palli, D., Panico, S., Tumino, R., Athersuch, T.J. i Vineis, P. (2011). The intake of grain fibers modulates cytokine levels in blood. *Biomarkers* 16(6): 504-10.

Chung, W.G., Miranda, C.L., Stevens, J.F. i Maier, C.S. (2009). Hop proanthocyanidins induce apoptosis, protein carbonylation, and cytoskeleton disorganization in human colorectal adenocarcinoma cells via reactive oxygen species. *Food Chem Toxicol* 47(4): 827-36.

Dang, C.V. (2012). MYC on the Path to Cancer. *Cell* 149(1): 22-35.

Dashwood, R.H. i Ho, E. (2007). Dietary histone deacetylase inhibitors: from cells to mice to man. *Semin Cancer Biol* 17(5): 363-9.

Dauer, A., Hensel, A., Lhoste, E., Knasmuller, S. i Mersch-Sundermann, V. (2003). Genotoxic and antigenotoxic effects of catechin and tannins from the bark of Hamamelis virginiana L. in metabolically competent, human hepatoma cells (Hep G2) using single cell gel electrophoresis. *Phytochemistry* 63(2): 199-207.

Davis, C.D. i Milner, J.A. (2009). Gastrointestinal microflora, food components and colon cancer prevention. *J Nutr Biochem* 20(10): 743-52.

DeBerardinis, R.J., Mancuso, A., Daikhin, E., Nissim, I., Yudkoff, M., Wehrli, S. i Thompson, C.B. (2007). Beyond aerobic glycolysis: transformed cells can engage in glutamine metabolism that exceeds the requirement for protein and nucleotide synthesis. *Proc Natl Acad Sci U S A* 104(49): 19345-50.

Deshpande, A., Sicinski, P. i Hinds, P.W. (2005). Cyclins and cdks in development and cancer: a perspective. *Oncogene* 24(17): 2909-15.

Duhon, D., Bigelow, R.L., Coleman, D.T., Steffan, J.J., Yu, C., Langston, W., Kevil, C.G. i Cardelli, J.A. (2010). The polyphenol epigallocatechin-3-gallate affects lipid rafts to block activation of the c-Met receptor in prostate cancer cells. *Mol Carcinog* 49(8): 739-49.

Dzubak, P., Hajduch, M., Vydra, D., Hustova, A., Kvasnica, M., Biedermann, D., Markova, L., Urban, M. i Sarek, J. (2006). Pharmacological activities of natural triterpenoids and their therapeutic implications. *Nat Prod Rep* 23(3): 394-411.

Engelbrecht, A.M., Mattheyse, M., Ellis, B., Loos, B., Thomas, M., Smith, R., Peters, S., Smith, C. i Myburgh, K. (2007). Proanthocyanidin from grape seeds inactivates the PI3-kinase/PKB pathway and induces apoptosis in a colon cancer cell line. *Cancer Lett* 258(1): 144-53.

Fantin, V.R., St-Pierre, J. i Leder, P. (2006). Attenuation of LDH-A expression uncovers a link between glycolysis, mitochondrial physiology, and tumor maintenance. *Cancer Cell* 9(6): 425-34.

Fearon, E.R. i Vogelstein, B. (1990). A genetic model for colorectal tumorigenesis. *Cell* 61(5): 759-67.

Fernandez-Navarro, M., Peragon, J., Amores, V., De La Higuera, M. i Lupianez, J.A. (2008). Maslinic acid added to the diet increases growth and protein-turnover rates in the white muscle of rainbow trout (Oncorhynchus mykiss). *Comp Biochem Physiol C Toxicol Pharmacol* 147(2): 158-67.

Fiehn, O. (2002). Metabolomics--the link between genotypes and phenotypes. *Plant Mol Biol* 48(1-2): 155-71.

Fini, L., Piazzi, G., Daoud, Y., Selgrad, M., Maegawa, S., Garcia, M., Fogliano, V., Romano, M., Graziani, G., Vitaglione, P., Carmack, S.W., Gasbarrini, A., Genta, R.M., Issa, J.P., Boland, C.R. i Ricciardiello, L. (2011). Chemoprevention of intestinal polyps in ApcMin/+ mice fed with western or balanced diets by drinking annurca apple polyphenol extract. *Cancer Prev Res (Phila)* 4(6): 907-15.

Forester, S.C. i Lambert, J.D. (2011). The role of antioxidant versus pro-oxidant effects of green tea polyphenols in cancer prevention. *Mol Nutr Food Res* 55(6): 844-54.

Forte, A., De Sanctis, R., Leonetti, G., Manfredelli, S., Urbano, V. i Bezzi, M. (2008). Dietary chemoprevention of colorectal cancer. *Ann Ital Chir* 79(4): 261-7.

Foulds, L. (1954). The experimental study of tumor progression: a review. *Cancer Res* 14(5): 327-39.

Galati, G. i O'Brien, P.J. (2004). Potential toxicity of flavonoids and other dietary phenolics: significance for their chemopreventive and anticancer properties. *Free Radic Biol Med* 37(3): 287-303.

Gao, P., Tchernyshyov, I., Chang, T.C., Lee, Y.S., Kita, K., Ochi, T., Zeller, K.I., De Marzo, A.M., Van Eyk, J.E., Mendell, J.T. i Dang, C.V. (2009). c-Myc suppression of miR-23a/b enhances mitochondrial glutaminase expression and glutamine metabolism. *Nature* 458(7239): 762-5.

Gatalica, Z. i Torlakovic, E. (2008). Pathology of the hereditary colorectal carcinoma. *Fam Cancer* 7(1): 15-26.

Ghavami, S., Hashemi, M., Ande, S.R., Yeganeh, B., Xiao, W., Eshraghi, M., Bus, C.J., Kadkhoda, K., Wiechec, E., Halayko, A.J. i Los, M. (2009). Apoptosis and cancer: mutations within caspase genes. *J Med Genet* 46(8): 497-510.

Ghosh, S., Matsuoka, Y., Asai, Y., Hsin, K.Y. i Kitano, H. (2011). Software for systems biology: from tools to integrated platforms. *Nat Rev Genet* 12(12): 821-32.

Gillies, R.J., Robey, I. i Gatenby, R.A. (2008). Causes and consequences of increased glucose metabolism of cancers. *J Nucl Med* 49 Suppl 2: 24S-42S.

Govardhan, K.S., Ramyasri, K., Kethora, D., Ravishekar, Y. i Prasenjit, M. (2011). Harnessing impaired energy metabolism in cancer cell: small molecule- mediated ways to regulate tumorigenesis. *Anticancer Agents Med Chem* 11(3): 272-9.

Grivennikov, S.I., Greten, F.R. i Karin, M. (2010a). Immunity, inflammation, and cancer. *Cell* 140(6): 883-99.

Grivennikov, S.I. i Karin, M. (2010b). Inflammation and oncogenesis: a vicious connection. *Curr Opin Genet Dev* 20(1): 65-71.

Guan, T., Qian, Y., Tang, X., Huang, M., Huang, L., Li, Y. i Sun, H. (2011). Maslinic acid, a natural inhibitor of glycogen phosphorylase, reduces cerebral ischemic injury in hyperglycemic rats by GLT-1 up-regulation. *J Neurosci Res* 89(11): 1829-39.

Gulhati, P., Zaytseva, Y.Y., Valentino, J.D., Stevens, P.D., Kim, J.T., Sasazuki, T., Shirasawa, S., Lee, E.Y., Weiss, H.L., Dong, J., Gao, T. i Evers, B.M. (2012). Sorafenib Enhances the Therapeutic Efficacy of Rapamycin in Colorectal Cancers Harboring Oncogenic Kras and Pik3ca. *Carcinogenesis*.

Habtemariam, S. (2002). Hamamelitannin from Hamamelis virginiana inhibits the tumour necrosis factor-alpha (TNF)-induced endothelial cell death in vitro. *Toxicon* 40(1): 83-8.

Hagedorn, M., Zilberberg, L., Lozano, R.M., Cuevas, P., Canron, X., Redondo-Horcajo, M., Gimenez-Gallego, G. i Bikfalvi, A. (2001). A short peptide domain of platelet factor 4 blocks angiogenic key events induced by FGF-2. *Faseb J* 15(3): 550-2.

Hahn, W.C. i Weinberg, R.A. (2002). Rules for making human tumor cells. *N Engl J Med* 347(20): 1593-603.

Halestrap, A.P. (2012). The monocarboxylate transporter family--Structure and functional characterization. *IUBMB Life* 64(1): 1-9.

Halliwell, B. (2008). Are polyphenols antioxidants or pro-oxidants? What do we learn from cell culture and in vivo studies? *Arch Biochem Biophys* 476(2): 107-12.

Hanahan, D. i Weinberg, R.A. (2000). The hallmarks of cancer. *Cell* 100(1): 57-70.

Hanahan, D. i Weinberg, R.A. (2011). Hallmarks of cancer: the next generation. *Cell* 144(5): 646-74.

Hartisch, C., Kolodziej, H. i von Bruchhausen, F. (1997). Dual inhibitory activities of tannins from Hamamelis virginiana and related polyphenols on 5-lipoxygenase and lyso-PAF: acetyl-CoA acetyltransferase. *Planta Med* 63(2): 106-10.

Ho, L.L., Chen, W.J., Lin-Shiau, S.Y. i Lin, J.K. (2002). Penta-O-galloyl-beta-D-glucose inhibits the invasion of mouse melanoma by suppressing metalloproteinase-9 through down-regulation of activator protein-1. *Eur J Pharmacol* 453(2-3): 149-58.

Hsu, C.P., Lin, Y.H., Chou, C.C., Zhou, S.P., Hsu, Y.C., Liu, C.L., Ku, F.M. i Chung, Y.C. (2009). Mechanisms of grape seed procyanidin-induced apoptosis in colorectal carcinoma cells. *Anticancer Res* 29(1): 283-9.

Hsum, Y.W., Yew, W.T., Hong, P.L., Soo, K.K., Hoon, L.S., Chieng, Y.C. i Mooi, L.Y. (2011). Cancer Chemopreventive Activity of Maslinic Acid: Suppression of COX-2 Expression and Inhibition of NF-kappaB and AP-1 Activation in Raji Cells. *Planta Med.*

Hu, S., Dong, T.S., Dalal, S.R., Wu, F., Bissonnette, M., Kwon, J.H. i Chang, E.B. (2011). The microbe-derived short chain fatty acid butyrate targets miRNA-dependent p21 gene expression in human colon cancer. *PLoS One* 6(1): e16221.

Huang, L., Guan, T., Qian, Y., Huang, M., Tang, X., Li, Y. i Sun, H. (2011). Anti-inflammatory effects of maslinic acid, a natural triterpene, in cultured cortical astrocytes via suppression of nuclear factor-kappa B. *Eur J Pharmacol* 672(1-3): 169-74.

Huh, J.E., Lee, E.O., Kim, M.S., Kang, K.S., Kim, C.H., Cha, B.C., Surh, Y.J. i Kim, S.H. (2005). Penta-O-galloyl-beta-D-glucose suppresses tumor growth via inhibition of angiogenesis and stimulation of apoptosis: roles of cyclooxygenase-2 and mitogen-activated protein kinase pathways. *Carcinogenesis* 26(8): 1436-45.

Humphreys, K.J., Cobiac, L., Le Leu, R.K., Van der Hoek, M.B. i Michael, M.Z. (2012). Histone deacetylase inhibition in colorectal cancer cells reveals competing roles for members of the oncogenic miR-17-92 cluster. *Mol Carcinog*.

Ingolfsson, H.I., Koeppe, R.E., 2nd i Andersen, O.S. (2011). Effects of green tea catechins on gramicidin channel function and inferred changes in bilayer properties. *FEBS Lett* 585(19): 3101-5.

Iwuchukwu, O.F. i Nagar, S. (2008). Resveratrol (trans-resveratrol, 3,5,4'-trihydroxy-trans-stilbene) glucuronidation exhibits atypical enzyme kinetics in various protein sources. *Drug Metab Dispos* 36(2): 322-30.

Jemal, A., Center, M.M., DeSantis, C. i Ward, E.M. (2010). Global patterns of cancer incidence and mortality rates and trends. *Cancer Epidemiol Biomarkers Prev* 19(8): 1893-907.

Jozwiak, P. i Lipinska, A. (2012). The role of glucose transporter 1 (GLUT1) in the diagnosis and therapy of tumors. *Postepy Hig Med Dosw (Online)* 66: 165-74.

Juskiewicz, J., Milala, J., Jurgonski, A., Krol, B. i Zdunczyk, Z. (2011). Consumption of polyphenol concentrate with dietary fructo-oligosaccharides enhances cecal metabolism of quercetin glycosides in rats. *Nutrition* 27(3): 351-7.

Juskiewicz, J., Zary-Sikorska, E., Zdunczyk, Z., Krol, B., Jaroslawska, J. i Jurgonski, A. (2012). Effect of dietary supplementation with unprocessed and ethanol-extracted apple pomaces on caecal fermentation, antioxidant and blood biomarkers in rats. *Br J Nutr* 107(8): 1138-46.

Kamarajugadda, S., Stemboroski, L., Cai, Q., Simpson, N.E., Nayak, S., Tan, M. i Lu, J. (2012). Glucose Oxidation Modulates Anoikis and Tumor Metastasis. *Mol Cell Biol*.

Kamath, K.S., Vasavada, M.S. i Srivastava, S. (2011). Proteomic databases and tools to decipher post-translational modifications. *J Proteomics* 75(1): 127-44.

Kanwar, J., Taskeen, M., Mohammad, I., Huo, C., Chan, T.H. i Dou, Q.P. (2012). Recent advances on tea polyphenols. *Front Biosci (Elite Ed)* 4: 111-31.

Katiyar, S.K. (2007). UV-induced immune suppression and photocarcinogenesis: chemoprevention by dietary botanical agents. *Cancer Lett* 255(1): 1-11.

Kaur, M., Singh, R.P., Gu, M., Agarwal, R. i Agarwal, C. (2006). Grape seed extract inhibits in vitro and in vivo growth of human colorectal carcinoma cells. *Clin Cancer Res* 12(20 Pt 1): 6194-202.

Kaur, M., Tyagi, A., Singh, R.P., Sclafani, R.A., Agarwal, R. i Agarwal, C. (2011). Grape seed extract upregulates p21 (Cip1) through redox-mediated activation of ERK1/2 and posttranscriptional regulation leading to cell cycle arrest in colon carcinoma HT29 cells. *Mol Carcinog*.

Kosmala, M., Kolodziejczyk, K., Zdunczyk, Z., Juskiewicz, J. i Boros, D. (2011). Chemical composition of natural and polyphenol-free apple pomace and the effect of this dietary ingredient on intestinal fermentation and serum lipid parameters in rats. *J Agric Food Chem* 59(17): 9177-85.

Kroemer, G. i Pouyssegur, J. (2008). Tumor cell metabolism: cancer's Achilles' heel. *Cancer Cell* 13(6): 472-82.

Kuo, P.T., Lin, T.P., Liu, L.C., Huang, C.H., Lin, J.K., Kao, J.Y. i Way, T.D. (2009). Penta-O-galloyl-beta-D-glucose suppresses prostate cancer bone metastasis by transcriptionally repressing EGF-induced MMP-9 expression. *J Agric Food Chem* 57(8): 3331-9.

Lee, W.N., Guo, P., Lim, S., Bassilian, S., Lee, S.T., Boren, J., Cascante, M., Go, V.L. i Boros, L.G. (2004). Metabolic sensitivity of pancreatic tumour cell apoptosis to glycogen phosphorylase inhibitor treatment. *Br J Cancer* 91(12): 2094-100.

Li, C., Allen, A., Kwagh, J., Doliba, N.M., Qin, W., Najafi, H., Collins, H.W., Matschinsky, F.M., Stanley, C.A. i Smith, T.J. (2006). Green tea polyphenols modulate insulin secretion by inhibiting glutamate dehydrogenase. *J Biol Chem* 281(15): 10214-21.

Li, C., Yang, Z., Zhai, C., Qiu, W., Li, D., Yi, Z., Wang, L., Tang, J., Qian, M., Luo, J. i Liu, M. (2010). Maslinic acid potentiates the anti-tumor activity of tumor necrosis factor alpha by inhibiting NF-kappaB signaling pathway. *Mol Cancer* 9: 73.

Li, F.Y. i Lai, M.D. (2009). Colorectal cancer, one entity or three. *J Zhejiang Univ Sci B* 10(3): 219-29.

Lin, C.C., Huang, C.Y., Mong, M.C., Chan, C.Y. i Yin, M.C. (2011). Antiangiogenic potential of three triterpenic acids in human liver cancer cells. *J Agric Food Chem* 59(2): 755-62.

Lizárraga, D., Lozano, C., Briede, J.J., van Delft, J.H., Touriño, S., Centelles, J.J., Torres, J.L. i Cascante, M. (2007). The importance of polymerization and galloylation for the antiproliferative properties of procyanidin-rich natural extracts. *Febs J* 274(18): 4802-11.

Lizárraga, D., Touriño, S., Reyes-Zurita, F.J., de Kok, T.M., van Delft, J.H., Maas, L.M., Briede, J.J., Centelles, J.J., Torres, J.L. i Cascante, M. (2008). Witch hazel (Hamamelis virginiana) fractions and the importance of gallate moieties--electron transfer capacities in their antitumoral properties. *J Agric Food Chem* 56(24): 11675-82.

Lizárraga, D., Vinardell, M.P., Noe, V., van Delft, J.H., Alcarraz-Vizan, G., van Breda, S.G., Staal, Y., Gunther, U.L., Reed, M.A., Ciudad, C.J., Torres, J.L. i Cascante, M. (2011). A Lyophilized Red Grape Pomace Containing Proanthocyanidin-Rich Dietary Fiber Induces Genetic and Metabolic Alterations in Colon Mucosa of Female C57BL/6J Mice. *J Nutr*.

Lopez-Oliva, M.E., Agis-Torres, A., Goni, I. i Munoz-Martinez, E. (2010). Grape antioxidant dietary fibre reduced apoptosis and induced a pro-reducing shift in the glutathione redox state of the rat proximal colonic mucosa. *Br J Nutr* 103(8): 1110-7.

Lunt, S.Y. i Vander Heiden, M.G. (2011). Aerobic glycolysis: meeting the metabolic requirements of cell proliferation. *Annu Rev Cell Dev Biol* 27: 441-64.

MacKenzie, S.H., Schipper, J.L. i Clark, A.C. (2010). The potential for caspases in drug discovery. *Curr Opin Drug Discov Devel* 13(5): 568-76.

Marin, S., Chiang, K., Bassilian, S., Lee, W.N., Boros, L.G., Fernandez-Novell, J.M., Centelles, J.J., Medrano, A., Rodriguez-Gil, J.E. i Cascante, M. (2003). Metabolic strategy of boar spermatozoa revealed by a metabolomic characterization. *FEBS Lett* 554(3): 342-6.

Marquez-Martin, A., De La Puerta, R., Fernandez-Arche, A., Ruiz-Gutierrez, V. i Yaqoob, P. (2006). Modulation of cytokine secretion by pentacyclic triterpenes from olive pomace oil in human mononuclear cells. *Cytokine* 36(5-6): 211-7.

Mashima, T., Seimiya, H. i Tsuruo, T. (2009). De novo fatty-acid synthesis and related pathways as molecular targets for cancer therapy. *Br J Cancer* 100(9): 1369-72.

Mathupala, S.P., Ko, Y.H. i Pedersen, P.L. (2010). The pivotal roles of mitochondria in cancer: Warburg and beyond and encouraging prospects for effective therapies. *Biochim Biophys Acta* 1797(6-7): 1225-30.

McCart, A.E., Vickaryous, N.K. i Silver, A. (2008). Apc mice: models, modifiers and mutants. *Pathol Res Pract* 204(7): 479-90.

Medema, J.P. i Vermeulen, L. (2011). Microenvironmental regulation of stem cells in intestinal homeostasis and cancer. *Nature* 474(7351): 318-26.

Mendler, A.N., Hu, B., Prinz, P.U., Kreutz, M., Gottfried, E. i Noessner, E. (2011). Tumor lactic acidosis suppresses CTL function by inhibition of p38 and JNK/c-Jun activation. *Int J Cancer*.

Menendez, J.A. (2010). Fine-tuning the lipogenic/lipolytic balance to optimize the metabolic requirements of cancer cell growth: molecular mechanisms and therapeutic perspectives. *Biochim Biophys Acta* 1801(3): 381-91.

Meng, M., Chen, S., Lao, T., Liang, D. i Sang, N. (2010). Nitrogen anabolism underlies the importance of glutaminolysis in proliferating cells. *Cell Cycle* 9(19): 3921-32.

Misikangas, M., Pajari, A.M., Paivarinta, E., Oikarinen, S.I., Rajakangas, J., Marttinen, M., Tanayama, H., Torronen, R. i Mutanen, M. (2007). Three Nordic berries inhibit intestinal tumorigenesis in multiple intestinal neoplasia/+ mice by modulating beta-catenin signaling in the tumor and transcription in the mucosa. *J Nutr* 137(10): 2285-90.

Miyamoto, K., Kishi, N., Koshiura, R., Yoshida, T., Hatano, T. i Okuda, T. (1987). Relationship between the structures and the antitumor activities of tannins. *Chem Pharm Bull (Tokyo)* 35(2): 814-22.

Moneriz, C., Marin-Garcia, P., Garcia-Granados, A., Bautista, J.M., Diez, A. i Puyet, A. (2011). Parasitostatic effect of maslinic acid. I. Growth arrest of Plasmodium falciparum intraerythrocytic stages. *Malar J* 10: 82.

Mutanen, M., Pajari, A.M. i Oikarinen, S.I. (2000). Beef induces and rye bran prevents the formation of intestinal polyps in Apc(Min) mice: relation to beta-catenin and PKC isozymes. *Carcinogenesis* 21(6): 1167-73.

Mutanen, M., Pajari, A.M., Paivarinta, E., Misikangas, M., Rajakangas, J., Marttinen, M. i Oikarinen, S. (2008). Berries as chemopreventive dietary constituents--a mechanistic approach with the ApcMin/+ mouse. *Asia Pac J Clin Nutr* 17 Suppl 1: 123-5.

Nair, S., Hebbar, V., Shen, G., Gopalakrishnan, A., Khor, T.O., Yu, S., Xu, C. i Kong, A.N. (2008). Synergistic effects of a combination of dietary factors sulforaphane and (-) epigallocatechin-3-gallate in HT-29 AP-1 human colon carcinoma cells. *Pharm Res* 25(2): 387-99.

Nakamura, K., Abu Lila, A.S., Matsunaga, M., Doi, Y., Ishida, T. i Kiwada, H. (2011). A double-modulation strategy in cancer treatment with a chemotherapeutic agent and siRNA. *Mol Ther* 19(11): 2040-7.

Negrini, S., Gorgoulis, V.G. i Halazonetis, T.D. (2010). Genomic instability--an evolving hallmark of cancer. *Nat Rev Mol Cell Biol* 11(3): 220-8.

Nowel, M.S. i Chapman, G.B. (1976). The ultrastructure of implanted trophoblast cells of the yellow agouti mouse. *J Anat* 122(Pt 1): 177-88.

Ogino, S., Chan, A.T., Fuchs, C.S. i Giovannucci, E. (2011). Molecular pathological epidemiology of colorectal neoplasia: an emerging transdisciplinary and interdisciplinary field. *Gut* 60(3): 397-411.

Oh, G.S., Pae, H.O., Oh, H., Hong, S.G., Kim, I.K., Chai, K.Y., Yun, Y.G., Kwon, T.O. i Chung, H.T. (2001). In vitro anti-proliferative effect of 1,2,3,4,6-penta-O-galloyl-beta-D-glucose on human hepatocellular carcinoma cell line, SK-HEP-1 cells. *Cancer Lett* 174(1): 17-24.

Ohtani, N., Takahashi, A., Mann, D.J. i Hara, E. (2012). Cellular senescence: a double-edged sword in the fight against cancer. *Exp Dermatol* 21 Suppl 1: 1-4.

Oliver, S.G., Winson, M.K., Kell, D.B. i Baganz, F. (1998). Systematic functional analysis of the yeast genome. *Trends Biotechnol* 16(9): 373-8.

Ortega, A.D., Sanchez-Arago, M., Giner-Sanchez, D., Sanchez-Cenizo, L., Willers, I. i Cuezva, J.M. (2009). Glucose avidity of carcinomas. *Cancer Lett* 276(2): 125-35.

Ozhan, M., Yilmaz, S., Aliyev, A., Varoglu, E., Halac, M. i Kantarci, F. (2012). Acute respiratory distress syndrome suggested by (18)F-FDG PET/CT. *Hell J Nucl Med* 15(1): 72-3.

Paez-Ribes, M., Allen, E., Hudock, J., Takeda, T., Okuyama, H., Vinals, F., Inoue, M., Bergers, G., Hanahan, D. i Casanovas, O. (2009). Antiangiogenic therapy elicits malignant progression of tumors to increased local invasion and distant metastasis. *Cancer Cell* 15(3): 220-31.

Parra, A., Rivas, F., Martin-Fonseca, S., Garcia-Granados, A. i Martinez, A. (2011). Maslinic acid derivatives induce significant apoptosis in b16f10 murine melanoma cells. *Eur J Med Chem* 46(12): 5991-6001.

Patra, S.K., Rizzi, F., Silva, A., Rugina, D.O. i Bettuzzi, S. (2008). Molecular targets of (-)-epigallocatechin-3-gallate (EGCG): specificity and interaction with membrane lipid rafts. *J Physiol Pharmacol* 59 Suppl 9: 217-35.

Phelps, R.A., Chidester, S., Dehghanizadeh, S., Phelps, J., Sandoval, I.T., Rai, K., Broadbent, T., Sarkar, S., Burt, R.W. i Jones, D.A. (2009). A two-step model for colon adenoma initiation and progression caused by APC loss. *Cell* 137(4): 623-34.

Porat, Y., Abramowitz, A. i Gazit, E. (2006). Inhibition of amyloid fibril formation by polyphenols: structural similarity and aromatic interactions as a common inhibition mechanism. *Chem Biol Drug Des* 67(1): 27-37.

Poznic, M. (2009). Retinoblastoma protein: a central processing unit. *J Biosci* 34(2): 305-12.

Ramos-Montoya, A., Lee, W.N., Bassilian, S., Lim, S., Trebukhina, R.V., Kazhyna, M.V., Ciudad, C.J., Noe, V., Centelles, J.J. i Cascante, M. (2006). Pentose phosphate cycle oxidative and nonoxidative balance: A new vulnerable target for overcoming drug resistance in cancer. *Int J Cancer* 119(12): 2733-41.

Ravindranath, M.H., Saravanan, T.S., Monteclaro, C.C., Presser, N., Ye, X., Selvan, S.R. i Brosman, S. (2006). Epicatechins Purified from Green Tea (Camellia sinensis) Differentially Suppress Growth of Gender-Dependent Human Cancer Cell Lines. *Evid Based Complement Alternat Med* 3(2): 237-47.

Raza, H. i John, A. (2005). Green tea polyphenol epigallocatechin-3-gallate differentially modulates oxidative stress in PC12 cell compartments. *Toxicol Appl Pharmacol* 207(3): 212-20.

Reyes-Zurita, F.J., Pachon-Pena, G., Lizárraga, D., Rufino-Palomares, E.E., Cascante, M. i Lupianez, J.A. (2011). The natural triterpene maslinic acid induces apoptosis in HT29 colon cancer cells by a JNK-p53-dependent mechanism. *BMC Cancer* 11: 154.

Reyes-Zurita, F.J., Rufino-Palomares, E.E., Lupianez, J.A. i Cascante, M. (2009). Maslinic acid, a natural triterpene from Olea europaea L., induces apoptosis in HT29 human colon-cancer cells via the mitochondrial apoptotic pathway. *Cancer Lett* 273(1): 44-54.

Reyes, F.J., Centelles, J.J., Lupianez, J.A. i Cascante, M. (2006). (2Alpha,3beta)-2,3-dihydroxyolean-12-en-28-oic acid, a new natural triterpene from Olea europea, induces caspase dependent apoptosis selectively in colon adenocarcinoma cells. *FEBS Lett* 580(27): 6302-10.

Roberts, P.J., Bisi, J.E., Strum, J.C., Combest, A.J., Darr, D.B., Usary, J.E., Zamboni, W.C., Wong, K.K., Perou, C.M. i Sharpless, N.E. (2012). Multiple roles of cyclin-dependent kinase 4/6 inhibitors in cancer therapy. *J Natl Cancer Inst* 104(6): 476-87.

Rustgi, A.K. (2007). The genetics of hereditary colon cancer. *Genes Dev* 21(20): 2525-38.

Saksena, S., Theegala, S., Bansal, N., Gill, R.K., Tyagi, S., Alrefai, W.A., Ramaswamy, K. i Dudeja, P.K. (2009). Mechanisms underlying modulation of monocarboxylate transporter 1 (MCT1) by somatostatin in human intestinal epithelial cells. *Am J Physiol Gastrointest Liver Physiol* 297(5): G878-85.

Saleh, M. i Trinchieri, G. (2011). Innate immune mechanisms of colitis and colitis-associated colorectal cancer. *Nat Rev Immunol* 11(1): 9-20.

Samudio, I., Fiegl, M. i Andreeff, M. (2009). Mitochondrial uncoupling and the Warburg effect: molecular basis for the reprogramming of cancer cell metabolism. *Cancer Res* 69(6): 2163-6.

Samudio, I., Harmancey, R., Fiegl, M., Kantarjian, H., Konopleva, M., Korchin, B., Kaluarachchi, K., Bornmann, W., Duvvuri, S., Taegtmeyer, H. i Andreeff, M. (2010). Pharmacologic inhibition of fatty acid oxidation sensitizes human leukemia cells to apoptosis induction. *J Clin Invest* 120(1): 142-56.

Sandulache, V.C., Ow, T.J., Pickering, C.R., Frederick, M.J., Zhou, G., Fokt, I., Davis-Malesevich, M., Priebe, W. i Myers, J.N. (2011). Glucose, not glutamine, is the dominant energy source required for proliferation and survival of head and neck squamous carcinoma cells. *Cancer* 117(13): 2926-38.

Sato, S. i Itamochi, H. (2012). Bevacizumab and ovarian cancer. *Curr Opin Obstet Gynecol* 24(1): 8-13.

Senanayake, T.H., Warren, G. i Vinogradov, S.V. (2011). Novel anticancer polymeric conjugates of activated nucleoside analogues. *Bioconjug Chem* 22(10): 1983-93.

Shay, J.W., Reddel, R.R. i Wright, W.E. (2012). Cancer. Cancer and telomeres--an ALTernative to telomerase. *Science* 336(6087): 1388-90.

Shen, G., Khor, T.O., Hu, R., Yu, S., Nair, S., Ho, C.T., Reddy, B.S., Huang, M.T., Newmark, H.L. i Kong, A.N. (2007). Chemoprevention of familial adenomatous polyposis by natural dietary compounds sulforaphane and dibenzoylmethane alone and in combination in ApcMin/+ mouse. *Cancer Res* 67(20): 9937-44.

Shen, W.J., Dai, D.Q., Teng, Y. i Liu, J. (2008). [Effects of sodium butyrate on proliferation of human gastric cancer cells and expression of p16 gene]. *Zhonghua Yi Xue Za Zhi* 88(17): 1192-6.

Shi, Q., Le, X., Wang, B., Abbruzzese, J.L., Xiong, Q., He, Y. i Xie, K. (2001). Regulation of vascular endothelial growth factor expression by acidosis in human cancer cells. *Oncogene* 20(28): 3751-6.

Shojaei, F. (2012). Anti-angiogenesis therapy in cancer: current challenges and future perspectives. *Cancer Lett* 320(2): 130-7.

Siddiqui, I.A., Malik, A., Adhami, V.M., Asim, M., Hafeez, B.B., Sarfaraz, S. i Mukhtar, H. (2008). Green tea polyphenol EGCG sensitizes human prostate carcinoma LNCaP cells to TRAIL-mediated apoptosis and synergistically inhibits biomarkers associated with angiogenesis and metastasis. *Oncogene* 27(14): 2055-63.

Singh, B.N., Shankar, S. i Srivastava, R.K. (2011). Green tea catechin, epigallocatechin-3-gallate (EGCG): Mechanisms, perspectives and clinical applications. *Biochem Pharmacol*.

Sobie, E.A., Lee, Y.S., Jenkins, S.L. i Iyengar, R. (2011). Systems biology--biomedical modeling. *Sci Signal* 4(190): tr2.

Sottnik, J.L., Lori, J.C., Rose, B.J. i Thamm, D.H. (2011). Glycolysis inhibition by 2-deoxy-D-glucose reverts the metastatic phenotype in vitro and in vivo. *Clin Exp Metastasis* 28(8): 865-75.

Sultana, N. i Lee, N.H. (2007). Antielastase and free radical scavenging activities of compounds from the stems of Cornus kousa. *Phytother Res* 21(12): 1171-6.

Sun, C., Rosendahl, A.H., Ansari, D. i Andersson, R. (2011a). Proteome-based biomarkers in pancreatic cancer. *World J Gastroenterol* 17(44): 4845-52.

Sun, R.C., Board, P.G. i Blackburn, A.C. (2011b). Targeting metabolism with arsenic trioxide and dichloroacetate in breast cancer cells. *Mol Cancer* 10: 142.

Swinnen, J.V., Brusselmans, K. i Verhoeven, G. (2006). Increased lipogenesis in cancer cells: new players, novel targets. *Curr Opin Clin Nutr Metab Care* 9(4): 358-65.

Tessitore, L., Davit, A., Sarotto, I. i Caderni, G. (2000). Resveratrol depresses the growth of colorectal aberrant crypt foci by affecting bax and p21(CIP) expression. *Carcinogenesis* 21(8): 1619-22.

Tian, B., Sun, Z., Xu, Z. i Hua, Y. (2007). Chemiluminescence analysis of the prooxidant and antioxidant effects of epigallocatechin-3-gallate. *Asia Pac J Clin Nutr* 16 Suppl 1: 153-7.

Tong, X., Zhao, F. i Thompson, C.B. (2009). The molecular determinants of de novo nucleotide biosynthesis in cancer cells. *Curr Opin Genet Dev* 19(1): 32-7.

Touriño, S., Lizárraga, D., Carreras, A., Lorenzo, S., Ugartondo, V., Mitjans, M., Vinardell, M.P., Julia, L., Cascante, M. i Torres, J.L. (2008). Highly galloylated tannin fractions from witch hazel (Hamamelis virginiana) bark: electron transfer capacity, in vitro antioxidant activity, and effects on skin-related cells. *Chem Res Toxicol* 21(3): 696-704.

Touriño, S., Perez-Jimenez, J., Mateos-Martin, M.L., Fuguet, E., Vinardell, M.P., Cascante, M. i Torres, J.L. (2011). Metabolites in Contact with the Rat Digestive Tract after Ingestion of a Phenolic-Rich Dietary Fiber Matrix. *J Agric Food Chem*.

Trzeciakiewicz, A., Habauzit, V. i Horcajada, M.N. (2009). When nutrition interacts with osteoblast function: molecular mechanisms of polyphenols. *Nutr Res Rev* 22(1): 68-81.

Vaiopoulos, A.G., Papachroni, K.K. i Papavassiliou, A.G. (2010). Colon carcinogenesis: Learning from NF-kappaB and AP-1. *Int J Biochem Cell Biol* 42(7): 1061-5.

Valet, G. (2005). Cytomics: an entry to biomedical cell systems biology. *Cytometry A* 63(2): 67-8.

Veldhoen, R.A., Banman, S.L., Hemmerling, D.R., Odsen, R., Simmen, T., Simmonds, A.J., Underhill, D.A. i Goping, I.S. (2012). The chemotherapeutic agent paclitaxel inhibits autophagy through two distinct mechanisms that regulate apoptosis. *Oncogene*.

Velmurugan, B., Singh, R.P., Agarwal, R. i Agarwal, C. (2010a). Dietary-feeding of grape seed extract prevents azoxymethane-induced colonic aberrant crypt foci formation in fischer 344 rats. *Mol Carcinog* 49(7): 641-52.

Velmurugan, B., Singh, R.P., Kaul, N., Agarwal, R. i Agarwal, C. (2010b). Dietary feeding of grape seed extract prevents intestinal tumorigenesis in APCmin/+ mice. *Neoplasia* 12(1): 95-102.

Vennat, B., Pourrat, H., Pouget, M.P., Gross, D. i Pourrat, A. (1988). Tannins from Hamamelis virginiana: Identification of Proanthocyanidins and Hamamelitannin Quantification in Leaf, Bark, and Stem Extracts. *Planta Med* 54(5): 454-7.

Verschoyle, R.D., Greaves, P., Cai, H., Edwards, R.E., Steward, W.P. i Gescher, A.J. (2007). Evaluation of the cancer chemopreventive efficacy of rice bran in genetic mouse models of breast, prostate and intestinal carcinogenesis. *Br J Cancer* 96(2): 248-54.

Vizan, P., Alcarraz-Vizan, G., Diaz-Moralli, S., Rodriguez-Prados, J.C., Zanuy, M., Centelles, J.J., Jauregui, O. i Cascante, M. (2007). Quantification of intracellular phosphorylated carbohydrates in HT29 human colon adenocarcinoma cell line using liquid chromatography-electrospray ionization tandem mass spectrometry. *Anal Chem* 79(13): 5000-5.

Vizan, P., Alcarraz-Vizan, G., Diaz-Moralli, S., Solovjeva, O.N., Frederiks, W.M. i Cascante, M. (2009a). Modulation of pentose phosphate pathway during cell cycle progression in human colon adenocarcinoma cell line HT29. *Int J Cancer* 124(12): 2789-96.

Vizán, P., Mazurek, S. i Cascante, M. (2008). Robust metabolic adaptation underlying tumor progression. *Metabolomics* 4(1): 1-12.

Vizan, P., Sanchez-Tena, S., Alcarraz-Vizan, G., Soler, M., Messeguer, R., Pujol, M.D., Paul Lee, W.N. i Cascante, M. (2009b). Characterization of the metabolic changes underlying growth factor angiogenic activation: identification of new potential therapeutic targets. *Carcinogenesis*.

Waldecker, M., Kautenburger, T., Daumann, H., Veeriah, S., Will, F., Dietrich, H., Pool-Zobel, B.L. i Schrenk, D. (2008). Histone-deacetylase inhibition and butyrate formation: Fecal slurry incubations with apple pectin and apple juice extracts. *Nutrition* 24(4): 366-74.

Walenta, S. i Mueller-Klieser, W.F. (2004). Lactate: mirror and motor of tumor malignancy. *Semin Radiat Oncol* 14(3): 267-74.

Wang, X., Spandidos, A., Wang, H. i Seed, B. (2012). PrimerBank: a PCR primer database for quantitative gene expression analysis, 2012 update. *Nucleic Acids Res* 40(Database issue): D1144-9.

Weinberg, F., Hamanaka, R., Wheaton, W.W., Weinberg, S., Joseph, J., Lopez, M., Kalyanaraman, B., Mutlu, G.M., Budinger, G.R. i Chandel, N.S. (2010). Mitochondrial metabolism and ROS generation are essential for Kras-mediated tumorigenicity. *Proc Natl Acad Sci U S A* 107(19): 8788-93.

White, E. i DiPaola, R.S. (2009). The double-edged sword of autophagy modulation in cancer. *Clin Cancer Res* 15(17): 5308-16.

Wise, D.R., DeBerardinis, R.J., Mancuso, A., Sayed, N., Zhang, X.Y., Pfeiffer, H.K., Nissim, I., Daikhin, E., Yudkoff, M., McMahon, S.B. i Thompson, C.B. (2008). Myc regulates a transcriptional program that stimulates mitochondrial glutaminolysis and leads to glutamine addiction. *Proc Natl Acad Sci U S A* 105(48): 18782-7.

Wong, J.J., Hawkins, N.J. i Ward, R.L. (2007). Colorectal cancer: a model for epigenetic tumorigenesis. *Gut* 56(1): 140-8.

Xu, H.X., Zeng, F.Q., Wan, M. i Sim, K.Y. (1996). Anti-HIV triterpene acids from Geum japonicum. *J Nat Prod* 59(7): 643-5.

Yang, C.S., Lambert, J.D. i Sang, S. (2009). Antioxidative and anti-carcinogenic activities of tea polyphenols. *Arch Toxicol* 83(1): 11-21.

Yang, C.S., Wang, H., Li, G.X., Yang, Z., Guan, F. i Jin, H. (2011). Cancer prevention by tea: Evidence from laboratory studies. *Pharmacol Res* 64(2): 113-22.

Yang, C.S. i Wang, X. (2010). Green tea and cancer prevention. *Nutr Cancer* 62(7): 931-7.

Yap, W.H., Khoo, K.S., Lim, S.H., Yeo, C.C. i Lim, Y.M. (2012). Proteomic analysis of the molecular response of Raji cells to maslinic acid treatment. *Phytomedicine* 19(2): 183-91.

Yun, J.W., Lee, W.S., Kim, M.J., Lu, J.N., Kang, M.H., Kim, H.G., Kim, D.C., Choi, E.J., Choi, J.Y., Kim, H.G., Lee, Y.K., Ryu, C.H., Kim, G., Choi, Y.H., Park, O.J. i Shin, S.C. (2010). Characterization of a profile of the anthocyanins isolated from Vitis coignetiae Pulliat and their anti-invasive activity on HT-29 human colon cancer cells. *Food Chem Toxicol* 48(3): 903-9.

Zhu, W.G. i Otterson, G.A. (2003). The interaction of histone deacetylase inhibitors and DNA methyltransferase inhibitors in the treatment of human cancer cells. *Curr Med Chem Anticancer Agents* 3(3): 187-99.

Ziech, D., Franco, R., Pappa, A. i Panayiotidis, M.I. (2011). Reactive oxygen species (ROS)--induced genetic and epigenetic alterations in human carcinogenesis. *Mutat Res* 711(1-2): 167-73.

PUBLICACIONS

CAPÍTOL 1

L'hamamelitanin d'*Hamamelis virginiana* mostra citotoxicitat específica contra cèl·lules de càncer de còlon

Els resultats presentats en aquest capítol han estat publicats a la revista *Journal of Natural Products* amb un índex d'impacte de 2,872.

Susana Sánchez-Tena[1], María L. Fernández-Cachón[1, ‡], Anna Carreras[2], M. Luisa Mateos-Martín[2], Noelia Costoya[3], Mary P. Moyer[4], María J. Nuñez[3], Josep L. Torres[2] i Marta Cascante[1, *]

[1]Facultat de Biologia, Universitat de Barcelona i IBUB, Unitat associada al CSIC, 08028 Barcelona, Espanya

[2]Institut de Química Avançada de Catalunya (IQAC-CSIC), 08034 Barcelona, Espanya

[3]Escola d'Enginyeria, USC, 15782 Santiago de Compostel·la, Espanya

[4]INCELL, San Antonio TX 78249, EUA

[‡]Adreça actual: Freiburg Institut for Advanced Studies. School of Life Sciences – LifeNet. Freiburg im Breisgau, Alemanya

RESUM

L'escorça d'*Hamamelis virginiana* (avellaner de bruixa) és una font rica en tanins condensats i hidrolitzables, els quals s'ha descrit que exerceixen una acció protectora envers el càncer de còlon. El present estudi caracteritza diferent tanins de l'avellaner de bruixa com agents citotòxics selectius contra el càncer de còlon. Per cobrir la diversitat estructural dels tanins presents a l'escorça d'*H. virginiana*, els tanins hidrolitzables, hamamelitanin i pentagaloilglucosa, juntament amb la fracció rica en proantocianidines o tanins condensats (F800H4), es van seleccionar per a l'estudi. El tractament amb aquests compostos va reduir la viabilitat i va induir apoptosi, necrosi i arrest en la fase S del cicle cel·lular en cèl·lules HT29, amb l'hamamelitanin sent el més eficaç. Per eliminar l'efecte artefactual degut a la formació de H_2O_2 en el medis de cultiu, l'efecte antiproliferatiu es va determinar en presència i absència de catalasa. La presència de catalasa només va canviar significativament l'IC_{50} de la fracció F800H4. A més, a concentracions que inhibeixen un 50% el creixement de les cèl·lules HT29, l'hamamelitanin no va tenir cap efecte nociu en colonòcits normals NCM460 mentre que la pentagaloilglucosa va inhibir ambdós tipus cel·lulars. Utilitzant l'assaig del TNPTM es va identificar una posició fenòlica altament reactiva present en l'hamamelitanin que pot explicar la seva eficàcia inhibint el creixement del càncer de còlon.

Hamamelitannin from Witch Hazel *(Hamamelis virginiana)* Displays Specific Cytotoxic Activity against Colon Cancer Cells

Susana Sánchez-Tena[1], María L. Fernández-Cachón[1, ‡], Anna Carreras[2], M. Luisa Mateos-Martín[2], Noelia Costoya[3], Mary P. Moyer[4], María J. Nuñez[3], Josep L. Torres[2] and Marta Cascante[1, *]

[1]Faculty of Biology, Universitat de Barcelona and IBUB, Unit Associated with CSIC, 08028 Barcelona, Spain

[2]Institute for Advanced Chemistry of Catalonia (IQAC-CSIC), 08034 Barcelona, Spain

[3]School of Engineering, USC, 15782 Santiago de Compostela, Spain

[4]INCELL Corporation, San Antonio TX 78249, USA

[‡]Present address: Freiburg Institute for Advanced Studies. School of Life Sciences – LifeNet. Freiburg im Breisgau, Germany;

ABSTRACT

Hamamelis virginiana (witch hazel) bark is a rich source of condensed and hydrolysable tannins reported to exert a protective action against colon cancer. The present study characterizes different witch hazel tannins as selective cytotoxic agents against colon cancer. To cover the structural diversity of the tannins that occur in *H. virginiana* bark, the hydrolysable tannins, hamamelitannin and pentagalloylglucose, together with a proanthocyanidin-rich fraction (F800H4) were selected for the study. Treatment with these compounds reduced tumor viability and induced apoptosis, necrosis, and S-phase arrest in the cell cycle of HT29 cells, with hamamelitannin the most efficient. Owing to polyphenol-mediated H_2O_2 formation in the incubation media, the antiproliferative effect was determined in the presence and absence of catalase to rule out any such interference. The presence of catalase only significantly changed the IC_{50} for F800H4. Furthermore, at concentrations that inhibit the growth of HT29 cells by 50%, hamamelitannin had no harmful effects on NCM460 normal colonocytes, whereas pentagalloylglucose inhibited both cancerous and normal cell growth. Using the TNPTM assay, we identified a highly reactive phenolic position in hamamelitannin which may explain its efficacy at inhibiting colon cancer growth.

INTRODUCTION

Several epidemiological studies have indicated that tannins may exert a protective effect against colon cancer, one of the most prevalent neoplastic diseases in the developed world (Theodoratou *et al.*, 2007; Cutler *et al.*, 2008). Witch hazel (*Hamamelis virginiana*) bark is a rich source of both proanthocyanidins, or condensed tannins, and hydrolysable tannins (Figure 1) such as hamamelitannin and pentagalloylglucose (Vennat *et al.*, 1988), whose capacity to regulate cell proliferation, cell cycle, and apoptosis have attracted much attention (Hu *et al.*, 2009a).

An inverse relation has been reported between proanthocyanidins and colorectal cancer (Mutanen *et al.*, 2008). An *in vitro* study demonstrated that a grape seed proanthocyanidin extract significantly inhibits cell viability and increases apoptosis in Caco-2 colon cancer cells, but does not alter the viability of the normal colon NCM460 cell line (Engelbrecht *et al.*, 2007). Other results show that proanthocyanidins from different sources are cytotoxic to human colorectal cells (Gosse *et al.*, 2005; Chung *et al.*, 2009; Hoverman *et al.*, 2011). In addition, several *in vitro* and *in vivo* studies have shown that hydrolysable tannins from witch hazel bark exhibit multiple biological activities, which may have potential in the prevention and treatment of cancer. *In vivo* preclinical studies of pentagalloylglucose, one of the major hydrolysable tannins in witch hazel, demonstrated inhibition of prostate cancer (Hu *et al.*, 2008; Kuo *et al.*, 2009), lung cancer (Huh *et al.*, 2005), and sarcoma (Miyamoto *et al.*, 1987) cells. *In vitro* inhibition of the growth and invasiveness of breast cancer, leukemia, melanoma, and liver cancer cells have also been reported (Oh *et al.*, 2001; Ho *et al.*, 2002; Chen *et al.*, 2003; Chen *et al.*, 2004). The other major hydrolysable tannin in witch hazel, hamamelitannin, inhibits TNF-mediated endothelial cell death and DNA fragmentation in EAhy926 endothelial cells (Habtemariam, 2002). Since TNFα/TNFR1 signaling may act as a tumor promoter for colon carcinogenesis (Sakai *et al.*, 2010), the anti-TNF activity of hamamelitannin may indicate a protective effect against colon cancer. Furthermore, hamamelitannin has been described to inhibit 5-lipoxygenase (5-LOX) (Hartisch *et al.*, 1997) and given that 5-LOX is an inflammatory enzyme involved in malignant transformation (Wasilewicz *et al.*, 2010), this inhibition could prevent cancer growth.

Moreover, various studies have analyzed the cytotoxicity and scavenging capacity of *H. virginiana* phenolic compounds. It has been reported that different witch hazel polyphenolic fractions are highly active as free radical scavengers against 2,2′-azinobis-(3-ethylbenzothiazoline-6-sulfonic acid) (ABTS), 1,1-diphenyl-2-picrylhydrazyl (DPPH), and tris-(2,4,6-trichloro-3,5-dinitrophenyl)-methyl (HNTTM). They also reduce tris(2,3,5,6-tetrachloro-4-nitrophenyl)-methyl

(TNPTM) radical to some extent, which indicates that they contain highly reactive hydroxy groups. In this way, witch hazel fractions protect red blood cells from free radical-induced hemolysis and also inhibit the proliferation of the SK-Mel 28 melanoma tumor cell line (Touriño *et al.*, 2008). Some of these fractions also inhibited cell proliferation, arrested the cell cycle at the S phase and induced apoptosis in HT29 human colon cancer cells (Lizárraga *et al.*, 2008). The witch hazel mixtures studied so far include those from highly heterogeneous mixtures containing both hydrolysable and condensed tannins of low molecular weight, as well as flavan-3-ol monomers (Touriño *et al.*, 2008; Lizárraga *et al.*, 2008); however, the activity of oligomeric structures from witch hazel bark has not been evaluated. Furthermore, Masaki et al. reported that hamamelitannin from *H. virginiana* posses protective activity to cell damage induced by superoxide anion radicals in murine dermal fibroblast (Masaki *et al.*, 1993; Masaki *et al.*, 1995).

To advance our understanding of the compounds responsible for the activity of *H. virginiana* bark, we evaluated the behavior of pure hamamelitannin and pentagalloylglucose (hydrolysable tannins of different size) and a highly purified proanthocyanidin-rich fraction (F800H4). First, we examined the viability, apoptosis, and cell cycle of the human colorectal adenocarcinoma HT29 cell line after treatment with these compounds. To identify products that inhibit cancer cell growth without harming normal cells, the antiproliferative capacity of *Hamamelis* compounds was also measured against the NCM460 cell line (human colonocytes). As several studies have reported that polyphenols can be oxidized under standard cell culture conditions, leading to the production of significant amounts of ROS such as H_2O_2, and that this can modulate cell functions (Halliwell, 2003), we supplemented the cell culture medium with catalase, which decomposes polyphenol-generated ROS, thus ruling out this possibility (Bellion *et al.*, 2009).

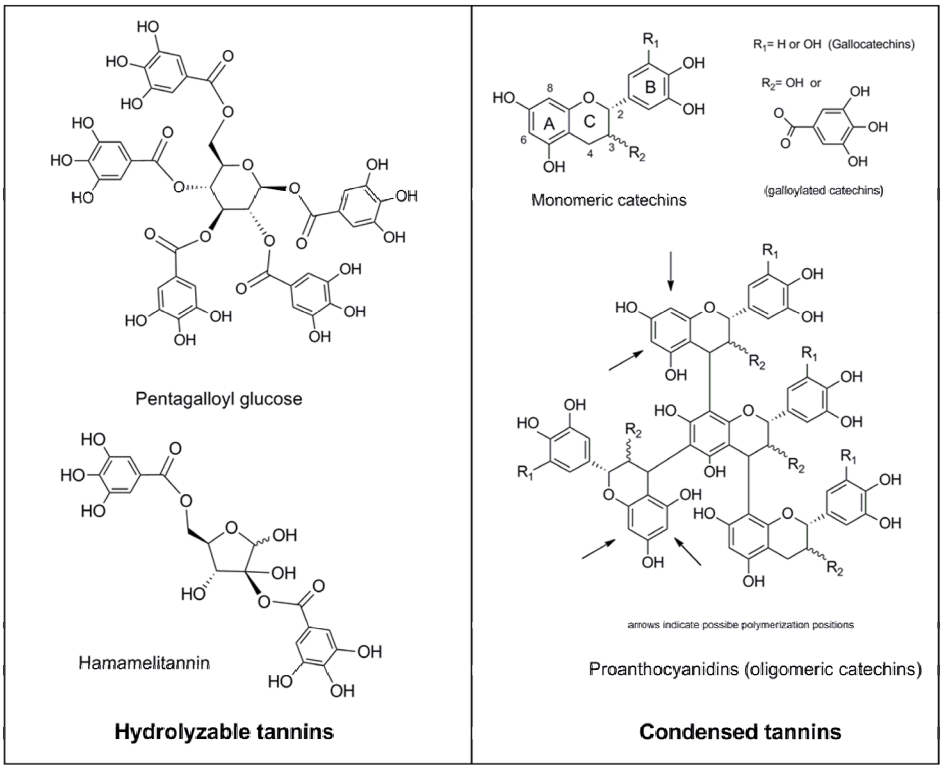

Figure 1. Structures of hydrolysable and condensed tannins in *Hamamelis virginiana* bark.

MATERIALS AND METHODS

General Experimental Procedures. UV measurements were made on a UV spectrophotometer Cary 50-Bio (Varian, Palo Alto, CA, USA). Semipreparative chromatography was conducted on a Waters system (Milford, MA, USA) using an X-Terra C18 (19 x 250 mm, 10 μm) column. HPLC was carried out on a Hitachi (San Jose, CA, USA) system equipped with a quaternary pump, autosampler and diode array detector (DAD), and an analytical Kromasil C_{18} (Teknokroma, Barcelona, Spain) column. All chemicals were purchased from Sigma-Aldrich Co (St Louis, MO, USA), unless otherwise specified. For extraction, we used deionized water, bulk EtOH (Momplet y Esteban, Barcelona, Spain), bulk acetone (Quimivita, Sant Adrià del Besòs, Spain), and bulk hexane (alkanes mixture) (Quimivita). For purification, deionized water, analytical grade MeOH (Panreac, Montcada i Reixac, Spain), analytical grade acetone (Carlo Erba, Milano, Italy), and preparative grade CH_3CN (E. Merck, Darmstadt, Germany) were used for semipreparative and preparative chromatography; milli-Q water and HPLC grade CH_3CN (E. Merck) were used for

analytical RP-HPLC. Analytical grade MeOH (Panreac) was used for thioacidolysis and free radical scavenging assays, and analytical grade CH_3Cl (Panreac) was used for the electron transfer assays. TFA (Fluorochem, Derbyshire, UK) biotech grade was distilled in-house. 37% HCl and HOAc were from E. Merck. Et_3N (E. Merck) was of buffer grade. Deuterated solvents for NMR were from SDS (Peypin, France). DPPH (95%) was from Aldrich (Gillingham-Dorset, UK), 6-hydroxy-2,5,7,8-tetramethylchroman-2-carboxylic acid (Trolox) (97%) was from Aldrich (Milwaukee, WI, USA). HNTTM and TNPTM radicals were synthesized as described elsewhere (Torres *et al.*, 2003; Torres *et al.*, 2007). Antibiotics (10000 U/mL penicillin, 10000 µg/mL streptomycin) were obtained from Gibco-BRL (Eggenstein, Germany), fetal calf serum (FCS) was from Invitrogen (Paisley, UK) and trypsin EDTA solution C (0.05% trypsin–0.02% EDTA) was from Biological Industries (Kibbutz Beit Haemet, Israel). The Annexin V/FITC kit was obtained from Bender System (Vienna, Austria). M3Base medium was purchased from INCELL (San Antonio, TX, USA).

Extraction, Fractionation and Characterization of F800H4. Polyphenols were obtained from witch hazel bark by extraction with acetone-water (7:3) and fractionation with EtOAc (Touriño *et al.*, 2008) that produced fraction OWH (polyphenols soluble in EtOAc and H_2O) and fraction AH (polyphenols only soluble in H_2O). To generate fraction F800H4, AH (800 mg) was dissolved in 50% MeOH and fractionated on a Sephadex LH-20 column (50 x 2.5 cm i.d.) using a gradient of MeOH in H_2O and a final step of washing with acetone, as previously reported (Jerez *et al.*, 2007). Five sub-fractions (800H1 to 800H5) were collected and their absorbance was measured at 280 and 400 nm; yield, 8% from fraction AH; 0.05% from witch hazel bark. Table 1 shows the chemical composition of fraction F800H4, which was estimated as previously described (Touriño *et al.*, 2008). The content of condensed tannins was estimated by thioacidolytic depolymerization in the presence of cysteamine and HPLC analysis of the cleaved units. The hydrolysable tannins were determined directly from the fraction by HPLC and standards.

Purification of Pentagalloylglucose. Pentagalloylglucose was purified from fraction OWH by semipreparative chromatography on a Waters system (Milford, MA, USA) using an X-Terra C18 (19 x 250 mm, 10 µm) column. A total amount of 2 g of OWH was processed in successive chromatographic runs with loads of 200 mg, 4 mL each, and elution by a binary system [solvent A, 0.1 % aqueous TFA; solvent B, 0.08 % TFA in H_2O/CH_3CN (1:4)] under the following conditions: 10 min at 16% B and two gradients, 16-36% B over 40 min and 36-55% B over 5 min, at a flow rate of 10 mL/min with detection at 235 nm. The purity of the pentagalloylglucose was ascertained by HPLC on a Hitachi (San Jose, CA, USA) system equipped with a quaternary pump, autosampler

and diode array detector (DAD) and an analytical Kromasil C18 (Teknokroma, Barcelona, Spain) column under the same elution conditions at a flow rate of 1 mL/min. Pentagalloylglucose was lyophilized and its identity was confirmed by chromatography coupled to high resolution mass spectrometry and NMR; purity, 95% by HPLC; yield, 3.8% from fraction OWH, 0.03% from witch hazel bark.

DPPH Assay. The antiradical capacity of the polyphenols was evaluated by the DPPH stable radical method (Brand-Williams *et al.*, 1995). Fresh MeOH solutions (2 mL) at concentrations ranging from 2 to 30 μM were added to a freshly prepared radical solution (2 mL, 120 μM) in deoxygenated MeOH. The mixture was incubated for 30 min at room temperature in the dark and the UV absorbance at 517 nm was measured. The results were plotted as the percentage of absorbance disappearance [(1 - A/A0) × 100] against the amount of sample divided by the initial concentration of DPPH. Each data point was the result of three independent determinations. A dose–response curve was obtained for every sample. The results are expressed as the efficient concentration, EC_{50}, given as the amount of polyphenols that consumes half the amount of free radical divided by the initial amount of DPPH in micromoles. The results are also expressed as antiradical power (ARP), which is the inverse of EC_{50}. UV measurements were made on a UV spectrophotometer Cary 50-Bio (Varian, Palo Alto, CA, USA).

Electron Transfer Capacity against the Stable Free Radicals HNTTM and TNPTM. Fresh solutions of the polyphenols (2 mL) at concentrations ranging from 2 to 62 μM were added to a freshly prepared solution of HNTTM (2 mL, 120 μM) in deoxygenated $CHCl_3$/MeOH (2:1). The mixture was incubated for 7 h at room temperature in the dark and the UV absorbance was measured at 384 nm. The results are plotted as the percentage of absorbance disappearance [(1 - A/A0) × 100] against the amount of sample divided by the initial amount of the radical in micromoles, as described for DPPH. Each data point was the result of three independent determinations. A dose–response curve was obtained for every sample. The results are expressed as the efficient concentration, EC_{50}, and as ARP. The working conditions with TNPTM were essentially those described for HNTTM (Torres *et al.*, 2007) with some differences. The concentration range was 10-120 μM, the incubation time was 48 h and the absorbance was measured at 378 nm. The results are plotted as described for HNTTM.

Cell Culture. Human colorectal adenocarcinoma HT29 cells (obtained from the American Type Culture Collection, HTB-38) were grown as a monolayer culture in Dulbecco's Modified Eagle's Medium (DMEM) in the presence of 10% heat-inactivated fetal calf serum and 0.1%

streptomycin/penicillin in standard culture conditions. NCM460 cells, obtained by a Material Transfer Agreement with INCELL, are from an epithelial cell line derived from the normal colon mucosa of a 68-year old Hispanic male (Moyer *et al.*, 1996). They were grown as a monolayer culture in M3Base medium (which contains growth supplements and antibiotics) supplemented with 10% heat-inactivated fetal calf serum and 2.5 mM of D-glucose (final concentration 5 mM glucose). The cells were cultured at 37ºC in a 95% air, 5% CO_2 humidified environment.

Determination of Cell Viability. The assay was performed using a variation of the MTT assay described by Mosmann (Mosmann, 1983). The assay is based upon the principle of reduction of MTT into blue formazan pigments by viable mitochondria in healthy cells. The cells were seeded at densities of 3×10^3 cells/well (HT29 cells) and 1×10^4 cells/well (NCM460 cells) in 96-well flat-bottom plates. After 24 h of incubation at 37ºC, the polyphenolic samples were added to the cells at different concentrations in fresh medium. Some experiments were performed in the presence of catalase (100 U/mL, from bovine liver) to examine the potential influence on extracellular H_2O_2. The use of an antioxidant enzyme in the cell medium allows us to rule out the effects of exogenous H_2O_2 generated during the incubation with polyphenols. The addition of this enzyme does not affect the cellular markers, since it does not enter the cells and is removed after incubation. In all cases the antitumor agent EGCG was used as standard. The culture was incubated for 72 h. Next the medium was removed and 50 μL of MTT (1 mg/mL in PBS) with 50 μL of fresh medium was added to each well and incubated for 1 h. The MTT reduced to blue formazan and the precipitate was dissolved in 100 μL of DMSO; absorbance values were measured on an ELISA plate reader (550 nM) (Tecan Sunrise MR20-301, TECAN, Salzburg, Austria). Absorbance was taken as proportional to the number of living cells. The concentrations that caused 50% cell growth inhibition (IC_{50}) were estimated from the dose–viability curves.

Cell Cycle Analysis by FACS. The cell cycle was analyzed by measuring the cellular DNA content using the fluorescent nucleic acid dye propidium iodide (PI) to identify the proportion of cells in each stage of the cell cycle. The assay was carried out using flow cytometry with a fluorescence-activated cell sorter (FACS). HT29 cells were plated in 6-well flat-bottom plates at a density of 87×10^3 cells/well. After 24 h of incubation at 37ºC, the polyphenolic fractions were added to the cells at their respective IC_{50} values. We used the G1/S cell cycle inhibitor HU at 1 mM as standard. The cultures were incubated for 72 h in the absence or presence of the polyphenolic fractions. The cells were trypsinized, pelleted by centrifugation (1500 rpm for 5 minutes), and stained in Tris buffered saline (TBS) containing 50 μg/mL PI, 10 μg/mL RNase free of DNase, and

0.1% Igepal CA-630. They were incubated in the dark for 1 h at 4ºC. Cell cycle analysis was performed by FACS (Epics XL flow cytometer, Coulter Corp., Hialeah, FL, USA) at 488 nm (Lozano *et al.*, 2005).

Apoptosis Analysis by FACS. Double staining with Annexin V-FITC and PI measured by FACS was used to determine the percentage of apoptotic cells. Annexin+/ PI- cells were considered early apoptotic cells. Annexin+/ PI+ and Annexin-/ PI+ cells were classed together as late apoptotic/necrotic cells, since this method does not differentiate necrotic cells from cells in late stages of apoptosis, which are also permeable to PI. The cells were seeded, treated, and collected as described in the previous section. ST 1 μM was utilized as a control of apoptosis induction. After centrifugation (1500 rpm for 5 minutes), they were washed in binding buffer (10 mM Hepes, pH 7.4, 140 mM NaCl, 2.5 mM $CaCl_2$) and re-suspended in the same buffer. Annexin V-FITC was added using the Annexin V-FITC kit. Afterwards, the cells were incubated for 30 minutes at room temperature in the dark. Next, PI was added 1 min before the FACS analysis at 20 μg/mL. Fluorescence was measured at 495 nm (Annexin V-FITC) and 488 nm (PI).

Determination of H_2O_2 (FOX Assay). H_2O_2 in the cell culture medium was determined using the ferrous oxidation xylenol orange (FOX) assay (Jiang *et al.*, 1992). After oxidation of Fe(II) to Fe(III) by H_2O_2, the resulting xylenol orange–Fe(III) complex was quantified spectrophotometrically (560 nm). The cells were incubated for 72 hours with a range of concentrations of witch hazel compounds in culture medium (DMEM or M3Base) either alone or in the presence of catalase (100 U/mL, from bovine liver) under cell culture conditions (96-well flat-bottom plate, in the absence of cells). EGCG was used as positive control in this assay given that it has already been reported that this product generates high levels of ROS in cell culture media. Next, 100 μL of medium was transferred to a new 96-well flat-bottom plate. FOX reagent (900 μL) was added to each aliquot: 100 μM of xylenol orange, 250 μM of ferrous ammonium sulfate, 25 mM of H_2SO_4 and 4 mM of BHT in 90% (v/v) MeOH. After 30 min, absorbance at 560 nm was measured in a microplate reader (Tecan Sunrise MR20-301, TECAN). Peroxides were quantified by comparing the absorbance to a standard curve (H_2O_2 concentrations: 0–150 μM).

Data Presentation and Statistical Analysis. Data are given as the means ± S.D. (standard deviation). For each assay, the parametric unpaired two-tailed independent sample t-test was used for statistical comparison with the untreated control cells and differences were considered to be significant when $p < 0.05$ and $p < 0.001$.

RESULTS AND DISCUSSION

Pentagalloylglucose and fraction F800H4 were extracted from the bark of witch hazel whereas the hydrolysable tannin hamamelitannin was obtained commercially. Both hydrolysable tannins presented a purity of 98% or more, as confirmed by HPLC. Once fraction F800H4 was obtained, its polyphenolic composition was characterized to ensure that it possessed a high percentage of condensed tannins. Table 1 summarizes the results of the HPLC analysis after thioacidolysis in the presence of cysteamine (condensed tannins) and direct HPLC analysis (gallic acid, pentagalloylglucose, and hamamelitannin). F800H4 was found to be composed of mostly condensed tannins (83.9% of the total tannins), both monomers and proanthocyanidins [(epi)catechin oligomers and polymers]. It also contained 16.1% of hydrolysable tannins, mainly hamamelitannin. Pentagalloylglucose was not detected in fraction F800H4. The condensed tannins had a mean degree of polymerization (mDP) of 2.6, 35% of galloylation, and 32% of pyrogallol. The total galloylation of the fraction was 45.5%.

Table 1. Polyphenolic Composition of F800H4

Composition of the condensed tannins (CTn) 83.9%					
mDP	**% G**	**% P**			
2,6	35,0	32,0			
% GC	**% EGC**	**% C**	**% EC**	**% EGCG**	**% ECG**
12,4	0,4	29,1	23,0	19,1	15,9

Composition of the hydrolysable tannins (HTn) 16.1%		
% GA	**% HT**	**% PGG**
10,0	90,0	0,0

[a]mDP: mean degree of polymerization; %G, percentage of galloylation; %P: percentage in pyrogallol. [b]GC, gallocatechin; EGC, epigllocatechin; C, catechin; EC, epicatechin; EGCG, epigallocatechin gallate; ECG, epicatechin gallate. [c]GA, gallic acid; HT, hamamelitannin; PGG, pentagalloylglucose.

Tannins regulate different cell functions through different actions that may or may not involve redox reactions (Sang *et al.*, 2005). Since polyphenols may act as antioxidants and prooxidants, we studied the redox activity of *H. virginiana* compounds and evaluated their free radical scavenging properties using different stable radicals like DPPH, HNTTM, and TNPTM. DPPH reacts with polyphenols by mechanisms that may include both hydrogen donation and electron transfer (Foti *et al.*, 2004), while HNTTM and TNPTM are only sensitive to electron transfer (Torres *et al.*, 2007). The reactions with DPPH and HNTTM gave information on the total capacity to scavenge radicals by hydrogen donation or concerted electron proton transfer (DPPH) and by electron transfer (HNTTM). The reaction with TNPTM revealed the presence of highly redox reactive positions. Table 2 summarizes the activities of pentagalloylglucose, hamamelitannin, and the proanthocyanidin fraction F800H4 against the stable free radicals. Overall, pentagalloylglucose, hamamelitannin, and the proanthocyanidin-rich fraction F800H4 showed a similar total scavenging capacity, as their number of phenolic hydroxy groups per unit of mass was similar. Interestingly, differences were detected with TNPTM. While the scavenging capacity of the polyphenols against TNPTM is low because only some of the hydroxy groups are able to donate electrons to this radical, the possible effects of these hydroxy groups may be biologically relevant because they are the most reactive positions. One of the phenolic hydroxy groups in hamamelitannin was reactive enough to transfer its electron to TNPTM while pentagalloylglucose was much less responsive (Table 2, last column). Hamamelitannin and pentagalloylglucose are structurally similar. In the case of hamamelitannin though, there is a hydroxy moiety geminal to one of the gallate esters and this might explain the differences detected in the reactivity against the TNPTM radical. The extra hydroxy group might participate in a hydrogen bond with the carbonyl group from the gallate moiety to form a six-membered ring. This could introduce a conformational restriction with loss of planarity and subsequent loss of conjugation within the gallate moiety. The extended conjugation of the carbonyl and aromatic groups is the reason why gallates are less reactive than pyrogallols (Sato *et al.,* 2010). The results with TNPTM indicate that hamamelitannin is particularly reactive and may even participate in the formation of ROS through electron transfer to oxygen to form the superoxide radical.

Table 2. Hydrogen Donation and Electron Transfer Capacity

	DPPH			HNTTM			TNPTM		
	EC_{50} [a]	ARP [b]	H/e [c]	EC_{50} [a]	ARP [b]	e [c]	EC_{50} [a]	ARP [b]	e [c]
PGG	23,8	42,0	19,8	54,8	18,2	8,6	2403,9	0,4	0,2
HT	27,8	36,2	8,8	71,2	14,0	3,4	116,2	2,2	1,0
F800H4	39,8	25,1	27,1	66,7	15,0	16,2	1761,6	0,6	0,7

[a] EC_{50} µg of polyphenol/µmol of radical. [b] ARP, $(1/EC_{50}) \times 10^3$. [c] Number of hydrogen atoms donated or electrons transferred to the stable radical per molecule of polyphenol, calculated as the inverse of 2 x molar EC_{50}.

Pentagalloylglucose has been shown to inhibit different malignancies (Miyamoto *et al.*, 1987; Hu *et al.*, 2008; Kuo *et al.*, 2009). Potential mechanisms for its anticancer activity include anti-angiogenesis, antiproliferation, S-phase and G1-phase cell-cycle arrest, induction of apoptosis, anti-inflammation and anti-oxidation. Putative molecular targets include p53, Stat3, Cox-2, VEGFR1, AP-1, SP-1, Nrf-2, and MMP-9. This study reports for the first time the role of pentagalloylglucose in colon cancer. We studied here the viability, the cell cycle, and apoptosis process in human colorectal adenocarcinoma HT29 cells. In these bioassays, different positive controls were used. Epigallocatechin gallate (EGCG), a major catechin in green tea described to have antitumor activity (Singh *et al.*, ; Yang *et al.*), was used as standard in cell viability assays; the cell cycle inhibitor hydroxyurea (HU) was used as standard in cell cycle experiments (Iacomino *et al.*, 2006) and staurosporine (ST) was utilized as a positive control in apoptosis assays (*Elsaba et al.,* 2010). Treatment with pentagalloylglucose reduced the viability of HT29 cells with an IC_{50} value of 28 ± 8.8 µg/mL (Figure 2a) and induced 11% apoptosis compared to control cells, 5% necrosis (Figure 3) and S-phase arrest in the cell cycle with 8% increase in the population of cells in the S phase and a concomitant decrease in the percentage of cells in G1 and G2 phases (Figure 4). Because pentagalloylglucose inhibits DNA replicative synthesis with greater efficacy than a known DNA polymerase-alpha inhibitor, aphidocolin,(Hu *et al.*, 2009b) this may explain the arrest in the S phase. The antitumor effects of hamamelitannin have not been examined, except for its antigenotoxic action in HepG2 human hepatoma cells reported by Dauer et al. (Dauer *et al.*, 2003), as well as its anti-TNF (Habtemariam, 2002) and anti-LOX activities (Hartisch *et al.*, 1997). The cellular mechanism that this hydrolysable tannin induces may be related to the inhibition of the tumor necrosis factor itself and its receptor, which affect apoptosis, necrosis, and cell cycle processes. As a result, after treatment with hamamelitannin, we observed a reduction in the viability

of HT29 cells with an IC_{50} of 20 ± 4.5 µg/mL (Figure 2a) and induction of 26% of apoptosis, 14% of necrosis (Figure 3) and S-phase arrest in the cell cycle with a 16% increase in the population of cells in this phase (Figure 4). With regard to condensed tannins, proanthocyanidins from various sources have been reported to inhibit colon cancer cells (Maldonado-Celisa *et al.*, 2008; McDougall *et al.*, 2008). Treatment of the human colon adenocarcinoma HT29 cell line with the proanthocyanidin-rich fraction F800H4 extracted from witch hazel bark was less effective at inhibiting cell viability (IC_{50} = 38 ± 4.4 µg/mL; Figure 2a), and inducing apoptosis (9%) and necrosis (6%) (Figure 3), than the same treatment with hydrolysable tannins. F800H4 had little effect on the normal cell-cycle distribution apart from a slight increase in the S- and G2-phases (Figure 4).

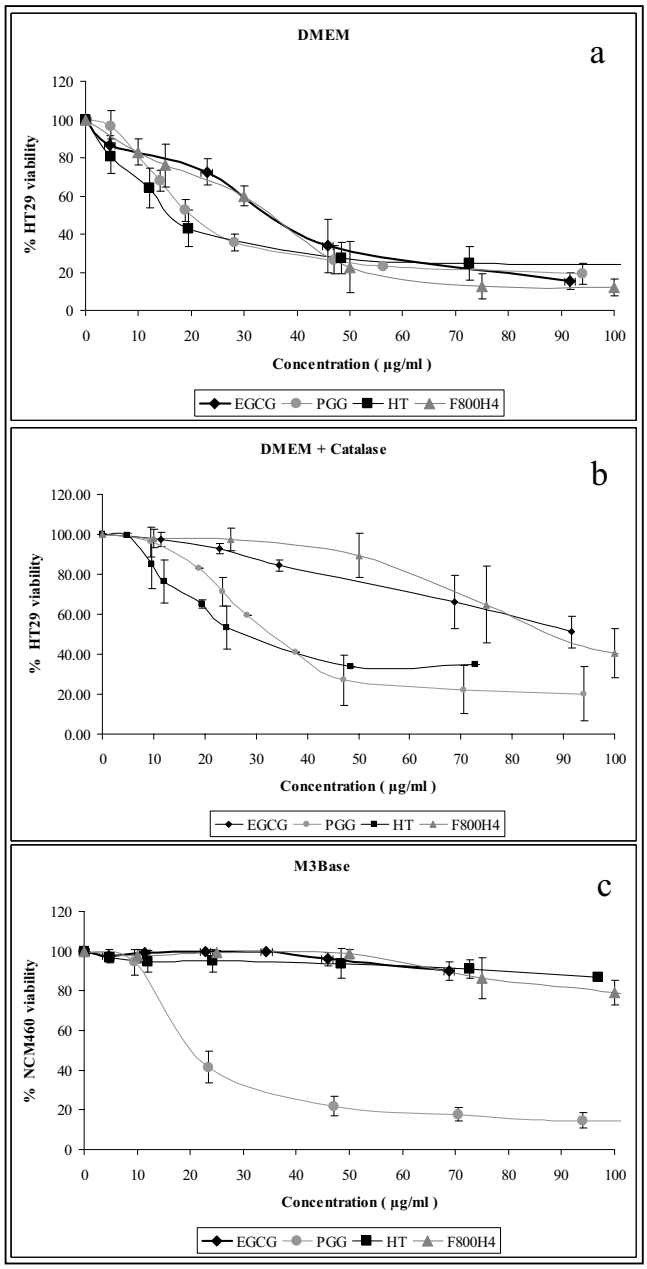

Figure 2. [a] Effect on HT29 cell viability of different concentrations of *Hamamelis virginiana* compounds in DMEM. [b] Effect on HT29 cell viability of witch hazel compounds in DMEM supplemented with catalase (100 U/mL). [c] Effect of Hamamelis products on NCM460 colonocyte growth. In all cases epigallocatechin gallate is used as standard. Values are represented as mean of percentage of cell viability with respect to control cells ± standard error of three independent experiments.

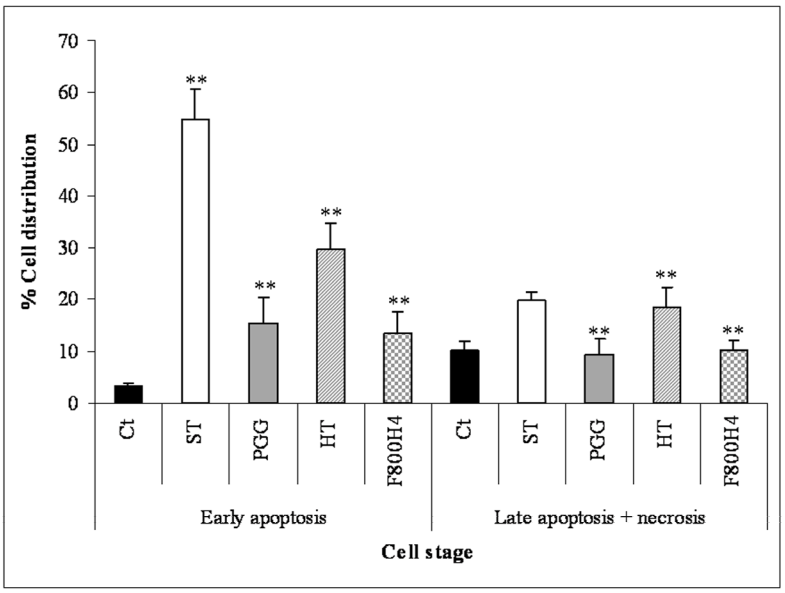

Figure 3. Early apoptotic cells: Annexin V+ PI-; late apoptotic/necrotic cells: Annexin V+/ PI+ and Annexin V-/ PI+. Staurosporine is utilized as positive control. Values are expressed as mean ± standard deviation of three separate experiments. **p < 0.001, significant difference with respect to the corresponding value in untreated cells (Ct).

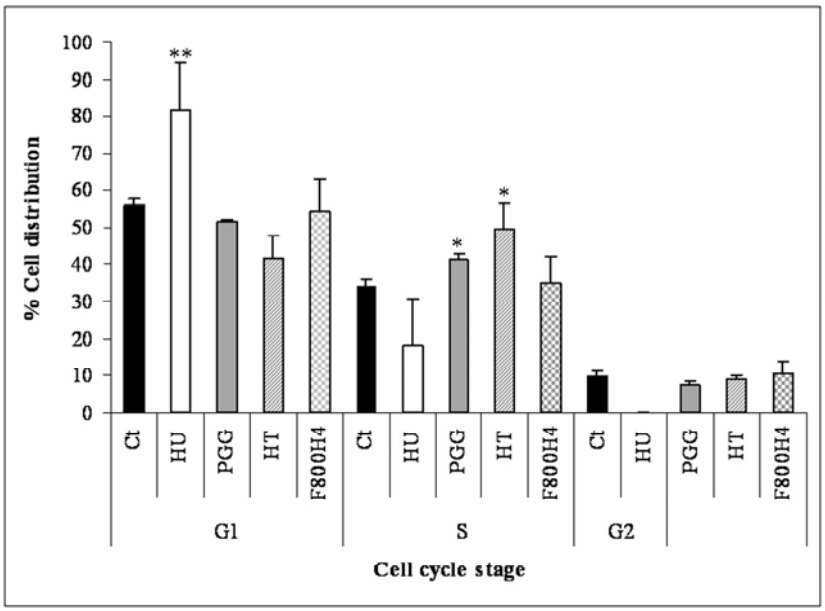

Figure 4. Normalized percentages of cells in different cell stages are shown. Cell phases analyzed: G1, S and G2. The cell cycle inhibitor hydroxyurea was used as standard. Mean ± standard deviation of three separate experiments. *p < 0.05; **p < 0.001, significant difference with respect to control cells (Ct).

Overall, the hydrolysable tannins were more effective than the condensed tannins. Interestingly, hamamelitannin, which includes a highly reactive position, as demonstrated by its reaction with TNPTM (Table 2), showed the strongest inhibition of cell viability, induction of apoptosis and necrosis, and cell-cycle arrest in the S phase in HT29 colon cancer cells (Figures 2a, 3, 4). The effect of this reactive position in hamamelitannin may even be prooxidant. The prooxidant effect of some polyphenols has been discussed extensively and it has been suggested that moderate generation of ROS may produce an antioxidant effect by fostering the endogenous defenses (Dhakshinamoorthy *et al.*, 2000; Ascensao *et al.*, 2005). Therefore, in our assays, hamamelitannin may exert its activity, at least in part, by providing mild prooxidant challenges through electron transfer reactions leading to moderate formation of ROS.

On the other hand, since it has been reported that an increase in endogenous ROS levels is required for the transition from the G1 to the S phase of the cell cycle (Havens *et al.*, 2006), the cell cycle arrest in the S phase induced by witch hazel compounds may be explained to some extent by its ROS scavenging capacity.

In the search for compounds or fractions that inhibit cancer cell growth without harming normal cells, the antiproliferative capacity of pentagalloylglucose, hamamelitannin, and the proanthocyanidin-rich fraction F800H4 was determined in NCM460 human colonocytes. NCM460 are non-tumorigenic cells derived from normal colon mucosa that has not been infected or transfected with any genetic information (Moyer *et al.*, 1996). This is the first comparison of the effects of witch hazel compounds on the growth of non-transformed colonocytes and cancerous colon cells. Our results show that the concentrations of hamamelitannin and F800H4 capable of inducing the death of HT29 cells (Figure 2a) had no harmful effects on normal colon cells (IC_{50} higher than 100 µg/mL for hamamelitannin and F800H4) (Figure 2c), whereas pentagalloylglucose inhibited both cancerous and normal cell growth (Figure 2a and 2c). Pentagalloylglucose inhibited NCM460 cell viability with an IC_{50} of 23 µg/mL ± 2.4 (Figure 2a, c).

It has been reported that polyphenol-mediated ROS formation in cell culture medium can lead to the artifactual modulation of cytotoxicity attributed to polyphenol exposure. Accordingly, Chai et al. reported that H_2O_2-mediated cytotoxicity, resulting from incubation of PC12 cells with green tea or red wine was completely prevented by the addition of bovine liver catalase to the culture medium (Chai *et al.*, 2003). All *Hamamelis* compounds tested together with the positive control used (EGCG) (Long *et al.*, 2000; Elbling *et al.*, 2005) generated H_2O_2 in a concentration-dependent manner in DMEM (Figure 5a). Hamamelitannin showed the highest H_2O_2 production at

100 µg/mL. As expected, supplementing the cell culture medium with 100 U/mL catalase resulted in almost complete decomposition of polyphenol generated H_2O_2 in all cases (Figure 5b). The next step was to study the antiproliferative capacity of *H. virginiana* polyphenolics by co-incubating with catalase. This enzyme had little effect on HT29 cells incubated with hydrolysable tannins (IC_{50} in DMEM = 28 µg/mL ± 8.8 (Figure 2a) / IC_{50} in DMEM with catalase = 34 µg/mL ± 1.2 (Figure 2b) for pentagalloylglucose and IC_{50} in DMEM = 20 µg/mL ± 4.5 (Figure 2a) / IC_{50} in DMEM with catalase = 13 µg/mL ± 4.6 (Figure 2b) for hamamelitannin), whereas F800H4 cytotoxicity was shown to be partially attributable to H_2O_2-mediated modulation (IC_{50} in DMEM = 38 µg/mL ± 4.4 (Figure 2a) / IC_{50} in DMEM with catalase = 95 µg/mL ± 8.7 (Figure 2b)). This effect is probably triggered by the highly reactive pyrogallol moieties in the condensed tannins. Interestingly, the results obtained for the positive control, EGCG, a flavan-3-ol with a pyrogallol B-ring, are in accordance with this hypothesis. Consequently, the difference between the IC_{50} value of F800H4 determined in HT29 cells incubated with catalase (Figure 2b) and the value established in NCM460 cells (Figure 2c) is not as high as when we compared the results obtained for HT29 without catalase (Figure 2a), which were artifactual, with NCM460 (Figure 2c). This demonstrates that, as with pentagalloylglucose, F800H4 is not completely specific against cancer cells. Interestingly, the cytotoxic activity of hamamelitannin was not modified by the addition of catalase to the medium.

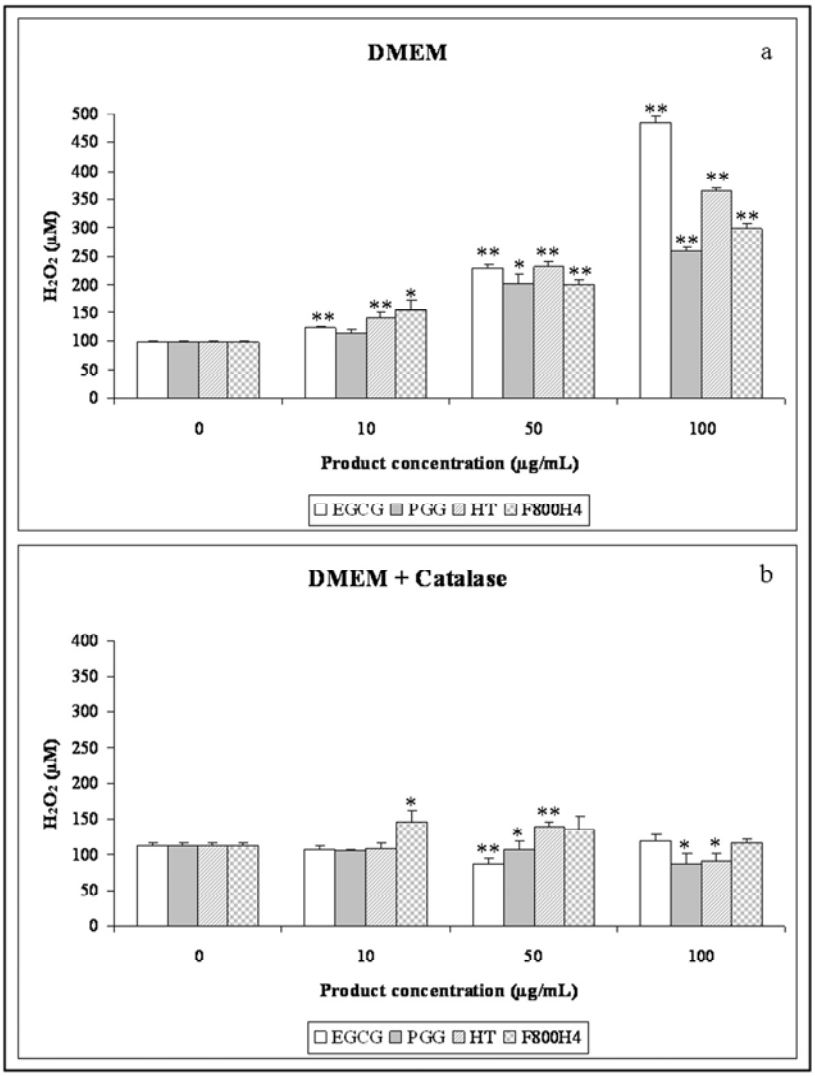

Figure 5. [a] H_2O_2 concentration in cell culture medium (DMEM + 10% FCS + 0.1% streptomycin/penicillin) with pentagalloyl glucose, hamamelitannin and the proanthocyanidin-rich fraction F800H4 in medium. [b] H_2O_2 concentration produced in DMEM culture medium with catalase (100 U/mL) after incubation with witch hazel compounds. Epigallocatechin gallate is used as positive control. Mean ± standard deviation of two independent experiments. $^{**}p < 0.001$ and $^{*}p < 0.05$, significant difference with respect to the corresponding value in untreated cells (Ct).

In summary, we conclude that pentagalloylglucose and the proanthocyanidin-rich fraction F800H4 do not show specificity for cancerous cells, whereas hamamelitannin is a promising chemotherapeutic agent, which might be used for the treatment of colon cancer without compromising the viability of normal colon cells. Hamamelitannin appears to contain a highly

reactive phenolic position that can be detected by the stable radical TNPTM, which may explain its efficacy at inhibiting colon cancer cell growth. These findings may lead to a better understanding of the structure–bioactivity relationship of tannins, which should be of assistance for formulations of chemopreventive and chemotherapeutic agents.

ACKNOWLEDGEMENT

Financial support was provided by grants SAF2008-00164, SAF2011-25726, AGL2006-12210-C03-02/ALI and AGL2009-12374-C03-03/ALI from the Spanish government Ministerio de Ciencia e Innovación and personal financial support (FPU program); from the Ministerio de Educación y Ciencia and from the Red Temática de Investigación Cooperativa en Cáncer, Instituto de Salud Carlos III, Spanish Ministry of Science and Innovation & European Regional Development Fund (ERDF) "Una manera de hacer Europa" (ISCIII-RTICC grants RD06/0020/0046). It has also received financial support from the AGAUR-Generalitat de Catalunya (grant 2009SGR1308, 2009 CTP 00026 and Icrea Academia award 2010 granted to M. Cascante), and the European Commission (FP7) ETHERPATHS KBBE-grant agreement nº22263.

REFERENCES

Ascensao, A.A., Magalhaes, J.F., Soares, J.M., Ferreira, R.M., Neuparth, M.J., Appell, H.J. i Duarte, J.A. (2005). Cardiac mitochondrial respiratory function and oxidative stress: the role of exercise. *Int J Sports Med* 26(4): 258-67.

Bellion, P., Olk, M., Will, F., Dietrich, H., Baum, M., Eisenbrand, G. i Janzowski, C. (2009). Formation of hydrogen peroxide in cell culture media by apple polyphenols and its effect on antioxidant biomarkers in the colon cell line HT-29. *Mol Nutr Food Res* 53(10): 1226-36.

Brand-Williams, W., Cuvelier, M.E. i Berset, C. (1995). Use of a free radical method to evaluate antioxidant activity. *LWT - Food Science and Technology* 28(1): 25-30.

Cutler, G.J., Nettleton, J.A., Ross, J.A., Harnack, L.J., Jacobs, D.R., Jr., Scrafford, C.G., Barraj, L.M., Mink, P.J. i Robien, K. (2008). Dietary flavonoid intake and risk of cancer in postmenopausal women: the Iowa Women's Health Study. *Int J Cancer* 123(3): 664-71.

Chai, P.C., Long, L.H. i Halliwell, B. (2003). Contribution of hydrogen peroxide to the cytotoxicity of green tea and red wines. *Biochem Biophys Res Commun* 304(4): 650-4.

Chen, W.J., Chang, C.Y. i Lin, J.K. (2003). Induction of G1 phase arrest in MCF human breast cancer cells by pentagalloylglucose through the down-regulation of CDK4 and CDK2 activities and up-regulation of the CDK inhibitors p27(Kip) and p21(Cip). *Biochem Pharmacol* 65(11): 1777-85.

Chen, W.J. i Lin, J.K. (2004). Induction of G1 arrest and apoptosis in human jurkat T cells by pentagalloylglucose through inhibiting proteasome activity and elevating p27Kip1, p21Cip1/WAF1, and Bax proteins. *J Biol Chem* 279(14): 13496-505.

Chung, W.G., Miranda, C.L., Stevens, J.F. i Maier, C.S. (2009). Hop proanthocyanidins induce apoptosis, protein carbonylation, and cytoskeleton disorganization in human colorectal adenocarcinoma cells via reactive oxygen species. *Food Chem Toxicol* 47(4): 827-36.

Dauer, A., Hensel, A., Lhoste, E., Knasmuller, S. i Mersch-Sundermann, V. (2003). Genotoxic and antigenotoxic effects of catechin and tannins from the bark of Hamamelis virginiana L. in metabolically competent, human hepatoma cells (Hep G2) using single cell gel electrophoresis. *Phytochemistry* 63(2): 199-207.

Dhakshinamoorthy, S., Long, D.J., 2nd i Jaiswal, A.K. (2000). Antioxidant regulation of genes encoding enzymes that detoxify xenobiotics and carcinogens. *Curr Top Cell Regul* 36: 201-16.

Elbling, L., Weiss, R.M., Teufelhofer, O., Uhl, M., Knasmueller, S., Schulte-Hermann, R., Berger, W. i Micksche, M. (2005). Green tea extract and (-)-epigallocatechin-3-gallate, the major tea catechin, exert oxidant but lack antioxidant activities. *Faseb J* 19(7): 807-9.

Elsaba, T.M., Martinez-Pomares, L., Robins, A.R., Crook, S., Seth, R., Jackson, D., McCart, A., Silver, A.R., Tomlinson, I.P. i Ilyas, M. (2010). The stem cell marker CD133 associates with enhanced colony formation and cell motility in colorectal cancer. *PLoS One* 5(5): e10714.

Engelbrecht, A.M., Mattheyse, M., Ellis, B., Loos, B., Thomas, M., Smith, R., Peters, S., Smith, C. i Myburgh, K. (2007). Proanthocyanidin from grape seeds inactivates the PI3-kinase/PKB pathway and induces apoptosis in a colon cancer cell line. *Cancer Lett* 258(1): 144-53.

Foti, M.C., Daquino, C. i Geraci, C. (2004). Electron-transfer reaction of cinnamic acids and their methyl esters with the DPPH(*) radical in alcoholic solutions. *J Org Chem* 69(7): 2309-14.

Gosse, F., Guyot, S., Roussi, S., Lobstein, A., Fischer, B., Seiler, N. i Raul, F. (2005). Chemopreventive properties of apple procyanidins on human colon cancer-derived metastatic SW620 cells and in a rat model of colon carcinogenesis. *Carcinogenesis* 26(7): 1291-5.

Habtemariam, S. (2002). Hamamelitannin from Hamamelis virginiana inhibits the tumour necrosis factor-alpha (TNF)-induced endothelial cell death in vitro. *Toxicon* 40(1): 83-8.

Halliwell, B. (2003). Oxidative stress in cell culture: an under-appreciated problem? *FEBS Lett* 540(1-3): 3-6.

Hartisch, C., Kolodziej, H. i von Bruchhausen, F. (1997). Dual inhibitory activities of tannins from Hamamelis virginiana and related polyphenols on 5-lipoxygenase and lyso-PAF: acetyl-CoA acetyltransferase. *Planta Med* 63(2): 106-10.

Havens, C.G., Ho, A., Yoshioka, N. i Dowdy, S.F. (2006). Regulation of late G1/S phase transition and APC Cdh1 by reactive oxygen species. *Mol Cell Biol* 26(12): 4701-11.

Ho, L.L., Chen, W.J., Lin-Shiau, S.Y. i Lin, J.K. (2002). Penta-O-galloyl-beta-D-glucose inhibits the invasion of mouse melanoma by suppressing metalloproteinase-9 through down-regulation of activator protein-1. *Eur J Pharmacol* 453(2-3): 149-58.

Hoverman, J.R., Cartwright, T.H., Patt, D.A., Espirito, J.L., Clayton, M.P., Garey, J.S., Kopp, T.J., Kolodziej, M., Neubauer, M.A., Fitch, K., Pyenson, B. i Beveridge, R.A. (2011). Pathways, outcomes, and costs in colon cancer: retrospective evaluations in 2 distinct databases. *Am J Manag Care* 17 Suppl 5 Developing: SP45-52.

Hu, H., Chai, Y., Wang, L., Zhang, J., Lee, H.J., Kim, S.H. i Lu, J. (2009a). Pentagalloylglucose induces autophagy and caspase-independent programmed deaths in human PC-3 and mouse TRAMP-C2 prostate cancer cells. *Mol Cancer Ther* 8(10): 2833-43.

Hu, H., Lee, H.J., Jiang, C., Zhang, J., Wang, L., Zhao, Y., Xiang, Q., Lee, E.O., Kim, S.H. i Lu, J. (2008). Penta-1,2,3,4,6-O-galloyl-beta-D-glucose induces p53 and inhibits STAT3 in prostate cancer cells in vitro and suppresses prostate xenograft tumor growth in vivo. *Mol Cancer Ther* 7(9): 2681-91.

Hu, H., Zhang, J., Lee, H.J., Kim, S.H. i Lu, J. (2009b). Penta-O-galloyl-beta-D-glucose induces S- and G(1)-cell cycle arrests in prostate cancer cells targeting DNA replication and cyclin D1. *Carcinogenesis* 30(5): 818-23.

Huh, J.E., Lee, E.O., Kim, M.S., Kang, K.S., Kim, C.H., Cha, B.C., Surh, Y.J. i Kim, S.H. (2005). Penta-O-galloyl-beta-D-glucose suppresses tumor growth via inhibition of angiogenesis and stimulation of apoptosis: roles of cyclooxygenase-2 and mitogen-activated protein kinase pathways. *Carcinogenesis* 26(8): 1436-45.

Iacomino, G., Medici, M.C., Napoli, D. i Russo, G.L. (2006). Effects of histone deacetylase inhibitors on p55CDC/Cdc20 expression in HT29 cell line. *J Cell Biochem* 99(4): 1122-31.

Jerez, M., Touriño, S., Sineiro, J., Torres, J.L. i Núñez, M.J. (2007). Procyanidins from pine bark: Relationships between structure, composition and antiradical activity. *Food Chemistry* 104(2): 518-527.

Jiang, Z.-Y., Hunt, J.V. i Wolff, S.P. (1992). Ferrous ion oxidation in the presence of xylenol orange for detection of lipid hydroperoxide in low density lipoprotein. *Analytical Biochemistry* 202(2): 384-389.

Kuo, P.T., Lin, T.P., Liu, L.C., Huang, C.H., Lin, J.K., Kao, J.Y. i Way, T.D. (2009). Penta-O-galloyl-beta-D-glucose suppresses prostate cancer bone metastasis by transcriptionally repressing EGF-induced MMP-9 expression. *J Agric Food Chem* 57(8): 3331-9.

Lizárraga, D., Touriño, S., Reyes-Zurita, F.J., de Kok, T.M., van Delft, J.H., Maas, L.M., Briede, J.J., Centelles, J.J., Torres, J.L. i Cascante, M. (2008). Witch hazel (Hamamelis virginiana) fractions and the importance of gallate moieties--electron transfer capacities in their antitumoral properties. *J Agric Food Chem* 56(24): 11675-82.

Long, L.H., Clement, M.V. i Halliwell, B. (2000). Artifacts in cell culture: rapid generation of hydrogen peroxide on addition of (-)-epigallocatechin, (-)-epigallocatechin gallate, (+)-catechin, and quercetin to commonly used cell culture media. *Biochem Biophys Res Commun* 273(1): 50-3.

Lozano, C., Torres, J.L., Julia, L., Jimenez, A., Centelles, J.J. i Cascante, M. (2005). Effect of new antioxidant cysteinyl-flavanol conjugates on skin cancer cells. *FEBS Lett* 579(20): 4219-25.

Maldonado-Celisa, M.E., Roussia, S., Foltzer-Jourdainne, C., Gosse, F., Lobstein, A., Habold, C., Roessner, A., Schneider-Stock, R. i Raul, F. (2008). Modulation by polyamines of apoptotic pathways triggered by procyanidins in human metastatic SW620 cells. *Cell Mol Life Sci* 65(9): 1425-34.

Masaki, H., Atsumi, T. i Sakurai, H. (1993). Evaluation of superoxide scavenging activities of hamamelis extract and hamamelitannin. *Free Radic Res Commun* 19(5): 333-40.

Masaki, H., Atsumi, T. i Sakurai, H. (1995). Protective activity of hamamelitannin on cell damage induced by superoxide anion radicals in murine dermal fibroblasts. *Biol Pharm Bull* 18(1): 59-63.

McDougall, G.J., Ross, H.A., Ikeji, M. i Stewart, D. (2008). Berry extracts exert different antiproliferative effects against cervical and colon cancer cells grown in vitro. *J Agric Food Chem* 56(9): 3016-23.

Miyamoto, K., Kishi, N., Koshiura, R., Yoshida, T., Hatano, T. i Okuda, T. (1987). Relationship between the structures and the antitumor activities of tannins. *Chem Pharm Bull (Tokyo)* 35(2): 814-22.

Mosmann, T. (1983). Rapid colorimetric assay for cellular growth and survival: application to proliferation and cytotoxicity assays. *J Immunol Methods* 65(1-2): 55-63.

Moyer, M.P., Manzano, L.A., Merriman, R.L., Stauffer, J.S. i Tanzer, L.R. (1996). NCM460, a normal human colon mucosal epithelial cell line. *In Vitro Cell Dev Biol Anim* 32(6): 315-7.

Mutanen, M., Pajari, A.M., Paivarinta, E., Misikangas, M., Rajakangas, J., Marttinen, M. i Oikarinen, S. (2008). Berries as chemopreventive dietary constituents--a mechanistic approach with the ApcMin/+ mouse. *Asia Pac J Clin Nutr* 17 Suppl 1: 123-5.

Oh, G.S., Pae, H.O., Oh, H., Hong, S.G., Kim, I.K., Chai, K.Y., Yun, Y.G., Kwon, T.O. i Chung, H.T. (2001). In vitro anti-proliferative effect of 1,2,3,4,6-penta-O-galloyl-beta-D-glucose on human hepatocellular carcinoma cell line, SK-HEP-1 cells. *Cancer Lett* 174(1): 17-24.

Sakai, H., Yamada, Y., Shimizu, M., Saito, K., Moriwaki, H. i Hara, A. (2010). Genetic ablation of Tnfalpha demonstrates no detectable suppressive effect on inflammation-related mouse colon tumorigenesis. *Chem Biol Interact* 184(3): 423-430.

Sang, S., Hou, Z., Lambert, J.D. i Yang, C.S. (2005). Redox properties of tea polyphenols and related biological activities. *Antioxid Redox Signal* 7(11-12): 1704-14.

Sato, M., Toyazaki, H., Yoshioka, Y., Yokoi, N. i Yamasaki, T. (2010). Structural characteristics for superoxide anion radical scavenging and productive activities of green tea polyphenols including proanthocyanidin dimers. *Chem Pharm Bull (Tokyo)* 58(1): 98-102.

Singh, B.N., Shankar, S. i Srivastava, R.K. (2011). Green tea catechin, epigallocatechin-3-gallate (EGCG): Mechanisms, perspectives and clinical applications. *Biochem Pharmacol*.

Theodoratou, E., Kyle, J., Cetnarskyj, R., Farrington, S.M., Tenesa, A., Barnetson, R., Porteous, M., Dunlop, M. i Campbell, H. (2007). Dietary flavonoids and the risk of colorectal cancer. *Cancer Epidemiol Biomarkers Prev* 16(4): 684-93.

Torres, J.L., Carreras, A., Jimenez, A., Brillas, E., Torrelles, X., Rius, J. i Julia, L. (2007). Reducing power of simple polyphenols by electron-transfer reactions using a new stable radical of the PTM series, tris(2,3,5,6-tetrachloro-4-nitrophenyl)methyl radical. *J Org Chem* 72(10): 3750-6.

Torres, J.L., Varela, B., Brillas, E. i Julia, L. (2003). Tris(2,4,6-trichloro-3,5-dinitrophenyl)methyl radical: a new stable coloured magnetic species as a chemosensor for natural polyphenols. *Chem Commun (Camb)*(1): 74-5.

Touriño, S., Lizárraga, D., Carreras, A., Lorenzo, S., Ugartondo, V., Mitjans, M., Vinardell, M.P., Julia, L., Cascante, M. i Torres, J.L. (2008). Highly galloylated tannin fractions from witch hazel (Hamamelis virginiana) bark: electron transfer capacity, in vitro antioxidant activity, and effects on skin-related cells. *Chem Res Toxicol* 21(3): 696-704.

Vennat, B., Pourrat, H., Pouget, M.P., Gross, D. i Pourrat, A. (1988). Tannins from Hamamelis virginiana: Identification of Proanthocyanidins and Hamamelitannin Quantification in Leaf, Bark, and Stem Extracts. *Planta Med* 54(5): 454-7.

Wasilewicz, M.P., Kolodziej, B., Bojulko, T., Kaczmarczyk, M., Sulzyc-Bielicka, V., Bielicki, D. i Ciepiela, K. (2010). Overexpression of 5-lipoxygenase in sporadic colonic adenomas and a possible new aspect of colon carcinogenesis. *Int J Colorectal Dis* 25(9): 1079-85.

Yang, C.S., Wang, H., Li, G.X., Yang, Z., Guan, F. i Jin, H. (2011). Cancer prevention by tea: Evidence from laboratory studies. *Pharmacol Res* 64(2): 113-22.

CAPÍTOL 2

Els polifenols majoritaris en té verd inhibeixen la diferenciació induïda per butirat mitjançant interacció amb el Transportador Monocarboxílic 1 (MCT1)

Susana Sánchez-Tena[1], Pedro Vizán[1, †], Pradeep K. Dudeja[2], Josep J. Centelles[1] i Marta Cascante[1]

[1]Departament de Bioquímica i Biologia Molecular, Facultat de Biologia, Universitat de Barcelona, Institut de Biomedicina de la Universitat de Barcelona (IBUB), Unitat associada al CSIC, Barcelona, Espanya

[2]Section of Digestive Diseases and Nutrition, Department of Medicine, University of Illinois at Chicago and Jesse Brown VA Medical Center, Chicago, USA

[†]Adreça actual: Laboratory of Developmental Signaling, Cancer Research UK. London Research Institute, London WC2A 3LY, United Kingdom

RESUM

Una dieta rica en fibra dietètica i compostos derivats de plantes com són els polifenols ha estat inversament relacionada amb el risc de càncer de còlon. L'efecte protector d'aquests compostos bioactius es veu afectat per la microbiota. Recentment, s'ha mostrat que els polifenols naturals augmenten la concentració intestinal de productes derivats de la fermentació microbiana de la fibra com és el butirat, un conegut inhibidor de les histones deacetilases (HDACs) que indueix diferenciació en cèl·lules de càncer de còlon. En aquest estudi, es va avaluar l'efecte de les catequines del té verd, (-)-epicatequina (EC) i (-)-epigal·locatequin gal·lat (EGCG), en la diferenciació de cèl·lules HT29 d'adenocarcinoma de còlon humà induïda per NaB. Tot i que el tractament amb polifenols sols no va modificar la diferenciació de les cèl·lules HT29, aquest va reduir la diferenciació induïda per NaB. L'ús d'un altre inhibidor de les HDACs, la Tricostatina A (TSA), el qual també va produir diferenciació que no va ser afectada pels polifenols, i la determinació de l'activitat HDAC *in vitro*, la qual no va ser afectada pels polifenols, van eliminar un mecanisme dependent d'HDAC. Estudis posteriors van revelar una disminució en l'entrada cel·lular de NaB produïda pel tractament amb polifenols. Això ens va portar a estudiar el Transportador Monocarboxílic 1 (MCT1 - *Monocarboxylate Transporter 1*), el qual ha estat descrit com a transportador intestinal del NaB. Mentre que les catequines del té verd no van produir canvis en l'expressió del MCT1, aquestes van regular la funció del MCT1 a través de la seva reorganització a la membrana plasmàtica augmentant la seva presència en fraccions no corresponents a *rafts* lípidics. Els nostres descobriments revelen que, per mantenir els seus efectes beneficiosos, el NaB i els polifenols del té verd han de ser utilitzats separadament. Aquesta informació s'hauria de tenir en compte per al disseny de noves intervencions terapèutiques en la prevenció o el tractament del càncer colorectal.

Green tea polyphenols inhibit butyrate-induced colon cancer cells differentiation by interacting with Monocarboxilate Transporter 1 (MCT1)

Susana Sánchez-Tena[1], Pedro Vizán[1, †], Pradeep K. Dudeja[2], Josep J. Centelles[1,] and Marta Cascante[1]

[1]Department of Biochemistry and Molecular Biology, Faculty of Biology, Universitat de Barcelona, Institute of Biomedicine of Universitat de Barcelona (IBUB) and CSIC-Associated Unit Barcelona, Spain

[2]Section of Digestive Diseases and Nutrition, Department of Medicine, University of Illinois at Chicago and Jesse Brown VA Medical Center, 820 South Damen Avenue, Chicago, IL 60612, USA.

[†]Present address: Laboratory of Developmental Signaling, Cancer Research UK

London Research Institute, London WC2A 3LY, United Kingdom.

ABSTRACT

A diet rich in dietetic fiber and plant-derived compounds such as polyphenols has been inversely related to colon cancer risk. The protective effects of these bioactive compounds are mediated by the microbiota. Recently, it has been shown that natural polyphenols increase dietary fiber microbial fermentation derived products such as butyrate, a well-described histone deacetylase (HDAC) inhibitor that induces differentiation in colon cancer cells. In this study, we evaluated the effect of the green tea polyphenols, (-)-epicatechin (EC) and (-)-epigallocatechin gallate (EGCG), on human colon adenocarcinoma HT29 cells NaB-induced differentiation. Although polyphenols treatment did not modify HT29 differentiation, it reduced NaB-induced differentiation. The use of another HDAC inhibitor, Trichostatin A (TSA), which also caused differentiation but was not affected by polyphenols, and *in vitro* HDAC activity determination, in which polyphenols did not shown any effect, rule out an HDAC-dependent mechanism. Posterior studies revealed uptake competition between NaB and polyphenols. This led us to study the Monocarboxilate Transporter 1 (MCT1), which has been described as a transporter for both NaB and poyphenols. Whereas green tea catechins did not produce changes in MCT1 expression, they resulted to modulate MCT1 function via its reorganization in the plasma membrane enhancing its presence in non-raft fractions. Our findings suggest that to maintain their beneficial effects, NaB and green tea polyphenols have to be used separately. This valuable information should be of assistance in choosing a rational design for more effective therapeutic interventions in the prevention or treatment of colorectal cancer.

INTRODUCTION

Colorectal cancer (CRC) constitutes one of the most frequent malignancies worldwide and is one of the prevalent causes of cancer-related mortality in the western world (Jemal *et al.*, 2010). Therefore, further development of therapeutic and preventive approaches to control this disease is clearly needed. A diet rich in fiber and plant-derived compounds present in tea, fruits and vegetables has been inversely associated with the risk of colorectal cancer (Ferguson *et al.*, 2001; Watson *et al.*, 2011). Furthermore, the protective effect of the bioactive compounds present in these aliments has been shown to be related to the human intestinal microbiota activity. In this regard, consumption of natural polyphenols has been described to be able to increase dietary fiber microbial fermentation derived products such as butyrate (NaB - Sodium butyrate) (Juskiewicz *et al.*, 2011; Kosmala *et al.*, 2011; Juskiewicz *et al.*, 2012), thus providing a beneficial effect to the host. However, how NaB and polyphenols interact at cellular level has not been satisfactorily addressed.

NaB has been described as a potent antitumoral agent against colon cancer that has been even used in clinical trials for treating cancers (Berni Canani *et al.*, 2012). NaB is a four-carbon short chain fatty acid that represents a major oxidative fuel for colon epithelial cells (Corfe *et al.*, 2009). Previous studies have demonstrated that deficiency in the availability or utilization of NaB causes colitis and may be involved in ulcerative colitis and colon carcinogenesis (Boren *et al.*, 2003; Alcarraz-Vizan *et al.*, 2010). Moreover, NaB induces apoptosis and a cell cycle arrest in the G1/G0 phase accompanied by terminal cell differentiation in several colon cancer cell lines (Shen *et al.*, 2008; Andriamihaja *et al.*, 2009; Humphreys *et al.*, 2012). The mechanisms of action of butyrate to induce differentiation involves mainly an epigenetic regulation of gene expression through the inhibition of histone deacetylases (HDACs) (Carafa *et al.*, 2011), which remove acetyl groups from lysine residues of histones and regulate the affinity of protein transcription complexes for DNA. Genes causing cell differentiation are normally downregulated by HDAC activity.

Numerous studies have evaluated the antitumor activities of green tea polyphenols in different experimental systems and the observations have shown that these tea components lead to cancer cell growth inhibition, apoptosis, and reduction in invasion, angiogenesis and metastasis (Kanwar *et al.*, 2012). A plethora of molecular mechanisms of tea polyphenols has been suggested, which include both anti-oxidant and pro-oxidant effects, inhibition of mitogen-activated protein kinases, or modulation of growth factor receptor tyrosine kinases and transporters activity through the alteration of lipid rafts by tea catechins (reviewed in ref. 16) (Yang *et al.*, 2010). However, little is known about the role of green tea polyphenols in

intestinal epithelial differentiation of colon cancer cells. Although they have been related to cell differentiation, their modulation is largely dependent on the cell type. For example, tea catechins have been shown to enhance the differentiation of normal human keratinocytes (Balasubramanian *et al.*, 2007). However, EGCG also has been reported to inhibit the formation and differentiation of osteoclasts (Oka *et al.*, 2012) and to reduce endothelial differentiation (Lamy *et al.*, 2002). In colon cancer cells, differentiation produced by polyphenols has been also reported to be dependent on the cell line (Lea *et al.*, 2010).

In the present study, we evaluated the effect of the major green tea polyphenols (-) -epigallocatechin gallate (EGCG) and (-)-epicatechin (EC) on differentiation induced by NaB in human colon adenocarcinoma HT29 cells. We demonstrate that polyphenols interfere with NaB induced differentiation and we propose a mechanism for this inhibition based on the re-localization of a monocarboxylate transporter in the plasma membrane.

MATERIALS AND METHODS

Chemicals and cell culture conditions. All chemicals were purchased from Sigma-Aldrich Co (St. Louis, MO), unless otherwise specified.

HT29 human colon adenocarcinoma cells (obtained from the American Type Culture Collection) were grown in Dulbecco's Modified Eagle's Medium (DMEM) 25 mM D-glucose supplemented with 10% heat-inactivated fetal calf serum (FCS) (PAA Laboratories, Pasching, Austria) and 0.1% antibiotics (100 U/mL penicillin and 100 µg/mL streptomycin) (Invitrogen, Paisley, UK). Caco-2 cells were maintained in DMEM 25 mM D-glucose, 20% FCS, 2 mM glutamine, and 1% antibiotics (100 U/mL penicillin and 100 µg/mL streptomycin). Cell cultures were carried out at 37 °C in a humidified atmosphere with 5% CO2.

Determination of cell viability. The assay is based upon the principle of reduction of MTT into blue formazan pigments by viable mitochondria in healthy cells. HT29 cells were seeded at 3×10^3 cells cells/well in 96-well flat-bottom plates. After 24 h of incubation at 37ºC, fresh media containing EC and EGCG at different concentrations were added. After 72 hours, the media was removed, and 50 µL of MTT (1 mg/mL in PBS) with 50 µL of fresh medium was added to each well and incubated for 1 h. The MTT reduced to blue formazan and the precipitate was dissolved in 100 µL of DMSO. Absorbance values were measured on an ELISA plate reader (550 nm) (Tecan Sunrise MR20-301, Tecan, Salzburg, Austria). Absorbance was taken as proportional to the number of living cells.

Alkaline Phosphatase Activity assay. Alkaline phosphatase activity was measured using p-nitrophenyl phosphate as substrate according to the published procedures (Bergmeyer, 1972). HT29 human colon adenocarcinoma cells were started in 60 cm^2 petri dishes with the same number of cells (6×10^5) and incubated for 24 h at 37°C. Then, new medium with polyphenols, NaB and NaB/polyphenols was added and incubated for 24, 48 and 72 h at 37°C. The medium was changed every 24 h. After incubation, the cells were washed with phosphate buffered saline (PBS), detached from the flasks using 0.025% trypsin-EDTA (Invitrogen) and then resuspended in lysis buffer (1 mM dithiothreitol, 1 mM EDTA, 0.02% Triton X-100, 0.02% sodium deoxycholate, 0.2 mM phenylmethylsulfonyl fluoride, 1% sodium azide and 20 mM Tris-HCl, pH 7.5). Cells were homogenized using a laboratory sonicator (1/2 Liter Branson 200 Ultrasonic bath, 5 min, 40 kHz, 4ºC) and immediately ultracentrifuged at 105,000g for 1 h at 4ºC. The supernatant was separated and used for the determination of alkaline phosphatase activity using a Cobas Mira Plus chemistry analyzer (HORIBA ABX, Montpellier, France). The enzyme activity was estimated by measuring the absorbance at 405 nm due to formation of p-nitrophenol and was expressed as mU/ml per mg of protein. Protein determination was performed in the same lysates using the BCA protein assay (Pierce Biotechnology, Rockford, IL).

Histone deacetylase (HDAC) assay. HT29 cells were incubated in 60 cm^2 petri dishes for 48-72 h at 37°C (65-85% confluence). Next, cells were washed in PBS pH 7.4 followed by incubation in hypotonic buffer (20 mM HEPES pH 7.6, 20% glycerol, 10 mM NaCl, 1.5 mM $MgCl_2$, 0.2 mM EDTA, 0.1% Triton X-100) for 5 min. Then, cells were collected and nuclei pelleted at 1000 rpm in microfuge for 10 minutes. Purified nuclei were resuspended in hypertonic buffer (20 mM HEPES pH 7.6, 20% glycerol, 450 mM NaCl, 1.5 mM $MgCl_2$, 0.2 mM EDTA, 0.1% Triton X-100) and rocked for 1 hour at 4ºC. After centrifuging at 13000 rpm in microfuge for 5 minutes at 4ºC, the supernatant obtained was the nuclear extract. Then, nuclear extracts of non-treated HT29 cells were quantified by using standard BCA Protein Assay (Pierce Biotechnology, Rockford, IL) and same quantity of protein was subjected to treatment with NaB and NaB/polyphenols for 30 min at 37°C. HDAC activity was measured employing a Fluorometric Assay Kit (Biovision), following manufacturer's instructions. The procedure involves the use of the HDAC substrate, which consists of an acetylated lysine side chain, and incubation with a sample containing nuclear extract. Deacetylation sensitizes the substrate, and treatment with the lysine developer produces a fluorophore, which can be analyzed with a fluorometer (Ex/Em = 350 - 380/440 - 460 nm). A HeLa cell nuclear extract was used as a positive control. Percent inhibition of treated cells was compared with HT29 untreated controls.

[^{14}C]-NaB uptake. HT29 cells were seeded at 2 × 10^4 cells/well in 24-well plates. After 24 h of incubation at 37ºC, fresh media containing NaB and NaB/polyphenols was added and incubated for 48 h at 37°C. The medium was changed after 24 h of incubation and left 24 h more. Next, cells were incubated at room temperature for 20 min in tracer-free buffer containing (in mM): 110 NaCl, 1 $CaCl_2$, 4 KCl, 0.44 K_2HPO_4, 1 $MgSO_4$, 5 glucose, 50 mannitol and 5 HEPES, pH 7.4. Cells were then washed and incubated with buffer containing (in mM): 259 mannitol, 20 HEPES, pH 6.5 and 1 [^{14}C]-NaB (1 μCi/ml) for a time period of 5 min. The uptake was stopped by washing the cells twice with ice-cold PBS. Finally, cells were solubilized with 0.5 N NaOH for at least 4 h. The protein concentration was measured by the method of BCA. Incorporated radioactivity was counted by a Tri-CARB 1600-TR liquid scintillation counter (Packard Instruments, Downers Grove, IL). The values were expressed as nmol/mg protein per 5 min.

Transient transfection and luciferase assay. Cloning of the MCT1 promoter region and preparation of its progressive 5′ deletion constructs in pGL2 reporter plasmid have been described earlier (Hadjiagapiou *et al.*, 2005). Caco-2 cells were transfected using the Amaxa Nucleofector System (Amaxa) according to the manufacturer's instructions. Briefly, 2 × 10^6 cells were harvested and then were electroporated in 100 μl of solution T (supplied by Amaxa) with MCT1 promoter-luciferase construct. The cells were then transferred to full media and plated on a 24-well plate. 24 hours after transfection, fresh medium containing NaB and polyphenols were added. After 24 h of incubation, cells were processed as indicated in Luciferase Assay System kit from Promega (Madison, WI). Luciferase activities were measured 48h post transfection using GLOMAX Luminometer (Promega) and expressed as percent of the control. Protein concentrations were determined using Bradford Assay (Bio-Rad). The promoter activity was expressed as a ratio of luciferase activity to protein in each sample.

Cell lysates and Western blotting. 6 × 10^5 HT29 cells were plated on 60 cm^2 petri dishes and incubated for 24 h. Then, fresh medium with NaB and NaB/polyphenols was added and incubated for 48 h. After incubation, the cells were washed with ice-cold PBS and lysed in 20 mM Tris·HCl, pH 7.5, 150 mM NaCl, 1% Triton X-100, 1 mM EDTA, 1 mM EGTA, and 1× complete protease inhibitor cocktail. The lysate was sonicated and centrifuged at 5000 g for 5 min at 4°C, and protein concentration was determined by Bradford. The samples obtained above were subjected to 10% SDS-PAGE and transferred to nitrocellulose membranes. MCT1 expression was detected utilizing human anti MCT1 antibody (Santa Cruz Biotechnology, sc-50324). Flotillin expression was analyzed using human anti flotillin antibody (BD Transduction Laboratories, 610820). Beta-actin was used as a loading control (MP Biomedicals, Eschwege, Germany, 69100).

Rafts isolation and biochemical characterization. Lipid rafts were isolated by flotation on OptiPrep density gradient as previously described (Qiu *et al.*, 2011). HT29 human colon adenocarcinoma cells were started in 60 cm^2 petri dishes with the same number of cells (6×10^5) and incubated for 24 h at 37°C. Then, cells were exposed to or not exposed to NaB or NaB/polyphenols for 48 h. After incubation, cells were resuspended, and incubated for 30 min at 4°C in TNE buffer containing (in mM) 25 Tris (pH 7.4), 150 NaCl, 5 EDTA, and 1% Triton X-100 supplemented with 1× Complete protease inhibitor cocktail. The membranes were then adjusted to 40% final concentration of OptiPrep and layered at the bottom of density gradient with steps of final concentrations of 35, 30, 25, and 20% of OptiPrep in TNE buffer. TNE buffer was laid on the top of the gradient, which was then centrifuged at 48,000 rpm for 4 h at 4°C. 1 ml fractions were collected from the top to the bottom of the gradient and then analyzed by Western blotting (see above). MCT1 and the described marker for lipid rafts, flotillin, were analyzed in each fraction (Zhao *et al.*, 2011).

Data Presentation and Statistical Analysis. Data are given as the means ± S.D. (standard deviation). For each assay, the parametric unpaired two-tailed independent sample t-test was used for statistical comparison with the untreated control cells and differences were considered to be significant when $p < 0.05$ or $p < 0.001$.

RESULTS

Inhibition of HT29 cell viability by EC and EGCG. To determine a non-toxic but still active concentration of EC and EGCG, HT29 cell viability was determined in the presence of different polyphenol concentrations (Figure 1). From the obtained dose-viability curve we estimated the inhibitory concentration 20 (IC_{20}) defined as the concentration of product that causes 20% of inhibition of cell viability respect to control non-treated cells viability after 72 hours. Although increasing concentrations of both EC and EGCG produced a dose-dependent decrease in cell viability, EGCG was much more efficient at doing so. The 72 hours IC_{20} values obtained were 100 μM for EC and 20 μM for EGCG. We used these concentrations along the study.

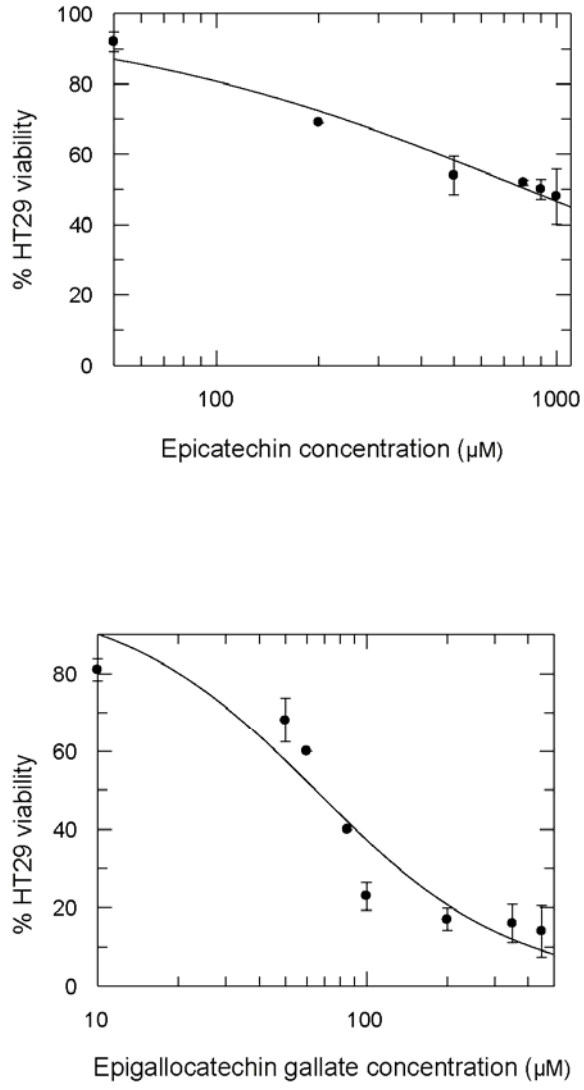

Figure 1. Dose-effect curves of EC and EGCG on cell viability. HT29 cell cultures were treated with increasing doses of EC (**A**) or EGCG (**B**) as indicated on the x axis for 72 hours. Cell viability was expressed as a percentage respect to untreated control. IC_{20} (EC) = 100 μM / IC_{20} (EGCG) = 20 μM.

Polyphenols reduce NaB-induced differentiation in colorectal adenocarcinoma cell lines. Firstly, we studied whether EC and EGCG affected NaB-induced differentiation. Cells were exposed to 2 mM NaB for 24, 48 and 72 hours, alone or in the presence of 100 μM EC and 20 μM EGCG. Measured as Alkaline Phosphatase (AP) activity, NaB-induced differentiation was reduced by both polyphenols at 48 and 72 hours of combined treatment (Figure 2A). EC was also able to reduce NaB-induced AP activity at 24 hours (Figure 2A). Worthy of note,

treatments with polyphenols alone did not have any impact on differentiation (Figure 2B). To discard a direct effect of the polyphenols on AP activity, we repeated the experiments measuring the activity of another differentiation marker (aminopeptidase N) at 48 hours. Consistently, polyphenols reduced NaB-induced differentiation (Supplemental Figure 1A) and did not show an increase in differentiation when used alone (Supplemental Figure 1B). This effect of polyphenols was also extended to another epithelial colorectal adenocarcinoma cell line, Caco-2, which showed the same differentiation profile regarding NaB and polyphenols treatment (Supplemental Figure 2A&B).

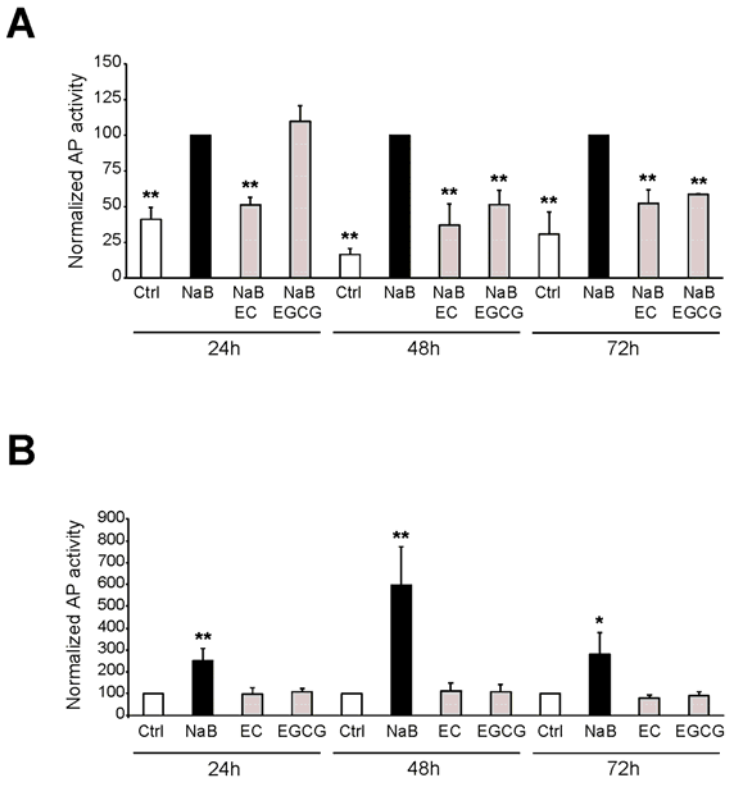

Figure 2. Polyphenols reduce butyrate-induced differentiation. (**A**) HT29 cells were treated with NaB 2 mM or with NaB and polyphenols EC 100 μM and EGCG 20 μM for 24, 48 and 72 hours and AP activity was measured and normalized by protein. The data are presented and statistically tested as AP activity normalized to NaB treated cells. (**B**) HT29 cells were treated with NaB 2 mM or with polyphenols alone (EC 100 μM and EGCG 20 μM) for 24, 48 and 72 hours and AP activity was measured. The data are presented and statistically tested as AP activity normalized to Ctr cells. All experiments were performed four times. * $p<0.05$, ** $p<0.01$.

Tea polyphenols effect on differentiation is not related to HDAC activity modulation. Given that the NaB-induced differentiation is provoked by its inhibitory capacity of HDAC activity (Waldecker *et al.*, 2008b), we decided to study the effects of EC and EGCG in HDAC-related differentiation. First, we studied whether polyphenols were able to modify the differentiation induced by Trichostatin A (TSA), another well-described HDAC inhibitor. HT29 cells were exposed to 180 nM TSA for 48 hours, alone or in presence of 100 μM EC and 20 μM EGCG. The addition of polyphenols to TSA did not have any impact on TSA-induced differentiation measured as AP activity (Figure 3A). Secondly, we determined directly the HDAC activity in nuclear extracts from HT29 cells after their incubation with NaB and polyphenols alone or in combination. In nuclear extracts from HT29 human colon adenocarcinoma cells, NaB was found to be a potent HDAC inhibitor, significantly decreasing the HDAC activity in a dose-dependent manner (55% and 67% reduction at 500 μM and 2 mM of NaB, respectively) (Figure 3B). On the contrary, none of the concentrations studied for EC and EGCG were able to inhibit significantly the HDAC activity in HT29 nuclear extracts (Figure 3B). Moreover, polyphenols do not produce any difference respect to the HDAC activity inhibition of NaB when cells were treated with both simultaneously (Figure 3C). These results led us to conclude that polyphenols are not affecting NaB differentiation by directly affecting HDAC activity.

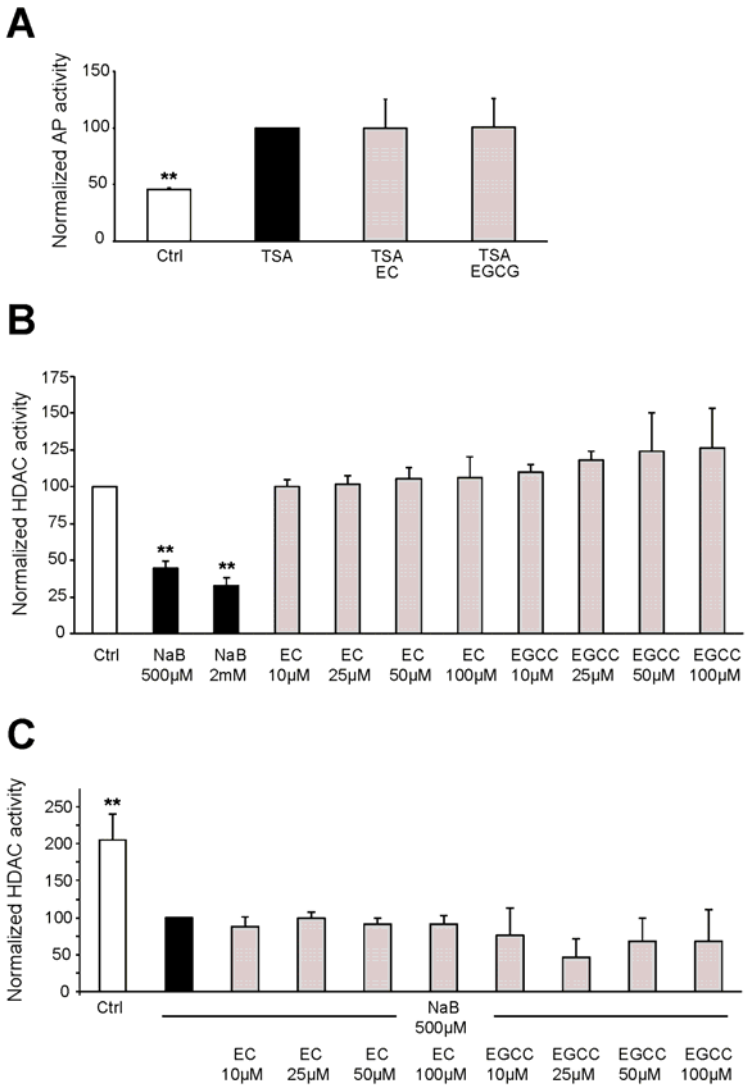

Figure 3. Polyphenols effect on differentiation is not HDAC-related. (**A**) HT29 human colon adenocarcinoma cells were treated with TSA at 180 nM or with TSA in the presence of polyphenols EC 100 μM and EGCG 20 μM for 48 hours and AP activity was measured. Data are presented as AP activity normalized and statistically tested to TSA treated cells. (**B**) HDAC activity determined in nuclear extracts from HT29 cells after treatment with NaB or NaB with polyphenols for X hours. The data are presented and statistically tested as HDAC activity normalized to non-treated (Ctr) cells. (**C**) HDAC activity determined in nuclear extracts from HT29 cells after treatment with NaB or polyphenols for X hours. The data are presented and statistically tested as HDAC activity normalized to Ctr cells. Mean ± S.D. from three independent experiments. * $p<0.05$, ** $p<0.01$.

Polyphenols impair NaB entry to the cell. To study the mechanism of interference between NaB and polyphenols we studied the cellular entry of NaB into HT29 cells. HT29 cells

were incubated with 2 mM NaB alone or in the presence of 100 μM EC and 20 μM EGCG for 48 hours and acute [^{14}C]-NaB incorporation was measured. NaB treatment slightly enhanced its own transport (Figure 4A). Interestingly, we observed a significant decrease in [^{14}C]-NaB cellular entry after NaB/polyphenols incubation respect to NaB-treated cells (Figure 4A).

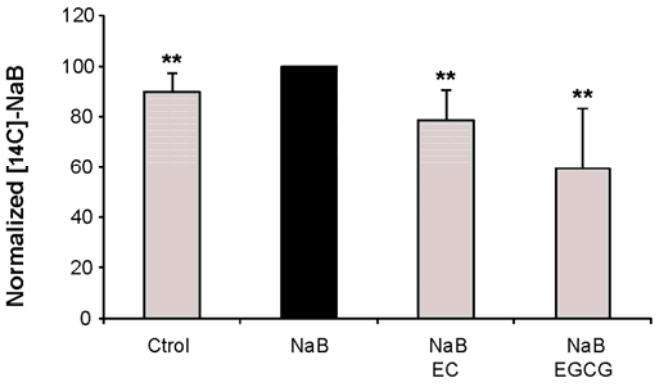

Figure 4. Polyphenols impair NaB entrance to the cell. HT29 cells were treated with NaB 2 mM or with NaB and polyphenols EC 100 μM and EGCG 20 μM for 72 hours. Acute [^{14}C]-NaB uptake was subsequently measured as described in Materials & Methods. Experiments were performed two times. ** $p<0.01$.

Tea polyphenols effect on NaB-induced differentiation is not related to MCT1 expression. Next, we decided to study the intestinal transporter Monocarboxilate Transporter 1 (MCT1) used for NaB transport (Saksena *et al.*, 2009). Firstly, we examined MCT1 promoter activity in response to NaB and polyphenols. Caco-2 cells were transiently transfected with MCT1 promoter-reporter construct. 24 hours posttransfection, cells were treated with NaB, polyphenols or a combination of both for 24 h and luciferase assays were performed 48 h posttransfection. Interestingly, NaB was able to significantly increase MCT1 promoter activity with an approximately fourfold augment compared with control (Figure 5A). In contrast, polyphenols alone did not affect MCT1 expression respect to the control cells (Figure 5A). When we combined NaB with polyphenols at IC_{20} concentration, the NaB-induced MCT1 expression was slightly but not significantly reduced (Figure 5A). Subsequently, we tested if these changes in expression could be also detected at protein level. Stinkingly, western blot

analysis of MCT1 showed that there were no differences at protein level in any of the treatments (Figure 5B), indicating post-transcriptional regulation of MCT1.

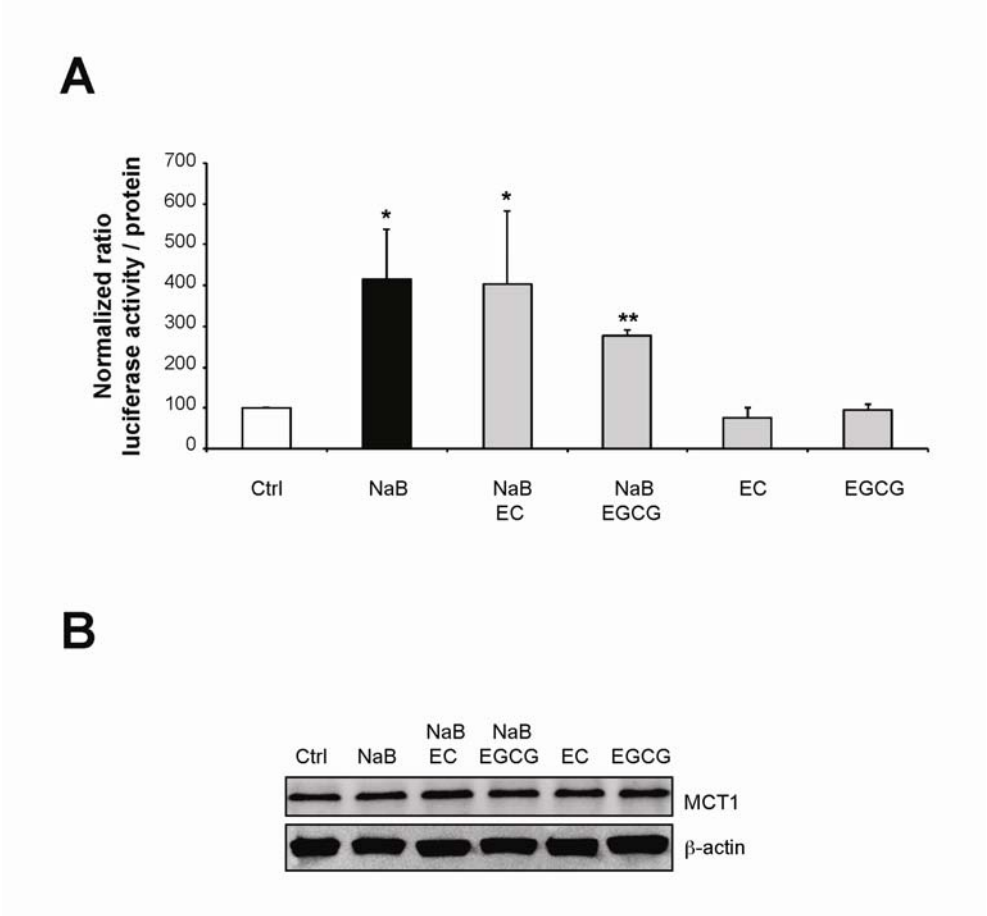

Figure 5. Effect of NaB and polyphenols on MCT1 expression. (**A**) Caco-2 cells were transiently transfected with the MCT1 promoter-luciferase construct, treated with NaB alone, polyphenols alone or a combination of both and the promoter activity was assessed by measuring luciferase activity and expressed as relative light units (RLU)/mg. Results represent means ± SD of two separate experiments performed in triplicate and are expressed as fold increase comparing treated transfected cells with transfected untreated ctr cells. * $p<0.05$, ** $p<0.01$ compared with control. (**B**) After X hours of NaB, polyphenols or both, Caco-2 lysates were probed against MCT-1 in a western blot, using beta-actin as a loading control. A representative blot is shown.

EC and EGCG reduce NaB-enhanced MCT1 raft localization in HT29 plasma membrane. Since polyphenols have been demonstrated to be lipid rafts regulators (Colin *et al.*, 2011), we next investigated whether EC and EGCG caused any alterations in the association of MCT1 with lipid rafts. Lipid-rich plasma membrane domains have been commonly isolated as

detergent-resistant membranes by flotation from denser material through a discontinuous or continuous density gradient. In this case, we used an OptiPrep density gradient. After centrifugation, proteins in the OptiPrep fractions can be directly analyzed by SDS-PAGE and Western Blot. As shown in Figure 6, MCT1 was predominantly expressed in high-density non-raft fractions of control HT29 cells, even though some MCT1 expression was found in lipid rafts-corresponding fractions. NaB treatment for 48 hours disrupted lipid raft organization partially, and at the same time enhanced the presence of MCT1 in low-density fractions representing lipid rafts. When polyphenols were added to NaB, MCT1 was redistributed in all fractions, counteracting NaB-induced localization of the transporter in the lipid rafts (Figure 6).

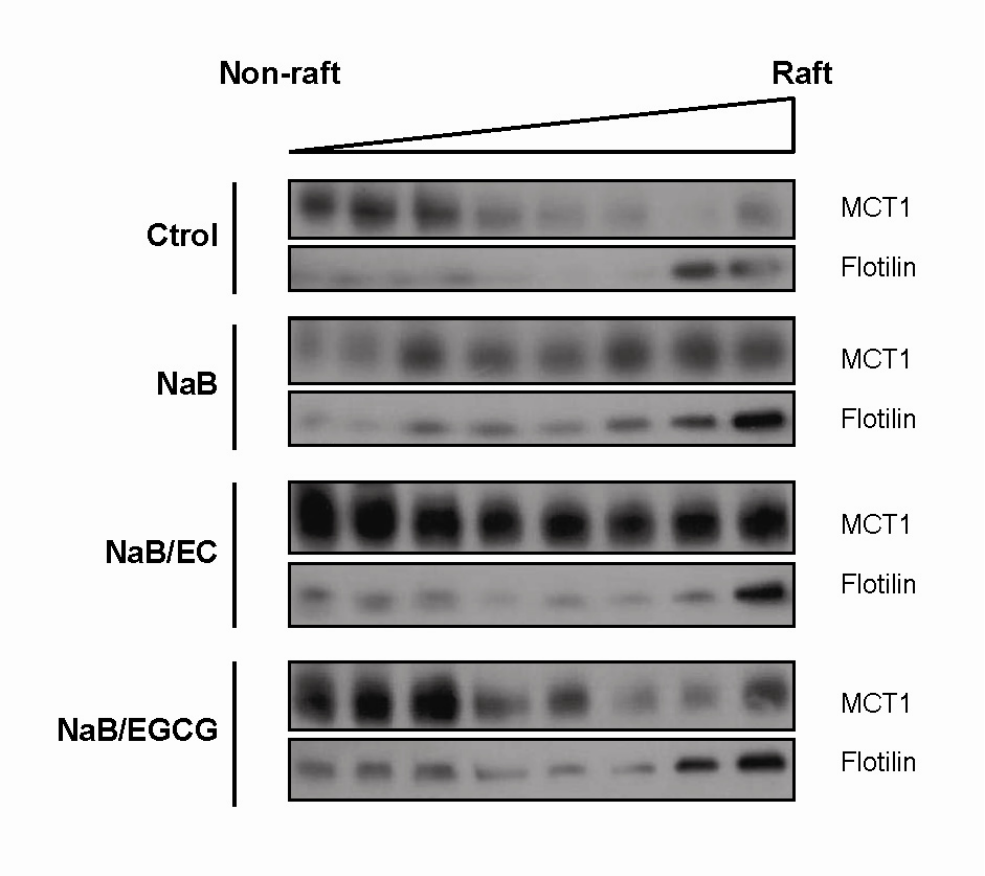

Figure 6. EC and EGCG antagonize plasma membrane redistribution of MCT1 caused by NaB. HT29 cells were incubated with NaB or NaB/polyphenols for 48 h and then lysed. Cellular membranes were laid at the bottom of OptiPrep density gradient and subjected to ultracentrifugation. Fractions were then collected from the top (low-density fractions) to the bottom of the gradient (high-density fractions). Proteins in the fractions were separated on 10% SDS-PAGE and blots were probed with anti-MCT1 or anti-flotillin antibodies.

DISCUSSION

In this study we analyze the effect of polyphenols on NaB-induced differentiation. We decided to use the IC_{20} concentrations at 72 hours (EC: 100μM, EGCG: 20μM) to avoid massive cell damage by polyphenols. Regarding NaB, we used a concentration of 2mM that has been described to be able to differentiate HT29 colon cancer cells (Alcarraz-Vizan *et al.*, 2010). Surprisingly, although treatment with EC and EGCG alone did not change cell differentiation, NaB-induced differentiation was reduced by both polyphenols. The mechanism of action of NaB in colon cancer mainly includes effects on differentiation via its inhibition of HDACs. EGCG has also been identified as an inhibitor of HDAC activity in prostate, skin and breast cancer cells (Waldecker *et al.*, 2008a). However, studies in HT29 cells revealed that there was no significant change in HDAC activity of cytoplasmic or nuclear fractions after sulforaphane and EGCG treatment (Nair *et al.*, 2008). Accordingly, we have not detected any significant inhibition of HDAC activity in vitro (Figure 3B), and the impairment of differentiation was not observed using TSA (Figure 3A), another well-known HDAC inhibitor also proposed as anti-tumor agent (Amoedo *et al.*, 2011).

The effect of polyphenols on NaB-induced differentiation could be due to an interaction between NaB and polyphenols that prevents the entry and cellular action of NaB. Determination of [^{14}C]-NaB uptake showed that whereas NaB treatment triggered its own transport, polyphenol treatment impaired NaB uptake (Figure 4). This result led us to study the activity of the aforementioned NaB intestinal transporter Monocarboxilate Transporter 1 (MCT1). It has been shown that MCT1 is located within the apical membrane of the intestinal tract where it is involved in the absorption of short chain fatty acids, such as NaB, into the colon. Short chain fatty acid can also enter cells rapidly by free diffusion of the undissociated acid, nevertheless its transport is strongly facilitated by MCT1 (Halestrap, 2012). As it has been mentioned before, NaB has antitumor properties in colorectal cancer and, as such, MCT1, which is involved in its transport, is considered a tumor suppressor gene. Hence, next step was the evaluation of MCT1 expression. MCT-1 luciferase reporter assays showed an increase in expression after NaB treatment, but not with the polyphenols alone (Figure 5A). This substrate-induced MCT1 activity by NaB has been previously demonstrated in AA/C1 human colonic epithelial cells (Cuff *et al.*, 2002) and colon cancer Caco-2 cells (Borthakur *et al.*, 2008). In contrast as expected, this reporter increase was not significantly inhibited by simultaneous treatment with polyphenols and, moreover, it not produced an increase in protein levels (Figure 5B).

Since we detected an increase in mRNA that did not result in an enhanced MCT1 protein, we sought for another mechanism to explain the effects on NaB-induced differentiation

produced by the polyphenols. Recent remarkable progresses indicate that optimal function of some transporters is dependent on its association with lipid rafts (Chen *et al.*, 2011). Interestingly, lipid rafts, defined as microdomains within the lipid bilayer of cellular membranes that assemble subsets of transmembrane or glycosylphosphatidylinisotol-anchored proteins and lipids (cholesterol and sphingolipids) and that experimentally resist extraction in cold detergent, have been related to some of the biological effects induced by tea polyphenols (Patra *et al.*, 2008). Concretely, EGCG has been shown to prevent activation of c-Met receptor (Duhon *et al.*, 2010) and epidermal growth factor receptor (EGFR) (Adachi *et al.*, 2007). Similarly, our analysis of lipid raft-dependent MCT1 function in HT29 cells indicated that NaB activate MCT1 function by enhancing its positioning in lipid rafts, and that tea polyphenols produce a redistribution of MCT1 in the non-lipid raft fractions (Figure 6). These observations made us to hypothesize that EGCG and EC might inhibit MCT1 NaB transport by altering lipid rafts organization. At the same time, this provides an explanation for the the observed increase in NaB uptake after NaB treatment (Figure 4), which could not be explained by changes in the quantity of protein MCT1 (Figure 5B), but due to the modulation of lipid rafts by 2 mM NaB (Figure 6).

It has been reported that the chemical structure of polyphenols is generally involved in their biological efficiency (Yang *et al.*, 2009). Concretely in green tea catechins, the most bioactive catechin has been describe to be EGCG containing a trihydroxyl structure in the D ring (gallate) and also a pyrogallol B-ring, followed closely by ECG with a gallate group, and then to a lesser extent EGC and EC that posses a basic structure (Ingolfsson *et al.*, 2011). However, our results for both green tea components, EC and EGCG, were very similar along the study.

The present study provides evidence that tea polyphenols EC and EGCG impair NaB uptake and the subsequent NaB-induced differentiation in HT29 cells. These novel findings suggest that although both NaB and green tea catechins have been reported to have a wide range of beneficial effects for human health, at cellular level they interfere, suggesting they may be used separately. Regarding the abovementioned studies about the increase in short chain fatty acids cecal concentration by polyphenols, when combined with a rich fiber diet, the raise in cecal NaB may compensate *in vivo* the inhibition of NaB uptake by polyphenols described here in case that NaB increase is related to a change of microbial activity enhancing NaB production. Moreover, the increased NaB cecal concentration may be also explained by the inhibitory action of polyphenols in NaB intestinal uptake. Further studies may be required to investigate the physiological relevance of our findings, which provides a better knowledge about the

interferences of prebiotics, and which should be of assistance in preparing a rational design for preventive and therapeutic interventions.

ACKNOWLEDGEMENTS

The authors thank Ursula Valls Benavides, Marta Camps Camprubi, Mireia Pérez Verdaguer and Anna Oliveras Martínez for technical support in the experiments. Financial support was provided by grants SAF2008-00164, SAF2011-25726, AGL2006-12210-C03-02/ALI, and AGL2009-12374-C03-03/ALI from the Spanish government Ministerio de Ciencia e Innovación and personal financial support (FPU program); from the Ministerio de Educación y Ciencia; and from the Red Temática de Investigación Cooperativa en Cáncer, Instituto de Salud Carlos III, Spanish Ministry of Science and Innovation & European Regional Development Fund (ERDF) "Una manera de hacer Europa" (ISCIII-RTICC grants RD06/0020/0046). We have also received financial support from the AGAUR-Generalitat de Catalunya (grant 2009SGR1308, 2009 CTP 00026, and Icrea Academia Award 2010 granted to M.C.) and the European Commission (FP7) ETHERPATHS KBBE-grant agreement no. 22263.

REFERENCES

Adachi, S., Nagao, T., Ingolfsson, H.I., Maxfield, F.R., Andersen, O.S., Kopelovich, L. i Weinstein, I.B. (2007). The inhibitory effect of (-)-epigallocatechin gallate on activation of the epidermal growth factor receptor is associated with altered lipid order in HT29 colon cancer cells. *Cancer Res* **67**(13): 6493-501.

Alcarraz-Vizan, G., Boren, J., Lee, W.N. i Cascante, M. (2010). Histone deacetylase inhibition results in a common metabolic profile associated with HT29 differentiation. *Metabolomics* **6**(2): 229-237.

Amoedo, N.D., Rodrigues, M.F., Pezzuto, P., Galina, A., da Costa, R.M., de Almeida, F.C., El-Bacha, T. i Rumjanek, F.D. (2011). Energy metabolism in H460 lung cancer cells: effects of histone deacetylase inhibitors. *PLoS One* **6**(7): e22264.

Andriamihaja, M., Chaumontet, C., Tome, D. i Blachier, F. (2009). Butyrate metabolism in human colon carcinoma cells: implications concerning its growth-inhibitory effect. *J Cell Physiol* **218**(1): 58-65.

Balasubramanian, S. i Ecker, R.L. (2007). Keratinocyte proliferation, differentiation, and apoptosis-Differential mechanisms of regulation by curcumin, EGCG and apigenin. *Toxicol Appl Pharmacol*.

Bergmeyer, H.U. (1972). Standardization of enzyme assays. *Clin Chem* **18**(11): 1305-11.

Berni Canani, R., Di Costanzo, M. i Leone, L. (2012). The epigenetic effects of butyrate: potential therapeutic implications for clinical practice. *Clin Epigenetics* **4**(1): 4.

Boren, J., Lee, W.N., Bassilian, S., Centelles, J.J., Lim, S., Ahmed, S., Boros, L.G. i Cascante, M. (2003). The stable isotope-based dynamic metabolic profile of butyrate-induced HT29 cell differentiation. *J Biol Chem* **278**(31): 28395-402.

Borthakur, A., Saksena, S., Gill, R.K., Alrefai, W.A., Ramaswamy, K. i Dudeja, P.K. (2008). Regulation of monocarboxylate transporter 1 (MCT1) promoter by butyrate in human intestinal epithelial cells: involvement of NF-kappaB pathway. *J Cell Biochem* **103**(5): 1452-63.

Carafa, V., Nebbioso, A. i Altucci, L. (2011). Histone deacetylase inhibitors: recent insights from basic to clinical knowledge & patenting of anti-cancer actions. *Recent Pat Anticancer Drug Discov* **6**(1): 131-45.

Colin, D., Limagne, E., Jeanningros, S., Jacquel, A., Lizard, G., Athias, A., Gambert, P., Hichami, A., Latruffe, N., Solary, E. i Delmas, D. (2011). Endocytosis of resveratrol via lipid rafts and activation of downstream signaling pathways in cancer cells. *Cancer Prev Res (Phila)* **4**(7): 1095-106.

Corfe, B.M., Williams, E.A., Bury, J.P., Riley, S.A., Croucher, L.J., Lai, D.Y. i Evans, C.A. (2009). A study protocol to investigate the relationship between dietary fibre intake and fermentation, colon cell turnover, global protein acetylation and early carcinogenesis: the FACT study. *BMC Cancer* **9**: 332.

Cuff, M.A., Lambert, D.W. i Shirazi-Beechey, S.P. (2002). Substrate-induced regulation of the human colonic monocarboxylate transporter, MCT1. *J Physiol* **539**(Pt 2): 361-71.

Chen, G., Howe, A.G., Xu, G., Frohlich, O., Klein, J.D. i Sands, J.M. (2011). Mature N-linked glycans facilitate UT-A1 urea transporter lipid raft compartmentalization. *Faseb J* **25**(12): 4531-9.

Duhon, D., Bigelow, R.L., Coleman, D.T., Steffan, J.J., Yu, C., Langston, W., Kevil, C.G. i Cardelli, J.A. (2010). The polyphenol epigallocatechin-3-gallate affects lipid rafts to block activation of the c-Met receptor in prostate cancer cells. *Mol Carcinog* **49**(8): 739-49.

Ferguson, L.R., Chavan, R.R. i Harris, P.J. (2001). Changing concepts of dietary fiber: implications for carcinogenesis. *Nutr Cancer* **39**(2): 155-69.

Hadjiagapiou, C., Borthakur, A., Dahdal, R.Y., Gill, R.K., Malakooti, J., Ramaswamy, K. i Dudeja, P.K. (2005). Role of USF1 and USF2 as potential repressor proteins for human intestinal monocarboxylate transporter 1 promoter. *Am J Physiol Gastrointest Liver Physiol* **288**(6): G1118-26.

Halestrap, A.P. (2012). The monocarboxylate transporter family--Structure and functional characterization. *IUBMB Life* **64**(1): 1-9.

Humphreys, K.J., Cobiac, L., Le Leu, R.K., Van der Hoek, M.B. i Michael, M.Z. (2012). Histone deacetylase inhibition in colorectal cancer cells reveals competing roles for members of the oncogenic miR-17-92 cluster. *Mol Carcinog*.

Ingolfsson, H.I., Koeppe, R.E., 2nd i Andersen, O.S. (2011). Effects of green tea catechins on gramicidin channel function and inferred changes in bilayer properties. *FEBS Lett* **585**(19): 3101-5.

Jemal, A., Center, M.M., DeSantis, C. i Ward, E.M. (2010). Global patterns of cancer incidence and mortality rates and trends. *Cancer Epidemiol Biomarkers Prev* **19**(8): 1893-907.

Juskiewicz, J., Milala, J., Jurgonski, A., Krol, B. i Zdunczyk, Z. (2011). Consumption of polyphenol concentrate with dietary fructo-oligosaccharides enhances cecal metabolism of quercetin glycosides in rats. *Nutrition* **27**(3): 351-7.

Juskiewicz, J., Zary-Sikorska, E., Zdunczyk, Z., Krol, B., Jaroslawska, J. i Jurgonski, A. (2012). Effect of dietary supplementation with unprocessed and ethanol-extracted apple pomaces on caecal fermentation, antioxidant and blood biomarkers in rats. *Br J Nutr* **107**(8): 1138-46.

Kanwar, J., Taskeen, M., Mohammad, I., Huo, C., Chan, T.H. i Dou, Q.P. (2012). Recent advances on tea polyphenols. *Front Biosci (Elite Ed)* **4**: 111-31.

Kosmala, M., Kolodziejczyk, K., Zdunczyk, Z., Juskiewicz, J. i Boros, D. (2011). Chemical composition of natural and polyphenol-free apple pomace and the effect of this dietary ingredient on intestinal fermentation and serum lipid parameters in rats. *J Agric Food Chem* **59**(17): 9177-85.

Lamy, S., Gingras, D. i Beliveau, R. (2002). Green tea catechins inhibit vascular endothelial growth factor receptor phosphorylation. *Cancer Res* **62**(2): 381-5.

Lea, M.A., Ibeh, C., Han, L. i Desbordes, C. (2010). Inhibition of growth and induction of differentiation markers by polyphenolic molecules and histone deacetylase inhibitors in colon cancer cells. *Anticancer Res* **30**(2): 311-8.

Nair, S., Hebbar, V., Shen, G., Gopalakrishnan, A., Khor, T.O., Yu, S., Xu, C. i Kong, A.N. (2008). Synergistic effects of a combination of dietary factors sulforaphane and (-) epigallocatechin-3-gallate in HT-29 AP-1 human colon carcinoma cells. *Pharm Res* **25**(2): 387-99.

Oka, Y., Iwai, S., Amano, H., Irie, Y., Yatomi, K., Ryu, K., Yamada, S., Inagaki, K. i Oguchi, K. (2012). Tea polyphenols inhibit rat osteoclast formation and differentiation. *J Pharmacol Sci* **118**(1): 55-64.

Patra, S.K., Rizzi, F., Silva, A., Rugina, D.O. i Bettuzzi, S. (2008). Molecular targets of (-)-epigallocatechin-3-gallate (EGCG): specificity and interaction with membrane lipid rafts. *J Physiol Pharmacol* **59 Suppl 9**: 217-35.

Qiu, Y., Wang, Y., Law, P.Y., Chen, H.Z. i Loh, H.H. (2011). Cholesterol regulates micro-opioid receptor-induced beta-arrestin 2 translocation to membrane lipid rafts. *Mol Pharmacol* **80**(1): 210-8.

Saksena, S., Theegala, S., Bansal, N., Gill, R.K., Tyagi, S., Alrefai, W.A., Ramaswamy, K. i Dudeja, P.K. (2009). Mechanisms underlying modulation of monocarboxylate transporter 1 (MCT1) by somatostatin in human intestinal epithelial cells. *Am J Physiol Gastrointest Liver Physiol* **297**(5): G878-85.

Shen, W.J., Dai, D.Q., Teng, Y. i Liu, J. (2008). [Effects of sodium butyrate on proliferation of human gastric cancer cells and expression of p16 gene]. *Zhonghua Yi Xue Za Zhi* **88**(17): 1192-6.

Waldecker, M., Kautenburger, T., Daumann, H., Busch, C. i Schrenk, D. (2008a). Inhibition of histone-deacetylase activity by short-chain fatty acids and some polyphenol metabolites formed in the colon. *J Nutr Biochem* **19**(9): 587-93.

Waldecker, M., Kautenburger, T., Daumann, H., Veeriah, S., Will, F., Dietrich, H., Pool-Zobel, B.L. i Schrenk, D. (2008b). Histone-deacetylase inhibition and butyrate formation: Fecal slurry incubations with apple pectin and apple juice extracts. *Nutrition* **24**(4): 366-74.

Watson, A.J. i Collins, P.D. (2011). Colon cancer: a civilization disorder. *Dig Dis* **29**(2): 222-8.

Yang, C.S., Lambert, J.D. i Sang, S. (2009). Antioxidative and anti-carcinogenic activities of tea polyphenols. *Arch Toxicol* **83**(1): 11-21.

Yang, C.S. i Wang, X. (2010). Green tea and cancer prevention. *Nutr Cancer* **62**(7): 931-7.

Zhao, F., Zhang, J., Liu, Y.S., Li, L. i He, Y.L. (2011). Research advances on flotillins. *Virol J* **8**: 479.

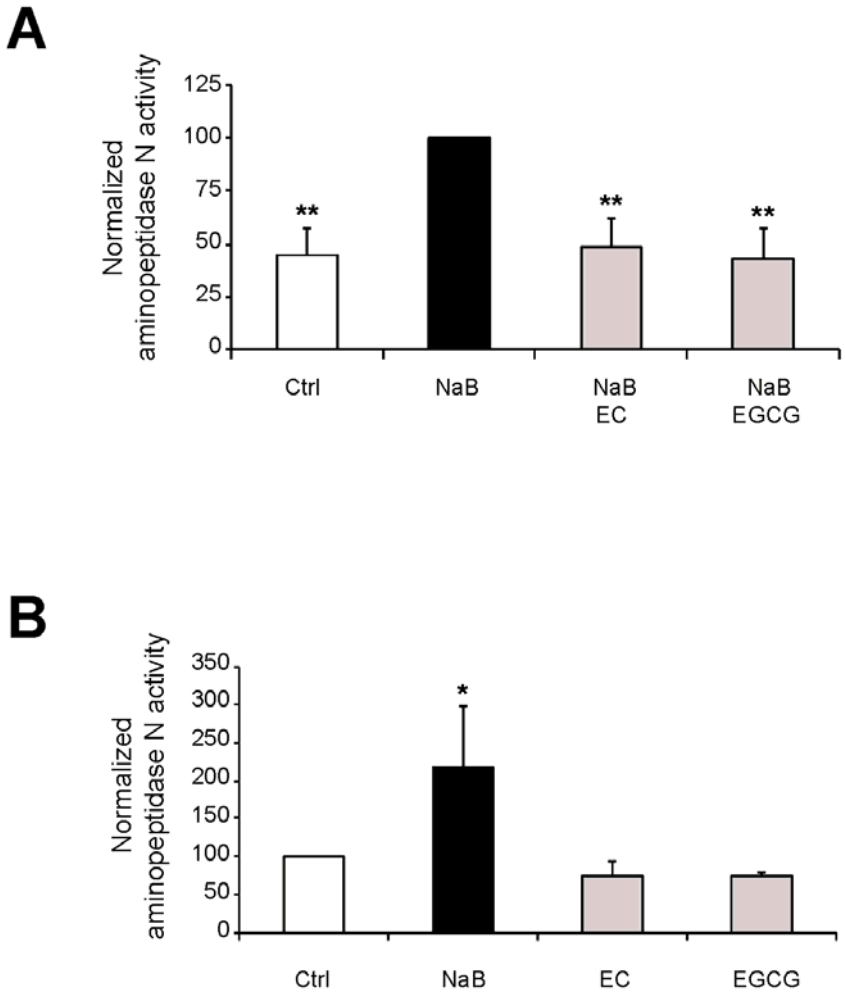

Supplemental Figure 1. Polyphenols reduce butyrate-induced HT29 differentiation measured as aminopeptidase N (AMN) activity. (**A**) HT29 cells were exposed to NaB at 2 mM for 48 hours, alone or in the presence of EC at 100 μM and EGCG at 20 μM and aminopeptidase N (AMN) activity was measured and normalized by protein. The data are presented and statistically tested as AMN activity normalized to NaB treated cells. NaB-induced differentiation was reduced by both polyphenols. (**B**) HT29 cells were treated with NaB 2 mM or with polyphenols alone (EC 100 μM and EGCG 20 μM) for 48 hours and AMN activity was measured. The data are presented and statistically tested as AMN activity normalized to Ctr cells. Polyphenols did not show an increase in differentiation when used alone All experiments were carried out four times. * $p<0.05$, ** $p<0.01$.

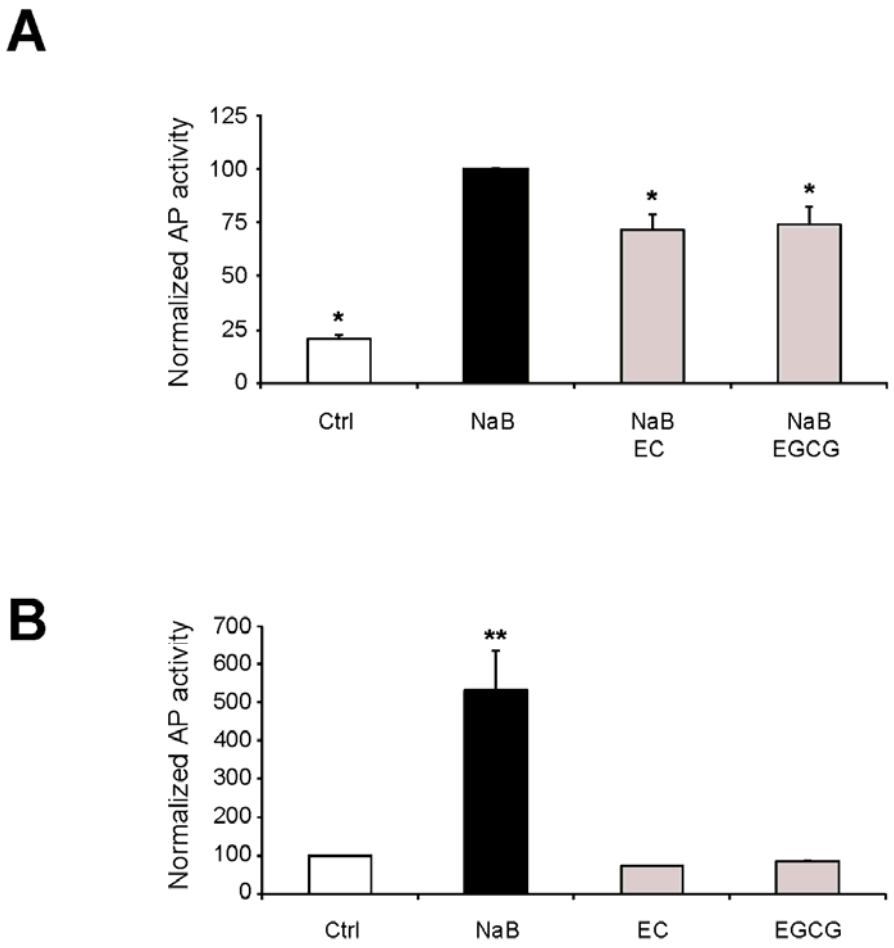

Supplemental Figure 2. Butyrate-induced Caco-2 differentiation is reduced by tea catechins. (**A**) Caco-2 cells were treated with NaB 2 mM or with NaB and polyphenols EC 100 μM and EGCG 20 μM for 48 hours and alkaline phosphatase (AP) activity was measured and normalized by protein. The data are presented and statistically tested as AP activity normalized to NaB treated cells. Polyphenols produced a slight no significant decrease in NaB-induced differentiation. (**B**) Caco-2 cells were treated with NaB 2 mM or with polyphenols alone (EC 100 μM and EGCG 20 μM) for 48 hours and alkaline phosphatase (AP) activity was measured. The data are presented and statistically tested as AP activity normalized to Ctr cells. Polyphenols alone did not have any impact on differentiation. This experiment was performed once using two cultures for each treatment. * $p<0.05$, ** $p<0.01$.

CAPÍTOL 3

L'epicatequin gal·lat interfereix amb la productivitat metabòlica en cèl·lules de càncer de colon

Susana Sánchez-Tena[1], Gema Alcarraz-Vizán[1, †], Pedro Vizán[1, ‡], Silvia Marín[1], Josep Lluís Torres[2] i Marta Cascante[1]

[1]Departament de Bioquímica i Biologia Molecular, Facultat de Biologia, Universitat de Barcelona, Institut de Biomedicina de la Universitat de Barcelona (IBUB), Unitat associada al CSIC, Barcelona, Espanya

[2]Institut de Química Avançada de Catalunya (IQAC-CSIC), Barcelona, Espanya

[†]Adreça actual: Laboratori de Diabetes i Obesitat, IDIBAPS, Barcelona, Espanya
[‡]Adreça actual: Laboratory of Developmental Signalling, Cancer Research UK, London Research Institute, London WC2A 3PX, UK

RESUM

Evidències experimentals i epidemiològiques demostren que els polifenols del raïm i del té verd són capaços d'inhibir la proliferació tumoral i modular el metabolisme cel·lular. L'adaptació metabòlica subjacent a la progressió tumoral confereix a les cèl·lules canceroses la capacitat per sobreviure, proliferar i envair. Per tant, la inhibició del perfil metabòlic tumoral es presenta com una nova i potent estratègia terapèutica. En aquest estudi, es van utilitzar determinacions espectrofotomètriques combinades amb un anàlisi de la distribució isotopomèrica de massa (MIDA - *Mass Isotopomer Distribution Analysis*) amb [1,2-$^{13}C_2$]-glucosa com traçador per revelar l'organització de la xarxa metabòlica en cèl·lules HT29 d'adenocarcinoma de còlon humà en resposta a diferents concentracions d'epicatequin gal·lat (ECG), una de les principals catequines en té verd i la més important en extractes de raïm. L'anàlisi bioquímic va revelar una disminució en el consum de glucosa i glutamina i també en la producció de lactat després del tractament amb ECG. A més, el metabolisme de la [1,2-$^{13}C_2$]-glucosa per part de les cèl·lules HT29 ens va permetre determinar que el cicle dels àcids tricarboxílics, la síntesi *de novo* d'àcids grassos i la ruta de les pentoses fosfat es trobaven reduïdes en les cèl·lules tractades amb ECG. Curiosament, l'ECG va inhibir l'activitat dels enzims clau de la via de les pentoses fosfat, la transcetolasa i la glucosa-6-fosfat deshidrogenasa. En conclusió, els nostres resultats suggereix que l'ECG interfereix amb l'adaptació metabòlica tumoral, disminuint les necessitats energètiques i biosintètiques associades amb una proliferació accelerada en cèl·lules HT29.

Epicatechin gallate impairs colon cancer cell metabolic productivity

Susana Sánchez-Tena[1], Gema Alcarraz-Vizán[1, †], Pedro Vizán[1, ‡], Silvia Marín[1], Josep Lluís Torres[2] and Marta Cascante[1]

[1]Department of Biochemistry and Molecular Biology, Faculty of Biology, Universitat de Barcelona, Institute of Biomedicine of Universitat de Barcelona (IBUB) and Unit associated with CSIC, Barcelona, Spain

[2]Institute for Advanced Chemistry of Catalonia (IIQAB-CSIC), Barcelona, Spain

[†]Present address: Laboratory of Diabetes and Obesity, IDIBAPS, Barcelona, Spain

[‡]Present address: Laboratory of Developmental Signalling, Cancer Research UK, London Research Institute, London WC2A 3PX, UK

ABSTRACT

Epidemiological and experimental evidences demonstrate that green tea and grape polyphenols have the ability to inhibit cancer growth and modulate cellular metabolism. The robust metabolic adaptation underlying tumor progression confers cancer cells the ability to survive, proliferate and invade. Therefore, targeting the tumor metabolic profile is a potential novel therapeutic approach. In our study, we used biochemical determinations combined with a mass isotopomer distribution analysis (MIDA) approach using [1,2-$^{13}C_2$]-glucose as a tracer to characterize human colon adenocarcinoma HT29 cells metabolic network in response to different concentrations of epicatechin gallate (ECG), one of the main catechins in green tea and the most important catechin in grape extracts. Biochemical analyses revealed a decrease in both glucose and glutamine consumption and in lactate production after ECG treatment. Moreover, the metabolization of [1,2-$^{13}C_2$]-glucose by HT29 cells allowed us to establish that the tricarboxylic acid cycle, the *de novo* synthesis of fatty acids and the pentose phosphate pathway were reduced in ECG-treated cells. Interestingly, ECG inhibited the activity of transketolase and glucose-6-phosphate dehydrogenase, the key enzymes of the pentose phosphate pathway. To sum up, our data suggest ECG as a promising chemotherapeutic agent for the treatment of colon cancer which targets metabolic tumor adaptation diminishing the energetic needs and the biosynthetic requirements associated with an increased proliferation of HT29 tumor cells.

INTRODUCTION

Colorectal cancer is one of the most prevalent causes of cancer-related mortality in the western world (Jemal *et al.*, 2010). Therefore, further development of therapeutic and preventive means of controlling this disease is clearly needed. Epidemiological and experimental studies have linked a diet rich in fruits, vegetables and beverages containing polyphenolic compounds to the prevention of colon cancer, among other diseases. In particular, epicatechin gallate (ECG), one of the major catechins in green tea and grape, has been described as a potent protector against colorectal cancer in a cell type dependent manner. ECG induced apoptosis in SW480 cells through the ERK activation, AKT inhibition, imbalance among anti- and pro- apoptotic protein levels and caspase-3 activation. However, in Caco2 cells, ECG only increased the antioxidant potential without affecting cell growth (Ramos *et al.*, 2011). Another study described that ECG induces G1 phase cell cycle arrest and apoptosis in HCT116 colon cancer cells (Baek *et al.*, 2004). Moreover, recent both *in vitro* and *in vivo* studies indicate that green tea and grape polyphenols have preventive effects against the development of metabolic diseases such as obesity, insulin resistance, hypertension and hypercholesterolemia (Chen *et al.*, 2012; Shimizu *et al.*, 2012).

Multiple lines of evidence show that tumorigenesis is often associated with a metabolic adaptation characterized by, among others, the broadly known Warburg effect (increased fermentation of glucose to lactate even in the presence of oxygen), a high glutamine uptake, the activation of biosynthetic pathways and the over-expression of some isoenzymes. These robust characteristics confer a common advantage to many different types of cancers, increasing the ability of cells to survive, proliferate and invade (Dang *et al.*, 2011). Therefore, a better knowledge of the tumor metabolic profile required to support proliferation is necessary for the development of novel therapeutic strategies against cancer. By studying how antiproliferative natural products alter this metabolic profile in cancer derived cell lines, we are revealing potential targets for therapeutic strategies against cancer.

Stable isotope tracing, using [1,2-$^{13}C_2$]-glucose as a source of carbon in combination with mass spectrometry to detect detailed substrate flow and specific distribution patterns in various ^{13}C isotopomers, allows the evaluation of metabolic fluxes through the main pathways that facilitate energy production and biosynthetic metabolism. Examples of the strength of this approach include the characterization of the metabolic adaptation underlying angiogenic activation (Vizan *et al.*, 2009) and the elucidation of distinctive metabolic phenotypes that correlate with different codon-specific mutations in K-ras in NIH3T3 mice fibroblasts (Vizan *et al.*, 2005).

In the present study we use this powerful methodology to gain insight into the targeting of the tumor metabolic profile present in human colon adenocarcinoma HT29 cells by ECG. Our data indicated that ECG impairs the metabolic productivity associated with an increased tumor proliferation.

MATERIALS AND METHODS

Chemicals. All chemicals were purchased from Sigma-Aldrich Co (St Louis, MO, USA), unless otherwise specified. Dulbecco's Modified Eagle´s Medium (DMEM) and antibiotic (10,000 U/mL penicillin, 10,000 µg/mL streptomycin) were obtained from Gibco-BRL (Eggenstein, Germany), fetal calf serum (FCS) and trypsin-EDTA solution C (0.05% trypsin-0.02% EDTA) from Invitrogen (Paisley, UK). Stable [1,2-$^{13}C_2$]-glucose isotope was obtained with >99% purity and 99% isotope enrichment for each position from Isotec Inc. (Miamisburg, OH).

Cell culture. Human colorectal adenocarcinoma HT29 cells (obtained from the American Type Culture Collection, HTB-38) were grown as a monolayer culture in DMEM (with 4 mM L-glutamine, without glucose and without sodium pyruvate) in the presence of 10% heat-inactivated fetal calf serum, 10 mM of glucose and 0.1% streptomycin/penicillin in standard culture conditions. Cell cultures were carried at 37ºC in 95% air, 5% CO_2 humidified environment. HT29 cell cultures were started with 3×10^5 cells in 60 cm^2 petri dishes which were achieved by using standard cell counting techniques. 24 h after seeding, cell medium was removed and fresh supplemented medium with [1,2-$^{13}C_2$]-D-glucose (50% isotope enrichment) was added with or without ECG. The cells were harvested 72 h after treatment.

Determination of cell viability. The assay was performed using a variation of the MTT assay (Sanchez-Tena *et al.*, 2012). The assay is based upon the principle of reduction of MTT into blue formazan pigments by viable mitochondria in healthy cells. HT29 cells were seeded at densities of 3×10^3 cells cells/well in 96-well flat-bottom plates. After 24 h of incubation at 37ºC, ECG was added to the cells at different concentrations in fresh medium. The culture was incubated for 72 h. Next, the medium was removed, and 50 µL of MTT (1 mg/mL in PBS) with 50 µL of fresh medium was added to each well and incubated for 1 h. The MTT reduced to blue formazan and the precipitate was dissolved in 100 µL of DMSO. Absorbance values were measured on an ELISA plate reader (550 nM) (Tecan Sunrise MR20-301, Tecan, Salzburg, Austria). Absorbance was taken as proportional to the number of living cells.

Glucose, lactate and glutamine concentration. The glucose, lactate and glutamine concentrations in the culture medium were measured spectrophotometrically using a Cobas Mira Plus chemistry analyzer (HORIBA ABX, Montpellier, France) at the beginning and at the end of the incubation time, to calculate glucose/glutamine consumption and lactate production.

Lactate mass isotopomer analysis. To measure lactate by gas chromatography coupled to mass spectrometry (GC/MS), this metabolite was extracted by ethyl acetate after acidification with HCl and derivatized to its propylamideheptafluorobutyric form (Lee *et al.*, 1998). The m/z 328 (carbons 1–3 of lactate, chemical ionization) was monitored for the detection of m0 (unlabeled species), m1 (lactate with one ^{13}C atom) and m2 (lactate with two ^{13}C atoms).

Glutamate mass isotopomer analysis. Glutamate was separated from the cell medium using ion-exchange chromatography as described elsewhere (Boren *et al.*, 2003). Glutamate was converted to its n-trifluoroacetyl-n-butyl derivative and the ion clusters m/z 198 (carbons 2–5 of glutamate, electron impact ionization) and m/z 152 (carbons 2–4 of glutamate, electron impact ionization) were monitored.

Fatty acids mass isotopomer analysis. Fatty acids were extracted by saponification of the Trizol (Invitrogen, Carlsbad, CA) cell extract after removal of the RNA-containing supernatant. Cell debris was treated with 30% KOH and 100% ethanol overnight, and the extraction was performed using petroleum ether (Lee *et al.*, 1998). Fatty acids were converted to its methyl ester derivative and the ion clusters m/z 269 (palmitate (C16), electronic impact ionization) and m/z 297 (stearate (C18), electronic impact ionization) were monitored.

RNA ribose mass isotopomer analysis. RNA ribose was isolated by acid hydrolysis of cellular RNA after Trizol purification of cell extracts. Ribose isolated from RNA was derivatized to its aldonitrile acetate form using hydroxyl-amine in pyridine and acetic anhydride (Lee *et al.*, 1998). The ion cluster around the m/z 256 (carbons 1–5 of ribose, chemical ionization) was monitored.

Gas chromatography/mass spectrometry. Mass spectral data were obtained on a GCMS-QP2010 selective detector connected to a GC-2010 gas chromatograph from Shimadzu. The settings were as follows: GC inlet 200 ºC, transfer line 280 ºC, MS Quad 150ºC. A HP-5MS capillary column (30 m length, 250 µm diameter and 0.25 µm film thickness) was used for the analysis of glucose, lactate, ribose and glutamate. On the other hand, for the analysis of fatty acids the GC inlet was set at 250 ºC and a bpx70 (SGE) column (30 m length, 250 µm diameter and 0.25 µm film thickness) was used.

Activities of the PPP enzymes glucose-6-phosphate dehydrogenase (G6PD) and transketolase (TKT). Cell cultures were washed with PBS and scrapped in lysis buffer (20 mM Tris–HCl, pH 7.5, 1 mM dithiothreitol, 1 mM EDTA, 0.02% Triton X-100, 0.02% sodium deoxycholate). Cells were homogenized on ice-cold buffer following 3 cycles of 10 s of sonication with a titanium probe and immediately centrifuged at 13,000×g for 20 minutes at 4ºC. The supernatant was used for the determination of enzyme activities adapting a previously described method (Boren et al. 2001) to a Cobas Mira Plus chemistry analyzer. Briefly, G6PD (EC 1.1.1.49) activity was evaluated by measuring 340 nm absorbance changes result of NADPH formation recorded for 15 minutes after the addition of 10 µL of sample to a cuvette containing 0.5 mM $NADP^+$ in 50 mM Tris–HCl, pH 7.6 at 37 °C. Reactions were initiated by the addition of G6P up to a final concentration of 2 mM. The method for TKT (EC 2.2.1.1) analysis is based on its product, glyceraldehyd-3-phosphate, which is isomerized to dihydroxyacetone-phosphate and in turn, its conversion to glycerol-phosphate consumes NADH that absorbs at 340 nm. Briefly, samples were added to a cuvette containing 5 mM $MgCl_2$, 0.2 U/ml triose phosphate isomerase, 0.2 mM NADH, 0.1 mM thiamine pyrophosphate in 50 mM Tris–HCl, and pH 7.6 at 37 °C. The reaction was initiated by the addition of a substrate mixture in 1:2 proportion (substrate mixture : final volume) prepared by dissolving 50 mM R5P in 50 mM Tris–HCl, pH 7.6 with 0.1 U/ml ribulose-5-phosphate-3-epimerase and 1.7 mU/ml phosphoriboisomerase. Later, protein concentration of cell extracts was determined using the BCA Protein Assay (Pierce Biotechnology, Rockford, IL). Enzyme activities are expressed as mU/mg prot.

Data analysis and statistical methods. *In vitro* experiments were carried out using three cultures each time for each treatment. Mass spectral analyses were carried out by three independent automatic injections of 1 µL of each sample by the automatic sampler. Statistical analyses were performed using the parametric unpaired, two-tailed independent sample t test with 95% or 99% confidence intervals. $p < 0.05$ (*) and $p < 0.01$ (**) were considered to indicate significant differences.

RESULTS

Inhibition of HT29 cell viability by ECG. HT29 cells were treated with different doses of ECG and cell viability was determined (Figure 1). According to the results, two doses of ECG were chosen: a concentration of 70 µM, which produced a reduction of viability of 18±4 and a higher concentration of 140 µM, which caused a more important reduction in HT29 cell viability of 70±11.

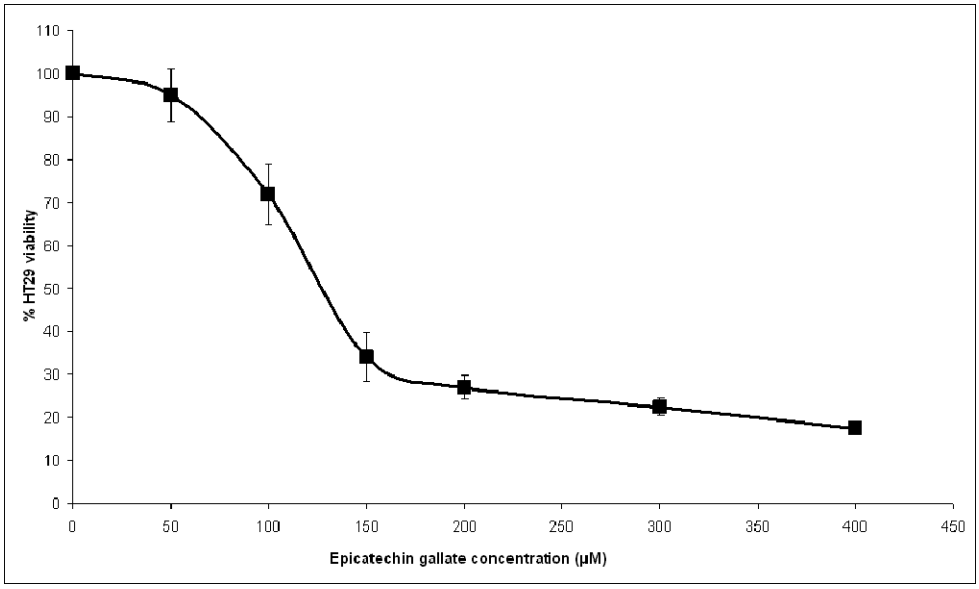

Figure 1. Effect of increasing concentrations of ECG on HT29 cell viability. Values are represented as mean of percentage of cell viability with respect to control cells ± standard error of three independent experiments.

Differences in glucose and glutamine consumption and lactate production in ECG-treated HT29 cells. Glucose and glutamine consumption and lactate production were estimated in HT29 cells before and after 72 h of ECG treatment. Figure 2 shows the values for glucose consumption (A), lactate production (B) and glutamine consumption (C) in ECG-treated cells and non-treated (control) cells. Treatment with 70 μM ECG did not show any effect in glucose and glutamine consumption and lactate production. However, 140 μM ECG treatment decreased 70% and 55% glucose and glutamine consumption, respectively. Similarly, lactate production was reduced by 46% after the incubation of human colon adenocarcinoma HT29 cells with 140 μM of ECG.

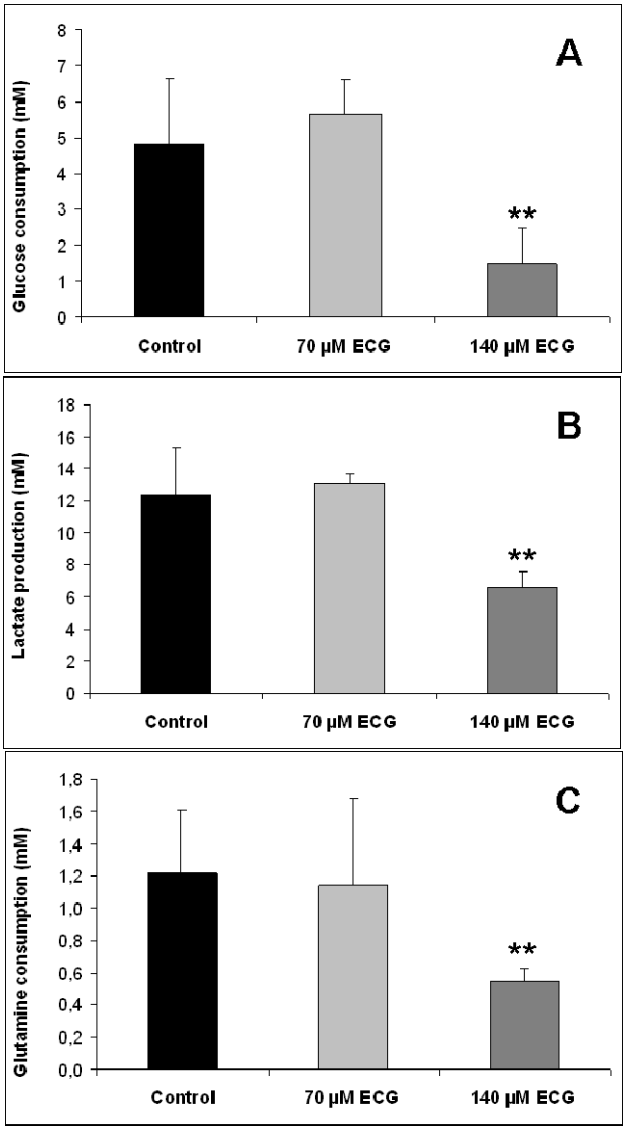

Figure 2. Effect of ECG on glucose (**A**) and glutamine (**C**) consumption and on lactate production (**B**). Mean ± standard deviation of three independent experiments. **p < 0.01, significant difference with respect to the corresponding value in untreated cells.

Lactate mass isotopomer distribution was not significantly affected by ECG. From lactate mass isotopomer distribution the total lactate enrichment measured as ∑mn=m1+m2×2 can be calculated. This parameter represents the average number of ^{13}C atoms per molecule and indicates the synthesis *de novo* from labeled glucose. The glycolytic rate (GR), which indicates the rate of lactate production versus glucose consumption, can be also estimated from m2 lactate*2/m2 glucose. In the experiments performed the initial m2 glucose represented 48.17 %. Table 1 shows that lactate label distribution was not significantly altered when HT29 cells were treated with 70 µM or 140 µM of ECG.

Table 1. Lactate mass isotopomer distribution

	m0	m1	m2	∑mn	GR (%)
Control	0,7854±0,0219	0,0203±0,0050	0,1897±0,0187	0,4134±0,0423	77,9227±7,7842
70 µM ECG	0,7927±0,0095	0,01588±0,0014	0,1891±0,0110	0,4009±0,0182	78,0257±5,5051
140 µM ECG	0,7822±0,01710	0,0269±0,0093	0,1850±0,01089	0,4144±0,0283	75,3152±4,7679

Table 1. Lactate mass isotopomer distribution, ^{13}C enrichment (∑mn) and glycolytic rate (GR) determined after 72 h treatment of HT29 cells with 70 µM and 140 µM ECG. Values are represented as mean ± standard error of three independent experiments.

ECG treatment reduced tricarboxylic acid cycle activity. Tricarboxylic acid (TCA) cycle activity was studied by means of glutamate mass isotopomer distribution analyses. Fluxes through pyruvate dehydrogenase (PDH) and pyruvate carboxylase (PC) pathways were estimated from the levels of m2 isotopomers of C2-C4 and C2-C5 fragments (%PC=m2 (C2-C4)/m2 (C2-C5) and %PDH=(m2 (C2-C5) - m2 (C2-C4))/m2 (C2-C5)) and ^{13}C glutamate enrichment was calculated as ∑mn=m1+m2×2+m3×3 for C2-C4 and C2-C5 glutamate fragments. Both 70 µM and 140 µM ECG-treated cells presented a lower TCA cycle activity compared to control cells as suggested by the reduction in glutamate enrichment (Table 2). Results also showed that whereas 140 µM ECG treatment increased PC contribution to TCA cycle, it decreased glucose utilization through PDH (Figure 3).

Table 2. Glutamate mass isotopomer distribution

C2-C4	m0	m1	m2	∑mn
Control	0,9573±0,0195	0,0389±0,0187	0,0026±0,0016	0,0477±0,0202
70 µM ECG	0,9763±0,0141	0,0213±0,0142*	0,0011±0,0006**	0,0276±0,0140*
140 µM ECG	0,9834±0,0044**	0,0122±0,0026**	0,0010±0,0004**	0,0240±0,0139**

C2-C5	m0	m1	m2	∑mn
Control	0,9486±0,0081	0,0154±0,0028	0,0339±0,0049	0,0901±0,0139
70 µM ECG	0,9659±0,0046**	0,0092±0,0024**	0,0241±0,0023**	0,0605±0,0072**
140 µM ECG	0,9861±0,0026**	0,0043±0,0012**	0,0075±0,0013**	0,0243±0,0043**

Table 2. Mass isotopomer distribution and ^{13}C enrichment (∑mn) in fragments C2-C4 (upper panel) and C2-C5 (lower panel) from glutamate secreted in the culture media after 72 h treatment of HT29 cells with 70 µM and 140 µM ECG. Values are expressed as mean ± standard error of three independent experiments. $p < 0.05$ (*) / $p < 0.01$ (**) versus the untreated condition.

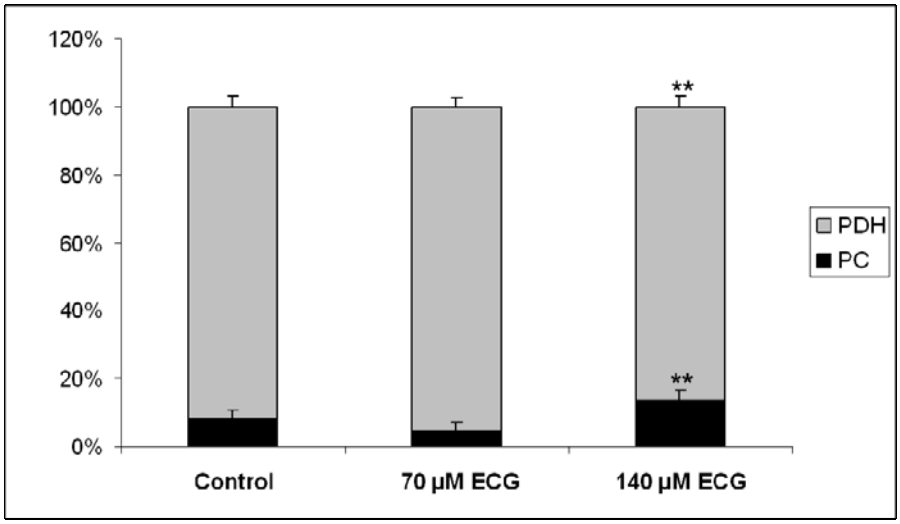

Figure 3. PC and PDH contributions to TCA cycle were estimated using m2 (C2–C4) and m2 (C2–C5) - m2 (C2–C4), respectively. Values are expressed as mean ± standard error of three independent experiments. $p < 0.01$ (**) versus the untreated condition.

ECG inhibited lipid synthesis. Lipid synthesis is dependent on glucose carbons, as they are the primary source of acetyl-CoA, which is then incorporated into fatty acids through *de novo* synthesis. Acetyl-CoA enrichment was calculated from the m4/m2 ratio using the formula m4/m2= (n–1)/2×(q/1- q), where n is the number of acetyl units and q is the labeled fraction with p being the unlabeled fraction (p+q=1). Therefore, to calculate palmitate (C16) labelled fraction, the formula is (m4/m2)/3.5= q/1-q= q/p, whereas to calculate it for stearate (C18) we used (m4/m2)/4= q/1-q= q/p. Next, we obtain the labeled fraction from q= (q/p)/(1+q/p). The contribution of glucose carbons to fatty acid synthesis was estimated dividing the obtained q by the theoretical enrichment derived from glucose. Finally, we determined the relative number of fatty acids synthesized *de novo* respect to the total number of *de novo* fatty acids (FNS) using the formula $m2/8q(1-q)^7$ for palmitate and $m2/9q(1-q)^8$ for stearate. Results shown in figure 4A revealed that 70 µM ECG was enough to reduce an 8% the contribution of glucose to stearate (Figure 4A) and that 140 µM ECG reduced a 9% the contribution of glucose to both palmitate and stearate synthesis. Figure 4B shows that stearate synthesis was lower than palmitate synthesis in HT29 cells. Moreover, the fraction of *de novo* synthesis or FNS was inhibited a 27% and a 35% for palmitate and stearate, respectively, after the treatment with 140 µM ECG (Figure 4B).

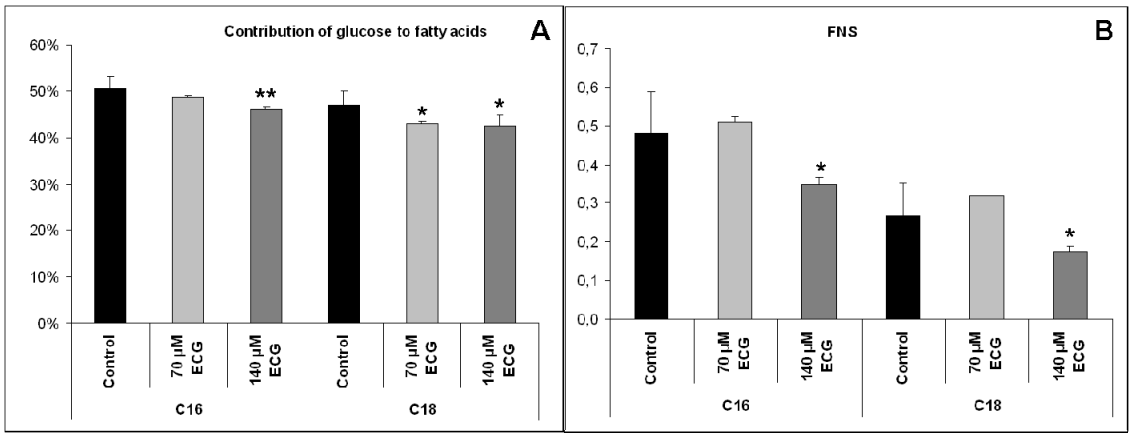

Figure 4. (A) Determination of the relative contribution of glucose carbons to palmitate (C16) and stearate (C18) synthesis. (**B)** Determination of the fraction of *de novo* synthesis of palmitate (C16) and stearate (C18) in ECG-treated cells and in control cells. Mean ± standard deviation of two independent experiments. $p < 0.05$ (*) / $p < 0.01$ (**), significant difference with respect to control cells.

Reduced *de novo* synthesis of RNA ribose from glucose in ECG-treated HT29 cells. Table 3 shows RNA ribose analysis. Whereas ribose mass isotopomer m1 is formed when [1,2-$^{13}C_2$]-glucose is decarboxylated by the oxidative branch of the pentose phosphate pathway (PPP), m2 mass isotopomer is synthesized by the reversible non-oxidative branch of the cycle. The combination of these two branches generates m3 and m4 species. Therefore, the ratio between fluxes through oxidative and non-oxidative branches of PPP can be estimated according to the formula ox:non-ox=(m1)/(m2) since m1 need the oxidative branch to be formed, whereas m2 specie require the non-oxidative branch. The total ribose label incorporation is estimated as $\sum mn=m1+m2\times2+m3\times3+m4\times4$. HT29 cells treated with 70 µM ECG did not present consistent differences in both ^{13}C enrichment and the ox:non-ox ratio respect to the control cells (Table 3). On the contrary, treatment with 140 µM ECG was able to diminish ribose total ^{13}C enrichment in HT29 cells and was also able to significantly modulate the flux balance through the two branches of the PPP (ox:non-ox ratio) in favor of the oxidative branch.

Table 3. Ribose mass isotopomer distribution

	m0	m1	m2	m3	m4	∑mn	ox:non-ox
Control	0,5521±0,0672	0,2597±0,0443	0,1288±0,0186	0,0438±0,0122	0,01558±0,0040	0,7109±0,1107	2,0163±0,3205
70 µM ECG	0,5237±0,0232	0,2736±0,0125	0,1310±0,0123	0,0513±0,0050	0,0202±0,0042	0,7743±0,0387	2,0885±0,2205
140 µM ECG	0,6666±0,0432**	0,2015±0,0372**	0,0940±0,0197**	0,0283±0,0075**	0,0095±0,0024**	0,5124±0,0481**	2,1436±0,5741*

Table 3. Mass isotopomer distribution, ^{13}C enrichment (∑mn) and the oxidative:non-oxidative ratio in RNA ribose in HT29 cells non-treated or treated with 70 µM and 140 µM ECG. Mean ± standard deviation of three separate experiments. $p < 0.05$ (*) / $p < 0.01$ (**), significant difference with respect to control cells.

ECG inhibited G6PD and TKT specific enzymatic activities. After discover a disbalance between the fluxes through the oxidative and the non-oxidative branches of the PPP, we decided to study the activity of the enzymes controlling this biosynthetic pathway, G6PD and TKT. The specific activities of these enzymes were measured for non-treated and ECG-treated cells and compared in figure 5. There were no significant changes in the G6PD and TKT activities after 70 µM ECG treatment in HT29 cells. However, decreases of 15 % in G6PD and 35 % in TKT specific activities were observed after treatment with 140 µM ECG.

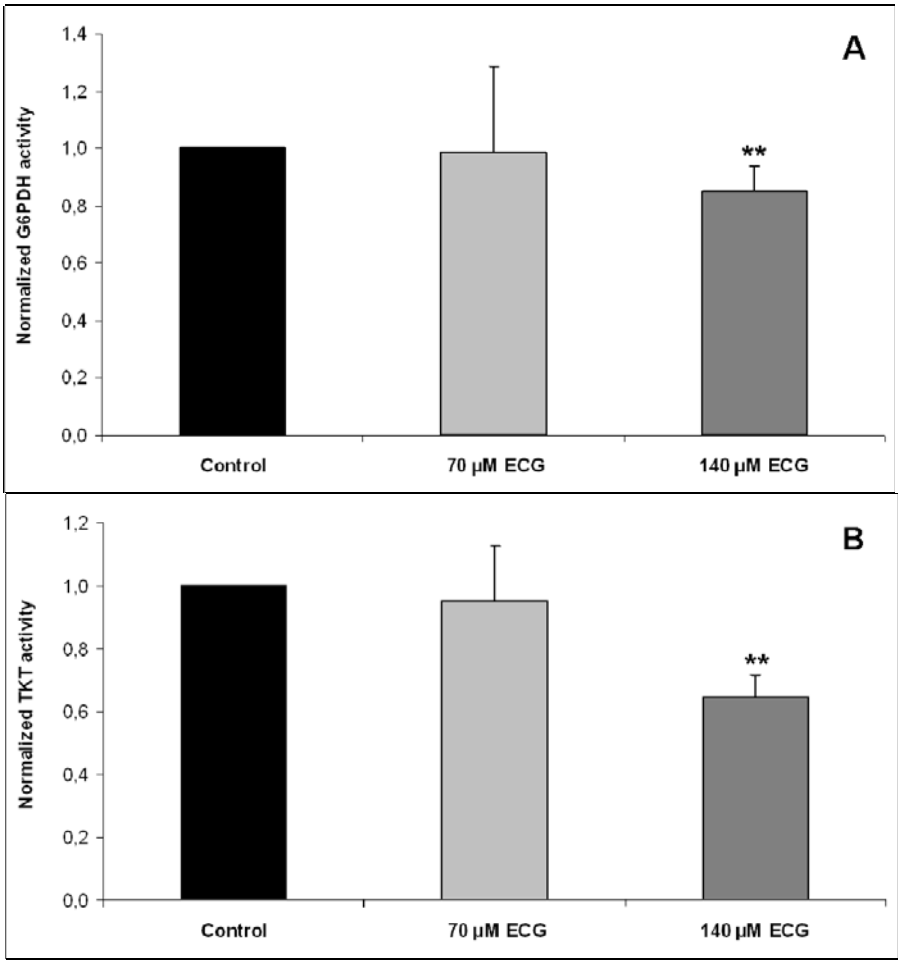

Figure 5. Plot of fold of ECG-treated respect non-treated HT29 cells of G6PD (**A**) and TKT (**B**) activities. Results show the mean ± standard error of four experiments. $p < 0.01$ (**) versus untreated cells.

DISCUSSION

The characteristic metabolic adaptation underlying tumor progression represents the end point of several signaling cascades, but it also actively enhances the degree of tumor malignancy. In this framework, tumor metabolism confers a novel potential target to inhibit cancer cell growth. Given that the green tea catechin ECG has been associated to both tumor inhibition and metabolic modulation, we decided to study the HT29 colon cancer cells metabolic network in response to different concentrations of this polyphenol.

Neoplastic cells increase glycolysis in order to produce anabolic precursors and energy (Vander Heiden *et al.*, 2009). In order to maintain this high rate of glycolysis, it is obligatory for the tumor cells to have access to an elevated supply of glucose. In this regard, our results showed that HT29 cells treated with 140 µM ECG exhibited a lower glucose uptake compared

to HT29 control cells (Figure 2). This result is in agreement with the anti-diabetic and anti-obesity activities of green tea, which have been related to the regulation of the gene expression in the glucose uptake function (Cao *et al.*, 2007). Moreover, the inhibition in substrate consumption was also accompanied by a reduced lactate production (Figure 2). Reduction in delivered lactate is, at least in part, a consequence of decreased glucose uptake. Interestingly, recent reports indicate that targeting lactate efflux is a new avenue to inhibit cancer growth; first, inhibiting the overall glycolytic pathway, and second, avoiding the acidic pH of the tumor microenvironment (Mathupala *et al.*, 2010). On the other hand, mass isotopomer distribution in lactate gave us additional information about the glycolytic pathway. Incubation with [1,2-$^{13}C_2$]-glucose as tracer resulted in specific mass isotopomer distributions in metabolites such as lactate secreted into the culture medium, which were analyzed by GC/MS techniques. The applied technique determined the fractions of different mass isotopomers: m0 (without any ^{13}C labels), m1 (one ^{13}C label), m2 (two ^{13}C labels), etc. These fractions for lactate present in the media in control and ECG-treated conditions are shown in Table 1 and showed no relevant changes after ECG treatment at the different concentrations studied. The estimated glycolytic flux (GR) did not show modifications, indicating that although the absolute values for glucose consumption and lactate production were reduced in 140 μM ECG-treated cells, the velocity of the pathway did not change after ECG treatment. This estimated GR indicated that in all cases a 75-78 % of the lactate came directly from glucose. Consistently, our calculations for glycolytic rate in HT29 cells are in agreement with previous from Alcarraz-Vizán et al. (Alcarraz-Vizan *et al.*, 2010). In this regard, taking into account the determined GR, lactate production is greater to the expected from glucose consumption, indicating that lactate is being produced from additional carbon sources, other than glucose, such as pyruvate, glutamine and aminoacids.

It has to be noted that the growth of cancer cells requires more than just glucose. Highly proliferative cells also require additional supplies such as glutamine for cell growth and biomass accumulation (Dang, 2012). Glutamine is used as a source of nitrogen and as a key anaplerotic carbon source to replenish metabolites depleted from the TCA cycle for biosynthesis. On one hand, glutamine can provide carbon for lipid synthesis by oxidative metabolism through the TCA cycle to produce malate that when is converted to pyruvate, can be decarboxylated by the PDH enzyme to yield acetyl-coA that will be exported to the cytosol. This route fuels mitochondrial ATP generation, serves as a source of NADPH by the action of the malic enzyme, and supplies anaplerotic carbon to the TCA cycle. On the other hand, the α-ketoglutarate obtained from glutamine can be reduced to generate citrate, which in turn can be used as a source of acetyl-coA in the cytosol where will be used for biosynthesis (Metallo *et al.*, 2011; Vander Heiden *et al.*, 2012). Interestingly, glutamine consumption was diminished in

HT29 cells after incubation with 140 μM of ECG (Figure 2). This decrease in glutamine uptake by ECG could be related to its ability to inhibit the mitochondrial glutamate dehydrogenase, which catalyzes an oxidative deamination of glutamate to α-ketoglutarate that feeds the TCA cycle (Li *et al.*, 2006).

Regarding glutamate mass isotopomer analysis, label distribution in fragments C2-C4 and C2-C5 allowed us to estimate the TCA cycle activity. The reduction in ^{13}C enrichment in all the fractions of glutamate after ECG treatments (Table 2) indicated an inhibition of the TCA cycle. On contrary to the historically thought, up-regulation of glycolysis exhibited by cancer cells does not necessarily imply a strict anaerobic metabolism nor a dysfunctional oxidative phosphorylation (Amoedo *et al.*, 2011). Recently, it has been reported that the tumorigenicity mediated by oncogens such as Myc and K-ras is dependent on mitochondrial metabolism and electron transport (Weinberg *et al.*, 2010; Le *et al.*, 2012) and also that metastatic breast cancer cells utilize aerobic glycolysis coupled with the TCA cycle and the oxidative phosphorylation to generate ATP (Chen *et al.*, 2007). In these cases the activation of the TCA cycle seems to be needed to supply energy and anabolic precursors required for the synthesis of cell building blocks. Therefore, the inhibition of the TCA cycle by ECG may act as reducing the metabolic precursors necessary for the biosynthesis of proteins, nucleic acids and lipids. Furthermore, the analysis of glutamate fragments allowed us to calculate the contributions of PC and PDH to TCA cycle (Figure 3). ^{13}C from [1,2-$^{13}C_2$]-glucose can enter into mitochondrial citrate by the abovementioned PDH or via the anaplerotic carboxylation of pyruvate catalyzed by PC. Then, transamination of α-ketoglutarate produces labeled glutamate that is excreted in the media. Depending on the route used to enter within the mitochondria, a different label pattern in C2-C4 and C2-C5 glutamate fragments is obtained. In HT29 cells both PDH and PC entry points are active, although the PDH flux is much more important (around 90 %) (Figure 3). Interestingly, 140 μM ECG produced a disequilibrium in glucose utilization through both routes, enhancing the contribution of the PC flux and reducing the characteristic high tumor flux through PDH.

A recent study described that simultaneous targeting of the glycolytic pathway with dichloroacetate and the mitochondrial activity with arsenic trioxide in breast cancer cells is more effective inhibiting cell proliferation and inducing cell death than either inhibition alone (Sun *et al.*, 2011). Therefore, our results suggest that ECG could be a good strategy to inhibit cancer cells by means of inhibiting the main energetic pathways necessaries to produce cellular ATP and also metabolic intermediaries.

Precursors for lipids and proteins are generated in the TCA cycle and removed from the mitochondria to participate in biosynthetic reactions. Therefore, next step was to determine label

incorporation into the fatty acids palmitate (C16) and stearate (C18) and calculate the contribution of glucose to lipid synthesis and the FNS. Results denoted a less active lipogenesis in ECG-treated cells, which could be related to an inhibition in the synthesis of essential components of the cellular membranes required for the accelerated proliferation in HT29 cells. Interestingly, both TCA cycle and lipogenesis were already reduced with 70 μM ECG treatment indicating a more sensitive and efficient effect of ECG targeting these pathways.

Finally, the analysis of ribose showed in Table 3 demonstrated that low ECG concentration did not cause significant changes in its mass isotopomer distribution. However, high ECG concentration reduced ribose ^{13}C enrichment indicating that the *de novo* synthesis of ribose from glucose was decreased. It is worth noting that pentose phosphate pathway inhibition in different tumor cell lines results in an effective decrease in tumor cell proliferation (Comin-Anduix *et al.*, 2001; Cascante *et al.*, 2002). Furthermore, inhibition of nucleic acid synthesis has been shown to be successful in chemotherapy (Purcell *et al.*, 2003). Ribose can be synthesized from the glycolytic intermediate glucose-6-phosphate via the oxidative branch of the PPP as well as from fructose-6-phosphate and glyceraldehyde-3-phosphate via the non-oxidative branch of the PPP. Mass isotopomer distribution analysis in ribose showed a significant increase in the ox:non-ox ratio after treatment with high concentrations of ECG. This fact prompted us to deepen in the PPP activity after ECG treatment. We analyzed the activities of the key enzymes in PPP: G6PD and TKT. Both enzymatic activities were reduced in 140 μM ECG-treated cells (Figure 5). Moreover, in agreement with the reported increase in the ox:non-ox ratio, the inhibition observed for TKT was more important than the reduction in G6PD. Given that the control coefficients on tumor cell growth for G6PD and TKT have been described to be 0.41 and 0.9, respectively (Boren *et al.*, 2002); the 35 % reduction in TKT activity could imply an important effect inhibiting nucleic acid synthesis and tumor growth. Interestingly, in several tumor-derived cell lines, the non-oxidative branch of the PPP was found to be the main source for ribose-5-phosphate synthesis (Cascante *et al.*, 2000), hence the importance of this inhibition is reinforced. Although in a lesser extent, G6PD activity showed also an inhibition (15 %) that could also be biologically important since the use of the oxidative branch of the PPP enables cells not only to synthesize more ribose for nucleic acid requirements, but also to recruit reducing power in the form of NADPH necessary to membrane lipid synthesis.

It has been described that the pattern of metabolic changes is associated with the type of cell death and growth inhibition involved in the cytotoxic action of a determined drug (Motrescu *et al.*, 2005). Moreover, the precise metabolic phenotype in cancer cells has been reported to be dependent on cell type and growth conditions (Telang *et al.*, 2007) and even on the microregions of the same tumor (dos Santos *et al.*, 2004). In our study, ECG acts mainly

reducing the synthesis of macromolecules needed to produce a new cell, hence inhibiting colon cancer cell viability. In future studies, it would be interesting to determine whether these metabolic changes induced by ECG are common to other colon cancer models.

In summary, incubation with different concentrations of ECG modified, in a dose-dependent manner, the metabolic profile in HT29 cells targeting the incorporation of nutrients into the biomass. ECG reduced substrate uptake and also the anabolic pathways needed to satisfy the metabolic requirements associated with an increased tumor proliferation (Figure 6). Our results indicate that bioactive compounds such as polyphenols may play a role in cancer therapy as nutritional supplements controlling tumor viability through the regulation of glucose carbon redistribution.

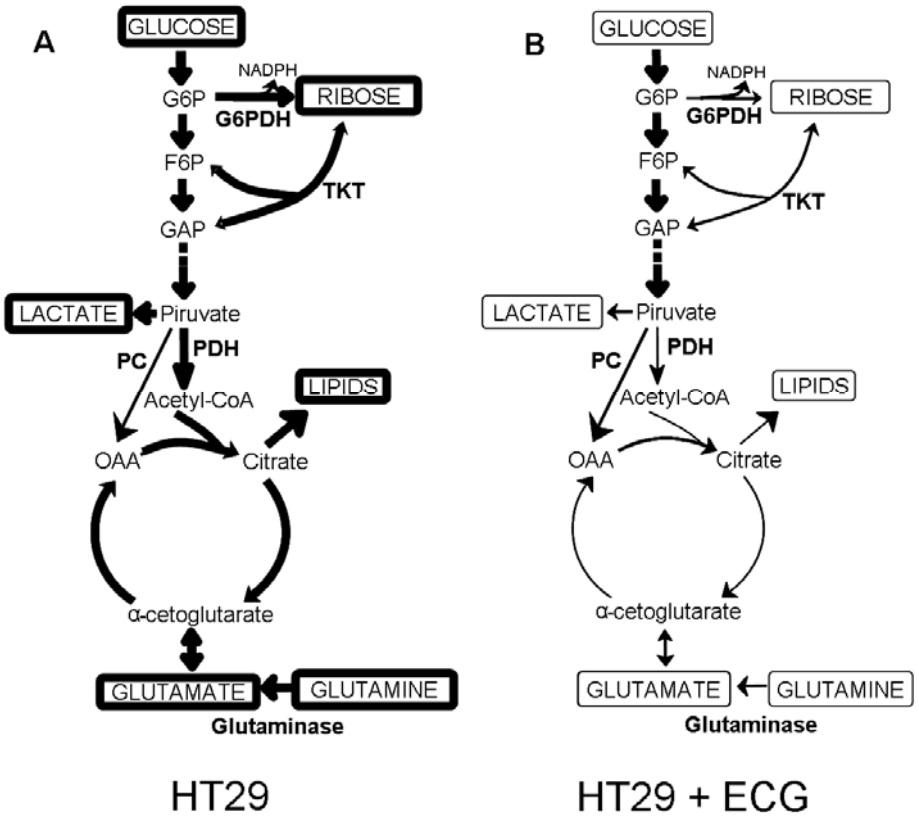

Figure 6. HT29s' metabolic network changes in response to ECG treatment. (**A**) Activated metabolic profile in HT29 cells to support tumor proliferation. (**B**) ECG treatment reduced glucose/glutamine uptake, lactate production, TCA cycle activity and lipid and ribose synthesis. G6P, glucose-6-phosphate; F6P, fructose-6-phosphate; GAP, glyceraldehyde-3-phosphate; OAA, oxaloacetate; G6PDH, glucose-6-phosphate dehydrogenase; TKT, transketolase.

ACKOWLEDGEMENTS

Financial support was provided by grants SAF2008-00164, SAF2011-25726, AGL2006-12210-C03-02/ALI, and AGL2009-12374-C03-03/ALI from the Spanish government Ministerio de Economía y Competitividad and personal financial support (FPU program); and from the Red Temática de Investigación Cooperativa en Cáncer, Instituto de Salud Carlos III, Spanish Ministry of Science and Innovation & European Regional Development Fund (ERDF) "Una manera de hacer Europa" (ISCIII-RTICC grants RD06/0020/0046). We have also received financial support from the AGAUR-Generalitat de Catalunya (grant 2009SGR1308, 2009 CTP 00026, and Icrea Academia Award 2010 granted to M.C.) and the European Commission (FP7) ETHERPATHS KBBE-grant agreement no. 22263.

REFERENCES

Alcarraz-Vizan, G., Boren, J., Lee, W.N. i Cascante, M. (2010). Histone deacetylase inhibition results in a common metabolic profile associated with HT29 differentiation. *Metabolomics* **6**(2): 229-237.

Amoedo, N.D., Rodrigues, M.F., Pezzuto, P., Galina, A., da Costa, R.M., de Almeida, F.C., El-Bacha, T. i Rumjanek, F.D. (2011). Energy metabolism in H460 lung cancer cells: effects of histone deacetylase inhibitors. *PLoS One* **6**(7): e22264.

Baek, S.J., Kim, J.S., Jackson, F.R., Eling, T.E., McEntee, M.F. i Lee, S.H. (2004). Epicatechin gallate-induced expression of NAG-1 is associated with growth inhibition and apoptosis in colon cancer cells. *Carcinogenesis* **25**(12): 2425-32.

Boren, J., Lee, W.N., Bassilian, S., Centelles, J.J., Lim, S., Ahmed, S., Boros, L.G. i Cascante, M. (2003). The stable isotope-based dynamic metabolic profile of butyrate-induced HT29 cell differentiation. *J Biol Chem* **278**(31): 28395-402.

Boren, J., Montoya, A.R., de Atauri, P., Comin-Anduix, B., Cortes, A., Centelles, J.J., Frederiks, W.M., Van Noorden, C.J. i Cascante, M. (2002). Metabolic control analysis aimed at the ribose synthesis pathways of tumor cells: a new strategy for antitumor drug development. *Mol Biol Rep* **29**(1-2): 7-12.

Cao, H., Hininger-Favier, I., Kelly, M.A., Benaraba, R., Dawson, H.D., Coves, S., Roussel, A.M. i Anderson, R.A. (2007). Green tea polyphenol extract regulates the expression of genes involved in glucose uptake and insulin signaling in rats fed a high fructose diet. *J Agric Food Chem* **55**(15): 6372-8.

Cascante, M., Boros, L.G., Comin-Anduix, B., de Atauri, P., Centelles, J.J. i Lee, P.W. (2002). Metabolic control analysis in drug discovery and disease. *Nat Biotechnol* **20**(3): 243-9.

Cascante, M., Centelles, J.J., Veech, R.L., Lee, W.N. i Boros, L.G. (2000). Role of thiamin (vitamin B-1) and transketolase in tumor cell proliferation. *Nutr Cancer* **36**(2): 150-4.

Comin-Anduix, B., Boren, J., Martinez, S., Moro, C., Centelles, J.J., Trebukhina, R., Petushok, N., Lee, W.N., Boros, L.G. i Cascante, M. (2001). The effect of thiamine supplementation on tumour proliferation. A metabolic control analysis study. *Eur J Biochem* **268**(15): 4177-82.

Chen, E.I., Hewel, J., Krueger, J.S., Tiraby, C., Weber, M.R., Kralli, A., Becker, K., Yates, J.R., 3rd i Felding-Habermann, B. (2007). Adaptation of energy metabolism in breast cancer brain metastases. *Cancer Res* **67**(4): 1472-86.

Chen, Y.K., Cheung, C., Reuhl, K.R., Liu, A.B., Lee, M.J., Lu, Y.P. i Yang, C.S. (2012). Effects of green tea polyphenol (-)-epigallocatechin-3-gallate on newly developed high-fat/Western-style diet-induced obesity and metabolic syndrome in mice. *J Agric Food Chem* **59**(21): 11862-71.

Dang, C.V. (2012). MYC on the Path to Cancer. *Cell* **149**(1): 22-35.

Dang, C.V., Hamaker, M., Sun, P., Le, A. i Gao, P. (2011). Therapeutic targeting of cancer cell metabolism. *J Mol Med (Berl)* **89**(3): 205-12.

dos Santos, M.A., Borges, J.B., de Almeida, D.C. i Curi, R. (2004). Metabolism of the microregions of human breast cancer. *Cancer Lett* **216**(2): 243-8.

Jemal, A., Center, M.M., DeSantis, C. i Ward, E.M. (2010). Global patterns of cancer incidence and mortality rates and trends. *Cancer Epidemiol Biomarkers Prev* **19**(8): 1893-907.

Le, A., Lane, A.N., Hamaker, M., Bose, S., Gouw, A., Barbi, J., Tsukamoto, T., Rojas, C.J., Slusher, B.S., Zhang, H., Zimmerman, L.J., Liebler, D.C., Slebos, R.J., Lorkiewicz, P.K., Higashi, R.M., Fan, T.W. i Dang, C.V. (2012). Glucose-independent glutamine metabolism via TCA cycling for proliferation and survival in B cells. *Cell Metab* **15**(1): 110-21.

Lee, W.N., Boros, L.G., Puigjaner, J., Bassilian, S., Lim, S. i Cascante, M. (1998). Mass isotopomer study of the nonoxidative pathways of the pentose cycle with [1,2-13C2]glucose. *Am J Physiol* **274**(5 Pt 1): E843-51.

Li, C., Allen, A., Kwagh, J., Doliba, N.M., Qin, W., Najafi, H., Collins, H.W., Matschinsky, F.M., Stanley, C.A. i Smith, T.J. (2006). Green tea polyphenols modulate insulin secretion by inhibiting glutamate dehydrogenase. *J Biol Chem* **281**(15): 10214-21.

Mathupala, S.P., Ko, Y.H. i Pedersen, P.L. (2010). The pivotal roles of mitochondria in cancer: Warburg and beyond and encouraging prospects for effective therapies. *Biochim Biophys Acta* **1797**(6-7): 1225-30.

Metallo, C.M., Gameiro, P.A., Bell, E.L., Mattaini, K.R., Yang, J., Hiller, K., Jewell, C.M., Johnson, Z.R., Irvine, D.J., Guarente, L., Kelleher, J.K., Vander Heiden, M.G., Iliopoulos, O. i Stephanopoulos, G. (2011). Reductive glutamine metabolism by IDH1 mediates lipogenesis under hypoxia. *Nature* **481**(7381): 380-4.

Motrescu, E.R., Otto, A.M., Brischwein, M., Zahler, S. i Wolf, B. (2005). Dynamic analysis of metabolic effects of chloroacetaldehyde and cytochalasin B on tumor cells using bioelectronic sensor chips. *J Cancer Res Clin Oncol* **131**(10): 683-91.

Purcell, W.T. i Ettinger, D.S. (2003). Novel antifolate drugs. *Curr Oncol Rep* **5**(2): 114-25.

Ramos, S., Rodriguez-Ramiro, I., Martin, M.A., Goya, L. i Bravo, L. (2011). Dietary flavanols exert different effects on antioxidant defenses and apoptosis/proliferation in Caco-2 and SW480 colon cancer cells. *Toxicol In Vitro* **25**(8): 1771-81.

Sanchez-Tena, S., Fernandez-Cachon, M.L., Carreras, A., Mateos-Martin, M.L., Costoya, N., Moyer, M.P., Nunez, M.J., Torres, J.L. i Cascante, M. (2012). Hamamelitannin from Witch Hazel (Hamamelis virginiana) Displays Specific Cytotoxic Activity against Colon Cancer Cells. *J Nat Prod* **75**(1): 26-33.

Shimizu, M., Kubota, M., Tanaka, T. i Moriwaki, H. (2012). Nutraceutical approach for preventing obesity-related colorectal and liver carcinogenesis. *Int J Mol Sci* **13**(1): 579-95.

Sun, R.C., Board, P.G. i Blackburn, A.C. (2011). Targeting metabolism with arsenic trioxide and dichloroacetate in breast cancer cells. *Mol Cancer* **10**: 142.

Telang, S., Lane, A.N., Nelson, K.K., Arumugam, S. i Chesney, J. (2007). The oncoprotein H-RasV12 increases mitochondrial metabolism. *Mol Cancer* **6**: 77.

Vander Heiden, M.G., Cantley, L.C. i Thompson, C.B. (2009). Understanding the Warburg effect: the metabolic requirements of cell proliferation. *Science* **324**(5930): 1029-33.

Vander Heiden, M.G., Lunt, S.Y., Dayton, T.L., Fiske, B.P., Israelsen, W.J., Mattaini, K.R., Vokes, N.I., Stephanopoulos, G., Cantley, L.C., Metallo, C.M. i Locasale, J.W. (2012). Metabolic Pathway Alterations that Support Cell Proliferation. *Cold Spring Harb Symp Quant Biol*.

Vizan, P., Boros, L.G., Figueras, A., Capella, G., Mangues, R., Bassilian, S., Lim, S., Lee, W.N. i Cascante, M. (2005). K-ras codon-specific mutations produce distinctive metabolic phenotypes in NIH3T3 mice [corrected] fibroblasts. *Cancer Res* **65**(13): 5512-5.

Vizan, P., Sanchez-Tena, S., Alcarraz-Vizan, G., Soler, M., Messeguer, R., Pujol, M.D., Paul Lee, W.N. i Cascante, M. (2009). Characterization of the metabolic changes underlying growth factor angiogenic activation: identification of new potential therapeutic targets. *Carcinogenesis*.

Weinberg, F., Hamanaka, R., Wheaton, W.W., Weinberg, S., Joseph, J., Lopez, M., Kalyanaraman, B., Mutlu, G.M., Budinger, G.R. i Chandel, N.S. (2010). Mitochondrial metabolism and ROS generation are essential for Kras-mediated tumorigenicity. *Proc Natl Acad Sci U S A* **107**(19): 8788-93.

CAPÍTOL 4

La fibra dietètica antioxidant de raïm inhibeix la poliposi intestinal en ratolins $Apc^{Min/+}$

Susana Sánchez-Tena[1], Daneida Lizárraga[1,§], Anibal Miranda[1], Maria Pilar Vinardell[2], Francisco García-García[3], Joaquín Dopazo[3], Josep Lluís Torres[4], Fulgencio Saura-Calixto[5], Gabriel Capellà[6] i Marta Cascante[1]

[1]Departament de Bioquímica i Biologia Molecular, Facultat de Biologia, Universitat de Barcelona, Institut de Biomedicina de la Universitat de Barcelona (IBUB), Unitat associada al CSIC, Barcelona, Espanya

[2]Departament de Fisiologia, Facultat de Farmacia, Universitat de Barcelona, Barcelona, Espanyaº

[3]Node de Genòmica Funcional, Institut Nacional de Bioinformatica, Departamento de Bioinformática, CIPF, Valencia, Espanya

[4]Institut de Química Avançada de Catalunya (IQAC-CSIC), Barcelona, Espanya

[5]Instituto de Ciencia y Tecnología de Alimentos y Nutrición (ICTAN-CSIC), Madrid, Espanya

[6]Laboratori de Recerca Translacional, IDIBELL-Institut Català d'Oncologia, Barcelona, Espanya

§ *Present address:* Department of Health Risk Analysis and Toxicology, Maastricht University, Maastricht, The Netherlands.

RESUM

Estudis epidemiològics i experimentals suggereixen que la fibra i els polifenols tenen un efecte protector contra del desenvolupament del càncer de còlon. Consegüentment, en aquest treball es va avaluar el l'eficàcia quimiopreventiva i els mecanismes d'acció associats de la fibra antioxidant de raïm (GADF – *Grape Antioxidante Dietary Fiber*) enfront la tumorigenesis intestinal espontània en el model de ratolí $Apc^{Min/+}$. Els ratolins es van alimentar amb un pinso estàndard (grup control) o bé amb pinso contenint un 1% (w/w) de GADF (grup GADF) durant 6 setmanes. La GADF va reduir la tumorigenesis intestinal, concretament va disminuir el número total de pòlips un 76% respecte els ratolins control. A més, l'anàlisi de pòlips per mida, va mostrar una reducció considerable en totes les categories [diàmetre <1 mm (65%), 1–2 mm (67%) i >2 mm (87%)]. Pel que fa a la formació de pòlips en les zones proximal, medial i distal, es va observar una disminució del 76%, 81% i 73%, respectivament. Els potencials mecanismes moleculars subjacents a la inhibició de la tumorigenesis intestinal es van investigar per comparació dels perfils d'expressió dels ratolins tractats o no amb GADF. Es va observar que els efectes de la GADF s'associen principalment amb la modulació de gens implicats en la progressió tumoral, incloent *Ccnd1*, *Gadd45a*, *Tgfb1*, *Plk3*, *kitl*, *Csnk1e*, *Lfng*, *Pold1* i *Rfc1*. Els nostres descobriments mostren per primer cop l'eficàcia i els mecanismes moleculars d'acció de la GADF contra la tumorigenesis intestinal en ratolins $Apc^{Min/+}$, suggerint el seu potencial per la prevenció envers el càncer colorectal.

Grape antioxidant dietary fiber (GADF) inhibits intestinal polyposis in $Apc^{Min/+}$ mice

Susana Sánchez-Tena[1], Daneida Lizárraga[1,§], Anibal Miranda[1], Maria Pilar Vinardell[2], Francisco García-García[3], Joaquín Dopazo[3] , Josep Lluís Torres[4], Fulgencio Saura-Calixto[5], Gabriel Capellà[6] and Marta Cascante[1,*].

[1] Department of Biochemistry and Molecular Biology, Faculty of Biology, Universitat de Barcelona, Institute of Biomedicine of Universitat de Barcelona (IBUB) and CSIC-Associated Unit Barcelona, Spain

[2] Departament de Fisiologia, Facultat de Farmacia, Universitat de Barcelona, Barcelona, Spain

[3] Functional Genomics Node, National Institute of Bioinformatics, Department of Bioinformatics, CIPF, Valencia, Spain

[4] Institute for Advanced Chemistry of Catalonia (IQAC-CSIC), Barcelona, Spain

[5] Department of Metabolism and Nutrition, Institute of Food Science and Technology and Nutrition (ICTAN-CSIC), Madrid, Spain

[6] Translational Research Laboratory, IDIBELL-Catalan Institute of Oncology, Barcelona, Spain

[§] *Present address:* Department of Health Risk Analysis and Toxicology, Maastricht University, Maastricht, The Netherlands.

ABSTRACT

Epidemiological and experimental studies suggest that fiber and polyphenolic compounds might have a protective effect on the development of colon cancer in humans. Accordingly, we assessed the chemopreventive efficacy and associated mechanisms of action of a lyophilized red grape pomace containing proanthocyanidin-rich dietary fiber (Grape Antioxidant Dietary Fiber, GADF) on spontaneous intestinal tumorigenesis in the $Apc^{Min/+}$ mouse model. Mice were fed a standard diet (control group) or a 1% (w/w) GADF-supplemented diet (GADF group) for 6 weeks. GADF supplementation greatly reduced intestinal tumorigenesis, significantly decreasing the total number of polyps by 76%. Moreover, size distribution analysis showed a considerable reduction in all polyp size categories [diameter <1 mm (65%), 1–2 mm (67%) and >2 mm (87%)]. In terms of polyp formation in the proximal, middle and distal portions of the small intestine a decrease of 76%, 81% and 73% was observed respectively. Putative molecular mechanisms underlying the inhibition of intestinal tumorigenesis were investigated by comparison of microarray expression profiles of GADF-treated and non-treated mice. We observed that the effects of GADF are mainly associated with the modulation of genes involved in cancer progression, including *Ccnd1*, *Gadd45a*, *Tgfb1*, *Plk3*, *kitl*, *Csnk1e*, *Lfng*, *Pold1* and *Rfc1*. Our findings show for the first time the efficacy and associated mechanisms of action of GADF against intestinal tumorigenesis in $Apc^{Min/+}$ mice, suggesting its potential for the prevention of colorectal cancer.

INTRODUCTION

Most grape dietary fibre and polyphenols accumulate in the fruit skins, seed and pulp, which after the manufacture of grape juice and wine remains as pomace. After production, this processed raw material becomes a by-product and is used as fertilizer, animal feed or disposed in dumps, being a great waste of health-promoting compounds. Given that there is great evidence suggesting that higher dietary intake of vegetables and fruits, rich in fibre and polyphenols, is associated with a lower risk of colorectal cancer (Forte *et al.*, 2008), further study of these by-products as colon cancer chemopreventive agents is still needed.

Grape Antioxidant Dietary Fiber (GADF), here in the form of lyophilized red grape pomace, is a wine processing by-product from red grape that is rich in dietary fibre and polyphenols. It contains a large amount (13% wt:wt) of non-extractable polymeric proanthocyanidins (PA), mainly (epi)catechin-based polymers that are part of the dietary fiber fraction together with lignins and polysaccharides. During its transit along the intestinal tract, the small soluble polyphenols are absorbed and the remaining PA progressively release (epi)catechin units that are then absorbed and metabolized. The remaining polymeric PA are cleaved by the intestinal microbiota into smaller species such as phenolic acids, which in turn are absorbed and metabolized (Touriño *et al.*, 2011). Previous studies in male Wistar rats have shown that GADF exerts a protective effect upon the large intestine mucosa, which has been attributed to modulation of the gluthathione redox system and endogenous antioxidant enzymes (Lopez-Oliva *et al.*, 2010). Recently, Lizárraga and colleagues reported that the inclusion of GADF in the mouse diet protects the normal colon tissue against polyp development through alterations in the expression of tumor suppressor genes and proto-oncogenes as well as the modulation of enzymes pertaining to the xenobiotic detoxifying system and endogenous antioxidant cell defenses (Lizárraga *et al.*, 2011). Together, these results suggest that GADF could be an effective chemopreventive agent against colorectal cancer. However, the efficacy of GADF as a chemopreventive agent needs to be established in well-defined preclinical models of colon cancer before embarking on clinical trials.

The $Apc^{Min/+}$ mouse is a model of colon cancer that harbors a dominant germline mutation at codon 850 of the homolog of the human adenomatous polyposis coli (*Apc)* gene, which results in a defective protein product that predisposes the mice to spontaneously develop pre-neoplastic intestinal polyps (Su *et al.*, 1992). APC function is linked to the Wnt signaling pathway, in which it operates by activating β-catenin degradation. Therefore, mutation of the *Apc* gene produces cytosolic accumulation and an increase in the nuclear translocation of β-catenin. In the nucleus, β-catenin activates the transcription factor T cell factor/lymphoid enhancer factor (TCF/LEF), giving

rise to an increase in the expression of genes regulating cell proliferation and predisposing the cells to the formation of tumors. Mutations in the *Apc* gene have been directly implicated in the development of both human familial adenomatous polyposis (FAP) and sporadic colorectal cancer (Hinoi *et al.*, 2007). Hence, the $Apc^{Min/+}$ mouse model is considered an analog of human intestinal tumorigenesis and has been widely used to study the effects of dietary and pharmaceutical agents on human colon cancer prevention. Here we assessed the efficacy and associated molecular mechanisms of action of GAFD consumption on spontaneous intestinal tumorigenesis in $Apc^{Min/+}$ mice.

MATERIAL AND METHODS

Grape antioxidant dietary fiber (GADF). GADF was obtained from red grapes (the *Cencibel* variety) harvested in the vintage year 2005 in *La Mancha* region in Spain, as described in the Spanish patents registered under the numbers 2259258 and 2130092. The percentage composition of GADF used in this work was as follows: dietary fiber, 73.48 ± 0.79 (57.95 ± 0.78 comprising an indigestible fraction of insoluble compounds such as lignin and proanthocyanidins and 15.53 ± 0.11 of a soluble fraction constituted by pectins and hemicellulose); polymeric proanthocyanidins associated with insoluble dietary fiber, 14.81 ± 0.19; fat, 7.69 ± 0.49; protein, 11.08 ± 0.46; and ash, 5.25 ± 0.19. More than 100 phenolic compounds (not associated with dietary fiber) such as phenolic acids, anthocyanidins, catechins and other flavonoids have been detected in GADF (Touriño *et al.*, 2008).

Animals and diet. We used male $Apc^{Min/+}$ mice aged 5 weeks from Jackson Laboratories (Bangor, ME). Animals were housed in plastic cages at 22 °C and 50% humidity, with a 12:12 h light/dark cycle, according to European Union Regulations. The experimental protocols were approved by the Experimental Animal Ethical Research Committee of the University of Barcelona in accordance with current regulations for the use and handling of experimental animals. After 7 days of acclimatization during which they received a standard diet (Teklad Global 18% Protein rodent diet), the animals were randomly divided into two groups, with 12 and 10 mice per group (Control and GADF respectively). Control mice continued to be fed the standard diet, and the GADF-treated group was fed a special diet comprising the basal diet (Teklad Global 18% Protein rodent diet) supplemented with GADF at 1% w/w in order to mimic the recommended fiber content in the diet (Ferguson, 2005). Diets were purchased from Harlan Interfauna Iberica S.L (Barcelona, Spain). Both food and water were supplied *ad libitum* throughout the experiment. Throughout the 6-week treatment period, mice were observed for any signs of toxicity, and body weight and food and

water intake were recorded weekly. At the end of the 6 weeks, the animals were starved overnight and then anesthetized with volatile isoflurane (ESTEVE, Barcelona, Spain). Blood samples were obtained by cardiac puncture. Finally, animals were sacrificed by an overdose of anesthesia.

Measurement of intestinal polyps. $Apc^{Min/+}$ mice develop polyps in both the small and large intestine, although more intestinal adenomas are observed in the small intestine. Therefore, after sacrifice, the small intestine was excised from each mouse. Immediately after sacrifice, the small intestine was cut longitudinally and rinsed with phosphate-buffered saline solution (pH 7.4) to remove the intestinal contents. The intestines were pinned flat on cardboard and then fixed for 1 day in 4% neutral buffered formalin solution (v/v; pH 7.4). Intestinal sections were stored at room temperature in 1% neutral buffered formalin solution (v/v) until further analysis. In order to facilitate tumor quantification and identification, the small intestine was divided into three equal sections: proximal, medial and distal. Thereafter the small intestine sections were stained in phosphate-buffered saline solution (pH 7.4) and 0.1% (v/v) methylene blue. Using a stereomicroscope and a measured grid, the number of tumors and their dimensions in each small intestine section were determined. The size of each tumor was categorized as <1 mm, 1–1.9 mm, or ≥2 mm.

RNA isolation and gene profiling by Affymetrix Microarrays. Large intestine was removed and placed on a plastic plate, which was kept at 4 °C on ice. After removal of the rectum, the colon was opened longitudinally with fine scissors, and mucus and feces were removed. The colonic mucosal layer was incubated in Trizol (Invitrogen, Carlsbad, CA) for 3 min and scraped off the muscle layer using the edge of a sterile glass slide. Cells were transferred into 800 µl Trizol, homogenized by pipetting, and stored at -80 °C until RNA isolation. Total RNA was isolated using a combination of two methods. First, total RNA was isolated using the Trizol method, according to the manufacturer´s protocol (Invitrogen, Carlsbad, CA). Next, RNA was purified using the RNeasy Mini kit and DNase I treatment (Qiagen, Germantown, MD) according to the manufacturer´s protocol. RNA was dissolved in DEPC-treated, RNase-free water. RNA purity and quantity were tested spectrophotometrically using the NanoDrop ND-1000 (NanoDrop Technologies) and were considered suitable for further processing if the ratio of absorbance at 260/280 > 1.9. Integrity was tested using lab-on-a-chip technology on the BioAnalyzer 2100 (Agilent, Palo Alto, CA, USA) and RNA was considered to be intact when showing a RNA integrity number (RIN) > 8. Affymetrix Microarrays using the Mouse Genome 430 2.0 platforms were performed according to the protocols published by the manufacturer (Affymetrix). We analyzed five RNA samples chosen at random from the control and GADF group.

Microarray data analyses. Data were standardized using the Robust Multi-array Average method (Bolstad *et al.*, 2003) and quantile normalization. Differential gene expression was assessed using the *limma* (Smyth, 2004) package from Bioconductor. Multiple testing adjustment of p-value was conducted according to Benjamini and Hochberg (Benjamini *et al.*, 2001). Biochemical pathway analysis was conducted using the Kyoto Encyclopedia of Genes and Genomes (KEGG) Mapper. This is a collection of KEGG mapping tools for KEGG pathway mapping. The tool "Search&Color Pathway" was used to overlay gene expression results from microarrays onto biochemical pathways found in the KEGG. Gene expression levels were denoted using color codes displayed along the pathway by gene symbol boxes. Different shapes and patterns were used to represent induced and suppressed gene expression. Enrichment analysis was based on MetaCore™, an integrated knowledge database and software suite for pathway analysis of experimental data and gene lists. Enrichment analysis consists of matching the gene IDs of possible targets for the "common", "similar" and "unique" sets with gene IDs in functional ontologies in MetaCore. The probability of a random intersection between a set of IDs the size of the target list with ontology entities is estimated by the p-value of the hypergeometric intersection. A lower p-value means higher relevance of the entity to the dataset, which results in higher rating for the entity. Use of the False Discovery Rate (adjusted p-value) allows processes with doubtful significance for the current experiment to be rejected, and ensures that the findings are not contaminated with false positives. Gene set analysis was carried out for the Gene Ontology terms using FatiScan (Al-Shahrour *et al.*, 2007) integrated in the Babelomics suite. This method detects significantly up- or down-regulated blocks of functionally related genes in lists of genes ordered by differential expression. FatiScan can search blocks of genes that are functionally related using different criteria such as gene ontology terms, KEGG pathways, and others. The core of the method proposed is based on an algorithm to test whether a set of genes, labeled with terms (biological information), contain significant enrichments in one or several of these terms with respect to another set of reference genes. FatiScan uses a Fisher's exact test for 2×2 contingency tables to compare two groups of genes and extract a list of GO terms whose distribution among groups is significantly different. Given that many GO terms are tested simultaneously, the results of the test are corrected for multiple testing to obtain an adjusted p-value. FatiScan returns adjusted p-value based on the False Discovery Rate (FDR) method (Benjamini *et al.*, 2001).

RT-real time PCR. cDNA was synthesized in a total volume of 20 µl from RNA samples by mixing 1 µg of total RNA, 125 ng of random hexamers (Roche), 0.01 M dithiothreitol (Invitrogen), 20 units of RNAsin (Promega), 0.5 mM dNTPs (Bioline), 200 units of M-MLV reverse transcriptase (Invitrogen) and 4 µl 5X First-Strand Buffer (375 mM KCl, 15 mM $MgCl_2$,

250 mM Tris-HCl, pH 8.3) (Invitrogen). The reaction mixture was incubated at 37 ºC for 60 min. The cDNA product was used for subsequent amplification by real time PCR. The mRNA levels for the selected genes were determined in an ABI Prism 7000 Sequence Detection System (Applied Biosystems) using 9 µL of the cDNA mixture and 11 µL of the specific primers in Master mix (all from Applied Biosystems). β2 microglobulin (B2M) RNA was used as an endogenous control. The reaction was performed following the manufacturer's recommendations. Fold-changes in gene expression were calculated using the standard ΔΔCt method.

RESULTS AND DISCUSSION

GADF supplementation inhibits spontaneous intestinal polyposis without affecting body weight in APC $^{Min/+}$ mice.

During the experiment the body weight and food and water consumption of all mice were monitored. Food consumption and body weight gain did not differ between the control and GADF groups throughout the study and no mortality was observed in any group (data not shown). GADF treatment did not result in macroscopic changes indicative of toxicity in any organs including the liver, lung and kidney.

GADF treatment resulted in a significant reduction in the formation of small intestine tumors. Control mice developed an average of 16 polyps per animal and GADF treatment decreased this number to 3.9 (Figure 1A). In fact, GADF induced a 76% reduction in intestinal polyposis with respect to the control. Interestingly, GADF exerted a higher anti-tumoral effect than observed in previous studies in Apc$^{Min/+}$ mice in similar conditions using dietary fiber or other individual polyphenolic compounds. For example, administration of 1% dibenzoylmethane reduced the total number of small intestinal tumors by 50% in Apc$^{Min/+}$ mice (Shen *et al.*, 2007). The best results obtained with fiber in similar studies were a reduction in small intestinal tumors of 25% after feeding on 10% rye bran (Mutanen *et al.*, 2000) and a decrease of 51% with 30% rice bran (Verschoyle *et al.*, 2007). As shown in Figure 1B, GADF treatment induced a decrease in the number of small intestine polyps in the proximal, medial and distal sections of 76% (4.6 ± 0.9 versus 1.1 ± 0.3), 81% (4.3 ± 1.0 versus 0.8 ± 0.3) and 73% (7.3 ± 2.4 versus 2.0 ± 0.4) respectively. These homogeneous values indicate that GADF exerts its anti-tumorigenic activity throughout the small intestine. GADF contains a complex mixture of polyphenols including monomers of catechins, anthocyanins, flavonols and hydroxycinnamic acids, as well as (epi)catechin oligomers and polymers (PA), all of which are associated with a fiber matrix of both soluble and insoluble polymers such as polysaccharides and lignins that may influence the

absorption of the putatively bioactive GADF components. Small polyphenols such as phenolic acids and monomeric (epi)catechins that are originally contained within the matrix or are derived from the partial depolymerization of oligomeric PA are absorbed in the small intestine; however, some of the PA are fermented by the intestinal microbiota and are absorbed in the form of smaller phenolic acids (Touriño *et al.*, 2009). The fact that GADF exerts its anti-tumorigenic function homogeneously throughout the intestine could thus be related to its composition, as the putatively bioactive polyphenolic compounds embedded in the fiber are gradually released and absorbed. Moreover, fiber increases the transit time through the gastrointestinal tract, which allows food polyphenols to be more extensively absorbed by enterocytes. Analysis of the size distribution of polyps revealed that GADF reduced the occurrence or growth of <1 mm diameter polyps by 65% (5.5 ± 1.2 versus 1.9 ± 0.4), of 1–2 mm by 67% (3.0 ± 1.1 versus 1.0 ± 0.3) and of >2 mm by 87% (7.7 ± 2.2 versus 1.0 ± 0.3) (Figure 1C). These results suggest that GADF inhibits both the appearance and development of intestinal polyps, although the most important inhibitory effect was observed in larger polyps indicating a major inhibition in polyp's progression.

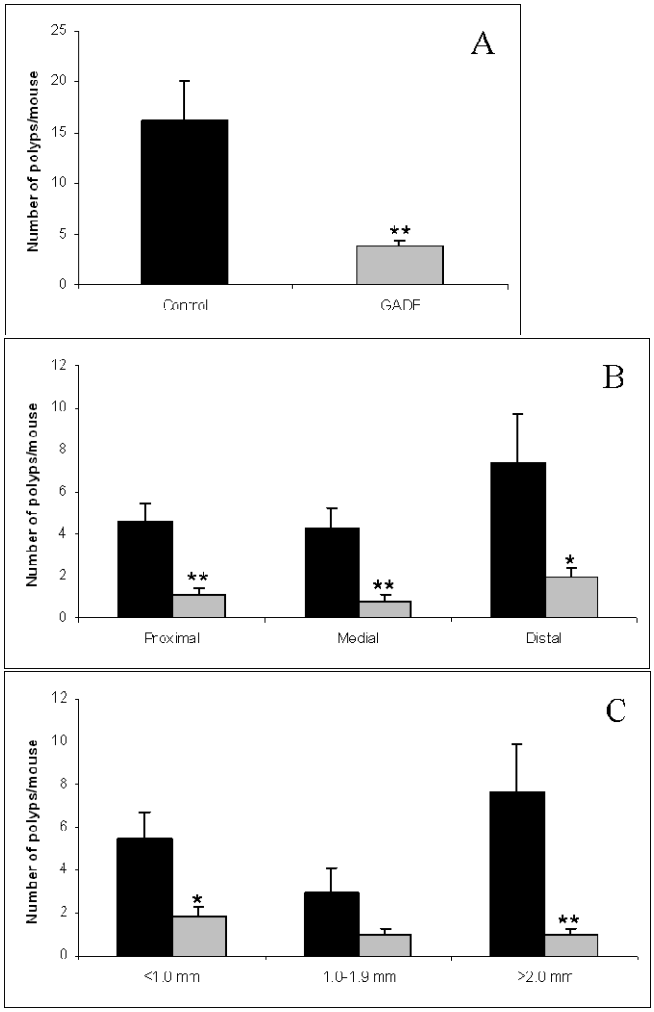

Figure 1. A) Total number of polyps/mouse in the small intestine of $Apc^{Min/+}$ mice. B) Number of polyps/mouse in proximal, medial and distal sections. C) Number of polyps/mouse shown by polyp size distribution (<1 mm diameter polyps, 1–2 mm and >2 mm). Data represented as mean ± SEM (*, $p > 0.05$) (**, $p > 0.01$).

Gene expression profile induced by GADF. To elucidate the underlying mechanisms by which GADF prevents carcinogenesis we determined the transcriptional profile of the $Apc^{Min/+}$ mouse colonic mucosa following GADF treatment using cDNA microarrays.

Of the 39,000 genes represented on the whole mouse genome cDNA microarray, 183 genes were differentially expressed between the control and GADF groups with a 1.5-fold change or more in expression. Of these 183 differentially expressed genes, 40 genes were up-regulated and 143

genes were down-regulated. A complete list of these differentially expressed genes is shown in supplemental data 1.

This list of differentially expressed genes associated with GADF consumption was subjected to a KEGG molecular pathway analysis using KEGG Mapper to identify any enrichment of genes with specific biological themes. This analysis mainly showed modifications in cancer-related pathways. Figure 2 presents the KEGG cell cycle pathway analysis using KEGG Mapper. This analysis suggests that GADF suppresses tumorigenesis in $Apc^{Min/+}$ mice by inducing cell cycle arrest. GADF treatment led to a reduction in the expression of the *Ccnd1* gene, which codes for cyclin D, which in turn is involved in regulating cell cycle progression and drives the G1/S phase transition. *Cyclin D* is under the transcriptional activation induced by β-catenin/TCF/LEF, hence the downregulation of this gene by GADF antagonizes the deregulated Wnt signaling pathway in $Apc^{Min/+}$ mice. Moreover, an increase in the expression of a regulator of this protein called *Gadd45a* was detected. The GADD45 protein interacts with many effectors, such as Cdc2/CyclinB1, PCNA (which regulates Cyclin D/Cdk4,6), and p21, thus mediating cell cycle arrest, differentiation or apoptosis (Hoffman *et al.*, 2009). These results are consistent with previous studies in which dietary supplementation with grape seed extract in $Apc^{Min/+}$ mice was found to down-regulate Cyclin D1 and up-regulate Cip1/p21 in small intestinal tissue samples according to immunohistochemical analysis (Velmurugan *et al.*, 2010). Likewise, another study reported that grape seed extract up-regulates p21, leading to G1 cell cycle arrest (Kaur *et al.*, 2011). Furthermore, study of the cell cycle pathway showed that the expression of *Tgfb1* is also down-regulated. Interestingly, TGF-beta1 has been reported to be involved in the progression of colorectal cancer, and therefore a reduction in its expression suggests higher sensitivity to anti-growth signals and a reduction in angiogenesis (Narai *et al.*, 2002; Langenskiold *et al.*, 2008). Additionally, the DNA replication pathway represented in KEGG Mapper (data not shown) was also down-regulated in the mucosa of $Apc^{Min/+}$ mice treated with GADF. This was due to inhibition of the expression of *Pold2* and *Rfc1*, two members of the DNA polymerase complex. Consequently, inhibition of DNA synthesis may also be involved in the induction of G1 arrest in the cell cycle (Takeda *et al.*, 2005).

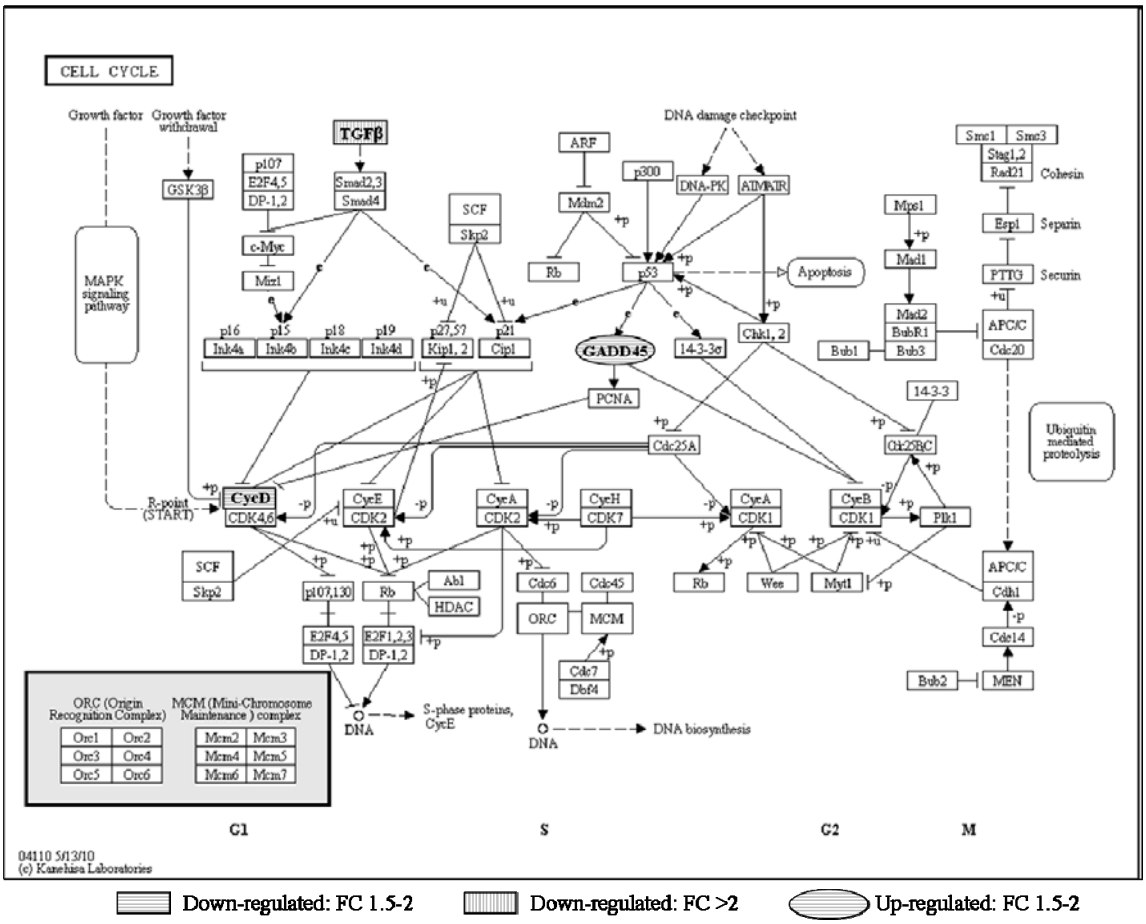

Figure 2. Adaptation of KEGG cell cycle pathway using KEGG Mapper. Circular pathway members were significantly up-regulated and rectangular members were found to be down-regulated in the intestinal mucosa of $Apc^{Min/+}$ mice treated with GADF. Horizontal lines indicate a fold change (FC) of between 1.5 and 2 and vertical lines a FC of more than 2.

KEGG Mapper analysis also showed the modulation of other genes related to cancer pathways (Figure 3). GADF supplementation modulated the expression of *Kitl*, which encodes the ligand of the tyrosine-kinase receptor KIT. The ligand for KIT is known as kit ligand or stem cell factor (SCF). Yasuda and colleagues reported that SCF-KIT signaling enhances proliferation and invasion in KIT-positive colorectal cancer cell lines (Yasuda *et al.*, 2007). Thus, the lower expression of kit ligand in GADF-treated mice may be related to the inhibition of intestinal polyp growth.

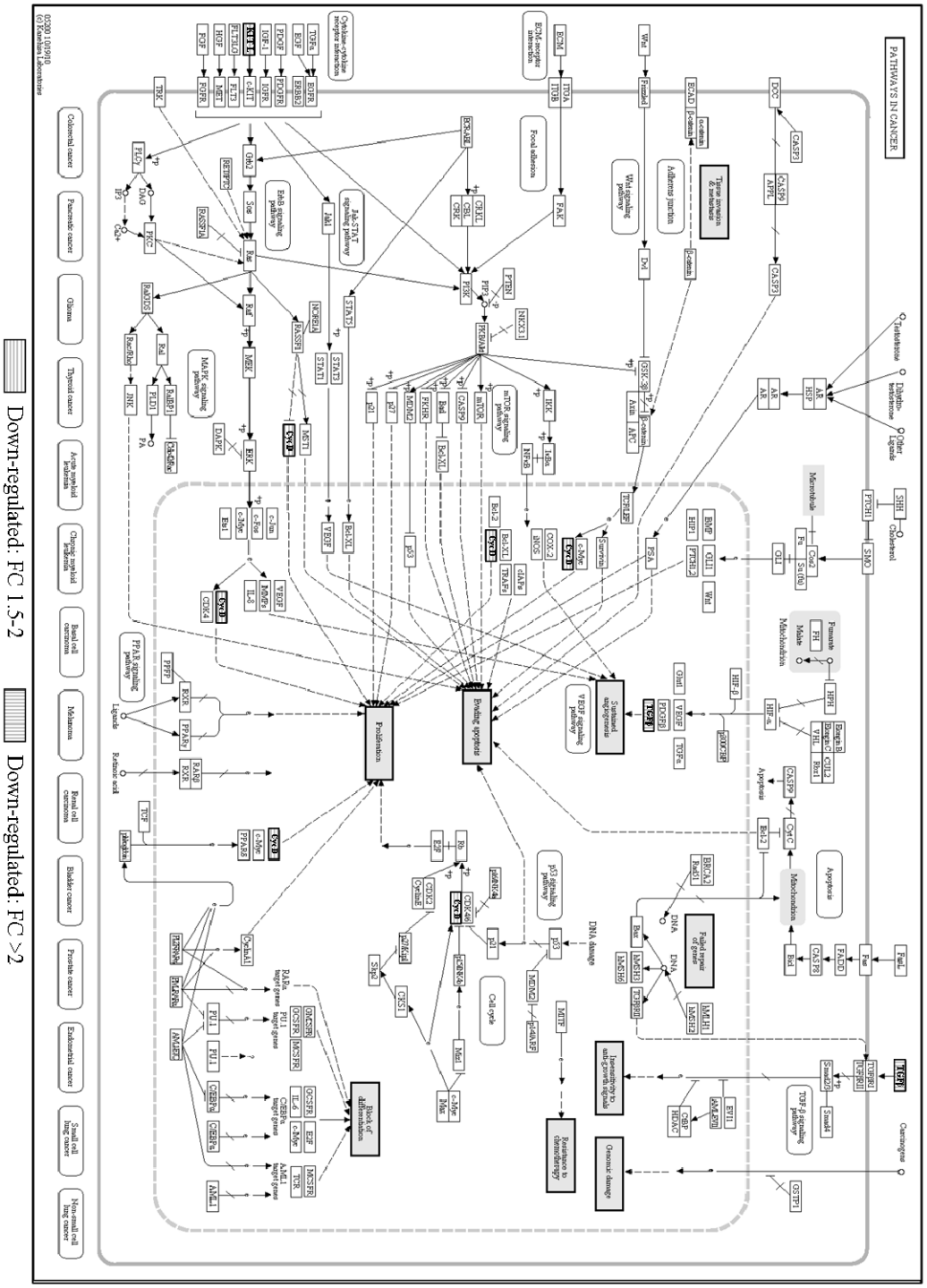

Figure 3. Relative transcript abundance of genes encoding proteins in cancer pathways, as determined by KEGG Mapper. Circular boxes represent up-regulated genes and rectangular boxes represent down-regulated genes following GADF supplementation. Horizontal lines indicate a FC of between 1.5 and 2 and vertical lines specify a FC of more than 2.

As mentioned earlier, $Apc^{Min/+}$ mice possess a mutation in the *Apc* gene that results in defective Wnt signaling. The representation of the KEGG Mapper Wnt signaling pathway (Figure 4) showed that GADF down-regulates the expression of *Csnk1e*, which encodes the CKI protein epsilon. This protein is a positive regulator of beta-catenin-driven transcription and is specifically required for the proliferation of breast cancer cells with activated beta-catenin (Kim *et al.*, 2010). Moreover, recent data indicate that Wnt and Notch signaling might play an equally important role in the maintenance of the undifferentiated state of *Apc*-deficient cells (Reedijk *et al.*, 2008). In fact, it has been reported that Notch signaling occurs downstream of Wnt through β-catenin-mediated transcriptional activation of the Notch-ligand Jagged1 (Rodilla *et al.*, 2009), suggesting that Notch is an alternative target for the treatment of *Apc*-mutant intestinal polyposis. Interestingly, GADF treatment also down-regulated *Lfng* (data not shown), which encodes Fringe, a glycosyltransferase that is involved in the elongation of O-ligands in the Notch pathway (Chen *et al.*, 2001). Therefore, GADF inhibits colon cancer growth through the simultaneous downregulation of Wnt and Notch signaling.

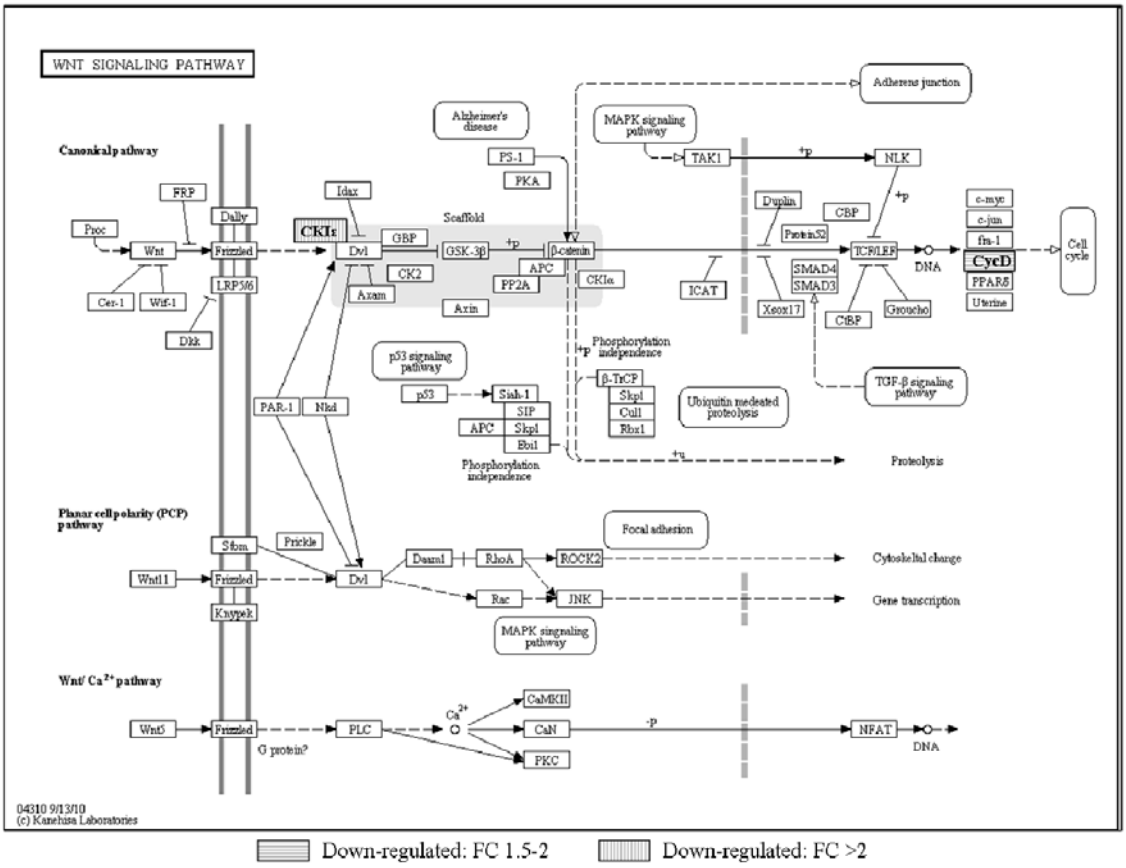

Figure 4. Adaptation of KEGG Wnt signaling pathway. Circular colored boxes represent up-regulated genes encoding that protein and rectangular boxes represent down-regulated genes in $Apc^{Min/+}$ mice following GADF treatment. Horizontal lines indicate a FC in expression of between 1.5 and 2 and vertical lines specify a FC of more than 2.

Pathway analysis performed using KEGG Mapper was complemented with an independent analysis by MetaCore to obtain the p-value of each pathway. Pathway analysis of significantly modulated genes using MetaCore showed significant changes in maps that contain several canonical pathways. Table 1 presents the top Maps according to Metacore, showing the greatest downregulation in the cell cycle, immune system responses and G-protein signaling, whereas cell adhesion, neurophysiological process and development were up-regulated. In addition to the above-mentioned cell-cycle-associated genes, Metacore analysis identified upregulation of the PLK3 gene, which is associated with cell cycle progression. Interestingly, PLK3 has been correlated with the development of certain cancers (Myer *et al.*, 2011), and therefore its downregulation by GADF could be involved in the anti-tumoral effect of the latter in $Apc^{Min/+}$ mice. Metacore analysis also

revealed the downregulation of immune-system-related genes by GADF (*Lck, Nfkbie, Cxcr4, H2-Ab1, Igh, Igl-V1,* and *Igkv1-117*). Inflammation and immune system responses have been reported to have dual effects in cancer, either by providing protection from tumor cells or, when inflammation becomes chronic, by promoting tumor growth. Grape polyphenols have been implicated in strengthening immune function (Katiyar, 2007), but their anti-inflammatory and immune-attenuating properties have recently attracted much attention (Misikangas *et al.*, 2007; Kawaguchi *et al.*, 2011). These functions may play an important role in $Apc^{Min/+}$ mice since the tumorigenesis initiated by intrinsic defects in pathways regulating cell proliferation, as observed in $Apc^{Min/+}$ mice, is driven by repeated inflammation and excessive immune signaling (Saleh *et al.*, 2011). Accordingly, a study identifying genes involved in tumorigenesis in $Apc^{Min/+}$ mice revealed the upregulation of various immune system and inflammation genes (Leclerc *et al.*, 2004). Therefore, in this case, diminished immune signaling may reduce tumor progression. Interestingly, apart from the immuno-attenuating properties of grape polyphenols mentioned above, a recent investigation concluded that high fiber intake may be inversely associated with the presence of a cytokine pro-inflammatory profile (Chuang *et al.*, 2011). Therefore, attenuation of the immune response in $Apc^{Min/+}$ mice treated with GADF could be due to the combined effect of soluble polyphenols, insoluble PA and other components of the dietary fiber fraction such as polysaccharides and lignins.

Table1

Effects in modulated pathways by GADF in colon mucosa of ApcMin/+ mice as found in Metacore

GeneGO Maps	Regulated pathways	p-value	Significant/total genes
Cell cycle and its regulation (↓)	Regulation of G1/S transition (part 1) (↓)	0,0010	2 (*Ccnd1, Tgfb1*)/38
	Nucleocytoplasmic transport of CDK/Cyclins (↓)	0,0023	1 (*Ccnd1*)/14
	ATM / ATR regulation of G2 / M checkpoint (↑)	0,0005	2 (*Gadd45a, Plk3*)/26
Immune response (↓)	CXCR4 signaling via second messenger (↓)	0,0007	3 (*Lck, Nfkbie, Cxcr4*)/34
	TCR and CD28 co-stimulation in activation of NF-kB (↓)	0,0012	3 (*H2-Ab1, Nfkbie, Lck*)/40
	ICOS pathway in T-helper cell (↓)	0,0017	3 (*H2-Ab1, Nfkbie, Lck*)/46
	NFAT in immune response (↓)	0,0023	4 (*H2-Ab1, Nfkbie, Lck, Ig*)/51
	T cell receptor signaling pathway (↓)	0,0025	3 (*H2-Ab1, Nfkbie, Lck*)/52
G-protein signaling (↓)	G-Protein alpha-q signaling cascades (↓)	0,0007	3 (*Rgs2, Plcb4, Nfkbie*)/34
	Proinsulin C-peptide signaling (↓)	0,0025	3 (*Ccnd1, Plcb4, Nfkbie*)/52
Cell adhesion (↑)	Tight junctions (↑)	0,0010	2 (*Ocln, Cldn4*)/36
	Ephrin signaling (↑)	0,0016	1 (*Epha2*)/45
Neurophysiological process (↑)	Receptor-mediated axon growth repulsion (↑)	0,0016	2 (*Epha2*)/45
Development (↑)	A3 receptor signaling (↓)	0,0021	3 (*H2-A, Nfkbie, Lck*)/49
	TGF-beta-dependent induction of EMT via SMADs (↓)	0,0008	2 (*Tgfb1, Ets1*)/35
	TGF-beta-dependent induction of EMT via SMADs (↑)	0,0009	2 (*Edn1, Ocln*)/35
	TGF-beta-dependent induction of EMT via MAPK (↑)	0,0017	2 (Edn1, Ocln)/47
	Regulation of epithelial-to-mesenchymal transition (EMT) (↑)	0,0031	2 (Edn1, Ocln)/64

↑/↓ Activated/Inhibited

In addition to modulation of the immune response, some of the down-regulated immune system/inflammation genes identified in the Metacore analysis (Table 1) have been associated with tumoral progression. For example, *Cxcr4,* a chemokine receptor specific for stromal cell-derived factor-1, has been reported to be involved in tumorigenicity in breast, pancreatic and colorectal cancer (Wang *et al.*, 2008; Yoshitake *et al.*, 2008; Holm *et al.*, 2009). Regarding colorectal cancer, the expression of both stromal cell-derived factor-1 and its receptor CXCR4 has been reported to predict lymph node metastasis. Therefore, lower expression of this protein in GADF-fed mice may be related to the inhibition of tumor growth. GADF supplementation also modulated the expression of *Nfkbie,* which has been reported to regulate cell viability and proliferation during transformation (Dooley *et al.*, 2011). Additionally, *Lck*, a Src-related tyrosine kinase that is expressed in certain tumors such as human colon carcinoma (Krystal *et al.*, 1998), was down-regulated in the mucosa of $Apc^{Min/+}$ mice treated with GADF.

Also, a promoting effect of GADF on enterocytic differentiation was shown by the upregulation of genes related to cell adhesion molecules such as *Ocln, Cldn4* and *Epha2* in polarized epithelial cells (Table 1).

To gain further insight into the biological processes related to the protective effects of fiber and grape polyphenols, we used a Gene set analysis of the KEGG pathways using the tool FatiScan in the Babelomics suite. In this case all genes in the array (significantly and non-significantly differentially expressed) were included in the analysis in order to detect which pathways were globally modulated. Substantial modulation of the KEGG cancer and immune system diseases/immune system subgroups was also independently identified by this analysis (Table 2). GADF was also found to modulate carbohydrate and lipid metabolism. This may be related to previous data that indicate that grape products reduce plasma lipids and benefit blood glucose control (Vislocky *et al.*, 2010). In terms of the possible effects produced by other components of the fiber, it has been shown that a diet containing pectin may help correct some disturbances in lipid metabolism, and that a diet containing cellulose may improve glycemic control (Krzysik *et al.*, 2011).

Table 2 (continued)

Blocks of functionally related genes after GADF treatment in $Apc^{Min/+}$ mice			
Down-regulated KEGG pathways			
ID KEGG	**KEGG annotation**	**Group**	**Subgroup**
mmu04210	Apoptosis	Cellular Processes	
mmu04115	p53 signaling pathway	Cellular Processes	
mmu04114	Oocyte meiosis	Cellular Processes	
mmu04110	Cell cycle	Cellular Processes	Cell Growth and Death
mmu04142	Lysosome	Cellular Processes	Transport and Catabolism
mmu04150	mTOR signaling pathway	Environmental Information Processing	
mmu04370	VEGF signaling pathway	Environmental Information Processing	
mmu04350	TGF-beta signaling pathway	Environmental Information Processing	
mmu04012	ErbB signaling pathway	Environmental Information Processing	Signal Transduction
mmu04512	ECM-receptor interaction	Environmental Information Processing	
mmu04514	Cell adhesion molecules (CAMs)	Environmental Information Processing	Signaling Molecules and Interaction
mmu04130	SNARE interactions in vesicular transport	Genetic Information Processing	
mmu03060	Protein export	Genetic Information Processing	
mmu03050	Proteasome	Genetic Information Processing	
mmu03018	RNA degradation	Genetic Information Processing	Folding, Sorting and Degradation
mmu03440	Homologous recombination	Genetic Information Processing	
mmu03410	Base excision repair	Genetic Information Processing	
mmu03430	Mismatch repair	Genetic Information Processing	
mmu03030	DNA replication	Genetic Information Processing	
mmu03420	Nucleotide excision repair	Genetic Information Processing	Replication and Repair
mmu03022	Basal transcription factors	Genetic Information Processing	
mmu03020	RNA polymerase	Genetic Information Processing	
mmu03040	Spliceosome	Genetic Information Processing	Transcription
mmu00970	Aminoacyl-tRNA biosynthesis	Genetic Information Processing	
mmu03010	Ribosome	Genetic Information Processing	Translation
mmu05215	Prostate cancer	Human Diseases	
mmu05216	Thyroid cancer	Human Diseases	
mmu05214	Glioma	Human Diseases	
mmu05222	Small cell lung cancer	Human Diseases	
mmu05221	Acute myeloid leukemia	Human Diseases	
mmu05223	Non-small cell lung cancer	Human Diseases	
mmu05219	Bladder cancer	Human Diseases	
mmu05211	Renal cell carcinoma	Human Diseases	
mmu05210	Colorectal cancer	Human Diseases	
mmu05220	Chronic myeloid leukemia	Human Diseases	
mmu05212	Pancreatic cancer	Human Diseases	Cancers
mmu05416	Viral myocarditis	Human Diseases	Cardiovascular Diseases
mmu05340	Primary immunodeficiency	Human Diseases	
mmu05320	Autoimmune thyroid disease	Human Diseases	
mmu05330	Allograft rejection	Human Diseases	
mmu05332	Graft-versus-host disease	Human Diseases	
mmu05322	Systemic lupus erythematosus	Human Diseases	
mmu05310	Asthma	Human Diseases	Immune System Diseases
mmu04940	Type I diabetes mellitus	Human Diseases	Metabolic Diseases
mmu05012	Parkinson´s disease	Human Diseases	Neurodegenerative Diseases
mmu00330	Arginine and proline metabolism	Metabolism	
mmu00280	Valine, leucine and isoleucine degradation	Metabolism	
mmu00310	Lysine degradation	Metabolism	Amino Acid Metabolism
mmu00030	Pentose phosphate pathway	Metabolism	
mmu00020	Citrate cycle (TCA cycle)	Metabolism	
mmu00010	Glycolysis / Gluconeogenesis	Metabolism	
mmu00620	Pyruvate metabolism	Metabolism	
mmu00640	Propanoate metabolism	Metabolism	
mmu00520	Amino sugar and nucleotide sugar metabolism	Metabolism	Carbohydrate Metabolism
mmu00190	Oxidative phosphorylation	Metabolism	Energy Metabolism
mmu00563	Glycosylphosphatidylinositol(GPI)-anchor biosynthesis	Metabolism	
mmu00510	N-Glycan biosynthesis	Metabolism	Glycan Biosynthesis and Metabolism
mmu00564	Glycerophospholipid metabolism	Metabolism	
mmu00071	Fatty acid metabolism	Metabolism	
mmu00592	alpha-Linolenic acid metabolism	Metabolism	
mmu00561	Glycerolipid metabolism	Metabolism	
mmu01040	Biosynthesis of unsaturated fatty acids	Metabolism	
mmu00565	Ether lipid metabolism	Metabolism	
mmu00062	Fatty acid elongation in mitochondria	Metabolism	
mmu00600	Sphingolipid metabolism	Metabolism	Lipid Metabolism
mmu00760	Nicotinate and nicotinamide metabolism	Metabolism	
mmu00740	Riboflavin metabolism	Metabolism	
mmu00670	One carbon pool by folate	Metabolism	
mmu00770	Pantothenate and CoA biosynthesis	Metabolism	
mmu00860	Porphyrin and chlorophyll metabolism	Metabolism	Metabolism of Cofactors and Vitamins
mmu00480	Glutathione metabolism	Metabolism	Metabolism of Other Amino Acids
mmu00230	Purine metabolism	Metabolism	
mmu00240	Pyrimidine metabolism	Metabolism	Nucleotide Metabolism
mmu00983	Drug metabolism	Metabolism	Xenobiotics Biodegradation and Metabolism
mmu04912	GnRH signaling pathway	Organismal Systems	
mmu04914	Progesterone-mediated oocyte maturation	Organismal Systems	Endocrine System
mmu04621	NOD-like receptor signaling pathway	Organismal Systems	
mmu04620	Toll-like receptor signaling pathway	Organismal Systems	
mmu04666	Fc gamma R-mediated phagocytosis	Organismal Systems	
mmu04623	Cytosolic DNA-sensing pathway	Organismal Systems	
mmu04664	Fc epsilon RI signaling pathway	Organismal Systems	
mmu04670	Leukocyte transendothelial migration	Organismal Systems	
mmu04612	Antigen processing and presentation	Organismal Systems	
mmu04662	B cell receptor signaling pathway	Organismal Systems	
mmu04640	Hematopoietic cell lineage	Organismal Systems	Immune System
mmu04730	Long-term depression	Organismal Systems	Nervous System

Table 2

Blocks of functionally related genes after GADF treatment in $Apc^{Min/+}$ mice			
Up-regulated KEGG pathways			
ID KEGG	**KEGG annotation**	**Group**	**Subgroup**
mmu04520	Adherens junction	Cellular Processes	Cell Communication
mmu05412	Arrhythmogenic right ventricular cardiomyopathy (ARVC)	Human Diseases	
mmu05414	Dilated cardiomyopathy	Human Diseases	
mmu05410	Hypertrophic cardiomyopathy (HCM)	Human Diseases	Cardiovascular Diseases
mmu00290	Valine, leucine and isoleucine biosynthesis	Metabolism	Amino Acid Metabolism
mmu00100	Steroid biosynthesis	Metabolism	Lipid Metabolism
mmu00830	Retinol metabolism	Metabolism	Metabolism of Cofactors and Vitamins
mmu04260	Cardiac muscle contraction	Organismal Systems	Circulatory System
mmu04360	Axon guidance	Organismal Systems	Development
mmu04740	Olfactory transduction	Organismal Systems	Sensory System

Interestingly, studies evaluating the consumption of GADF by normal C57BL/6J mice showed many changes in the expression of genes involved in antioxidant activity and xenobiotic metabolism. GADF up-regulated genes encoding enzymes implicated in phase I (biotransformation) of the xenobiotic metabolism that convert hydrophobic compounds to more water-soluble moieties, as well as genes from phase II (detoxifying metabolism) that catalyze several conjugation reactions, and genes encoding for peroxiredoxins, members of the family of mammalian proteins that neutralize reactive oxygen species (Lizárraga *et al.*, 2011). Surprisingly, in $Apc^{Min/+}$ mice, GADF had no significant effect on the antioxidant and detoxifying machinery, apart from upregulation of the *Cyp2c54* gene (supplemental data 1) which encodes a cytochrome P450, demonstrating the importance of the regulation of cell growth and maintenance functions to the detriment of antioxidant and xenobiotic systems in tumor progression.

We hypothesize that the changes in the gene expression profile induced in the intestinal mucosa of $Apc^{Min/+}$ mice treated with GADF and the associated inhibition of spontaneous intestinal polyposis may be a result of the action of polyphenolic compounds (both soluble and insoluble fiber-like PA) and other components of the dietary fiber fraction. It is likely that the polyphenols contained in GADF act through molecular mechanisms such as the modulation of gene expression, as previously reported (Yun *et al.*, 2010), whereas the insoluble polysaccharides in the fiber act via the short chain fatty acids (SCFA) released from their fermentation by the gut microflora. SCFA do more than just provide an important source of energy to the colonic epithelium, as they also possess a wide range of physiological functions. For instance, acetate has been shown to bind a G-protein-coupled receptor, GPR43, which is expressed on immune cells (Maslowski *et al.*, 2009), and butyrate has been reported to inhibit histone deacetylase enzymes and alter microRNA expression, consequently preventing malignant transformation by reducing cell proliferation and inducing differentiation and apoptosis (Hu *et al.*, 2011).

Validation of microarray data by RT-PCR. The changes in mRNA expression observed in the microarrays for *Ccnd1*, *Kitl, Csnk1e, Lfng* and *Cxcr4* were further validated by RT-real time PCR (Figure 5). These targets were selected for RT-real time PCR analysis based on their participation in the pathways that were significantly modulated by GADF supplementation.

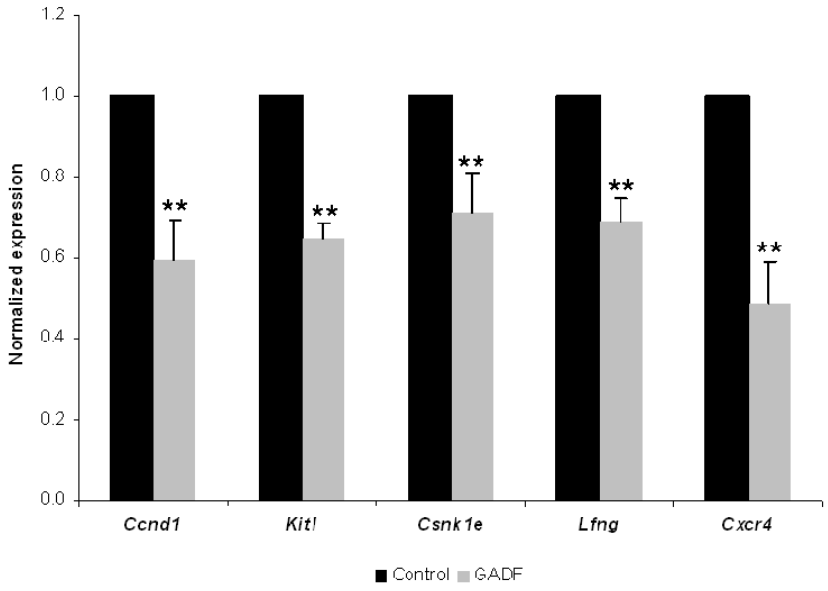

Figure 5. Validation of genes that were differentially expressed in the colon mucosa of $Apc^{Min/+}$ mice after GADF treatment by RT-PCR. Data represented as mean ± SEM (* *, $p > 0.01$).

In summary, the present study shows for the first time that dietary administration of GADF prevents spontaneous intestinal polyposis in the $Apc^{Min/+}$ mouse model. The cancer chemopreventive effects of GADF were mainly related to the modulation of cancer progression-related genes, suggesting the induction of G1 cell cycle arrest and the downregulation of genes related to the immune response and inflammation, and thus a protective effect against chronic inflammation and excessive immune signaling in $Apc^{Min/+}$ mice. The powerful anti-tumoral effect of GADF may be the result of synergy between the different compounds in the dietary fiber, including soluble and insoluble grape polyphenols and insoluble polysaccharides and lignins. The fact that GADF is a by-product of the wine industry makes it of particular economic and health interest. Taken together, our findings show that GADF is a promising nutraceutical for the prevention of colon cancer in high-risk populations.

ACKNOWLEDGEMENTS

The authors thank Miquel Borràs, Joaquín de Lapuente, Javier González and Joan Serret from CERETOX for support in the experiments. Financial support was provided by grants SAF2008-00164, AGL2006-12210-C03-02/ALI and AGL2009-12374-C03-03/ALI from the Spanish government Ministerio de Ciencia e Innovación and personal financial support (FPU program); from the Ministerio de Educación y Ciencia and from the Red Temática de Investigación Cooperativa en Cáncer, Instituto de Salud Carlos III, Spanish Ministry of Science and Innovation & European Regional Development Fund (ERDF) "Una manera de hacer Europa" (ISCIII-RTICC grants RD06/0020/0046). It has also received financial support from the AGAUR-Generalitat de Catalunya (grant 2009SGR1308, 2009 CTP 00026 and Icrea Academia award 2010 granted to M. Cascante), and the European Commission (FP7) ETHERPATHS KBBE-grant agreement nº22263.

REFERENCES

Al-Shahrour, F., Arbiza, L., Dopazo, H., Huerta-Cepas, J., Minguez, P., Montaner, D. i Dopazo, J. (2007). From genes to functional classes in the study of biological systems. *BMC Bioinformatics* **8**: 114.

Benjamini, Y., Drai, D., Elmer, G., Kafkafi, N. i Golani, I. (2001). Controlling the false discovery rate in behavior genetics research. *Behav Brain Res* **125**(1-2): 279-84.

Bolstad, B.M., Irizarry, R.A., Astrand, M. i Speed, T.P. (2003). A comparison of normalization methods for high density oligonucleotide array data based on variance and bias. *Bioinformatics* **19**(2): 185-93.

Chen, J., Moloney, D.J. i Stanley, P. (2001). Fringe modulation of Jagged1-induced Notch signaling requires the action of beta 4galactosyltransferase-1. *Proc Natl Acad Sci U S A* **98**(24): 13716-21.

Chuang, S.C., Vermeulen, R., Sharabiani, M.T., Sacerdote, C., Fatemeh, S.H., Berrino, F., Krogh, V., Palli, D., Panico, S., Tumino, R., Athersuch, T.J. i Vineis, P. (2011). The intake of grain fibers modulates cytokine levels in blood. *Biomarkers* **16**(6): 504-10.

Dooley, A.L., Winslow, M.M., Chiang, D.Y., Banerji, S., Stransky, N., Dayton, T.L., Snyder, E.L., Senna, S., Whittaker, C.A., Bronson, R.T., Crowley, D., Barretina, J., Garraway, L., Meyerson, M. i Jacks, T. (2011). Nuclear factor I/B is an oncogene in small cell lung cancer. *Genes Dev* **25**(14): 1470-5.

Ferguson, L.R. (2005). Does a diet rich in dietary fibre really reduce the risk of colon cancer? *Dig Liver Dis* **37**(3): 139-41.

Forte, A., De Sanctis, R., Leonetti, G., Manfredelli, S., Urbano, V. i Bezzi, M. (2008). Dietary chemoprevention of colorectal cancer. *Ann Ital Chir* **79**(4): 261-7.

Hinoi, T., Akyol, A., Theisen, B.K., Ferguson, D.O., Greenson, J.K., Williams, B.O., Cho, K.R. i Fearon, E.R. (2007). Mouse model of colonic adenoma-carcinoma progression based on somatic Apc inactivation. *Cancer Res* **67**(20): 9721-30.

Hoffman, B. i Liebermann, D.A. (2009). Gadd45 modulation of intrinsic and extrinsic stress responses in myeloid cells. *J Cell Physiol* **218**(1): 26-31.

Holm, N.T., Abreo, F., Johnson, L.W., Li, B.D. i Chu, Q.D. (2009). Elevated chemokine receptor CXCR4 expression in primary tumors following neoadjuvant chemotherapy predicts poor outcomes for patients with locally advanced breast cancer (LABC). *Breast Cancer Res Treat* **113**(2): 293-9.

Hu, S., Dong, T.S., Dalal, S.R., Wu, F., Bissonnette, M., Kwon, J.H. i Chang, E.B. (2011). The microbe-derived short chain fatty acid butyrate targets miRNA-dependent p21 gene expression in human colon cancer. *PLoS One* **6**(1): e16221.

Katiyar, S.K. (2007). UV-induced immune suppression and photocarcinogenesis: chemoprevention by dietary botanical agents. *Cancer Lett* **255**(1): 1-11.

Kaur, M., Tyagi, A., Singh, R.P., Sclafani, R.A., Agarwal, R. i Agarwal, C. (2011). Grape seed extract upregulates p21 (Cip1) through redox-mediated activation of ERK1/2 and posttranscriptional regulation leading to cell cycle arrest in colon carcinoma HT29 cells. *Mol Carcinog*.

Kawaguchi, K., Matsumoto, T. i Kumazawa, Y. (2011). Effects of antioxidant polyphenols on TNF-alpha-related diseases. *Curr Top Med Chem* **11**(14): 1767-79.

Kim, S.Y., Dunn, I.F., Firestein, R., Gupta, P., Wardwell, L., Repich, K., Schinzel, A.C., Wittner, B., Silver, S.J., Root, D.E., Boehm, J.S., Ramaswamy, S., Lander, E.S. i Hahn, W.C. (2010). CK1epsilon is required for breast cancers dependent on beta-catenin activity. *PLoS One* **5**(2): e8979.

Krystal, G.W., DeBerry, C.S., Linnekin, D. i Litz, J. (1998). Lck associates with and is activated by Kit in a small cell lung cancer cell line: inhibition of SCF-mediated growth by the Src family kinase inhibitor PP1. *Cancer Res* **58**(20): 4660-6.

Krzysik, M., Grajeta, H., Prescha, A. i Weber, R. (2011). Effect of cellulose, pectin and chromium(III) on lipid and carbohydrate metabolism in rats. *J Trace Elem Med Biol*.

Langenskiold, M., Holmdahl, L., Falk, P., Angenete, E. i Ivarsson, M.L. (2008). Increased TGF-beta 1 protein expression in patients with advanced colorectal cancer. *J Surg Oncol* **97**(5): 409-15.

Leclerc, D., Deng, L., Trasler, J. i Rozen, R. (2004). ApcMin/+ mouse model of colon cancer: gene expression profiling in tumors. *J Cell Biochem* **93**(6): 1242-54.

Lizárraga, D., Vinardell, M.P., Noe, V., van Delft, J.H., Alcarraz-Vizan, G., van Breda, S.G., Staal, Y., Gunther, U.L., Reed, M.A., Ciudad, C.J., Torres, J.L. i Cascante, M. (2011). A Lyophilized Red Grape Pomace Containing Proanthocyanidin-Rich Dietary Fiber Induces Genetic and Metabolic Alterations in Colon Mucosa of Female C57BL/6J Mice. *J Nutr*.

Lopez-Oliva, M.E., Agis-Torres, A., Goni, I. i Munoz-Martinez, E. (2010). Grape antioxidant dietary fibre reduced apoptosis and induced a pro-reducing shift in the glutathione redox state of the rat proximal colonic mucosa. *Br J Nutr* **103**(8): 1110-7.

Maslowski, K.M., Vieira, A.T., Ng, A., Kranich, J., Sierro, F., Yu, D., Schilter, H.C., Rolph, M.S., Mackay, F., Artis, D., Xavier, R.J., Teixeira, M.M. i Mackay, C.R. (2009). Regulation of inflammatory responses by gut microbiota and chemoattractant receptor GPR43. *Nature* **461**(7268): 1282-6.

Misikangas, M., Pajari, A.M., Paivarinta, E., Oikarinen, S.I., Rajakangas, J., Marttinen, M., Tanayama, H., Torronen, R. i Mutanen, M. (2007). Three Nordic berries inhibit intestinal tumorigenesis in multiple intestinal neoplasia/+ mice by modulating beta-catenin signaling in the tumor and transcription in the mucosa. *J Nutr* **137**(10): 2285-90.

Mutanen, M., Pajari, A.M. i Oikarinen, S.I. (2000). Beef induces and rye bran prevents the formation of intestinal polyps in Apc(Min) mice: relation to beta-catenin and PKC isozymes. *Carcinogenesis* **21**(6): 1167-73.

Myer, D.L., Robbins, S.B., Yin, M., Boivin, G.P., Liu, Y., Greis, K.D., Bahassi, E.M. i Stambrook, P.J. (2011). Absence of polo-like kinase 3 in mice stabilizes Cdc25A after DNA damage but is not sufficient to produce tumors. *Mutat Res*.

Narai, S., Watanabe, M., Hasegawa, H., Nishibori, H., Endo, T., Kubota, T. i Kitajima, M. (2002). Significance of transforming growth factor beta1 as a new tumor marker for colorectal cancer. *Int J Cancer* **97**(4): 508-11.

Reedijk, M., Odorcic, S., Zhang, H., Chetty, R., Tennert, C., Dickson, B.C., Lockwood, G., Gallinger, S. i Egan, S.E. (2008). Activation of Notch signaling in human colon adenocarcinoma. *Int J Oncol* **33**(6): 1223-9.

Rodilla, V., Villanueva, A., Obrador-Hevia, A., Robert-Moreno, A., Fernandez-Majada, V., Grilli, A., Lopez-Bigas, N., Bellora, N., Alba, M.M., Torres, F., Dunach, M., Sanjuan, X., Gonzalez, S., Gridley, T., Capella, G., Bigas, A. i Espinosa, L. (2009). Jagged1 is the pathological link between Wnt and Notch pathways in colorectal cancer. *Proc Natl Acad Sci U S A* **106**(15): 6315-20.

Saleh, M. i Trinchieri, G. (2011). Innate immune mechanisms of colitis and colitis-associated colorectal cancer. *Nat Rev Immunol* **11**(1): 9-20.

Shen, G., Khor, T.O., Hu, R., Yu, S., Nair, S., Ho, C.T., Reddy, B.S., Huang, M.T., Newmark, H.L. i Kong, A.N. (2007). Chemoprevention of familial adenomatous polyposis by natural dietary compounds

sulforaphane and dibenzoylmethane alone and in combination in ApcMin/+ mouse. *Cancer Res* **67**(20): 9937-44.

Smyth, G.K. (2004). Linear models and empirical bayes methods for assessing differential expression in microarray experiments. *Stat Appl Genet Mol Biol* **3**: Article3.

Su, L.K., Kinzler, K.W., Vogelstein, B., Preisinger, A.C., Moser, A.R., Luongo, C., Gould, K.A. i Dove, W.F. (1992). Multiple intestinal neoplasia caused by a mutation in the murine homolog of the APC gene. *Science* **256**(5057): 668-70.

Takeda, D.Y. i Dutta, A. (2005). DNA replication and progression through S phase. *Oncogene* **24**(17): 2827-43.

Touriño, S., Fuguet, E., Jauregui, O., Saura-Calixto, F., Cascante, M. i Torres, J.L. (2008). High-resolution liquid chromatography/electrospray ionization time-of-flight mass spectrometry combined with liquid chromatography/electrospray ionization tandem mass spectrometry to identify polyphenols from grape antioxidant dietary fiber. *Rapid Commun Mass Spectrom* **22**(22): 3489-500.

Touriño, S., Fuguet, E., Vinardell, M.P., Cascante, M. i Torres, J.L. (2009). Phenolic metabolites of grape antioxidant dietary fiber in rat urine. *J Agric Food Chem* **57**(23): 11418-26.

Touriño, S., Perez-Jimenez, J., Mateos-Martin, M.L., Fuguet, E., Vinardell, M.P., Cascante, M. i Torres, J.L. (2011). Metabolites in Contact with the Rat Digestive Tract after Ingestion of a Phenolic-Rich Dietary Fiber Matrix. *J Agric Food Chem*.

Velmurugan, B., Singh, R.P., Kaul, N., Agarwal, R. i Agarwal, C. (2010). Dietary feeding of grape seed extract prevents intestinal tumorigenesis in APCmin/+ mice. *Neoplasia* **12**(1): 95-102.

Verschoyle, R.D., Greaves, P., Cai, H., Edwards, R.E., Steward, W.P. i Gescher, A.J. (2007). Evaluation of the cancer chemopreventive efficacy of rice bran in genetic mouse models of breast, prostate and intestinal carcinogenesis. *Br J Cancer* **96**(2): 248-54.

Vislocky, L.M. i Fernandez, M.L. (2010). Biomedical effects of grape products. *Nutr Rev* **68**(11): 656-70.

Wang, Z., Ma, Q., Liu, Q., Yu, H., Zhao, L., Shen, S. i Yao, J. (2008). Blockade of SDF-1/CXCR4 signalling inhibits pancreatic cancer progression in vitro via inactivation of canonical Wnt pathway. *Br J Cancer* **99**(10): 1695-703.

Yasuda, A., Sawai, H., Takahashi, H., Ochi, N., Matsuo, Y., Funahashi, H., Sato, M., Okada, Y., Takeyama, H. i Manabe, T. (2007). Stem cell factor/c-kit receptor signaling enhances the proliferation and invasion of colorectal cancer cells through the PI3K/Akt pathway. *Dig Dis Sci* **52**(9): 2292-300.

Yoshitake, N., Fukui, H., Yamagishi, H., Sekikawa, A., Fujii, S., Tomita, S., Ichikawa, K., Imura, J., Hiraishi, H. i Fujimori, T. (2008). Expression of SDF-1 alpha and nuclear CXCR4 predicts lymph node metastasis in colorectal cancer. *Br J Cancer* **98**(10): 1682-9.

Yun, J.W., Lee, W.S., Kim, M.J., Lu, J.N., Kang, M.H., Kim, H.G., Kim, D.C., Choi, E.J., Choi, J.Y., Kim, H.G., Lee, Y.K., Ryu, C.H., Kim, G., Choi, Y.H., Park, O.J. i Shin, S.C. (2010). Characterization of a profile of the anthocyanins isolated from Vitis coignetiae Pulliat and their anti-invasive activity on HT-29 human colon cancer cells. *Food Chem Toxicol* **48**(3): 903-9.

Supplemental data 1

Differentially expressed genes GADF_vs_CTL

Affimetrix ID	Symbol	Gene description	Fold change	Adjusted p-value
1418283_at	Cldn4	claudin 4	2,0	0,047
1449133_at	Sprr1a	small proline-rich protein 1A	2,0	0,035
1451924_a_at	Edn1	endothelin 1	1,9	0,049
1419911_at	Coro1c	coronin, actin binding protein 1C	1,8	0,047
1443208_at			1,8	0,035
1441115_at	D18Ertd232e	DNA segment, Chr 18, ERATO Doi 232, expressed	1,8	0,041
1439124_at	Wdr91	WD repeat domain 91	1,8	0,049
1417133_at	Pmp22	peripheral myelin protein 22	1,7	0,022
1433205_at	Ndfip2	Nedd4 family interacting protein 2	1,7	0,039
1436520_at	Ahnak2	AHNAK nucleoprotein 2	1,7	0,044
1436750_a_at	Oxct1	3-oxoacid CoA transferase 1	1,7	0,049
1424339_at	Oasl1	2'-5' oligoadenylate synthetase-like 1	1,7	0,036
1455180_at	Gcom1	GRINL1A complex locus	1,7	0,047
1455457_at	Cyp2c54	cytochrome P450, family 2, subfamily c, polypeptide 54	1,7	0,049
1436614_at			1,7	0,046
1430191_at	9130004J05Rik	RIKEN cDNA 9130004J05 gene	1,7	0,045
1434496_at	Plk3	polo-like kinase 3 (Drosophila)	1,7	0,022
1458279_at			1,7	0,022
1455804_x_at	Oxct1	3-oxoacid CoA transferase 1	1,6	0,049
1422823_at	Eps8	epidermal growth factor receptor pathway substrate 8	1,6	0,044
1441030_at	Rai14	retinoic acid induced 14	1,6	0,044
1426818_at	Arrdc4	arrestin domain containing 4	1,6	0,035
1437868_at	Fam46a	family with sequence similarity 46, member A	1,6	0,035
1435059_at	Asap1	ArfGAP with SH# domain, ankyrin repeat and PH domain1	1,6	0,036
1436101_at	Pank2	pantothenate kinase 2 (Hallervorden-Spatz syndrome)	1,6	0,047
1438581_at	Cytsa	cytospin A	1,6	0,047
1425837_a_at	Ccrn4l	CCR4 carbon catabolite repression 4-like (S. cerevisiae)	1,6	0,049
1417732_at	Anxa8	annexin A8	1,6	0,049
1421151_a_at	Epha2	Eph receptor A2	1,6	0,035
1439598_at			1,5	0,036
1458591_at	Rasef	RAS and EF hand domain containing	1,5	0,044
1417335_at	Sult2b1	sulfotransferase family, cytosolic, 2B, member 1	1,5	0,049
1452385_at	Usp53	ubiquitin specific peptidase 53	1,5	0,044
1449519_at	Gadd45a	growth arrest and DNA-damage-inducible 45 alpha	1,5	0,050
1448873_at	Ocln	occludin	1,5	0,044
1455033_at	Fam102b	family with sequence similarity 102, member B	1,5	0,047
1426894_s_at	Fam102a	family with sequence similarity 102, member A	1,5	0,049
1435265_at			1,5	0,035
1458453_at	Lmo7	LIM domain only 7	1,5	0,048
1422824_s_at	Eps8	epidermal growth factor receptor pathway substrate 8	1,5	0,049
1418459_at	Ccdc91	coiled-coil domain containing 91	-1,5	0,035
1420249_s_at	Ccl6	chemokine (C-C motif) ligand 6	-1,5	0,049
1449342_at	Ptplb	protein tyrosine phosphatase-like (proline instead of catalytic arginine), member b	-1,5	0,047
1452191_at	Prcp	prolylcarboxypeptidase (angiotensinase C)	-1,5	0,047
1430514_a_at	Cd99	CD99 antigen	-1,5	0,044
1430656_a_at	Asnsd1	asparagine synthetase domain containing 1	-1,5	0,049
1435864_a_at	1810063B05Rik	RIKEN cDNA 1810063B05 gene	-1,5	0,047
1451091_at	Txndc5	thioredoxin domain containing 5	-1,5	0,049
1433831_at	4833418A01Rik	RIKEN cDNA 4833418A01 gene	-1,5	0,047
1422029_at	Ccl20	chemokine (C-C motif) ligand 20	-1,5	0,049
1451987_at	Arrb2	arrestin, beta 2	-1,5	0,035
1428340_s_at	Atp13a2	ATPase type 13A2	-1,5	0,039
1453550_a_at	Far1	fatty acyl CoA reductase 1	-1,5	0,036
1436038_a_at	Pigp	phosphatidylinositol glycan anchor biosynthesis, class P	-1,5	0,049
1434955_at	March1	membrane-associated ring finger (C3HC4) 1	-1,5	0,049
1421022_x_at	Acyp1	acylphosphatase 1, erythrocyte (common) type	-1,5	0,047
1426801_at	39692	septin 8	-1,6	0,046
1419463_at	Clca2	chloride channel calcium activated 2	-1,6	0,036
1437341_x_at	Cnp	2',3'-cyclic nucleotide 3' phosphodiesterase	-1,6	0,044
1454930_at	Tbcel	tubulin folding cofactor E-like	-1,6	0,036
1457817_at			-1,6	0,049
1437354_at	Ube3a	ubiquitin protein ligase E3A	-1,6	0,046
1443167_at			-1,6	0,049
1423966_at	Cd99l2	CD99 antigen-like 2	-1,6	0,044
1436212_at	Tmem71	transmembrane protein 71	-1,6	0,035
1423306_at	2010002N04Rik	RIKEN cDNA 2010002N04 gene	-1,6	0,047
1425206_a_at	Ube3a	ubiquitin protein ligase E3A	-1,6	0,049
1417619_at	Gadd45gip1	growth arrest and DNA-damage-inducible, gamma interacting protein 1	-1,6	0,050
1417176_at	Csnk1e	casein kinase 1, epsilon	-1,6	0,048
1460486_at	Rabgap1	RAB GTPase activating protein 1	-1,6	0,049
1443894_at	Evi2a	ecotropic viral integration site 2a	-1,6	0,036
1428850_x_at	Cd99	CD99 antigen	-1,6	0,044
1453761_at	Phf6	PHD finger protein 6	-1,6	0,047
1433496_at	Glt25d1	glycosyltransferase 25 domain containing 1	-1,6	0,047
1426555_at	Scpep1	serine carboxypeptidase 1	-1,6	0,041
1418513_at	Stk3	serine/threonine kinase 3 (Ste20, yeast homolog)	-1,6	0,049
1452888_at	1110034G24Rik	RIKEN cDNA 1110034G24 gene	-1,6	0,050
1451249_at	Trmt1	TRM1 tRNA methyltransferase 1 homolog (S. cerevisiae)	-1,6	0,048
1420975_at	Baz1b	bromodomain adjacent to zinc finger domain, 1B	-1,6	0,044
1439305_at			-1,6	0,036
1456064_at	Kcna3	potassium voltage-gated channel, shaker-related subfamily, member 3	-1,6	0,049
1451920_a_at	Rfc1	replication factor C (activator 1) 1	-1,6	0,047
1429847_a_at	4833418A01Rik	RIKEN cDNA 4833418A01 gene	-1,6	0,047
1425338_at	Plcb4	phospholipase C, beta 4	-1,6	0,047
1431430_s_at	Trim59	tripartite motif-containing 59	-1,6	0,045
1453485_s_at	1110005A03Rik	RIKEN cDNA 1110005A03 gene	-1,6	0,044
1425986_a_at	Dcun1d1	DCN1, defective in cullin neddylation 1, domain containing 1 (S. cerevisiae)	-1,6	0,047
1428900_s_at	Mett5d1	methyltransferase 5 domain containing 1	-1,6	0,049
1449749_s_at	Tfb1m	transcription factor B1, mitochondrial	-1,6	0,050
1451730_at	Zfp62	zinc finger protein 62	-1,6	0,047
1417419_at	Ccnd1	cyclin D1	-1,6	0,035
1450377_at	Thbs1	thrombospondin 1	-1,6	0,035
1421018_at	1110018J18Rik	RIKEN cDNA 1110018J18 gene	-1,6	0,047

1418980_a_at	Cnp	2',3'-cyclic nucleotide 3' phosphodiesterase	-1.6	0.050
1419279_at	Pip4k2a	phosphatidylinositol-5-phosphate 4-kinase, type II, alpha	-1.6	0.039
1426550_at	Sidt1	SID1 transmembrane family, member 1	-1.6	0.044
1450095_a_at	Acyp1	acylphosphatase 1, erythrocyte (common) type	-1.6	0.047
1434450_s_at	Adrbk2	adrenergic receptor kinase, beta 2	-1.7	0.049
1460468_s_at	Dnajc22	DnaJ (Hsp40) homolog, subfamily C, member 22	-1.7	0.035
1417568_at	Ncald	neurocalcin delta	-1.7	0.049
1451386_at	Blvrb	biliverdin reductase B (flavin reductase (NADPH))	-1.7	0.046
1448277_at	Pold2	polymerase (DNA directed), delta 2, regulatory subunit	-1.7	0.036
1433485_x_at	Gpr56	G protein-coupled receptor 56	-1.7	0.047
1448288_at	Nfib	nuclear factor I/B	-1.7	0.044
1446508_at			-1.7	0.047
1425477_x_at	H2-Ab1	histocompatibility 2, class II antigen A, beta 1	-1.7	0.047
1433466_at	AI467606	expressed sequence AI467606	-1.7	0.044
1439819_at	AU015263	expressed sequence AU015263	-1.7	0.047
1419247_at	Rgs2	regulator of G-protein signaling 2	-1.7	0.049
1455095_at	Hist2h2be	histone cluster 2, H2be	-1.7	0.050
1427680_a_at	Nfib	nuclear factor I/B	-1.7	0.049
1448012_at	C76336	expressed sequence C76336	-1.7	0.050
1454850_at	Tbc1d10c	TBC1 domain family, member 10c	-1.7	0.048
1436515_at	Bach2	BTB and CNC homology 2	-1.7	0.048
1418776_at	5830443L24Rik	RIKEN cDNA 5830443L24 gene	-1.7	0.048
1442325_at	Tbc1d24	TBC1 domain family, member 24	-1.7	0.035
1443353_at			-1.8	0.048
1417852_x_at	Clca1	chloride channel calcium activated 1	-1.8	0.047
1436171_at	Arhgap30	Rho GTPase activating protein 30	-1.8	0.035
1448482_at	Slc39a8	solute carrier family 39 (metal ion transporter), member 8	-1.8	0.049
1425396_a_at	Lck	lymphocyte protein tyrosine kinase	-1.8	0.040
1437756_at	Gimap9	GTPase, IMAP family member 9	-1.8	0.047
1425247_a_at	Igh	immunoglobulin heavy chain complex	-1.8	0.016
1418181_at	Ptp4a3	protein tyrosine phosphatase 4a3	-1.8	0.045
1417219_s_at	Tmsb10	thymosin, beta 10	-1.8	0.047
1425854_x_at	Tcrb-J	T-cell receptor beta, joining region	-1.8	0.035
1442338_at			-1.9	0.047
1458299_s_at	Nfkbie	nuclear factor of kappa light polypeptide gene enhancer in B-cells inhibitor, epsilon	-1.9	0.044
1429672_at	5830407E08Rik	RIKEN cDNA 5830407E08 gene	-1.9	0.035
1460279_a_at	Gtf2i	general transcription factor II I	-1.9	0.047
1420653_at	Tgfb1	transforming growth factor, beta 1	-1.9	0.044
1448698_at	Ccnd1	cyclin D1	-1.9	0.036
1420643_at	Lfng	LFNG O-fucosylpeptide 3-beta-N-acetylglucosaminyltransferase	-1.9	0.048
1416021_a_at	Fabp5	fatty acid binding protein 5, epidermal	-2.0	0.050
1423847_at	Ncapd2	non-SMC condensin I complex, subunit D2	-2.0	0.050
1423520_at	Lmnb1	lamin B1	-2.0	0.005
1448117_at	Kitl	kit ligand	-2.0	0.049
1436902_x_at	Tmsb10	thymosin, beta 10	-2.0	0.037
1417420_at	Ccnd1	cyclin D1	-2.0	0.049
1449005_at	Slc16a3	solute carrier family 16 (monocarboxylic acid transporters), member 3	-2.0	0.049
1450648_s_at	Rmcs5	response to metastatic cancers 5	-2.1	0.049
1438858_x_at	H2-Aa	histocompatibility 2, class II antigen A, alpha	-2.1	0.049
1417025_at	H2-Eb1	histocompatibility 2, class II antigen E beta	-2.1	0.050
1419248_at	Rgs2	regulator of G-protein signaling 2	-2.1	0.047
1450379_at	Msn	moesin	-2.1	0.047
1429065_at	1200009F10Rik	RIKEN cDNA 1200009F10 gene	-2.1	0.044
1416022_at	Fabp5	fatty acid binding protein 5, epidermal	-2.1	0.039
1419647_a_at	Ier3	immediate early response 3	-2.2	0.034
1447774_x_at	5730469M10Rik	RIKEN cDNA 5730469M10 gene	-2.2	0.048
1434067_at	AI662270	expressed sequence AI662270	-2.2	0.047
1430388_a_at	Sulf2	sulfatase 2	-2.2	0.035
1417290_at	Lrg1	leucine-rich alpha-2-glycoprotein 1	-2.2	0.036
1419004_s_at	Bcl2a1a	B-cell leukemia/lymphoma 2 related protein A1a	-2.2	0.039
1419480_at	Sell	selectin, lymphocyte	-2.2	0.039
1454268_a_at	Cyba	cytochrome b-245, alpha polypeptide	-2.2	0.036
1418296_at	Fxyd5	FXYD domain-containing ion transport regulator 5	-2.2	0.047
1433783_at	Ldb3	LIM domain binding 3	-2.3	0.049
1452716_at	5730469M10Rik	RIKEN cDNA 5730469M10 gene	-2.3	0.047
1460259_s_at	Clca2	chloride channel calcium activated 2	-2.3	0.045
1415854_at	Kitl	kit ligand	-2.3	0.047
1452431_s_at	H2-Aa	histocompatibility 2, class II antigen A, alpha	-2.5	0.047
1419549_at	Arg1	arginase, liver	-2.5	0.050
1419186_a_at	St8sia4	ST8 alpha-N-acetyl-neuraminide alpha-2,8-sialyltransferase 4	-2.5	0.047
1455966_s_at	Nudt21	nudix (nucleoside diphosphate linked moiety X)-type motif 21	-2.5	0.049
1451721_a_at	H2-Ab1	histocompatibility 2, class II antigen A, beta 1	-2.6	0.045
1436713_s_at	Meg3	maternally expressed 3	-2.6	0.046
1440196_at			-2.6	0.027
1449071_at	Myl7	myosin, light polypeptide 7, regulatory	-2.7	0.048
1424375_s_at	Gimap4	GTPase, IMAP family member 4	-2.8	0.050
1415983_at	Lcp1	lymphocyte cytosolic protein 1	-2.9	0.047
1420699_at	Clec7a	C-type lectin domain family 7, member a	-3.1	0.035
1448710_at	Cxcr4	chemokine (C-X-C motif) receptor 4	-3.1	0.022
1424931_s_at	Igl-V1	immunoglobulin lambda chain, variable 1	-3.3	0.049
1450792_at	Tyrobp	TYRO protein tyrosine kinase binding protein	-3.4	0.036
1455269_a_at	Coro1a	coronin, actin binding protein 1A	-3.5	0.049
1448617_at	Cd53	CD53 antigen	-3.7	0.047
1452163_at	Ets1	E26 avian leukemia oncogene 1, 5' domain	-3.9	0.044
1460218_at	Cd52	CD52 antigen	-4.0	0.044
1416246_a_at	Coro1a	coronin, actin binding protein 1A	-4.5	0.039
1417426_at	Srgn	serglycin	-4.6	0.050
1427747_a_at	Lcn2	lipocalin 2	-4.8	0.047
1460423_x_at	Igkv1-117	immunoglobulin kappa chain variable 1-117	-5.5	0.035
1455869_at			-6.2	0.047

CAPÍTOL 5

Efecte quimiopreventiu de l'àcid maslínic contra la tumorigenesi intestinal en ratolins $Apc^{Min/+}$

Susana Sánchez-Tena[1], Fernando Reyes[2], Santiago Díaz-Moralli[1], Maria Pilar Vinardell[3], Michelle Reed[4], Francisco García-García[5], Joaquín Dopazo[5], José Antonio Lupiáñez[2], Ulrich Günther[4] i Marta Cascante[1]

[1]Departament de Bioquímica i Biologia Molecular, Facultat de Biologia, Universitat de Barcelona, Institut de Biomedicina de la Universitat de Barcelona (IBUB), Unitat associada al CSIC, Barcelona, Espanya

[2]Departamento de Bioquímica y Biología Molecular, Universidad de Granada, Granada, Espanya

[3]Departament de Fisiologia, Facultat de Farmàcia, Universitat de Barcelona, Barcelona, Espanya

[4]Henry Wellcome Building for Biomolecular NMR Spectroscopy, CR UK Institute for Cancer Studies, University of Birmingham, Birmingham, U.K.

[5]Node de Genòmica Funcional, Institut Nacional de Bioinformática, Departamento de Bioinformática, CIPF, Valencia, Espanya

RESUM

La quimioprevenció és una estratègia per reduir el risc de càncer colorectal, una de les principals causes de mort als països occidentals. Pel que fa a això, l'àcid maslínic (MA-*Maslinic Acid*), un triterpè pentacíclic extret de la cera que recobreix les olives, s'ha descrit que es capaç d'inhibir la proliferació i d'induir apoptosi en línies cel·lulars de càncer de còlon, sense afectar cèl·lules intestinals normals. El present estudi va avaluar l'eficàcia quimiopreventiva i els mecanismes associats de l'MA envers la tumorigenesis intestinal espontania en ratolins $Apc^{Min/+}$. Els ratolins es van alimentar amb una dieta estàndard (grup control) o amb una dieta suplementada amb MA (grup MA) durant sis setmanes. El tractament amb MA va reduir el nombre total de pòlips intestinals en un 45% ($P < 0.01$). Els mecanismes d'acció associats a aquesta activitat quimiopreventiva es van investigar per comparació dels perfils d'expressió dels ratolins control i els ratolins tractats amb MA mitjançant *microarrays* i també per anàlisi del perfil metabòlic en el sèrum dels ratolins utilitzant tècniques de ressonància magnètica nuclear. El fenotip d'expressió induït per l'MA va suggerir que aquest producte actua inhibint les senyals de creixement i la inflamació. Finalment, aquests canvis resulten en un arrest en la fase G1 del cicle cel·lular i una inducció d'apoptosi. A més, el tractament amb MA va induir un perfil metabòlic protector contra la tumorigenesis intestinal. Aquests resultats mostren per primer cop l'eficàcia i els mecanismes moleculars d'acció de l'MA enfront el desenvolupament de tumors intestinals en el model de ratolins $Apc^{Min/+}$, suggerint el seu potencial quimiopreventiu contra el càncer colorectal.

Chemoprevention of intestinal tumorigenesis in $Apc^{Min/+}$ mice by maslinic acid from olive pomace

Susana Sánchez-Tena[1], Fernando Reyes[2], Santiago Díaz-Moralli[1], Maria Pilar Vinardell[3], Michelle Reed[4], Francisco García-García[5], Joaquín Dopazo[5], José Antonio Lupiáñez[2], Ulrich Günther[4] and Marta Cascante[1]

[1]Department of Biochemistry and Molecular Biology, Faculty of Biology, Universitat de Barcelona, Institute of Biomedicine of Universitat de Barcelona (IBUB) and CSIC-Associated Unit Barcelona, Spain

[2]Department of Biochemistry and Molecular Biology, University of Granada, Granada, Spain

[3]Department of Physiology, Faculty of Pharmacy, University of Barcelona, Barcelona, Spain

[4]Henry Wellcome Building for Biomolecular NMR Spectroscopy, CR UK Institute for Cancer Studies, University of Birmingham, Birmingham, U.K.

[5]Functional Genomics Node, National Institute of Bioinformatics, Department of Bioinformatics, CIPF, Valencia, Spain

ABSTRACT

Chemoprevention is a pragmatic approach to reduce the risk of colorectal cancer, one of the leading causes of cancer-related death in western countries. In this regard, maslinic acid (MA), a pentacyclic triterpene extracted from wax-like coatings of olives, is known to inhibit proliferation and induce apoptosis in colon cancer cell lines without affecting normal intestinal cells. The present study evaluated the chemopreventive efficacy and associated mechanisms of maslinic acid treatment on spontaneous intestinal tumorigenesis in $Apc^{Min/+}$ mice. Mice were fed with a standard diet (control group) or a maslinic acid-supplemented diet (MA group) for six weeks. MA feeding reduced total intestinal polyp formation by 45% ($P<0.01$). Putative molecular mechanisms associated with suppressing intestinal polyposis in $Apc^{Min/+}$ mice were investigated by comparing microarray expression profiles of MA-treated and control mice and by analyzing the serum metabolic profile using NMR techniques. The different expression phenotype induced by MA suggested that it exerts its chemopreventive action mainly by inhibiting cell-survival signaling and inflammation. These changes eventually induce G1-phase cell cycle arrest and apoptosis. Moreover, the metabolic changes induced by MA treatment were associated with a protective profile against intestinal tumorigenesis. These results show the efficacy and underlying mechanisms of MA against intestinal tumor development in the $Apc^{Min/+}$ mice model, suggesting its chemopreventive potential against colorectal cancer.

INTRODUCTION

Chemoprevention based on the use of bioactive plant compounds has emerged as a practical approach to decrease the risk of various cancers, including colorectal cancer, which is one of the most frequent malignancies and one of the leading causes of cancer-related death in western countries. Familial adenomatous polyposis (FAP), a hereditary colorectal cancer predisposition syndrome, is caused by a mutated adenomatous polyposis coli (*Apc*) gene. FAP patients develop numerous colonic adenomas progressing to colorectal cancer and small intestinal adenomas in most cases. Interestingly, the $Apc^{Min/+}$ mouse, a common animal model of intestinal tumorigenesis, harbors a mutation in the same gene that causes FAP and, like FAP patients, develops large numbers of intestinal tumors at an early age (Su *et al.*, 1992). Therefore, the $Apc^{Min/+}$ mouse model is considered to be an analog of human intestinal tumorigenesis and is extensively used to study chemotherapeutic agents for humans.

Natural products have been exploited for treatment of human diseases for thousands of years. Maslinic acid (MA), a natural pentacyclic triterpene, is widely present in dietary plants, especially in olive fruit skins. This compound has attracted much interest due to its proven pharmacologic safety and its many biological activities, such as anti-viral (Xu *et al.*, 1996) and antidiabetogenic (Fernandez-Navarro *et al.*, 2008) functions. More recently, some studies have shown that MA has anti-cancer capacity in different cell types, including melanoma (Parra *et al.*, 2011), liver cancer (Lin *et al.*, 2011), astrocytoma (Martin *et al.*, 2007) and colon cancer. Specifically in colon malignancies, MA possesses potent differentiating and anti-proliferation properties, inducing cell-cycle arrest in the G0/G1 phase and apoptosis in colon cancer cells without affecting non-tumor cells (Reyes *et al.*, 2006). However, because only a few, mainly *in vitro*, studies have aimed to characterize the mechanisms of action of olive components in colon cancer, further research is required.

Therefore, the main objective of the current study was to determine the efficacy of MA consumption in preventing spontaneous intestinal tumorigenesis in $Apc^{Min/+}$ mice and to characterize the mechanisms by which MA executes its function.

MATERIALS AND METHODS

Animals and treatment. A total of 22 male 4-week-old $Apc^{Min/+}$ mice were purchased from the Jackson Laboratories (Bar Harbor, ME) and maintained in the animal facility at the University of Barcelona. Animal care was strictly in accordance with the European Union Regulations. The experimental protocols were approved by the Experimental Animal Ethical

Research Committee of the University of Barcelona in accordance with current regulations for animal care and use for experimental purposes. MA was obtained from olive pomace by using the method described by Garcia-Granados et al. (Garcia-Granados *et al.*, 2003). The extract used was a white powder comprising 98% maslinic acid and 2% oleanolic acid. This extract is stable when stored at 4 ºC. After a 7-day acclimatization period receiving the standard diet (Teklad Global 18% Protein rodent diet), animals were randomly divided into two groups of 12 and 10 mice per group (Control and MA, respectively). Control mice were fed with the standard diet, and the MA-treated group was fed with the same diet supplemented with 100 mg of MA/kg feed (15 mg MA/kg body weight). Diets were purchased from Harlan Interfauna Iberica S.L (Barcelona, Spain). Animals were maintained for 12 h light/dark cycles, with free access to water and food. Throughout the 6-week treatment period, animals were observed for any signs of toxicity; body weights and food and water intake were recorded weekly. At the end of the 6 weeks, the animals were starved overnight and anesthetized with volatile isoflurane (ESTEVE, Barcelona, Spain) before blood samples were obtained by cardiac puncture. Finally, mice were killed by an overdose of anesthesia.

Measurement of intestinal polyps. $Apc^{Min/+}$ mice develop polyps in both the small and large intestine, with an increased incidence of intestinal adenomas observed in the former. Therefore, immediately after the mice were killed, the small intestine was excised from each mouse, cut longitudinally, and rinsed with phosphate-buffered saline solution (pH 7.4) to remove intestinal contents. Intestines were pinned flat on cardboard and then were fixed for 1 day in 4% neutral-buffered formalin solution (v/v; pH 7.4). Intestinal sections were stored at room temperature in 1% neutral buffered formalin solution (v/v) until further analysis. To facilitate tumor quantification and identification, the small intestine was divided into three equal-length sections: proximal, medial, and distal. Thereafter, the small-intestine sections were stained in phosphate-buffered saline solution (pH 7.4) containing 0.1% (v/v) methylene blue. By using a stereomicroscope and a measured grid, tumor number and dimensions were determined for each small-intestine section. The size of each intestine tumor was categorized as <1 mm, 1–1.9 mm, or ≥2 mm.

RNA isolation and gene profiling by Affymetrix Microarrays. The large intestine of each dead mouse was removed and placed on a plastic plate, which was kept at 4 °C. After removal of the rectum, the colon was opened longitudinally with fine scissors, and mucus and feces were washed away. The colonic mucosal layer was incubated in Trizol (Invitrogen, Carlsbad, CA) for 3 min and scraped off of the muscle layer with the edge of a sterile glass slide. Cells were transferred into 800 μL Trizol, homogenized by pipetting, and stored at −80°C until RNA extraction. RNA was isolated by using a combination of two methods. First, total

RNA was isolated by using the Trizol method according to the manufacturer's protocol (Invitrogen, Carlsbad, CA). Subsequently, it was purified by using the RNeasy Mini kit and digesting it with DNase I (Qiagen, Germantown, MD) according to the manufacturer's protocol. RNA pellets were resuspended in DEPC-treated, RNase-free water, and their purity and quantity were determined spectrophotometrically by using the NanoDrop ND-1000 (NanoDrop Technologies). RNA samples were considered suitable for further processing if their absorbance ratio 260/280 was higher than 1.9. Integrity was tested by using lab-on-a-chip technology on the BioAnalyzer 2100 (Agilent, Palo Alto, CA, USA). Samples were considered intact if they had an RNA integrity number (RIN) above 8. Affymetrix microarrays on the Mouse Genome 430 2.0 platforms were performed according to the protocols published by the manufacturer (Affymetrix). Five RNA samples chosen randomly from the control and the MA group were analyzed.

Microarray data analyses. Data was standardized by using the Robust Multi-array Average method (Bolstad *et al.*, 2003) and quantile normalization. Differential gene expression was assessedusing the *limma* (Smyth, 2004) package from Bioconductor. Multiple testing adjustment of p-values was carried out as described by Benjamini and Hochberg (Benjamini *et al.*, 2001). Biochemical pathway analysis was conducted using Kyoto Encyclopedia of Genes and Genomes (KEGG) Mapper, a collection of KEGG mapping tools for KEGG pathway mapping. The Search&Color Pathway tool was used to overlay gene expression results from microarrays onto biochemical pathways found in KEGG. Gene expression levels were denoted by color codes displayed on the pathway by gene symbol boxes. Different shapes and pattern boxes were used to represent induced and suppressed gene expression. Enrichment analysis was based on MetaCore, an integrated knowledge database and software suite for pathway analysis of experimental data and gene lists. Enrichment analysis consisted of matching gene IDs of possible targets for the "common", "similar", and "unique" sets with gene IDs in functional ontologies in MetaCore. The probability of a random intersection between a set of IDs and the size of target list with ontology entities was estimated by the p-value of hypergeometric intersection. A lower p-value indicates higher relevance of the entity to the dataset, which shows in a higher rating for the entity. The use of the False Discovery Rate (adjusted p-value) allowed processes with doubtful significance in the experiment to be rejected and ensures that findings are not contaminated with false positives.

RT Real-Time PCR. The cDNA was synthesized in a total volume of 20 µL by mixing 1 µg of total RNA, 125 ng of random hexamers (Roche), 0.01 M dithiothreitol (Invitrogen), 20 units of RNAsin (Promega), 0.5 mM dNTPs (Bioline), 200 units of M-MLV reverse transcriptase (Invitrogen), and 4 µL 5X First-Strand Buffer (375 mM KCl, 15 mM $MgCl_2$, 250

mM Tris-HCl, pH 8.3) (Invitrogen). The reaction mixture was incubated at 37ºC for 60 min. The cDNA product was used for subsequent real-time PCR amplification. The mRNA levels of the selected genes were determined in an ABI Prism 7000 Sequence Detection System (Applied Biosystems) by using 9 μL of the cDNA mixture and 11 μL of the specific primers in Master mix (all from Applied Biosystems). β2 microglobulin (B2M) RNA was used as an endogenous control. The reaction was performed following the manufacturers recommendations. Fold-changes in gene expression were calculated by using the standard ΔΔCt method.

Serum sampling and NMR metabolic analysis. Blood samples were obtained by cardiopuncture of anesthetized mice, and serum samples were obtained by centrifuging blood at 600 g at 4ºC for 10 min. Macromolecules were removed from the serum samples by using the ultrafiltration method described by Günther et al. (Gunther *et al.*, 2005). Briefly, NanoSep 3K Omega centrifugal devices were prepared by washing them 10 times with 0.5 mL water + 0.75 g/L sodium azide at 1100 g and 30ºC for 1 h. Prior to use, the mouse samples were stored at −80ºC. When needed, samples were thawed, filtered, and then spun at 9000 g at 4ºC for 45 min. Then, 150 μL of the filtrate was diluted to obtain a 600-μL NMR sample in buffer (60 mmol/L sodium phosphate, 10 mmol/L sodium azide, 0.5 mmol/LTMSP, 10% D_2O, pH 7.0). The samples were analyzed by using a Varian 600 Direct Drive spectrometer operating at 599.36 MHz with a 5 mm triple resonance probe at 25ºC. One-dimensional ^1H NMR spectra were obtained by using 1024 transients, 16 steady-state scans, a spectral width of 6313 Hz, 16384 complex data points, and a 4 s recycling time. Excitation sculpting was used for water suppression. The data were processed in NMRLab (Gunther *et al.*, 2000). An exponential line-broadening function of 0.3 Hz was applied, and the dataset was zero-filled to 32768 data points prior to Fourier transformation. Both spectra were phase-corrected manually and referenced to TMSP (at 0 ppm). Regions containing residual water signal and a TMSP signal were removed, and the data were binned, normalized, log-transformed, and mean-centered prior to principal component analysis. Loadings were then exported to Chenomx NMR Suite with associated libraries (version 4.5; Chenomx), which was used to identify metabolites contributing to signals in the loadings plots.

RESULTS AND DISCUSSION

MA inhibits intestinal tumorigenesis without affecting body weight in $APC^{Min/+}$ mice. During the experiment, all mice were monitored for body weight, diet, and water consumption. For the last three weeks, $Apc^{Min/+}$ mice fed with MA showed significantly lower body weight gains than did controls (Figure 1A). However, there were no significant differences in water

(data not shown) or food intake (Figure 1B) between control and MA-fed mice. Therefore, the loss of weight in MA-treated mice may not be attributed to differences in food and drink intake and may not be related to a satiety effect either. In fact, weight loss could be related to the antiobesity and antidiabetogenic features of MA (Liu *et al.*, 2007). Furthermore, none of the animals fed with MA produced any sign of toxicity or any gross changes in any organ, including liver, lung, and kidney.

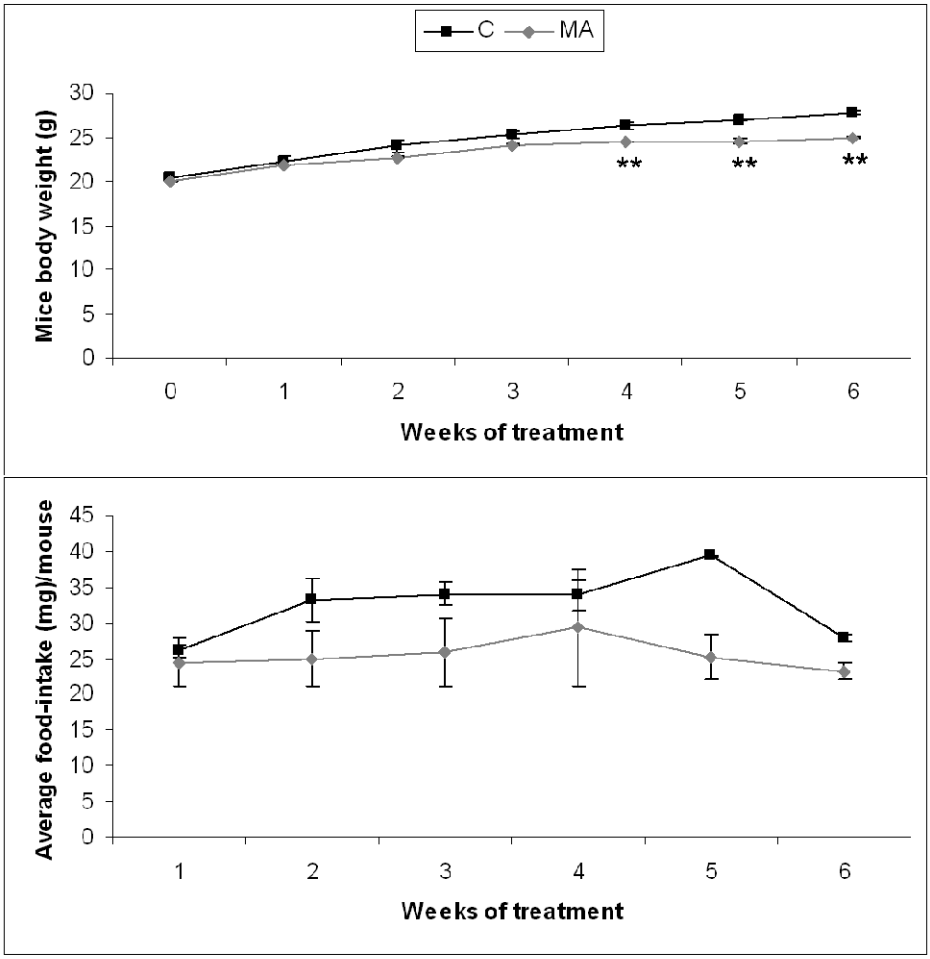

Figure 1. A) Effects of maslinic acid treatment on body weight. B) Effects of MA feeding in food intake. Data represented as mean ± SEM (* *, p > 0.01).

As shown in Figure 2A, MA prevented spontaneous intestinal polyposis in $Apc^{Min/+}$ mice. Dietary feeding with MA at 100 mg/kg of feed significantly ($P<0.01$) suppressed intestinal polyp formation by about 45% (9 tumors per mouse) when compared with the control diet group (16 tumors per mouse). Although MA significantly reduced the total number of polyps in small

intestine, this effect was statistically nonsignificant (due to fewer polyps and high variability) when polyps are classified by size or zone, except for polyps in the proximal small intestine (Figure 2B & C). MA showed differential efficacy depending on small-intestine segment. The most important MA chemopreventive effect was observed on proximal polyps (69%), followed by medial (4%) and distal polyps (28%) (Figure 2B). This is in agreement with previous evidence that some dietary and pharmaceutical compounds provide cancer protection only in parts of the small intestine (Corpet *et al.*, 2003). These effects could be related to several physiologic conditions through the gastrointestinal tract, such as pH, expression pattern of several enzymes, microbiota, and concentration due to intestinal content. All these conditions can modify the chemical structure of a chemopreventive agent and influence its final metabolism and, consequently, its anticancer effect. For example, resveratrol is almost completely conjugated upon oral administration, and the most bioactive metabolites are its glucuronide and sulfate derivatives (Tessitore *et al.*, 2000; Iwuchukwu *et al.*, 2008). The inhibitory efficacy depending on polyp size was more homogeneous, suggesting that MA inhibits both the appearance and development of intestinal polyps. In size distribution analysis of polyps, MA reduced the occurrence or growth of <1 mm diameter polyps by 44%, of 1–2 mm diameter polyps by 33%, and of >2 mm diameter polyps by 50% (Figure 2C).

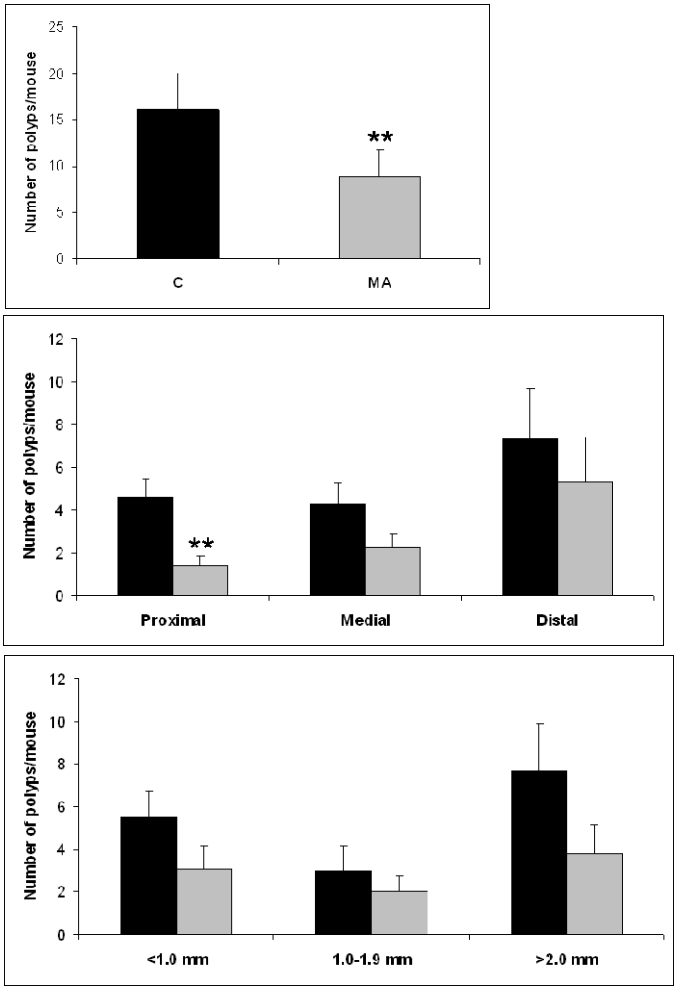

Figure 2. A) Total number of polyps/mouse in the small intestine of $Apc^{Min/+}$ mice. B) Number of polyps/mouse in proximal, medial and distal sections. C) Number of polyps/mouse shown by polyp size distribution (<1 mm diameter polyps, 1–2 mm and >2 mm). Data represented as mean ± SEM (* *, p > 0.01).

Gene expression profile induced by MA. To elucidate the underlying mechanisms by which MA inhibits intestinal tumorigenesis in $Apc^{Min/+}$ mice, we determined the transcriptional profile of the $Apc^{Min/+}$ mice's colonic mucosa by performing cDNA microarray analysis after MA feeding.

In the present study, we analyzed the expression profile of 45 101 genes by performing whole mouse genome cDNA microarrays. MA supplementation changed the expression of 2375 genes (p-value < 0.05), with an absolute fold-change of 1.5 or more. Of these 2375 differentially expressed genes, 193 were upregulated, and 2182 were downregulated (Supplemental data 1).

First, the list of differentially expressed genes between non-treated and MA-treated mice was subjected to a KEGG molecular pathway analysis using the KEGG Mapper tool to identify possible enrichment of genes with specific biological activities. The results of this study showed modifications mainly in cancer-related pathways. Figure 3 depicts the KEGG colorectal cancer pathway using KEGG Mapper and shows that MA downregulates glycogen synthase kinase 3β (*Gsk3b*), a protein involved in Wnt signaling that is affected in $Apc^{Min/+}$ mice. As mentioned above, $Apc^{Min/+}$ mice contain a mutation in APC that, together with Axin and GSK3β, operates by activating β-catenin degradation. Therefore, the mutation of the *Apc* gene present in the $Apc^{Min/+}$ mouse produces a cytosolic accumulation and an increase in nuclear translocation of β-catenin. In the nucleus, β-catenin interacts with the transcription factor T cell factor/lymphoid enhancer factor (TCF/LEF), leading to an increase in the expression of survival genes, including *c-Myc*, *Cyclin D1*, and *Cyclooxygenase-2* (*Cox-2*) (Phelps *et al.*, 2009). However, GSK3β has also been linked to a prosurvival signal in a Wnt/β-catenin-independent manner. In this regard, GSK3β is constitutively activated in colon cancer cells, where it is implicated in tumorigenesis and cancer progression. Accordingly, the downregulation of GSK3β inhibits proliferation and enhances apoptotic cell death in chronic lymphocytic leukemia B cells, renal cancer cells, pancreatic cancer cells, and colon cancer cells (Min *et al.*, 2009; Ban *et al.*, 2010). These results may indicate that MA confers a protective effect by inhibiting GSK3β. Interestingly, MA also inhibited Cyclin D *(Ccnd1)*, a gene expressed after the transcriptional activation of β-catenin/TCF/LEF. Cyclin D is involved in regulating cell-cycle progression and drives the G1/S phase transition. In agreement with this result, the results of other studies have related MA antitumor activity to an inhibition of cyclin D1 expression (Li *et al.*, 2010).

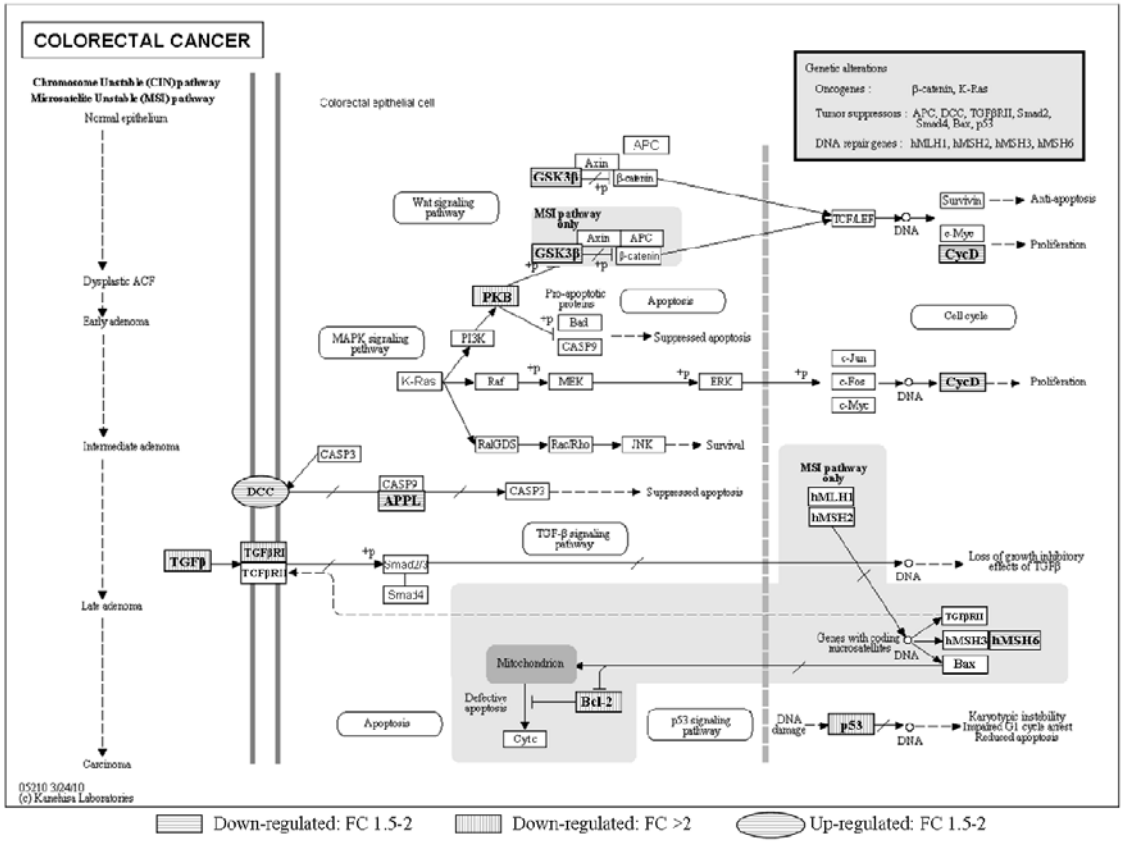

Figure 3. Adaptation of KEGG colorectal cancer pathway using KEGG Mapper. Circular pathway members were significantly up-regulated and rectangular members were found to be down-regulated in the intestinal mucosa of $Apc^{Min/+}$ mice treated with MA. Horizontal lines indicate a fold change (FC) of between 1.5 and 2 and vertical lines a FC of more than 2.

Moreover, MA treatment downregulated the expression of the *Akt1* gene, which codes for the protein AKT (protein kinase B, PKB), a serine/threonine kinase critical in controlling cell survival, insulin signaling, angiogenesis, and tumor formation. Overexpression of *Akt* is an early event in colorectal carcinogenesis (Colakoglu *et al.*, 2008), thus the lower expression of *Akt* in MA-treated mice may be related to the inhibition of intestinal polyp growth in $Apc^{Min/+}$ mice.

Another common clinicopathologic feature of colorectal carcinoma is the presence of mutations in p53 (*Tpr53*). This gene encodes protein p53, which regulates cell cycle, apoptosis, senescence, metabolism, and DNA repair. The mutated form of p53 is highly expressed in more than 50% of all cancers, including colon cancer. The existence of overexpressed p53 in $APC^{Min/+}$ mice may explain the downregulation of p53 by MA. In $APC^{Min/+}$ mice, p53 inactivation does has been reported to have little effect on the incidence or the progression and apoptosis of

adenomas (Qiu *et al.*, 2009). Nevertheless, inhibition of p53 in mice treated with MA indicates that the death process is p53-independent.

The genes of the post-replicative DNA mismatch repair system (MMR) are also involved in DNA repair. One of these genes, *Msh6,* was inhibited by MA. DNA repair is associated with the prevention of mutagenesis and cancer but can also be associated with the detection and repair of mismatches derived from chemically induced DNA damage with genotoxic agents. In this regard, the utility of genotoxic drugs is often limited by the enhanced ability of cancer cells to repair their DNA. Therefore, attenuation of the DNA repair system sensitizes tumor cells to DNA-damaging agents (Abuzeid *et al.*, 2009). Notably, MA has been reported to interfere with DNA integrity in HT29 cells (Reyes-Zurita *et al.*, 2011); hence, it could be acting, at least in part, as a genotoxic agent. In this case, *Msh6* downregulation could trigger DNA damage and posterior apoptosis. Anyway, inhibition of only one DNA repair system would hardly affect final repairing activity due to the functional redundancy of MMR proteins.

Furthermore, MA supplementation downregulated the expression of *Tgfb1* and its receptor (*Tgfb1r1*). Advanced colorectal adenomas usually present changes in transforming growth factor beta (TGFβ) signaling. Generally, cancerous cells increase their production of TGFβ, which acts on the secreting cancerous cells themselves and on surrounding cells regulating cell growth, differentiation, and apoptosis (Shiou *et al.*, 2006). Thus, reduction of TGFβ signaling by MA may be involved in the inhibition of tumorigenesis in $Apc^{Min/+}$ mice.

In the advanced stages of colorectal pathogenesis, deleted in colorectal carcinoma (*Dcc)* gene expression appears to be lost or markedly reduced. This gene encodes a netrin 1 receptor that functions as a tumor suppressor via its ability to trigger tumor cell apoptosis (Castets *et al.*, 2011). MA caused upregulation of DCC, indicating a pro-apoptotic effect. However, a mediator of the DCC apoptotic pathway, DIP13α (*Appl1*) was downregulated by MA treatment. DIP13α interacts with a region on the DCC cytoplasmic domain that is required for the induction of apoptosis (Liu *et al.*, 2002). However, DIP13α also binds many other proteins, including RAB5A, AKT2, PI3KCA, and adiponectin receptors to regulate cell proliferation and adiponectin and insulin signaling. Given that little is known about DIP13α, its inhibition by MA could indicate a beginning of MA-resistance in $Apc^{Min/+}$ mice, antagonizing DCC apoptotic activation but also modulating other DIP13α biological functions.

Furthermore, MA modulated the expression of another apoptosis-related protein called Bcl-2, an integral outer mitochondrial membrane protein that suppresses apoptosis by controlling mitochondrial membrane permeability. Bcl-2 inhibits caspase activity either by preventing the release of cytochrome c from the mitochondria and/or by binding to the

apoptosis-activating factor. Downregulation of *Bcl-2* by MA acts as a pro-apoptotic stimulus. This finding is in agreement with that of a recent study where western blotting analysis showed that the treatment of the HT29 human colon adenocarcinoma cell line with MA induced the repression of Bcl2 (Reyes-Zurita *et al.*, 2011).

Pathway analysis performed using KEGG Mapper was complemented with an independent analysis by MetaCore to obtain a p-value for each pathway. According to the GeneGO Maps Folder in Metacore, the maps containing genes corresponding to cytoskeleton remodeling, transcription, cell cycle, cell adhesion, immune response, apoptosis, and survival in normal and pathologic TGF-β-mediated regulation of cell proliferation were the most significantly modulated (Table 1).

Table 1. Effects in modulated pathways by MA in colon mucosa of ApcMin/+ mice as found in Metacore

GeneGO Maps	Regulated pathways	p-value	significant/total genes	Modulated genes
Cytoskeleton remodeling	TGF, WNT and cytoskeletal remodeling (↓)	3,57E-09	23/111	Ncl, Tgfb1, Tgfbr1, Wnt5a, Fzd7, Dvl1, Dock1, Akt1, Gsk3b, Map3k7, Mapk14, Limk2, Ppard, Trp53, Ccnd1, Cfl1, Actn1, Arpc4, Sos1,Grb2, Pxn , Tln1, Shc1
	Cytoskeleton remodeling (↓)	4,91E-07	19/102	Ncl, Tgfb1, Tgfbr1, Dock1, Gsk3b, Map3k7, Mapk14, Limk2, Cfl1, Actn1, Arpc4, Sos1,Grb2, Pxn , Tln1, Shc1
Transcription	CREB pathway (↓)	1,18E-07	13/44	Akt1, Mapk14, Ccnd1, Sos1, Grb2, Shc1, Clca2, Camk2g, Gprc5a, Prkcb, Prkar2b, Rps6ka2, Cdo1, Prkaca, Fbxw5, Fbxw11
Cell cycle	Regulation of G1/S transition (part 1) (↓)	1,61E-07	12/38	Cdk4, Cdk6, Junb, Btrc, Ppp2r4, Tgfb1, Tgfbr1, Gsk3b, Ccnd1, Ccnd2
Cell adhesion	Chemokines and adhesion (↓)	3,55E-07	19/100	Dock1, Akt1, Gsk3b, Limk2, Cfl1, Actn1, Arpc4, Sos1,Grb2, Pxn , Tln1, Shc1, Thbs1, Cd44, Cd47, Itga3, Msn, Flot2, Eif4g1
Immune response	Signaling pathway mediated by IL-6 and IL-1 (↓)	3,56E-06	9/27	Sos1,Grb2, Shc1, Il6st, Jak1, Ikbkap, Nfkbie, Irak1, Cebpb
	IL-15 signaling (↓)	2,19E-06	14/64	Akt1, Mapk14, Sos1,Grb2, Shc1, Il2rg, Adam17, Nfkbie, Prkce, Ets1, Bcl2, Bcl2l1
	MIF - the neuroendocrine-macrophage connector (↑)	1,92E-04	4/46	Plcb2, Pla2g4c, Itpr2
	PIP3 signaling in B lymphocytes (↑)	1,34E-04	4/42	Plcb2, Pik3r1, Itpr2, Foxo3, Igh-6
Apoptosis and survival	BAD phosphorylation (↓)	4,21E-06	11/42	Bcl2, Bcl2l1, Sos1, Grb2, Shc2, Rps6ka2, Ywhae, Ywhag, Prkar2b, Prkaca
Normal and pathological TGF-beta-mediated regulation of cell prolif.	Normal and pathological TGF-beta-mediated regulation of cell prolif. (↓)	2,71E-06	10/33	Tgfb1, Tgfbr1, Gsk3b, Mapk14, Trp53, Ccnd1,Sos1,Grb2, Shc1, Map2k6

↑/↓ Activated/Inhibited

In addition to the aforementioned cell-cycle-associated genes, Metacore analysis identified downregulation of *Cdk4*, *Cdk6*, *Btrc*, *Junb*, and *Ppp2r4* (Table 1, cell cycle). Cell-cycle progression is highly controlled by a complex network of signaling pathways that eventually converge to regulate the activity of cyclin/cyclin-dependent kinase (CDK) complexes. There are different members of the CDK family, and each CDK is dependent on a particular cyclin; therefore, the activity of each CDK can be controlled by the availability of its cyclin partner (Ballabeni *et al.*, 2011). In this regard, in addition to the downregulation of cyclin D mentioned previously, MA inhibited the expression of its partners during G1 phase, Cdk4 and Cdk6, inhibiting the G1 cyclin-CDK complexes and leading to G1-phase cell-cycle arrest. Specific and timely proteolysis of cell-cycle regulators by the ubiquitin-proteasome system represents an important mechanism that ensures proper progression through the cell cycle in a unidirectional and irreversible manner. Moreover, in cancer cells, deregulation or suppression of the proteasome is supposed to induce uncontrolled proteolysis and is linked to having a more sensitive profile to drugs than that of normal cells (Roberti *et al.*). MA inhibited the ubiquitin ligase SKP1–CUL1–F-box-protein (SCF) complex by downregulating the *Btrc* gene. BetaTrCP protein pertaining to the F-box family is the substrate-recognition component of the SCF ubiquitin ligase complex, which mediates the ubiquitination and subsequent proteasomal

degradation of target proteins involved in cell-cycle checkpoints, protein translation, cell growth, and survival. Interestingly, βTrCP mediates the degradation of the pro-apoptotic protein BimEL to promote cell survival (Dehan *et al.*, 2009) and has been reported to be overexpressed in colorectal tumors (Ougolkov *et al.*, 2004). Hence, its downregulation by MA could be related to the inhibition of spontaneous polyposis in $Apc^{Min/+}$. Additionally, MA modulates other cell-cycle regulatory proteins. For example, MA suppresses the expression of the gene encoding the oncogenic protein JunB, which is an essential component of the activating protein-1 (AP-1) transcription factor that is involved in the control of cell growth, differentiation, inflammation, and neoplastic transformation. It is noteworthy that a recent study demonstrated that the chemopreventive effects of MA in Raji cells depends on the inhibition of nuclear factor-κB (NF-κB) and the activation of Activator protein (AP-1) (Hsum *et al.*, 2011). Another protein controlling cell growth and division that was downregulated in $Apc^{Min/+}$ mice after treatment with MA was a regulatory subunit of protein phosphatase 2A (PP2A) (*Ppp2r4*). This protein has been described to dephosphorylate β-catenin, acting as a positive regulator of Wnt signaling (Eichhorn *et al.*, 2009; Zhang *et al.*, 2009). Moreover, *Ppp2r4* function is essential for cell survival (Eichhorn *et al.*, 2009; Zhang *et al.*, 2009). Therefore, MA's downregulation of the gene encoding this protein could be involved in its antitumor effect.

Apart from the apoptosis-related genes already mentioned, Metacore analysis revealed that the induction of apoptosis by MA was also based on the downregulation of the anti-apoptotic gene *Bcl2l1* (Bcl-XL) (Table 1, apoptosis and survival). Moreover, different signal transduction pathways that save cells from apoptosis have been shown to be modulated in MA-treated mice. For instance, MA downregulates epidermal growth factor receptor (EGFR) signaling, which is related to mitogenesis and tumorigenesis. After EGFR activation, a trimeric complex between tyrosine phosphorylated Shc, Grb2, and Sos is formed and this, in turn, triggers downstream mitogenic signaling (Koizumi *et al.*, 2005). MA exerted this action by downregulating *Shc1*, *Grb2*, and *Sos1* gene expression. Furthermore, MA treatment reduced the expression of the *Rps6ka2* gene, coding for the protein p90Rsk, a downstream mediator of the mitogen-activated protein kinase (MAPK) pathway, which has been reported to inhibit apoptosis via the stimulation of binding of Bad to 14-3-3 and the inactivation of Bad-mediated cell death (Tan *et al.*, 1999). Interestingly, MA also triggered this apoptotic action by inhibiting the expression of *Ywhae* and *Ywhag*, which code for different members of the family of 14-3-3 proteins, and thus reducing Bad sequestration and increasing Bad-induced apoptosis via the mitochondrial death pathway (Wu *et al.*, 2009). In addition, MA reduced the expression of *Prkar2b* and *Prkaca* coding for the regulatory subunit type II-beta of the cAMP-dependent protein kinase (PKA RII-beta) and the catalytic subunit alpha of the cAMP-dependent protein

kinase (PKA C-alpha), respectively. PKA is a serine/threonine kinase that is activated by cyclic adenosine monophosphate (cAMP). Effects of PKA on apoptosis are likely to be largely dependent on the cell type and the mechanisms by which apoptosis is induced (Franklin *et al.*, 2000). In the case of $Apc^{Min/+}$ mice, treatment with a PKA antagonist, Rp-8-Br-cAMPS, reduces tumor promotion and β-catenin levels, nuclear translocation, and expression of some of its target genes, such as *c-Myc* and *cyclooxygenase-2* (*Cox-2*) (Brudvik *et al.*, 2011).

In addition, evidence is accumulating to suggest that proteins involved in regulating actin cytoskeleton and cell adhesion also participate in mitogenesis, either as unique transducers of growth signals or as monitors of anti-apoptotic conditions, or both (Honda *et al.*, 2005; Rosano *et al.*, 2006). In this regard, Metacore analysis showed that MA downregulated the maps containing genes corresponding to cytoskeleton remodeling and cell adhesion (Table 1, cytoskeleton remodeling and cell adhesion). Amongst the modulated genes, it is important to highlight *Cd44*, which encodes a transmembrane protein associated with tumor invasion, metastasis, and acquisition of resistance to apoptosis. A recent study using short hairpin RNA against CD44 to silence its expression in SW620 colon cancer cells showed that reduced expression of the protein inhibited cell proliferation, migration, and invasion. In agreement with our results, reduced expression of CD44 induced cell cycle arrest in the G1 phase and apoptosis via the downregulation of Bcl-2 and Bcl-xL and the upregulation of BAX (Park *et al.*, 2012).

Therefore, expression data in cancer signaling indicate that, as suggested by our polyp analysis, MA inhibits both the appearance and development of intestinal polyps in $Apc^{Min/+}$ mice by inducing a cell-cycle arrest in the G1 phase and p53-independent apoptosis.

Finally, Metacore also revealed the downregulation of immune system–related genes by MA (Table 1, immune response). Inflammation and immune system responses have controversial effects in cancer, either by preventing and inhibiting tumor development or, when inflammation becomes chronic, by promoting the growth and progression of cancer (Zamarron *et al.*, 2011). In this regard, chronic inflammation plays a decisive role in the development and sustenance of intestinal adenomatous polyps in the $Apc^{Min/+}$ mice (McClellan *et al.*, 2012). Accordingly, MA has been implicated in anti-inflammatory and immune-attenuating actions via suppression of NFkB (Huang *et al.*, 2011). Therefore, in this case, the downregulation of immune system responses by MA may reduce tumor growth.

Validation of microarray data by RT-PCR. The changes in mRNA expression observed in the microarrays for *Ccnd1*, *Cdk4, Bcl2, Shc1, Cd44* and *Sorbs 1* were validated by performing RT real-time PCR assays (Figure 4). These targets were selected for RT real-time

PCR analysis on the basis of their significant participation in the chemopreventive effects produced in $Apc^{Min/+}$ mice by MA supplementation.

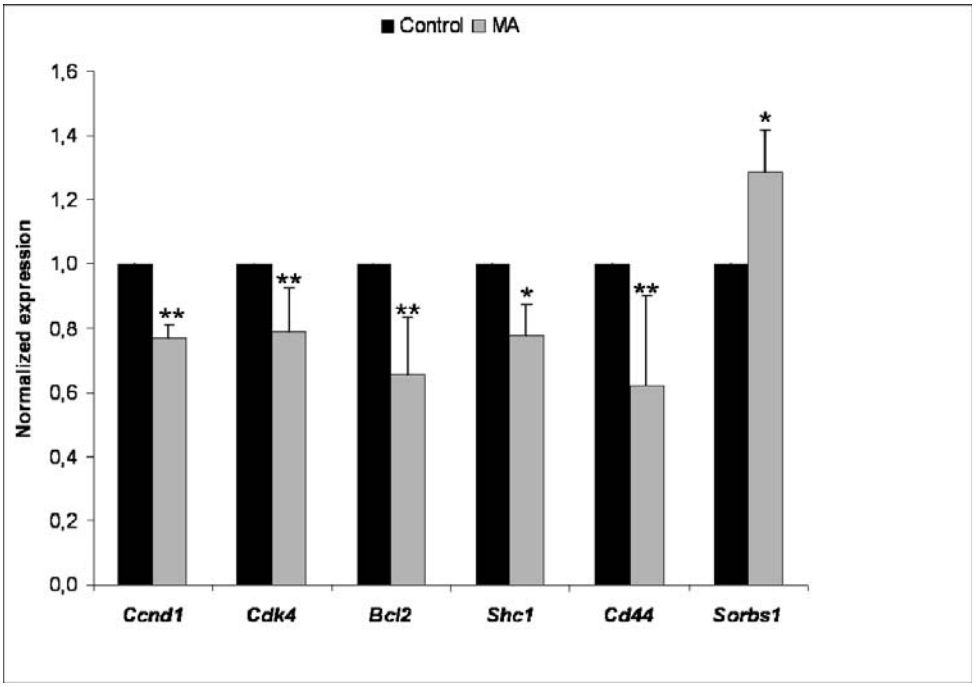

Figure 4. Validation of genes that were differentially expressed in the colon mucosa of $Apc^{Min/+}$ mice after MA treatment by RT-PCR. Data represented as mean ± SEM (*, $p > 0.05$; * *, $p > 0.01$).

Metabolic profile of blood serum induced by MA. ^{1}H NMR spectroscopy detected a wide range of metabolites in mouse serum. Principal component analysis revealed a clear difference between controls and MA-fed mice, with little variation between the replicates (Figure 5). This result reflects the observation in NMR spectra (Figure 6) in which replicates are almost indistinguishable but significant differences are observed between MA-treated and control mice. Comparison of the NMR spectra of serum from control and MA-fed mice showed that MA supplementation produced an increase in ketone bodies, whereas it reduced the levels of glucose relative to that in untreated mice (Figure 6). Interestingly, the genetic modulations induced by MA can explain the altered metabolic profile. The decrease in serum glucose concentration in ApcMin/+ mice treated with MA could be a consequence of the upregulation of the c-Cbl–associated protein (CAP) encoded by *Sorbs1*. CAP plays a critical role in insulin-regulated GLUT4 translocation (Zhang *et al.*, 2003) and hence, its activation by MA promotes glucose cellular uptake. Moreover, low glucose levels in mice serum can be due to a glycogen accumulation triggered by MA treatment. First, glycogen reservoirs are regulated by the aforementioned GSK3. This protein, apart from its role in Wnt and pro-survival signaling, is

able to phosphorylate and inhibit glycogen synthase activity, impairing glycogen synthesis. Thus, inhibiting GSK3 by MA implies an activation of glycogen accumulation. Second, MA also reduced *Phka1* expression. Because the *Phka1* gene encodes PHK protein, which activates glycogen phosphorylase and leads to the conversion of glycogen into glucose-1-phosphate, downregulating PHK inhibits glycogen degradation. In addition to these transcriptional modifications, MA has been described to be a potent inhibitor of glycogen phosphorylase activity, thus triggering glycogen reservoir accumulation (Guan *et al.*, 2011). An increase in ketone bodies was also found in serum from MA-treated mice. Ketone bodies consisted of 3-hydroxybutyrate and acetoacetate. The decrease in serum glucose may contribute to the increase in serum ketone body concentrations because, although ketone body synthesis occurs normally under all conditions, its formation increases as glucose availability drops. To support the elevated ketone body synthesis in MA-treated mice, high fatty acid oxidation is necessary for the production of acetyl-CoA used as substrate. In mice treated with MA, fatty acid degradation is activated by the upregulation of *Cpt1*, which encodes carnitine palmitoyltransferase I (CPT I), the mitochondrial gateway for fatty acid entry into the matrix and, thus, the main controller of fatty acid oxidation. It is noteworthy that this observation may be involved in the loss of weight detected in $Apc^{Min/+}$ mice after MA treatment. Given that accumulating evidence suggests that obesity (Mutoh *et al.*, 2011) and hyperglycemia (Erbach *et al.*, 2012) are associated with increased risk of colorectal cancer, the metabolic changes induced by MA treatment are potentiating its chemoprotective effect in $Apc^{Min/+}$ mice.

Taken together, our data show that MA is a nontoxic agent that effectively inhibits intestinal polyposis in genetically predisposed $Apc^{Min/+}$ mice. The cancer chemopreventive effects of MA are mainly related to the modulation of cancer progression–related genes, suggesting an induction of a G1-phase cell-cycle arrest and activation of apoptosis by a p53-independent mechanism. Moreover, the expression of genes related to energy metabolism is altered by MA to support a protective metabolic profile. In summary, our findings provide the first *in vivo* evidence that MA is a promising nutraceutical for colon cancer prevention.

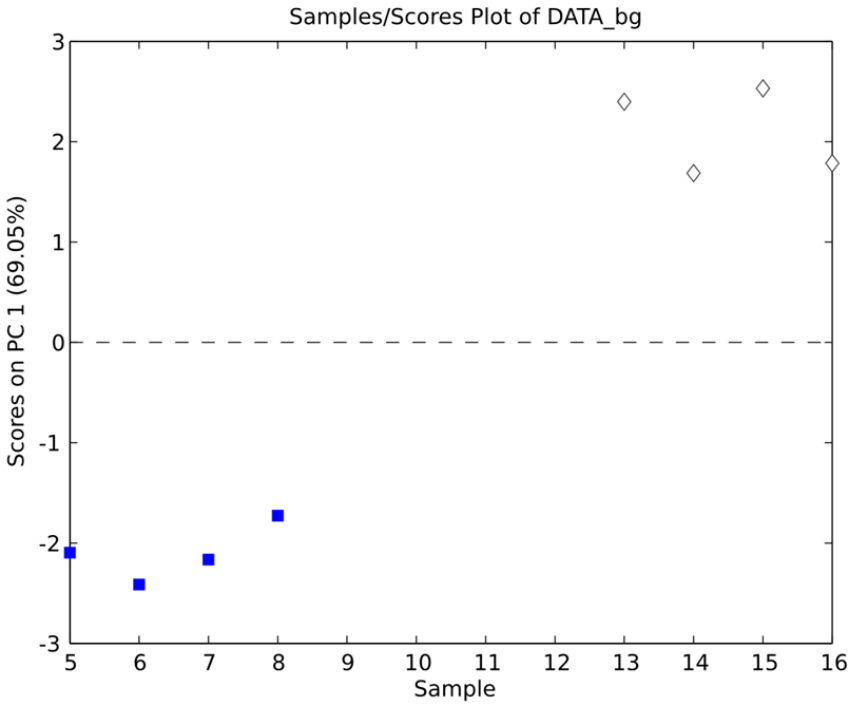

Figure 5. Principal component analysis revealed a clear difference between controls and MA-treated mice with little variation between the replicates.

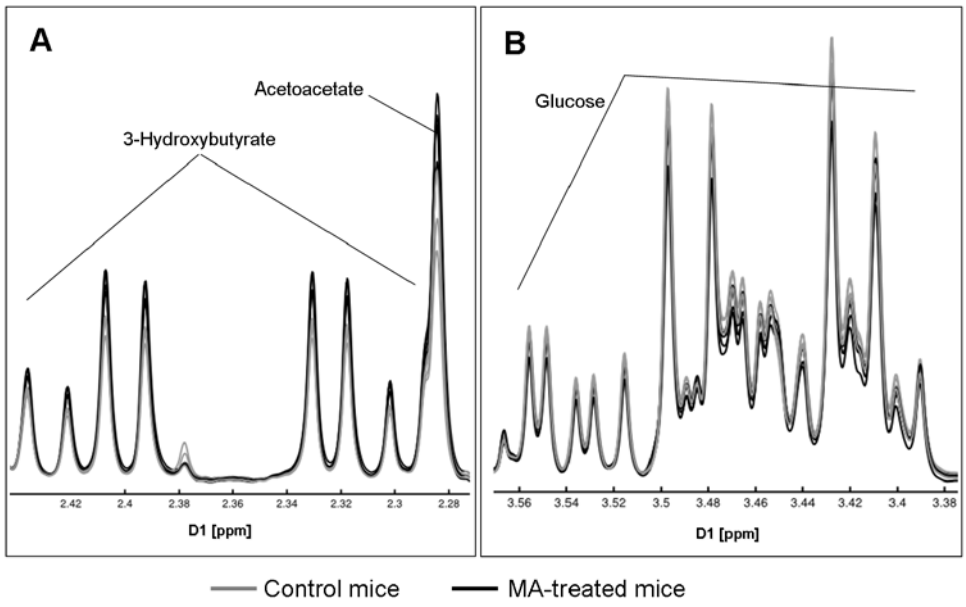

Figure 6. Overlaid ^{1}H NMR spectra of sera from Apc$^{Min/+}$ mice in the control and MA-treated groups. (A) Spectra fragment from 2.28 to 2.44 ppm. (B) Spectra fragment from 3.38 to 3.56 ppm.

ACKNOWLEDGEMENTS

The authors thank Anibal Miranda and Ursula Valls from the Universitat de Barcelona and Miquel Borràs, Joaquín de Lapuente, Javier González and Joan Serret from CERETOX for their technical support in the experiments. Financial support was provided by grant SAF2011-25726 and personal financial support (FPU program) from the Spanish government and also from the Red Temática de Investigación Cooperativa en Cáncer, Instituto de Salud Carlos III, Spanish Ministry of Science and Innovation & European Regional Development Fund (ERDF) "Una manera de hacer Europa" (ISCIII-RTICC grants RD06/0020/004 and RD06/0020/1019 and BIO2011-27069, MICINN). We have also received financial support from the AGAUR-Generalitat de Catalunya (grant 2009SGR1308, 2009 CTP 00026 and Icrea Academia Award 2010 granted to M.C.) and the European Commission (FP7) ETHERPATHS KBBE-grant agreement no. 22263. We thank the Bio-NMR EU project (Contract # 261863) for providing NMR access to the HWB-NMR facility. Finally, the authors are grateful for the financial support from Biomaslinic S.L. (Granada, Spain). Biomaslinic had also supplied the Maslinic Acid required for the investigation purpose.

REFERENCES

Abuzeid, W.M., Jiang, X., Shi, G., Wang, H., Paulson, D., Araki, K., Jungreis, D., Carney, J., O'Malley, B.W., Jr. i Li, D. (2009). Molecular disruption of RAD50 sensitizes human tumor cells to cisplatin-based chemotherapy. *J Clin Invest* **119**(7): 1974-85.

Ballabeni, A., Park, I.H., Zhao, R., Wang, W., Lerou, P.H., Daley, G.Q. i Kirschner, M.W. (2011). Cell cycle adaptations of embryonic stem cells. *Proc Natl Acad Sci U S A* **108**(48): 19252-7.

Ban, J.O., Kwak, D.H., Oh, J.H., Park, E.J., Cho, M.C., Song, H.S., Song, M.J., Han, S.B., Moon, D.C., Kang, K.W. i Hong, J.T. (2010). Suppression of NF-kappaB and GSK-3beta is involved in colon cancer cell growth inhibition by the PPAR agonist troglitazone. *Chem Biol Interact* **188**(1): 75-85.

Benjamini, Y., Drai, D., Elmer, G., Kafkafi, N. i Golani, I. (2001). Controlling the false discovery rate in behavior genetics research. *Behav Brain Res* **125**(1-2): 279-84.

Bolstad, B.M., Irizarry, R.A., Astrand, M. i Speed, T.P. (2003). A comparison of normalization methods for high density oligonucleotide array data based on variance and bias. *Bioinformatics* **19**(2): 185-93.

Brudvik, K.W., Paulsen, J.E., Aandahl, E.M., Roald, B. i Tasken, K. (2011). Protein kinase A antagonist inhibits beta-catenin nuclear translocation, c-Myc and COX-2 expression and tumor promotion in ApcMin/+ mice. *Mol Cancer* **10**: 149.

Castets, M., Broutier, L., Molin, Y., Brevet, M., Chazot, G., Gadot, N., Paquet, A., Mazelin, L., Jarrosson-Wuilleme, L., Scoazec, J.Y., Bernet, A. i Mehlen, P. (2011). DCC constrains tumour progression via its dependence receptor activity. *Nature*.

Colakoglu, T., Yildirim, S., Kayaselcuk, F., Nursal, T.Z., Ezer, A., Noyan, T., Karakayali, H. i Haberal, M. (2008). Clinicopathological significance of PTEN loss and the phosphoinositide 3-kinase/Akt pathway in sporadic colorectal neoplasms: is PTEN loss predictor of local recurrence? *Am J Surg* **195**(6): 719-25.

Corpet, D.E. i Pierre, F. (2003). Point: From animal models to prevention of colon cancer. Systematic review of chemoprevention in min mice and choice of the model system. *Cancer Epidemiol Biomarkers Prev* **12**(5): 391-400.

Dehan, E., Bassermann, F., Guardavaccaro, D., Vasiliver-Shamis, G., Cohen, M., Lowes, K.N., Dustin, M., Huang, D.C., Taunton, J. i Pagano, M. (2009). betaTrCP- and Rsk1/2-mediated degradation of BimEL inhibits apoptosis. *Mol Cell* **33**(1): 109-16.

Eichhorn, P.J., Creyghton, M.P. i Bernards, R. (2009). Protein phosphatase 2A regulatory subunits and cancer. *Biochim Biophys Acta* **1795**(1): 1-15.

Erbach, M., Mehnert, H. i Schnell, O. (2012). Diabetes and the risk for colorectal cancer. *J Diabetes Complications*.

Fernandez-Navarro, M., Peragon, J., Amores, V., De La Higuera, M. i Lupianez, J.A. (2008). Maslinic acid added to the diet increases growth and protein-turnover rates in the white muscle of rainbow trout (Oncorhynchus mykiss). *Comp Biochem Physiol C Toxicol Pharmacol* **147**(2): 158-67.

Franklin, R.A. i McCubrey, J.A. (2000). Kinases: positive and negative regulators of apoptosis. *Leukemia* **14**(12): 2019-34.

Garcia-Granados, A., Lopez, P.E., Melguizo, E., Moliz, J.N., Parra, A., Simeo, Y. i Dobado, J.A. (2003). Epoxides, cyclic sulfites, and sulfate from natural pentacyclic triterpenoids: theoretical calculations and chemical transformations. *J Org Chem* **68**(12): 4833-44.

Guan, T., Qian, Y., Tang, X., Huang, M., Huang, L., Li, Y. i Sun, H. (2011). Maslinic acid, a natural inhibitor of glycogen phosphorylase, reduces cerebral ischemic injury in hyperglycemic rats by GLT-1 up-regulation. *J Neurosci Res* **89**(11): 1829-39.

Gunther, R.W., Neuerburg, J., Mossdorf, A., Pfeffer, J., Hoj, A.R., Molgaard-Nielsen, A., Bucker, A. i Schmitz-Rode, T. (2005). New optional IVC filter for percutaneous retrieval--in vitro evaluation of embolus capturing efficiency. *Rofo* **177**(5): 632-6.

Gunther, U.L., Ludwig, C. i Ruterjans, H. (2000). NMRLAB-Advanced NMR data processing in matlab. *J Magn Reson* **145**(2): 201-8.

Honda, K., Yamada, T., Hayashida, Y., Idogawa, M., Sato, S., Hasegawa, F., Ino, Y., Ono, M. i Hirohashi, S. (2005). Actinin-4 increases cell motility and promotes lymph node metastasis of colorectal cancer. *Gastroenterology* **128**(1): 51-62.

Hsum, Y.W., Yew, W.T., Hong, P.L., Soo, K.K., Hoon, L.S., Chieng, Y.C. i Mooi, L.Y. (2011). Cancer Chemopreventive Activity of Maslinic Acid: Suppression of COX-2 Expression and Inhibition of NF-kappaB and AP-1 Activation in Raji Cells. *Planta Med.*

Huang, L., Guan, T., Qian, Y., Huang, M., Tang, X., Li, Y. i Sun, H. (2011). Anti-inflammatory effects of maslinic acid, a natural triterpene, in cultured cortical astrocytes via suppression of nuclear factor-kappa B. *Eur J Pharmacol* **672**(1-3): 169-74.

Iwuchukwu, O.F. i Nagar, S. (2008). Resveratrol (trans-resveratrol, 3,5,4'-trihydroxy-trans-stilbene) glucuronidation exhibits atypical enzyme kinetics in various protein sources. *Drug Metab Dispos* **36**(2): 322-30.

Koizumi, F., Shimoyama, T., Taguchi, F., Saijo, N. i Nishio, K. (2005). Establishment of a human non-small cell lung cancer cell line resistant to gefitinib. *Int J Cancer* **116**(1): 36-44.

Li, C., Yang, Z., Zhai, C., Qiu, W., Li, D., Yi, Z., Wang, L., Tang, J., Qian, M., Luo, J. i Liu, M. (2010). Maslinic acid potentiates the anti-tumor activity of tumor necrosis factor alpha by inhibiting NF-kappaB signaling pathway. *Mol Cancer* **9**: 73.

Lin, C.C., Huang, C.Y., Mong, M.C., Chan, C.Y. i Yin, M.C. (2011). Antiangiogenic potential of three triterpenic acids in human liver cancer cells. *J Agric Food Chem* **59**(2): 755-62.

Liu, J., Sun, H., Duan, W., Mu, D. i Zhang, L. (2007). Maslinic acid reduces blood glucose in KK-Ay mice. *Biol Pharm Bull* **30**(11): 2075-8.

Liu, J., Yao, F., Wu, R., Morgan, M., Thorburn, A., Finley, R.L., Jr. i Chen, Y.Q. (2002). Mediation of the DCC apoptotic signal by DIP13 alpha. *J Biol Chem* **277**(29): 26281-5.

Martin, R., Carvalho-Tavares, J., Ibeas, E., Hernandez, M., Ruiz-Gutierrez, V. i Nieto, M.L. (2007). Acidic triterpenes compromise growth and survival of astrocytoma cell lines by regulating reactive oxygen species accumulation. *Cancer Res* **67**(8): 3741-51.

McClellan, J.L., Davis, J.M., Steiner, J.L., Day, S.D., Steck, S.E., Carmichael, M.D. i Murphy, E.A. (2012). Intestinal inflammatory cytokine response in relation to tumorigenesis in the Apc(Min/+) mouse. *Cytokine* **57**(1): 113-9.

Min, H.J., Koh, S.S., Cho, I.R., Srisuttee, R., Park, E.H., Jhun, B.H., Kim, Y.G., Oh, S., Kwak, J.E., Johnston, R.N. i Chung, Y.H. (2009). Inhibition of GSK-3beta enhances reovirus-induced apoptosis in colon cancer cells. *Int J Oncol* **35**(3): 617-24.

Mutoh, M., Teraoka, N., Takasu, S., Takahashi, M., Onuma, K., Yamamoto, M., Kubota, N., Iseki, T., Kadowaki, T., Sugimura, T. i Wakabayashi, K. (2011). Loss of adiponectin promotes intestinal carcinogenesis in Min and wild-type mice. *Gastroenterology* **140**(7): 2000-8, 2008 e1-2.

Ougolkov, A., Zhang, B., Yamashita, K., Bilim, V., Mai, M., Fuchs, S.Y. i Minamoto, T. (2004). Associations among beta-TrCP, an E3 ubiquitin ligase receptor, beta-catenin, and NF-kappaB in colorectal cancer. *J Natl Cancer Inst* **96**(15): 1161-70.

Park, Y.S., Huh, J.W., Lee, J.H. i Kim, H.R. (2012). shRNA against CD44 inhibits cell proliferation, invasion and migration. *Oncol Rep* **27**(2): 339-46.

Parra, A., Rivas, F., Martin-Fonseca, S., Garcia-Granados, A. i Martinez, A. (2011). Maslinic acid derivatives induce significant apoptosis in b16f10 murine melanoma cells. *Eur J Med Chem* **46**(12): 5991-6001.

Phelps, R.A., Chidester, S., Dehghanizadeh, S., Phelps, J., Sandoval, I.T., Rai, K., Broadbent, T., Sarkar, S., Burt, R.W. i Jones, D.A. (2009). A two-step model for colon adenoma initiation and progression caused by APC loss. *Cell* **137**(4): 623-34.

Qiu, W., Carson-Walter, E.B., Kuan, S.F., Zhang, L. i Yu, J. (2009). PUMA suppresses intestinal tumorigenesis in mice. *Cancer Res* **69**(12): 4999-5006.

Reyes-Zurita, F.J., Pachon-Pena, G., Lizarraga, D., Rufino-Palomares, E.E., Cascante, M. i Lupianez, J.A. (2011). The natural triterpene maslinic acid induces apoptosis in HT29 colon cancer cells by a JNK-p53-dependent mechanism. *BMC Cancer* **11**: 154.

Reyes, F.J., Centelles, J.J., Lupianez, J.A. i Cascante, M. (2006). (2Alpha,3beta)-2,3-dihydroxyolean-12-en-28-oic acid, a new natural triterpene from Olea europea, induces caspase dependent apoptosis selectively in colon adenocarcinoma cells. *FEBS Lett* **580**(27): 6302-10.

Roberti, A., Rizzolio, F., Lucchetti, C., de Leval, L. i Giordano, A. (2011). Ubiquitin-mediated protein degradation and methylation-induced gene silencing cooperate in the inactivation of the INK4/ARF locus in Burkitt lymphoma cell lines. *Cell Cycle* **10**(1): 127-34.

Rosano, L., Spinella, F., Di Castro, V., Dedhar, S., Nicotra, M.R., Natali, P.G. i Bagnato, A. (2006). Integrin-linked kinase functions as a downstream mediator of endothelin-1 to promote invasive behavior in ovarian carcinoma. *Mol Cancer Ther* **5**(4): 833-42.

Shiou, S.R., Datta, P.K., Dhawan, P., Law, B.K., Yingling, J.M., Dixon, D.A. i Beauchamp, R.D. (2006). Smad4-dependent regulation of urokinase plasminogen activator secretion and RNA stability associated with invasiveness by autocrine and paracrine transforming growth factor-beta. *J Biol Chem* **281**(45): 33971-81.

Smyth, G.K. (2004). Linear models and empirical bayes methods for assessing differential expression in microarray experiments. *Stat Appl Genet Mol Biol* **3**: Article3.

Su, L.K., Kinzler, K.W., Vogelstein, B., Preisinger, A.C., Moser, A.R., Luongo, C., Gould, K.A. i Dove, W.F. (1992). Multiple intestinal neoplasia caused by a mutation in the murine homolog of the APC gene. *Science* **256**(5057): 668-70.

Tan, Y., Ruan, H., Demeter, M.R. i Comb, M.J. (1999). p90(RSK) blocks bad-mediated cell death via a protein kinase C-dependent pathway. *J Biol Chem* **274**(49): 34859-67.

Tessitore, L., Davit, A., Sarotto, I. i Caderni, G. (2000). Resveratrol depresses the growth of colorectal aberrant crypt foci by affecting bax and p21(CIP) expression. *Carcinogenesis* **21**(8): 1619-22.

Wu, K.K. i Liou, J.Y. (2009). Cyclooxygenase inhibitors induce colon cancer cell apoptosis Via PPARdelta --> 14-3-3epsilon pathway. *Methods Mol Biol* **512**: 295-307.

Xu, H.X., Zeng, F.Q., Wan, M. i Sim, K.Y. (1996). Anti-HIV triterpene acids from Geum japonicum. *J Nat Prod* **59**(7): 643-5.

Zamarron, B.F. i Chen, W. (2011). Dual roles of immune cells and their factors in cancer development and progression. *Int J Biol Sci* **7**(5): 651-8.

Zhang, M., Kimura, A. i Saltiel, A.R. (2003). Cloning and characterization of Cbl-associated protein splicing isoforms. *Mol Med* **9**(1-2): 18-25.

Zhang, W., Yang, J., Liu, Y., Chen, X., Yu, T., Jia, J. i Liu, C. (2009). PR55 alpha, a regulatory subunit of PP2A, specifically regulates PP2A-mediated beta-catenin dephosphorylation. *J Biol Chem* **284**(34): 22649-56.

Supplemental data 1

Genes differentially expressed MA_vs_CTL

Affimetrix ID	Symbol	Gene description	Fold change	Adjusted p-value
1437438_x_at	Pnliprp2	pancreatic lipase-related protein 2	5,8	0,009521
1447802_x_at	AV099323	expressed sequence AV099323	3,8	0,000000
1437812_x_at	Ganab	alpha glucosidase 2 alpha neutral subunit	3,6	0,000000
1447007_at	1700008I05Rik	RIKEN cDNA 1700008I05 gene	2,6	0,000000
1447882_x_at	Ddx54	DEAD (Asp-Glu-Ala-Asp) box polypeptide 54	2,5	0,000000
1450875_at	Gpr37	G protein-coupled receptor 37	2,5	0,000000
1441935_at	Ankra2	ankyrin repeat, family A (RFXANK-like), 2	2,4	0,000000
1440180_x_at	Zbtb3	zinc finger and BTB domain containing 3	2,3	0,000000
1440383_at	Dclre1b	DNA cross-link repair 1B, PSO2 homolog (S. cerevisiae)	2,3	0,000001
1420132_s_at	Pttg1ip	pituitary tumor-transforming 1 interacting protein	2,1	0,000003
1447902_at	1810013A23Rik	RIKEN cDNA 1810013A23 gene	2,1	0,000000
1455792_x_at	Ndn	necdin	2,1	0,000002
1439296_at	Prickle3	prickle homolog 3 (Drosophila)	2,1	0,000000
1452538_at	Igh-6	immunoglobulin heavy chain 6 (heavy chain of IgM)	2,0	0,000001
1418913_at	Bhmt2	betaine-homocysteine methyltransferase 2	2,0	0,000005
1419911_at	Coro1c	coronin, actin binding protein 1C	2,0	0,000002
1439224_at			2,0	0,001574
1451600_s_at	EG13909	predicted gene, EG13909	2,0	0,001412
1459047_x_at			1,9	0,000004
1436383_at	Cplx2	complexin 2	1,9	0,000000
1456120_at	Secisbp2l	SECIS binding protein 2-like	1,9	0,002064
1417197_at	Wwc2	WW, C2 and coiled-coil domain containing 2	1,9	0,000000
1439124_at	Wdr91	WD repeat domain 91	1,9	0,000001
1456868_at			1,9	0,000002
1440159_at	1700010B09Rik	RIKEN cDNA 1700010B09 gene	1,9	0,000317
1420175_at	Tax1bp1	Tax1 (human T-cell leukemia virus type I) binding protein 1	1,9	0,000134
1422425_at	Sprr2k	small proline-rich protein 2K	1,9	0,004129
1458626_at	Nos1	nitric oxide synthase 1, neuronal	1,9	0,000009
1422973_a_at	Thrsp	thyroid hormone responsive SPOT14 homolog (Rattus)	1,9	0,000001
1439144_at	Cwf19l1	CWF19-like 1, cell cycle control (S. pombe)	1,9	0,000002
1425824_a_at	Pcsk4	proprotein convertase subtilisin/kexin type 4	1,8	0,000003
1435906_x_at	Gbp2	guanylate binding protein 2	1,8	0,003678
1438956_x_at	Pim3	proviral integration site 3	1,8	0,000032
1459115_at			1,8	0,000000
1422162_at	Dcc	deleted in colorectal carcinoma	1,8	0,000002
1452481_at	Plcb2	phospholipase C, beta 2	1,8	0,000007
1441160_at	D330050G23Rik	RIKEN cDNA D330050G23 gene	1,8	0,000000
1419349_a_at	Cyp2d9	cytochrome P450, family 2, subfamily d, polypeptide 9	1,8	0,006830
1419975_at	Scp2	sterol carrier protein 2, liver	1,8	0,000381
1443152_at	Ptcd3	pentatricopeptide repeat domain 3	1,8	0,000058
1447892_at			1,8	0,000034
1429983_at	2010002M09Rik	RIKEN cDNA 2010002M09 gene	1,8	0,000010
1458250_at	Fam13c	family with sequence similarity 13, member C	1,8	0,000002
1450260_at	Grpr	gastrin releasing peptide receptor	1,8	0,008580
1423804_a_at	Idi1	isopentenyl-diphosphate delta isomerase	1,8	0,005388
1439834_at	2400009B08Rik	RIKEN cDNA 2400009B08 gene	1,8	0,000001
1455457_at	Cyp2c54	cytochrome P450, family 2, subfamily c, polypeptide 54	1,7	0,000046
1456003_a_at	Slc1a4	solute carrier family 1 (glutamate/neutral amino acid transporte	1,7	0,000006
1459243_at	100042016	predicted gene, 100042016	1,7	0,000258
1440642_at	D630042P16Rik	RIKEN cDNA D630042P16 gene	1,7	0,000005
1443827_x_at	Fam20c	family with sequence similarity 20, member C	1,7	0,000069
1438615_x_at	2010317E24Rik	RIKEN cDNA 2010317E24 gene	1,7	0,000000
1439404_x_at	Zfx	zinc finger protein X-linked	1,7	0,000025
1441840_x_at	Sbno2	strawberry notch homolog 2 (Drosophila)	1,7	0,000002
1442027_at	Nbeal1	neurobeachin like 1	1,7	0,000084
1451635_at	AB056442	cDNA sequence AB056442	1,7	0,000016
1436991_x_at	Gsn	gelsolin	1,7	0,000197
1432731_at	5830437K03Rik	RIKEN cDNA 5830437K03 gene	1,7	0,000216
1426520_at	Btg4	B-cell translocation gene 4	1,7	0,000015
1416023_at	Fabp3	fatty acid binding protein 3, muscle and heart	1,7	0,000011
1443799_at			1,7	0,000078
1436750_a_at	Oxct1	3-oxoacid CoA transferase 1	1,7	0,000589
1437671_x_at	Prss23	protease, serine, 23	1,7	0,001541
1459788_at	Gpr107	G protein-coupled receptor 107	1,7	0,002566
1436737_a_at	Sorbs1	sorbin and SH3 domain containing 1	1,7	0,000611
1439822_at			1,7	0,000002
1423544_at	Ptpn5	protein tyrosine phosphatase, non-receptor type 5	1,7	0,001058
1423635_at	Bmp2	bone morphogenetic protein 2	1,7	0,002040
1417461_at	Cap1	CAP, adenylate cyclase-associated protein 1 (yeast)	1,7	0,004914
1451547_at	Iyd	iodotyrosine deiodinase	1,7	0,008053
1460055_at			1,7	0,000055
1418623_at	Rab2a	RAB2A, member RAS oncogene family	1,7	0,000017
1444254_at	Tns4	tensin 4	1,7	0,000004
1439887_at			1,7	0,000619
1456701_at	B230208H17Rik	RIKEN cDNA B230208H17 gene	1,7	0,000001
1440824_at			1,7	0,000001
1455226_at	Spnb1	spectrin beta 1	1,7	0,000066
1448301_s_at	Serpinb1a	serine (or cysteine) peptidase inhibitor, clade B, member 1a	1,7	0,000317
1454789_x_at	Prpf6	PRP6 pre-mRNA splicing factor 6 homolog (yeast)	1,7	0,000003
1431189_a_at	Fahd2a	fumarylacetoacetate hydrolase domain containing 2A	1,7	0,000000
1441009_at	4732491K20Rik	RIKEN cDNA 4732491K20 gene	1,7	0,000148
1458335_x_at	Urm1	ubiquitin related modifier 1 homolog (S. cerevisiae)	1,7	0,000029
1436099_at	AI836003	expressed sequence AI836003	1,7	0,000036
1418069_at	Apoc2	apolipoprotein C-II	1,7	0,000867
1422533_at	Cyp51	cytochrome P450, family 51	1,7	0,003016
1455912_x_at	Unc45a	unc-45 homolog A (C. elegans)	1,7	0,000000
1449687_at	D10Ertd610e	DNA segment, Chr 10, ERATO Doi 610, expressed	1,6	0,001949
1424014_at	2900092E17Rik	RIKEN cDNA 2900092E17 gene	1,6	0,000007
1429935_at	Lcn12	lipocalin 12	1,6	0,000005
1419972_at	Slc35a5	solute carrier family 35, member A5	1,6	0,000001
1445125_at	D8Ertd107e	DNA segment, Chr 8, ERATO Doi 107, expressed	1,6	0,000027
1416854_at	Slc34a2	solute carrier family 34 (sodium phosphate), member 2	1,6	0,015000
1446978_at			1,6	0,000011
1437140_at	4930412F15Rik	RIKEN cDNA 4930412F15 gene	1,6	0,000027
1436155_at	Nmnat2	nicotinamide nucleotide adenylyltransferase 2	1,6	0,000116
1427267_at	Tnrc18	trinucleotide repeat containing 18	1,6	0,000029
1438156_x_at	Cpt1a	carnitine palmitoyltransferase 1a, liver	1,6	0,001922
1455033_at	Fam102b	family with sequence similarity 102, member B	1,6	0,000012
1418113_at	Cyp2d10	cytochrome P450, family 2, subfamily d, polypeptide 10	1,6	0,001799
1437342_x_at	Pttg1ip	pituitary tumor-transforming 1 interacting protein	1,6	0,000007
1438588_at	Plagl1	pleiomorphic adenoma gene-like 1	1,6	0,000017
1418602_at	Cdh15	cadherin 15	1,6	0,000025
1441026_at	Parp4	poly (ADP-ribose) polymerase family, member 4	1,6	0,005460

1431688_at	LOC73899	**hypothetical LOC73899**	**1,6**	0,001015
1425514_at	Pik3r1	**phosphatidylinositol 3-kinase, regulatory subunit, polypeptide**	**1,6**	0,000034
1456569_x_at	Gsn	**gelsolin**	**1,6**	0,000037
1425848_a_at	Dusp26	**dual specificity phosphatase 26 (putative)**	**1,6**	0,000089
1447227_at			**1,6**	0,000474
1439451_x_at	Gpr172b	**G protein-coupled receptor 172B**	**1,6**	0,000119
1445708_x_at	3110021A11Rik	**RIKEN cDNA 3110021A11 gene**	**1,6**	0,000029
1422320_x_at	Phxr5	**per-hexamer repeat gene 5**	**1,6**	0,000026
1427780_at	Defb35	**defensin beta 35**	**1,6**	0,000003
1459658_at	Mcm5	**minichromosome maintenance deficient 5, cell division cycle 4**	**1,6**	0,000849
1423037_at	Aplnr	**apelin receptor**	**1,6**	0,000295
1452460_at	Ankrd26	**ankyrin repeat domain 26**	**1,6**	0,000190
1419918_at	Tmed7	**transmembrane emp24 protein transport domain containing 7**	**1,6**	0,000864
1456397_at	Cdh4	**cadherin 4**	**1,6**	0,000576
1445556_at			**1,6**	0,000049
1450361_at	Prop1	**paired like homeodomain factor 1**	**1,6**	0,000003
1417485_at	Ibsp	**integrin binding sialoprotein**	**1,6**	0,000083
1445566_at			**1,6**	0,000047
1439427_at	Cldn9	**claudin 9**	**1,6**	0,000003
1424386_at	Reep2	**receptor accessory protein 2**	**1,6**	0,000003
1433681_x_at	Capn3	**calpain 3**	**1,6**	0,000343
1433855_at	Abat	**4-aminobutyrate aminotransferase**	**1,6**	0,000174
1441910_x_at	Ccne1	**cyclin E1**	**1,6**	0,000003
1427970_at	Zfp689	**zinc finger protein 689**	**1,6**	0,000043
1422904_at	Fmo2	**flavin containing monooxygenase 2**	**1,6**	0,011499
1424722_at	1300017J02Rik	**RIKEN cDNA 1300017J02 gene**	**1,6**	0,000350
1435084_at	C730049O14Rik	**RIKEN cDNA C730049O14 gene**	**1,6**	0,001418
1429427_s_at	Tcf7l2	**transcription factor 7-like 2, T-cell specific, HMG-box**	**1,6**	0,003920
1419439_at	Stk22s1	**serine/threonine kinase 22 substrate 1**	**1,6**	0,000014
1440144_x_at	C330046E03	**hypothetical protein C330046E03**	**1,6**	0,000014
1445352_at			**1,6**	0,000045
1456844_at	Camk2d	**calcium/calmodulin-dependent protein kinase II, delta**	**1,6**	0,002838
1445662_x_at			**1,6**	0,000003
1436408_at	Rprml	**reprimo-like**	**1,6**	0,000887
1434831_a_at	Foxo3	**forkhead box O3**	**1,6**	0,000767
1444662_at	Pla2g4c	**phospholipase A2, group IVC (cytosolic, calcium-independent)**	**1,6**	0,000069
1424610_at	Trub2	**TruB pseudouridine (psi) synthase homolog 2 (E. coli)**	**1,6**	0,000275
1434426_at	Ncapd3	**non-SMC condensin II complex, subunit D3**	**1,6**	0,000974
1435964_a_at	Taok3	**TAO kinase 3**	**1,6**	0,000768
1418580_at	Rtp4	**receptor transporter protein 4**	**1,6**	0,005278
1443792_at	Tsga14	**testis specific gene A14**	**1,6**	0,000189
1437171_x_at	Gsn	**gelsolin**	**1,6**	0,000778
1433888_at	Atp2b2	**ATPase, Ca++ transporting, plasma membrane 2**	**1,6**	0,000003
1450255_at	Cdgap	**CDC42 GTPase-activating protein**	**1,6**	0,000141
1442241_at			**-1,6**	0,006507
1428234_at	Cpsf6	**cleavage and polyadenylation specific factor 6**	**-1,6**	0,002954
1447062_at			**-1,6**	0,000054
1434507_at	Npepl1	**aminopeptidase-like 1**	**-1,6**	0,000041
1434807_s_at	Mtx3	**metaxin 3**	**-1,6**	0,000388
1416835_s_at	Amd1	**S-adenosylmethionine decarboxylase 1**	**-1,6**	0,001681
1426232_at	BC024479	**cDNA sequence BC024479**	**-1,6**	0,008209
1433430_s_at	Cdc23	**CDC23 (cell division cycle 23, yeast, homolog)**	**-1,6**	0,000190
1441362_at			**-1,6**	0,000106
1451182_s_at	Ankrd54	**ankyrin repeat domain 54**	**-1,6**	0,000038
1456327_at			**-1,6**	0,005953
1428689_at	Tysnd1	**trypsin domain containing 1**	**-1,6**	0,000005
1449186_at	Bag4	**BCL2-associated athanogene 4**	**-1,6**	0,000052
1440715_s_at	Cdkn2aipnl	**CDKN2A interacting protein N-terminal like**	**-1,6**	0,005335
1418340_at	Fcer1g	**Fc receptor, IgE, high affinity I, gamma polypeptide**	**-1,6**	0,000389
1437410_at	Aldh2	**aldehyde dehydrogenase 2, mitochondrial**	**-1,6**	0,003684
1451794_at	Tmcc3	**transmembrane and coiled coil domains 3**	**-1,6**	0,005110
1427580_a_at	Rian	**RNA imprinted and accumulated in nucleus**	**-1,6**	0,002773
1439819_at	AU015263	**expressed sequence AU015263**	**-1,6**	0,008601
1430144_at	Avl9	**AVL9 homolog (S. cerevisiase)**	**-1,6**	0,004688
1442989_at			**-1,6**	0,000046
1443331_at			**-1,6**	0,000068
1418528_a_at	Dad1	**defender against cell death 1**	**-1,6**	0,001564
1452676_a_at	Pnpt1	**polyribonucleotide nucleotidyltransferase 1**	**-1,6**	0,012741
1420142_s_at	Pa2g4	**proliferation-associated 2G4**	**-1,6**	0,000783
1433174_a_at	5430440L12Rik	**RIKEN cDNA 5430440L12 gene**	**-1,6**	0,000295
1455863_at	Spata5l1	**spermatogenesis associated 5-like 1**	**-1,6**	0,000953
1417716_at	Got2	**glutamate oxaloacetate transaminase 2, mitochondrial**	**-1,6**	0,000002
1428707_at	Ptms	**parathymosin**	**-1,6**	0,000003
1423795_at	Sfpq	**splicing factor proline/glutamine rich (polypyrimidine tract binc**	**-1,6**	0,003932
1454842_a_at	B3galnt2	**UDP-GalNAc:betaGlcNAc beta 1,3-galactosaminyltransferase, p**	**-1,6**	0,009871
1439797_at	Ppard	**peroxisome proliferator activator receptor delta**	**-1,6**	0,001178
1460678_at	Klhdc2	**kelch domain containing 2**	**-1,6**	0,000825
1429725_at	Zfhx3	**zinc finger homeobox 3**	**-1,6**	0,000181
1434493_at	1810022K09Rik	**RIKEN cDNA 1810022K09 gene**	**-1,6**	0,010362
1451127_at	AW146242	**expressed sequence AW146242**	**-1,6**	0,000286
1425204_s_at	Ddx19a	**DEAD (Asp-Glu-Ala-Asp) box polypeptide 19a**	**-1,6**	0,000078
1429180_at	Gmpr2	**guanosine monophosphate reductase 2**	**-1,6**	0,010788
1425551_at	Hip1r	**huntingtin interacting protein 1 related**	**-1,6**	0,000366
1444478_at	Appl1	**adaptor protein, phosphotyrosine interaction, PH domain and l**	**-1,6**	0,002613
1422779_at	Smpd3	**sphingomyelin phosphodiesterase 3, neutral**	**-1,6**	0,000134
1418596_at	Fgfr4	**fibroblast growth factor receptor 4**	**-1,6**	0,000096
1416487_a_at	Yap1	**yes-associated protein 1**	**-1,6**	0,000094
1456386_at			**-1,6**	0,000602
1418253_a_at	Hspa4l	**heat shock protein 4 like**	**-1,6**	0,000243
1430415_at	Phf6	**PHD finger protein 6**	**-1,6**	0,001624
1444459_at			**-1,6**	0,002404
1458031_at			**-1,6**	0,000008
1431374_at	6330407A03Rik	**RIKEN cDNA 6330407A03 gene**	**-1,6**	0,000642
1448140_at	Ciapin1	**cytokine induced apoptosis inhibitor 1**	**-1,6**	0,000431
1428429_at	Rgmb	**RGM domain family, member B**	**-1,6**	0,000709
1440234_at	1810012P15Rik	**RIKEN cDNA 1810012P15 gene**	**-1,6**	0,000031
1425315_at	Dock7	**dedicator of cytokinesis 7**	**-1,6**	0,000952
1446447_at			**-1,6**	0,000056
1424923_at	Serpina3g	**serine (or cysteine) peptidase inhibitor, clade A, member 3G**	**-1,6**	0,013360
1449157_at	Nr2c1	**nuclear receptor subfamily 2, group C, member 1**	**-1,6**	0,000048
1448668_a_at	Irak1	**interleukin-1 receptor-associated kinase 1**	**-1,6**	0,000017
1423617_at	Pdf	**peptide deformylase (mitochondrial)**	**-1,6**	0,000105
1424197_s_at	Fance	**Fanconi anemia, complementation group E**	**-1,6**	0,000018
1435325_at	Usp46	**ubiquitin specific peptidase 46**	**-1,6**	0,000334
1456250_x_at	Tgfbi	**transforming growth factor, beta induced**	**-1,6**	0,001768
1441112_at	LOC667118	**similar to Zinc finger BED domain containing protein 4**	**-1,6**	0,006783

1443649_at			**-1,6**	0,001631
1428749_at	Dmxl2	**Dmx-like 2**	**-1,6**	0,001329
1453251_at	Dhx30	**DEAH (Asp-Glu-Ala-His) box polypeptide 30**	**-1,6**	0,001845
1443628_at			**-1,6**	0,000866
1426025_s_at	Laptm5	**lysosomal-associated protein transmembrane 5**	**-1,6**	0,000056
1423053_at	Arf4	**ADP-ribosylation factor 4**	**-1,6**	0,000010
1432384_a_at	Mettl6	**methyltransferase like 6**	**-1,6**	0,002797
1439201_at	Usp14	**ubiquitin specific peptidase 14**	**-1,6**	0,000053
1440068_at			**-1,6**	0,000192
1417311_at	Crip2	**cysteine rich protein 2**	**-1,6**	0,004015
1451091_at	Txndc5	**thioredoxin domain containing 5**	**-1,6**	0,000150
1458812_at			**-1,6**	0,000288
1438725_at	Med13	**mediator complex subunit 13**	**-1,6**	0,000222
1448585_at	Gtf2h4	**general transcription factor II H, polypeptide 4**	**-1,6**	0,000156
1429368_at	Lrig3	**leucine-rich repeats and immunoglobulin-like domains 3**	**-1,6**	0,000424
1440690_at			**-1,6**	0,001323
1418440_at	Col8a1	**collagen, type VIII, alpha 1**	**-1,6**	0,006082
1452381_at	Creb3l2	**cAMP responsive element binding protein 3-like 2**	**-1,6**	0,009036
1453228_at	Stx11	**syntaxin 11**	**-1,6**	0,000271
1456927_at	Mast2	**microtubule associated serine/threonine kinase 2**	**-1,6**	0,004584
1456933_at			**-1,6**	0,003023
1439622_at	Rassf4	**Ras association (RalGDS/AF-6) domain family member 4**	**-1,6**	0,000859
1429504_at	Rnpc3	**RNA-binding region (RNP1, RRM) containing 3**	**-1,6**	0,011502
1457641_at			**-1,6**	0,000869
1415888_at	Hdgf	**hepatoma-derived growth factor**	**-1,6**	0,000281
1420817_at	Ywhag	**tyrosine 3-monooxygenase/tryptophan 5-monooxygenase activ**	**-1,6**	0,000073
1441033_at	Tmtc2	**transmembrane and tetratricopeptide repeat containing 2**	**-1,6**	0,000172
1452182_at	Galnt2	**UDP-N-acetyl-alpha-D-galactosamine:polypeptide N-acetylgala**	**-1,6**	0,000001
1423345_at	Degs1	**degenerative spermatocyte homolog 1 (Drosophila)**	**-1,6**	0,000035
1426575_at	Sgms1	**sphingomyelin synthase 1**	**-1,6**	0,000448
1442511_at	Ipo7	**importin 7**	**-1,6**	0,015435
1430996_at	Etnk1	**ethanolamine kinase 1**	**-1,6**	0,001020
1451391_at	2700050L05Rik	**RIKEN cDNA 2700050L05 gene**	**-1,6**	0,000963
1452869_at	Prpf38b	**PRP38 pre-mRNA processing factor 38 (yeast) domain containi**	**-1,6**	0,002673
1430108_at	9030622M22Rik	**RIKEN cDNA 9030622M22 gene**	**-1,6**	0,000041
1439974_at	Fkbp15	**FK506 binding protein 15**	**-1,6**	0,003129
1432207_a_at	Toe1	**target of EGR1, member 1 (nuclear)**	**-1,6**	0,000064
1423982_at	Fusip1	**FUS interacting protein (serine-arginine rich) 1**	**-1,6**	0,005725
1458969_at	AU019559	**expressed sequence AU019559**	**-1,6**	0,000659
1450264_a_at	Chka	**choline kinase alpha**	**-1,6**	0,000606
1423321_at	Myadm	**myeloid-associated differentiation marker**	**-1,6**	0,000014
1418925_at	Celsr1	**cadherin, EGF LAG seven-pass G-type receptor 1 (flamingo ho**	**-1,6**	0,000053
1438442_at	5730470L24Rik	**RIKEN cDNA 5730470L24 gene**	**-1,6**	0,000385
1458737_at	C77097	**expressed sequence C77097**	**-1,6**	0,004714
1424232_a_at	Ftsjd1	**FtsJ methyltransferase domain containing 1**	**-1,6**	0,000011
1448794_s_at	Dnajc2	**DnaJ (Hsp40) homolog, subfamily C, member 2**	**-1,6**	0,006114
1438454_at	B430203M17Rik	**RIKEN cDNA B430203M17 gene**	**-1,6**	0,001666
1429586_at	4930558N01Rik	**RIKEN cDNA 4930558N01 gene**	**-1,6**	0,000029
1443156_at			**-1,6**	0,002082
1442494_at	Ubr2	**ubiquitin protein ligase E3 component n-recognin 2**	**-1,6**	0,002266
1418222_at	2610024G14Rik	**RIKEN cDNA 2610024G14 gene**	**-1,6**	0,000299
1441253_at			**-1,6**	0,013109
1448500_a_at	Lime1	**Lck interacting transmembrane adaptor 1**	**-1,6**	0,008299
1443068_at	D130084N16Rik	**RIKEN cDNA D130084N16 gene**	**-1,6**	0,004081
1452020_a_at	Siva1	**SIVA1, apoptosis-inducing factor**	**-1,6**	0,001373
1417602_at	Per2	**period homolog 2 (Drosophila)**	**-1,6**	0,000205
1429359_s_at	Rbpms	**RNA binding protein gene with multiple splicing**	**-1,6**	0,015601
1415689_s_at	Zkscan3	**zinc finger with KRAB and SCAN domains 3**	**-1,6**	0,000827
1439787_at	P2rx7	**purinergic receptor P2X, ligand-gated ion channel, 7**	**-1,6**	0,000070
1425424_at	MGC7817	**hypothetical protein LOC620031**	**-1,6**	0,000408
1450480_a_at	Grk6	**G protein-coupled receptor kinase 6**	**-1,6**	0,000083
1458602_at	Bbx	**bobby sox homolog (Drosophila)**	**-1,6**	0,000106
1439953_at	Pmm2	**phosphomannomutase 2**	**-1,6**	0,000711
1425348_a_at	Srprb	**signal recognition particle receptor, B subunit**	**-1,6**	0,000077
1417807_at	Ufsp1	**UFM1-specific peptidase 1**	**-1,6**	0,000070
1460548_a_at	Eral1	**Era (G-protein)-like 1 (E. coli)**	**-1,6**	0,000297
1456413_at	Pde4dip	**phosphodiesterase 4D interacting protein (myomegalin)**	**-1,6**	0,002884
1456476_at	Atxn2l	**ataxin 2-like**	**-1,6**	0,000106
1456897_at			**-1,6**	0,000874
1429963_at	Mapk6	**mitogen-activated protein kinase 6**	**-1,6**	0,000619
1453051_at	Zkscan1	**zinc finger with KRAB and SCAN domains 1**	**-1,6**	0,000001
1440635_at	Palld	**palladin, cytoskeletal associated protein**	**-1,6**	0,002672
1418475_at	Scnn1b	**sodium channel, nonvoltage-gated 1 beta**	**-1,6**	0,003407
1430992_s_at	Cisd2	**CDGSH iron sulfur domain 2**	**-1,6**	0,000044
1451591_a_at	Efnb1	**ephrin B1**	**-1,6**	0,000594
1428100_at	Sfrs1	**splicing factor, arginine/serine-rich 1 (ASF/SF2)**	**-1,6**	0,001974
1448691_at	Ubqln4	**ubiquilin 4**	**-1,6**	0,000001
1443630_at			**-1,6**	0,000308
1447465_at			**-1,6**	0,000011
1426764_at	Oaz2	**ornithine decarboxylase antizyme 2**	**-1,6**	0,000100
1455135_at	Ccdc9	**coiled-coil domain containing 9**	**-1,6**	0,000093
1443162_at			**-1,6**	0,000350
1419247_at	Rgs2	**regulator of G-protein signaling 2**	**-1,6**	0,000247
1440009_at	Olfr78	**olfactory receptor 78**	**-1,6**	0,010247
1420866_at	Zfp161	**zinc finger protein 161**	**-1,6**	0,000075
1460366_at	Eml3	**echinoderm microtubule associated protein like 3**	**-1,6**	0,000046
1426744_at	Srebf2	**sterol regulatory element binding factor 2**	**-1,6**	0,000002
1451927_a_at	Mapk14	**mitogen-activated protein kinase 14**	**-1,6**	0,004047
1436305_at	Rnf217	**ring finger protein 217**	**-1,6**	0,000080
1443148_at			**-1,6**	0,001245
1436665_a_at	Ltbp4	**latent transforming growth factor beta binding protein 4**	**-1,6**	0,001262
1425118_at	Spire2	**spire homolog 2 (Drosophila)**	**-1,6**	0,001311
1451667_at	Fam20b	**family with sequence similarity 20, member B**	**-1,6**	0,003868
1423879_at	D030056L22Rik	**RIKEN cDNA D030056L22 gene**	**-1,6**	0,000213
1455208_at	Pex19	**peroxisomal biogenesis factor 19**	**-1,6**	0,000053
1435923_at	Ado	**2-aminoethanethiol (cysteamine) dioxygenase**	**-1,6**	0,000536
1423450_a_at	Hs3st1	**heparan sulfate (glucosamine) 3-O-sulfotransferase 1**	**-1,6**	0,000054
1417254_at	Spata5	**spermatogenesis associated 5**	**-1,6**	0,000965
1455439_a_at	Lgals1	**lectin, galactose binding, soluble 1**	**-1,6**	0,007017
1419403_at	BC017612	**cDNA sequence BC017612**	**-1,6**	0,000869
1425845_a_at	Shoc2	**soc-2 (suppressor of clear) homolog (C. elegans)**	**-1,6**	0,000008
1416657_at	Akt1	**thymoma viral proto-oncogene 1**	**-1,6**	0,000003
1426790_at	Ssrp1	**structure specific recognition protein 1**	**-1,6**	0,000492
1434282_at	Ibtk	**inhibitor of Bruton agammaglobulinemia tyrosine kinase**	**-1,6**	0,000075
1442704_at			**-1,6**	0,001341
1434133_s_at	Wdr42a	**WD repeat domain 42A**	**-1,6**	0,000029

1430175_at	4930588G05Rik	**RIKEN cDNA 4930588G05 gene**	**-1,6**	0,001061
1451538_at	Sox9	**SRY-box containing gene 9**	**-1,6**	0,001053
1435916_at	Zfp84	**zinc finger protein 84**	**-1,6**	0,002291
1433506_at	Lrrc8d	**leucine rich repeat containing 8D**	**-1,6**	0,000309
1451099_at	Mbc2	**membrane bound C2 domain containing protein**	**-1,6**	0,000074
1443593_at			**-1,6**	0,001363
1434404_at	Fam73a	**family with sequence similarity 73, member A**	**-1,6**	0,005473
1449122_at	Ubxn2b	**UBX domain protein 2B**	**-1,6**	0,001017
1427417_at	Scml4	**sex comb on midleg-like 4 (Drosophila)**	**-1,6**	0,001056
1454743_at	Nup205	**nucleoporin 205**	**-1,6**	0,004080
1445885_at	Ube2d2	**ubiquitin-conjugating enzyme E2D 2**	**-1,6**	0,001509
1459648_at			**-1,6**	0,000043
1422793_at	Pafah1b2	**platelet-activating factor acetylhydrolase, isoform 1b, alpha2 s**	**-1,6**	0,000651
1458205_at			**-1,6**	0,001652
1428174_x_at	Khsrp	**KH-type splicing regulatory protein**	**-1,6**	0,000011
1451644_a_at	H2-gs10	**MHC class I like protein GS10**	**-1,6**	0,004917
1451514_at	Usp43	**ubiquitin specific peptidase 43**	**-1,6**	0,000005
1421784_a_at	Efna4	**ephrin A4**	**-1,6**	0,014561
1422551_at	Zkscan3	**zinc finger with KRAB and SCAN domains 3**	**-1,6**	0,000124
1447575_at			**-1,6**	0,000038
1426945_at	Ipo5	**importin 5**	**-1,6**	0,000623
1458974_at			**-1,6**	0,000017
1429464_at	Prkaa2	**protein kinase, AMP-activated, alpha 2 catalytic subunit**	**-1,6**	0,005457
1428168_at	Mpzl1	**myelin protein zero-like 1**	**-1,6**	0,001206
1416548_at	Slc35b4	**solute carrier family 35, member B4**	**-1,6**	0,000021
1458290_at			**-1,6**	0,002360
1456209_x_at			**-1,6**	0,001079
1437491_at	Bicd2	**bicaudal D homolog 2 (Drosophila)**	**-1,6**	0,000012
1427153_at	Bckdhb	**branched chain ketoacid dehydrogenase E1, beta polypeptide**	**-1,6**	0,008209
1418284_at	Vps72	**vacuolar protein sorting 72 (yeast)**	**-1,6**	0,000001
1422532_at	Xpc	**xeroderma pigmentosum, complementation group C**	**-1,6**	0,000014
1441732_at			**-1,6**	0,009311
1448623_at	Tmem123	**transmembrane protein 123**	**-1,6**	0,006826
1430515_s_at	Aasdhppt	**aminoadipate-semialdehyde dehydrogenase-phosphopantethe**	**-1,6**	0,006239
1457334_at	C130057M05Rik	**RIKEN cDNA C130057M05 gene**	**-1,6**	0,000352
1424078_s_at	Pex6	**peroxisomal biogenesis factor 6**	**-1,6**	0,000184
1449504_at	Kpna1	**karyopherin (importin) alpha 1**	**-1,6**	0,000323
1434680_at	Plekhg3	**pleckstrin homology domain containing, family G (with RhoGe**	**-1,6**	0,000003
1450519_a_at	Prkaca	**protein kinase, cAMP dependent, catalytic, alpha**	**-1,6**	0,000064
1427476_a_at	Trim32	**tripartite motif-containing 32**	**-1,6**	0,000190
1443905_at			**-1,6**	0,002877
1429846_at	9030411K21Rik	**RIKEN cDNA 9030411K21 gene**	**-1,6**	0,000719
1426781_at	Tyw1	**tRNA-yW synthesizing protein 1 homolog (S. cerevisiae)**	**-1,6**	0,000242
1421908_a_at	Tcf12	**transcription factor 12**	**-1,6**	0,000532
1444827_at			**-1,6**	0,001417
1455065_x_at	Gnpda1	**glucosamine-6-phosphate deaminase 1**	**-1,6**	0,001509
1417551_at	Cln3	**ceroid lipofuscinosis, neuronal 3, juvenile (Batten, Spielmeyer-**	**-1,6**	0,000472
1448392_at	Sparc	**secreted acidic cysteine rich glycoprotein**	**-1,6**	0,012991
1419072_at	Gstm7	**glutathione S-transferase, mu 7**	**-1,6**	0,000164
1448446_at	Deaf1	**deformed epidermal autoregulatory factor 1 (Drosophila)**	**-1,6**	0,000021
1449523_at	Bcl7c	**B-cell CLL/lymphoma 7C**	**-1,6**	0,000001
1418118_at	Slc22a1	**solute carrier family 22 (organic cation transporter), member 1**	**-1,6**	0,000162
1426518_at	Tubgcp5	**tubulin, gamma complex associated protein 5**	**-1,6**	0,000229
1417753_at	Pkd2	**polycystic kidney disease 2**	**-1,6**	0,002062
1426548_a_at	Atpbd4	**ATP binding domain 4**	**-1,6**	0,012039
1416075_at	Sav1	**salvador homolog 1 (Drosophila)**	**-1,6**	0,000002
1436007_a_at	Thumpd1	**THUMP domain containing 1**	**-1,6**	0,001071
1438419_at	Rbm16	**RNA binding motif protein 16**	**-1,6**	0,001261
1449947_s_at	Zfhx3	**zinc finger homeobox 3**	**-1,6**	0,013826
1452831_s_at	Ppat	**phosphoribosyl pyrophosphate amidotransferase**	**-1,6**	0,013337
1421052_a_at	Sms	**spermine synthase**	**-1,6**	0,000663
1452099_at	AA408296	**expressed sequence AA408296**	**-1,6**	0,001646
1444705_at			**-1,6**	0,000240
1417606_a_at	Calr	**calreticulin**	**-1,6**	0,000014
1424201_a_at	Seh1l	**SEH1-like (S. cerevisiae**	**-1,6**	0,000140
1422993_s_at	Refbp2	**RNA and export factor binding protein 2**	**-1,6**	0,009750
1416235_at	Lrrc59	**leucine rich repeat containing 59**	**-1,6**	0,000001
1452191_at	Prcp	**prolylcarboxypeptidase (angiotensinase C)**	**-1,6**	0,000050
1440408_at	B830008J18Rik	**RIKEN cDNA B830008J18 gene**	**-1,6**	0,001675
1455987_at	Sec61a1	**Sec61 alpha 1 subunit (S. cerevisiae)**	**-1,6**	0,000751
1444530_at			**-1,6**	0,000558
1423765_at	Athl1	**ATH1, acid trehalase-like 1 (yeast)**	**-1,6**	0,000069
1449117_at	Jund	**Jun proto-oncogene related gene d**	**-1,6**	0,000422
1451168_a_at	Arhgdia	**Rho GDP dissociation inhibitor (GDI) alpha**	**-1,6**	0,000044
1460692_at	Ehmt2	**euchromatic histone lysine N-methyltransferase 2**	**-1,6**	0,000002
1452045_at	Zfp281	**zinc finger protein 281**	**-1,6**	0,003080
1424660_s_at	Crtc2	**CREB regulated transcription coactivator 2**	**-1,6**	0,000003
1446929_at	D130062J21Rik	**RIKEN cDNA D130062J21 gene**	**-1,6**	0,004314
1439349_at	Sbno2	**strawberry notch homolog 2 (Drosophila)**	**-1,6**	0,000049
1451360_at	Ergic2	**ERGIC and golgi 2**	**-1,6**	0,000078
1439097_at			**-1,6**	0,000917
1416240_at	Psmb7	**proteasome (prosome, macropain) subunit, beta type 7**	**-1,6**	0,000219
1422493_at	Cpox	**coproporphyrinogen oxidase**	**-1,6**	0,000047
1448620_at	Fcgr3	**Fc receptor, IgG, low affinity III**	**-1,6**	0,012327
1457062_at	1700081L11Rik	**RIKEN cDNA 1700081L11 gene**	**-1,6**	0,000270
1416397_at	Mesdc1	**mesoderm development candidate 1**	**-1,6**	0,000055
1421832_at	Twsg1	**twisted gastrulation homolog 1 (Drosophila)**	**-1,6**	0,000081
1455841_s_at	Grwd1	**glutamate-rich WD repeat containing 1**	**-1,6**	0,000290
1451221_at	BC018507	**cDNA sequence BC018507**	**-1,6**	0,000980
1418644_a_at	Stk11	**serine/threonine kinase 11**	**-1,6**	0,000007
1426627_at	Map3k7	**mitogen-activated protein kinase kinase kinase 7**	**-1,6**	0,000332
1443109_at			**-1,6**	0,003648
1425592_at	Tnpo2	**transportin 2 (importin 3, karyopherin beta 2b)**	**-1,6**	0,000047
1427490_at	Abcb7	**ATP-binding cassette, sub-family B (MDR/TAP), member 7**	**-1,6**	0,001867
1435514_at	Lztfl1	**leucine zipper transcription factor-like 1**	**-1,6**	0,000522
1444185_at			**-1,6**	0,000027
1457154_at			**-1,6**	0,004512
1450570_a_at	Cd19	**CD19 antigen**	**-1,6**	0,002726
1446860_at			**-1,6**	0,000716
1450269_a_at	Pfkl	**phosphofructokinase, liver, B-type**	**-1,6**	0,001577
1429984_at	5730455O13Rik	**RIKEN cDNA 5730455O13 gene**	**-1,6**	0,000069
1457500_at	Depdc5	**DEP domain containing 5**	**-1,6**	0,008561
1438270_at	AI846148	**expressed sequence AI846148**	**-1,6**	0,000090
1459237_at			**-1,6**	0,001505
1426118_a_at	Tomm40	**translocase of outer mitochondrial membrane 40 homolog (yea**	**-1,6**	0,000000
1416637_at	Slc4a2	**solute carrier family 4 (anion exchanger), member 2**	**-1,6**	0,001438

1445830_at	Ctnnd1	**catenin (cadherin associated protein), delta 1**	**-1,6**	0,000297
1456973_at			**-1,6**	0,006071
1456775_at	Ints8	**integrator complex subunit 8**	**-1,6**	0,000013
1417740_at	Cdc37l1	**cell division cycle 37 homolog (S. cerevisiae)-like 1**	**-1,6**	0,000014
1427987_at	Safb2	**scaffold attachment factor B2**	**-1,6**	0,000025
1435965_at	Cnot3	**CCR4-NOT transcription complex, subunit 3**	**-1,6**	0,000443
1419330_a_at	Gpa33	**glycoprotein A33 (transmembrane)**	**-1,6**	0,000202
1418763_at	Nit2	**nitrilase family, member 2**	**-1,6**	0,001825
1447240_at			**-1,6**	0,000594
1428881_at	Klc1	**kinesin light chain 1**	**-1,6**	0,000741
1457834_at	Yy1	**YY1 transcription factor**	**-1,6**	0,000111
1419054_a_at	Ptpn21	**protein tyrosine phosphatase, non-receptor type 21**	**-1,6**	0,000012
1436039_at	Cmah	**cytidine monophospho-N-acetylneuraminic acid hydroxylase**	**-1,6**	0,004274
1449976_a_at	Gpr35	**G protein-coupled receptor 35**	**-1,6**	0,001441
1436660_at	Rrbp1	**ribosome binding protein 1**	**-1,6**	0,000069
1416750_at	Sigmar1	**sigma non-opioid intracellular receptor 1**	**-1,6**	0,000003
1450015_x_at	Sgpp1	**sphingosine-1-phosphate phosphatase 1**	**-1,6**	0,000157
1452989_at	2900009J20Rik	**RIKEN cDNA 2900009J20 gene**	**-1,6**	0,000006
1434558_at	Wdr47	**WD repeat domain 47**	**-1,6**	0,000427
1438762_at			**-1,6**	0,001358
1426574_a_at	Add3	**adducin 3 (gamma)**	**-1,6**	0,000523
1423358_at	Ece2	**endothelin converting enzyme 2**	**-1,6**	0,000045
1453993_a_at	Bnip2	**BCL2/adenovirus E1B interacting protein 2**	**-1,6**	0,003541
1420917_at	Prpf40a	**PRP40 pre-mRNA processing factor 40 homolog A (yeast)**	**-1,6**	0,003315
1423446_at	Dapk3	**death-associated protein kinase 3**	**-1,6**	0,000111
1436372_a_at	Pdxdc1	**pyridoxal-dependent decarboxylase domain containing 1**	**-1,6**	0,000000
1433804_at	Jak1	**Janus kinase 1**	**-1,6**	0,001153
1437532_at	Rnf216	**ring finger protein 216**	**-1,6**	0,000014
1425660_at	Btbd3	**BTB (POZ) domain containing 3**	**-1,6**	0,000098
1458934_at	D5Ertd505e	**DNA segment, Chr 5, ERATO Doi 505 , expressed**	**-1,6**	0,000130
1452500_at			**-1,6**	0,000413
1418565_at	Serbp1	**serpine1 mRNA binding protein 1**	**-1,6**	0,000069
1421889_a_at	Aplp2	**amyloid beta (A4) precursor-like protein 2**	**-1,6**	0,000002
1416032_at	Tmem109	**transmembrane protein 109**	**-1,6**	0,000005
1420930_s_at	Ctnnal1	**catenin (cadherin associated protein), alpha-like 1**	**-1,6**	0,000221
1424056_at	Usp48	**ubiquitin specific peptidase 48**	**-1,6**	0,000033
1424982_a_at	2700078E11Rik	**RIKEN cDNA 2700078E11 gene**	**-1,6**	0,000015
1416589_at	Sparc	**secreted acidic cysteine rich glycoprotein**	**-1,6**	0,003182
1420684_at	Acox3	**acyl-Coenzyme A oxidase 3, pristanoyl**	**-1,6**	0,000980
1450869_at	Fgf1	**fibroblast growth factor 1**	**-1,6**	0,004437
1457970_at	Actr1a	**ARP1 actin-related protein 1 homolog A, centractin alpha (yeas**	**-1,6**	0,000068
1460724_at	Ap2a1	**adaptor protein complex AP-2, alpha 1 subunit**	**-1,6**	0,000011
1447016_at	Tbc1d1	**TBC1 domain family, member 1**	**-1,6**	0,011490
1430103_at	9030607L20Rik	**RIKEN cDNA 9030607L20 gene**	**-1,6**	0,000139
1429847_a_at	4833418A01Rik	**RIKEN cDNA 4833418A01 gene**	**-1,6**	0,000131
1419550_a_at	Stk39	**serine/threonine kinase 39, STE20/SPS1 homolog (yeast)**	**-1,6**	0,000124
1438900_at	Sacm1l	**SAC1 (suppressor of actin mutations 1, homolog)-like (S. cerev**	**-1,6**	0,000024
1419573_a_at	Lgals1	**lectin, galactose binding, soluble 1**	**-1,6**	0,004722
1417568_at	Ncald	**neurocalcin delta**	**-1,6**	0,000054
1417295_at	Mta1	**metastasis associated 1**	**-1,6**	0,000002
1457304_at	D13Ertd787e	**DNA segment, Chr 13, ERATO Doi 787, expressed**	**-1,6**	0,000663
1425680_a_at	Btrc	**beta-transducin repeat containing protein**	**-1,6**	0,001617
1415899_at	Junb	**Jun-B oncogene**	**-1,6**	0,000475
1448604_at	Uck2	**uridine-cytidine kinase 2**	**-1,6**	0,000137
1431752_a_at	Urm1	**ubiquitin related modifier 1 homolog (S. cerevisiae)**	**-1,6**	0,000000
1437476_at	Rrm2b	**ribonucleotide reductase M2 B (TP53 inducible)**	**-1,6**	0,000047
1440305_at			**-1,6**	0,006857
1418982_at	Cebpa	**CCAAT/enhancer binding protein (C/EBP), alpha**	**-1,6**	0,000543
1426293_at	Zfp790	**zinc finger protein 790**	**-1,6**	0,000058
1448398_s_at	Rpl22	**ribosomal protein L22**	**-1,6**	0,000077
1416172_at	Pes1	**pescadillo homolog 1, containing BRCT domain (zebrafish)**	**-1,6**	0,002955
1456880_at			**-1,6**	0,000453
1456103_at	Pml	**promyelocytic leukemia**	**-1,6**	0,000070
1446735_at	Itsn2	**intersectin 2**	**-1,6**	0,000339
1452826_s_at	Fbxl20	**F-box and leucine-rich repeat protein 20**	**-1,6**	0,000029
1439639_at			**-1,6**	0,000795
1430161_at	Dlst	**dihydrolipoamide S-succinyltransferase (E2 component of 2-o**	**-1,6**	0,000007
1441707_at	Psma3	**proteasome (prosome, macropain) subunit, alpha type 3**	**-1,6**	0,001559
1426384_a_at	Ywhae	**tyrosine 3-monooxygenase/tryptophan 5-monooxygenase activ**	**-1,6**	0,000002
1457489_at			**-1,6**	0,000753
1442622_at			**-1,6**	0,000348
1436917_s_at	D2Bwg1335e	**DNA segment, Chr 2, Brigham & Women's Genetics 1335 expre**	**-1,6**	0,014286
1453589_a_at	6820431F20Rik	**RIKEN cDNA 6820431F20 gene**	**-1,6**	0,002311
1453380_a_at	Xrcc6bp1	**XRCC6 binding protein 1**	**-1,6**	0,000067
1458508_at	Matr3	**matrin 3**	**-1,6**	0,000577
1445438_at	Ddhd1	**DDHD domain containing 1**	**-1,6**	0,000413
1423045_at	Ncbp2	**nuclear cap binding protein subunit 2**	**-1,6**	0,005012
1431680_a_at	Ptprk	**protein tyrosine phosphatase, receptor type, K**	**-1,6**	0,000127
1425650_at	Tle4	**transducin-like enhancer of split 4, homolog of Drosophila E(sp**	**-1,6**	0,000057
1416386_a_at	M6pr	**mannose-6-phosphate receptor, cation dependent**	**-1,6**	0,000004
1444409_at	Rph3al	**rabphilin 3A-like (without C2 domains)**	**-1,6**	0,005737
1433932_x_at	C030046I01Rik	**RIKEN cDNA C030046I01 gene**	**-1,6**	0,000314
1442163_at			**-1,6**	0,000232
1439342_at	Clpx	**caseinolytic peptidase X (E.coli)**	**-1,6**	0,004189
1452406_x_at	Erdr1	**erythroid differentiation regulator 1**	**-1,6**	0,010460
1441351_at			**-1,6**	0,000444
1441372_at	5930405F01Rik	**RIKEN cDNA 5930405F01 gene**	**-1,6**	0,007282
1430538_at	2210013O21Rik	**RIKEN cDNA 2210013O21 gene**	**-1,6**	0,000028
1425919_at	Ndufa12	**NADH dehydrogenase (ubiquinone) 1 alpha subcomplex, 12**	**-1,6**	0,001849
1422719_s_at	Nup50	**nucleoporin 50**	**-1,6**	0,000147
1424614_at	Frag1	**FGF receptor activating protein 1**	**-1,6**	0,000005
1425805_a_at	Usp12	**ubiquitin specific peptidase 12**	**-1,6**	0,000330
1459144_at			**-1,6**	0,000573
1417187_at	Ube2k	**ubiquitin-conjugating enzyme E2K (UBC1 homolog, yeast)**	**-1,6**	0,000090
1442244_at	Inadl	**InaD-like (Drosophila)**	**-1,6**	0,000061
1423229_at	Inpp5e	**inositol polyphosphate-5-phosphatase E**	**-1,6**	0,000005
1418133_at	Bcl3	**B-cell leukemia/lymphoma 3**	**-1,6**	0,000163
1439125_at			**-1,6**	0,000315
1447973_at	Trip11	**thyroid hormone receptor interactor 11**	**-1,6**	0,000046
1443896_at	Tbc1d5	**TBC1 domain family, member 5**	**-1,6**	0,000817
1439467_at			**-1,6**	0,003673
1435695_a_at	Ggct	**gamma-glutamyl cyclotransferase**	**-1,6**	0,000102
1456388_at	Atp11a	**ATPase, class VI, type 11A**	**-1,6**	0,000083
1455591_at	Zfp618	**zinc fingerprotein 618**	**-1,6**	0,004499
1425326_at	Acly	**ATP citrate lyase**	**-1,6**	0,000080
1448569_at	Mlec	**malectin**	**-1,6**	0,000018

1441769_at			**-1,6**	0,000676
1443535_at	Rabgap1	**RAB GTPase activating protein 1**	**-1,6**	0,000641
1438345_at			**-1,6**	0,000016
1434196_at	Dnaja4	**DnaJ (Hsp40) homolog, subfamily A, member 4**	**-1,6**	0,002299
1435353_a_at	Sfi1	**Sfi1 homolog, spindle assembly associated (yeast)**	**-1,6**	0,000370
1434499_a_at	Ldhb	**lactate dehydrogenase B**	**-1,6**	0,000298
1415770_at	Wdr6	**WD repeat domain 6**	**-1,6**	0,001511
1448883_at	Lgmn	**legumain**	**-1,6**	0,000034
1417188_s_at	Ube2k	**ubiquitin-conjugating enzyme E2K (UBC1 homolog, yeast)**	**-1,6**	0,001320
1426365_at	2810403A07Rik	**RIKEN cDNA 2810403A07 gene**	**-1,6**	0,001233
1428656_at	Rnasen	**ribonuclease III, nuclear**	**-1,6**	0,000014
1423741_at	Rbm10	**RNA binding motif protein 10**	**-1,6**	0,000059
1456865_x_at	Rrs1	**RRS1 ribosome biogenesis regulator homolog (S. cerevisiae)**	**-1,6**	0,003150
1444343_at	A130064L14Rik	**RIKEN cDNA A130064L14 gene**	**-1,6**	0,003213
1437182_at	Dido1	**death inducer-obliterator 1**	**-1,6**	0,001909
1423584_at	Polr2b	**polymerase (RNA) II (DNA directed) polypeptide B**	**-1,6**	0,009277
1432262_at	Fam63a	**family with sequence similarity 63, member A**	**-1,6**	0,000079
1421148_a_at	Tial1	**Tia1 cytotoxic granule-associated RNA binding protein-like 1**	**-1,6**	0,000095
1460304_a_at	Ubtf	**upstream binding transcription factor, RNA polymerase I**	**-1,6**	0,000021
1435242_at	Pds5b	**PDS5, regulator of cohesion maintenance, homolog B (S. cerev**	**-1,6**	0,001820
1437184_at	Guf1	**GUF1 GTPase homolog (S. cerevisiae)**	**-1,6**	0,005107
1436779_at	Cybb	**cytochrome b-245, beta polypeptide**	**-1,6**	0,000232
1442731_at	Pds5a	**PDS5, regulator of cohesion maintenance, homolog A (S. cerev**	**-1,6**	0,004188
1450407_a_at	Anp32a	**acidic (leucine-rich) nuclear phosphoprotein 32 family, membe**	**-1,6**	0,001097
1450677_at	Chek1	**checkpoint kinase 1 homolog (S. pombe)**	**-1,6**	0,009464
1456706_at	4833441D16Rik	**RIKEN cDNA 4833441D16 gene**	**-1,6**	0,000346
1444458_at			**-1,6**	0,002502
1426631_at	Pus7	**pseudouridylate synthase 7 homolog (S. cerevisiae)**	**-1,6**	0,001195
1444728_at			**-1,6**	0,008412
1451347_at	Ino80e	**INO80 complex subunit E**	**-1,6**	0,000042
1447683_x_at	Mettl1	**methyltransferase like 1**	**-1,6**	0,000725
1430942_at	8430437O03Rik	**RIKEN cDNA 8430437O03 gene**	**-1,6**	0,000774
1417949_at	Ilf2	**interleukin enhancer binding factor 2**	**-1,6**	0,001094
1458292_at	Psma1	**proteasome (prosome, macropain) subunit, alpha type 1**	**-1,6**	0,001097
1431425_a_at	Rprd2	**regulation of nuclear pre-mRNA domain containing 2**	**-1,6**	0,000358
1452688_at	Prpf39	**PRP39 pre-mRNA processing factor 39 homolog (yeast)**	**-1,6**	0,006016
1441498_at			**-1,6**	0,002558
1425944_a_at	Rad51l3	**RAD51-like 3 (S. cerevisiae)**	**-1,6**	0,000028
1424603_at	Sumf1	**sulfatase modifying factor 1**	**-1,6**	0,013069
1460077_at	Ttc3	**tetratricopeptide repeat domain 3**	**-1,6**	0,002865
1428046_a_at	Zfx	**zinc finger protein X-linked**	**-1,6**	0,002966
1426053_a_at	Xpr1	**xenotropic and polytropic retrovirus receptor 1**	**-1,6**	0,000149
1431042_at	Paqr8	**progestin and adipoQ receptor family member VIII**	**-1,6**	0,007594
1435904_at	Eif2c3	**eukaryotic translation initiation factor 2C, 3**	**-1,6**	0,000064
1452055_at	Ctdsp1	**CTD (carboxy-terminal domain, RNA polymerase II, polypeptide**	**-1,6**	0,000014
1449046_a_at	Josd2	**Josephin domain containing 2**	**-1,6**	0,000006
1442178_at			**-1,6**	0,000687
1460486_at	Rabgap1	**RAB GTPase activating protein 1**	**-1,6**	0,000638
1444858_at			**-1,6**	0,000082
1457281_at	Dnajc21	**DnaJ (Hsp40) homolog, subfamily C, member 21**	**-1,6**	0,000036
1428924_at	Mocs3	**molybdenum cofactor synthesis 3**	**-1,6**	0,000010
1440894_at	Tmtc3	**transmembrane and tetratricopeptide repeat containing 3**	**-1,6**	0,000030
1458706_at			**-1,6**	0,001636
1436420_a_at	Ipo4	**importin 4**	**-1,6**	0,000992
1432910_at	Btbd7	**BTB (POZ) domain containing 7**	**-1,6**	0,000320
1443216_at			**-1,6**	0,001614
1430702_at	5830427D03Rik	**RIKEN cDNA 5830427D03 gene**	**-1,6**	0,000345
1456668_at			**-1,6**	0,000370
1434660_at	Alkbh1	**alkB, alkylation repair homolog 1 (E. coli)**	**-1,6**	0,009354
1417289_at	Plekha2	**pleckstrin homology domain-containing, family A (phosphoino**	**-1,6**	0,000003
1457480_at			**-1,6**	0,000711
1446736_at			**-1,6**	0,002671
1449582_at	Cdx1	**caudal type homeo box 1**	**-1,6**	0,000055
1438138_a_at	Pex6	**peroxisomal biogenesis factor 6**	**-1,6**	0,000029
1459884_at	Cox7c	**cytochrome c oxidase, subunit VIIc**	**-1,6**	0,006762
1434979_at	4933403F05Rik	**RIKEN cDNA 4933403F05 gene**	**-1,6**	0,000145
1437129_at	E330018D03Rik	**RIKEN cDNA E330018D03 gene**	**-1,6**	0,000635
1425114_at	Rbbp6	**retinoblastoma binding protein 6**	**-1,6**	0,002342
1429061_at	1810063B05Rik	**RIKEN cDNA 1810063B05 gene**	**-1,6**	0,000121
1455334_at	D330038O06Rik	**RIKEN cDNA D330038O06 gene**	**-1,6**	0,004763
1417848_at	Zfp704	**zinc finger protein 704**	**-1,6**	0,001610
1428720_s_at	2010309G21Rik	**RIKEN cDNA 2010309G21 gene**	**-1,6**	0,001547
1449608_a_at			**-1,6**	0,000524
1432472_a_at	Mccc2	**methylcrotonoyl-Coenzyme A carboxylase 2 (beta)**	**-1,6**	0,000141
1453304_s_at	Ly6e	**lymphocyte antigen 6 complex, locus E**	**-1,6**	0,000924
1448170_at	Siah2	**seven in absentia 2**	**-1,6**	0,000132
1442407_at			**-1,6**	0,000169
1456255_at	AI314180	**expressed sequence AI314180**	**-1,6**	0,008396
1456689_at	Rnf10	**ring finger protein 10**	**-1,6**	0,000344
1433931_at	C030046I01Rik	**RIKEN cDNA C030046I01 gene**	**-1,6**	0,000143
1439920_at			**-1,6**	0,000003
1417604_at	Camk1	**calcium/calmodulin-dependent protein kinase I**	**-1,6**	0,000003
1433769_at	Als2cl	**ALS2 C-terminal like**	**-1,6**	0,000604
1447099_at			**-1,6**	0,002973
1432352_at	Ccny	**cyclin Y**	**-1,6**	0,000935
1415972_at	Marcks	**myristoylated alanine rich protein kinase C substrate**	**-1,6**	0,000076
1419132_at	Tlr2	**toll-like receptor 2**	**-1,6**	0,002427
1451480_at	E2f4	**E2F transcription factor 4**	**-1,6**	0,000011
1430514_a_at	Cd99	**CD99 antigen**	**-1,6**	0,000026
1424033_at	Sfrs7	**splicing factor, arginine/serine-rich 7**	**-1,6**	0,000804
1423479_at	Nol11	**nucleolar protein 11**	**-1,6**	0,000682
1437916_at			**-1,6**	0,000810
1443773_at	Ylpm1	**YLP motif containing 1**	**-1,6**	0,000663
1441829_s_at	Akap10	**A kinase (PRKA) anchor protein 10**	**-1,6**	0,000009
1442235_at	Plagl2	**pleiomorphic adenoma gene-like 2**	**-1,6**	0,008748
1420682_at	Chrnb1	**cholinergic receptor, nicotinic, beta polypeptide 1 (muscle)**	**-1,6**	0,004715
1419191_at	Hipk3	**homeodomain interacting protein kinase 3**	**-1,6**	0,000053
1444224_at			**-1,6**	0,003078
1442445_at	2610027H17Rik	**RIKEN cDNA 2610027H17 gene**	**-1,6**	0,000919
1450678_at	Itgb2	**integrin beta 2**	**-1,6**	0,000404
1425964_x_at	Hspb1	**heat shock protein 1**	**-1,6**	0,000514
1455657_at	Smg1	**SMG1 homolog, phosphatidylinositol 3-kinase-related kinase (**	**-1,6**	0,000372
1437492_at	Mkx	**mohawk homeobox**	**-1,6**	0,000978
1441823_at	Zmiz1	**zinc finger, MIZ-type containing 1**	**-1,6**	0,001297
1422491_a_at	Bnip2	**BCL2/adenovirus E1B interacting protein 2**	**-1,6**	0,002041
1436509_at	Mlec	**malectin**	**-1,6**	0,000017

1416190_a_at	Sec61a1	**Sec61 alpha 1 subunit (S. cerevisiae)**	**-1,6**	0,000001
1438879_at			**-1,6**	0,001736
1459009_at			**-1,6**	0,001212
1417213_a_at	Rbm6	**RNA binding motif protein 6**	**-1,6**	0,000001
1430774_at	A430106A12Rik	**RIKEN cDNA A430106A12 gene**	**-1,6**	0,000049
1453524_at	Kif5b	**kinesin family member 5B**	**-1,6**	0,001314
1439139_at	D2Ertd640e	**DNA segment, Chr 2, ERATO Doi 640, expressed**	**-1,6**	0,000107
1418526_at	Fusip1	**FUS interacting protein (serine-arginine rich) 1**	**-1,6**	0,000291
1428949_at	Xpot	**exportin, tRNA (nuclear export receptor for tRNAs)**	**-1,6**	0,000021
1418860_a_at	Letmd1	**LETM1 domain containing 1**	**-1,6**	0,000007
1428698_at	Dpp8	**dipeptidylpeptidase 8**	**-1,6**	0,000001
1452463_x_at	Igk	**immunoglobulin kappa chain complex**	**-1,6**	0,008891
1417971_at	Nrm	**nurim (nuclear envelope membrane protein)**	**-1,6**	0,000070
1440287_at			**-1,6**	0,000211
1417500_a_at	Tgm2	**transglutaminase 2, C polypeptide**	**-1,6**	0,001019
1441547_at			**-1,6**	0,008346
1435426_s_at	Pisd	**phosphatidylserine decarboxylase**	**-1,6**	0,004280
1424776_a_at	Slc25a28	**solute carrier family 25, member 28**	**-1,6**	0,000045
1450916_at	Stau2	**staufen (RNA binding protein) homolog 2 (Drosophila)**	**-1,6**	0,000004
1435271_at	Irf3	**interferon regulatory factor 3**	**-1,6**	0,002310
1421895_at	Eif2s3x	**eukaryotic translation initiation factor 2, subunit 3, structural g**	**-1,6**	0,000067
1452036_a_at	Tmpo	**thymopoietin**	**-1,6**	0,003940
1440671_at	A130012E19Rik	**RIKEN cDNA A130012E19 gene**	**-1,6**	0,001119
1421819_a_at	Set	**SET translocation**	**-1,6**	0,006512
1438674_a_at	Sfrs8	**splicing factor, arginine/serine-rich 8**	**-1,6**	0,000122
1452280_at	Farp1	**FERM, RhoGEF (Arhgef) and pleckstrin domain protein 1 (chor**	**-1,6**	0,000698
1445545_at	Tmem77	**transmembrane protein 77**	**-1,6**	0,000037
1442834_at			**-1,6**	0,002241
1455472_at	A630071D13Rik	**RIKEN cDNA A630071D13 gene**	**-1,6**	0,002588
1442911_at	Riok2	**RIO kinase 2 (yeast)**	**-1,6**	0,000389
1442338_at			**-1,6**	0,000364
1423966_at	Cd99l2	**CD99 antigen-like 2**	**-1,6**	0,000003
1451465_at	Ubl7	**ubiquitin-like 7 (bone marrow stromal cell-derived)**	**-1,6**	0,000012
1416019_at	Dr1	**down-regulator of transcription 1**	**-1,6**	0,000157
1451518_at	Zfp709	**zinc finger protein 709**	**-1,6**	0,000061
1446548_at			**-1,6**	0,000903
1435561_at	Erf	**Ets2 repressor factor**	**-1,6**	0,000001
1429897_a_at	D16Ertd472e	**DNA segment, Chr 16, ERATO Doi 472, expressed**	**-1,6**	0,003804
1426756_at	Galnt2	**UDP-N-acetyl-alpha-D-galactosamine:polypeptide N-acetylgala**	**-1,6**	0,000010
1428506_at	Atic	**5-aminoimidazole-4-carboxamide ribonucleotide formyltransfe**	**-1,6**	0,000054
1459856_at			**-1,6**	0,003912
1434436_at	Morc4	**microrchidia 4**	**-1,6**	0,003481
1418230_a_at	Lims1	**LIM and senescent cell antigen-like domains 1**	**-1,6**	0,000188
1453852_at	Ddx50	**DEAD (Asp-Glu-Ala-Asp) box polypeptide 50**	**-1,6**	0,000630
1442971_at	Baz2b	**bromodomain adjacent to zinc finger domain, 2B**	**-1,6**	0,000586
1416389_a_at	Rcbtb2	**regulator of chromosome condensation (RCC1) and BTB (POZ)**	**-1,6**	0,000143
1418901_at	Cebpb	**CCAAT/enhancer binding protein (C/EBP), beta**	**-1,6**	0,008045
1429207_at	5730408K05Rik	**RIKEN cDNA 5730408K05 gene**	**-1,6**	0,003856
1431026_at	Nat12	**N-acetyltransferase 12**	**-1,6**	0,000034
1431196_at	Atp2c1	**ATPase, Ca++-sequestering**	**-1,6**	0,000022
1421260_a_at	Srm	**spermidine synthase**	**-1,6**	0,004647
1431287_at	Pcm1	**pericentriolar material 1**	**-1,6**	0,005889
1460035_at	Phb2	**prohibitin 2**	**-1,6**	0,000018
1450076_at	4933411K20Rik	**RIKEN cDNA 4933411K20 gene**	**-1,6**	0,000185
1452187_at	Rbm5	**RNA binding motif protein 5**	**-1,6**	0,000363
1452433_at			**-1,6**	0,000121
1443880_at	Zbtb39	**zinc finger and BTB domain containing 39**	**-1,6**	0,000003
1416536_at	Mum1	**melanoma associated antigen (mutated) 1**	**-1,6**	0,000021
1430135_at	Dnase2a	**deoxyribonuclease II alpha**	**-1,6**	0,004152
1428129_at	Lman1	**lectin, mannose-binding, 1**	**-1,6**	0,000003
1452024_a_at	Ldb1	**LIM domain binding 1**	**-1,6**	0,000059
1448103_s_at	Nono	**non-POU-domain-containing, octamer binding protein**	**-1,6**	0,001794
1437449_at	Rsad1	**radical S-adenosyl methionine domain containing 1**	**-1,6**	0,000210
1457673_at	6820431F20Rik	**RIKEN cDNA 6820431F20 gene**	**-1,6**	0,002976
1438887_a_at	Gmcl1	**germ cell-less homolog 1 (Drosophila)**	**-1,6**	0,000146
1424290_at	Osgin2	**oxidative stress induced growth inhibitor family member 2**	**-1,6**	0,000019
1449037_at	Crem	**cAMP responsive element modulator**	**-1,6**	0,000214
1453247_at	Zfp618	**zinc fingerprotein 618**	**-1,6**	0,005570
1448013_at	Usp24	**ubiquitin specific peptidase 24**	**-1,6**	0,000150
1439302_at	Uba6	**ubiquitin-like modifier activating enzyme 6**	**-1,6**	0,000322
1438072_at			**-1,6**	0,000934
1455336_at	Thap2	**THAP domain containing, apoptosis associated protein 2**	**-1,6**	0,001068
1448307_at	Psmg1	**proteasome (prosome, macropain) assembly chaperone 1**	**-1,6**	0,000476
1440847_at	Mtss1	**metastasis suppressor 1**	**-1,6**	0,001205
1448230_at	Usp10	**ubiquitin specific peptidase 10**	**-1,6**	0,000478
1457802_at	B930012P20Rik	**RIKEN cDNA B930012P20 gene**	**-1,6**	0,000492
1449044_at	Eef1e1	**eukaryotic translation elongation factor 1 epsilon 1**	**-1,6**	0,005174
1427040_at	Mdfic	**MyoD family inhibitor domain containing**	**-1,6**	0,003302
1448274_at	C1qbp	**complement component 1, q subcomponent binding protein**	**-1,6**	0,000608
1422718_at	Ap3s2	**adaptor-related protein complex 3, sigma 2 subunit**	**-1,6**	0,000007
1437067_at	Phtf2	**putative homeodomain transcription factor 2**	**-1,6**	0,007632
1455496_at	Pfas	**phosphoribosylformylglycinamidine synthase (FGAR amidotra**	**-1,6**	0,000077
1448667_x_at	Tob2	**transducer of ERBB2, 2**	**-1,6**	0,000190
1436422_at	BC026590	**cDNA sequence BC026590**	**-1,6**	0,000047
1444856_at			**-1,6**	0,002741
1452426_x_at			**-1,6**	0,007162
1429110_a_at	Nsun4	**NOL1/NOP2/Sun domain family, member 4**	**-1,6**	0,000818
1442023_at	A530030E21Rik	**RIKEN cDNA A530030E21 gene**	**-1,6**	0,013231
1445267_at			**-1,6**	0,000258
1451154_a_at	Cugbp2	**CUG triplet repeat, RNA binding protein 2**	**-1,6**	0,007877
1452916_at	Wbp7	**WW domain binding protein 7**	**-1,6**	0,000014
1449861_at	Nek4	**NIMA (never in mitosis gene a)-related expressed kinase 4**	**-1,6**	0,000002
1435037_at	Perld1	**per1-like domain containing 1**	**-1,6**	0,001369
1456648_at			**-1,6**	0,007836
1422145_at	Mgat3	**mannoside acetylglucosaminyltransferase 3**	**-1,6**	0,007613
1452799_at	Fggy	**FGGY carbohydrate kinase domain containing**	**-1,6**	0,000360
1421337_at	ENSMUSG00000053512	**predicted gene, ENSMUSG00000053512**	**-1,6**	0,000013
1417948_s_at	Ilf2	**interleukin enhancer binding factor 2**	**-1,6**	0,003070
1444744_at			**-1,6**	0,000034
1428187_at	Cd47	**CD47 antigen (Rh-related antigen, integrin-associated signal tr**	**-1,7**	0,000338
1442078_at			**-1,7**	0,000050
1425940_a_at	Ssbp3	**single-stranded DNA binding protein 3**	**-1,7**	0,000165
1415900_a_at	Kit	**kit oncogene**	**-1,7**	0,000522
1439276_at	Adar	**adenosine deaminase, RNA-specific**	**-1,7**	0,001449
1423334_at	Ergic1	**endoplasmic reticulum-golgi intermediate compartment (ERGI(**	**-1,7**	0,000022
1416158_at	Nr2f2	**nuclear receptor subfamily 2, group F, member 2**	**-1,7**	0,000004

1415761_at	Mrpl52	**mitochondrial ribosomal protein L52**	**-1,7**	0,000361
1436177_at	Plekha2	**pleckstrin homology domain-containing, family A (phosphoino**	**-1,7**	0,000003
1452402_at			**-1,7**	0,001166
1426888_at	Ehmt2	**euchromatic histone lysine N-methyltransferase 2**	**-1,7**	0,000284
1428466_at	Chd3	**chromodomain helicase DNA binding protein 3**	**-1,7**	0,000126
1442126_at			**-1,7**	0,000568
1424055_at	Ncoa5	**nuclear receptor coactivator 5**	**-1,7**	0,000003
1453736_s_at	B230219D22Rik	**RIKEN cDNA B230219D22 gene**	**-1,7**	0,000064
1446703_at			**-1,7**	0,000403
1440268_at	Trim41	**tripartite motif-containing 41**	**-1,7**	0,000079
1415956_a_at	Pctk1	**PCTAIRE-motif protein kinase 1**	**-1,7**	0,000001
1418274_at	Nutf2	**nuclear transport factor 2**	**-1,7**	0,001755
1435328_at	Cyhr1	**cysteine and histidine rich 1**	**-1,7**	0,000001
1422954_at	Zfp60	**zinc finger protein 60**	**-1,7**	0,000873
1422167_at	Sema5a	**sema domain, seven thrombospondin repeats (type 1 and type**	**-1,7**	0,000024
1455095_at	Hist2h2be	**histone cluster 2, H2be**	**-1,7**	0,000017
1443546_at			**-1,7**	0,002365
1449939_s_at	Dlk1	**delta-like 1 homolog (Drosophila)**	**-1,7**	0,010905
1422492_at	Cpox	**coproporphyrinogen oxidase**	**-1,7**	0,000038
1447156_at			**-1,7**	0,002139
1442580_at	A530020G20Rik	**RIKEN cDNA A530020G20 gene**	**-1,7**	0,000550
1434054_at	Sirt7	**sirtuin 7 (silent mating type information regulation 2, homolog)**	**-1,7**	0,015511
1432901_at	Etl4	**enhancer trap locus 4**	**-1,7**	0,000591
1435319_at	Ip6k2	**inositol hexaphosphate kinase 2**	**-1,7**	0,000004
1459187_at			**-1,7**	0,003124
1441404_at			**-1,7**	0,000697
1457510_at			**-1,7**	0,000739
1415773_at	Ncl	**nucleolin**	**-1,7**	0,004947
1441415_at			**-1,7**	0,000301
1418128_at	Adcy6	**adenylate cyclase 6**	**-1,7**	0,000062
1426850_a_at	Map2k6	**mitogen-activated protein kinase kinase 6**	**-1,7**	0,000446
1443551_at	Atp2a2	**ATPase, Ca++ transporting, cardiac muscle, slow twitch 2**	**-1,7**	0,004350
1438326_at	Trmt6	**tRNA methyltransferase 6 homolog (S. cerevisiae)**	**-1,7**	0,003491
1450400_at	Tgs1	**trimethylguanosine synthase homolog (S. cerevisiae)**	**-1,7**	0,000408
1426988_at	Klhdc5	**kelch domain containing 5**	**-1,7**	0,000307
1419295_at	Creb3l1	**cAMP responsive element binding protein 3-like 1**	**-1,7**	0,004428
1439209_at	Tcf12	**transcription factor 12**	**-1,7**	0,000963
1423522_at	Npm3	**nucleoplasmin 3**	**-1,7**	0,000952
1428301_at	ENSMUSG00000068790	**predicted gene, ENSMUSG00000068790**	**-1,7**	0,001189
1425087_at	2310003F16Rik	**RIKEN cDNA 2310003F16 gene**	**-1,7**	0,001249
1452764_at	Socs6	**suppressor of cytokine signaling 6**	**-1,7**	0,001346
1434067_at	AI662270	**expressed sequence AI662270**	**-1,7**	0,002259
1418915_at	Mmachc	**methylmalonic aciduria cblC type, with homocystinuria**	**-1,7**	0,000066
1424622_at	Hsf1	**heat shock factor 1**	**-1,7**	0,000009
1440892_at			**-1,7**	0,012066
1445966_at			**-1,7**	0,000375
1421955_a_at	Nedd4	**neural precursor cell expressed, developmentally down-regula**	**-1,7**	0,000079
1444001_at			**-1,7**	0,000862
1425373_a_at	Psmg2	**proteasome (prosome, macropain) assembly chaperone 2**	**-1,7**	0,000655
1420894_at	Tgfbr1	**transforming growth factor, beta receptor I**	**-1,7**	0,000027
1441274_at			**-1,7**	0,000484
1422680_at	Ctr9	**Ctr9, Paf1/RNA polymerase II complex component, homolog (S**	**-1,7**	0,000013
1438941_x_at	Ampd2	**adenosine monophosphate deaminase 2 (isoform L)**	**-1,7**	0,002520
1425227_a_at	Atp6v0a1	**ATPase, H+ transporting, lysosomal V0 subunit A1**	**-1,7**	0,000210
1420887_a_at	Bcl2l1	**BCL2-like 1**	**-1,7**	0,000349
1415682_at	Xpo7	**exportin 7**	**-1,7**	0,000007
1435136_at	Whsc1	**Wolf-Hirschhorn syndrome candidate 1 (human)**	**-1,7**	0,009310
1423084_at	B3galt2	**UDP-Gal:betaGlcNAc beta 1,3-galactosyltransferase, polypepti**	**-1,7**	0,003250
1442216_at			**-1,7**	0,000038
1429961_at	1700021C14Rik	**RIKEN cDNA 1700021C14 gene**	**-1,7**	0,001116
1437965_at	Heatr1	**HEAT repeat containing 1**	**-1,7**	0,000474
1429344_at	9,13E+15	**hypothetical 9130022E09**	**-1,7**	0,003841
1457479_at			**-1,7**	0,003516
1437756_at	Gimap9	**GTPase, IMAP family member 9**	**-1,7**	0,000628
1423726_at	Vat1	**vesicle amine transport protein 1 homolog (T californica)**	**-1,7**	0,000017
1427983_at	Zfp280c	**zinc finger protein 280C**	**-1,7**	0,008125
1424423_at	Lenep	**lens epithelial protein**	**-1,7**	0,000010
1431960_at	Wwox	**WW domain-containing oxidoreductase**	**-1,7**	0,000012
1443365_at	Htr4	**5 hydroxytryptamine (serotonin) receptor 4**	**-1,7**	0,000076
1415872_at	Hnrnph1	**heterogeneous nuclear ribonucleoprotein H1**	**-1,7**	0,008223
1428414_at	Ccny	**cyclin Y**	**-1,7**	0,010028
1417619_at	Gadd45gip1	**growth arrest and DNA-damage-inducible, gamma interacting p**	**-1,7**	0,000158
1451026_at	Ftsj3	**FtsJ homolog 3 (E. coli)**	**-1,7**	0,004494
1428354_at	Foxk2	**forkhead box K2**	**-1,7**	0,000019
1460555_at	Fam65b	**family with sequence similarity 65, member B**	**-1,7**	0,002909
1441960_x_at	5730494M16Rik	**RIKEN cDNA 5730494M16 gene**	**-1,7**	0,005162
1438076_at	Rpl30	**ribosomal protein L30**	**-1,7**	0,003279
1445963_at			**-1,7**	0,000007
1438683_at	Wasf2	**WAS protein family, member 2**	**-1,7**	0,000113
1448348_at	Caprin1	**cell cycle associated protein 1**	**-1,7**	0,000028
1459961_a_at	Stat3	**signal transducer and activator of transcription 3**	**-1,7**	0,000047
1442006_at			**-1,7**	0,000001
1418980_a_at	Cnp	**2',3'-cyclic nucleotide 3' phosphodiesterase**	**-1,7**	0,000002
1419477_at	Clec2d	**C-type lectin domain family 2, member d**	**-1,7**	0,005793
1451849_a_at	Lmnb2	**lamin B2**	**-1,7**	0,000493
1415957_a_at	Rrp1	**ribosomal RNA processing 1 homolog (S. cerevisiae)**	**-1,7**	0,000001
1427884_at	Col3a1	**collagen, type III, alpha 1**	**-1,7**	0,015212
1437359_at	Rnps1	**ribonucleic acid binding protein S1**	**-1,7**	0,002052
1437789_at	Birc6	**baculoviral IAP repeat-containing 6**	**-1,7**	0,001125
1452508_x_at	Ptms	**parathymosin**	**-1,7**	0,000115
1423048_a_at	Tollip	**toll interacting protein**	**-1,7**	0,001738
1418527_a_at	Fusip1	**FUS interacting protein (serine-arginine rich) 1**	**-1,7**	0,001000
1428158_at	Akt1s1	**AKT1 substrate 1 (proline-rich)**	**-1,7**	0,000002
1459143_at	Chchd3	**coiled-coil-helix-coiled-coil-helix domain containing 3**	**-1,7**	0,000021
1439933_at	B430316J06Rik	**RIKEN cDNA B430316J06 gene**	**-1,7**	0,003674
1450246_at	Fut2	**fucosyltransferase 2**	**-1,7**	0,004580
1459196_at			**-1,7**	0,001851
1445919_at	AA409261	**expressed sequence AA409261**	**-1,7**	0,000207
1439148_a_at	Pfkl	**phosphofructokinase, liver, B-type**	**-1,7**	0,001722
1455092_at	LOC100043601	**hypothetical protein LOC100043601**	**-1,7**	0,002534
1430971_a_at	Aqr	**aquarius**	**-1,7**	0,000005
1430089_at	5830469G19Rik	**RIKEN cDNA 5830469G19 gene**	**-1,7**	0,000043
1416014_at	Abce1	**ATP-binding cassette, sub-family E (OABP), member 1**	**-1,7**	0,002350
1438800_at	Nagk	**N-acetylglucosamine kinase**	**-1,7**	0,000159
1448123_s_at	Tgfbi	**transforming growth factor, beta induced**	**-1,7**	0,002235
1426897_at	Rcc2	**regulator of chromosome condensation 2**	**-1,7**	0,013166

1418851_at	Trim39	**tripartite motif-containing 39**	**-1,7**	0,000439
1440736_at	AI131651	**expressed sequence AI131651**	**-1,7**	0,000018
1454823_at	Wdr37	**WD repeat domain 37**	**-1,7**	0,000004
1444760_at	Ncor1	**nuclear receptor co-repressor 1**	**-1,7**	0,001322
1438353_at			**-1,7**	0,000356
1441141_at	Amn1	**antagonist of mitotic exit network 1 homolog (S. cerevisiae)**	**-1,7**	0,001109
1439093_at			**-1,7**	0,001304
1424333_at	Rg9mtd1	**RNA (guanine-9-) methyltransferase domain containing 1**	**-1,7**	0,000903
1424874_a_at	Ptbp1	**polypyrimidine tract binding protein 1**	**-1,7**	0,000003
1458460_at			**-1,7**	0,000516
1439126_at	1110007A13Rik	**RIKEN cDNA 1110007A13 gene**	**-1,7**	0,001467
1430152_at	Eps15	**epidermal growth factor receptor pathway substrate 15**	**-1,7**	0,000344
1417420_at	Ccnd1	**cyclin D1**	**-1,7**	0,001049
1447166_at			**-1,7**	0,007471
1447491_at			**-1,7**	0,000108
1458056_at	Sfrs12	**splicing factor, arginine/serine-rich 12**	**-1,7**	0,006472
1450082_s_at	Etv5	**ets variant gene 5**	**-1,7**	0,000807
1451687_a_at	Hnf1b	**HNF1 homeobox B**	**-1,7**	0,000007
1452247_at	Fxr1	**fragile X mental retardation gene 1, autosomal homolog**	**-1,7**	0,001184
1452974_at	Nol8	**nucleolar protein 8**	**-1,7**	0,006437
1423909_at	Tmem176a	**transmembrane protein 176A**	**-1,7**	0,001463
1435018_at	5930434B04Rik	**RIKEN cDNA 5930434B04 gene**	**-1,7**	0,000001
1446982_at			**-1,7**	0,000029
1418296_at	Fxyd5	**FXYD domain-containing ion transport regulator 5**	**-1,7**	0,000210
1453556_x_at	Cd99	**CD99 antigen**	**-1,7**	0,000026
1433972_at	Camta1	**calmodulin binding transcription activator 1**	**-1,7**	0,002059
1441477_at	Calu	**calumenin**	**-1,7**	0,000018
1433621_at	Wdr41	**WD repeat domain 41**	**-1,7**	0,000005
1457588_at	C76213	**expressed sequence C76213**	**-1,7**	0,001053
1441624_at	Sorbs2	**sorbin and SH3 domain containing 2**	**-1,7**	0,010746
1449155_at	Polr3g	**polymerase (RNA) III (DNA directed) polypeptide G**	**-1,7**	0,000203
1416355_at	Rbmx	**RNA binding motif protein, X chromosome**	**-1,7**	0,000245
1460642_at	Traf4	**TNF receptor associated factor 4**	**-1,7**	0,000018
1459897_a_at	Sbsn	**suprabasin**	**-1,7**	0,000142
1439159_at	Rere	**arginine glutamic acid dipeptide (RE) repeats**	**-1,7**	0,007589
1426873_s_at	Jup	**junction plakoglobin**	**-1,7**	0,000423
1432360_a_at	Tmtc4	**transmembrane and tetratricopeptide repeat containing 4**	**-1,7**	0,001587
1419964_s_at	Hdgf	**hepatoma-derived growth factor**	**-1,7**	0,000111
1446345_at			**-1,7**	0,000394
1438065_at	Rprd1a	**regulation of nuclear pre-mRNA domain containing 1A**	**-1,7**	0,001320
1417988_at	Resp18	**regulated endocrine-specific protein 18**	**-1,7**	0,000506
1425544_at	Plekha5	**pleckstrin homology domain containing, family A member 5**	**-1,7**	0,000576
1426051_a_at	Cenpb	**centromere protein B**	**-1,7**	0,000004
1446172_at			**-1,7**	0,001986
1435036_at	Aspg	**asparaginase homolog (S. cerevisiae)**	**-1,7**	0,003065
1441487_at	Trim2	**tripartite motif-containing 2**	**-1,7**	0,000155
1427439_s_at	Prmt5	**protein arginine N-methyltransferase 5**	**-1,7**	0,000072
1428636_at	Steap2	**six transmembrane epithelial antigen of prostate 2**	**-1,7**	0,000409
1419460_at	Rpp14	**ribonuclease P 14 subunit (human)**	**-1,7**	0,002587
1450124_a_at	Atp2a3	**ATPase, Ca++ transporting, ubiquitous**	**-1,7**	0,000133
1418280_at	Klf6	**Kruppel-like factor 6**	**-1,7**	0,004401
1450873_at	Gtpbp4	**GTP binding protein 4**	**-1,7**	0,006135
1423271_at	Gjb2	**gap junction protein, beta 2**	**-1,7**	0,001044
1426085_a_at	Pxn	**paxillin**	**-1,7**	0,000200
1429096_at	2810455D13Rik	**RIKEN cDNA 2810455D13 gene**	**-1,7**	0,000106
1446090_at			**-1,7**	0,000273
1422735_at	Foxq1	**forkhead box Q1**	**-1,7**	0,007640
1438257_at			**-1,7**	0,000012
1429900_at	5330406M23Rik	**RIKEN cDNA 5330406M23 gene**	**-1,7**	0,001830
1426550_at	Sidt1	**SID1 transmembrane family, member 1**	**-1,7**	0,000009
1426958_at	Rps9	**ribosomal protein S9**	**-1,7**	0,012268
1442139_at			**-1,7**	0,001937
1453077_a_at	Snapc3	**small nuclear RNA activating complex, polypeptide 3**	**-1,7**	0,007419
1441117_at			**-1,7**	0,002135
1423333_at	Ergic1	**endoplasmic reticulum-golgi intermediate compartment (ERGI**	**-1,7**	0,000001
1446475_at			**-1,7**	0,000295
1456661_at			**-1,7**	0,000075
1429058_at	Tmem107	**transmembrane protein 107**	**-1,7**	0,000004
1427193_at	Brd8	**bromodomain containing 8**	**-1,7**	0,000346
1424620_at	Nop16	**NOP16 nucleolar protein homolog (yeast)**	**-1,7**	0,000467
1460633_at	Prpf19	**PRP19/PSO4 pre-mRNA processing factor 19 homolog (S. cere**	**-1,7**	0,000073
1419647_a_at	Ier3	**immediate early response 3**	**-1,7**	0,006508
1430417_s_at	Neurl4	**neuralized homolog 4 (Drosophila)**	**-1,7**	0,000018
1417852_x_at	Clca1	**chloride channel calcium activated 1**	**-1,7**	0,000018
1436145_at			**-1,7**	0,000264
1460351_at	S100a11	**S100 calcium binding protein A11 (calgizzarin)**	**-1,7**	0,006176
1430780_a_at	Pmm1	**phosphomannomutase 1**	**-1,7**	0,001289
1421839_at	Abca1	**ATP-binding cassette, sub-family A (ABC1), member 1**	**-1,7**	0,007149
1438915_at	6720401G13Rik	**RIKEN cDNA 6720401G13 gene**	**-1,7**	0,003665
1440295_at	1110057K04Rik	**RIKEN cDNA 1110057K04 gene**	**-1,7**	0,000103
1439871_at			**-1,7**	0,000572
1428233_at	Cpsf6	**cleavage and polyadenylation specific factor 6**	**-1,7**	0,000193
1440543_at	Heatr5a	**HEAT repeat containing 5A**	**-1,7**	0,000063
1458393_at	Srr	**serine racemase**	**-1,7**	0,000043
1428404_at	2410025L10Rik	**RIKEN cDNA 2410025L10 gene**	**-1,7**	0,000006
1429545_at	Ube2i	**ubiquitin-conjugating enzyme E2I**	**-1,7**	0,001341
1456296_at	5830418K08Rik	**RIKEN cDNA 5830418K08 gene**	**-1,7**	0,005295
1430038_at	Gphn	**gephyrin**	**-1,7**	0,000065
1452498_at			**-1,7**	0,000130
1456040_at	Sf3b2	**splicing factor 3b, subunit 2**	**-1,7**	0,000000
1435134_at	Aadacl1	**arylacetamide deacetylase-like 1**	**-1,7**	0,015496
1455945_at	Zfp58	**zinc finger protein 58**	**-1,7**	0,000326
1449011_at	Slc12a7	**solute carrier family 12, member 7**	**-1,7**	0,000043
1457806_at	B830028B13Rik	**RIKEN cDNA B830028B13 gene**	**-1,7**	0,002936
1416915_at	Msh6	**mutS homolog 6 (E. coli)**	**-1,7**	0,000625
1431430_s_at	Trim59	**tripartite motif-containing 59**	**-1,7**	0,000525
1451109_a_at	Nedd4	**neural precursor cell expressed, developmentally down-regula**	**-1,7**	0,000149
1449653_at			**-1,7**	0,000039
1422743_at	Phka1	**phosphorylase kinase alpha 1**	**-1,7**	0,000134
1448815_at	Ogg1	**8-oxoguanine DNA-glycosylase 1**	**-1,7**	0,000093
1437219_at			**-1,7**	0,000443
1432978_at	9030607L02Rik	**RIKEN cDNA 9030607L02 gene**	**-1,7**	0,000052
1426297_at	Tcfe2a	**transcription factor E2a**	**-1,7**	0,007518
1445933_at			**-1,7**	0,000078
1440717_at	AA407881	**expressed sequence AA407881**	**-1,7**	0,000016
1417927_at	Ddx19a	**DEAD (Asp-Glu-Ala-Asp) box polypeptide 19a**	**-1,7**	0,000001

1450927_at	Lztr1	**leucine-zipper-like transcriptional regulator, 1**	**-1,7**	0,000064
1448592_at	Crtap	**cartilage associated protein**	**-1,7**	0,000021
1456952_at			**-1,7**	0,000321
1440954_at			**-1,7**	0,000204
1435550_at	C430014K11Rik	**RIKEN cDNA C430014K11 gene**	**-1,7**	0,000001
1454699_at	Sesn1	**sestrin 1**	**-1,7**	0,000530
1441195_at	6030487A22Rik	**RIKEN cDNA 6030487A22 gene**	**-1,7**	0,000672
1440905_at	Hs2st1	**heparan sulfate 2-O-sulfotransferase 1**	**-1,7**	0,002719
1430045_at	Tsnax	**translin-associated factor X**	**-1,7**	0,000373
1458079_at	Usp40	**ubiquitin specific peptidase 40**	**-1,7**	0,000039
1446071_at	Steap2	**six transmembrane epithelial antigen of prostate 2**	**-1,7**	0,001433
1431102_at	Cep350	**centrosomal protein 350**	**-1,7**	0,000047
1427079_at	Mapre3	**microtubule-associated protein, RP/EB family, member 3**	**-1,7**	0,002856
1427680_a_at	Nfib	**nuclear factor I/B**	**-1,7**	0,001155
1435078_at	Tanc2	**tetratricopeptide repeat, ankyrin repeat and coiled-coil containi**	**-1,7**	0,005879
1441718_at			**-1,7**	0,001455
1451249_at	Trmt1	**TRM1 tRNA methyltransferase 1 homolog (S. cerevisiae)**	**-1,7**	0,000013
1443114_at	Zmym4	**zinc finger, MYM-type 4**	**-1,7**	0,000923
1446472_at	Ahctf1	**AT hook containing transcription factor 1**	**-1,7**	0,000070
1418181_at	Ptp4a3	**protein tyrosine phosphatase 4a3**	**-1,7**	0,000980
1455627_at	Col8a1	**collagen, type VIII, alpha 1**	**-1,7**	0,009892
1456377_x_at	Limd2	**LIM domain containing 2**	**-1,7**	0,014421
1440637_at			**-1,7**	0,000150
1446164_at	Tgs1	**trimethylguanosine synthase homolog (S. cerevisiae)**	**-1,7**	0,001164
1418374_at	Fxyd3	**FXYD domain-containing ion transport regulator 3**	**-1,7**	0,001537
1438165_x_at	Vat1	**vesicle amine transport protein 1 homolog (T californica)**	**-1,7**	0,001023
1448277_at	Pold2	**polymerase (DNA directed), delta 2, regulatory subunit**	**-1,7**	0,000034
1435244_at	Vav2	**vav 2 oncogene**	**-1,7**	0,012505
1459537_at			**-1,7**	0,001081
1455606_at	N4bp1	**NEDD4 binding protein 1**	**-1,7**	0,000022
1421298_a_at	Hipk1	**homeodomain interacting protein kinase 1**	**-1,7**	0,000677
1436034_at	Cep68	**centrosomal protein 68**	**-1,7**	0,002122
1452175_at	1810026J23Rik	**RIKEN cDNA 1810026J23 gene**	**-1,7**	0,000007
1421271_at	Sh3rf1	**SH3 domain containing ring finger 1**	**-1,7**	0,000411
1459973_x_at	Dpp4	**dipeptidylpeptidase 4**	**-1,7**	0,000383
1424222_s_at	Rad23b	**RAD23b homolog (S. cerevisiae)**	**-1,7**	0,000001
1416283_at	Gart	**phosphoribosylglycinamide formyltransferase**	**-1,7**	0,001354
1451456_at	6430706D22Rik	**RIKEN cDNA 6430706D22 gene**	**-1,7**	0,000274
1419186_a_at	St8sia4	**ST8 alpha-N-acetyl-neuraminide alpha-2,8-sialyltransferase 4**	**-1,7**	0,007986
1419270_a_at	Dut	**deoxyuridine triphosphatase**	**-1,7**	0,007152
1434707_at	Sbf1	**SET binding factor 1**	**-1,7**	0,000001
1423493_a_at	Nfix	**nuclear factor I/X**	**-1,7**	0,000001
1438816_at	Ahctf1	**AT hook containing transcription factor 1**	**-1,7**	0,000768
1443526_at			**-1,7**	0,000935
1418991_at	Bak1	**BCL2-antagonist/killer 1**	**-1,7**	0,000075
1421033_a_at	Tcerg1	**transcription elongation regulator 1 (CA150)**	**-1,7**	0,000539
1453212_at	Zfp383	**zinc finger protein 383**	**-1,7**	0,003130
1440028_at			**-1,7**	0,010176
1429739_a_at	Patz1	**POZ (BTB) and AT hook containing zinc finger 1**	**-1,7**	0,010323
1441185_at	Msi2	**Musashi homolog 2 (Drosophila)**	**-1,7**	0,000569
1427353_at	Clasp1	**CLIP associating protein 1**	**-1,7**	0,005378
1416846_a_at	Pdzrn3	**PDZ domain containing RING finger 3**	**-1,7**	0,000443
1460253_at	Cmtm7	**CKLF-like MARVEL transmembrane domain containing 7**	**-1,7**	0,000210
1428873_a_at	Msl1	**male-specific lethal 1 homolog (Drosophila)**	**-1,7**	0,000003
1436539_at	Clmn	**calmin**	**-1,7**	0,000145
1451574_at	Bcl9	**B-cell CLL/lymphoma 9**	**-1,7**	0,000006
1457392_at			**-1,7**	0,000160
1425329_a_at	Cyb5r3	**cytochrome b5 reductase 3**	**-1,7**	0,000016
1424082_at	Tbc1d13	**TBC1 domain family, member 13**	**-1,7**	0,000005
1459358_at			**-1,7**	0,000020
1421809_at	Dgcr2	**DiGeorge syndrome critical region gene 2**	**-1,7**	0,000052
1443238_at			**-1,7**	0,000170
1428383_a_at	2310021P13Rik	**RIKEN cDNA 2310021P13 gene**	**-1,7**	0,000000
1450012_x_at	Ywhag	**tyrosine 3-monooxygenase/tryptophan 5-monooxygenase activ**	**-1,7**	0,000088
1459344_at	9630019E01Rik	**RIKEN cDNA 9630019E01 gene**	**-1,7**	0,001207
1444466_at	Ncald	**neurocalcin delta**	**-1,7**	0,000095
1439895_at	AU021025	**expressed sequence AU021025**	**-1,7**	0,000098
1451377_a_at	Aaas	**achalasia, adrenocortical insufficiency, alacrimia**	**-1,7**	0,000231
1420836_at	Slc25a30	**solute carrier family 25, member 30**	**-1,7**	0,000534
1438433_at	Whamm	**WAS protein homolog associated with actin, golgi membranes**	**-1,7**	0,000022
1416237_at	Mpzl2	**myelin protein zero-like 2**	**-1,7**	0,000003
1421038_a_at	Kcnn4	**potassium intermediate/small conductance calcium-activated c**	**-1,7**	0,000054
1419033_at	Papola	**poly (A) polymerase alpha**	**-1,7**	0,002305
1421574_at	Rap2a	**RAS related protein 2a**	**-1,7**	0,000094
1434209_at	Prmt6	**protein arginine N-methyltransferase 6**	**-1,7**	0,000003
1447024_at			**-1,7**	0,001172
1426403_at	Actr1b	**ARP1 actin-related protein 1 homolog B, centractin beta (yeast**	**-1,7**	0,000001
1440622_at			**-1,7**	0,000179
1442052_at			**-1,7**	0,000733
1422799_at	Bat2	**HLA-B associated transcript 2**	**-1,7**	0,000010
1425206_a_at	Ube3a	**ubiquitin protein ligase E3A**	**-1,7**	0,007761
1433266_at	2810416A17Rik	**RIKEN cDNA 2810416A17 gene**	**-1,7**	0,014343
1425483_at	LOC100044677	**similar to thymus high mobility group box protein TOX**	**-1,7**	0,001173
1434360_s_at	Ptprg	**protein tyrosine phosphatase, receptor type, G**	**-1,7**	0,000097
1448656_at	Cacnb3	**calcium channel, voltage-dependent, beta 3 subunit**	**-1,7**	0,000014
1450537_at	Mid2	**midline 2**	**-1,7**	0,001323
1459670_at			**-1,7**	0,000571
1453193_s_at	Kif12	**kinesin family member 12**	**-1,7**	0,008514
1441642_at			**-1,7**	0,000272
1423847_at	Ncapd2	**non-SMC condensin I complex, subunit D2**	**-1,7**	0,001182
1440317_at	C130068B02Rik	**RIKEN cDNA C130068B02 gene**	**-1,7**	0,000933
1430075_at	Sf3b3	**splicing factor 3b, subunit 3**	**-1,7**	0,001748
1417786_a_at	Rgs19	**regulator of G-protein signaling 19**	**-1,7**	0,003598
1436518_at	Usp46	**ubiquitin specific peptidase 46**	**-1,7**	0,000069
1438862_at	A630005I04Rik	**RIKEN cDNA A630005I04 gene**	**-1,7**	0,000571
1416050_a_at	Scarb1	**scavenger receptor class B, member 1**	**-1,7**	0,000022
1448541_at	Klc1	**kinesin light chain 1**	**-1,7**	0,000057
1424866_at	Usp43	**ubiquitin specific peptidase 43**	**-1,7**	0,000000
1422088_at	Mycl1	**v-myc myelocytomatosis viral oncogene homolog 1, lung carci**	**-1,7**	0,000254
1437797_at	Atp2a2	**ATPase, Ca++ transporting, cardiac muscle, slow twitch 2**	**-1,7**	0,000623
1415869_a_at	Trim28	**tripartite motif-containing 28**	**-1,7**	0,000077
1436320_at			**-1,7**	0,000000
1458159_at			**-1,7**	0,003186
1423543_at	Swap70	**SWA-70 protein**	**-1,7**	0,000094
1423952_a_at	Krt7	**keratin 7**	**-1,7**	0,002401
1449116_a_at	Dtymk	**deoxythymidylate kinase**	**-1,7**	0,010033

1448101_s_at	Trim27	**tripartite motif-containing 27**	**-1,7**	0,000000
1445598_at			**-1,7**	0,003769
1423520_at	Lmnb1	**lamin B1**	**-1,7**	0,000144
1426532_at	Zmynd11	**zinc finger, MYND domain containing 11**	**-1,7**	0,000009
1452629_at	Safb2	**scaffold attachment factor B2**	**-1,7**	0,000006
1430043_at	Ttc19	**tetratricopeptide repeat domain 19**	**-1,7**	0,000090
1433647_s_at	Rhobtb3	**Rho-related BTB domain containing 3**	**-1,7**	0,004853
1457466_at	AA409368	**expressed sequence AA409368**	**-1,7**	0,009349
1460164_at	Spin1	**spindlin 1**	**-1,7**	0,000006
1443991_at	Dock1	**dedicator of cytokinesis 1**	**-1,7**	0,000055
1428672_at	Snrpf	**small nuclear ribonucleoprotein polypeptide F**	**-1,7**	0,004049
1439127_at	AI314180	**expressed sequence AI314180**	**-1,7**	0,003002
1460237_at	Trim8	**tripartite motif protein 8**	**-1,7**	0,000002
1438001_x_at	Reep5	**receptor accessory protein 5**	**-1,7**	0,000000
1426296_at	Rad52	**RAD52 homolog (S. cerevisiae)**	**-1,7**	0,000040
1416853_at	Ncdn	**neurochondrin**	**-1,7**	0,000004
1445152_at			**-1,7**	0,001997
1457189_at			**-1,7**	0,003540
1436791_at	Wnt5a	**wingless-related MMTV integration site 5A**	**-1,7**	0,004496
1441020_at			**-1,7**	0,006760
1426513_at	Rbm28	**RNA binding motif protein 28**	**-1,7**	0,000349
1448138_at	Ppp2r4	**protein phosphatase 2A, regulatory subunit B (PR 53)**	**-1,7**	0,000001
1427831_s_at	Zfp260	**zinc finger protein 260**	**-1,7**	0,001617
1446926_at	Pycard	**PYD and CARD domain containing**	**-1,7**	0,000026
1455087_at	D7Ertd715e	**DNA segment, Chr 7, ERATO Doi 715, expressed**	**-1,7**	0,012384
1451987_at	Arrb2	**arrestin, beta 2**	**-1,7**	0,000023
1417542_at	Rps6ka2	**ribosomal protein S6 kinase, polypeptide 2**	**-1,7**	0,000226
1449110_at	Rhob	**ras homolog gene family, member B**	**-1,7**	0,000016
1452400_a_at	Hoxa11as	**HOXA11 antisense RNA (non-protein coding)**	**-1,7**	0,000540
1442824_at	8030497I03Rik	**RIKEN cDNA 8030497I03 gene**	**-1,7**	0,001292
1442959_at	Birc6	**baculoviral IAP repeat-containing 6**	**-1,7**	0,000926
1426385_x_at	Ywhae	**tyrosine 3-monooxygenase/tryptophan 5-monooxygenase activ**	**-1,7**	0,000000
1448788_at	Cd200	**CD200 antigen**	**-1,7**	0,000036
1416124_at	Ccnd2	**cyclin D2**	**-1,7**	0,001347
1425932_a_at	Cugbp1	**CUG triplet repeat, RNA binding protein 1**	**-1,7**	0,000005
1452772_at	Tnks2	**tankyrase, TRF1-interacting ankyrin-related ADP-ribose polyme**	**-1,7**	0,000196
1429065_at	1200009F10Rik	**RIKEN cDNA 1200009F10 gene**	**-1,7**	0,000538
1424570_at	Ddx46	**DEAD (Asp-Glu-Ala-Asp) box polypeptide 46**	**-1,7**	0,000068
1440896_at			**-1,7**	0,001443
1452430_s_at	Sfrs1	**splicing factor, arginine/serine-rich 1 (ASF/SF2)**	**-1,7**	0,000047
1436796_at	Matr3	**matrin 3**	**-1,7**	0,000039
1431173_at	Fam53b	**family with sequence similarity 53, member B**	**-1,7**	0,001602
1454311_at			**-1,7**	0,002262
1424203_at	Ncln	**nicalin homolog (zebrafish)**	**-1,7**	0,000002
1458213_at			**-1,7**	0,000040
1442843_at	4933411D12Rik	**RIKEN cDNA 4933411D12 gene**	**-1,7**	0,000370
1433742_at	Kank1	**KN motif and ankyrin repeat domains 1**	**-1,7**	0,000023
1430134_a_at	Yars2	**tyrosyl-tRNA synthetase 2 (mitochondrial)**	**-1,7**	0,000295
1446510_at			**-1,7**	0,000197
1428543_at	Ppat	**phosphoribosyl pyrophosphate amidotransferase**	**-1,7**	0,008199
1442111_at	D430033H22Rik	**RIKEN cDNA D430033H22 gene**	**-1,7**	0,000009
1448126_at	Fam60a	**family with sequence similarity 60, member A**	**-1,7**	0,002786
1428854_at	Tmed8	**transmembrane emp24 domain containing 8**	**-1,7**	0,001523
1418032_at	Itfg2	**integrin alpha FG-GAP repeat containing 2**	**-1,7**	0,000020
1418397_at	Zfp275	**zinc finger protein 275**	**-1,7**	0,000184
1446504_at			**-1,7**	0,000063
1423488_at	Mmd	**monocyte to macrophage differentiation-associated**	**-1,7**	0,000643
1457173_at			**-1,8**	0,002016
1442464_at	Fbxl20	**F-box and leucine-rich repeat protein 20**	**-1,8**	0,000040
1448630_a_at	Sdhc	**succinate dehydrogenase complex, subunit C, integral membra**	**-1,8**	0,000001
1458156_at	E230012J19Rik	**RIKEN cDNA E230012J19 gene**	**-1,8**	0,009952
1423750_a_at	Sf1	**splicing factor 1**	**-1,8**	0,000000
1460579_at	Dnpep	**aspartyl aminopeptidase**	**-1,8**	0,001726
1416774_at	Wee1	**WEE 1 homolog 1 (S. pombe)**	**-1,8**	0,000739
1425587_a_at	Ptprj	**protein tyrosine phosphatase, receptor type, J**	**-1,8**	0,000558
1457468_at			**-1,8**	0,000428
1434034_at	Cerk	**ceramide kinase**	**-1,8**	0,000005
1423832_at	Prkag2	**protein kinase, AMP-activated, gamma 2 non-catalytic subunit**	**-1,8**	0,000982
1416140_a_at	Dhx30	**DEAH (Asp-Glu-Ala-His) box polypeptide 30**	**-1,8**	0,000004
1424407_s_at	Cbx6	**chromobox homolog 6**	**-1,8**	0,010261
1424665_at	Gpatch8	**G patch domain containing 8**	**-1,8**	0,000116
1417062_at	Armc10	**armadillo repeat containing 10**	**-1,8**	0,001520
1430808_at	Tbc1d5	**TBC1 domain family, member 5**	**-1,8**	0,000006
1417686_at	Lgals12	**lectin, galactose binding, soluble 12**	**-1,8**	0,000105
1427049_s_at	Smo	**smoothened homolog (Drosophila)**	**-1,8**	0,002885
1428560_at	Xpo5	**exportin 5**	**-1,8**	0,000296
1455030_at	Ptprj	**protein tyrosine phosphatase, receptor type, J**	**-1,8**	0,000244
1434618_at	Crebzf	**CREB/ATF bZIP transcription factor**	**-1,8**	0,001334
1425273_s_at	Emp2	**epithelial membrane protein 2**	**-1,8**	0,000817
1434741_at	Rreb1	**ras responsive element binding protein 1**	**-1,8**	0,000022
1448124_at	Gusb	**glucuronidase, beta**	**-1,8**	0,007636
1422576_at	Atxn10	**ataxin 10**	**-1,8**	0,001026
1428708_x_at	Ptms	**parathymosin**	**-1,8**	0,000000
1420650_at	Zfhx3	**zinc finger homeobox 3**	**-1,8**	0,001803
1443721_x_at	Sbno2	**strawberry notch homolog 2 (Drosophila)**	**-1,8**	0,000067
1430485_at	Trpc2	**transient receptor potential cation channel, subfamily C, memb**	**-1,8**	0,008250
1460016_at	Tmem164	**transmembrane protein 164**	**-1,8**	0,000029
1439553_s_at	Nutf2	**nuclear transport factor 2**	**-1,8**	0,001274
1442358_at	AA409587	**expressed sequence AA409587**	**-1,8**	0,001122
1459150_at			**-1,8**	0,002729
1430163_at	Rab43	**RAB43, member RAS oncogene family**	**-1,8**	0,000088
1435934_at	Ndufab1	**NADH dehydrogenase (ubiquinone) 1, alpha/beta subcomplex,**	**-1,8**	0,002395
1444520_at	Fryl	**furry homolog-like (Drosophila)**	**-1,8**	0,000002
1447109_at			**-1,8**	0,002409
1421972_s_at	Hcfc1	**host cell factor C1**	**-1,8**	0,000007
1439705_at			**-1,8**	0,000038
1447944_at	Zkscan1	**zinc finger with KRAB and SCAN domains 1**	**-1,8**	0,000271
1442603_at			**-1,8**	0,000696
1441445_at	Per3	**period homolog 3 (Drosophila)**	**-1,8**	0,001139
1435087_at	Zfp362	**zinc finger protein 362**	**-1,8**	0,000023
1454686_at	6430706D22Rik	**RIKEN cDNA 6430706D22 gene**	**-1,8**	0,000001
1448698_at	Ccnd1	**cyclin D1**	**-1,8**	0,000144
1448796_s_at	Tbrg4	**transforming growth factor beta regulated gene 4**	**-1,8**	0,000009
1426863_at	Rbmx	**RNA binding motif protein, X chromosome**	**-1,8**	0,007141
1444973_at			**-1,8**	0,001317
1458111_at	Fam20b	**family with sequence similarity 20, member B**	**-1,8**	0,000017

1441411_at	Lims1	**LIM and senescent cell antigen-like domains 1**	**-1,8**	0,000340
1450843_a_at	Serpinh1	**serine (or cysteine) peptidase inhibitor, clade H, member 1**	**-1,8**	0,000266
1441140_at			**-1,8**	0,001100
1458069_at			**-1,8**	0,000596
1438244_at	Nfib	**nuclear factor I/B**	**-1,8**	0,000130
1426956_a_at	Trp53bp1	**transformation related protein 53 binding protein 1**	**-1,8**	0,002049
1440965_at	Pigl	**phosphatidylinositol glycan anchor biosynthesis, class L**	**-1,8**	0,001863
1427251_at	Atp2a2	**ATPase, Ca++ transporting, cardiac muscle, slow twitch 2**	**-1,8**	0,000007
1423924_s_at	Tspan14	**tetraspanin 14**	**-1,8**	0,000052
1452251_at	Nbea	**neurobeachin**	**-1,8**	0,001815
1430700_a_at	Pla2g7	**phospholipase A2, group VII (platelet-activating factor acetylhy**	**-1,8**	0,012075
1426555_at	Scpep1	**serine carboxypeptidase 1**	**-1,8**	0,000002
1451364_at	Polr3gl	**polymerase (RNA) III (DNA directed) polypeptide G like**	**-1,8**	0,000002
1434448_at	Txlna	**taxilin alpha**	**-1,8**	0,000001
1447150_at	Mycbp2	**MYC binding protein 2**	**-1,8**	0,002113
1422769_at	Syncrip	**synaptotagmin binding, cytoplasmic RNA interacting protein**	**-1,8**	0,001346
1440513_at	C80258	**expressed sequence C80258**	**-1,8**	0,001075
1417176_at	Csnk1e	**casein kinase 1, epsilon**	**-1,8**	0,002135
1455854_a_at	Ssh1	**slingshot homolog 1 (Drosophila)**	**-1,8**	0,000101
1422064_a_at	Zbtb20	**zinc finger and BTB domain containing 20**	**-1,8**	0,000003
1452057_at	Actr1b	**ARP1 actin-related protein 1 homolog B, centractin beta (yeast**	**-1,8**	0,000004
1438839_a_at	Ywhae	**tyrosine 3-monooxygenase/tryptophan 5-monooxygenase activ**	**-1,8**	0,000000
1417623_at	Slc12a2	**solute carrier family 12, member 2**	**-1,8**	0,009263
1421018_at	1110018J18Rik	**RIKEN cDNA 1110018J18 gene**	**-1,8**	0,000070
1438437_a_at	4933439C10Rik	**RIKEN cDNA 4933439C10 gene**	**-1,8**	0,001174
1446719_at	Atad2b	**ATPase family, AAA domain containing 2B**	**-1,8**	0,000050
1454120_a_at	Pcgf6	**polycomb group ring finger 6**	**-1,8**	0,009071
1458299_s_at	Nfkbie	**nuclear factor of kappa light polypeptide gene enhancer in B-c**	**-1,8**	0,000033
1459003_at	Fhl1	**four and a half LIM domains 1**	**-1,8**	0,000324
1423141_at	Lipa	**lysosomal acid lipase A**	**-1,8**	0,006750
1442556_at			**-1,8**	0,000503
1416203_at	Aqp1	**aquaporin 1**	**-1,8**	0,001984
1426801_at	sep-08	**septin 8**	**-1,8**	0,000002
1453740_a_at	Ccnl2	**cyclin L2**	**-1,8**	0,001109
1416514_a_at	Fscn1	**fascin homolog 1, actin bundling protein (Strongylocentrotus p**	**-1,8**	0,013679
1439090_at	Tbc1d23	**TBC1 domain family, member 23**	**-1,8**	0,000114
1448767_s_at	Gjb1	**gap junction protein, beta 1**	**-1,8**	0,000008
1457292_at	Taf1d	**TATA box binding protein (Tbp)-associated factor, RNA polyme**	**-1,8**	0,014550
1442470_at			**-1,8**	0,000096
1436366_at	Ppp1r15b	**protein phosphatase 1, regulatory (inhibitor) subunit 15b**	**-1,8**	0,000455
1417975_at	Kpna4	**karyopherin (importin) alpha 4**	**-1,8**	0,000001
1449271_a_at	Hebp2	**heme binding protein 2**	**-1,8**	0,015176
1442811_at	Rgmb	**RGM domain family, member B**	**-1,8**	0,001520
1440416_at			**-1,8**	0,000015
1445900_at			**-1,8**	0,000075
1440660_at			**-1,8**	0,003431
1417030_at	Tmem206	**transmembrane protein 206**	**-1,8**	0,004206
1418499_a_at	Kcne3	**potassium voltage-gated channel, Isk-related subfamily, gene 3**	**-1,8**	0,012274
1439041_at	Slc39a10	**solute carrier family 39 (zinc transporter), member 10**	**-1,8**	0,002271
1429719_at	Foxp4	**forkhead box P4**	**-1,8**	0,000000
1440038_at	B430007K19Rik	**RIKEN cDNA B430007K19 gene**	**-1,8**	0,002023
1420816_at	Ywhag	**tyrosine 3-monooxygenase/tryptophan 5-monooxygenase activ**	**-1,8**	0,000000
1416818_at	Parva	**parvin, alpha**	**-1,8**	0,000126
1459315_at			**-1,8**	0,000082
1416661_at	Eif3a	**eukaryotic translation initiation factor 3, subunit A**	**-1,8**	0,000022
1458385_at	Hspa4l	**heat shock protein 4 like**	**-1,8**	0,000148
1436907_at	Nav1	**neuron navigator 1**	**-1,8**	0,004198
1424062_at	Ube2d1	**ubiquitin-conjugating enzyme E2D 1, UBC4/5 homolog (yeast)**	**-1,8**	0,000084
1439580_at	B930053N05Rik	**RIKEN cDNA B930053N05 gene**	**-1,8**	0,003301
1455218_at	6330503K22Rik	**RIKEN cDNA 6330503K22 gene**	**-1,8**	0,004536
1442107_at	Flnb	**filamin, beta**	**-1,8**	0,003276
1424772_at	H2afj	**H2A histone family, member J**	**-1,8**	0,000004
1456043_at	Usp22	**ubiquitin specific peptidase 22**	**-1,8**	0,000064
1458708_at			**-1,8**	0,000623
1449041_a_at	Trip6	**thyroid hormone receptor interactor 6**	**-1,8**	0,000495
1427152_at	Qser1	**glutamine and serine rich 1**	**-1,8**	0,000910
1448056_at	Huwe1	**HECT, UBA and WWE domain containing 1**	**-1,8**	0,000048
1456553_at			**-1,8**	0,002069
1460032_at			**-1,8**	0,000112
1455101_at	Phactr2	**phosphatase and actin regulator 2**	**-1,8**	0,000009
1460549_a_at	Cdc23	**CDC23 (cell division cycle 23, yeast, homolog)**	**-1,8**	0,000011
1458414_at	D2Ertd93e	**DNA segment, Chr 2, ERATO Doi 93, expressed**	**-1,8**	0,000070
1455655_a_at	Tardbp	**TAR DNA binding protein**	**-1,8**	0,002629
1424332_at	Rab40c	**Rab40c, member RAS oncogene family**	**-1,8**	0,001473
1457214_at			**-1,8**	0,000312
1435343_at	Dock10	**dedicator of cytokinesis 10**	**-1,8**	0,013942
1460403_at	Psip1	**PC4 and SFRS1 interacting protein 1**	**-1,8**	0,006355
1430039_at	Cdkal1	**CDK5 regulatory subunit associated protein 1-like 1**	**-1,8**	0,000014
1450983_at	Akap8	**A kinase (PRKA) anchor protein 8**	**-1,8**	0,000091
1428430_at	Rgmb	**RGM domain family, member B**	**-1,8**	0,000002
1443258_at	Foxp1	**forkhead box P1**	**-1,8**	0,000013
1452708_a_at	Luc7l	**Luc7 homolog (S. cerevisiae)-like**	**-1,8**	0,005856
1440465_at			**-1,8**	0,000039
1452482_at	Erbb3	**v-erb-b2 erythroblastic leukemia viral oncogene homolog 3 (av**	**-1,8**	0,003235
1419654_at	Tle3	**transducin-like enhancer of split 3, homolog of Drosophila E(sp**	**-1,8**	0,000004
1426692_at	Ccdc97	**coiled-coil domain containing 97**	**-1,8**	0,000002
1432344_a_at	Aplp2	**amyloid beta (A4) precursor-like protein 2**	**-1,8**	0,000214
1454636_at	Cbx5	**chromobox homolog 5 (Drosophila HP1a)**	**-1,8**	0,000211
1426849_at	Sec24b	**Sec24 related gene family, member B (S. cerevisiae)**	**-1,8**	0,000356
1453319_at	Ccar1	**cell division cycle and apoptosis regulator 1**	**-1,8**	0,006277
1416792_at	Ppm1g	**protein phosphatase 1G (formerly 2C), magnesium-dependent,**	**-1,8**	0,000001
1425461_at	Fbxw11	**F-box and WD-40 domain protein 11**	**-1,8**	0,000003
1450781_at	Hmga2	**high mobility group AT-hook 2**	**-1,8**	0,000065
1440139_at			**-1,8**	0,003256
1447615_at			**-1,8**	0,000864
1443522_s_at	Phip	**pleckstrin homology domain interacting protein**	**-1,8**	0,001687
1460342_s_at	Mprip	**myosin phosphatase Rho interacting protein**	**-1,8**	0,000120
1445618_at			**-1,8**	0,003776
1448012_at	C76336	**expressed sequence C76336**	**-1,8**	0,000018
1427956_at	Pcgf1	**polycomb group ring finger 1**	**-1,8**	0,000006
1439802_at	Stk35	**serine/threonine kinase 35**	**-1,8**	0,000006
1433776_at	Lhfp	**lipoma HMGIC fusion partner**	**-1,8**	0,004187
1446892_at			**-1,8**	0,002123
1441894_s_at	Grasp	**GRP1 (general receptor for phosphoinositides 1)-associated sc**	**-1,8**	0,000073
1427844_a_at	Cebpb	**CCAAT/enhancer binding protein (C/EBP), beta**	**-1,8**	0,004515
1428732_at	1700008J07Rik	**RIKEN cDNA 1700008J07 gene**	**-1,8**	0,000003

1440586_at	B430203I24Rik	**RIKEN cDNA B430203I24 gene**	**-1,8**	0,000060
1455084_x_at	Shmt2	**serine hydroxymethyltransferase 2 (mitochondrial)**	**-1,8**	0,000303
1437775_at	Dlst	**dihydrolipoamide S-succinyltransferase (E2 component of 2-o**	**-1,8**	0,000077
1427414_at	Prkar2a	**protein kinase, cAMP dependent regulatory, type II alpha**	**-1,8**	0,000015
1435460_at	Prkg2	**protein kinase, cGMP-dependent, type II**	**-1,8**	0,013502
1434922_at	Phf12	**PHD finger protein 12**	**-1,8**	0,000026
1436508_at	Mlec	**malectin**	**-1,8**	0,000009
1448780_at	Slc12a2	**solute carrier family 12, member 2**	**-1,8**	0,003922
1454881_s_at	Upk3b	**uroplakin 3B**	**-1,8**	0,005580
1458703_at			**-1,8**	0,000194
1455874_at	Tmem179b	**transmembrane protein 179B**	**-1,8**	0,002335
1416959_at	Nr1d2	**nuclear receptor subfamily 1, group D, member 2**	**-1,8**	0,000328
1435349_at	Nrp2	**neuropilin 2**	**-1,8**	0,000558
1417293_at	Hs6st1	**heparan sulfate 6-O-sulfotransferase 1**	**-1,8**	0,000002
1450382_at	Nf2	**neurofibromatosis 2**	**-1,8**	0,000001
1449554_at	Tle3	**transducin-like enhancer of split 3, homolog of Drosophila E(s**	**-1,8**	0,000018
1449268_at	Gfpt1	**glutamine fructose-6-phosphate transaminase 1**	**-1,8**	0,000014
1440490_at			**-1,8**	0,000001
1427397_at	2810046L04Rik	**RIKEN cDNA 2810046L04 gene**	**-1,8**	0,000014
1443153_at			**-1,8**	0,000031
1444764_at	A130022J21Rik	**RIKEN cDNA A130022J21 gene**	**-1,8**	0,000023
1435905_at	D3Ertd300e	**DNA segment, Chr 3, ERATO Doi 300, expressed**	**-1,8**	0,000025
1439344_at			**-1,8**	0,000359
1435889_at	Mark2	**MAP/microtubule affinity-regulating kinase 2**	**-1,8**	0,000222
1417057_a_at	Ppid	**peptidylprolyl isomerase D (cyclophilin D)**	**-1,8**	0,000674
1446299_at			**-1,8**	0,000745
1435122_x_at	Dnmt1	**DNA methyltransferase (cytosine-5) 1**	**-1,8**	0,009088
1428065_at	Slc44a2	**solute carrier family 44, member 2**	**-1,8**	0,000125
1438208_at	Taok2	**TAO kinase 2**	**-1,8**	0,000008
1422681_at	Ctr9	**Ctr9, Paf1/RNA polymerase II complex component, homolog (S**	**-1,8**	0,000015
1417476_at	Fbxw5	**F-box and WD-40 domain protein 5**	**-1,8**	0,000011
1447034_at			**-1,8**	0,002261
1426381_at	Pprc1	**peroxisome proliferative activated receptor, gamma, coactivat**	**-1,8**	0,001866
1460259_s_at	Clca2	**chloride channel calcium activated 2**	**-1,8**	0,000009
1444785_at			**-1,8**	0,000094
1435338_at	Cdk6	**cyclin-dependent kinase 6**	**-1,8**	0,000631
1438888_at	Gmcl1	**germ cell-less homolog 1 (Drosophila)**	**-1,8**	0,000255
1424048_a_at	Cyb5r1	**cytochrome b5 reductase 1**	**-1,8**	0,000032
1452237_at	Agfg1	**ArfGAP with FG repeats 1**	**-1,8**	0,002759
1436524_at	4833438C02Rik	**RIKEN cDNA 4833438C02 gene**	**-1,8**	0,000007
1454106_a_at	Cxxc1	**CXXC finger 1 (PHD domain)**	**-1,8**	0,000002
1424556_at	Pycr1	**pyrroline-5-carboxylate reductase 1**	**-1,8**	0,002415
1431530_a_at	Tspan5	**tetraspanin 5**	**-1,8**	0,000135
1439572_at			**-1,8**	0,001152
1422474_at	Pde4b	**phosphodiesterase 4B, cAMP specific**	**-1,8**	0,000361
1425993_a_at	Hsph1	**heat shock 105kDa/110kDa protein 1**	**-1,8**	0,006020
1457339_at			**-1,8**	0,001687
1419838_s_at	Plk4	**polo-like kinase 4 (Drosophila)**	**-1,8**	0,013632
1426117_a_at	Slc19a2	**solute carrier family 19 (thiamine transporter), member 2**	**-1,8**	0,000009
1419248_at	Rgs2	**regulator of G-protein signaling 2**	**-1,8**	0,000197
1442171_at	Prpf40a	**PRP40 pre-mRNA processing factor 40 homolog A (yeast)**	**-1,8**	0,000252
1460113_at	B930093H17Rik	**RIKEN cDNA B930093H17 gene**	**-1,8**	0,000005
1439931_at	Gsk3b	**glycogen synthase kinase 3 beta**	**-1,8**	0,000012
1428850_x_at	Cd99	**CD99 antigen**	**-1,8**	0,000007
1439305_at			**-1,8**	0,000026
1451956_a_at	Sigmar1	**sigma non-opioid intracellular receptor 1**	**-1,8**	0,000007
1433751_at	Slc39a10	**solute carrier family 39 (zinc transporter), member 10**	**-1,8**	0,010990
1424375_s_at	Gimap4	**GTPase, IMAP family member 4**	**-1,8**	0,009208
1437283_at	Tnpo2	**transportin 2 (importin 3, karyopherin beta 2b)**	**-1,8**	0,000000
1438916_x_at	6720401G13Rik	**RIKEN cDNA 6720401G13 gene**	**-1,8**	0,005139
1418727_at	Nup155	**nucleoporin 155**	**-1,8**	0,009575
1439773_at	Ly6e	**lymphocyte antigen 6 complex, locus E**	**-1,8**	0,004133
1423430_at	Mybbp1a	**MYB binding protein (P160) 1a**	**-1,8**	0,000042
1441482_at	Map2k6	**mitogen-activated protein kinase kinase 6**	**-1,8**	0,012957
1443115_at			**-1,8**	0,001503
1444231_at			**-1,8**	0,000892
1454817_at	Utp18	**UTP18, small subunit (SSU) processome component, homolog**	**-1,8**	0,004522
1438802_at	Foxp1	**forkhead box P1**	**-1,8**	0,000580
1424760_a_at	Smyd2	**SET and MYND domain containing 2**	**-1,8**	0,000319
1437667_a_at	Bach2	**BTB and CNC homology 2**	**-1,8**	0,000086
1452905_at	Meg3	**maternally expressed 3**	**-1,8**	0,001167
1451104_a_at	Snrnp70	**small nuclear ribonucleoprotein 70 (U1)**	**-1,8**	0,001109
1416295_a_at	Il2rg	**interleukin 2 receptor, gamma chain**	**-1,8**	0,005165
1420505_a_at	Stxbp1	**syntaxin binding protein 1**	**-1,8**	0,000097
1451115_at	Pias3	**protein inhibitor of activated STAT 3**	**-1,8**	0,000003
1434031_at	Zfp692	**zinc finger protein 692**	**-1,8**	0,000115
1432372_a_at	Spr	**sepiapterin reductase**	**-1,8**	0,000029
1419185_a_at	Mlxipl	**MLX interacting protein-like**	**-1,8**	0,000007
1431031_at	Arid4b	**AT rich interactive domain 4B (RBP1-like)**	**-1,8**	0,000311
1444150_at	Epb4.1	**erythrocyte protein band 4.1**	**-1,8**	0,000135
1441145_at	Phf21a	**PHD finger protein 21A**	**-1,8**	0,002293
1430920_at	Trmt11	**tRNA methyltransferase 11 homolog (S. cerevisiae)**	**-1,8**	0,000019
1442538_at			**-1,8**	0,000296
1455269_a_at	Coro1a	**coronin, actin binding protein 1A**	**-1,8**	0,009756
1456758_at	9930017N22Rik	**RIKEN cDNA 9930017N22 gene**	**-1,8**	0,000014
1428281_at	Trub1	**TruB pseudouridine (psi) synthase homolog 1 (E. coli)**	**-1,8**	0,000051
1458648_at	AU042950	**expressed sequence AU042950**	**-1,8**	0,000049
1456659_at	LOC552902	**hypothetical LOC552902**	**-1,8**	0,001805
1457047_at			**-1,8**	0,000981
1424544_at	Nrbp2	**nuclear receptor binding protein 2**	**-1,9**	0,000183
1443755_at			**-1,9**	0,000039
1423831_at	Prkag2	**protein kinase, AMP-activated, gamma 2 non-catalytic subunit**	**-1,9**	0,000013
1448881_at	Hp	**haptoglobin**	**-1,9**	0,005092
1434296_at	BC049349	**cDNA sequence BC049349**	**-1,9**	0,000012
1447096_at			**-1,9**	0,001918
1442309_at			**-1,9**	0,000034
1423723_s_at	Tardbp	**TAR DNA binding protein**	**-1,9**	0,004280
1451799_at	Ccdc25	**coiled-coil domain containing 25**	**-1,9**	0,000296
1458426_at			**-1,9**	0,000289
1438751_at	Slc30a10	**solute carrier family 30, member 10**	**-1,9**	0,001175
1448096_at	Ogfod1	**2-oxoglutarate and iron-dependent oxygenase domain containi**	**-1,9**	0,000826
1455521_at	Klf12	**Kruppel-like factor 12**	**-1,9**	0,002764
1448646_at	Wdr12	**WD repeat domain 12**	**-1,9**	0,002206
1424040_at	Mtap7d1	**microtubule-associated protein 7 domain containing 1**	**-1,9**	0,000015
1446474_at			**-1,9**	0,000007
1459701_x_at			**-1,9**	0,000019

1443489_at			**-1,9**	0,000070
1431118_at	6720427H10Rik	**RIKEN cDNA 6720427H10 gene**	**-1,9**	0,000009
1434847_at	Cnnm4	**cyclin M4**	**-1,9**	0,000627
1416184_s_at	Hmga1	**high mobility group AT-hook 1**	**-1,9**	0,000003
1457746_at			**-1,9**	0,000005
1452154_at	Iars	**isoleucine-tRNA synthetase**	**-1,9**	0,000848
1448346_at	Cfl1	**cofilin 1, non-muscle**	**-1,9**	0,000002
1457913_at	5730601F06Rik	**RIKEN cDNA 5730601F06 gene**	**-1,9**	0,011078
1427708_a_at	Nf2	**neurofibromatosis 2**	**-1,9**	0,000663
1432108_at	Pcgf6	**polycomb group ring finger 6**	**-1,9**	0,001312
1443167_at			**-1,9**	0,000982
1440799_s_at	Farp2	**FERM, RhoGEF and pleckstrin domain protein 2**	**-1,9**	0,000384
1416484_at	Ttc3	**tetratricopeptide repeat domain 3**	**-1,9**	0,000505
1445867_at	AL023008	**expressed sequence AL023008**	**-1,9**	0,000084
1415836_at	Aldh18a1	**aldehyde dehydrogenase 18 family, member A1**	**-1,9**	0,000002
1433806_x_at	Calr	**calreticulin**	**-1,9**	0,000004
1424927_at	Glipr1	**GLI pathogenesis-related 1 (glioma)**	**-1,9**	0,012266
1447929_at	Ssh3	**slingshot homolog 3 (Drosophila)**	**-1,9**	0,000000
1427978_at	4732418C07Rik	**RIKEN cDNA 4732418C07 gene**	**-1,9**	0,000000
1460096_at			**-1,9**	0,000042
1417655_a_at	Ars2	**arsenate resistance protein 2**	**-1,9**	0,000022
1456328_at	Bank1	**B-cell scaffold protein with ankyrin repeats 1**	**-1,9**	0,007419
1426533_at	Nop56	**NOP56 ribonucleoprotein homolog (yeast)**	**-1,9**	0,004610
1457356_at			**-1,9**	0,000244
1444372_at			**-1,9**	0,000092
1440464_at	Elavl1	**ELAV (embryonic lethal, abnormal vision, Drosophila)-like 1 (H**	**-1,9**	0,001259
1443624_at			**-1,9**	0,000344
1418167_at	Tcfap4	**transcription factor AP4**	**-1,9**	0,000001
1423161_s_at	Spred1	**sprouty protein with EVH-1 domain 1, related sequence**	**-1,9**	0,000092
1442239_at			**-1,9**	0,000125
1456514_at			**-1,9**	0,000117
1436729_at	Afap1	**actin filament associated protein 1**	**-1,9**	0,000979
1447122_at	Psmd1	**proteasome (prosome, macropain) 26S subunit, non-ATPase, 1**	**-1,9**	0,000228
1436456_at	Slc38a9	**solute carrier family 38, member 9**	**-1,9**	0,000630
1456916_at	Nsd1	**nuclear receptor-binding SET-domain protein 1**	**-1,9**	0,000736
1444506_at			**-1,9**	0,001276
1423143_at	Gtpbp4	**GTP binding protein 4**	**-1,9**	0,001747
1430388_a_at	Sulf2	**sulfatase 2**	**-1,9**	0,000006
1425634_a_at	Tnk1	**tyrosine kinase, non-receptor, 1**	**-1,9**	0,000024
1416871_at	Adam8	**a disintegrin and metallopeptidase domain 8**	**-1,9**	0,015271
1448019_at	Taok3	**TAO kinase 3**	**-1,9**	0,000254
1437917_at	D530037H12Rik	**RIKEN cDNA D530037H12 gene**	**-1,9**	0,000418
1448221_at	Bat1a	**HLA-B-associated transcript 1A**	**-1,9**	0,000071
1428207_at	Bcl7a	**B-cell CLL/lymphoma 7A**	**-1,9**	0,005081
1435381_at	2610110G12Rik	**RIKEN cDNA 2610110G12 gene**	**-1,9**	0,000605
1421958_at	L1cam	**L1 cell adhesion molecule**	**-1,9**	0,000799
1443554_at	Ssbp3	**single-stranded DNA binding protein 3**	**-1,9**	0,003256
1442473_at			**-1,9**	0,001107
1420881_at	Acd	**adrenocortical dysplasia**	**-1,9**	0,000001
1458309_at			**-1,9**	0,000012
1434118_at	Mul1	**mitochondrial ubiquitin ligase activator of NFKB 1**	**-1,9**	0,000019
1433491_at	Epb4.1l2	**erythrocyte protein band 4.1-like 2**	**-1,9**	0,000923
1418070_at	Cdyl	**chromodomain protein, Y chromosome-like**	**-1,9**	0,000010
1457302_at			**-1,9**	0,002339
1442632_at			**-1,9**	0,001868
1450854_at	Pa2g4	**proliferation-associated 2G4**	**-1,9**	0,000402
1446001_at			**-1,9**	0,003211
1458618_at			**-1,9**	0,000144
1434908_at	Scaf1	**SR-related CTD-associated factor 1**	**-1,9**	0,000014
1417381_at	C1qa	**complement component 1, q subcomponent, alpha polypeptid**	**-1,9**	0,009906
1428772_at	Xpot	**exportin, tRNA (nuclear export receptor for tRNAs)**	**-1,9**	0,001310
1419032_at	Papola	**poly (A) polymerase alpha**	**-1,9**	0,000144
1441558_at	D230044B12Rik	**RIKEN cDNA D230044B12 gene**	**-1,9**	0,000351
1416814_at	Tia1	**cytotoxic granule-associated RNA binding protein 1**	**-1,9**	0,008406
1454665_at	Irf2bp2	**interferon regulatory factor 2 binding protein 2**	**-1,9**	0,000985
1446861_at	Gns	**glucosamine (N-acetyl)-6-sulfatase**	**-1,9**	0,000035
1450704_at	Ihh	**Indian hedgehog**	**-1,9**	0,000011
1450839_at	D0H4S114	**DNA segment, human D4S114**	**-1,9**	0,003908
1434191_at	Tmem195	**transmembrane protein 195**	**-1,9**	0,004079
1457072_at	Bcl11a	**B-cell CLL/lymphoma 11A (zinc finger protein)**	**-1,9**	0,010050
1457369_at			**-1,9**	0,000000
1445340_at	Mycbp2	**MYC binding protein 2**	**-1,9**	0,004028
1427322_at	Brwd1	**bromodomain and WD repeat domain containing 1**	**-1,9**	0,000486
1415798_at	Ddr1	**discoidin domain receptor family, member 1**	**-1,9**	0,000017
1419655_at	Tle3	**transducin-like enhancer of split 3, homolog of Drosophila E(s**	**-1,9**	0,000009
1421026_at	Gna12	**guanine nucleotide binding protein, alpha 12**	**-1,9**	0,000201
1427883_a_at	Col3a1	**collagen, type III, alpha 1**	**-1,9**	0,010875
1457593_at	2610202C22Rik	**RIKEN cDNA 2610202C22 gene**	**-1,9**	0,000018
1442916_at			**-1,9**	0,000798
1416614_at	Eid1	**EP300 interacting inhibitor of differentiation 1**	**-1,9**	0,000005
1452690_at	Khsrp	**KH-type splicing regulatory protein**	**-1,9**	0,000003
1449944_a_at	Sec61a2	**Sec61, alpha subunit 2 (S. cerevisiae)**	**-1,9**	0,000067
1452560_a_at	Nfya	**nuclear transcription factor-Y alpha**	**-1,9**	0,000009
1453399_at	Ccnt2	**cyclin T2**	**-1,9**	0,000011
1431993_a_at	Rnf38	**ring finger protein 38**	**-1,9**	0,000008
1448375_at	Tm9sf3	**transmembrane 9 superfamily member 3**	**-1,9**	0,000002
1448117_at	Kitl	**kit ligand**	**-1,9**	0,000121
1449202_at	Sema4g	**sema domain, immunoglobulin domain (Ig), transmembrane do**	**-1,9**	0,000001
1425233_at	2210407C18Rik	**RIKEN cDNA 2210407C18 gene**	**-1,9**	0,010084
1452336_at	Zfp395	**zinc finger protein 395**	**-1,9**	0,000002
1452377_at	Mll1	**myeloid/lymphoid or mixed-lineage leukemia 1**	**-1,9**	0,000293
1450116_at	D3Ertd300e	**DNA segment, Chr 3, ERATO Doi 300, expressed**	**-1,9**	0,000131
1418893_at	Pbx2	**pre B-cell leukemia transcription factor 2**	**-1,9**	0,000001
1442150_at			**-1,9**	0,000058
1450757_at	Cdh11	**cadherin 11**	**-1,9**	0,001662
1448617_at	Cd53	**CD53 antigen**	**-1,9**	0,013069
1437500_at	Noc3l	**nucleolar complex associated 3 homolog (S. cerevisiae)**	**-1,9**	0,000027
1454254_s_at	1600029D21Rik	**RIKEN cDNA 1600029D21 gene**	**-1,9**	0,003318
1437188_at	Gabbr1	**gamma-aminobutyric acid (GABA-B) receptor, 1**	**-1,9**	0,000008
1445201_at	Zfp53	**zinc finger protein 53**	**-1,9**	0,000905
1420984_at	Pctp	**phosphatidylcholine transfer protein**	**-1,9**	0,000029
1426501_a_at	Tifa	**TRAF-interacting protein with forkhead-associated domain**	**-1,9**	0,000568
1460205_at	Dcakd	**dephospho-CoA kinase domain containing**	**-1,9**	0,000010
1418202_a_at	Wiz	**widely-interspaced zinc finger motifs**	**-1,9**	0,000001
1450986_at	Nop58	**NOP58 ribonucleoprotein homolog (yeast)**	**-1,9**	0,008738
1456170_x_at	Calr	**calreticulin**	**-1,9**	0,000000

1438058_s_at	Ptov1	**prostate tumor over expressed gene 1**	**-1,9**	0,000000
1426458_at	Slmap	**sarcolemma associated protein**	**-1,9**	0,000007
1441684_at	Ttc3	**tetratricopeptide repeat domain 3**	**-1,9**	0,003045
1420834_at	Vamp2	**vesicle-associated membrane protein 2**	**-1,9**	0,000003
1422321_a_at	Sf1	**splicing factor 1**	**-1,9**	0,000001
1427099_at	Maz	**MYC-associated zinc finger protein (purine-binding transcriptic**	**-1,9**	0,000001
1458233_at	Fryl	**furry homolog-like (Drosophila)**	**-1,9**	0,001041
1420924_at	Timp2	**tissue inhibitor of metalloproteinase 2**	**-1,9**	0,000909
1422440_at	Cdk4	**cyclin-dependent kinase 4**	**-1,9**	0,008642
1455831_at	Fus	**fusion, derived from t(12;16) malignant liposarcoma (human)**	**-1,9**	0,000554
1456715_at			**-1,9**	0,003593
1422850_at	Pabpn1	**poly(A) binding protein, nuclear 1**	**-1,9**	0,001545
1430356_at	2210402A03Rik	**RIKEN cDNA 2210402A03 gene**	**-1,9**	0,000007
1439545_at			**-1,9**	0,000020
1420824_at	Sema4d	**sema domain, immunoglobulin domain (Ig), transmembrane do**	**-1,9**	0,000011
1419276_at	Enpp1	**ectonucleotide pyrophosphatase/phosphodiesterase 1**	**-1,9**	0,000011
1426963_at	Pacs2	**phosphofurin acidic cluster sorting protein 2**	**-1,9**	0,000653
1444716_at	Mettl2	**methyltransferase like 2**	**-1,9**	0,000724
1455778_at	Zfp192	**zinc finger protein 192**	**-1,9**	0,001502
1420479_a_at	Nap1l1	**nucleosome assembly protein 1-like 1**	**-1,9**	0,009219
1459442_at			**-1,9**	0,000001
1459091_at			**-1,9**	0,000955
1435744_at	6720401G13Rik	**RIKEN cDNA 6720401G13 gene**	**-1,9**	0,003917
1453311_at	2310008B10Rik	**RIKEN cDNA 2310008B10 gene**	**-1,9**	0,000679
1420619_a_at	Aes	**amino-terminal enhancer of split**	**-1,9**	0,000000
1456526_at	C130034I24Rik	**RIKEN cDNA C130034I24 gene**	**-1,9**	0,000126
1415983_at	Lcp1	**lymphocyte cytosolic protein 1**	**-1,9**	0,000005
1435520_at	Msi2	**Musashi homolog 2 (Drosophila)**	**-1,9**	0,000005
1451229_at	Hdac11	**histone deacetylase 11**	**-1,9**	0,000021
1448127_at	Rrm1	**ribonucleotide reductase M1**	**-1,9**	0,010715
1437000_at	Dgkq	**diacylglycerol kinase, theta**	**-1,9**	0,000009
1417015_at	Rassf3	**Ras association (RalGDS/AF-6) domain family member 3**	**-1,9**	0,000015
1437078_at	Vps52	**vacuolar protein sorting 52 (yeast)**	**-1,9**	0,000108
1454142_a_at	Pwp1	**PWP1 homolog (S. cerevisiae)**	**-1,9**	0,000047
1429246_a_at	Anxa6	**annexin A6**	**-1,9**	0,012762
1449401_at	C1qc	**complement component 1, q subcomponent, C chain**	**-1,9**	0,008703
1426538_a_at	Trp53	**transformation related protein 53**	**-1,9**	0,000001
1440381_at	2410085M17Rik	**RIKEN cDNA 2410085M17 gene**	**-1,9**	0,000408
1421355_at	Tgm3	**transglutaminase 3, E polypeptide**	**-1,9**	0,000069
1423162_s_at	Spred1	**sprouty protein with EVH-1 domain 1, related sequence**	**-2,0**	0,000001
1453414_at	Ypel2	**yippee-like 2 (Drosophila)**	**-2,0**	0,000281
1453988_a_at	Ide	**insulin degrading enzyme**	**-2,0**	0,000005
1446598_at			**-2,0**	0,000166
1442761_at			**-2,0**	0,000273
1424794_at	Rnf186	**ring finger protein 186**	**-2,0**	0,000291
1421070_at	D3Ertd300e	**DNA segment, Chr 3, ERATO Doi 300, expressed**	**-2,0**	0,000299
1431362_a_at	Smoc2	**SPARC related modular calcium binding 2**	**-2,0**	0,008301
1449120_a_at	Pcm1	**pericentriolar material 1**	**-2,0**	0,000002
1430177_at	Ube2b	**ubiquitin-conjugating enzyme E2B, RAD6 homology (S. cerevis**	**-2,0**	0,000571
1454268_a_at	Cyba	**cytochrome b-245, alpha polypeptide**	**-2,0**	0,000417
1445387_at	Senp6	**SUMO/sentrin specific peptidase 6**	**-2,0**	0,000036
1424281_at	Ubap2	**ubiquitin-associated protein 2**	**-2,0**	0,000000
1457793_a_at	Whsc1l1	**Wolf-Hirschhorn syndrome candidate 1-like 1 (human)**	**-2,0**	0,000001
1449029_at	Mknk2	**MAP kinase-interacting serine/threonine kinase 2**	**-2,0**	0,000000
1451034_at	Zfp36l2	**zinc finger protein 36, C3H type-like 2**	**-2,0**	0,000004
1447402_at			**-2,0**	0,000011
1442484_at	D9Ertd306e	**DNA segment, Chr 9, ERATO Doi 306, expressed**	**-2,0**	0,000468
1450914_at	Ppp1r14b	**protein phosphatase 1, regulatory (inhibitor) subunit 14B**	**-2,0**	0,001316
1441956_s_at	Cux1	**cut-like homeobox 1**	**-2,0**	0,000677
1453074_at	Dusp23	**dual specificity phosphatase 23**	**-2,0**	0,000259
1436902_x_at	Tmsb10	**thymosin, beta 10**	**-2,0**	0,000001
1456904_at			**-2,0**	0,000145
1428869_at	Nolc1	**nucleolar and coiled-body phosphoprotein 1**	**-2,0**	0,000527
1443534_at			**-2,0**	0,000078
1434804_at	Exoc6b	**exocyst complex component 6B**	**-2,0**	0,000004
1456223_at			**-2,0**	0,000095
1429477_at	Ncaph2	**non-SMC condensin II complex, subunit H2**	**-2,0**	0,000704
1452226_at	Rcc2	**regulator of chromosome condensation 2**	**-2,0**	0,004644
1423757_x_at	Igfbp4	**insulin-like growth factor binding protein 4**	**-2,0**	0,013663
1416572_at	Mmp14	**matrix metallopeptidase 14 (membrane-inserted)**	**-2,0**	0,000266
1434166_at	9330151L19Rik	**RIKEN cDNA 9330151L19 gene**	**-2,0**	0,000520
1416362_a_at	Fkbp4	**FK506 binding protein 4**	**-2,0**	0,000051
1457848_at			**-2,0**	0,000002
1423746_at	Txndc5	**thioredoxin domain containing 5**	**-2,0**	0,000001
1457944_at			**-2,0**	0,000534
1449005_at	Slc16a3	**solute carrier family 16 (monocarboxylic acid transporters), me**	**-2,0**	0,000306
1416998_at	Rrs1	**RRS1 ribosome biogenesis regulator homolog (S. cerevisiae)**	**-2,0**	0,000101
1446621_at			**-2,0**	0,000093
1448748_at	Plek	**pleckstrin**	**-2,0**	0,012564
1424259_at	Lmf1	**lipase maturation factor 1**	**-2,0**	0,000011
1436427_at	Prpf4b	**PRP4 pre-mRNA processing factor 4 homolog B (yeast)**	**-2,0**	0,002367
1415977_at	Isyna1	**myo-inositol 1-phosphate synthase A1**	**-2,0**	0,000027
1416365_at	Hsp90ab1	**heat shock protein 90 alpha (cytosolic), class B member 1**	**-2,0**	0,000015
1417175_at	Csnk1e	**casein kinase 1, epsilon**	**-2,0**	0,000770
1439537_at			**-2,0**	0,000090
1429332_at	4632427E13Rik	**RIKEN cDNA 4632427E13 gene**	**-2,0**	0,000006
1459433_at	C130051F05Rik	**RIKEN cDNA C130051F05 gene**	**-2,0**	0,000139
1450377_at	Thbs1	**thrombospondin 1**	**-2,0**	0,000056
1424938_at	Steap1	**six transmembrane epithelial antigen of the prostate 1**	**-2,0**	0,004091
1435981_at	Nav2	**neuron navigator 2**	**-2,0**	0,000167
1430418_at	Tmem57	**transmembrane protein 57**	**-2,0**	0,000288
1458972_at	9330112F22Rik	**RIKEN cDNA 9330112F22 gene**	**-2,0**	0,000036
1421267_a_at	Cited2	**Cbp/p300-interacting transactivator, with Glu/Asp-rich carboxy**	**-2,0**	0,000001
1439619_at	Tcf12	**transcription factor 12**	**-2,0**	0,002775
1452139_at	Slc35c1	**solute carrier family 35, member C1**	**-2,0**	0,000002
1446692_at			**-2,0**	0,000013
1417219_s_at	Tmsb10	**thymosin, beta 10**	**-2,0**	0,000000
1460116_s_at	Spred1	**sprouty protein with EVH-1 domain 1, related sequence**	**-2,0**	0,000065
1442418_at	B930096F20Rik	**RIKEN cDNA B930096F20 gene**	**-2,0**	0,000141
1434077_at	Wdr37	**WD repeat domain 37**	**-2,0**	0,000003
1448842_at	Cdo1	**cysteine dioxygenase 1, cytosolic**	**-2,0**	0,012853
1460210_at	Pkd1	**polycystic kidney disease 1 homolog**	**-2,0**	0,000000
1435162_at	Prkg2	**protein kinase, cGMP-dependent, type II**	**-2,0**	0,010413
1454247_a_at	Gpa33	**glycoprotein A33 (transmembrane)**	**-2,0**	0,000001
1446508_at			**-2,0**	0,000001
1419257_at	Tcea1	**transcription elongation factor A (SII) 1**	**-2,0**	0,000074

1443332_at			**-2,0**	0,004935
1460565_at	Slc41a1	**solute carrier family 41, member 1**	**-2,0**	0,000295
1440294_at			**-2,0**	0,000071
1434784_s_at	Tmem106c	**transmembrane protein 106C**	**-2,0**	0,000001
1451199_at	Qtrtd1	**queuine tRNA-ribosyltransferase domain containing 1**	**-2,0**	0,002877
1419522_at	Zmynd19	**zinc finger, MYND domain containing 19**	**-2,0**	0,000040
1429870_at	Tnik	**TRAF2 and NCK interacting kinase**	**-2,0**	0,006291
1436919_at	Trp53i11	**transformation related protein 53 inducible protein 11**	**-2,0**	0,000011
1422972_s_at	Kat2a	**K(lysine) acetyltransferase 2A**	**-2,0**	0,000001
1442056_at			**-2,0**	0,001717
1417658_at	Tbrg4	**transforming growth factor beta regulated gene 4**	**-2,0**	0,000001
1420653_at	Tgfb1	**transforming growth factor, beta 1**	**-2,0**	0,000026
1440615_at	Dusp16	**dual specificity phosphatase 16**	**-2,0**	0,000020
1431096_at	Ints8	**integrator complex subunit 8**	**-2,0**	0,000175
1454090_at	Pdss1	**prenyl (solanesyl) diphosphate synthase, subunit 1**	**-2,0**	0,000000
1420833_at	Vamp2	**vesicle-associated membrane protein 2**	**-2,0**	0,000016
1419168_at	Mapk6	**mitogen-activated protein kinase 6**	**-2,0**	0,000000
1444042_at	Trip11	**thyroid hormone receptor interactor 11**	**-2,0**	0,000003
1423325_at	Pnn	**pinin**	**-2,0**	0,000193
1449080_at	Hdac2	**histone deacetylase 2**	**-2,0**	0,002875
1457188_at			**-2,0**	0,000012
1417814_at	Pla2g5	**phospholipase A2, group V**	**-2,0**	0,000185
1428557_a_at	Ormdl1	**ORM1-like 1 (S. cerevisiae)**	**-2,0**	0,000437
1452427_s_at	Ptplad1	**protein tyrosine phosphatase-like A domain containing 1**	**-2,0**	0,000129
1438686_at	Eif4g1	**eukaryotic translation initiation factor 4, gamma 1**	**-2,0**	0,000001
1431061_s_at	Peli1	**pellino 1**	**-2,0**	0,000000
1458065_at			**-2,0**	0,000239
1455548_at	Dlgap4	**discs, large homolog-associated protein 4 (Drosophila)**	**-2,0**	0,000000
1421224_a_at	Hnf1b	**HNF1 homeobox B**	**-2,0**	0,000000
1450747_at	Keap1	**kelch-like ECH-associated protein 1**	**-2,0**	0,000032
1436871_at	Sfrs7	**splicing factor, arginine/serine-rich 7**	**-2,0**	0,003940
1429088_at	Lbh	**limb-bud and heart**	**-2,0**	0,000001
1460218_at	Cd52	**CD52 antigen**	**-2,0**	0,003816
1424198_at	Dlg5	**discs, large homolog 5 (Drosophila)**	**-2,0**	0,000010
1448590_at	Col6a1	**collagen, type VI, alpha 1**	**-2,0**	0,001071
1439123_at			**-2,0**	0,000202
1433586_at	Rgmb	**RGM domain family, member B**	**-2,0**	0,000005
1436318_at	Tardbp	**TAR DNA binding protein**	**-2,0**	0,000556
1443846_x_at			**-2,0**	0,000015
1436232_a_at	Gabpb1	**GA repeat binding protein, beta 1**	**-2,0**	0,000000
1444445_at	C77648	**expressed sequence C77648**	**-2,0**	0,000086
1421811_at	Thbs1	**thrombospondin 1**	**-2,0**	0,006431
1445827_at	Prkcbp1	**protein kinase C binding protein 1**	**-2,0**	0,000206
1445178_at	Sh3rf1	**SH3 domain containing ring finger 1**	**-2,0**	0,002888
1456063_at	Fam120c	**family with sequence similarity 120, member C**	**-2,0**	0,000102
1423087_a_at	Tomm6	**translocase of outer mitochondrial membrane 6 homolog (yeas**	**-2,0**	0,000000
1451331_at	Ppp1r1b	**protein phosphatase 1, regulatory (inhibitor) subunit 1B**	**-2,0**	0,000001
1417253_at	Frg1	**FSHD region gene 1**	**-2,0**	0,000000
1448603_at	Srpk2	**serine/arginine-rich protein specific kinase 2**	**-2,0**	0,000001
1424668_a_at	Cux1	**cut-like homeobox 1**	**-2,0**	0,000000
1423121_at	Ide	**insulin degrading enzyme**	**-2,0**	0,000001
1443355_at			**-2,0**	0,000636
1422249_s_at	Zfa	**zinc finger protein, autosomal**	**-2,0**	0,000612
1428142_at	Etv5	**ets variant gene 5**	**-2,0**	0,010199
1423004_at	Vipr1	**vasoactive intestinal peptide receptor 1**	**-2,0**	0,000153
1440040_at			**-2,0**	0,003431
1441359_at	Zcchc11	**zinc finger, CCHC domain containing 11**	**-2,0**	0,000012
1441505_at			**-2,1**	0,000049
1427408_a_at	Thrap3	**thyroid hormone receptor associated protein 3**	**-2,1**	0,000000
1441125_at	Setd5	**SET domain containing 5**	**-2,1**	0,000039
1436321_at	B3gnt7	**UDP-GlcNAc:betaGal beta-1,3-N-acetylglucosaminyltransferase**	**-2,1**	0,000292
1434644_at	Tbl1x	**transducin (beta)-like 1 X-linked**	**-2,1**	0,000006
1457262_at	Smg1	**SMG1 homolog, phosphatidylinositol 3-kinase-related kinase (**	**-2,1**	0,000000
1417232_at	Cldn2	**claudin 2**	**-2,1**	0,000321
1444333_at			**-2,1**	0,000100
1420699_at	Clec7a	**C-type lectin domain family 7, member a**	**-2,1**	0,002664
1457812_at	Trp53bp1	**transformation related protein 53 binding protein 1**	**-2,1**	0,005441
1453234_at	1300002K09Rik	**RIKEN cDNA 1300002K09 gene**	**-2,1**	0,000033
1441475_at			**-2,1**	0,000131
1451884_a_at	Lsm2	**LSM2 homolog, U6 small nuclear RNA associated (S. cerevisia**	**-2,1**	0,000000
1422528_a_at	Zfp36l1	**zinc finger protein 36, C3H type-like 1**	**-2,1**	0,000000
1445341_at			**-2,1**	0,000227
1423357_at	2610209A20Rik	**RIKEN cDNA 2610209A20 gene**	**-2,1**	0,001263
1441272_at	Matr3	**matrin 3**	**-2,1**	0,000029
1428069_at	Cdca7	**cell division cycle associated 7**	**-2,1**	0,002715
1446182_at			**-2,1**	0,000103
1449845_a_at	Ephb4	**Eph receptor B4**	**-2,1**	0,000000
1456955_at			**-2,1**	0,000029
1431235_at	Matr3	**matrin 3**	**-2,1**	0,000000
1427048_at	Smo	**smoothened homolog (Drosophila)**	**-2,1**	0,000069
1440372_at			**-2,1**	0,000021
1438700_at	Fnbp4	**formin binding protein 4**	**-2,1**	0,000193
1415871_at	Tgfbi	**transforming growth factor, beta induced**	**-2,1**	0,000038
1420762_a_at	Ybx2	**Y box protein 2**	**-2,1**	0,000000
1422705_at	Pmepa1	**prostate transmembrane protein, androgen induced 1**	**-2,1**	0,006721
1424081_at	Pcgf6	**polycomb group ring finger 6**	**-2,1**	0,000316
1442224_at			**-2,1**	0,000022
1446143_at			**-2,1**	0,000002
1436515_at	Bach2	**BTB and CNC homology 2**	**-2,1**	0,000072
1440123_at			**-2,1**	0,000007
1418824_at	Arf6	**ADP-ribosylation factor 6**	**-2,1**	0,000007
1422854_at	Shc1	**src homology 2 domain-containing transforming protein C1**	**-2,1**	0,000003
1421118_a_at	Gpr56	**G protein-coupled receptor 56**	**-2,1**	0,000000
1434554_at	Trim37	**tripartite motif-containing 37**	**-2,1**	0,001400
1437798_at	6720422M22Rik	**RIKEN cDNA 6720422M22 gene**	**-2,1**	0,003899
1452899_at	Rian	**RNA imprinted and accumulated in nucleus**	**-2,1**	0,000419
1443444_at			**-2,1**	0,000012
1440254_at	100041277	**predicted gene, 100041277**	**-2,1**	0,001202
1449551_at	Myo1c	**myosin IC**	**-2,1**	0,000000
1431830_at	Zfp329	**zinc finger protein 329**	**-2,1**	0,000160
1456547_at			**-2,1**	0,000049
1420946_at	Atrx	**alpha thalassemia/mental retardation syndrome X-linked homo**	**-2,1**	0,000899
1438069_a_at	Rbm5	**RNA binding motif protein 5**	**-2,1**	0,000356
1433485_x_at	Gpr56	**G protein-coupled receptor 56**	**-2,1**	0,000000
1418835_at	Phlda1	**pleckstrin homology-like domain, family A, member 1**	**-2,1**	0,008178
1450089_a_at	Srprb	**signal recognition particle receptor, B subunit**	**-2,1**	0,000000

1430837_a_at	Mbd1	**methyl-CpG binding domain protein 1**	**-2,1**	0,000000
1425711_a_at	Akt1	**thymoma viral proto-oncogene 1**	**-2,1**	0,000000
1417632_at	Atp6v0a1	**ATPase, H+ transporting, lysosomal V0 subunit A1**	**-2,1**	0,000001
1444890_at			**-2,1**	0,000464
1427739_a_at	Trp53	**transformation related protein 53**	**-2,1**	0,000001
1418830_at	Cd79a	**CD79A antigen (immunoglobulin-associated alpha)**	**-2,1**	0,004599
1452811_at	Atic	**5-aminoimidazole-4-carboxamide ribonucleotide formyltransfe**	**-2,1**	0,000000
1431175_at	1810019D21Rik	**RIKEN cDNA 1810019D21 gene**	**-2,1**	0,000467
1436736_x_at	D0H4S114	**DNA segment, human D4S114**	**-2,1**	0,007208
1428319_at	Pdlim7	**PDZ and LIM domain 7**	**-2,1**	0,002488
1420975_at	Baz1b	**bromodomain adjacent to zinc finger domain, 1B**	**-2,1**	0,000001
1443158_at			**-2,1**	0,000017
1425276_at	Fbrs	**fibrosin**	**-2,1**	0,000000
1442336_at			**-2,2**	0,000000
1442316_x_at	Trp53bp1	**transformation related protein 53 binding protein 1**	**-2,2**	0,000155
1420893_a_at	Tgfbr1	**transforming growth factor, beta receptor I**	**-2,2**	0,000027
1460279_a_at	Gtf2i	**general transcription factor II I**	**-2,2**	0,000027
1428513_at	Calcoco1	**calcium binding and coiled coil domain 1**	**-2,2**	0,000000
1435477_s_at	Fcgr2b	**Fc receptor, IgG, low affinity IIb**	**-2,2**	0,004341
1446618_at	LOC432971	**hypothetical gene supported by AK038224**	**-2,2**	0,000009
1437431_at	Cux1	**cut-like homeobox 1**	**-2,2**	0,000057
1439948_at	BC046401	**cDNA sequence BC046401**	**-2,2**	0,000626
1443509_at			**-2,2**	0,000058
1450743_s_at	Syncrip	**synaptotagmin binding, cytoplasmic RNA interacting protein**	**-2,2**	0,000197
1434852_at	Pla2g2f	**phospholipase A2, group IIF**	**-2,2**	0,000005
1442700_at	Pde4b	**phosphodiesterase 4B, cAMP specific**	**-2,2**	0,001242
1456849_at			**-2,2**	0,000025
1438245_at	Nfib	**nuclear factor I/B**	**-2,2**	0,000039
1420747_at	Ppnr	**per-pentamer repeat gene**	**-2,2**	0,000198
1428909_at	A130040M12Rik	**RIKEN cDNA A130040M12 gene**	**-2,2**	0,000066
1439950_at	Dync1h1	**dynein cytoplasmic 1 heavy chain 1**	**-2,2**	0,000006
1438402_at	Fam171a1	**family with sequence similarity 171, member A1**	**-2,2**	0,000010
1427037_at	Eif4g1	**eukaryotic translation initiation factor 4, gamma 1**	**-2,2**	0,000000
1415922_s_at	Marcksl1	**MARCKS-like 1**	**-2,2**	0,008574
1455878_at	2700023E23Rik	**RIKEN cDNA 2700023E23 gene**	**-2,2**	0,004043
1448692_at	Ubqln4	**ubiquilin 4**	**-2,2**	0,000000
1448916_at	Mafg	**v-maf musculoaponeurotic fibrosarcoma oncogene family, pro**	**-2,2**	0,000145
1439136_at			**-2,2**	0,000090
1456632_at	Bcl11a	**B-cell CLL/lymphoma 11A (zinc finger protein)**	**-2,2**	0,006576
1415824_at	Scd2	**stearoyl-Coenzyme A desaturase 2**	**-2,2**	0,000024
1445866_at	Mast4	**microtubule associated serine/threonine kinase family membe**	**-2,2**	0,000004
1417326_a_at	Anapc11	**anaphase promoting complex subunit 11**	**-2,2**	0,000000
1426596_a_at	Smn1	**survival motor neuron 1**	**-2,2**	0,000000
1431206_at	5730601F06Rik	**RIKEN cDNA 5730601F06 gene**	**-2,2**	0,000424
1421354_at	Prkg2	**protein kinase, cGMP-dependent, type II**	**-2,2**	0,007489
1436967_at	Ankrd11	**ankyrin repeat domain 11**	**-2,2**	0,000029
1452021_a_at	Hes6	**hairy and enhancer of split 6 (Drosophila)**	**-2,2**	0,003228
1450379_at	Msn	**moesin**	**-2,2**	0,000014
1425359_at	Mall	**mal, T-cell differentiation protein-like**	**-2,2**	0,001021
1433587_at	Rgmb	**RGM domain family, member B**	**-2,2**	0,000030
1441373_at			**-2,2**	0,000512
1460672_at	2410002F23Rik	**RIKEN cDNA 2410002F23 gene**	**-2,2**	0,000592
1435608_at	Znrf3	**zinc and ring finger 3**	**-2,2**	0,012041
1459316_at			**-2,2**	0,000035
1448018_at			**-2,2**	0,001874
1445200_at			**-2,2**	0,000725
1453623_a_at	Rad23a	**RAD23a homolog (S. cerevisiae)**	**-2,2**	0,000000
1416106_at	Kti12	**KTI12 homolog, chromatin associated (S. cerevisiae)**	**-2,2**	0,000015
1425698_a_at	Crebzf	**CREB/ATF bZIP transcription factor**	**-2,2**	0,000002
1436869_at	Shh	**sonic hedgehog**	**-2,2**	0,001881
1458358_at	Pank2	**pantothenate kinase 2 (Hallervorden-Spatz syndrome)**	**-2,2**	0,000007
1441481_at	Mfap3l	**microfibrillar-associated protein 3-like**	**-2,2**	0,014794
1434316_at	Chsy1	**chondroitin sulfate synthase 1**	**-2,2**	0,001377
1447408_at			**-2,2**	0,000136
1422846_at	Rbp2	**retinol binding protein 2, cellular**	**-2,2**	0,000001
1442535_at			**-2,2**	0,000091
1428462_at	Ppp2r5e	**protein phosphatase 2, regulatory subunit B (B56), epsilon isof**	**-2,3**	0,000002
1440841_at			**-2,3**	0,000062
1438164_x_at	Flot2	**flotillin 2**	**-2,3**	0,000035
1446550_at	Gspt1	**G1 to S phase transition 1**	**-2,3**	0,000319
1444260_at			**-2,3**	0,001108
1451169_at	Nomo1	**nodal modulator 1**	**-2,3**	0,000000
1440621_at			**-2,3**	0,000039
1438559_x_at	Slc44a2	**solute carrier family 44, member 2**	**-2,3**	0,000107
1458018_at			**-2,3**	0,000025
1439477_at	5430406J06Rik	**RIKEN cDNA 5430406J06 gene**	**-2,3**	0,000002
1419480_at	Sell	**selectin, lymphocyte**	**-2,3**	0,000182
1442992_at	130004C03	**hypothetical LOC403343**	**-2,3**	0,000326
1455060_at	G3bp1	**Ras-GTPase-activating protein SH3-domain binding protein 1**	**-2,3**	0,000008
1427110_at	Raver1	**ribonucleoprotein, PTB-binding 1**	**-2,3**	0,000004
1427797_s_at			**-2,3**	0,000005
1437486_at	Gprc5a	**G protein-coupled receptor, family C, group 5, member A**	**-2,3**	0,000007
1416200_at	Il33	**interleukin 33**	**-2,3**	0,006724
1418587_at	Traf3	**TNF receptor-associated factor 3**	**-2,3**	0,000000
1422559_at	Ube2n	**ubiquitin-conjugating enzyme E2N**	**-2,3**	0,000000
1456993_at	D2Ertd640e	**DNA segment, Chr 2, ERATO Doi 640, expressed**	**-2,3**	0,000016
1460302_at	Thbs1	**thrombospondin 1**	**-2,3**	0,000810
1429192_at	Ski	**ski sarcoma viral oncogene homolog (avian)**	**-2,3**	0,000000
1424667_a_at	Cux1	**cut-like homeobox 1**	**-2,3**	0,000000
1428694_at	5033413D16Rik	**RIKEN cDNA 5033413D16 gene**	**-2,3**	0,001549
1444140_at			**-2,3**	0,000180
1421709_a_at	Fmo5	**flavin containing monooxygenase 5**	**-2,3**	0,003287
1421164_a_at	Arhgef1	**Rho guanine nucleotide exchange factor (GEF) 1**	**-2,3**	0,000009
1440196_at			**-2,3**	0,000182
1442071_at	Abce1	**ATP-binding cassette, sub-family E (OABP), member 1**	**-2,3**	0,001526
1417460_at	Ifitm2	**interferon induced transmembrane protein 2**	**-2,3**	0,000999
1420948_s_at	Atrx	**alpha thalassemia/mental retardation syndrome X-linked homo**	**-2,3**	0,000397
1450834_at	Fut4	**fucosyltransferase 4**	**-2,3**	0,000000
1417426_at	Srgn	**serglycin**	**-2,3**	0,006102
1424117_at	BC056474	**cDNA sequence BC056474**	**-2,3**	0,000000
1442067_at			**-2,3**	0,000176
1423129_at	Shoc2	**soc-2 (suppressor of clear) homolog (C. elegans)**	**-2,3**	0,000000
1421149_a_at	Atn1	**atrophin 1**	**-2,3**	0,000000
1422439_a_at	Cdk4	**cyclin-dependent kinase 4**	**-2,3**	0,007011
1442903_at	4732423E21Rik	**RIKEN cDNA 4732423E21 gene**	**-2,4**	0,001925
1440773_at			**-2,4**	0,000003

1427903_at	Phpt1	**phosphohistidine phosphatase 1**	**-2,4**	0,000009
1427008_at	Rnf43	**ring finger protein 43**	**-2,4**	0,009681
1436222_at	Gas5	**growth arrest specific 5**	**-2,4**	0,009639
1450792_at	Tyrobp	**TYRO protein tyrosine kinase binding protein**	**-2,4**	0,000007
1417063_at	C1qb	**complement component 1, q subcomponent, beta polypeptide**	**-2,4**	0,007557
1437733_at	Eif4ebp2	**eukaryotic translation initiation factor 4E binding protein 2**	**-2,4**	0,000000
1428777_at	Spred1	**sprouty protein with EVH-1 domain 1, related sequence**	**-2,4**	0,000000
1423566_a_at	Hsph1	**heat shock 105kDa/110kDa protein 1**	**-2,4**	0,000379
1448797_at	Elk3	**ELK3, member of ETS oncogene family**	**-2,4**	0,011654
1448160_at	Lcp1	**lymphocyte cytosolic protein 1**	**-2,4**	0,000003
1418591_at	Dnaja4	**DnaJ (Hsp40) homolog, subfamily A, member 4**	**-2,4**	0,000196
1433756_at	S100pbp	**S100P binding protein**	**-2,4**	0,000046
1448766_at	Gjb1	**gap junction protein, beta 1**	**-2,4**	0,000001
1423760_at	Cd44	**CD44 antigen**	**-2,4**	0,007276
1441615_at	Cbfa2t2	**core-binding factor, runt domain, alpha subunit 2, translocated**	**-2,4**	0,000085
1458676_at	Nktr	**natural killer tumor recognition sequence**	**-2,4**	0,000001
1457383_at			**-2,4**	0,000000
1449956_at	Prkce	**protein kinase C, epsilon**	**-2,4**	0,000241
1420394_s_at	Lilrb4	**leukocyte immunoglobulin-like receptor, subfamily B, member**	**-2,4**	0,009649
1429169_at	Rbm3	**RNA binding motif protein 3**	**-2,4**	0,015359
1417821_at	D17H6S56E-5	**DNA segment, Chr 17, human D6S56E 5**	**-2,4**	0,005630
1420643_at	Lfng	**LFNG O-fucosylpeptide 3-beta-N-acetylglucosaminyltransferas**	**-2,4**	0,000009
1415935_at	Smoc2	**SPARC related modular calcium binding 2**	**-2,4**	0,008087
1447147_at			**-2,4**	0,003647
1452911_at	Spred1	**sprouty protein with EVH-1 domain 1, related sequence**	**-2,4**	0,000002
1437400_at	Nedd4l	**neural precursor cell expressed, developmentally down-regula**	**-2,5**	0,000001
1452841_at	Pgm2l1	**phosphoglucomutase 2-like 1**	**-2,5**	0,011822
1421789_s_at	Arf3	**ADP-ribosylation factor 3**	**-2,5**	0,000033
1432646_a_at	2900097C17Rik	**RIKEN cDNA 2900097C17 gene**	**-2,5**	0,000022
1454904_at	Mtm1	**X-linked myotubular myopathy gene 1**	**-2,5**	0,001372
1422135_at	Zfp146	**zinc finger protein 146**	**-2,5**	0,000165
1429555_at	Cldnd1	**claudin domain containing 1**	**-2,5**	0,000004
1443095_at			**-2,5**	0,000059
1448710_at	Cxcr4	**chemokine (C-X-C motif) receptor 4**	**-2,5**	0,000002
1424179_at	Plekhj1	**pleckstrin homology domain containing, family J member 1**	**-2,5**	0,000000
1455904_at	Gas5	**growth arrest specific 5**	**-2,5**	0,008137
1442675_at			**-2,5**	0,002387
1436541_at	2310008H09Rik	**RIKEN cDNA 2310008H09 gene**	**-2,5**	0,000012
1418468_at	Anxa11	**annexin A11**	**-2,5**	0,000001
1437052_s_at	Slc2a3	**solute carrier family 2 (facilitated glucose transporter), membe**	**-2,5**	0,004548
1417470_at	Apobec3	**apolipoprotein B mRNA editing enzyme, catalytic polypeptide 3**	**-2,5**	0,000168
1443027_at			**-2,5**	0,000386
1417228_at	Capn1	**calpain 1**	**-2,5**	0,000001
1459942_at			**-2,5**	0,000005
1448482_at	Slc39a8	**solute carrier family 39 (metal ion transporter), member 8**	**-2,5**	0,000037
1448749_at	Plek	**pleckstrin**	**-2,5**	0,000826
1445390_at	Pawr	**PRKC, apoptosis, WT1, regulator**	**-2,5**	0,000000
1455246_at	Smarcc1	**SWI/SNF related, matrix associated, actin dependent regulator**	**-2,5**	0,000405
1437627_at	Mex3d	**mex3 homolog D (C. elegans)**	**-2,5**	0,000235
1428010_at	Timm9	**translocase of inner mitochondrial membrane 9 homolog (yeas**	**-2,5**	0,000112
1452235_at	Man1b1	**mannosidase, alpha, class 1B, member 1**	**-2,6**	0,000000
1435655_at	Rpl12	**ribosomal protein L12**	**-2,6**	0,000424
1446130_at			**-2,6**	0,000266
1418524_at	Pcm1	**pericentriolar material 1**	**-2,6**	0,000002
1435152_at	Leng8	**leukocyte receptor cluster (LRC) member 8**	**-2,6**	0,000004
1416246_a_at	Coro1a	**coronin, actin binding protein 1A**	**-2,6**	0,000506
1459443_at			**-2,6**	0,000430
1457781_at	Kcnq1ot1	**KCNQ1 overlapping transcript 1**	**-2,6**	0,000585
1437325_x_at	Aldh18a1	**aldehyde dehydrogenase 18 family, member A1**	**-2,6**	0,000006
1431385_a_at	Mbtps1	**membrane-bound transcription factor peptidase, site 1**	**-2,6**	0,000002
1427747_a_at	Lcn2	**lipocalin 2**	**-2,6**	0,000740
1425716_s_at	Bak1	**BCL2-antagonist/killer 1**	**-2,6**	0,000003
1423754_at	Ifitm3	**interferon induced transmembrane protein 3**	**-2,6**	0,011114
1441797_at			**-2,6**	0,000021
1452483_a_at	Cd44	**CD44 antigen**	**-2,6**	0,000409
1448029_at	Tbx3	**T-box 3**	**-2,7**	0,002106
1455195_at	Rps24	**ribosomal protein S24**	**-2,7**	0,001936
1434357_a_at	Kpnb1	**karyopherin (importin) beta 1**	**-2,7**	0,000000
1443837_x_at	Bcl2	**B-cell leukemia/lymphoma 2**	**-2,7**	0,000362
1455740_at	Hnrnpa1	**heterogeneous nuclear ribonucleoprotein A1**	**-2,7**	0,000306
1421262_at	Lipg	**lipase, endothelial**	**-2,7**	0,000006
1419728_at	Cxcl5	**chemokine (C-X-C motif) ligand 5**	**-2,7**	0,005692
1430332_a_at	Gusb	**glucuronidase, beta**	**-2,7**	0,000122
1460650_at	Atp6v0a1	**ATPase, H+ transporting, lysosomal V0 subunit A1**	**-2,7**	0,000007
1434376_at	Cd44	**CD44 antigen**	**-2,7**	0,005388
1457084_at	Nlrp9b	**NLR family, pyrin domain containing 9B**	**-2,7**	0,000001
1419398_a_at	Reep5	**receptor accessory protein 5**	**-2,8**	0,000000
1418015_at	Pum2	**pumilio 2 (Drosophila)**	**-2,8**	0,000000
1452163_at	Ets1	**E26 avian leukemia oncogene 1, 5' domain**	**-2,8**	0,003713
1443341_at			**-2,8**	0,000000
1416568_a_at	Acin1	**apoptotic chromatin condensation inducer 1**	**-2,8**	0,000000
1427979_at	4732418C07Rik	**RIKEN cDNA 4732418C07 gene**	**-2,8**	0,000000
1436713_s_at	Meg3	**maternally expressed 3**	**-2,8**	0,000003
1418570_at	Ncstn	**nicastrin**	**-2,8**	0,000000
1441480_at	7120451J01Rik	**RIKEN cDNA 7120451J01 gene**	**-2,8**	0,000000
1458161_at	Kcnq1ot1	**KCNQ1 overlapping transcript 1**	**-2,8**	0,000088
1437405_a_at	Igfbp4	**insulin-like growth factor binding protein 4**	**-2,9**	0,008826
1450903_at	Rad23b	**RAD23b homolog (S. cerevisiae)**	**-2,9**	0,000000
1422853_at	Shc1	**src homology 2 domain-containing transforming protein C1**	**-2,9**	0,000000
1426208_x_at	Plagl1	**pleiomorphic adenoma gene-like 1**	**-2,9**	0,010471
1439068_at	Erap1	**endoplasmic reticulum aminopeptidase 1**	**-2,9**	0,000000
1439740_s_at	Uck2	**uridine-cytidine kinase 2**	**-2,9**	0,000006
1417440_at	Arid1a	**AT rich interactive domain 1A (SWI-like)**	**-3,0**	0,000000
1431214_at	LOC67527	**murine leukemia retrovirus**	**-3,1**	0,000000
1427385_s_at	Actn1	**actinin, alpha 1**	**-3,1**	0,000000
1445111_at			**-3,1**	0,000004
1423756_s_at	Igfbp4	**insulin-like growth factor binding protein 4**	**-3,1**	0,008142
1419313_at	Ccnt1	**cyclin T1**	**-3,2**	0,000000
1449370_at	Sox4	**SRY-box containing gene 4**	**-3,2**	0,003259
1417229_at	Capn1	**calpain 1**	**-3,2**	0,000000
1423060_at	Pa2g4	**proliferation-associated 2G4**	**-3,2**	0,000000
1450188_s_at	Lipg	**lipase, endothelial**	**-3,2**	0,000000
1437443_at	EG620382	**predicted gene, EG620382**	**-3,2**	0,000000
1460423_x_at	Igkv1-117	**immunoglobulin kappa chain variable 1-117**	**-3,2**	0,000431
1435664_at	Zfp397	**zinc finger protein 397**	**-3,3**	0,000011
1416239_at	Ass1	**argininosuccinate synthetase 1**	**-3,3**	0,000000

1415854_at	Kitl	**kit ligand**	**-3,3**	0,000000
1449184_at	Pglyrp1	**peptidoglycan recognition protein 1**	**-3,4**	0,000000
1446595_at	Itsn2	**intersectin 2**	**-3,5**	0,000000
1424254_at	Ifitm1	**interferon induced transmembrane protein 1**	**-3,5**	0,011034
1452415_at	Actn1	**actinin, alpha 1**	**-3,6**	0,000000
1416521_at	Sepw1	**selenoprotein W, muscle 1**	**-3,6**	0,000000
1431213_a_at	LOC67527	**murine leukemia retrovirus**	**-3,7**	0,000000
1459556_at			**-3,8**	0,000000
1419157_at	Sox4	**SRY-box containing gene 4**	**-3,8**	0,002579
1437479_x_at	Tbx3	**T-box 3**	**-3,9**	0,002979
1444258_at			**-3,9**	0,000000
1436780_at	Ogt	**O-linked N-acetylglucosamine (GlcNAc) transferase (UDP-N-ac**	**-4,0**	0,000000
1449552_at	Zfr	**zinc finger RNA binding protein**	**-4,1**	0,000000
1458617_at	Prkcbp1	**protein kinase C binding protein 1**	**-4,5**	0,000003
1426936_at	LOC215866	**hypothetical protein LOC215866**	**-4,7**	0,000698
1442626_at			**-4,8**	0,000000
1418078_at	Psme3	**proteaseome (prosome, macropain) 28 subunit, 3**	**-5,3**	0,000000

CAPÍTOL 6

Caracterització dels canvis metabòlics associats a l'activació angiogènica: identificació de potencials dianes terapèutiques

Els resultats presentats en aquest capítol han estat publicats a la revista *Carcinogenesis* amb un índex d'impacte de 5,402.

Pedro Vizán[1,†], Susana Sánchez-Tena[1], Gema Alcarraz-Vizán[1], Marta Soler[2,‡], Ramon Messeguer[2], M.Dolors Pujol[3], Wai-Nang Paul Lee[4] i Marta Cascante[1]

[1]Facultat de Biologia, Universitat de Barcelona i IBUB, unitat associada al CSIC, 08028 Barcelona, Espanya

[2]Divisió Biomed, Centre Tecnològic Leitat, Parc Científic de Barcelona, 08028 Barcelona, Espanya

[3]Departament de Farmacologia i Química Farmacèutica, Facultat de Farmàcia,

Universitat de Barcelona, 08028 Barcelona, Espanya

[4]Department of Pediatrics and Research and Education Institute, UCLA School of Medicine, Torrance, CA 90502, USA

[†]Adreça actual: Laboratory of Developmental Signalling, Cancer Research UK, London Research Institute, London WC2A 3PX, UK

[‡]Adreça actual: Institut d'Investigació Biomèdica de Bellvitge (IDIBELL), Hospital Duran i Reynals, 08907 1'Hospitalet de Llobregat, Espanya

RESUM

L'angiogènesi és un procés que consisteix en el reclutament de cèl·lules endotelials cap a un estímul angiogènic. Les cèl·lules subsegüentment proliferen i es diferencien per formar capil·lars sanguinis. Es coneix molt poc sobre l'adaptació metabòlica que pateixen les cèl·lules endotelials durant aquesta transformació. En aquest treball es van estudiar els canvis metabòlics en cèl·lules endotelials HUVEC (*Human Umbilical Vascular Endothelial Cells*) activades per factors de creixement, [1,2-$^{13}C_2$]-glucosa i un anàlisi de la distribució isotopomèrica de massa. El metabolisme de la [1,2-$^{13}C_2$]-glucosa per part de les cèl·lules HUVEC ens va permetre traçar les principals vies metabòliques de la glucosa, incloent la síntesi de glicogen, el cicle de les pentoses fosfat i la glicòlisi. L'estimulació endotelial amb VEGF (*Vascular Endothelial Growth Factor*) o FGF (*Fibroblast Growth Factor*) va mostrar una adaptació metabòlica comú basada en aquestes vies. Posteriorment, un inhibidor específic del receptor 2 del VEGF va demostrar la importància de metabolisme de glicogen i del cicle de les pentoses fosfat. A més, es va mostrar que el glicogen era exhaurit en un medi amb glucosa baixa, però, en canvi, era conservat sota condicions d'hipòxia. Finalment, es va demostrar que la inhibició directa dels enzims clau del metabolisme de glicogen i de la ruta de les pentoses fosfat reduïa la viabilitat i la migració de les cèl·lules HUVEC. En aquest sentit, inhibidors d'aquests vies han estat descrits com agents antitumorals. Per tant, els nostres resultats suggereixen que la inhibició d'aquestes vies metabòliques ofereix una nova i potent estratègia terapèutica que simultàniament inhibeix proliferació tumoral i angiogènesi.

Characterization of the metabolic changes underlying growth factor angiogenic activation: identification of new potential therapeutic targets

Pedro Vizán[1], Susana Sánchez-Tena[1], Gema Alcarraz-Vizán[1], Marta Soler[1], Ramón Messeguer[2], M. Dolors Pujol[3], Wai-Nang Paul Lee[4] and Marta Cascante[1,*]

[1]Department of Biochemistry and Molecular Biology, University of Barcelona, Faculty of Biology, Av Diagonal 645, 08028 Barcelona, Spain

[2]Biomed Division, Leitat Technological Center, Parc Científic Barcelona, C/ Baldiri i Reixach 15-21, 08028 Barcelona, Spain

[3]Department of Pharmacology and Pharmaceutical Chemistry, University of Barcelona, Faculty of Pharmacy, Av. Diagonal 643, 08028-Barcelona, Spain

[4]Department of Pediatrics, Research and Education Institute, UCLA School of Medicine, RB1, 1124 West Carson Street, Torrance, California 90502, USA

[†]Present address: Laboratory of Developmental Signalling, Cancer Research UK, London Research Institute, London WC2A 3PX, UK

[‡]Present address: Institut d'Investigació Biomèdica de Bellvitge (IDIBELL), Hospital Duran i Reynals, 08907 1'Hospitalet de Llobregat, Espanya

ABSTRACT

Angiogenesis is a fundamental process to normal and abnormal tissue growth and repair, which consists of recruiting endothelial cells toward an angiogenic stimulus. The cells subsequently proliferate and differentiate to form endothelial tubes and capillary-like structures. Little is known about the metabolic adaptation of endothelial cells through such a transformation. We studied the metabolic changes of endothelial cell activation by growth factors using human umbilical vein endothelial cells (HUVEC), [1,2-$^{13}C_2$]-glucose and mass isotopomer distribution analysis (MIDA). The metabolism of [1,2-$^{13}C_2$]-glucose by HUVEC allows us to trace many of the main glucose metabolic pathways, including glycogen synthesis, the pentose cycle and the glycolytic pathways. So we established that these pathways were crucial to endothelial cell proliferation under vascular endothelial growth factor (VEGF) and fibroblast growth factor (FGF) stimulation. A specific VEGF receptor 2 (VEGFR-2) inhibitor demonstrated the importance of glycogen metabolism and pentose cycle pathway. Furthermore, we showed that glycogen was depleted in a low glucose medium, but conserved under hypoxic conditions. Finally, we demonstrated that direct inhibition of key enzymes to glycogen metabolism and pentose phosphate pathways reduced HUVEC cell viability and migration. In this regard, inhibitors of these pathways have been shown to be effective antitumoral agents. To sum up, our data suggest that the inhibition of metabolic pathways offers a novel and powerful therapeutic approach, which simultaneously inhibits tumor cell proliferation and tumor-induced angiogenesis.

INTRODUCTION

One of the critical stages in tumor growth is neovascularization. The angiogenic impulse is promoted by tumor expression of proangiogenic proteins, including vascular endothelial growth factor (VEGF), fibroblast growth factor (FGF), interleukin-8 (IL-8), platelet-derived growth factor (PDGF) and transforming growth factor beta (TGF-beta), among others. The combined action of these factors on endothelial cells leads to the acquisition of a specific phenotype, which allows endothelial cells to migrate towards an angiogenic stimulus, proliferate and differentiate into capillary-like structures. Concretely, VEGF, which is highly upregulated in most human cancers (Ferrara, 1999), has emerged in the last few years as the crucial rate-limiting step in the regulation of normal and abnormal angiogenesis (Ferrara, 2002). Therefore, VEGF and its receptor have been exploited in antiangiogenic therapies that are already successfully applied in clinical settings (Brekken *et al.*, 2000; Ferrara, 2005; Ferrara *et al.*, 2005). However, although patients treated with VEGF inhibitors may survive longer, there is emerging evidence that VEGF may be replaced by other angiogenic pathways as the disease progresses. Thus, a better understanding of the underlying metabolic changes that supports tumor angiogenesis downstream of VEGF activation is necessary to design complementary strategies that can overcome resistance to angiogenic therapies. In fact, in spite of the increasing recognition that the metabolome represents the end point of many cellular events (Boros *et al.*, 2002; Kell *et al.*, 2005), little is known about the metabolic changes underlying endothelial cell activation during angiogenesis (Dagher *et al.*, 1999; Ido *et al.*, 2002; Gatenby *et al.*, 2003; Mori *et al.*, 2003). A better knowledge of the specific adaptation of metabolic network fluxes occurring downstream of the growth factor activation of endothelial cells could aid identification of metabolic enzyme drug targets. Such targets might help to overcome the developing resistance to VEGF-targeted therapies. Accurate substrate flow characterization of the activated endothelial cells in the angiogenic process may permit the design of effective, targeted antiangiogenic drugs acting downstream of the VEGF receptors.

Metabolic changes underlying tumor cell metabolism have been extensively studied in recent decades (Dang *et al.*, 1999; Mazurek *et al.*, 2003) and successful strategies for inhibiting the pathways on which cancer cells are strongly dependent have been proposed. In particular, inhibition of nucleic acid synthesis has been shown to be successful in chemotherapy (Purcell *et al.*, 2003). Recently, it has been demonstrated in different tumor cell lines that pentose phosphate pathway (PPP) inhibition results in an effective decrease in tumor cell proliferation (Boros *et al.*, 1997; Rais *et al.*, 1999; Comin-Anduix *et al.*, 2001; Boren *et al.*, 2002; Cascante *et al.*, 2002). Moreover, it has been proposed that inhibition of normally enhanced tumor cell glycolysis can be a novel strategy for anticancer treatment (Pelicano *et al.*, 2006) or for

overcoming the drug resistance associated with mitochondrial respiratory defects and hypoxia (Xu *et al.*, 2005; Pelicano *et al.*, 2006).

Stable isotope-based dynamic metabolic profiling using gas chromatography/mass spectrometry (GC/MS) is a powerful new tool of great use in drug development (Boros *et al.*, 2002). In particular, the use of glucose labelled at the first two carbon positions with the stable isotope ^{13}C has been shown to be effective in revealing detailed substrate flow and distribution patterns in the complex metabolic network of different tumoral and non-tumoral cells. Recent examples of the strength of this approach include the elucidation of the metabolic mechanism underlying butyrate-induced cell differentiation (Boren *et al.*, 2003), and the characterization of distinctive metabolic profiles that correlate with different point mutations in K-ras oncogene, which confer different degrees of aggressiveness in vivo, proving how the most aggressive mutations had an increased glycolytic rate (Vizan *et al.*, 2005). In the present study, we used human umbilical vein endothelial cells (HUVEC) as an angiogenic model. We adopted a metabolic isotope distribution analysis (MIDA) approach with [1,2-$^{13}C_2$]-glucose tracer labelling to reveal the mechanisms of endothelial cells' metabolic network in response to the activation produced by the angiogenic stimulus of different growth factors. The metabolism of [1,2-$^{13}C_2$]-glucose by HUVEC allows us to trace many of the main glucose metabolic pathways, including glycogen synthesis, the pentose cycle pathways and the glycolytic pathways. To examine the downstream effect of VEGF, we used a well-known VEGFR-2 (VEGF receptor 2) inhibitor, 5-diarylurea-oxy-benzimidazole, which has also shown effects on Tie-2 receptors (Miyazaki *et al.*, 2007). This inhibitor allowed us to analyze the flux changes downstream of a specific inhibition of the angiogenic stimulus. The characterization of the effects of VEGFR-2 inhibitors at metabolic level contributes to the design of new therapeutic strategies for overcoming drug resistance. Such strategies are based on targeting the appropriate metabolic pathways, which mimic the effect of direct receptor inhibition on the metabolic network.

MATERIALS AND METHODS

Cell culture conditions. Human umbilical vein endothelial cells (HUVEC) (AdvanCell) were cultured on gelatin at 37ºC in a humidified atmosphere of 5% CO_2 and 95% air in endothelial cell basal medium (EBM) (Clonetics), supplemented with EGM SingleQuots (Clonetics) and 10% FCS (Biological Industries). In these standard conditions, a 7.4-fold change with respect to the initial cell number was observed at 72 hours.

Specifically activated cell growth assay for the MIDA analysis. Cells grown to 80-90% confluence were removed from the flask using 0.025% trypsin/EDTA (Gibco) at room

temperature. Cells were seeded at a density of 4×10^5 onto gelatine-precoated 75cm^2 Petri dishes (Falcon) in EGM (5mmol/L glucose), supplemented with EGM SingleQuots and 10% FCS for 24h. The incubation medium was then removed and the plates washed twice with HBSS (Clonetics). Specifically activated cell growth media was then added to the cell culture. This media contained EBM supplemented with 10 ng/ml vascular endothelial growth factor (VEGF) (R&D systems) or 0.3 ng/ml basic fibroblast growth factor (bFGF) plus 2% FCS supplemented with 3 µg/ml heparin, 1µg/ml hydrocortisone and 10 mmol/L of [1,2-$^{13}C_2$]-glucose (50% isotope enrichment, Isotec). The inhibitor of VEGFR-2 5-diarylurea-oxy-benzimidazole was used at a final concentration of 85 nM. Cell cultures were incubated for 72 hours. After the incubations, cells were centrifuged (1350 rpm for 5 minutes) to obtain the incubation medium and cell pellets. At the end of the experiment, the final cell numbers were measured with a haemocytometer. To determine glycogen content, cells were immediately frozen in liquid nitrogen before being processed.

Glucose and lactate concentration. The glucose and lactate concentrations in the culture medium were determined as previously described (Gutmann *et al.*, 1974) using a Cobas Mira Plus chemistry analyzer (HORIBA ABX) at the beginning and the end of the incubation time, to calculate glucose consumption and lactate production.

Lactate isotopomeric analysis. Lactate from the cell culture medium was extracted by ethyl acetate after acidification with HCl. Lactate was derivatized to its propylamide-heptafluorobutyric form and the m/z 328 (carbons 1–3 of lactate, chemical ionization) was monitored as described (Lee *et al.*, 1998).

RNA ribose isotopomeric analysis. RNA ribose was isolated by acid hydrolysis of cellular RNA after Trizol (Invitrogen) purification of cell extracts. Ribose isolated from RNA was derivatized to its aldonitrile acetate form, using hydroxyl-amine in pyridine and acetic anhydride. The ion cluster around the m/z 256 (carbons 1–5 of ribose, chemical ionization) was monitored to find the molar enrichment and positional distribution of ^{13}C labels in ribose (Lee *et al.*, 1998).

Glycogen content determination and isotopomeric analysis. The glycogen content in frozen cell monolayers obtained from HUVEC was extracted as described previously (Boros *et al.*, 2001), by direct digestion of sonicated extracts with amyloglucosidase (Sigma). The glycogen was then purified using a tandem set of Dowex-1X8/ Dowex-50WX8 (Sigma) ion-exchange columns. For the isotopomeric analysis, the glycogen was converted to its glucose aldonitrile pentaacetate derivative, as described previously (Szafranek *et al.*, 1974) and the ion cluster around m/z 328 was monitored. Measurement of the glycogen content was carried out

using the isotopomer [U-^{13}C-D_7]-glucose as the recovery standard and internal standard quantification procedures. The ion cluster for the [U-^{13}C-D_7]-glucose of the glucose aldonitrile pentaacetate derivative was monitored from m/z 339 to m/z 341. Glucose from glycogen was corrected by million of cells.

Gas chromatography/mass spectrometry. Mass spectral data were obtained on an HP5973 mass selective detector connected to an HP6890 gas chromatograph. The settings were as follows: GC inlet 230 °C, transfer line 280 °C, MS source 230 °C, MS quad 150 °C. An HP-5 capillary column (30 m length, 250 mm diameter and 0.25 mm film thickness) was used to analyse glucose, ribose and lactate.

Hypoxic or hypoglycaemic conditions. To determine glycogen content under hypoxic or hypoglycaemic conditions, HUVEC cells were seeded at a density of 1×10^6 onto 75cm^2 Petri dishes (Falcon) in EGM (5 mmol/L glucose) supplemented with EGM SingleQuots and 10% FCS for 24h. The incubation medium was then removed and specifically activated cell growth media added in normoxic (37ºC in a humidified atmosphere of 5% CO_2 and 95% air), hypoxic (37ºC in a humidified atmosphere of 5% CO_2, 1% O_2) or hypoglycaemic conditions (EGM 10 mmol/L glucose as a positive control, DMEM (Sigma) 10 mmol/L glucose supplemented with EGM SingleQuots and 10% FCS as a negative control and DMEM without glucose supplemented with EGM SingleQuots and 10% FCS). Cells were counted after 24 hours. The medium was stored for subsequent analyses of glucose consumption and lactate production, as described above. In parallel, cell monolayers were immediately frozen in liquid nitrogen for glycogen determinations. Glycogen was extracted and quantified as described previously (Lerin *et al.*, 2004), with 30% (w/v) KOH and Whatman 31ET paper to precipitate the glycogen. Glucose released from glycogen was measured enzymatically in a Cobas Mira Plus chemistry analyzer (HORIBA ABX) and then corrected by protein content.

Cell viability assay. This assay was performed using a variation of the method described by Mosmann (Mosmann, 1983), as specified in Matito (Matito *et al.*, 2003). For this assay, 3×10^3 HUVEC cells/well were cultured on 96 well plates. Inhibitors CP-320626, G5 and O1 were added from 10 to 100 μM for 48 hours. Relative cell viability was measured by absorbance on an ELISA plate reader (Tecan Sunrise MR20-301, TECAN) at 550 nm.

Inhibitor CP-320626, kindly provided by Pfizer, is an indole-2-carboxamide that binds at the dimmer interface site of glycogen phosphorylase, which was recently identified as a new allosteric site by X-ray crystallographic analysis (Ekstrom *et al.*, 2002). G5 and O1 were kindly supplied by Jaime Rubio from the University of Barcelona. Molecular modeling has been used

in the development of these novel compounds inhibitors of glucose-6-phosphate dehydrogenase and transketolase, respectively.

Migration assay. Migration assays were performed as described previously (Keely, 2001), with the following modifications: 24-well cell culture plates (Falcon) were used with light-opaque PET membrane filter inserts with 8 mm-pores (Transwell HTS FluoroBlokTM Multiwell Insert Systems from Becton Dickinson). The upper and lower surfaces of the Transwell membranes were coated for 2 hours at 37ºC with 15 µg/ml type I Collagen. HUVEC cells (5×10^4 cells) suspended in 100 µl of EBM, and in absence of serum or other supplements, were seeded after coating onto the upper side of each Transwell chamber and placed 4 hours at 37ºC. Then, 500 µl of the inhibitors at IC50 (i.e. concentration at which the cell viability is 50% of the control calculated from figure 4A: 40 µM of CP-320626, 30 µM of G5 and 25 µM of O1) and at 10×IC50 in EBM with 10% FCS and supplements were added to the lower compartment of the 24-well plates to test their inhibitory effect. After 4 hours at 37ºC, cells that had migrated to the lower side of the transwell were incubated with 5 mM Calcein-AM (Calbiochem) for 25-30 minutes at 37ºC. Migrated cells were counted under a light microscope at a magnification of 10X.

RESULTS

VEGF and FGF trigger a common characteristic metabolic changes in HUVEC cells. Lactate in the cell culture medium, the secreted product of glycolysis, was used to determine the contribution of glycolysis and the oxidative pentose phosphate pathway (PPP) to the central glucose metabolism. The unlabeled species (m0) represents the corrected lactate mass isotopomer distribution without the ^{13}C label; m1 represents the distribution with one ^{13}C label; and m2 with two ^{13}C labels. The species m2 originates from glucose that is converted to lactate directly by glycolysis. In contrast, m1 originates from glucose metabolized by direct oxidation via the oxidative steps of the pentose phosphate pathway, which is then recycled to glycolysis via the nonoxidative pentose cycle. Thus, we can calculate the PC parameter, which gives us an idea of pentose cycle use (as a percentage) with respect to glycolysis (Lee *et al.*, 1998). FGF activation provoked greater proliferation than VEGF activation (Figure 1). Therefore, the concentration of lactate secreted into the medium was higher in FGF-activated HUVEC cells (data not shown). Consequently, we observed a slight increase in ^{13}C-enriched lactate after FGF activation, with respect to VEGF (Table 1A, upper panel), measured as $\sum mn = m1 + 2 \times m2$, a parameter that represents the average number of ^{13}C atoms per molecule. However, the flux balance (PC parameter) was not significantly altered, indicating a similar

metabolic lactate pattern after both FGF and VEGF activation. Moreover, unlabelled lactate (m0) accumulated in similar amounts. This confirmed that the utilization of other carbon sources via degradation of the amino acids glutamine (glutaminolysis) and serine (serinolysis) is also maintained in HUVEC cells independently of the two growth factor activation pathways.

Due to the characteristics of the pentose phosphate pathway, label incorporation into ribose occurred with the isotopomers m1 and m2 but also m3 and m4 species. m1 is formed when [1,2-$^{13}C_2$]-glucose is decarboxylated by the oxidative branch of the pentose phosphate pathway. m2 is synthesized by the reversible nonoxidative branch of the cycle. The combination of these two branches generates m3 and m4 species. The total label incorporation or ^{13}C enrichment is measured as $\sum mn=m1+2\times m2+3\times m3+4\times m4$. To assess the contribution of each pentose phosphate pathway branch, the oxidative versus nonoxidative ratio was used, measured as $ox/nonox=(m1+m3)/(m2+m3+2\times m4)$, since m1 and m3 need the oxidative branch to be formed, and m2, m3 and m4 species require the nonoxidative branch (twice in m4). In Table 1B (upper panel), a representative isotopomeric distribution of a single experiment is displayed. Significant, similar traffic of glucose through the pentose phosphate pathway was observed after either FGF or VEGF activation. As we noticed for lactate, the higher proliferation rate caused by FGF activation (Figure 1) caused a slight increase in ^{13}C enrichment ($\sum mn$), with respect to VEGF activated cells. However, the flux balance through the two branches of the pentose cycle (ox/nonox ratio) was very similar and did not present consistent differences in the replicates performed.

High, similar glycogen concentrations were found in HUVEC cells under all the culture conditions. ^{13}C labelling was found in glycogen reservoirs. The analysis of glucose isotopomer distribution obtained from glycogen displayed only m0 and m2 species, indicating that the glycogen carbon source is glucose from the culture medium. A representative ^{13}C enrichment of glycogen after FGF or VEGF activation, measured as $\sum mn=2\times m2$, is depicted in Figure 2A (black bars). Since initial glycogen reservoirs were not labelled, ^{13}C incorporation into glycogen from glucose increases with time and is dependent on the proliferation rate, as the cells have to replenish their glycogen content. Thus, as observed for lactate and ribose, there was a higher concentration of labelled glucose in glycogen after FGF activation than after VEGF activation, due to its higher proliferation rate (Figure 1).

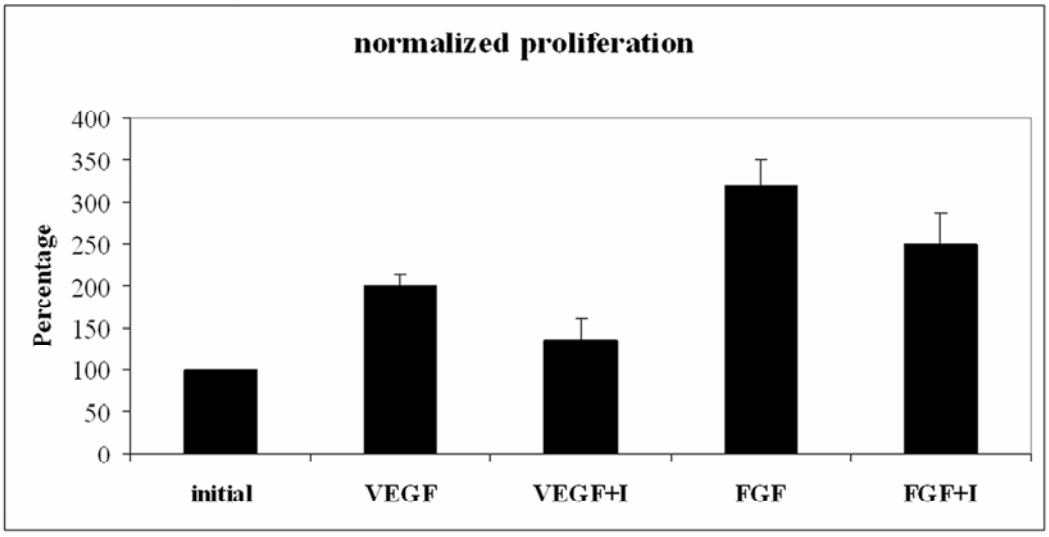

Figure 1. Normalized cell counts with respect to the initial cell number. FGF activation induced higher proliferation rates than VEGF activation. The inhibitor (I: 5-diarylurea-oxy-benzimidazole) caused a decrease in both VEGF and FGF treated cells. However, this was relatively more pronounced when VEGF was used to activate HUVEC cells. Data are presented as mean ± standard deviation of three independent experiments.

Inhibition of VEGFR-2 decreases HUVEC cell proliferation via specific pathways activated by VEGF. 5-Diarylurea-oxy-benzimidazole is a well-known VEGFR-2 (vascular endothelial growth factor receptor 2) inhibitor. It is often used to investigate the link between receptor activation and signalling pathways. The use of 5-diarylurea-oxy-benzimidazole allows us to study whether the characteristic, activated HUVEC metabolic pattern described above is the downstream effect of receptor activation signalling pathways. The inhibitor caused approximately 30% of proliferation inhibition when HUVEC cells were activated with VEGF and, unexpectedly, 20% of proliferation inhibition when cells were activated with FGF (Figure 1). Interestingly, inhibitor treatment did not affect the metabolic network when HUVEC activation was mediated by FGF, meanwhile VEGF-activated cells suffered changes in ribose and glycogen metabolism. Thus, meanwhile the RNA ribose isotopomeric distribution was not affected by the inhibitor in the three experiments performed when FGF was the activator (Table 1B, lower panel - in the single experiment depicted in Table 1B, there was a slight increase in ribose ^{13}C enrichment when 5-diarylurea-oxy-benzimidazole was added to FGF-activated HUVEC cells, but this increase was not statistically significant in the replicates), RNA ribose showed a significant and consistent decrease in ^{13}C enrichment ($\sum mn$) when 5-diarylurea-oxy-benzimidazole was added to VEGF activated cells (Table 1B, lower panel). Similar isotopomeric distribution patterns were found in all the experiments performed. Whereas the m2

proportion did not present significant changes, m1 decreased after the treatment with 5-diarylurea-oxy-benzimidazole, which caused a small but significant decrease in ox/nonox ratio of PPP.

Table 1. Isotopomeric distribution

A. Lactate isotopomeric distribution

HUVEC specific activation

	m0	m1	m2	Σmn	PC (%)
VEGF	0.8157 ± 0.006	0.0164 ± 0.001	0.1668 ± 0.0032	0.3532 ± 0.0073	3.17 ± 0.14
FGF	0.803 ± 0.007	0.0185 ± 0.0034	0.1772 ± 0.0039	0.3766 ± 0.0103	3.36 ± 0.53

VEGFR-2 inhibitor treatment

	m0	m1	m2	Σmn	PC (%)
VEGF+I	0.8202 ± 0.006	0.0156 ± 0.0014	0.1629 ± 0.0044	0.3451 ± 0.011	3.09 ± 0.20
FGF+I	0.8024 ± 0.0019	0.0174 ± 0.0008	0.179 ± 0.00126	0.379 ± 0.0027	3.13 ± 0.12

B. Ribose isotopomeric distribution

HUVEC specific activation

	m1	m2	m3	m4	Σmn	ox/nonox
VEGF	0.1887 ± 0.0014	0.1262 ± 0.0012	0.0332 ± 0.0004	0.0198 ± 0.0007	0.6208 ± 0.0061	1.1151 ± 0.0203
FGF	0.2015 ± 0.0021	0.1354 ± 0.0004	0.0303 ± 0.001	0.0163 ± 0.0008	0.6314 ± 0.0132	1.1697 ± 0.0056

VEGFR-2 inhibitor treatment

	m1	m2	m3	m4	Σmn	ox/nonox
VEGF+I	0.1664 ± 0.0007	0.1253 ± 0.002	0.0297 ± 0.0005	0.0207 ± 0.0005	0.5879 ± 0.0125**	0.9986 ± 0.0119**
FGF+I	0.1993 ± 0.0016	0.1466 ± 0.0018	0.0306 ± 0.0005	0.0180 ± 0.0004	0.6594 ± 0.0088	1.0784 ± 0.0062

Isotopomeric distribution in lactate and RNA ribose after growth factor-activated and 5-diarylurea-oxy benzimidazole-treated HUVEC cells. A, representative isotopomeric distribution and ^{13}C enrichment (∑mn) in lactate. No significant differences were found in lactate after activation with VEGF or FGF (upper panel). The introduction of the inhibitor (I: 5-diarylurea-oxy-benzimidazole) (lower panel) did not cause any relevant changes. B, representative isotopomeric distribution, ^{13}C enrichment (∑mn) and the oxidative/nonoxidative ratio in RNA ribose. HUVEC cells activated by either VEGF or FGF activation use the pentose phosphate pathway in a similar way (upper panel). Inhibitor I treatment (lower panel) caused a significant decrease in the total incorporation from glucose to ribose (∑mn) in VEGF activation. This decrease was mainly determined by the inhibition of the oxidative branch of the pentose phosphate pathway. Significance was tested using a nonparametric Mann-Whitney W test to compare the medians of each independent experiment, considering 99% as a confident level. Significant differences (**) were consistent in the three independent experiments.

Similarly, although the inhibitor caused proliferation decrease in VEGF and FGF-activated cells (Figure 2A), glycogen synthesis and turnover was also only affected by 5-diarylurea-oxy-benzimidazole in VEGF activated cells. The ^{13}C enrichment of glycogen decreased significantly and consistently when the inhibitor was added. To deeper study of this

marked decrease in label incorporation into glycogen when 5-diarylurea-oxy-benzimidazole was added to VEGF-activated HUVEC cells, the glycogen content was measured by GC/MS procedures, using an internal standard. Figure 2B shows that the glycogen content of VEGF-activated cells increased when the cells were treated with 5-diarylurea-oxy-benzimidazole, indicating that glycogen degradation was inhibited.

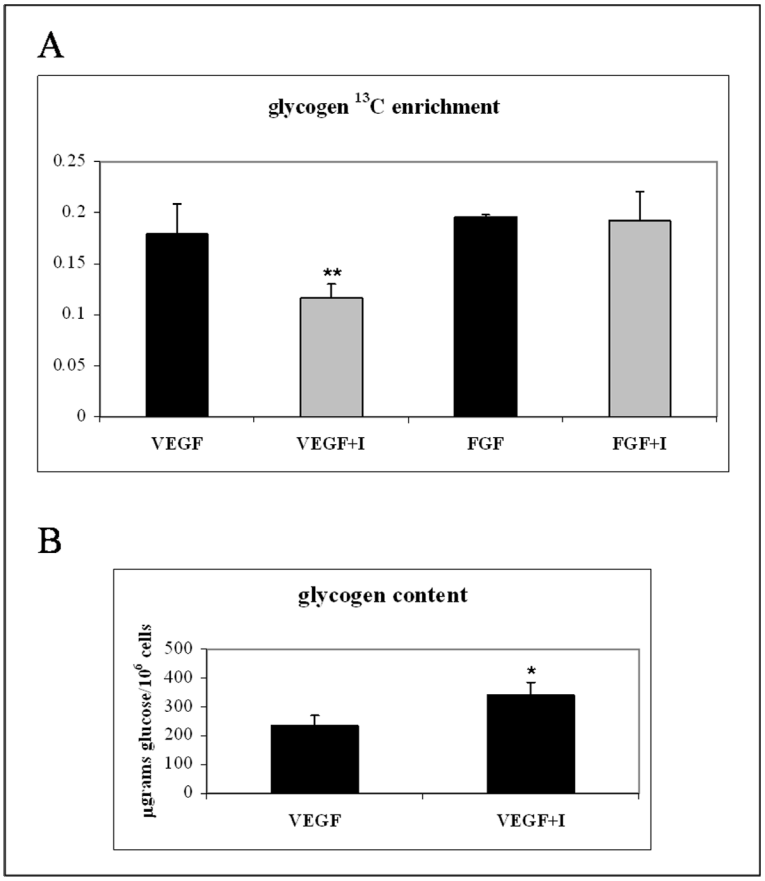

Figure 2. ^{13}C enrichment of glycogen reservoirs and glycogen content in growth factor-activated and 5-diarylurea-oxy-benzimidazole- treated HUVEC cells. A, glycogen ^{13}C enrichment, calculated as ∑mn=2×m2, shows similar glycogen-glucose turnover after activation with both VEGF and FGF (black bars). The inhibitor (I: 5-diarylurea-oxy-benzimidazole) produced a significant decrease in glycogen turnover from glucose after VEGF-specific HUVEC activation (grey bars). After the FGF activation, the inhibitor did not significantly affect the total ^{13}C incorporation into glycogen. Significance was tested using a nonparametric Mann-Whitney W test to compare the medians of each independent experiment, considering 99% as a confident level. Significant differences (**) were consistent in the three independent experiments. B, glycogen content expressed in µg of glucose released from glycogen with respect to 10^6 cells. The inhibitor I promoted a significant accumulation of glycogen reservoirs. Significance (*) was tested using a nonparametric Mann-Whitney W test to compare the medians of seven samples from two independent experiments, considering 95% as a confident level.

Curiously, the VEGFR-2 inhibitor treatment did not affect lactate label distribution. Moreover, neither ^{13}C enrichment nor flux balance (PC parameter) presented significant differences after either VEGF- or FGF-activation, indicating that the metabolic pattern detected in lactate was not dependent on specific endothelial activation (Table 1A, lower panel).

Glycogen reservoirs are mobilized under hypoglycaemic conditions, but not under hypoxic conditions. Activated endothelial cells induced by tumors are recruited towards hypoxic and hypoglycaemic environments. To better understand the role of HUVEC glycogen reservoirs in physiological conditions, cells were cultured in a glucose-free medium. For this specific culture condition, 10 mM glucose Dulbecco's Modified Eagle Medium (DMEM) was used as a control versus glucose-free DMEM. After 24 hours of incubation, glycogen was extracted, measured and corrected by protein content. Figure 3A shows that there was a total absence of glycogen content in HUVEC cells when glucose was absent from the culture medium. This dramatic decrease of glycogen content in glucose-free medium has been previously reported in other human endothelial cells (Artwohl *et al.*, 2007). Lactate production was also measured after 24 hours. Its concentration decreased sharply in hypoglycaemic conditions (data not shown), indicating that glycogen reservoirs are not large enough to support glycolysis for 24 hours.

Effects of hypoxia on HUVEC glycogen usage was also assessed. Corroboration of hypoxia impact in HUVEC metabolism was assessed by determining glucose and lactate from the culture medium, and the glycolytic rate was calculated as the rate of lactate production *versus* glucose consumption. As expected, after 24 hours under hypoxic conditions (1% O_2), the glycolytic rate increased by 20%. This was also confirmed by a 37% increase in intracellular concentration of fructose-1,6-bisphosphate, measured as described previously (Vizan *et al.*, 2007) (data not shown). Glycogen content, however, was not metabolized in HUVEC cells under hypoxic condition, as observed in hypoglycaemia, but an increase in glycogen reservoirs were observed (Figure 3B).

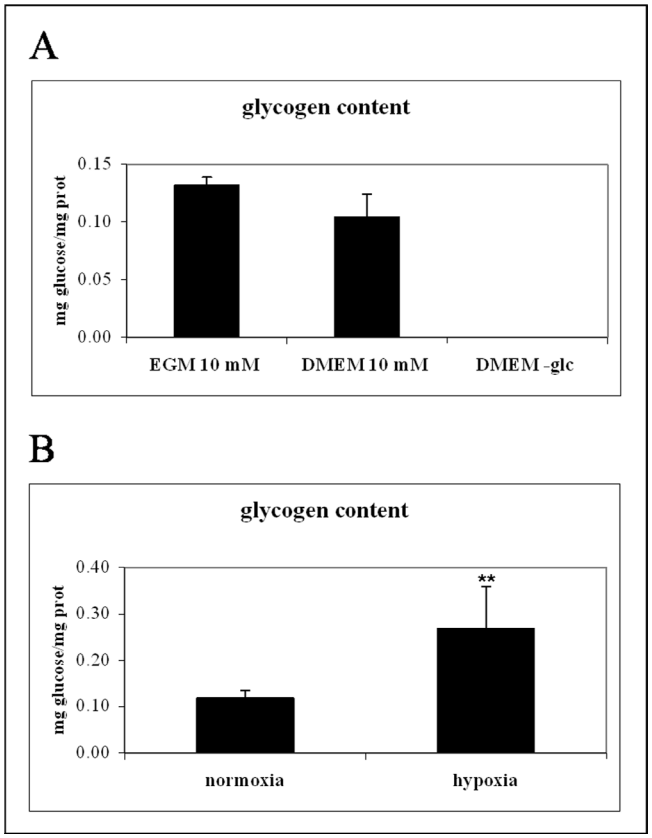

Figure 3. Glycogen content, expressed as mg glucose released from glycogen with respect to mg of protein content, in HUVEC cells under hypoglycaemic or hypoxic culture conditions after 24 hours. A, hypoglycaemic conditions: the substitution of endothelial growth medium (EGM) containing 10 mM of initial glucose by Dulbecco's Modified Eagle's Medium (DMEM), 10 mM of initial glucose slightly affected the glycogen content in HUVEC cells. However, when glucose-free DMEM was used, HUVEC cells lost all of their glycogen reservoirs. B, hypoxic conditions (24 hours at low O_2 concentration) did not provoke the use of glycogen reservoirs, but caused a significant increase in cellular glycogen content. Significance (**) was tested using a nonparametric Mann-Whitney W test to compare the medians of five samples from two independent experiments, considering 99% as a confident level.

Pentose phosphate pathway and glycogen metabolism are good antiangiogenic targets. Previously reported results suggested that glycogen metabolism and the pentose phosphate pathway (PPP) may be good targets for metabolic interventions (Lee *et al.*, 2004; Ramos-Montoya *et al.*, 2006). Therefore, HUVEC cells were treated with CP-320626, an inhibitor of the key enzyme in glycogen degradation, glycogen phosphorylase (Oikonomakos *et al.*, 2000), as well as with G5 and O1, inhibitors of glucose-6-phosphate dehydrogenase and transketolase, the key enzymes of the oxidative and nonoxidative branches of PPP respectively (Boren *et al.*, 2002). After 48 hours, dose-escalating treatment with CP-320626 and both G5 and

O1 caused dose-dependent inhibition of cell viability (Figure 4A), confirming the importance of these two metabolic pathways in HUVEC cells.

Moreover, the inhibitors of glycogen metabolism and pentose phosphate pathway also impair the capacity of HUVEC to migrate (fig 4B). After just 4 hours of incubation, the addition of CP-320626 caused a decrease of migration of 12% and 84% at its respective IC50 and 10xIC50 concentration. Similar dose-response inhibition of PPP was observed, with a decrease of 40% and 66% for O1 and of 12% and 19% for G5 at their respective IC50 and 10xIC50 concentration. Consistent with proliferation assays, the inhibitor of the non oxidative branch of PPP O1 decreased the migration capacity in a larger extend that G5, inhibitor of the oxidative branch of PPP. It could be explained by the metabolic characteristic of PPP: the non oxidative branch of PPP is a reversible pathway with the capacity of buffering pentose with hexose phosphates, so the inhibition of the oxidative branch could be eventually compensated by the non oxidative, provoking that increasing concentrations of G5 did not cause an massive increase in migration inhibition, as well as is observed in viability assays.

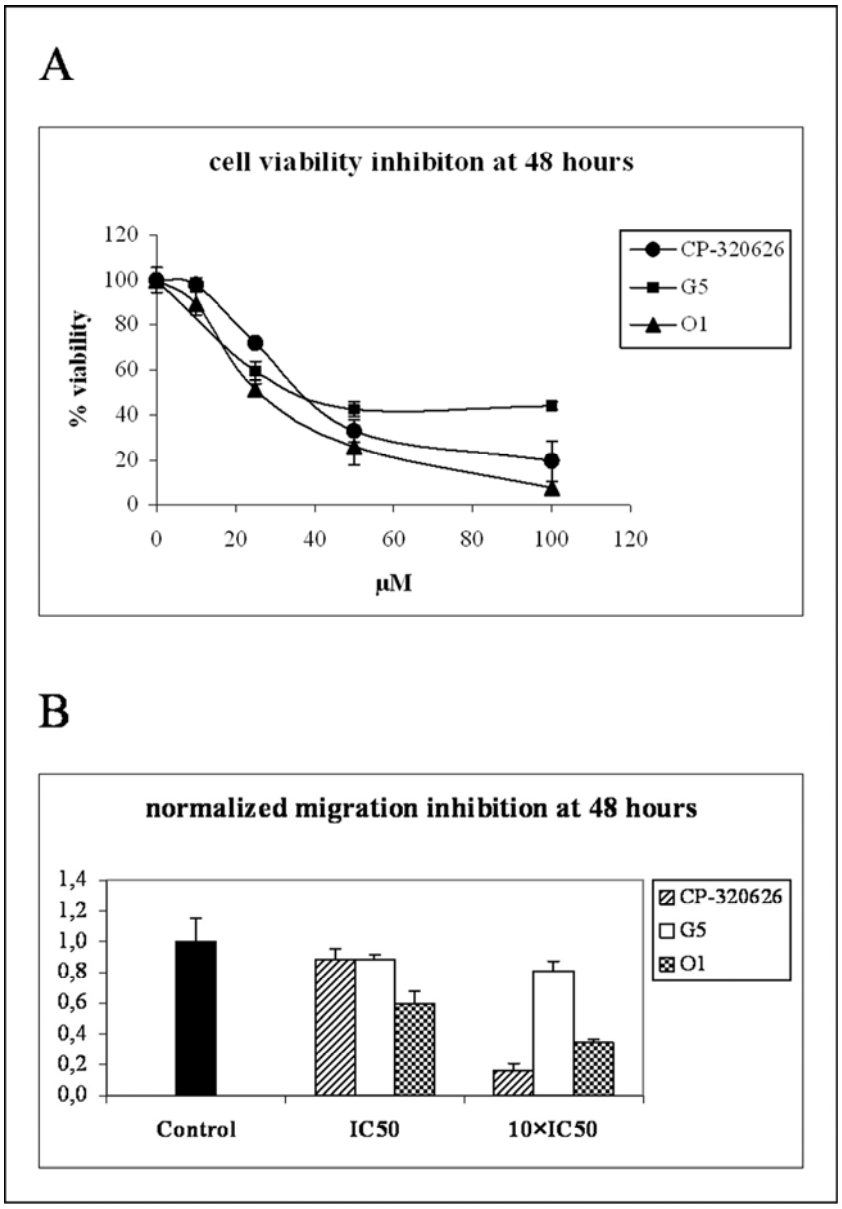

Figure 4. (A) Cell viability of HUVECs after treatment with glycogen phosphorylase inhibitor CP-320626, glucose-6-phosphate dehydrogenase inhibitor G5 and transketolase inhibitor O1. After 48 hours, dose-escalating treatment with the three compounds caused dose-dependent inhibition of cell proliferation. Data are presented as mean ± standard deviation of three independent experiments performed. **(B)** Migration capacity of HUVECs after the treatment with CP-320626, G5 and O1. Data are normalized with respect control (media without drug).

DISCUSSION

Cancer is an extremely complex and heterogeneous disease that exhibits a high level of robustness against a range of therapeutic efforts (Kitano, 2004). Looking for new targets to arrest cancer progression and invasion is one of the main current research challenges. With the

development of systems biology, it has became more evident that a system level understanding of cancer cells and vascular endothelial cells that provide tumor vascularization could contribute to developing new drugs and therapies. Moreover, the recognition that the phenotype and function of mammalian cells largely depends on metabolic adaptation has greatly stimulated research initiatives in the field of metabolomics and fluxomics (Cascante *et al.*, 2002; de la Fuente *et al.*, 2002).

Although the central role of VEGF in the activation of angiogenesis has been clearly established, prior to the present study little was known about the metabolic network modulation required to support the angiogenic process. Results reported in this paper, using the [1,2-$^{13}C_2$]-glucose stable isotope as a carbon source and a tracer-based metabolomics approach, reveal a characteristic metabolic flux pattern downstream of endothelial cells activation, regardless of whether HUVEC cells are activated by VEGF or FGF. Thus, this common metabolic adaptation may be required to support endothelial cell function in the angiogenic process and includes a high flux of glucose through the pentose phosphate pathway and an active glycogen metabolism. Lactate isotopomeric distribution is not significantly different when either VEGF or FGF are used to activate HUVEC cells (Table 1A). RNA ribose ^{13}C enrichment is slightly higher after FGF activation than after VEGF activation of HUVEC cells, probably due to a higher proliferation rate (Figure 1). However, fluxes through oxidative and nonoxidative branches of the pentose cycle are not significantly altered, as the oxidative/nonoxidative ratio was similar in all the experiments (Table 1B, upper panel). Glycogen ^{13}C enrichment was around 10% higher after FGF activation than after VEGF activation (Figure 2A). This also correlates with a higher proliferation rate. This, and the fact that high, similar glycogen concentrations were found in VEGF- or FGF-activated HUVEC cells indicates that glycogen deposits are important for HUVEC cell proliferation.

This strong dependence of activated HUVEC cell metabolism on glycogen and the pentose phosphate pathway (PPP) could be essential to supporting the angiogenic process. Consequently, glycogen and the PPP could be targets within the angiogenic cell metabolic network for potential novel therapies. In order to check whether this common metabolic pattern is a consequence of the angiogenic HUVEC cell activation that may be essential for the angiogenic process, we analysed the effects of a well-known VEGFR-2 (vascular endothelial growth factor receptor 2) inhibitor, 5-diarylurea-oxy-benzimidazole, on HUVEC cells' metabolic network. This inhibitor acts on the intracellular part of the VEGFR-2 and impedes phosphorylation through its tyrosine kinase activity, causing a decrease in the VEGF-activated phosphorylation cascade and the HUVEC proliferation rate (Figure 1).

The lactate isotopomeric distribution did not change significantly when the inhibitor was added to either VEGF-activated or FGF-activated HUVEC cells (Table 1A), suggesting that glycolytic flux does not depend on signal transduction from the VEGF receptor. However, the results show that treatment with the inhibitor in VEGF-activated cells cause a decrease in PPP flux, as there was a significant decrease in ^{13}C ribose enrichment ($\sum$mn) (Table 1B). This decrease was mainly determined by the inhibition of the oxidative branch of the pentose phosphate pathway. Worthy of note, MIDA experiments were performed at 72 hours, when metabolic enrichment of ^{13}C from [1,2-$^{13}C_2$]-glucose is almost saturated. Therefore, the differences in proliferation rate caused by VEGF or FGF activation hardly led to a relevant difference in ^{13}C ribose enrichment. The specificity of this metabolic response is corroborated by the fact that the inhibitor treatment, which caused a 30% and 20% decrease in proliferation when HUVEC cells were activated with VEGF and FGF respectively, only significantly decreased RNA ribose enrichment when VEGF was used as angiogenic activator. This leads us to conclude that the inhibitor acts specifically on its target receptor VEGFR-2, which causes a specific metabolic effect on PPP.

Interestingly, it has been demonstrated that activation of the pentose cycle is downregulated during the differentiation process (Boren *et al.*, 2003), whereas its activation is a common characteristic of tumor cells (Boros *et al.*, 1998). These results reinforce the emergence of the PPP as a promising therapeutic target, since actions on this pathway could inhibit tumor proliferation and impede angiogenic progression. Thus, metabolic inhibition of both the oxidative and nonoxidative branch of this pathway has been described as a good antitumoral strategy (Boros *et al.*, 1997; Rais *et al.*, 1999; Comin-Anduix *et al.*, 2001; Boren *et al.*, 2002; Cascante *et al.*, 2002). Moreover, it has been recently demonstrated that disruption of the unbalance between oxidative and nonoxidative branches of pentose-phosphate metabolism using a multiple hit drug strategy results in colon cancer adenocarcinoma cell death (Ramos-Montoya *et al.*, 2006). Additionally, several studies have demonstrated that downregulation of these pathways decreases the migration capacity of bovine aortic endothelial cells (Ascher *et al.*, 2001; Leopold *et al.*, 2003).

The results also show that 5-diarylurea-oxy-benzimidazole inhibitor impairs ^{13}C enrichment of glycogen reservoirs when the inhibitor is added to VEGF-activated cells, but not when it is added to FGF-activated cells (Figure 2A, grey bars), which led us to hypothesize a reducing glycogen mobilization specifically provoked by the inhibitor. This is confirmed by the accumulation of glycogen reservoirs when the inhibitor is present (Figure 2B).

The physiological impact of huge glycogen reservoirs on HUVEC cells could be explained by the needs of endothelial cells during the formation of new vessels, after their recruitment by solid tumors, in which there is a hypoglycaemic and hypoxic environment. Accordingly, by forcing physiological hypoglycaemic conditions, we observed how HUVEC glycogen reservoirs are totally catabolized (Figure 3A). Hypoxia does not lead to the use of glycogen reservoirs. On the contrary, it does cause an increase in the cellular glycogen content (Figure 3B). In hypoxic conditions, the glycolytic rate increases provoking an increase of the intracellular concentration of sugar phosphate glycolytic intermediates. Therefore, we hypostatize that the observed increase in glycogen content under hypoxic conditions could be explained by the metabolic equilibrium between glycolytic intermediates and glycogen reservoirs. Interestingly, glycogen metabolism has also been described as an antitumoral target in MIA pancreatic cells (Lee *et al.*, 2004), again providing a common, attackable metabolic characteristic in tumors and in the endothelial cells activated by them.

In summary, we have described high activity of pentose phosphate metabolism, large glycogen deposits and high glycogen turnover as a common adaptive metabolic pattern associated with angiogenic activation, regardless of the activation pathway. This proves the robustness of the angiogenic process (Figure 5A). Specific inhibition of the angiogenic stimulus using 5-diarylurea-oxy-benzimidazole resulted in a decrease in the pentose phosphate pathway and glycogen metabolism, which confirms that the activation of these two pathways is one of the mechanisms resulting in angiogenic activation downstream of growth factor stimulation (Figure 5B). Thus, these results offer new insight into the vulnerability of the angiogenic cell metabolic network and indicate potential new antiangiogenic targets. To prove this hypothesis, we corroborated the importance of the aforementioned metabolic characteristics by inhibiting key enzymes to glycogen metabolism and PPP (Figure 4) and corroborating that they inhibition affect both viability and migration capacity of HUVEC cells. Further work is needed to provide molecular evidence that directly links the observed metabolic changes to growth factor signalling pathways and validates the new targets. Nevertheless, in this paper we have demonstrated that metabolic studies can reliably provide a systemic view of a biological process, such as angiogenesis activation by growth factors, as well as the potential use of such processes for antiproliferative and antimigration interventions. It is of crucial importance to note that the endothelial metabolic targets proposed here also promising anticancer targets (Rais *et al.*, 1999; Lee *et al.*, 2004; Ramos-Montoya *et al.*, 2006). Thus, metabolic interventions that could affect at the same time solid tumors and vessels formation should be seriously considered in integrate actions against carcinogenic process.

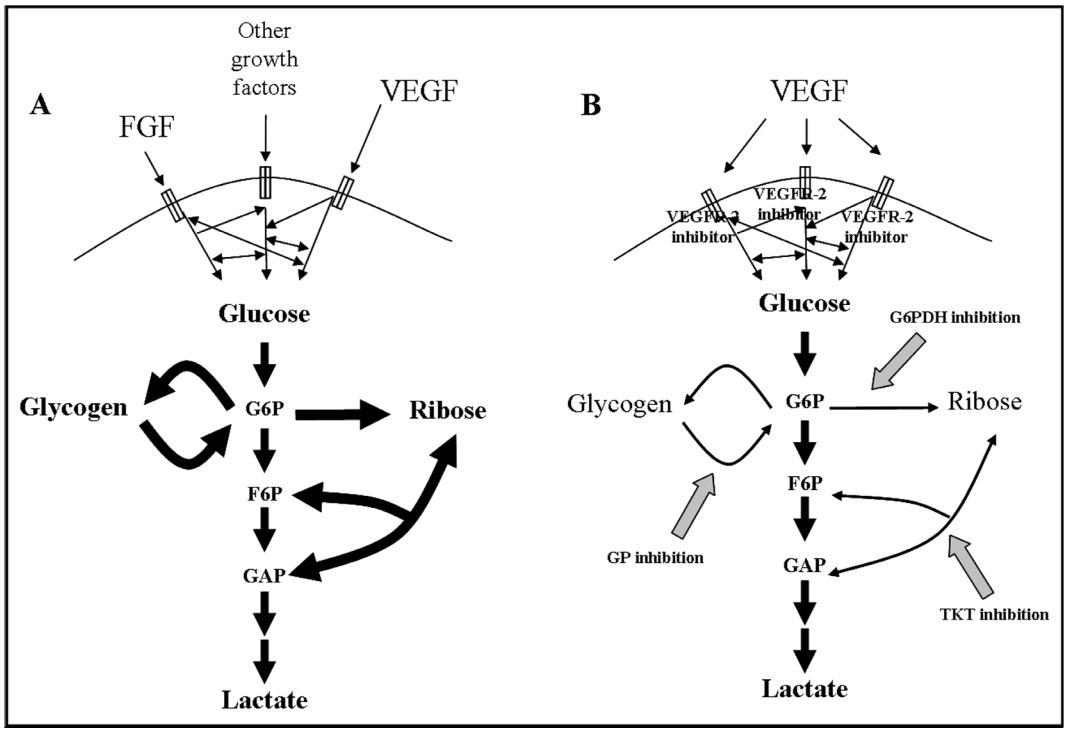

Figure 5. HUVEC cells' metabolic network adaptation in response to the activation produced by the angiogenic stimulus of different growth factors (VEGF and FGF) and after specific inhibition of the angiogenic stimulus using a VEGFR-2 inhibitor. A, the induction of angiogenic stimulus by growth factor metabolically activated HUVEC cells, producing a similar pattern of glucose usage. B, the inhibition of the VEGF receptor caused a decrease in the proliferation rate, which was accompanied by a decrease in the pentose phosphate pathway activity and glycogen metabolism. Actions on these metabolic points also impaired the angiogenic process. Abbreviations: G6P, glucose-6-phosphate; F6P, fructose-6-phosphate; GAP, glyceraldehyde-3-phosphate; GP, glycogen phosphorylase; G6PDH, glucose-6-phosphate dehydrogenase; TKT, transketolase.

ACKNOWLEDGEMENTS

This work was supported by SAF2005-01627 and SAF2008-00164 to MC from the Spanish Ministry of Science and Technology and European Union FEDER funds; the General Clinical Research Center (PHS M01-RR00425); the UCLA Center for Excellence in Pancreatic Diseases, Metabolomics Core (1 P01 AT003960-01A1); ISCIII-RTICC (RD06/0020/0046) from the Spanish Ministry of Health and Consumption; and 2005SGR00204 from the government of Catalonia.

REFERENCES

Artwohl, M., Brunmair, B., Furnsinn, C., Holzenbein, T., Rainer, G., Freudenthaler, A., Porod, E.M., Huttary, N. i Baumgartner-Parzer, S.M. (2007). Insulin does not regulate glucose transport and metabolism in human endothelium. *Eur J Clin Invest* **37**(8): 643-50.

Ascher, E., Gade, P.V., Hingorani, A., Puthukkeril, S., Kallakuri, S., Scheinman, M. i Jacob, T. (2001). Thiamine reverses hyperglycemia-induced dysfunction in cultured endothelial cells. *Surgery* **130**(5): 851-8.

Boren, J., Lee, W.N., Bassilian, S., Centelles, J.J., Lim, S., Ahmed, S., Boros, L.G. i Cascante, M. (2003). The stable isotope-based dynamic metabolic profile of butyrate-induced HT29 cell differentiation. *J Biol Chem* **278**(31): 28395-402.

Boren, J., Montoya, A.R., de Atauri, P., Comin-Anduix, B., Cortes, A., Centelles, J.J., Frederiks, W.M., Van Noorden, C.J. i Cascante, M. (2002). Metabolic control analysis aimed at the ribose synthesis pathways of tumor cells: a new strategy for antitumor drug development. *Mol Biol Rep* **29**(1-2): 7-12.

Boros, L.G., Brandes, J.L., Yusuf, F.I., Cascante, M., Williams, R.D. i Schirmer, W.J. (1998). Inhibition of the oxidative and nonoxidative pentose phosphate pathways by somatostatin: a possible mechanism of antitumor action. *Medical Hypotheses* **50**(6): 501-506.

Boros, L.G., Cascante, M. i Paul Lee, W.-N. (2002). Metabolic profiling of cell growth and death in cancer: applications in drug discovery. *Drug Discovery Today* **7**(6): 364-372.

Boros, L.G., Lapis, K., Szende, B., Tomoskozi-Farkas, R., Balogh, A., Boren, J., Marin, S., Cascante, M. i Hidvegi, M. (2001). Wheat germ extract decreases glucose uptake and RNA ribose formation but increases fatty acid synthesis in MIA pancreatic adenocarcinoma cells. *Pancreas* **23**(2): 141-7.

Boros, L.G., Puigjaner, J., Cascante, M., Lee, W.N., Brandes, J.L., Bassilian, S., Yusuf, F.I., Williams, R.D., Muscarella, P., Melvin, W.S. i Schirmer, W.J. (1997). Oxythiamine and dehydroepiandrosterone inhibit the nonoxidative synthesis of ribose and tumor cell proliferation. *Cancer Res* **57**(19): 4242-8.

Brekken, R.A., Overholser, J.P., Stastny, V.A., Waltenberger, J., Minna, J.D. i Thorpe, P.E. (2000). Selective inhibition of vascular endothelial growth factor (VEGF) receptor 2 (KDR/Flk-1) activity by a monoclonal anti-VEGF antibody blocks tumor growth in mice. *Cancer Res* **60**(18): 5117-24.

Cascante, M., Boros, L.G., Comin-Anduix, B., de Atauri, P., Centelles, J.J. i Lee, P.W. (2002). Metabolic control analysis in drug discovery and disease. *Nat Biotechnol* **20**(3): 243-9.

Comin-Anduix, B., Boren, J., Martinez, S., Moro, C., Centelles, J.J., Trebukhina, R., Petushok, N., Lee, W.N., Boros, L.G. i Cascante, M. (2001). The effect of thiamine supplementation on tumour proliferation. A metabolic control analysis study. *Eur J Biochem* **268**(15): 4177-82.

Dagher, Z., Ruderman, N., Tornheim, K. i Ido, Y. (1999). The effect of AMP-activated protein kinase and its activator AICAR on the metabolism of human umbilical vein endothelial cells. *Biochem Biophys Res Commun* **265**(1): 112-5.

Dang, C.V. i Semenza, G.L. (1999). Oncogenic alterations of metabolism. *Trends Biochem Sci* **24**(2): 68-72.

de la Fuente, A., Snoep, J.L., Westerhoff, H.V. i Mendes, P. (2002). Metabolic control in integrated biochemical systems. *Eur J Biochem* **269**(18): 4399-408.

Ekstrom, J.L., Pauly, T.A., Carty, M.D., Soeller, W.C., Culp, J., Danley, D.E., Hoover, D.J., Treadway, J.L., Gibbs, E.M., Fletterick, R.J., Day, Y.S., Myszka, D.G. i Rath, V.L. (2002). Structure-activity analysis of the purine binding site of human liver glycogen phosphorylase. *Chem Biol* **9**(8): 915-24.

Ferrara, N. (1999). Molecular and biological properties of vascular endothelial growth factor. *J Mol Med* **77**(7): 527-43.

Ferrara, N. (2002). VEGF and the quest for tumour angiogenesis factors. *Nat Rev Cancer* **2**(10): 795-803.

Ferrara, N. (2005). VEGF as a therapeutic target in cancer. *Oncology* **69 Suppl 3**: 11-6.

Ferrara, N. i Kerbel, R.S. (2005). Angiogenesis as a therapeutic target. *Nature* **438**(7070): 967-74.

Gatenby, R.A. i Gawlinski, E.T. (2003). The glycolytic phenotype in carcinogenesis and tumor invasion: insights through mathematical models. *Cancer Res* **63**(14): 3847-54.

Gutmann, I. i Wahlefeld, A.W. (1974). L-(+)-lactate. In: Methods of Enzymatic Analysis. New York, Bergmeyer HU.

Ido, Y., Carling, D. i Ruderman, N. (2002). Hyperglycemia-induced apoptosis in human umbilical vein endothelial cells: inhibition by the AMP-activated protein kinase activation. *Diabetes* **51**(1): 159-67.

Keely, P.J. (2001). Ras and Rho protein induction of motility and invasion in T47D breast adenocarcinoma cells. *Methods Enzymol* **333**: 256-66.

Kell, D.B., Brown, M., Davey, H.M., Dunn, W.B., Spasic, I. i Oliver, S.G. (2005). Metabolic footprinting and systems biology: the medium is the message. *Nat Rev Microbiol* **3**(7): 557-65.

Kitano, H. (2004). Cancer as a robust system: implications for anticancer therapy. *Nat Rev Cancer* **4**(3): 227-35.

Lee, W.N., Boros, L.G., Puigjaner, J., Bassilian, S., Lim, S. i Cascante, M. (1998). Mass isotopomer study of the nonoxidative pathways of the pentose cycle with [1,2-13C2]glucose. *Am J Physiol* **274**(5 Pt 1): E843-51.

Lee, W.N., Guo, P., Lim, S., Bassilian, S., Lee, S.T., Boren, J., Cascante, M., Go, V.L. i Boros, L.G. (2004). Metabolic sensitivity of pancreatic tumour cell apoptosis to glycogen phosphorylase inhibitor treatment. *Br J Cancer* **91**(12): 2094-100.

Leopold, J.A., Walker, J., Scribner, A.W., Voetsch, B., Zhang, Y.Y., Loscalzo, A.J., Stanton, R.C. i Loscalzo, J. (2003). Glucose-6-phosphate dehydrogenase modulates vascular endothelial growth factor-mediated angiogenesis. *J Biol Chem* **278**(34): 32100-6.

Lerin, C., Montell, E., Nolasco, T., Garcia-Rocha, M., Guinovart, J.J. i Gomez-Foix, A.M. (2004). Regulation of glycogen metabolism in cultured human muscles by the glycogen phosphorylase inhibitor CP-91149. *Biochem J* **378**(Pt 3): 1073-7.

Matito, C., Mastorakou, F., Centelles, J.J., Torres, J.L. i Cascante, M. (2003). Antiproliferative effect of antioxidant polyphenols from grape in murine Hepa-1c1c7. *Eur J Nutr* **42**(1): 43-9.

Mazurek, S. i Eigenbrodt, E. (2003). The tumor metabolome. *Anticancer Res* **23**(2A): 1149-54.

Miyazaki, Y., Tang, J., Maeda, Y., Nakano, M., Wang, L., Nolte, R.T., Sato, H., Sugai, M., Okamoto, Y., Truesdale, A.T., Hassler, D.F., Nartey, E.N., Patrick, D.R., Ho, M.L. i Ozawa, K. (2007). Orally active 4-amino-5-diarylurea-furo[2,3-d]pyrimidine derivatives as anti-angiogenic agent inhibiting VEGFR2 and Tie-2. *Bioorg Med Chem Lett* **17**(6): 1773-8.

Mori, N., Natarajan, K., Chacko, V.P., Artemov, D. i Bhujwalla, Z.M. (2003). Choline phospholipid metabolites of human vascular endothelial cells altered by cyclooxygenase inhibition, growth factor depletion, and paracrine factors secreted by cancer cells. *Mol Imaging* **2**(2): 124-30.

Mosmann, T. (1983). Rapid colorimetric assay for cellular growth and survival: application to proliferation and cytotoxicity assays. *J Immunol Methods* **65**(1-2): 55-63.

Oikonomakos, N.G., Skamnaki, V.T., Tsitsanou, K.E., Gavalas, N.G. i Johnson, L.N. (2000). A new allosteric site in glycogen phosphorylase b as a target for drug interactions. *Structure* **8**(6): 575-84.

Pelicano, H., Martin, D.S., Xu, R.H. i Huang, P. (2006). Glycolysis inhibition for anticancer treatment. *Oncogene* **25**(34): 4633-46.

Purcell, W.T. i Ettinger, D.S. (2003). Novel antifolate drugs. *Curr Oncol Rep* **5**(2): 114-25.

Rais, B., Comin, B., Puigjaner, J., Brandes, J.L., Creppy, E., Saboureau, D., Ennamany, R., Paul Lee, W.-N., Boros, L.G. i Cascante, M. (1999). Oxythiamine and dehydroepiandrosterone induce a G1 phase cycle arrest in Ehrlich's tumor cells through inhibition of the pentose cycle. *FEBS Letters* **456**(1): 113-118.

Ramos-Montoya, A., Lee, W.N., Bassilian, S., Lim, S., Trebukhina, R.V., Kazhyna, M.V., Ciudad, C.J., Noe, V., Centelles, J.J. i Cascante, M. (2006). Pentose phosphate cycle oxidative and nonoxidative balance: A new vulnerable target for overcoming drug resistance in cancer. *Int J Cancer* **119**(12): 2733-41.

Szafranek, J., Pfaffenberger, C.D. i Horning, E.C. (1974). The mass spectra of some per-O-acetylaldononitriles. *Carbohydr Res* **38**: 97-105.

Vizan, P., Alcarraz-Vizan, G., Diaz-Moralli, S., Rodriguez-Prados, J.C., Zanuy, M., Centelles, J.J., Jauregui, O. i Cascante, M. (2007). Quantification of intracellular phosphorylated carbohydrates in HT29 human colon adenocarcinoma cell line using liquid chromatography-electrospray ionization tandem mass spectrometry. *Anal Chem* **79**(13): 5000-5.

Vizan, P., Boros, L.G., Figueras, A., Capella, G., Mangues, R., Bassilian, S., Lim, S., Lee, W.N. i Cascante, M. (2005). K-ras codon-specific mutations produce distinctive metabolic phenotypes in NIH3T3 mice [corrected] fibroblasts. *Cancer Res* **65**(13): 5512-5.

Xu, R.H., Pelicano, H., Zhou, Y., Carew, J.S., Feng, L., Bhalla, K.N., Keating, M.J. i Huang, P. (2005). Inhibition of glycolysis in cancer cells: a novel strategy to overcome drug resistance associated with mitochondrial respiratory defect and hypoxia. *Cancer Res* **65**(2): 613-21.

ANNEX

ANNEX 1 (CAPÍTOL 1)

L'hamamelitanin d'*Hamamelis virginiana* mostra citotoxicitat específica contra cèl·lules de càncer de còlon

Publicació a la revista *Journal of Natural Products* amb un índex d'impacte de 2,872.

Susana Sánchez-Tena[1], María L. Fernández-Cachón[1, ‡], Anna Carreras[2], M. Luisa Mateos-Martín[2], Noelia Costoya[3], Mary P. Moyer[4], María J. Nuñez[3], Josep L. Torres[2] i Marta Cascante[1, *]

[1]Facultat de Biologia, Universitat de Barcelona i IBUB, unitat associada al CSIC, 08028 Barcelona, Espanya

[2]Institut de Química Avançada de Catalunya (IQAC-CSIC), 08034 Barcelona, Espanya

[3]Escola d'Enginyeria, USC, 15782 Santiago de Compostel·la, Espanya

[4]INCELL, San Antonio TX 78249, EUA

[‡]Adreça actual: Freiburg Institut for Advanced Studies. School of Life Sciences – LifeNet. Freiburg im Breisgau, Alemanya

RESUM

L'escorça d'*Hamamelis virginiana* (avellaner de bruixa) és una font rica en tanins condensats i hidrolitzables, els quals s'ha descrit que exerceixen una acció protectora envers el càncer de còlon. El present estudi caracteritza diferent tanins de l'avellaner de bruixa com agents citotòxics selectius contra el càncer de còlon. Per cobrir la diversitat estructural dels tanins presents a l'escorça d'*H. virginiana*, els tanins hidrolitzables, hamamelitanin i pentagaloilglucosa, juntament amb la fracció rica en proantocianidines o tanins condensats (F800H4), es van seleccionar per a l'estudi. El tractament amb aquests compostos va reduir la viabilitat i va induir apoptosi, necrosi i arrest en la fase S del cicle cel·lular en cèl·lules HT29, amb l'hamamelitanin sent el més eficaç. Per eliminar l'efecte artefactual degut a la formació de H_2O_2 en el medis de cultiu, l'efecte antiproliferatiu es va determinar en presència i absència de catalasa. La presència de catalasa només va canviar significativament l'IC_{50} de la fracció F800H4. A més, a concentracions que inhibeixen un 50% el creixement de les cèl·lules HT29, l'hamamelitanin no va tenir cap efecte nociu en colonòcits normals NCM460 mentre que la pentagaloilglucosa va inhibir ambdós tipus cel·lulars. Utilitzant l'assaig del TNPTM es va identificar una posició fenòlica altament reactiva present en l'hamamelitanin que pot explicar la seva eficàcia inhibint el creixement del càncer de còlon.

JOURNAL OF NATURAL PRODUCTS

Article

pubs.acs.org/jnp

Hamamelitannin from Witch Hazel (*Hamamelis virginiana*) Displays Specific Cytotoxic Activity against Colon Cancer Cells

Susana Sánchez-Tena,[†] María L. Fernández-Cachón,[†,‡] Anna Carreras,[§] M. Luisa Mateos-Martín,[§] Noelia Costoya,[⊥] Mary P. Moyer,[∥] María J. Nuñez,[⊥] Josep L. Torres,[§] and Marta Cascante*[,†]

[†]Faculty of Biology, Universitat de Barcelona, IBUB, Unit Associated with CSIC, 08028 Barcelona, Spain

[§]Institute for Advanced Chemistry of Catalonia (IQAC-CSIC), 08034 Barcelona, Spain

[⊥]School of Engineering, Universidade de Santiago de Compostela, 15782 Santiago de Compostela, Spain

[∥]INCELL Corporation, San Antonio, Texas 78249, United States

ABSTRACT: *Hamamelis virginiana* (witch hazel) bark is a rich source of condensed and hydrolyzable tannins reported to exert a protective action against colon cancer. The present study characterizes different witch hazel tannins as selective cytotoxic agents against colon cancer. To cover the structural diversity of the tannins that occur in *H. virginiana* bark, the hydrolyzable tannins, hamamelitannin and pentagalloylglucose, together with a proanthocyanidin-rich fraction (F800H4) were selected for the study. Treatment with these compounds reduced tumor viability and induced apoptosis, necrosis, and S-phase arrest in the cell cycle of HT29 cells, with hamamelitannin being the most efficient. Owing to polyphenol-mediated H_2O_2 formation in the incubation media, the antiproliferative effect was determined in the presence and absence of catalase to rule out any such interference. The presence of catalase significantly changed the IC_{50} only for F800H4. Furthermore, at concentrations that inhibit the growth of HT29 cells by 50%, hamamelitannin had no harmful effects on NCM460 normal colonocytes, whereas pentagalloylglucose inhibited both cancerous and normal cell growth. Using the TNPTM assay, we identified a highly reactive phenolic position in hamamelitannin, which may explain its efficacy at inhibiting colon cancer growth.

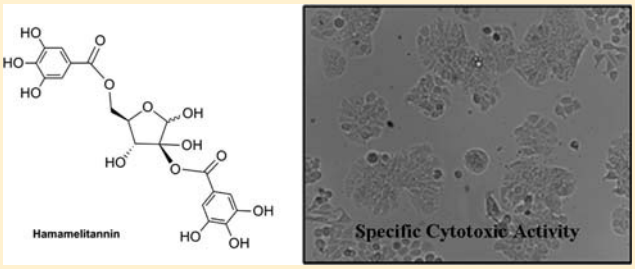

Several epidemiological studies have indicated that tannins may exert a protective effect against colon cancer, one of the most prevalent neoplastic diseases in the developed world.[1,2] Witch hazel (*Hamamelis virginiana*) bark is a rich source of both proanthocyanidins, or condensed tannins, and hydrolyzable tannins (Figure 1) such as hamamelitannin and pentagalloylglucose,[3] whose capacity to regulate cell proliferation, cell cycle, and apoptosis has attracted much attention.[4] An inverse relation has been reported between proanthocyanidins and colorectal cancer.[5] An in vitro study demonstrated that a grape seed proanthocyanidin extract significantly inhibits cell viability and increases apoptosis in Caco-2 colon cancer cells, but does not alter the viability of the normal colon NCM460 cell line.[6] Other results show that proanthocyanidins from different sources are cytotoxic to human colorectal cells.[7−9] In addition, several in vitro and in vivo studies have shown that hydrolyzable tannins from witch hazel bark exhibit multiple biological activities, which may have potential in the prevention and treatment of cancer. In vivo preclinical studies of pentagalloylglucose, one of the major hydrolyzable tannins in witch hazel, demonstrated inhibition of prostate cancer,[10,11] lung cancer,[12] and sarcoma[13] cells. In vitro inhibition of the growth and invasiveness of breast cancer, leukemia, melanoma, and liver cancer cells has also been reported.[14−17] The other major hydrolyzable tannin in witch hazel, hamamelitannin, inhibits TNF-mediated endothelial cell death and DNA fragmentation in EAhy926 endothelial cells.[18] Since TNFα/TNFR1 signaling may act as a tumor promoter for colon carcinogenesis,[19] the anti-TNF activity of hamamelitannin may indicate a protective effect against colon cancer. Furthermore, hamamelitannin has been described to inhibit 5-lipoxygenase (5-LOX),[20] and given that 5-LOX is an inflammatory enzyme involved in malignant transformation,[21] this inhibition could prevent cancer growth.

Moreover, various studies have analyzed the cytotoxicity and scavenging capacity of *H. virginiana* phenolic compounds. It has been reported that different witch hazel polyphenolic fractions are highly active as free radical scavengers against 2,2′-azinobis(3-ethylbenzothiazoline-6-sulfonic acid) (ABTS), 1,1-diphenyl-2-picrylhydrazyl (DPPH), and tris(2,4,6-trichloro-3,5-dinitrophenyl)methyl (HNTTM). They also reduce tris-(2,3,5,6-tetrachloro-4-nitrophenyl)methyl (TNPTM) radical to some extent, which indicates that they contain highly reactive hydroxy groups. In this way, witch hazel fractions protect red blood cells from free radical-induced hemolysis and also inhibit the proliferation of the SK-Mel 28 melanoma tumor cell line.[22] Some of these fractions also inhibited cell proliferation, arrested the cell cycle at the S phase, and induced

Received: May 20, 2011

dx.doi.org/10.1021/np200426k | *J. Nat. Prod.* XXXX, XXX, XXX−XXX

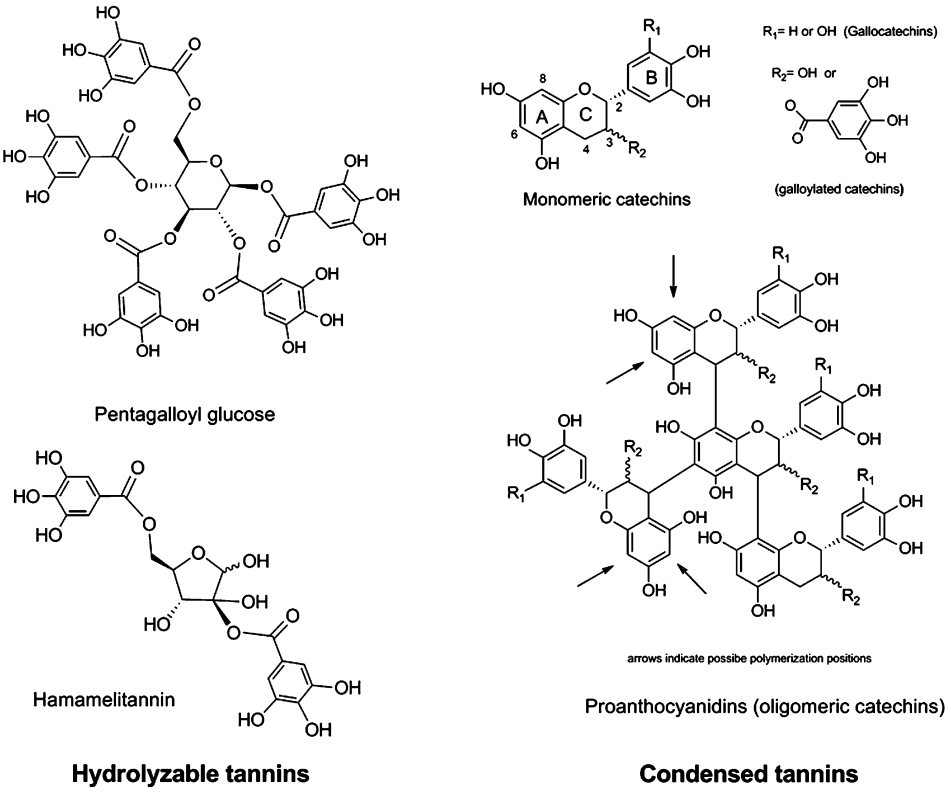

Figure 1. Structures of hydrolyzable and condensed tannins in *Hamamelis virginiana* bark.

apoptosis in HT29 human colon cancer cells.[23] The witch hazel mixtures studied so far include those from highly heterogeneous mixtures containing both hydrolyzable and condensed tannins of low molecular weight, as well as flavan-3-ol monomers;[22,23] however, the activity of oligomeric structures from witch hazel bark has not been evaluated. Furthermore, Masaki et al. reported that hamamelitannin from *H. virginiana* possesses protective activity from cell damage induced by superoxide anion radicals in murine dermal fibroblasts.[24,25]

To advance our understanding of the compounds responsible for the activity of *H. virginiana* bark, we evaluated the behavior of pure hamamelitannin and pentagalloylglucose (hydrolyzable tannins of different size) and a highly purified proanthocyanidin-rich fraction (F800H4). First, we examined the viability, apoptosis, and cell cycle of the human colorectal adenocarcinoma HT29 cell line after treatment with these compounds. To identify products that inhibit cancer cell growth without harming normal cells, the antiproliferative capacity of *Hamamelis* compounds was also measured against the NCM460 cell line (human colonocytes). As several studies have reported that polyphenols can be oxidized under standard cell culture conditions, leading to the production of significant amounts of ROS such as H_2O_2, and that this can modulate cell functions,[26] we supplemented the cell culture medium with catalase, which decomposes polyphenol-generated ROS, thus ruling out this possibility.[27]

RESULTS AND DISCUSSION

Pentagalloylglucose and fraction F800H4 were extracted from the bark of witch hazel, whereas the hydrolyzable tannin hamamelitannin was obtained commercially. Both hydrolyzable tannins presented a purity of 98% or more, as confirmed by HPLC. Once fraction F800H4 was obtained, its polyphenolic composition was characterized to ensure that it possessed a high percentage of condensed tannins. Table 1 summarizes the results of the HPLC analysis after thioacidolysis in the presence of cysteamine (condensed tannins) and direct HPLC analysis (gallic acid, pentagalloylglucose, and hamamelitannin). F800H4 was found to be composed of mostly condensed tannins (83.9% of the total tannins), both monomers and proanthocyanidins [(epi)catechin oligomers and polymers]. It also contained 16.1% hydrolyzable tannins, mainly hamamelitannin. Pentagalloylglucose was not detected in fraction F800H4. The condensed tannins had a mean degree of polymerization (mDP) of 2.6, 35% galloylation and 32% pyrogallol. The total galloylation of the fraction was 45.5%.

Table 1. Polyphenolic Composition of F800H4[a]

Composition of the Condensed Tannins (CTn) 83.9%					
mDP	% G	% P			
2.6	35.0	32.0			
% GC	% EGC	% C	% EC	% EGCG	% ECG
12.4	0.4	29.1	23.0	19.1	15.9
Composition of the Hydrolyzable Tannins (HTn) 16.1%					
% GA		% HT		% PGG	
10.0		90.0		0.0	

[a]mDP, mean degree of polymerization; % G, percentage of galloylation; % P, percentage in pyrogallol; GC, gallocatechin; EGC, epigllocatechin; C, catechin; EC, epicatechin; EGCG, epigallocatechin gallate; ECG, epicatechin gallatel; GA, gallic acid; HT, hamamelitannin; PGG, pentagalloylglucose.

Tannins regulate different cell functions through different actions that may or may not involve redox reactions.[28] Since

dx.doi.org/10.1021/np200426k | J. Nat. Prod. XXXX, XXX, XXX–XXX

Table 2. Hydrogen Donation and Electron Transfer Capacity

	DPPH			HNTTM			TNPTM		
	EC_{50}[a]	ARP[b]	H/e[c]	EC_{50}[a]	ARP[b]	e[c]	EC_{50}[a]	ARP[b]	e[c]
PGG	23.8	42.0	19.8	54.8	18.2	8.6	2403.9	0.4	0.2
HT	27.8	36.2	8.8	71.2	14.0	3.4	116.2	2.2	1.0
F800H4	39.8	25.1	27.1	66.7	15.0	16.2	1761.6	0.6	0.7

[a]EC_{50}, μg of polyphenol/μmol of radical. [b]ARP, $(1/EC_{50}) \times 10^3$. [c]Number of hydrogen atoms donated or electrons transferred to the stable radical per molecule of polyphenol, calculated as the inverse of 2 × molar EC_{50}.

polyphenols may act as antioxidants and prooxidants, we studied the redox activity of *H. virginiana* compounds and evaluated their free radical scavenging properties using different stable radicals such as DPPH, HNTTM, and TNPTM. DPPH reacts with polyphenols by mechanisms that may include both hydrogen donation and electron transfer,[29] while HNTTM and TNPTM are sensitive only to electron transfer.[30] The reactions with DPPH and HNTTM gave information on the total capacity to scavenge radicals by hydrogen donation or concerted electron proton transfer (DPPH) and by electron transfer (HNTTM). The reaction with TNPTM revealed the presence of highly redox reactive positions. Table 2 summarizes the activities of pentagalloylglucose, hamamelitannin, and the proanthocyanidin fraction F800H4 against the stable free radicals. Overall, pentagalloylglucose, hamamelitannin, and the proanthocyanidin-rich fraction F800H4 showed a similar total scavenging capacity, as their number of phenolic hydroxy groups per unit of mass was similar. Interestingly, differences were detected with TNPTM. While the scavenging capacity of the polyphenols against TNPTM is low because only some of the hydroxy groups are able to donate electrons to this radical, the possible effects of these hydroxy groups may be biologically relevant because they are the most reactive positions. One of the phenolic hydroxy groups in hamamelitannin was reactive enough to transfer its electron to TNPTM, while pentagalloylglucose was much less responsive (Table 2, last column). Hamamelitannin and pentagalloylglucose are structurally similar. In the case of hamamelitannin though, there is a hydroxy moiety geminal to one of the gallate esters, and this might explain the differences detected in the reactivity against the TNPTM radical. The extra hydroxy group might participate in a hydrogen bond with the carbonyl group from the gallate moiety to form a six-membered ring. This could introduce a conformational restriction with loss of planarity and subsequent loss of conjugation within the gallate moiety. The extended conjugation of the carbonyl and aromatic groups is the reason that gallates are less reactive than pyrogallols.[31] The results with TNPTM indicate that hamamelitannin is particularly reactive and may even participate in the formation of ROS through electron transfer to oxygen to form the superoxide radical.

Pentagalloylglucose has been shown to inhibit different malignancies.[10,11,13] Potential mechanisms for its anticancer activity include antiangiogenesis, antiproliferation, S-phase and G1-phase cell cycle arrest, induction of apoptosis, and anti-inflammatory and antioxidative effects . Putative molecular targets include p53, Stat3, Cox-2, VEGFR1, AP-1, SP-1, Nrf-2, and MMP-9. This study reports for the first time the role of pentagalloylglucose in colon cancer. We studied here the viability, the cell cycle, and the apoptosis process in human colorectal adenocarcinoma HT29 cells. In these bioassays, different positive controls were used. Epigallocatechin gallate (EGCG), a major catechin in green tea described to have antitumor activity,[32,33] was used as a standard in the cell viability assays; the cell cycle inhibitor hydroxyurea (HU) was used as a standard in the cell cycle experiments,[34] and staurosporine (ST) was utilized as a positive control in the apoptosis assays.[35] Treatment with pentagalloylglucose reduced the viability of HT29 cells with an IC_{50} value of 28 ± 8.8 μg/mL (Figure 2a) and induced 11% apoptosis compared to control cells, 5% necrosis (Figure 3), and S-phase arrest in the cell cycle with 8% increase in the population of cells in the S phase and a concomitant decrease in the percentage of cells in the G1 and G2 phases (Figure 4). Because pentagalloylglucose inhibits DNA replicative synthesis with greater efficacy than a known DNA polymerase-alpha inhibitor, aphidocolin,[36] this may explain the arrest in the S phase. The antitumor effects of hamamelitannin have not been examined, except for its antigenotoxic action in HepG2 human hepatoma cells reported by Dauer et al.,[37] as well as its anti-TNF[18] and anti-LOX activities.[20] The cellular mechanism that this hydrolyzable tannin induces may be related to the inhibition of the tumor necrosis factor itself and its receptor, which affect apoptosis, necrosis, and cell cycle processes. As a result, after treatment with hamamelitannin, we observed a reduction in the viability of HT29 cells with an IC_{50} of 20 ± 4.5 μg/mL (Figure 2a) and induction of 26% apoptosis, 14% necrosis (Figure 3), and S-phase arrest in the cell cycle with a 16% increase in the population of cells in this phase (Figure 4). With regard to condensed tannins, proanthocyanidins from various sources have been reported to inhibit colon cancer cells.[38,39] Treatment of the human colon adenocarcinoma HT29 cell line with the proanthocyanidin-rich fraction F800H4 extracted from witch hazel bark was less effective at inhibiting cell viability (IC_{50} = 38 ± 4.4 μg/mL; Figure 2a) and inducing apoptosis (9%) and necrosis (6%) (Figure 3) than the same treatment with hydrolyzable tannins. F800H4 had little effect on the normal cell cycle distribution apart from a slight increase in the S and G2 phases (Figure 4).

Overall, the hydrolyzable tannins were more effective than the condensed tannins. Interestingly, hamamelitannin, which includes a highly reactive position, as demonstrated by its reaction with TNPTM (Table 2), showed the strongest inhibition of cell viability, induction of apoptosis and necrosis, and cell cycle arrest in the S phase in HT29 colon cancer cells (Figures 2a, 3, 4). The effect of this reactive position in hamamelitannin may even be prooxidant. The prooxidant effect of some polyphenols has been discussed extensively, and it has been suggested that moderate generation of ROS may produce an antioxidant effect by fostering the endogenous defenses.[40,41] Therefore, in our assays, hamamelitannin may exert its activity, at least in part, by providing mild prooxidant challenges through electron transfer reactions leading to moderate formation of ROS.

On the other hand, since it has been reported that an increase in endogenous ROS levels is required for the transition from the G1 to the S phase of the cell cycle,[42] the cell cycle

dx.doi.org/10.1021/np200426k | J. Nat. Prod. XXXX, XXX, XXX–XXX

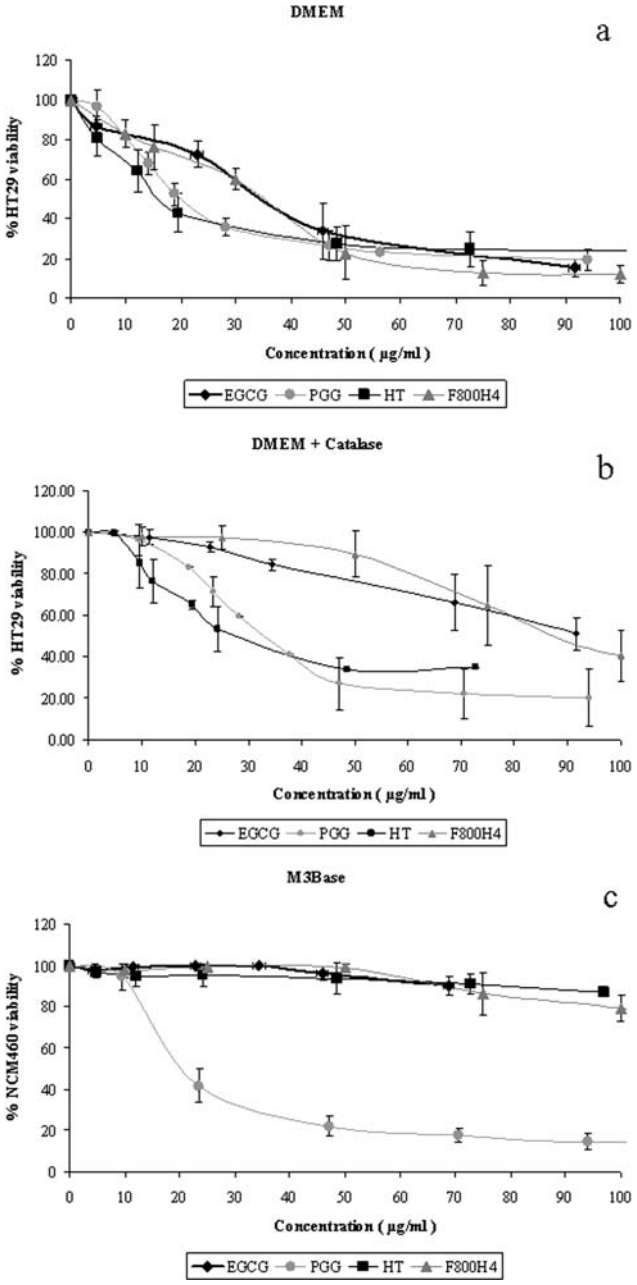

Figure 2. (a) Effect on HT29 cell viability of different concentrations of *Hamamelis virginiana* compounds in DMEM. (b) Effect on HT29 cell viability of witch hazel compounds in DMEM supplemented with catalase (100 U/mL). (c) Effect of Hamamelis products on NCM460 colonocyte growth. In all cases epigallocatechin gallate is used as a standard. Values are represented as mean of percentage of cell viability with respect to control cells ± standard error of three independent experiments.

arrest in the S phase induced by witch hazel compounds may be explained to some extent by its ROS scavenging capacity.

In the search for compounds or fractions that inhibit cancer cell growth without harming normal cells, the antiproliferative capacity of pentagalloylglucose, hamamelitannin, and the proanthocyanidin-rich fraction F800H4 was determined in NCM460 human colonocytes. NCM460 are nontumorigenic cells derived from normal colon mucosa that has not been infected or transfected with any genetic information.[43] This is

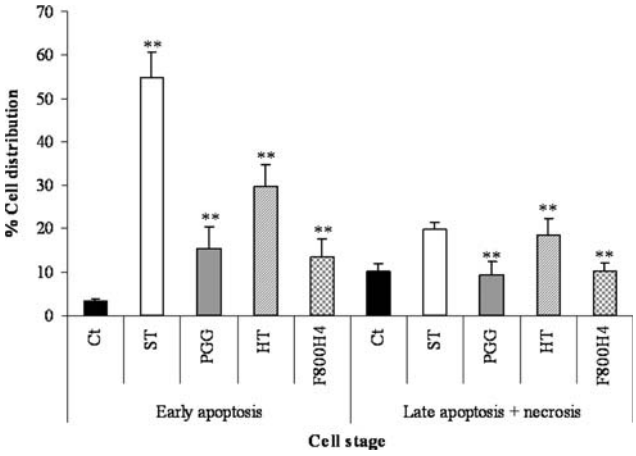

Figure 3. Early apoptotic cells: annexin V+/PI−. Late apoptotic/necrotic cells: annexin V+/PI+ and annexin V−/PI+. Staurosporine is utilized as a positive control. Values are expressed as mean ± standard deviation of three separate experiments. $^{**}p < 0.001$, significant difference with respect to the corresponding value in untreated cells (Ct).

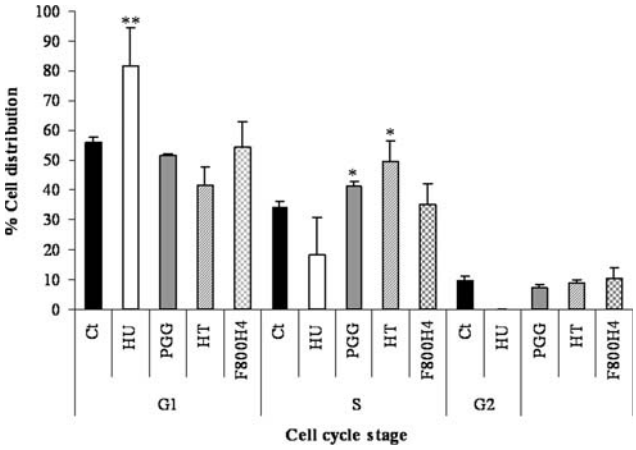

Figure 4. Normalized percentages of cells in different cell stages. Cell phases analyzed: Gl, S, and G2. The cell cycle inhibitor hydroxyurea was used as a standard. Mean ± standard deviation of three separate experiments. $^{*}p < 0.05$; $^{**}p < 0.001$, significant difference with respect to control cells (Ct).

the first comparison of the effects of witch hazel compounds on the growth of nontransformed colonocytes and cancerous colon cells. Our results show that the concentrations of hamamelitannin and F800H4 capable of inducing the death of HT29 cells (Figure 2a) had no harmful effects on normal colon cells (IC_{50} higher than 100 μg/mL for hamamelitannin and F800H4) (Figure 2c), whereas pentagalloylglucose inhibited both cancerous and normal cell growth (Figure 2a, c). Pentagalloylglucose inhibited NCM460 cell viability with an IC_{50} of 23 μg/mL ± 2.4 (Figure 2a, c).

It has been reported that polyphenol-mediated ROS formation in cell culture medium can lead to the artifactual modulation of cytotoxicity attributed to polyphenol exposure. Accordingly, Chai et al. reported that H_2O_2-mediated cytotoxicity, resulting from incubation of PC12 cells with green tea or red wine, was completely prevented by the addition of bovine liver catalase to the culture medium.[44] All *Hamamelis* compounds tested together with the positive

dx.doi.org/10.1021/np200426k | *J. Nat. Prod.* XXXX, XXX, XXX−XXX

control used (EGCG)[45,46] generated H_2O_2 in a concentration-dependent manner in DMEM (Figure 5a). Hamamelitannin showed the highest H_2O_2 production, at 100 μg/mL. As expected, supplementing the cell culture medium with 100 U/mL catalase resulted in almost complete decomposition of polyphenol-generated H_2O_2 in all cases (Figure 5b). The next step was to study the antiproliferative capacity of *H. virginiana* polyphenolics by co-incubating with catalase. This enzyme had little effect on HT29 cells incubated with hydrolyzable tannins (IC_{50} in DMEM = 28 μg/mL ± 8.8 (Figure 2a)/IC_{50} in DMEM with catalase = 34 μg/mL ± 1.2 (Figure 2b) for pentagalloylglucose and IC_{50} in DMEM = 20 μg/mL ± 4.5 (Figure 2a)/IC_{50} in DMEM with catalase =13 μg/mL ± 4.6 (Figure 2b) for hamamelitannin), whereas F800H4 cytotoxicity was shown to be partially attributable to H_2O_2-mediated modulation (IC_{50} in DMEM = 38 μg/mL ± 4.4 (Figure 2a)/IC_{50} in DMEM with catalase = 95 μg/mL ± 8.7 (Figure 2b)). This effect is probably triggered by the highly reactive pyrogallol moieties in the condensed tannins. Interestingly, the results obtained for the positive control, EGCG, a flavan-3-ol with a pyrogallol B-ring, are in accordance with this hypothesis. Consequently, the difference between the IC_{50} value of F800H4 determined in HT29 cells incubated with catalase (Figure 2b) and the value established in NCM460 cells (Figure 2c) is not as high as when we compared the results obtained for HT29 without catalase (Figure 2a), which were artifactual, with NCM460 (Figure 2c). This demonstrates that, as with pentagalloylglucose, F800H4 is not completely specific against cancer cells. Interestingly, the cytotoxic activity of hamamelitannin was not modified by the addition of catalase to the medium.

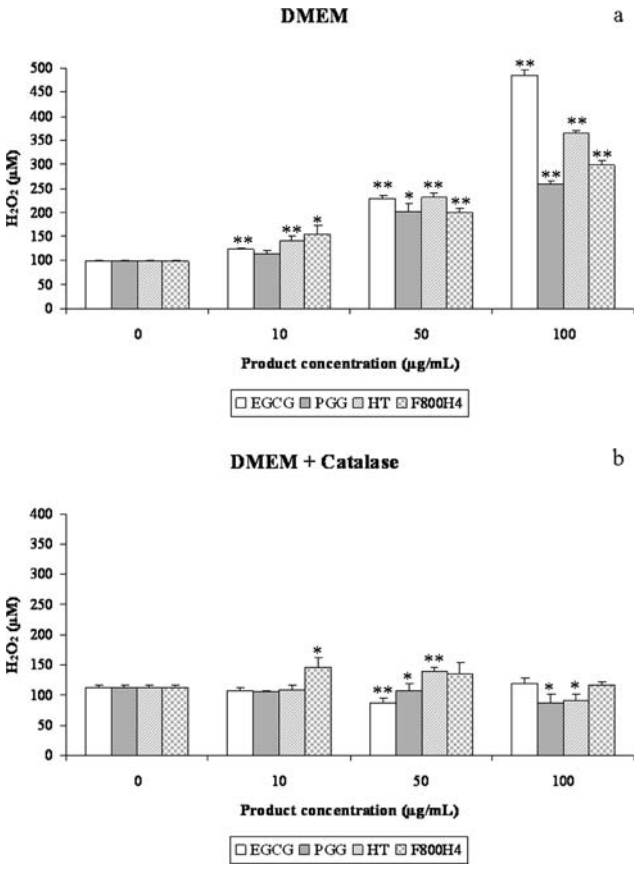

Figure 5. (a) H_2O_2 concentration in cell culture medium (DMEM + 10% FCS + 0.1% streptomycin/penicillin) with pentagalloyl glucose, hamamelitannin, and the proanthocyanidin-rich fraction F800H4 in medium. (b) H_2O_2 concentration produced in DMEM culture medium with catalase (100 U/mL) after incubation with witch hazel compounds. Epigallocatechin gallate is used as a positive control. Mean ± standard deviation of two independent experiments. $^{**}p < 0.001$ and $^{*}p < 0.05$, significant difference with respect to the corresponding value in untreated cells (Ct).

In summary, we conclude that pentagalloylglucose and the proanthocyanidin-rich fraction F800H4 do not show specificity for cancerous cells, whereas hamamelitannin is a promising chemotherapeutic agent, which might be used for the treatment of colon cancer without compromising the viability of normal colon cells. Hamamelitannin appears to contain a highly reactive phenolic position that can be detected by the stable radical TNPTM, which may explain its efficacy at inhibiting colon cancer cell growth. These findings may lead to a better understanding of the structure–bioactivity relationship of tannins, which should be of assistance for formulations of chemopreventive and chemotherapeutic agents.

EXPERIMENTAL SECTION

General Experimental Procedures. UV measurements were made on a Cary 50-Bio UV spectrophotometer (Varian, Palo Alto, CA, USA). Semipreparative chromatography was conducted on a Waters system (Milford, MA, USA) using an X-Terra C_{18} (19 × 250 mm, 10 μm) column. HPLC was carried out on a Hitachi (San Jose, CA, USA) system equipped with a quaternary pump, autosampler, and diode array detector and an analytical Kromasil C_{18} (Teknokroma, Barcelona, Spain) column. All chemicals were purchased from Sigma-Aldrich Co. (St Louis, MO, USA), unless otherwise specified. For extraction, we used deionized water, bulk EtOH (Momplet y Esteban, Barcelona, Spain), bulk acetone (Quimivita, Sant Adrià del Besòs, Spain), and bulk hexane (alkanes mixture) (Quimivita). For purification, deionized water, analytical grade MeOH (Panreac, Montcada i Reixac, Spain), analytical grade acetone (Carlo Erba, Milano, Italy), and preparative grade CH_3CN (E. Merck, Darmstadt, Germany) were used for semipreparative and preparative chromatography; milli-Q water and HPLC grade CH_3CN (E. Merck) were used for analytical RP-HPLC. Analytical grade MeOH (Panreac) was used for thioacidolysis and free radical scavenging assays, and analytical grade CH_3Cl (Panreac) was used for the electron transfer assays. TFA (Fluorochem, Derbyshire, UK) biotech grade was distilled in-house. HCl (37%) and HOAc were from E. Merck. Et_3N (E. Merck) was of buffer grade. Deuterated solvents for NMR were from SDS (Peypin, France). DPPH (95%) was from Aldrich (Gillingham-Dorset, UK), and 6-hydroxy-2,5,7,8-tetramethylchroman-2-carboxylic acid (Trolox) (97%) was from Aldrich (Milwaukee, WI, USA). HNTTM and TNPTM radicals were synthesized as described elsewhere.[30,47] Antibiotics (10 000 U/mL penicillin, 10 000 μg/mL streptomycin) were obtained from Gibco-BRL (Eggenstein, Germany), fetal calf serum (FCS) was from Invitrogen (Paisley, UK), and trypsin EDTA solution C (0.05% trypsin–0.02% EDTA) was from Biological Industries (Kibbutz Beit Haemet, Israel). The annexin V/FITC kit was obtained from Bender System (Vienna, Austria). M3Base medium was purchased from INCELL (San Antonio, TX, USA).

Extraction, Fractionation, and Characterization of F800H4. Polyphenols were obtained from witch hazel bark by extraction with acetone–water (7:3) and fractionation with EtOAc,[22] which produced fraction OWH (polyphenols soluble in EtOAc and H_2O) and fraction AH (polyphenols only soluble in H_2O). To generate fraction F800H4, AH (800 mg) was dissolved in 50% MeOH and fractionated on a Sephadex LH-20 column (50 × 2.5 cm i.d.) using a gradient of MeOH in H_2O and a final step of washing with acetone, as previously reported.[48] Five subfractions (800H1 to 800H5) were collected, and their absorbance was measured at 280 and 400 nm; yield, 8% from

dx.doi.org/10.1021/np200426k | J. Nat. Prod. XXXX, XXX, XXX–XXX

fraction AH; 0.05% from witch hazel bark. Table 1 shows the chemical composition of fraction F800H4, which was estimated as previously described.[22] The content of condensed tannins was estimated by thioacidolytic depolymerization in the presence of cysteamine and HPLC analysis of the cleaved units. The hydrolyzable tannins were determined directly from the fraction by HPLC and standards.

Purification of Pentagalloylglucose. Pentagalloylglucose was purified from fraction OWH by semipreparative chromatography on a Waters system (Milford, MA, USA) using an X-Terra C_{18} (19 × 250 mm, 10 μm) column. A total amount of 2 g of OWH was processed in successive chromatographic runs with loads of 200 mg, 4 mL each, and elution by a binary system [solvent A, 0.1% aqueous TFA; solvent B, 0.08% TFA in H_2O−CH_3CN (1:4)] under the following conditions: 10 min at 16% B and two gradients, 16−36% B over 40 min, and 36−55% B over 5 min, at a flow rate of 10 mL/min with detection at 235 nm. The purity of the pentagalloylglucose was ascertained by HPLC on a Hitachi (San Jose, CA, USA) system equipped with a quaternary pump, autosampler, and diode array detector and an analytical Kromasil C_{18} (Teknokroma, Barcelona, Spain) column under the same elution conditions at a flow rate of 1 mL/min. Pentagalloylglucose was lyophilized, and its identity was confirmed by chromatography coupled to high-resolution mass spectrometry and NMR; purity, 95% by HPLC; yield, 3.8% from fraction OWH, 0.03% from witch hazel bark.

DPPH Assay. The antiradical capacity of the polyphenols was evaluated by the DPPH stable radical method.[49] Fresh MeOH solutions (2 mL) at concentrations ranging from 2 to 30 μM were added to a freshly prepared radical solution (2 mL, 120 μM) in deoxygenated MeOH. The mixture was incubated for 30 min at room temperature in the dark, and the UV absorbance at 517 nm was measured. The results were plotted as the percentage of absorbance disappearance $[(1 - A/A_0) \times 100]$ against the amount of sample divided by the initial concentration of DPPH. Each data point was the result of three independent determinations. A dose−response curve was obtained for every sample. The results are expressed as the efficient concentration, EC_{50}, given as the amount of polyphenols that consumes half the amount of free radical divided by the initial amount of DPPH in micromoles. The results are also expressed as antiradical power (ARP), which is the inverse of EC_{50}. UV measurements were made on a Cary 50-Bio UV spectrophotometer (Varian, Palo Alto, CA, USA).

Electron Transfer Capacity against the Stable Free Radicals HNTTM and TNPTM. Fresh solutions of the polyphenols (2 mL) at concentrations ranging from 2 to 62 μM were added to a freshly prepared solution of HNTTM (2 mL, 120 μM) in deoxygenated $CHCl_3$−MeOH (2:1). The mixture was incubated for 7 h at room temperature in the dark, and the UV absorbance was measured at 384 nm. The results are plotted as the percentage of absorbance disappearance $[(1 - A/A_0) \times 100]$ against the amount of sample divided by the initial amount of the radical in micromoles, as described for DPPH. Each data point was the result of three independent determinations. A dose−response curve was obtained for every sample. The results are expressed as the efficient concentration, EC_{50}, and as ARP. The working conditions with TNPTM were essentially those described for HNTTM[30] with some differences. The concentration range was 10−120 μM, the incubation time was 48 h, and the absorbance was measured at 378 nm. The results are plotted as described for HNTTM.

Cell Culture. Human colorectal adenocarcinoma HT29 cells (obtained from the American Type Culture Collection, HTB-38) were grown as a monolayer culture in Dulbecco's modified Eagle's medium (DMEM) in the presence of 10% heat-inactivated fetal calf serum and 0.1% streptomycin/penicillin in standard culture conditions. NCM460 cells, obtained by a Material Transfer Agreement with INCELL, are from an epithelial cell line derived from the normal colon mucosa of a 68-year-old Hispanic male.[43] They were grown as a monolayer culture in M3Base medium (which contains growth supplements and antibiotics) supplemented with 10% heat-inactivated fetal calf serum and 2.5 mM D-glucose (final concentration 5 mM glucose). The cells were cultured at 37 °C in a 95% air, 5% CO_2 humidified environment.

Determination of Cell Viability. The assay was performed using a variation of the MTT assay described by Mosmann.[50] The assay is based upon the principle of reduction of MTT into blue formazan pigments by viable mitochondria in healthy cells. The cells were seeded at densities of 3×10^3 cells/well (HT29 cells) and 1×10^4 cells/well (NCM460 cells) in 96-well flat-bottom plates. After 24 h of incubation at 37 °C, the polyphenolic samples were added to the cells at different concentrations in fresh medium. Some experiments were performed in the presence of catalase (100 U/mL, from bovine liver) to examine the potential influence on extracellular H_2O_2. The use of an antioxidant enzyme in the cell medium allows us to rule out the effects of exogenous H_2O_2 generated during the incubation with polyphenols. The addition of this enzyme does not affect the cellular markers, since it does not enter the cells and is removed after incubation. In all cases the antitumor agent EGCG was used as standard. The culture was incubated for 72 h. Next the medium was removed, and 50 μL of MTT (1 mg/mL in PBS) with 50 μL of fresh medium was added to each well and incubated for 1 h. The MTT reduced to blue formazan, and the precipitate was dissolved in 100 μL of DMSO; absorbance values were measured on an ELISA plate reader (550 nM) (Tecan Sunrise MR20-301, Tecan, Salzburg, Austria). Absorbance was taken as proportional to the number of living cells. The concentrations that caused 50% cell growth inhibition (IC_{50}) were estimated from the dose−viability curves.

Cell Cycle Analysis by FACS. The cell cycle was analyzed by measuring the cellular DNA content using the fluorescent nucleic acid dye propidium iodide (PI) to identify the proportion of cells in each stage of the cell cycle. The assay was carried out using flow cytometry with a fluorescence-activated cell sorter (FACS). HT29 cells were plated in six-well flat-bottom plates at a density of 87×10^3 cells/well. After 24 h of incubation at 37 °C, the polyphenolic fractions were added to the cells at their respective IC_{50} values. We used the G1/S cell cycle inhibitor HU at 1 mM as standard. The cultures were incubated for 72 h in the absence or presence of the polyphenolic fractions. The cells were trypsinized, pelleted by centrifugation (1500 rpm for 5 min), and stained in Tris-buffered saline containing 50 μg/mL PI, 10 μg/mL RNase free of DNase, and 0.1% Igepal CA-630. They were incubated in the dark for 1 h at 4 °C. Cell cycle analysis was performed by FACS (Epics XL flow cytometer, Coulter Corp., Hialeah, FL, USA) at 488 nm.[51]

Apoptosis Analysis by FACS. Double staining with annexin V-FITC and PI measured by FACS was used to determine the percentage of apoptotic cells. Annexin+/PI− cells were considered early apoptotic cells. Annexin+/PI+ and annexin−/PI+ cells were classed together as late apoptotic/necrotic cells, since this method does not differentiate necrotic cells from cells in late stages of apoptosis, which are also permeable to PI. The cells were seeded, treated, and collected as described in the previous section. ST (1 μM) was utilized as a control of apoptosis induction. After centrifugation (1500 rpm for 5 min), they were washed in binding buffer (10 mM Hepes, pH 7.4, 140 mM NaCl, 2.5 mM $CaCl_2$) and resuspended in the same buffer. Annexin V-FITC was added using the annexin V-FITC kit. Afterward, the cells were incubated for 30 min at room temperature in the dark. Next, PI was added 1 min before the FACS analysis at 20 μg/mL. Fluorescence was measured at 495 nm (annexin V-FITC) and 488 nm (PI).

Determination of H_2O_2 (FOX Assay). H_2O_2 in the cell culture medium was determined using the ferrous oxidation xylenol orange (FOX) assay.[52] After oxidation of Fe(II) to Fe(III) by H_2O_2, the resulting xylenol orange−Fe(III) complex was quantified spectrophotometrically (560 nm). The cells were incubated for 72 h with a range of concentrations of witch hazel compounds in culture medium (DMEM or M3Base) either alone or in the presence of catalase (100 U/mL, from bovine liver) under cell culture conditions (96-well flat-bottom plate, in the absence of cells). EGCG was used as a positive control in this assay given that it has already been reported that this product generates high levels of ROS in cell culture media. Next, 100 μL of medium was transferred to a new 96-well flat-bottom plate. FOX reagent (900 μL) was added to each aliquot: 100 μM xylenol orange, 250 μM ferrous ammonium sulfate, 25 mM H_2SO_4 and 4 mM BHT in

90% (v/v) MeOH. After 30 min, absorbance at 560 nm was measured in a microplate reader (Tecan Sunrise MR20-301, Tecan). Peroxides were quantified by comparing the absorbance to a standard curve (H_2O_2 concentrations: 0−150 μM).

Data Presentation and Statistical Analysis. Data are given as the means ± SD (standard deviation). For each assay, the parametric unpaired two-tailed independent sample *t* test was used for statistical comparison with the untreated control cells, and differences were considered to be significant when $p < 0.05$ and $p < 0.001$.

AUTHOR INFORMATION

Corresponding Author

*Phone: 0034 934021593. Fax: 0034 934021559. E-mail: martacascante@ub.edu.

Present Address

‡Freiburg Institute for Advanced Studies. School of Life Sciences−LifeNet, Freiburg im Breisgau, Germany.

ACKNOWLEDGMENTS

Financial support was provided by grants SAF2008-00164, SAF2011-25726, AGL2006-12210-C03-02/ALI, and AGL2009-12374-C03-03/ALI from the Spanish government Ministerio de Ciencia e Innovación and personal financial support (FPU program); from the Ministerio de Educación y Ciencia; and from the Red Temática de Investigación Cooperativa en Cáncer, Instituto de Salud Carlos III, Spanish Ministry of Science and Innovation & European Regional Development Fund (ERDF) "Una manera de hacer Europa" (ISCIII-RTICC grants RD06/0020/0046). We have also received financial support from the AGAUR-Generalitat de Catalunya (grant 2009SGR1308, 2009 CTP 00026, and Icrea Academia Award 2010 granted to M.C.) and the European Commission (FP7) ETHERPATHS KBBE-grant agreement no. 22263.

REFERENCES

(1) Theodoratou, E.; Kyle, J.; Cetnarskyj, R.; Farrington, S. M.; Tenesa, A.; Barnetson, R.; Porteous, M.; Dunlop, M.; Campbell, H. *Cancer Epidemiol. Biomarkers Prev.* **2007**, *16*, 684−693.

(2) Cutler, G. J.; Nettleton, J. A.; Ross, J. A.; Harnack, L. J.; Jacobs, D. R. Jr.; Scrafford, C. G.; Barraj, L. M.; Mink, P. J.; Robien, K. *Int. J. Cancer.* **2008**, *123*, 664−671.

(3) Vennat, B.; Pourrat, H.; Pouget, M. P.; Gross, D.; Pourrat, A. *Planta Med.* **1988**, *54*, 454−457.

(4) Hu, H.; Chai, Y.; Wang, L.; Zhang, J.; Lee, H. J.; Kim, S. H.; Lu, J. *Mol. Cancer Ther.* **2009**, *8*, 2833−2843.

(5) Mutanen, M.; Pajari, A. M.; Paivarinta, E.; Misikangas, M.; Rajakangas, J.; Marttinen, M.; Oikarinen, S. *Asia Pac. J. Clin. Nutr.* **2008**, *17* (Suppl 1), 123−125.

(6) Engelbrecht, A. M.; Mattheyse, M.; Ellis, B.; Loos, B.; Thomas, M.; Smith, R.; Peters, S.; Smith, C.; Myburgh, K. *Cancer Lett.* **2007**, *258*, 144−153.

(7) Chung, W. G.; Miranda, C. L.; Stevens, J. F.; Maier, C. S. *Food Chem. Toxicol.* **2009**, *47*, 827−836.

(8) Gosse, F.; Guyot, S.; Roussi, S.; Lobstein, A.; Fischer, B.; Seiler, N.; Raul, F. *Carcinogenesis* **2005**, *26*, 1291−1295.

(9) Kolodziel, H.; Heberland, C.; Woerdenbag, H. J.; Konings, A. W. T. *Phytother. Res.* **1995**, *9*, 410−415.

(10) Hu, H.; Lee, H. J.; Jiang, C.; Zhang, J.; Wang, L.; Zhao, Y.; Xiang, Q.; Lee, E. O.; Kim, S. H.; Lu, J. *Mol. Cancer Ther.* **2008**, *7*, 2681−2691.

(11) Kuo, P. T.; Lin, T. P.; Liu, L. C.; Huang, C. H.; Lin, J. K.; Kao, J. Y.; Way, T. D. *J. Agric. Food Chem.* **2009**, *57*, 3331−3339.

(12) Huh, J. E.; Lee, E. O.; Kim, M. S.; Kang, K. S.; Kim, C. H.; Cha, B. C.; Surh, Y. J.; Kim, S. H. *Carcinogenesis* **2005**, *26*, 1436−1445.

(13) Miyamoto, K.; Kishi, N.; Koshiura, R.; Yoshida, T.; Hatano, T.; Okuda, T. *Chem. Pharm. Bull. (Tokyo)* **1987**, *35*, 814−822.

(14) Chen, W. J.; Chang, C. Y.; Lin, J. K. *Biochem. Pharmacol.* **2003**, *65*, 1777−1785.

(15) Chen, W. J.; Lin, J. K. *J. Biol. Chem.* **2004**, *279*, 13496−13505.

(16) Oh, G. S.; Pae, H. O.; Oh, H.; Hong, S. G.; Kim, I. K.; Chai, K. Y.; Yun, Y. G.; Kwon, T. O.; Chung, H. T. *Cancer Lett.* **2001**, *174*, 17−24.

(17) Ho, L. L.; Chen, W. J.; Lin-Shiau, S. Y.; Lin, J. K. *Eur. J. Pharmacol.* **2002**, *453*, 149−158.

(18) Habtemariam, S. *Toxicon* **2002**, *40*, 83−88.

(19) Sakai, H.; Yamada, Y.; Shimizu, M.; Saito, K.; Moriwaki, H.; Hara, A. *Chem. Biol. Interact.* **2010**, *184*, 423−430.

(20) Hartisch, C.; Kolodziej, H.; von Bruchhausen, F. *Planta Med.* **1997**, *63*, 106−110.

(21) Wasilewicz, M. P.; Kolodziej, B.; Bojulko, T.; Kaczmarczyk, M.; Sulzyc-Bielicka, V.; Bielicki, D.; Ciepiela, K. *Int. J. Colorectal Dis.* **2010**, *25*, 1079−1085.

(22) Touriño, S.; Lizarraga, D.; Carreras, A.; Lorenzo, S.; Ugartondo, V.; Mitjans, M.; Vinardell, M. P.; Julia, L.; Cascante, M.; Torres, J. L. *Chem. Res. Toxicol.* **2008**, *21*, 696−704.

(23) Lizarraga, D.; Tourino, S.; Reyes-Zurita, F. J.; de Kok, T. M.; van Delft, J. H.; Maas, L. M.; Briede, J. J.; Centelles, J. J.; Torres, J. L.; Cascante, M. *J. Agric. Food Chem.* **2008**, *56*, 11675−11682.

(24) Masaki, H.; Atsumi, T.; Sakurai, H. *Free Radical Res. Commun.* **1993**, *19*, 333−340.

(25) Masaki, H.; Atsumi, T.; Sakurai, H. *Biol. Pharm. Bull.* **1995**, *18*, 59−63.

(26) Halliwell, B. *FEBS Lett.* **2003**, *540*, 3−6.

(27) Bellion, P.; Olk, M.; Will, F.; Dietrich, H.; Baum, M.; Eisenbrand, G.; Janzowski, C. *Mol. Nutr. Food Res.* **2009**, *53*, 1226−1236.

(28) Sang, S.; Hou, Z.; Lambert, J. D.; Yang, C. S. *Antioxid. Redox Signal.* **2005**, *7*, 1704−1714.

(29) Foti, M. C.; Daquino, C.; Geraci, C. *J. Org. Chem.* **2004**, *69*, 2309−2314.

(30) Torres, J. L.; Carreras, A.; Jimenez, A.; Brillas, E.; Torrelles, X.; Rius, J.; Julia, L. *J. Org. Chem.* **2007**, *72*, 3750−3756.

(31) Sato, M.; Toyazaki, H.; Yoshioka, Y.; Yokoi, N.; Yamasaki, T. *Chem. Pharm. Bull. (Tokyo)* **2010**, *58*, 98−102.

(32) Singh, B. N.; Shankar, S.; Srivastava, R. K. *Biochem. Pharmacol.* **2011**, *82*, 1807−1821.

(33) Yang, C. S.; Wang, H.; Li, G. X.; Yang, Z.; Guan, F.; Jin, H. *Pharmacol. Res.* **2011**, *64*, 113−122.

(34) Iacomino, G.; Medici, M. C.; Napoli, D.; Russo, G. L. *J. Cell. Biochem.* **2006**, *99*, 1122−1131.

(35) Elsaba, T. M.; Martinez-Pomares, L.; Robins, A. R.; Crook, S.; Seth, R.; Jackson, D.; McCart, A.; Silver, A. R.; TomLinson, I. P.; Ilyas, M. *PLoS One.* **2010**, *5*, e10714.

(36) Hu, H.; Zhang, J.; Lee, H. J.; Kim, S. H.; Lu, J. *Carcinogenesis* **2009**, *30*, 818−823.

(37) Dauer, A.; Hensel, A.; Lhoste, E.; Knasmuller, S.; Mersch-Sundermann, V. *Phytochemistry* **2003**, *63*, 199−207.

(38) McDougall, G. J.; Ross, H. A.; Ikeji, M.; Stewart, D. *J. Agric. Food Chem.* **2008**, *56*, 3016−3023.

(39) Maldonado-Celisa, M. E.; Roussia, S.; Foltzer-Jourdainne, C.; Gosse, F.; Lobstein, A.; Habold, C.; Roessner, A.; Schneider-Stock, R.; Raul, F. *Cell. Mol. Life Sci.* **2008**, *65*, 1425−1434.

(40) Ascensao, A. A.; Magalhaes, J. F.; Soares, J. M.; Ferreira, R. M.; Neuparth, M. J.; Appell, H. J.; Duarte, J. A. *Int. J. Sports Med.* **2005**, *26*, 258−267.

(41) Dhakshinamoorthy, S.; Long, D. J. 2nd; Jaiswal, A. K. *Curr. Top Cell Regul.* **2000**, *36*, 201−216.

(42) Havens, C. G.; Ho, A.; Yoshioka, N.; Dowdy, S. F. *Mol. Cell. Biol.* **2006**, *26*, 4701−4711.

(43) Moyer, M. P.; Manzano, L. A.; Merriman, R. L.; Stauffer, J. S.; Tanzer, L. R. *In Vitro Cell Dev. Biol. Anim.* **1996**, *32*, 315−317.

(44) Chai, P. C.; Long, L. H.; Halliwell, B. *Biochem. Biophys. Res. Commun.* **2003**, *304*, 650−654.

(45) Elbling, L.; Weiss, R. M.; Teufelhofer, O.; Uhl, M.; Knasmueller, S.; Schulte-Hermann, R.; Berger, W.; Micksche, M. *FASEB J.* **2005**, *19*, 807−809.
(46) Long, L. H.; Clement, M. V.; Halliwell, B. *Biochem. Biophys. Res. Commun.* **2000**, *273*, 50−53.
(47) Torres, J. L.; Varela, B.; Brillas, E.; Julia, L. *Chem. Commun. (Cambridge, U.K.).* **2003**, 74−75.
(48) Jerez, M.; Touriño, S.; Sineiro, J.; Torres, J. L.; Núñez, M. J. *Food Chem.* **2007**, *104*, 518−527.
(49) Brand-Williams, W.; Cuvelier, M. E.; Berset, C. *LWT−Food Sci. Technol.* **1995**, *28*, 25−30.
(50) Mosmann, T. *J. Immunol. Methods* **1983**, *65*, 55−63.
(51) Lozano, C.; Torres, J. L.; Julia, L.; Jimenez, A.; Centelles, J. J.; Cascante, M. *FEBS Lett.* **2005**, *579*, 4219−4225.
(52) Jiang, Z.-Y.; Hunt, J. V.; Wolff, S. P. *Anal. Biochem.* **1992**, *202*, 384−389.

ANNEX 2 (CAPÍTOL 6)

Caracterització dels canvis metabòlics associats a l'activació angiogènica: identificació de potencials dianes terapèutiques

Publicació a la revista *Carcinogenesis* amb un índex d'impacte de 5,402.

Pedro Vizán[1,†], Susana Sánchez-Tena[1], Gema Alcarraz-Vizán[1], Marta Soler[2,‡], Ramon Messeguer[2], M.Dolors Pujol[3], Wai-Nang Paul Lee[4] i Marta Cascante[1]

[1]Facultat de Biologia, Universitat de Barcelona i IBUB, unitat associada al CSIC, 08028 Barcelona, Espanya

[2]Divisió Biomed, Centre Tecnològic Leitat, Parc Científic de Barcelona, 08028 Barcelona, Espanya

[3]Departament de Farmacologia i Química Farmacèutica, Facultat de Farmàcia,

Universitat de Barcelona, 08028 Barcelona, Espanya

[4]Department of Pediatrics and Research and Education Institute, UCLA School of Medicine, Torrance, CA 90502, USA

[†]Adreça actual: Laboratory of Developmental Signalling, Cancer Research UK, London Research Institute, London WC2A 3PX, UK

[‡]Adreça actual: Institut d'Investigació Biomèdica de Bellvitge (IDIBELL), Hospital Duran i Reynals, 08907 1'Hospitalet de Llobregat, Espanya

RESUM

L'angiogènesi és un procés que consisteix en el reclutament de cèl·lules endotelials cap a un estímul angiogènic. Les cèl·lules subsegüentment proliferen i es diferencien per formar capil·lars sanguinis. Es coneix molt poc sobre l'adaptació metabòlica que pateixen les cèl·lules endotelials durant aquesta transformació. En aquest treball es van estudiar els canvis metabòlics en cèl·lules endotelials HUVEC (*Human Umbilical Vascular Endothelial Cells*) activades per factors de creixement, [1,2-$^{13}C_2$]-glucosa i un anàlisi de la distribució isotopomèrica de massa. El metabolisme de la [1,2-$^{13}C_2$]-glucosa per part de les cèl·lules HUVEC ens va permetre traçar les principals vies metabòliques de la glucosa, incloent la síntesi de glicogen, el cicle de les pentoses fosfat i la glicòlisi. L'estimulació endotelial amb VEGF (*Vascular Endothelial Growth Factor*) o FGF (*Fibroblast Growth Factor*) va mostrar una adaptació metabòlica comú basada en aquestes vies. Posteriorment, un inhibidor específic del receptor 2 del VEGF va demostrar la importància de metabolisme de glicogen i del cicle de les pentoses fosfat. A més, es va mostrar que el glicogen era exhaurit en un medi amb glucosa baixa, però, en canvi, era conservat sota condicions d'hipòxia. Finalment, es va demostrar que la inhibició directa dels enzims clau del metabolisme de glicogen i de la ruta de les pentoses fosfat reduïa la viabilitat i la migració de les cèl·lules HUVEC. En aquest sentit, inhibidors d'aquests vies han estat descrits com agents antitumorals. Per tant, els nostres resultats suggereixen que la inhibició d'aquestes vies metabòliques ofereix una nova i potent estratègia terapèutica que simultàniament inhibeix proliferació tumoral i angiogènesi.

Carcinogenesis vol.30 no.6 pp.946–952, 2009
doi:10.1093/carcin/bgp083
Advance Access publication April 15, 2009

Characterization of the metabolic changes underlying growth factor angiogenic activation: identification of new potential therapeutic targets

Pedro Vizán[4], Susana Sánchez-Tena, Gema Alcarraz-Vizán, Marta Soler[5], Ramon Messeguer[1], M.Dolors Pujol[2], Wai-Nang Paul Lee[3] and Marta Cascante*

Department of Biochemistry and Molecular Biology, Faculty of Biology, University of Barcelona, Avenue Diagonal 645, 08028 Barcelona, Spain, [1]Biomed Division, Leitat Technological Center, Parc Científic Barcelona, C/Baldiri i Reixach, 15-21, 08028 Barcelona, Spain, [2]Department of Pharmacology and Pharmaceutical Chemistry, Faculty of Pharmacy, University of Barcelona, Avenue Diagonal 643, 08028 Barcelona, Spain and [3]Department of Pediatrics and Research and Education Institute, UCLA School of Medicine, 1124 West Carson Street, RB1, Torrance, CA 90502, USA

[4]Present address: Laboratory of Developmental Signalling, Cancer Research UK London Research Institute, 44 Lincoln's Inn Fields, London WC2A 3PX, UK and [5]Present address: Cancer Biology and Epigenetics Program (PEBC), Institut d'Investigació Biomèdica de Bellvitge (IDIBELL), Hospital Duran i Reynals, Avinguda Gran Via de L'Hospitalet, 199-203, 08907 l'Hospitalet de Llobregat, Spain

*To whom correspondence should be addressed. Tel: +34 93 402 1217; Fax: +34 93 402 1219;
Email: martacascante@ub.edu

Angiogenesis is a fundamental process to normal and abnormal tissue growth and repair, which consists of recruiting endothelial cells toward an angiogenic stimulus. The cells subsequently proliferate and differentiate to form endothelial tubes and capillary-like structures. Little is known about the metabolic adaptation of endothelial cells through such a transformation. We studied the metabolic changes of endothelial cell activation by growth factors using human umbilical vein endothelial cells (HUVECs), [1,2-$^{13}C_2$]-glucose and mass isotopomer distribution analysis. The metabolism of [1,2-$^{13}C_2$]-glucose by HUVEC allows us to trace many of the main glucose metabolic pathways, including glycogen synthesis, the pentose cycle and the glycolytic pathways. So we established that these pathways were crucial to endothelial cell proliferation under vascular endothelial growth factor (VEGF) and fibroblast growth factor (FGF) stimulation. A specific VEGF receptor-2 inhibitor demonstrated the importance of glycogen metabolism and pentose cycle pathway. Furthermore, we showed that glycogen was depleted in a low glucose medium, but conserved under hypoxic conditions. Finally, we demonstrated that direct inhibition of key enzymes to glycogen metabolism and pentose phosphate pathways reduced HUVEC viability and migration. In this regard, inhibitors of these pathways have been shown to be effective antitumoral agents. To sum up, our data suggest that the inhibition of metabolic pathways offers a novel and powerful therapeutic approach, which simultaneously inhibits tumor cell proliferation and tumor-induced angiogenesis.

Introduction

One of the critical stages in tumor growth is neovascularization. The angiogenic impulse is promoted by tumor expression of proangiogenic proteins, including vascular endothelial growth factor (VEGF), fibroblast growth factor (FGF), interleukin-8, platelet-derived growth factor and transforming growth factor-beta, among others. The combined action of these factors on endothelial cells leads to the acquisition of a specific phenotype, which allows endothelial cells to migrate toward an angiogenic stimulus, proliferate and differentiate into capillary-like structures. Concretely, VEGF, which is highly upregulated in most human cancers (1), has emerged in the last few years as the crucial rate-limiting step in the regulation of normal and abnormal angiogenesis (2). Therefore, VEGF and its receptor have been exploited in antiangiogenic therapies that are already successfully applied in clinical settings (3–5). However, although patients treated with VEGF inhibitors may survive longer, there is emerging evidence that VEGF may be replaced by other angiogenic pathways as the disease progresses (5,6). Thus, a better understanding of the underlying metabolic changes that supports tumor angiogenesis downstream of VEGF activation is necessary to design complementary strategies that can overcome resistance to angiogenic therapies. In fact, in spite of the increasing recognition that the metabolome represents the end point of many cellular events (7–9), little is known about the metabolic changes underlying endothelial cell activation during angiogenesis (10–13). A better knowledge of the specific adaptation of metabolic network fluxes occurring downstream of the growth factor activation of endothelial cells could aid identification of metabolic enzyme drug targets. Such targets might help to overcome the developing resistance to VEGF-targeted therapies. Accurate substrate flow characterization of the activated endothelial cells in the angiogenic process may permit the design of effective, targeted antiangiogenic drugs acting downstream of the VEGF receptors.

Metabolic changes underlying tumor cell metabolism have been extensively studied in recent decades (14–16) and successful strategies for inhibiting the pathways on which cancer cells are strongly dependent have been proposed. In particular, inhibition of nucleic acid synthesis has been shown to be successful in chemotherapy (17). Recently, it has been demonstrated in different tumor cell lines that pentose phosphate pathway (PPP) inhibition results in an effective decrease in tumor cell proliferation (18–22). Moreover, it has been proposed that inhibition of normally enhanced tumor cell glycolysis can be a novel strategy for anticancer treatment (23,24) or for overcoming the drug resistance associated with mitochondrial respiratory defects and hypoxia (23,25).

Stable isotope-based dynamic metabolic profiling using gas chromatography/mass spectrometry is a powerful new tool of great use in drug development (8). In particular, the use of glucose labeled at the first two carbon positions with the stable isotope ^{13}C has been shown to be effective in revealing detailed substrate flow and distribution patterns in the complex metabolic network of different tumoral and non-tumoral cells. Recent examples of the strength of this approach include the elucidation of the metabolic mechanism underlying butyrate-induced cell differentiation (26) and the characterization of distinctive metabolic profiles that correlate with different point mutations in K-ras oncogene, which confer different degrees of aggressiveness *in vivo*, proving how the most aggressive mutations had an increased glycolytic rate (27). In the present study, we used human umbilical vein endothelial cells (HUVECs) as an angiogenic model. We adopted a mass isotope distribution analysis approach with [1,2-$^{13}C_2$]-glucose tracer labeling to reveal the mechanisms of endothelial cells' metabolic network in response to the activation produced by the angiogenic stimulus of different growth factors. The metabolism of [1,2-$^{13}C_2$]-glucose by HUVEC allows us to trace many of the main glucose metabolic pathways, including glycogen synthesis, the pentose cycle pathways and the glycolytic pathways. To examine the downstream effect of VEGF, we used a well-known vascular endothelial growth factor receptor-2 (VEGFR-2) inhibitor, 5-diarylureaoxy-benzimidazole, which has also shown effects on Tie-2 receptors (28). This inhibitor allowed us to analyze the flux changes downstream of a specific inhibition of the angiogenic stimulus. The

Abbreviations: DMEM, Dulbecco's modified Eagle's medium; EBM, endothelial cell basal medium; EGM, endothelial cell growth medium; FCS, fetal calf serum; FGF, fibroblast growth factor; HUVEC, human umbilical vein endothelial cell; PPP, pentose phosphate pathway; VEGF, vascular endothelial growth factor; VEGFR-2, vascular endothelial growth factor receptor-2.

characterization of the effects of VEGFR-2 inhibitors at metabolic level contributes to the design of new therapeutic strategies for overcoming drug resistance. Such strategies are based on targeting the appropriate metabolic pathways, which mimic the effect of direct receptor inhibition on the metabolic network.

Materials and methods

Cell culture conditions

HUVECs (AdvanCell, Barcelona, Spain) were cultured on gelatin at 37°C in a humidified atmosphere of 5% CO_2 and 95% air in endothelial cell basal medium (EBM) (Clonetics, San Diego, CA) and supplemented with endothelial cell growth medium (EGM) SingleQuots (Clonetics) and 10% fetal calf serum (FCS) (Biological Industries, Kibbutz Beit Ha'Emek, Israel). In these standard conditions, a 7.4-fold change with respect to the initial cell number was observed at 72 h.

Specifically activated cell growth assay for the mass isotopomer distribution analysis analysis

Cells grown to 80–90% confluence were removed from the flask using 0.025% trypsin/ethylenediaminetetraacetic acid (Gibco, Invitrogen, Carlsbad, CA) at room temperature. Cells were seeded at a density of 4×10^5 onto gelatine-precoated 75 cm^2 petri dishes (Falcon, BD biosciences, Franklin Lakes, NJ) in EGM (5 mmol/l glucose) and supplemented with EGM SingleQuots and 10% FCS for 24 h. The incubation medium was then removed and the plates were washed twice with Hanks' balanced salt solution (Clonetics). Specifically activated cell growth media was then added to the cell culture. This media contained EBM supplemented with 10 ng/ml VEGF (R&D systems, Minneapolis, MN) or 0.3 ng/ml basic FGF plus 2% FCS supplemented with 3 μg/ml heparin, 1 μg/ml hydrocortisone and 10 mmol/l of [1,2-$^{13}C_2$]-glucose (50% isotope enrichment, Isotec, Sigma-Aldrich, St. Louis, MO). The inhibitor of VEGFR-2, 5-diarylurea-oxy-benzimidazole, was used at a final concentration of 85 nM. Cell cultures were incubated for 72 h. After the incubations, cells were centrifuged (1350 r.p.m. for 5 min) to obtain the incubation medium and cell pellets. At the end of the experiment, the final cell numbers were measured with a hemocytometer. To determine glycogen content, cells were immediately frozen in liquid nitrogen before being processed.

Glucose and lactate concentration

The glucose and lactate concentrations in the culture medium were determined as described previously (29,30) using a Cobas Mira Plus chemistry analyzer (HORIBA ABX, Montpellier, France) at the beginning and at the end of the incubation time, to calculate glucose consumption and lactate production.

Lactate isotopomeric analysis

Lactate from the cell culture medium was extracted by ethyl acetate after acidification with HCl. Lactate was derivatized to its propylamide-heptafluorobutyric form and the m/z 328 (carbons 1–3 of lactate, chemical ionization) was monitored as described (31).

RNA ribose isotopomeric analysis

RNA ribose was isolated by acid hydrolysis of cellular RNA after Trizol (Invitrogen, Carlsbad, CA) purification of cell extracts. Ribose isolated from RNA was derivatized to its aldonitrile acetate form using hydroxylamine in pyridine and acetic anhydride. The ion cluster around the m/z 256 (carbons 1–5 of ribose, chemical ionization) was monitored to find the molar enrichment and positional distribution of ^{13}C labels in ribose (31).

Glycogen content determination and isotopomeric analysis

The glycogen content in frozen cell monolayers obtained from HUVEC was extracted as described previously (32), by direct digestion of sonicated extracts with amyloglucosidase (Sigma-Aldrich, St. Louis, MO). The glycogen was then purified using a tandem set of Dowex-1X8/ Dowex-50WX8 (Sigma) ion exchange columns. For the isotopomeric analysis, the glycogen was converted to its glucose aldonitrile pentaacetate derivative as described previously (33) and the ion cluster around m/z 328 was monitored. Measurement of the glycogen content was carried out using the isotopomer [U-^{13}C-D_7]-glucose as the recovery standard and internal standard quantification procedures. The ion cluster for the [U-^{13}C-D_7]-glucose of the glucose aldonitrile pentaacetate derivative was monitored from m/z 339 to m/z 341. Glucose from glycogen was corrected by million of cells.

Gas chromatography/mass spectrometry

Mass spectral data were obtained on an HP5973 mass selective detector connected to an HP6890 gas chromatograph. The settings were as follows: gas chromatography inlet 230°C; transfer line 280°C; mass spectrometry source 230°C and mass spectrometry quad 150°C. An HP-5 capillary column (30 m length, 250 mm diameter and 0.25 mm film thickness) was used to analyze glucose, ribose and lactate.

Hypoxic or hypoglycaemic conditions

To determine glycogen content under hypoxic or hypoglycaemic conditions, HUVECs were seeded at a density of 1×10^6 onto 75 cm^2 petri dishes (Falcon) in EGM (5 mmol/l glucose) supplemented with EGM SingleQuots and 10% FCS for 24 h. The incubation medium was then removed and specifically activated cell growth media added in normoxic (37°C in a humidified atmosphere of 5% CO_2 and 95% air), hypoxic (37°C in a humidified atmosphere of 5% CO_2, 1% O_2) or hypoglycaemic conditions [EGM 10 mmol/l glucose as a positive control, Dulbecco's modified Eagle's medium (DMEM; Sigma) 10 mmol/l glucose supplemented with EGM SingleQuots and 10% FCS as a negative control and DMEM without glucose supplemented with EGM SingleQuots and 10% FCS]. Cells were counted after 24 h. The medium was stored for subsequent analyses of glucose consumption and lactate production, as described above. In parallel, cell monolayers were immediately frozen in liquid nitrogen for glycogen determinations. Glycogen was extracted and quantified as described previously (34), with 30% (wt/vol) KOH and Whatman 31ET paper to precipitate the glycogen. Glucose released from glycogen was measured enzymatically in a Cobas Mira Plus chemistry analyzer (HORIBA ABX) and then corrected by protein content.

Cell viability assay

This assay was performed using a variation of the method described by Mosmann (35), as specified in Matito *et al*. (36). For this assay, 3×10^3 HUVEC cells/well were cultured on 96-well plates. Inhibitors CP-320626, G5 and O1 were added from 10 to 100 μM for 48 h. Relative cell viability was measured by absorbance on an enzyme-linked immunosorbent assay plate reader (Tecan Sunrise MR20-301, TECAN, Männedorf, Switzerland) at 550 nm.

Inhibitor CP-320626, kindly provided by Pfizer (New York City, NY) is an indole-2-carboxamide that binds at the dimmer interface site of glycogen phosphorylase, which was recently identified as a new allosteric site by X-ray crystallographic analysis (37,38). G5 and O1 were kindly supplied by Jaime Rubio from the University of Barcelona. Molecular modeling has been used in the development of these novel compound inhibitors of glucose-6-phosphate dehydrogenase and transketolase, respectively.

Migration assay

Migration assays were performed as described previously (39), with the following modifications: 24-well cell culture plates (Falcon) were used with light-opaque polyethylene terephthalate membrane filter inserts with 8 mm pores (Transwell HTS FluoroBlokTM Multiwell Insert Systems from Becton Dickinson, Franklin Lakes, NJ). The upper and lower surfaces of the Transwell membranes were coated for 2 h at 37°C with 15 μg/ml type I Collagen. HUVECs were (5×10^4 cells) suspended in 100 μl of EBM, and in absence of serum or other supplements, were seeded after coating onto the upper side of each Transwell chamber and placed 4 h at 37°C. Then, 500 μl of the inhibitors at IC50 (i.e. concentration at which the cell viability is 50% of the control calculated from Figure 4A: 40 μM of CP-320626, 30 μM of G5 and 25 μM of O1) and at 10 × IC50 in EBM with 10% FCS and supplements were added to the lower compartment of the 24-well plates to test their inhibitory effect. After 4 h at 37°C, cells that had migrated to the lower side of the transwell were incubated with 5 mM Calcein-AM (Calbiochem, MERCK, Whitehouse Station, NJ) for 25–30 min at 37°C. Migrated cells were counted under a light microscope at a magnification of ×10.

Results

VEGF and FGF trigger a common characteristic metabolic changes in HUVECs

Lactate in the cell culture medium, the secreted product of glycolysis, was used to determine the contribution of glycolysis and the oxidative PPP to the central glucose metabolism. The unlabeled species (m0) represents the corrected lactate mass isotopomer distribution without the ^{13}C label; m1 represents the distribution with one ^{13}C label and m2 with two ^{13}C labels. The species m2 originates from glucose that is converted to lactate directly by glycolysis. In contrast, m1 originates from glucose metabolized by direct oxidation via the oxidative steps of the PPP, which is then recycled to glycolysis via the non-oxidative pentose cycle. Thus, we can calculate the PC parameter, which gives us an idea of pentose cycle use (as a percentage) with respect to glycolysis (31). FGF activation provoked greater proliferation than

VEGF activation (Figure 1). Therefore, the concentration of lactate secreted into the medium was higher in FGF-activated HUVECs (data not shown). Consequently, we observed a slight increase in ^{13}C-enriched lactate after FGF activation, with respect to VEGF (Table 1A, upper panel), measured as $\sum$mn = m1 + 2 × m2, a parameter that represents the average number of ^{13}C atoms per molecule. However, the flux balance (PC parameter) was not significantly altered, indicating a similar metabolic lactate pattern after both FGF and VEGF activation. Moreover, unlabeled lactate (m0) accumulated in similar amounts. This confirmed that the utilization of other carbon sources via degradation of the amino acids glutamine (glutaminolysis) and serine (serinolysis) is also maintained in HUVECs independently of the two growth factor activation pathways.

Due to the characteristics of the PPP, label incorporation into ribose occurred with the isotopomers m1 and m2 but also m3 and m4 species can be found. m1 is formed when [1,2-$^{13}C_2$]-glucose is decarboxylated by the oxidative branch of the PPP. m2 is synthesized by the reversible non-oxidative branch of the cycle. The combination of these two branches generates m3 and m4 species. The total label incorporation or ^{13}C enrichment is measured as $\sum$mn = m1 + 2 × m2 + 3 × m3 + 4 × m4. To assess the contribution of each PPP branch, the oxidative versus non-oxidative ratio was used, measured as ox:non-ox = (m1 + m3)/(m2 + m3 + 2 × m4), since m1 and m3 need the oxidative branch to be formed, and m2, m3 and m4 species require the non-oxidative branch (twice in m4). In Table IB (upper panel), a representative isotopomeric distribution of a single experiment is displayed. Significantly, similar traffic of glucose through the PPP was observed after either FGF or VEGF activation. As we noticed for lactate, the higher proliferation rate caused by FGF activation (Figure 1) caused a slight increase in ^{13}C enrichment ($\sum$mn), with respect to VEGF-activated cells. However, the flux balance through the two branches of the pentose cycle (ox:non-ox ratio) was very similar and did not present consistent differences in the replicates performed.

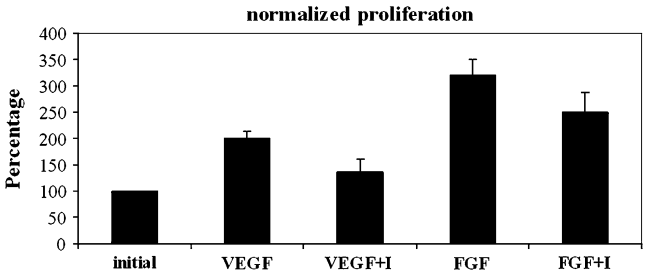

Fig. 1. Normalized cell counts with respect to the initial cell number. FGF activation induced higher proliferation rates than VEGF activation. The inhibitor (I: 5-diarylurea-oxy-benzimidazole) caused a decrease in both VEGF- and FGF-treated cells. However, this was relatively more pronounced when VEGF was used to activate HUVECs. Data are presented as mean ± SD of three independent experiments, 221 × 113 mm (600 × 600 DPI).

High, similar glycogen concentrations were found in HUVECs under all the culture conditions. ^{13}C labeling was found in glycogen reservoirs. The analysis of glucose isotopomer distribution obtained from glycogen displayed only m0 and m2 species, indicating that the glycogen carbon source is glucose from the culture medium. A representative ^{13}C enrichment of glycogen after FGF or VEGF activation, measured as $\sum$mn = 2 × m2, is depicted in Figure 2A (black bars). Since initial glycogen reservoirs were not labeled, ^{13}C incorporation into glycogen from glucose increases with time and is dependent on the proliferation rate, as the cells have to replenish their glycogen content. Thus, as observed for lactate and ribose, there was a higher concentration of labeled glucose in glycogen after FGF activation than after VEGF activation, due to its higher proliferation rate (Figure 1).

Inhibition of VEGFR-2 decreases HUVEC proliferation via specific pathways activated by VEGF

5-Diarylurea-oxy-benzimidazole is a well-known VEGFR-2 inhibitor. It is often used to investigate the link between receptor activation and signaling pathways. The use of 5-diarylurea-oxy-benzimidazole allows us to study whether the characteristic, activated HUVEC metabolic pattern described above is the downstream effect of receptor activation-signaling pathways. The inhibitor caused ∼30% of proliferation inhibition when HUVECs were activated with VEGF and, unexpectedly, 20% of proliferation inhibition when cells were activated with FGF (Figure 1). Interestingly, inhibitor treatment did not affect the metabolic network when HUVEC activation was mediated by FGF; meanwhile, VEGF-activated cells suffered changes in ribose and glycogen metabolism. Thus, meanwhile, the RNA ribose isotopomeric distribution was not affected by the inhibitor in the three experiments performed when FGF was the activator (Table IB, lower

Table I. Isotopomeric distribution

A. Lactate isotopomeric distribution

	m0	m1	m2	Σmn	PC (%)
HUVEC specific activation					
VEGF	0.8157 ± 0.006	0.0164 ± 0.001	0.1668 ± 0.0032	0.3532 ± 0.0073	3.17 ± 0.14
FGF	0.803 ± 0.007	0.0185 ± 0.0034	0.1772 ± 0.0039	0.3766 ± 0.0103	3.36 ± 0.53
VEGFR-2 inhibitor treatment					
VEGF+I	0.8202 ± 0.006	0.0156 ± 0.0014	0.1629 ± 0.0044	0.3451 ± 0.011	3.09 ± 0.20
FGF+I	0.8024 ± 0.0019	0.0174 ± 0.0008	0.179 ± 0.00126	0.379 ± 0.0027	3.13 ± 0.12

B. Ribose isotopomeric distribution

	m1	m2	m3	m4	Σmn	ox:non-ox
HUVEC specific activation						
VEGF	0.1887 ± 0.0014	0.1262 ± 0.0012	0.0332 ± 0.0004	0.0198 ± 0.0007	0.6208 ± 0.0061	1.1151 ± 0.0203
FGF	0.2015 ± 0.0021	0.1354 ± 0.0004	0.0303 ± 0.001	0.0163 ± 0.0008	0.6314 ± 0.0132	1.1697 ± 0.0056
VEGFR-2 inhibitor treatment						
VEGF+I	0.1664 ± 0.0007	0.1253 ± 0.002	0.0297 ± 0.0005	0.0207 ± 0.0005	0.5879 ± 0.0125**	0.9986 ± 0.0119**
FGF+I	0.1993 ± 0.0016	0.1466 ± 0.0018	0.0306 ± 0.0005	0.0180 ± 0.0004	0.6594 ± 0.0088	1.0784 ± 0.0062

Isotopomeric distribution in lactate and RNA ribose after growth factor-activated and 5-diarylurea-oxy benzimidazole-treated HUVECs. (**A**) Representative isotopomeric distribution and ^{13}C enrichment ($\sum$mn) in lactate. No significant differences were found in lactate after activation with VEGF or FGF (upper panel). The introduction of the inhibitor (I: 5-diarylurea-oxy-benzimidazole) (lower panel) did not cause any relevant changes. (**B**) Representative isotopomeric distribution, ^{13}C enrichment ($\sum$mn) and the oxidative:non-oxidative ratio in RNA ribose. HUVECs activated by either VEGF or FGF activation use the PPP in a similar way (upper panel). Inhibitor I treatment (lower panel) caused a significant decrease in the total incorporation from glucose to ribose ($\sum$mn) in VEGF activation. This decrease was mainly determined by the inhibition of the oxidative branch of the PPP. Significance was tested using a non-parametric Mann–Whitney *W*-test to compare the medians of each independent experiment, considering 99% as a confident level. Significant differences (**) were consistent in the three independent experiments.

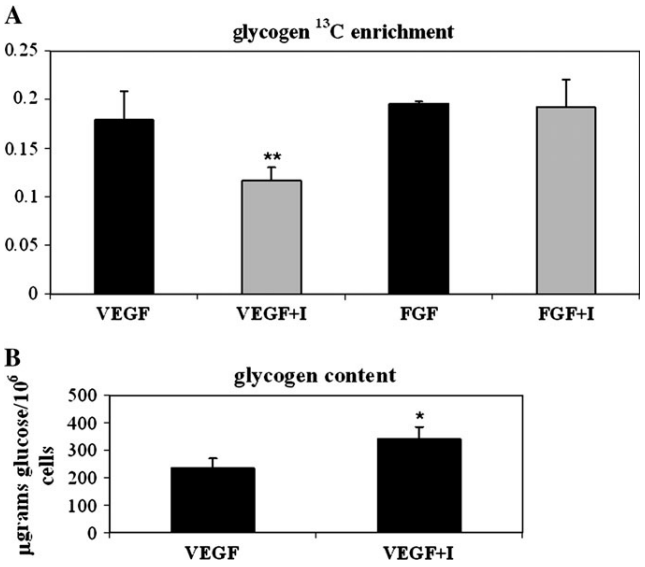

Fig. 2. ^{13}C enrichment of glycogen reservoirs and glycogen content in growth factor-activated and 5-diarylurea-oxy-benzimidazole-treated HUVECs. (**A**) Glycogen ^{13}C enrichment, calculated as $\Sigma mn = 2 \times m2$, shows similar glycogen–glucose turnover after activation with both VEGF and FGF (black bars). The inhibitor (I: 5-diarylurea-oxy-benzimidazole) produced a significant decrease in glycogen turnover from glucose after VEGF-specific HUVEC activation (gray bars). After the FGF activation, the inhibitor did not significantly affect the total ^{13}C incorporation into glycogen. Significance was tested using a non-parametric Mann–Whitney *W*-test to compare the medians of each independent experiment, considering 99% as a confident level. Significant differences (**) were consistent in the three independent experiments. (**B**) Glycogen content expressed in mg of glucose with respect to 10^6 cells. The inhibitor I promoted a significant accumulation of glycogen reservoirs. Significance (*) was tested using a non-parametric Mann–Whitney *W*-test to compare the medians of seven samples from two independent experiments, considering 95% as a confident level, 146 × 168 mm (600 × 600 DPI).

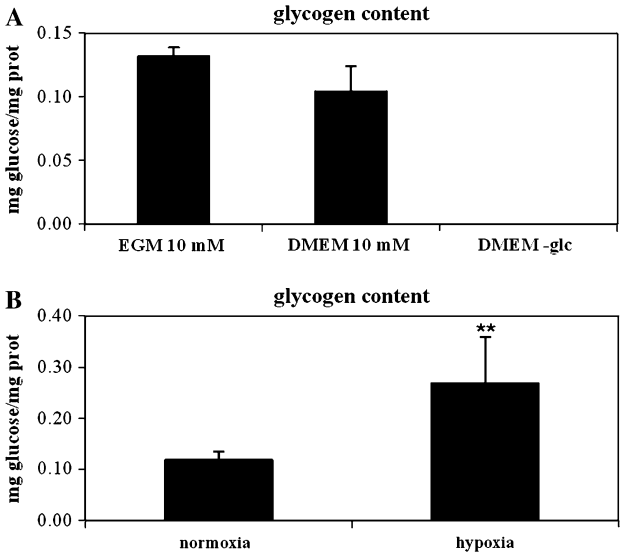

Fig. 3. Glycogen content, expressed as mg glucose released from glycogen with respect to mg of protein content, in HUVECs under hypoglycaemic or hypoxic culture conditions after 24 h. (**A**) hypoglycaemic conditions: the substitution of endothelial growth medium containing 10 mM of initial glucose by DMEM, 10 mM of initial glucose slightly affected the glycogen content in HUVECs. However, when glucose-free DMEM was used, HUVECs lost all of their glycogen reservoirs. (**B**) Hypoxic conditions (24 h at low O2 concentration) did not provoke the use of glycogen reservoirs, but caused a significant increase in cellular glycogen content. Significance (**) was tested using a non-parametric Mann–Whitney *W*-test to compare the medians of five samples from two independent experiments, considering 99% as a confident level, 132 × 170 mm (600 × 600 DPI).

panel—in the single experiment depicted in Table IB, there was a slight increase in ribose ^{13}C enrichment when 5-diarylurea-oxy-benzimidazole was added to FGF-activated HUVECs, but this increase was not statistically significant in the replicates), RNA ribose showed a significant and consistent decrease in ^{13}C enrichment ($\sum$mn) when 5-diarylurea-oxy-benzimidazole was added to VEGF-activated cells (Table IB, lower panel). Similar isotopomeric distribution patterns were found in all the experiments performed. Whereas the m2 proportion did not present significant changes, m1 decreased after the treatment with 5-diarylurea-oxy-benzimidazole, which caused a small but significant decrease in ox:non-ox ratio of PPP.

Similarly, although the inhibitor caused proliferation decrease in VEGF- and FGF-activated cells (Figure 1), glycogen synthesis and turnover was also only affected by 5-diarylurea-oxy-benzimidazole in VEGF-activated cells. The ^{13}C enrichment of glycogen decreased significantly and consistently when the inhibitor was added. To deeper study of this marked decrease in label incorporation into glycogen when 5-diarylurea-oxy-benzimidazole was added to VEGF-activated HUVECs, the glycogen content was measured by gas chromatography/mass spectrometry procedures using an internal standard. Figure 2B shows that the glycogen content of VEGF-activated cells increased when the cells were treated with 5-diarylurea-oxy-benzimidazole, indicating that glycogen degradation was inhibited.

Curiously, the VEGFR-2 inhibitor treatment did not affect lactate label distribution. Moreover, neither ^{13}C enrichment nor flux balance (PC parameter) presented significant differences after either VEGF or FGF activation, indicating that the metabolic pattern detected in lactate was not dependent on specific endothelial activation (Table IA, lower panel).

Glycogen reservoirs are mobilized under hypoglycaemic conditions, but not under hypoxic conditions

Activated endothelial cells induced by tumors are recruited toward hypoxic and hypoglycaemic environments. To better understand the role of HUVEC glycogen reservoirs in physiological conditions, cells were cultured in a glucose-free medium. For this specific culture condition, 10 mM glucose DMEM was used as a control versus glucose-free DMEM. After 24 h of incubation, glycogen was extracted, measured and corrected by protein content. Figure 3A shows that there was a total absence of glycogen content in HUVECs when glucose was absent from the culture medium. This dramatic decrease of glycogen content in glucose-free medium has been previously reported in other human endothelial cells (40). Lactate production was also measured after 24 h. Its concentration decreased sharply in hypoglycaemic conditions (data not shown), indicating that glycogen reservoirs are not large enough to support glycolysis for 24 h.

Effects of hypoxia on HUVEC glycogen usage were also assessed. Corroboration of hypoxia impact in HUVEC metabolism was assessed by determining glucose and lactate from the culture medium, and the glycolytic rate was calculated as the rate of lactate production versus glucose consumption. As expected, after 24 h under hypoxic conditions (1% O_2), the glycolytic rate increased by 20%. This was also confirmed by a 37% increase in intracellular concentration of fructose-1,6-bisphosphate and measured as described previously (41) (data not shown). Glycogen content, however, was not metabolized in HUVECs under hypoxic condition, as observed in hypoglycaemia, but an increase in glycogen reservoirs was observed (Figure 3B).

PPP and glycogen metabolism are good antiangiogenic targets

Previously reported results suggested that glycogen metabolism and the PPP may be good targets for metabolic interventions (42–44). Therefore, HUVECs were treated with CP-320626, an inhibitor of

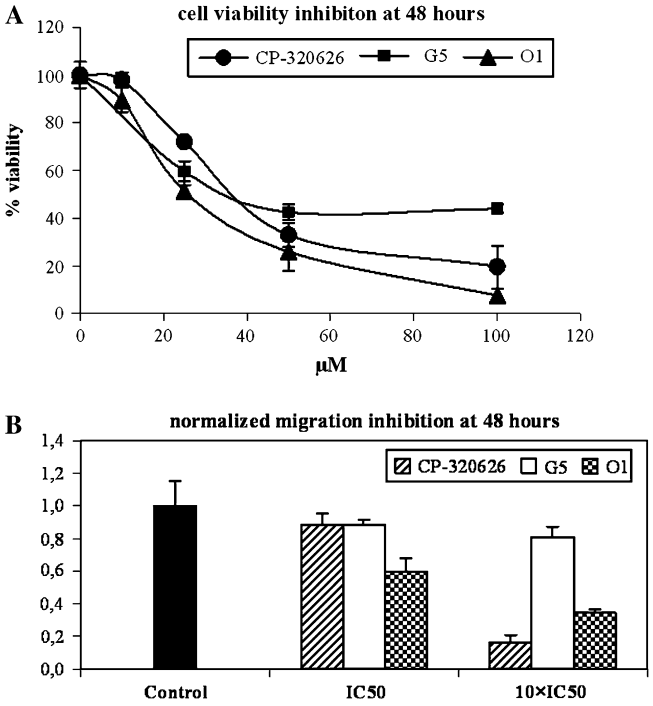

Fig. 4. (**A**) Cell viability of HUVECs after treatment with glycogen phosphorylase inhibitor CP-320626, glucose-6-phosphate dehydrogenase inhibitor G5 and transketolase inhibitor O1. After 48 h, dose-escalating treatment with the three compounds caused dose-dependent inhibition of cell proliferation. Data are presented as mean ± SD of three independent experiments performed. (**B**) Migration capacity of HUVECs after the treatment with CP-320626, G5 and O1. Data are normalized with respect control (media without drug), 142 × 206 mm (600 × 600 DPI).

the key enzyme in glycogen degradation, glycogen phosphorylase (45), as well as with G5 and O1, inhibitors of glucose-6-phosphate dehydrogenase and transketolase, the key enzymes of the oxidative and non-oxidative branches of PPP (18), respectively. After 48 h, dose-escalating treatment with CP-320626 and both G5 and O1 caused dose-dependent inhibition of cell viability (Figure 4A), confirming the importance of these two metabolic pathways in HUVECs.

Moreover, the inhibitors of glycogen metabolism and PPP also impair the capacity of HUVEC to migrate (Figure 4B). After just 4 h of incubation, the addition of CP-320626 caused a decrease of migration of 12 and 84% at its respective IC50 and 10 × IC50 concentration. Similar dose-response inhibition of PPP was observed, with a decrease of 40 and 66% for O1 and of 12 and 19% for G5 at their respective IC50 and 10 × IC50 concentration. Consistent with proliferation assays, the inhibitor of the non-oxidative branch of PPP O1 decreased the migration capacity in a larger extend that G5 inhibitor of the oxidative branch of PPP. It could be explained by the metabolic characteristic of PPP: the non-oxidative branch of PPP is a reversible pathway with the capacity of buffering pentose with hexose phosphates, so the inhibition of the oxidative branch could be eventually compensated by the non-oxidative, provoking that increasing concentrations of G5 did not cause an massive increase in migration inhibition, as well as is observed in viability assays.

Discussion

Cancer is an extremely complex and heterogenous disease that exhibits a high level of robustness against a range of therapeutic efforts (46). Looking for new targets to arrest cancer progression and invasion is one of the main current research challenges. With the development of systems biology, it has became more evident that a system level understanding of cancer cells and vascular endothelial cells that provide tumor vascularization could contribute to developing new drugs and therapies. Moreover, the recognition that the phenotype and function of mammalian cells largely depends on metabolic adaptation has greatly stimulated research initiatives in the field of metabolomics and fluxomics (20,47).

Although the central role of VEGF in the activation of angiogenesis has been clearly established, prior to the present study little was known about the metabolic network modulation required to support the angiogenic process. Results reported in this paper, using the [1,2-$^{13}C_2$]-glucose stable isotope as a carbon source and a tracer-based metabolomics approach, reveal a characteristic metabolic flux pattern downstream of endothelial cells activation, regardless of whether HUVECs are activated by VEGF or FGF. Thus, this common metabolic adaptation may be required to support endothelial cell function in the angiogenic process and includes a high flux of glucose through the PPP and an active glycogen metabolism. Lactate isotopomeric distribution is not significantly different when either VEGF or FGF is used to activate HUVECs (Table IA). RNA ribose ^{13}C enrichment is slightly higher after FGF activation than after VEGF activation of HUVECs, probably due to a higher proliferation rate (Figure 1). However, fluxes through oxidative and non-oxidative branches of the pentose cycle are not significantly altered, as the oxidative:non-oxidative ratio was similar in all the experiments (Table IB, upper panel). Glycogen ^{13}C enrichment was ~10% higher after FGF activation than after VEGF activation (Figure 2A). This also correlates with a higher proliferation rate. This, and the fact that high, similar glycogen concentrations were found in VEGF- or FGF-activated HUVECs indicates that glycogen deposits are important for HUVEC proliferation.

This strong dependence of activated HUVEC metabolism on glycogen and the PPP could be essential to supporting the angiogenic process. Consequently, glycogen and the PPP could be targets within the angiogenic cell metabolic network for potential novel therapies. In order to check whether this common metabolic pattern is a consequence of the angiogenic HUVEC activation that may be essential for the angiogenic process, we analyzed the effects of a well-known VEGFR-2 inhibitor, 5-diarylurea-oxy-benzimidazole, on HUVECs' metabolic network. This inhibitor acts on the intracellular part of the VEGFR-2 and impedes phosphorylation through its tyrosine kinase activity, causing a decrease in the VEGF-activated phosphorylation cascade and the HUVEC proliferation rate (Figure 1).

The lactate isotopomeric distribution did not change significantly when the inhibitor was added to either VEGF-activated or FGF-activated HUVECs (Table IA), suggesting that glycolytic flux does not depend on signal transduction from the VEGF receptor. However, the results show that treatment with the inhibitor in VEGF-activated cells cause a decrease in PPP flux, as there was a significant decrease in ^{13}C ribose enrichment ($\sum$mn) (Table IB). This decrease was mainly determined by the inhibition of the oxidative branch of the PPP. Worthy of note, mass isotopomer distribution analysis experiments were performed at 72 h, when metabolic enrichment of ^{13}C from [1,2-$^{13}C_2$]-glucose is almost saturated. Therefore, the differences in proliferation rate caused by VEGF or FGF activation hardly led to a relevant difference in ^{13}C ribose enrichment. The specificity of this metabolic response is corroborated by the fact that the inhibitor treatment, which caused a 30 and 20% decrease in proliferation when HUVEC cells were activated with VEGF and FGF, respectively, only significantly decreased RNA ribose enrichment when VEGF was used as angiogenic activator. This leads us to conclude that the inhibitor acts specifically on its target receptor VEGFR-2, which causes a specific metabolic effect on PPP.

Interestingly, it has been demonstrated that activation of the pentose cycle is downregulated during the differentiation process (26), whereas its activation is a common characteristic of tumor cells (48). These results reinforce the emergence of the PPP as a promising therapeutic target, since actions on this pathway could inhibit tumor proliferation and impede angiogenic progression. Thus, metabolic

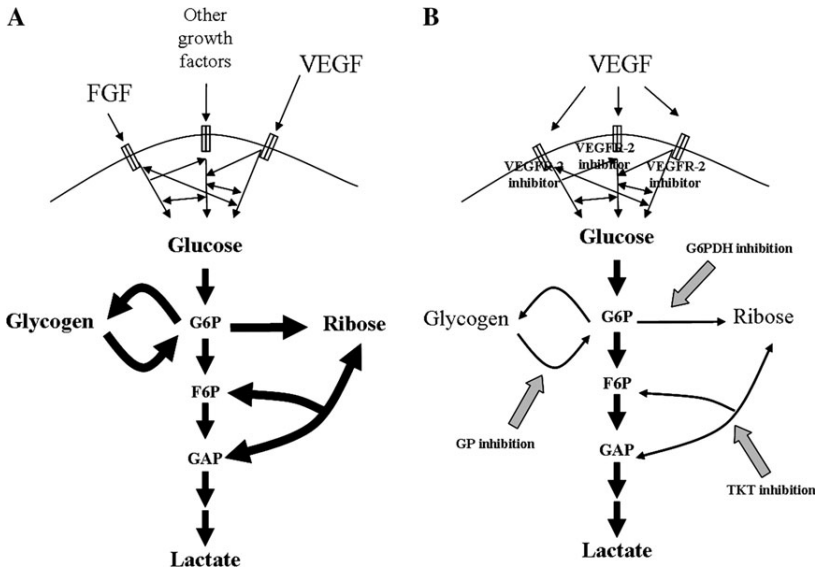

Fig. 5. HUVECs' metabolic network changes in response to the activation produced by the angiogenic stimulus of different growth factors (VEGF and FGF) and after specific inhibition of the angiogenic stimulus using a VEGFR-2 inhibitor. (**A**) The induction of angiogenic stimulus by growth factor metabolically activated HUVECs, producing a similar pattern of glucose usage. (**B**) The inhibition of the VEGF receptor caused a decrease in the proliferation rate, which was accompanied by a decrease in the PPP activity and glycogen metabolism. Actions on these metabolic points also impaired the angiogenic process. F6P, fructose-6-phosphate; G6P, glucose-6-phosphate; GAP, glyceraldehyde-3-phosphate; GP, glycogen phosphorylase; G6PDH, glucose-6-phosphate dehydrogenase; TKT, transketolase, 220 × 150 mm (600 × 600 DPI).

inhibition of both the oxidative and non-oxidative branches of this pathway has been described as a good antitumoral strategy (18–22). Moreover, it has been recently demonstrated that disruption of the balance between oxidative and non-oxidative branches of pentose phosphate metabolism using a multiple hit drug strategy results in colon cancer adenocarcinoma cell death (43). Additionally, several studies have demonstrated that downregulation of these pathways decreases the migration capacity of bovine aortic endothelial cells (49,50).

The results also show that 5-diarylurea-oxy-benzimidazole inhibitor impairs ^{13}C enrichment of glycogen reservoirs when the inhibitor is added to VEGF-activated cells, but not when it is added to FGF-activated cells (Figure 2A, gray bars), which led us to hypothesize a reducing glycogen mobilization specifically provoked by the inhibitor. This is confirmed by the accumulation of glycogen reservoirs when the inhibitor is present (Figure 2B).

The physiological impact of huge glycogen reservoirs on HUVECs could be explained by the needs of endothelial cells during the formation of new vessels, after their recruitment by solid tumors, in which there is a hypoglycaemic and hypoxic environment. Accordingly, by forcing physiological hypoglycaemic conditions, we observed how HUVEC glycogen reservoirs are totally catabolized (Figure 3A). Hypoxia does not lead to the use of glycogen reservoirs. On the contrary, it does cause an increase in the cellular glycogen content (Figure 3B). In hypoxic conditions, the glycolytic rate increases provoking an increase of the intracellular concentration of sugar phosphate glycolytic intermediates. Therefore, we hypothesize that the observed increase in glycogen content under hypoxic conditions could be explained by the metabolic equilibrium between glycolytic intermediates and glycogen reservoirs. Interestingly, glycogen metabolism has also been described as an antitumoral target in MIA pancreatic cells (42), again providing a common, attackable metabolic characteristic in tumors and in the endothelial cells activated by them.

In summary, we have described high activity of pentose phosphate metabolism, large glycogen deposits and high glycogen turnover as a common adaptive metabolic pattern associated with angiogenic activation, regardless of the activation pathway. This proves the robustness of the angiogenic process (Figure 5A). Specific inhibition of the angiogenic stimulus using 5-diarylurea-oxy-benzimidazole resulted in a decrease in the PPP and glycogen metabolism, which confirms that the activation of these two pathways is one of the mechanisms resulting in angiogenic activation downstream of growth factor stimulation (Figure 5B). Thus, these results offer new insight into the vulnerability of the angiogenic cell metabolic network and indicate potential new antiangiogenic targets. To prove this hypothesis, we corroborated the importance of the aforementioned metabolic characteristics by inhibiting key enzymes to glycogen metabolism and PPP (Figure 4) and corroborating that the inhibition affect both viability and migration capacity of HUVECs. Further work is needed to provide molecular evidence that directly links the observed metabolic changes to growth factor-signaling pathways and validates the new targets. Nevertheless, in this paper, we have demonstrated that metabolic studies can reliably provide a systemic view of a biological process, such as angiogenesis activation by growth factors, as well as the potential use of such processes for antiproliferative and anti-migration interventions. It is of crucial importance to note that the endothelial metabolic targets proposed here also promising anticancer targets (22,42,43). Thus, metabolic interventions that could affect at the same time solid tumors and vessels formation should be seriously considered in integrating actions against carcinogenic process.

Funding

Spanish Ministry of Science and Technology and European Union Fondo Europeo de Desarrollo Regional (SAF2005-01627, SAF2008-00164 to M.C.); General Clinical Research Center (PHS M01-RR00425); University of California, Los Angeles, Center for Excellence in Pancreatic Diseases, Metabolomics Core (1 P01 AT003960-01A1); Spanish Ministry of Health and Consumption, ISCIII-RTICC (RD06/0020/0046); Government of Catalonia (2005SGR00204).

Acknowledgements

Conflict of Interest Statement: None declared.

References

1. Ferrara,N. (1999) Molecular and biological properties of vascular endothelial growth factor. *J. Mol. Med.*, **77**, 527–543.
2. Ferrara,N. (2002) VEGF and the quest for tumour angiogenesis factors. *Nat. Rev. Cancer*, **2**, 795–803.
3. Brekken,R.A. *et al*. (2000) Selective inhibition of vascular endothelial growth factor (VEGF) receptor 2 (KDR/Flk-1) activity by a monoclonal anti-VEGF antibody blocks tumor growth in mice. *Cancer Res.*, **60**, 5117–5124.
4. Ferrara,N. *et al*. (2005) Angiogenesis as a therapeutic target. *Nature*, **438**, 967–974.
5. Ferrara,N. (2005) VEGF as a therapeutic target in cancer. *Oncology*, **69** (suppl. 3), 11–16.
6. Kerbel,R. *et al*. (2002) Clinical translation of angiogenesis inhibitors. *Nat. Rev. Cancer*, **2**, 727–739.
7. Kell,D.B. *et al*. (2005) Metabolic footprinting and systems biology: the medium is the message. *Nat. Rev. Microbiol.*, **3**, 557–565.
8. Boros,L.G. *et al*. (2002) Metabolic profiling of cell growth and death in cancer: applications in drug discovery. *Drug Discov. Today*, **7**, 364–372.
9. Nicholson,J.K. *et al*. (2002) Metabonomics: a platform for studying drug toxicity and gene function. *Nat. Rev. Drug Discov.*, **1**, 153–161.
10. Dagher,Z. *et al*. (1999) The effect of AMP-activated protein kinase and its activator AICAR on the metabolism of human umbilical vein endothelial cells. *Biochem. Biophys. Res. Commun.*, **265**, 112–115.
11. Ido,Y. *et al*. (2002) Hyperglycemia-induced apoptosis in human umbilical vein endothelial cells: inhibition by the AMP-activated protein kinase activation. *Diabetes*, **51**, 159–167.
12. Mori,N. *et al*. (2003) Choline phospholipid metabolites of human vascular endothelial cells altered by cyclooxygenase inhibition, growth factor depletion, and paracrine factors secreted by cancer cells. *Mol. Imaging*, **2**, 124–130.
13. Gatenby,R.A. *et al*. (2003) The glycolytic phenotype in carcinogenesis and tumor invasion: insights through mathematical models. *Cancer Res.*, **63**, 3847–3854.
14. Dang,C.V. *et al*. (1999) Oncogenic alterations of metabolism. *Trends Biochem. Sci.*, **24**, 68–72.
15. Mazurek,S. *et al*. (2003) The tumor metabolome. *Anticancer Res.*, **23**, 1149–1154.
16. Vizán,P. *et al*. (2008) Robust metabolic adaptation underlying tumor progression. *Metabolomics*, **4**, 1–12.
17. Purcell,W.T. *et al*. (2003) Novel antifolate drugs. *Curr. Oncol. Rep.*, **5**, 114–125.
18. Boren,J. *et al*. (2002) Metabolic control analysis aimed at the ribose synthesis pathways of tumor cells: a new strategy for antitumor drug development. *Mol. Biol. Rep.*, **29**, 7–12.
19. Boros,L.G. *et al*. (1997) Oxythiamine and dehydroepiandrosterone inhibit the nonoxidative synthesis of ribose and tumor cell proliferation. *Cancer Res.*, **57**, 4242–4248.
20. Cascante,M. *et al*. (2002) Metabolic control analysis in drug discovery and disease. *Nat. Biotechnol.*, **20**, 243–249.
21. Comin-Anduix,B. *et al*. (2001) The effect of thiamine supplementation on tumour proliferation. A metabolic control analysis study. *Eur. J. Biochem.*, **268**, 4177–4182.
22. Rais,B. *et al*. (1999) Oxythiamine and dehydroepiandrosterone induce a G1 phase cycle arrest in Ehrlich's tumor cells through inhibition of the pentose cycle. *FEBS Lett.*, **456**, 113–118.
23. Pelicano,H. *et al*. (2006) Glycolysis inhibition for anticancer treatment. *Oncogene*, **25**, 4633–4646.
24. Gatenby,R.A. *et al*. (2007) Glycolysis in cancer: a potential target for therapy. *Int. J. Biochem. Cell Biol.*, **39**, 1358–1366.
25. Xu,R.H. *et al*. (2005) Inhibition of glycolysis in cancer cells: a novel strategy to overcome drug resistance associated with mitochondrial respiratory defect and hypoxia. *Cancer Res.*, **65**, 613–621.
26. Boren,J. *et al*. (2003) The stable isotope-based dynamic metabolic profile of butyrate-induced HT29 cell differentiation. *J. Biol. Chem.*, **278**, 28395–28402.
27. Vizan,P. *et al*. (2005) K-ras codon-specific mutations produce distinctive metabolic phenotypes in NIH3T3 mice [corrected] fibroblasts. *Cancer Res.*, **65**, 5512–5515.
28. Miyazaki,Y. *et al*. (2007) Orally active 4-amino-5-diarylurea-furo[2,3-d]pyrimidine derivatives as anti-angiogenic agent inhibiting VEGFR2 and Tie-2. *Bioorg. Med. Chem. Lett.*, **17**, 1773–1778.
29. Kunst,A. *et al*. (1984) D-Glucose: UV-methods with hexokinase and glucose-6-phosphate dehydrogenase. In: Bergmeyer,H.U. (ed.), *Methods of Enzymatic Analysis,* **Vol. VI**, Verlag Chemie, Weinheim, Germany, pp. 163–172.
30. Passoneau,J.V. *et al*. (1974) L-(+)-lactate: fluorometric method. In: Bergmeyer,H.U. (ed.), *Methods of Enzymatic Analysis,* **Vol. III**, Academic press, New york, pp. 1468–1472.
31. Lee,W.N. *et al*. (1998) Mass isotopomer study of the nonoxidative pathways of the pentose cycle with [1,2-13C2]glucose. *Am. J. Physiol.*, **274**, E843–E851.
32. Boros,L.G. *et al*. (2001) Wheat germ extract decreases glucose uptake and RNA ribose formation but increases fatty acid synthesis in MIA pancreatic adenocarcinoma cells. *Pancreas*, **23**, 141–147.
33. Szafranek,J. *et al*. (1974) The mass spectra of some per-O-acetylaldononitriles. *Carbohydr. Res.*, **38**, 97–105.
34. Lerin,C. *et al*. (2004) Regulation of glycogen metabolism in cultured human muscles by the glycogen phosphorylase inhibitor CP-91149. *Biochem. J.*, **378**, 1073–1077.
35. Mosmann,T. (1983) Rapid colorimetric assay for cellular growth and survival: application to proliferation and cytotoxicity assays. *J. Immunol. Methods*, **65**, 55–63.
36. Matito,C. *et al*. (2003) Antiproliferative effect of antioxidant polyphenols from grape in murine Hepa-1c1c7. *Eur. J. Nutr.*, **42**, 43–49.
37. Deng,Q. *et al*. (2005) Modeling aided design of potent glycogen phosphorylase inhibitors. *J. Mol. Graph. Model.*, **23**, 457–464.
38. Hoover,D.J. *et al*. (1998) Indole-2-carboxamide inhibitors of human liver glycogen phosphorylase. *J. Med. Chem.*, **41**, 2934–2938.
39. Keely,P.J. *et al*. (1997) Cdc42 and Rac1 induce integrin-mediated cell motility and invasiveness through PI(3)K. *Nature*, **390**, 632–636.
40. Artwohl,M. *et al*. (2007) Insulin does not regulate glucose transport and metabolism in human endothelium. *Eur. J. Clin. Invest.*, **37**, 643–650.
41. Vizan,P. *et al*. (2007) Quantification of intracellular phosphorylated carbohydrates in HT29 human colon adenocarcinoma cell line using liquid chromatography-electrospray ionization tandem mass spectrometry. *Anal. Chem.*, **79**, 5000–5005.
42. Lee,W.N. *et al*. (2004) Metabolic sensitivity of pancreatic tumour cell apoptosis to glycogen phosphorylase inhibitor treatment. *Br. J. Cancer*, **91**, 2094–2100.
43. Ramos-Montoya,A. *et al*. (2006) Pentose phosphate cycle oxidative and nonoxidative balance: a new vulnerable target for overcoming drug resistance in cancer. *Int. J. Cancer*, **119**, 2733–2741.
44. Frederiks,W.M. *et al*. (2008) Elevated activity of the oxidative and nonoxidative pentose phosphate pathway in (pre)neoplastic lesions in rat liver. *Int. J. Exp. Pathol.*, **89**, 232–240.
45. Oikonomakos,N.G. *et al*. (2000) A new allosteric site in glycogen phosphorylase b as a target for drug interactions. *Structure*, **8**, 575–584.
46. Kitano,H. (2004) Cancer as a robust system: implications for anticancer therapy. *Nat. Rev. Cancer*, **4**, 227–235.
47. de la Fuente,A. *et al*. (2002) Metabolic control in integrated biochemical systems. *Eur. J. Biochem.*, **269**, 4399–4408.
48. Boros,L.G. *et al*. (1998) Inhibition of the oxidative and nonoxidative pentose phosphate pathways by somatostatin: a possible mechanism of antitumor action. *Med. Hypotheses*, **50**, 501–506.
49. Leopold,J.A. *et al*. (2003) Glucose-6-phosphate dehydrogenase modulates vascular endothelial growth factor-mediated angiogenesis. *J. Biol. Chem.*, **278**, 32100–32106.
50. Ascher,E. *et al*. (2001) Thiamine reverses hyperglycemia-induced dysfunction in cultured endothelial cells. *Surgery*, **130**, 851–858.

Received October 16, 2008; revised March 19, 2009; accepted April 4, 2009

ANNEX 3

Efecte protector de diferents fraccions polifenòliques de raïm envers els danys i la mort cel·lular induïts per la radiació UV

Publicació a la revista *Journal of Agricultural and Food Chemistry* amb un factor d'impacte 2,816.

Cecilia Matito[1], Neus Agell[2], Susana Sanchez-Tena[1], Josep L. Torres[3] i Marta Cascante[1]

[1]Facultat de Biologia, Universitat de Barcelona i IBUB, unitat associada al CSIC, 08028 Barcelona, Espanya

[2]Departament de Biologia Cel·lular, Immunologia i Neurociències, Facultat de Medicina, Universitat de Barcelona, IDIBAPS, 08036 Barcelona, Espanya

[3]Institut de Química Avançada de Catalunya (IQAC-CSIC), 08034 Barcelona, Espanya

RESUM

La radiació ultraviolada (UV) porta a la generació de d'espècies reactives d'oxigen (ROS - *Reactive Oxygen Species*). Aquestes molècules alteren diferents funcions cel·lulars clau i poden resultar en la mort cel·lular. Diversos estudis han descrit que els antioxidants naturals poden protegir la pell contra aquests efectes nocius de la radiació UV. En aquest treball es va avaluar la capacitat *in vitro* de diverses fraccions polifenòliques de raïm, les quals diferien en el grau de polimerització i el percentatge de gal.loització, per protegir els queratinòcits humans HaCaT contra el dany oxidatiu produït per la radiació UV. Aquestes fraccions van inhibir els nivells basals i els ROS intracel·lulars generats per la radiació UVB i UVA en aquesta línia cel·lular. Consegüentment, les mateixes fraccions van inhibir l'activació de les proteïnes p38 i JNK1/2 induïda per la radiació UVB i UVA. L'efecte protector més elevat va correspondre a les fraccions riques en oligòmers i esters de gal·lat. Aquests resultats haurien de ser considerats en la farmacologia clínica per la utilització d'extractes polifenòlics com nous agents fotoprotectors per a la pell.

JOURNAL OF AGRICULTURAL AND FOOD CHEMISTRY

ARTICLE

pubs.acs.org/JAFC

Protective Effect of Structurally Diverse Grape Procyanidin Fractions against UV-Induced Cell Damage and Death

Cecilia Matito,[†,‡] Neus Agell,[§] Susana Sanchez-Tena,[†] Josep L. Torres,[‡] and Marta Cascante*[,†]

[†]Department of Biochemistry and Molecular Biology, Faculty of Biology, University of Barcelona and IBUB, Unit Associated with CSIC, Diagonal 645, 08028 Barcelona, Spain

[‡]Institute for Advanced Chemistry of Catalonia (IQAC−CSIC), Jordi Girona 18-26, 08034 Barcelona, Spain

[§]Department of Cell Biology, Immunology and Neurosciences, Faculty of Medicine, University of Barcelona, IDIBAPS, Casanova 143, 08036 Barcelona, Spain

ABSTRACT: UV radiation leads to the generation of reactive oxygen species (ROS). These molecules exert a variety of harmful effects by altering key cellular functions and may result in cell death. Several studies have demonstrated that human skin can be protected against UV radiation by using plant-derived antioxidants. Here we evaluated the *in vitro* capacity of several antioxidant polyphenolic fractions from grape, which differ in their degree of polymerization and percentage of galloylation, to protect HaCaT human keratinocytes against UV-induced oxidative damage. These fractions inhibited both basal and UVB- or UVA-induced intracellular ROS generation in this cell line. Consequently, the same fractions inhibited p38 and JNK1/2 activation induced by UVB or UVA radiation. The highest protective effect was for fractions rich in procyanidin oligomers and gallate esters. These encouraging *in vitro* results support further research and should be taken into consideration into the clinical pharmacology of plant-derived polyphenolic extracts as novel agents for skin photoprotection.

KEYWORDS: grape, polyphenols, antioxidant, UV radiation, reactive oxygen species (ROS), mitogen-activated protein (MAP) kinases (MAPKs)

INTRODUCTION

UV radiation from sunlight is the main environmental cause of skin damage.[1] Excessive exposure to UV radiation has several adverse effects on human health, such as skin carcinogenesis, immunosuppression, solar erythema and premature skin aging.[2] Many harmful effects of short-wavelength UVB (290−320 nm) and long-wavelength UVA (320−400 nm) are associated with the generation of reactive oxygen species (ROS), for instance superoxide radical ($O_2^{\bullet-}$) and hydrogen peroxide (H_2O_2). An integrated defense system comprising nonenzymatic and enzymatic antioxidants, including catalase, glutathione, and superoxide dismutase, is thus crucial in protecting the skin from oxidative stress.[3] Severe depletion of endogenous skin antioxidants during oxidative stress caused by prolonged exposure to UV radiation results in insufficient protection and hence extensive cellular damage and eventual cell death by apoptosis.[4,5] Excessive levels of ROS not only damage cells directly by oxidizing macromolecules such as DNA and lipids but also indirectly by triggering stress-sensitive signaling pathways such as that of c-Jun N-terminal kinase (JNK)/stress-activated protein kinase (SAPK) and p38 mitogen-activated protein kinase (MAPK).[6] The activation of these intracellular cascades increases expression of various proteins related to the induction of apoptosis.[7] Moreover, activation of JNK and p38 pathways has been described in keratinocytes in response to exposure to UVB[8] and UVA.[9,10]

The current approach to protecting human skin against solar UV-induced oxidative damage relies heavily on the avoidance of excessive exposure to sunlight and the use of sunscreens. Topical and oral supplementation of phytochemicals may complement these strategies.[11,12] Several studies have recently demonstrated the efficacy of naturally occurring botanical antioxidants, such as green tea polyphenols,[13] rosmarinic acid,[14] resveratrol,[15] genistein,[16] and grape seed proanthocyanidins, against the adverse effects of UV radiation on skin. In particular, dietary grape seed proanthocyanidins have been reported to inhibit photocarcinogenesis in SKH-1 hairless mice,[17] to show anti-inflammatory activity in mouse skin,[18] and to reduce UV-induced oxidative stress by inhibiting MAPKs and NF-κB signaling in human epidermal keratinocytes and in mice.[19] However, several questions remain as to the relevance of the polyphenolic structure of grape extracts and their photoprotective capacity. In this study, we tested the polyphenolic fractions from a grape by-product. These contained monomers and oligomers of catechins with some galloylation and mainly polymerized procyanidins.[20] Lizárraga and colleagues described that the mean degree of polymerization and the percentage of galloylation of grape polyphenolic fractions affect their antiproliferative potential and their scavenging capacity in colon cancer cells.[21] Moreover, the most widely studied natural catechin, epigallocatechin-3 gallate, is a potent antioxidant and skin photoprotector.[19] These and other results suggest that the degree of polymerization and the percentage of galloylation in natural extracts are crucial chemical characteristics for biological activity.[22,23] These parameters may be useful indicators to evaluate the potential of natural plant extracts to protect skin against UV-induced damage.

Here we studied the relationship between key structural characteristics of grape procyanidins, such as the mean degree

Received: November 17, 2010
Accepted: March 15, 2011
Revised: March 9, 2011
Published: March 15, 2011

of polymerization and percentage of galloylation, and the capacity of these compounds to protect skin against photodamage. To examine whether these polyphenols, which are potent free radical scavengers,[24,25] exert a protective effect against UV-induced oxidative stress in human keratinocytes, we used immortalized, but not tumorigenic, HaCaT cells from human adult skin keratinocytes.[26] This cell line provides a suitable experimental model to assess the response of epidermal components of the skin to UV-induced oxidative stress.

Thus, we examined the potential protective effects of grape-derived phenolic fractions against ROS formation and against the activation of JNK1/2 and p38 MAPKs induced by UVB and UVA radiation. At concentrations between 5 and 20 μg/mL, these fractions had a protective effect against UV-induced ROS generation and MAPK activation. Moreover, we demonstrate that the degree of polymerization and percentage of galloylation are crucial to the protective effect of these fractions.

MATERIALS AND METHODS

Natural Products. The polyphenolic fractions were obtained from pressing destemmed Parellada grapes (*Vitis vinifera*) as described before.[27] Fractions contained flavanols (catechins) that differed in the mean degree of polymerization (mDP) and percentage of galloylation (% G). Total fraction OW, which was soluble in ethyl acetate and in water, was obtained by solvent fractionation, and it contained gallic acid (GA), (+)-catechin (Cat), (−)-epicatechin (EC), glycosylated flavonols and procyanidin oligomers (the latter with mDP 1.7 and % G 15%). The other fractions were derived from OW by column chromatography using either reverse-phase, absorption/exclusion, or a combination of both techniques. These derived fractions contained mainly flavanols and were as follows: IV (formed by flavanol oligomers with mDP = 2.7, % G = 25); XI (formed by flavanol oligomers with mDP = 3.7, % G = 31); and V (formed only by nongalloylated flavanol monomers). To analyze their effects, the fractions were dissolved in sterilized PBS at concentrations of 5 mg/mL and subjected to nitrogen gas immediately prior to use.

Materials and Chemicals. The UV source was a BIO-SUN system illuminator (Vilbert Lourmat; Torcy, France) consisting of two UV lamps that delivered uniform UVA (365 nm) and UVB (312 nm) radiation at a distance of about 10 cm.

All chemicals were purchased from Sigma (St. Louis, MO, USA) unless otherwise specified.

Cell Culture. The HaCaT cell line comprising spontaneously transformed but nonmalignant human skin keratinocytes was used.[26] Cells were cultured at 37 °C in Dulbecco's modified Eagle medium (DMEM) containing 25 mM glucose (Cambrex Bioscience; Verviers, Belgium) and supplemented with 10% heat-inactivated fetal calf serum (FCS) (PAA Laboratories GmbH; Pasching, Austria), L-glutamine 2 mM, Hepes 10 mM and 0.2% antibiotic (Gibco-BRL; Eggenstein, Germany). 22,600 cells/cm^2 were grown for 24 h to 80−90% confluence and fed with standard medium (without serum) for 48 h to induce quiescence and basal levels of phospho-p38 and JNK 1/2.

Treatment with Polyphenols and UV Radiation. Quiescent keratinocytes, cultured as described above, were pretreated with various concentrations of polyphenolic fractions (5, 10, and 20 μg/mL for the total fraction OW and 5 μg/mL for the derived fractions IV, V and XI) for 6 h. After washing with PBS, plates without cover were placed in the BIO-SUN system and cells in PBS were UVB-irradiated at 312 nm and doses of 0.03 or 0.05 J/cm^2 (less than 1 min of radiation) or UVA-irradiated at 365 nm and doses of 10, 20, or 30 J/cm^2 (radiation times were 30 min, 1 or 2 h respectively). The conditions used for UVA and UVB radiation were adapted from previous publications.[28,29] After UV exposure, cells were fed with fresh serum-free medium and postincubated for 24 h for viability assays or for 30 min for the analysis of MAPK activation and ROS release. Furthermore, control nonirradiated cells were treated in the same way.

Detection of Intracellular ROS. Intracellular ROS in UVB- or UVA-irradiated cells pretreated or not with the polyphenolic fractions was analyzed by flow cytometry using dihydrorhodamine 123 (DHR) as a specific fluorescent dye probe, since the intracellular release of ROS irreversibly oxidizes DHR, which is then converted to the red fluorescent compound rhodamine 123.[30−32] Thus, 83,000 cells were cultured in 12-well microtiter plates in standard culture medium. After 24 h this medium was replaced by another without serum, and cells were incubated for 48 h prior to the 6 h treatment with the corresponding polyphenolic fraction. Cells were loaded with 5 μM DHR for 30 min and washed in PBS before being exposed to UVB or UVA radiation at 0.05 or 20 J/cm2, respectively. After 30 min of postincubation, cells were washed in PBS, trypsinized and collected by centrifugation at 500*g*. Pellets were then washed in PBS before fixing cells with 400 μL of 0.5% formaldehyde in PBS. Finally, cells were placed on ice and analyzed by measuring the fluorescence intensity of 10,000 cells at 488 nm in an Epics XL flow cytometer. The results were expressed as a percentage of mean fluorescence intensity of nonirradiated DHR-stained cells, considering them as 100%.

Western Blot Analysis of MAPK Activity. Cells cultured in 22.1 cm^2 plates were pretreated with or without the corresponding polyphenolic fraction, and irradiated as described in the previous section. After UV radiation, cells were postincubated at 37 °C and 5% CO2 for a range of times (30 min, 1 and 2 h) for the activation time course assay or collected at 30 min for the protection assays. Thus, cells were washed in PBS and extracted with 300 μL of lysis buffer containing 81.5 mM Tris pH 6.8, 2% (w/v) SDS and protease inhibitors (10 μg/mL leupeptin, aprotinin and PMSF and 1 μg/mL ortovanadate). After sonicating the cells, we quantified the protein content using the Lowry assay.[33] Equal amounts of protein (25 μg) in loading buffer containing 50 mM Tris pH 6.8, 2% (w/v) SDS, 10 mM DTT, 10% (v/v) glycerol and 0.2% (w/v) bromophenol blue were boiled for 5 min, separated by SDS−PAGE (4% stacking and 10% resolving) and transferred to PVDF membrane (Bio-Rad Laboratories, CA, USA). After blocking in TBS-Tween (0.1%) and 5% (w/v) of BSA for 1 h at room temperature, blots were incubated overnight at 4 °C with the corresponding primary antibody in TBS-T with 5% (w/v) BSA at 1:1000 dilutions. For phosphorylated MAPK analysis, we used polyclonal antiphospho-p38 and monoclonal antiphospho-JNK antibodies (Cell Signaling, Beverly, MA, USA). For total MAPK analysis, polyclonal anti-p38 and anti-JNK antibodies were used (Cell Signaling). Afterward, the blots were washed in TBS-T three times for 5 min each, and incubated with HRP-conjugated goat anti-rabbit (Amersham Biosciences AB, Uppsala, Sweden) or HRP-conjugated rabbit anti-mouse (DAKO, Copenhagen, Denmark) for polyclonal and monoclonal primary antibodies respectively. Secondary antibodies were prepared in TBS-T and 2% (w/v) dry milk at 1:3000 dilutions and incubated for 1 h at room temperature. After incubation with secondary antibody, blots were again washed three times for 5 min in TBS-T, followed by one washing step in TBS. They were then visualized on film by enhanced chemiluminescence with an ECL kit (Biological Industries, Kibbutz Beit Haemek, Israel).

RESULTS

UV-Induced and Basal ROS Generation Is Inhibited by the Polyphenolic Fractions. The polyphenolic fractions lowered baseline ROS levels in a significant manner in non-UV-irradiated cells (Figure 1A). In addition, this reduction was dose-dependent as observed for the total fraction OW and was lower for the fraction V at 5 μg/mL with respect to IV and XI at the same concentration (about 20% vs 40−50% reduction for IV and XI) (Figure 1A). Moreover, the decrease in ROS levels observed for

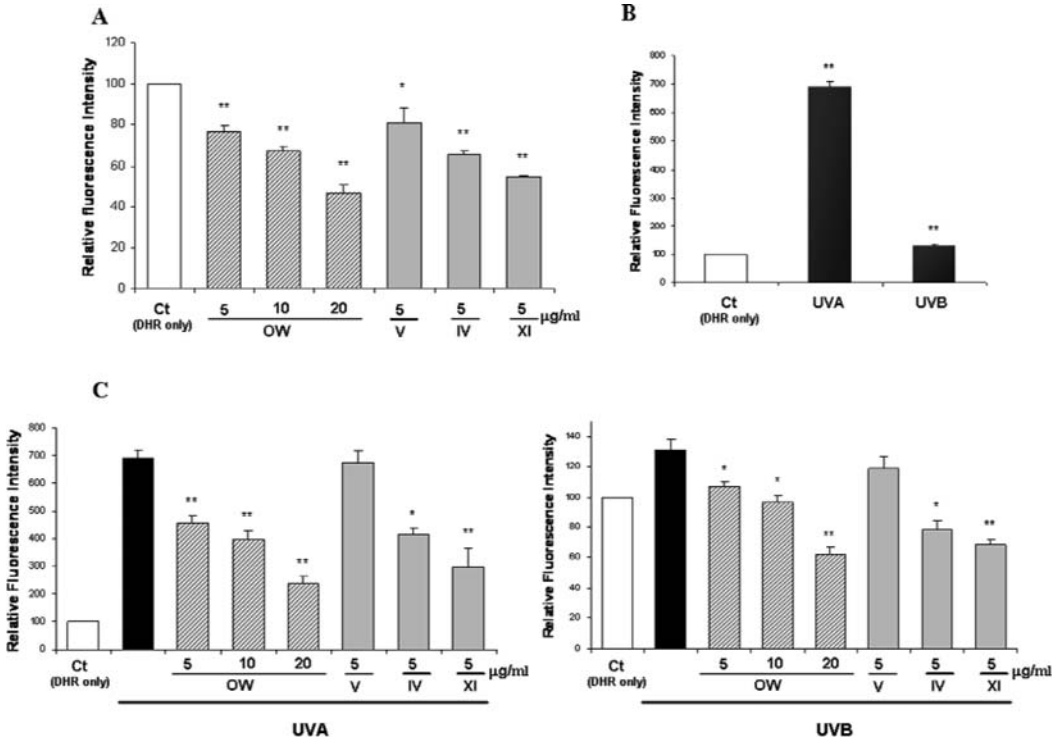

Figure 1. Inhibition of basal and UV-induced ROS production by polyphenolic fractions. (A) To determine intracellular ROS generation, HaCaT keratinocytes treated with total or derived polyphenolic fractions (OW, IV, V and XI) at the indicated concentrations for 6 h were incubated with DHR, followed by 30 min of postincubation, and analyzed by flow cytometry as indicated in Materials and Methods. (B) UV-induced ROS production in nontreated HaCaT cells after exposure to 20 J/cm^2 UVA or 0.05 J/cm^2 UVB. (C) Cells were pretreated with total or derived polyphenolic fractions (OW, IV, V and XI) at the indicated concentrations for 6 h previous to UVA or UVB irradiation, and ROS production was determined as stated above. Results are representative of three independent experiments (mean ± SEM). * $p < 0.05$, ** $p < 0.001$ versus control.

5 μg/mL of fractions IV and XI was achieved only by 10−20 μg/mL of the total fraction OW (Figure 1A). UV-irradiated HaCaT cells showed an increase in intracellular ROS after UV radiation. This increase was about 6-fold higher after UVA exposure and less than 2-fold higher after UVB radiation compared to the baseline levels of ROS. (Figure 1B) Pretreatment of cells with the polyphenolic fractions reduced ROS levels in a significant manner after UVB and UVA radiation, regardless of the concentration tested, except fraction V, which failed to exert a protective effect at 5 μg/mL (the concentration studied for the derived fractions) (Figure 1C). Moreover, ROS generated after UVA and UVB exposure decreased in the total fraction OW in a dose-dependent manner. A reduction in ROS of about 50−60% was achieved with 10−20 μg/mL of this fraction. A similar decrease (50−60%) was induced by only 5 μg/mL of the fractions IV and XI (Figure 1C). In addition, when cells were exposed to UVB radiation, all the fractions, except V, reduced the generation of ROS to lower values than the control nonirradiated cells (Figure 1C, right section). Since the increase in ROS production was much higher after UVA radiation, the extent of the decrease exerted by fractions OW, IV and XI for this source of radiation was not as large as for UVB radiation (Figure 1C).

Time Course of p38 and JNK1/2 Activation after UVA or UVB Irradiation. Activation of the MAPKs p38 and JNK1/2 was analyzed at a range of time points after exposure to 20 J/cm^2 UVA or 0.05 J/cm^2 UVB. A 30 min incubation of cells after exposure to the two kinds of UV radiation was sufficient to activate p38 and JNK1/2 (Figure 2). Moreover, this activation was more accentuated after UVA radiation (Figure 2). The phospho levels of the two MAPKs (phospho-p38 and phospho-JNK1/2) decreased with longer postirradiation incubation times, the reduction being greater after UVA radiation (Figure 2).

Inhibition of UV-Induced p38 and JNK1/2 Activation by the Polyphenolic Fractions. Having determined that the optimum postirradiation incubation time with the fractions was 30 min, we studied the capacity of the total polyphenolic fraction OW and the derived fractions V, IV and XI to prevent the activation of p38 and JNK1/2. For OW, we tested 5, 10, and 20 μg/mL while 5 μg/mL was used for all the other fractions.

A 6 h pretreatment with the fractions protected cells against p38 and JNK1/2 activation. When cells were irradiated with UVA, this effect was clearer for the highest concentration of OW (20 μg/mL) and 5 μg/mL for fractions V, IV and XI (Figure 3A, right). Similar results were obtained for UVB radiation, except for fraction V at 5 μg/mL, which did not inhibit p38 activation (Figure 3A, left). In addition, the amount of total MAPKs was identical for nonirradiated cells and cells irradiated with UVB and UVA (Figure 3A). Given this observation, the decrease observed in protein phosphorylation levels was specific.

The active forms of MAPKs (phospho-p38 and -JNK1/2) (Figure 3B) were quantified by referring the density of phospho-p38 or -JNK1/2 to that of the corresponding α-actin bands and considering the density of UV-radiated nontreated cell bands as 100% activation. The OW fraction demonstrated a dose-dependent protective effect against p38 activation. This effect was

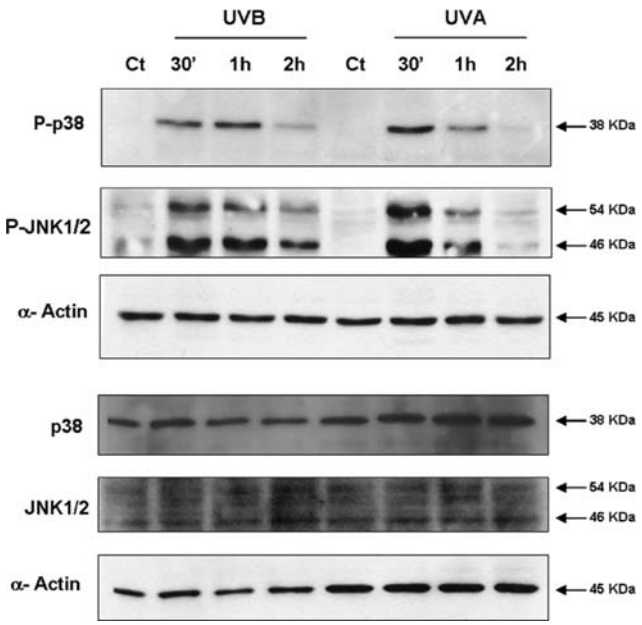

Figure 2. Time course of p38 and JNK1/2 phosphorylation induced by UV radiation. HaCaT cells were cultured for 48 h in the absence of serum followed by exposure to 20 J/cm^2 UVA or 0.05 J/cm^2 UVB. Cells were collected at a range of times, as indicated. The levels of phosphorylated and total p38 and JNK1/2 were determined by Western blot analysis using phospho- and total-specific antibodies. Actin expression was used as loading control.

higher for UVB radiation, where all the concentrations tested decreased activation in a significant manner (Figure 3B, upper section). Moreover, the protective effect of fractions V, IV and XI was quite similar for UVB- and UVA-irradiated cells. Fractions IV and XI showed the greatest protection, presenting about a 50−60% reduction in p38 activation at 5 μg/mL, while the same concentration of fraction V resulted in only a 25% decrease (Figure 3B, upper section). Furthermore, the 50−60% decrease in UVB-induced p38 activation achieved by 5 μg/mL of IV and XI was obtained only at a concentration 2-fold higher of OW (Figure 3B, upper section). When cells were UVA-irradiated, the highest concentration of OW (20 μg/mL) did not reduce p38 activation to the same extent as IV and XI at 5 μg/mL (Figure 3B, upper section). As observed for p38, protection against UV-induced JNK1/2 activation by the fractions was generally higher for UVB-irradiated cells and was dose-dependent, as observed for OW (Figure 3B, lower section). However, in contrast to the findings for p38 activation, the protective effect of OW and V, IV and XI did not differ greatly, showing a 20−40% decrease in JNK1/2 activation at 5 μg/mL for all the fractions and about a 60% reduction only for the highest concentration of OW (20 μg/mL) (Figure 3B).

DISCUSSION

UV radiation-induced oxidative stress in skin cells caused by the generation of intracellular ROS results in cell damage and ultimately in apoptosis. Several studies using *in vitro* and *in vivo* systems have demonstrated that grape proanthocyanidins prevent UV-induced skin damage.[19] However, much less is known about the relationship between the structure of polyphenols and their photoprotective capacity. Here we tested the protective effect of several grape-derived polyphenolic fractions, previously characterized in our group,[27] against UV-induced oxidative damage. Particular attention was paid to the differences in polymerization and galloylation, measured as mean degree of polymerization and percentage of galloylation. Thus, we used fractions (IV and XI) composed of large oligomers (mDP 2.7 and 3.7, respectively) and a high percentage of galloylation (% G 25 and 31, respectively), a fraction (V) that contained only monomers without gallate groups, and a fraction with moderate characteristics from which the other fractions were generated (OW, mDP 1.7 and % G 15%). We demonstrate a statistically significant increase in intracellular ROS in keratinocytes HaCaT exposed to either UVA or UVB radiation, although this increase was much more marked after UVA exposure. Our results show that the polyphenolic fractions acted through a free radical scavenging dependent pathway to inhibit UV-induced oxidative stress. Thus, a 6 h pretreatment of cells with these fractions resulted in a decrease in UVA- or UVB-induced ROS generation, except for the monomeric nongalloylated fraction V, which failed to exert a protective effect. Similar results were obtained for nonirradiated cells pretreated with the fractions. This observation indicates the powerful radical scavenger capacity of these grape polyphenolic fractions, which also decreased the baseline levels of intracellular ROS. We propose that the level of photoprotection is related to the procyanidin size and galloylation from inactive nongalloylated monomers (fraction V) to the most efficient oligomers (mDP 3.7) with 31% galloylation (fraction XI) (Figures 1A and 1C). Fractions IV and OW, having intermediate galloylation and polymerization levels, showed a moderate capacity to decrease intracellular ROS. We detected a clear relationship between radical scavenging activity and the prevention of ROS formation. Therefore, exogenous supplementation of grape fractions may reverse the oxidative imbalance produced by UV-radiation through the scavenging and quenching of ROS. The concentrations of polyphenolic fractions used (5, 10, and 20 μg/mL for the total fraction OW and 5 μg/mL for the derived fractions IV, V and XI) are more efficient at protecting HaCaT cells than other natural products. For instance, 30 μg/mL of a red orange extract protects human keratinocytes from UVB-induced damage[34] and 15 μg/mL of quercetin has been proved to protect these cells from UVA-induced oxidative stress.[35] Moreover, the concentrations assayed can be easily reached *in vivo*. Since 1 to 5% of topically applied catechin samples penetrate the epidermis,[36] preparations containing 1% of catechins would deliver the active concentrations used here. Nonetheless, the observation that the monomers did not protect keratinocytes from radiation may indicate that they do not penetrate the cellular membrane as efficiently as the oligomers. This notion is consistent with previous experiments that stressed the relevance of procyanidin size for surface effects.[37]

JNK and p38 are activated by oxidative stress, thus suggesting that ROS serve as second messengers.[38] These intracellular cascades trigger many transcription factors, such as the activator protein-1 (AP-1), the signal transducers and activators of transcription-1 (STAT-1) and the tumor protein p53, which regulate the expression of genes implicated in cell differentiation, survival and apoptosis.[39,40] Here we demonstrate that UVA and UVB radiation induced p38 and JNK1/2 activation in HaCaT and that this activation was higher after UVA exposure (Figure 2), correlating with their capacity to induce ROS generation (Figure 1B). As the total amount of MAPKs did not decrease during the postirradiation incubation times, we propose that the

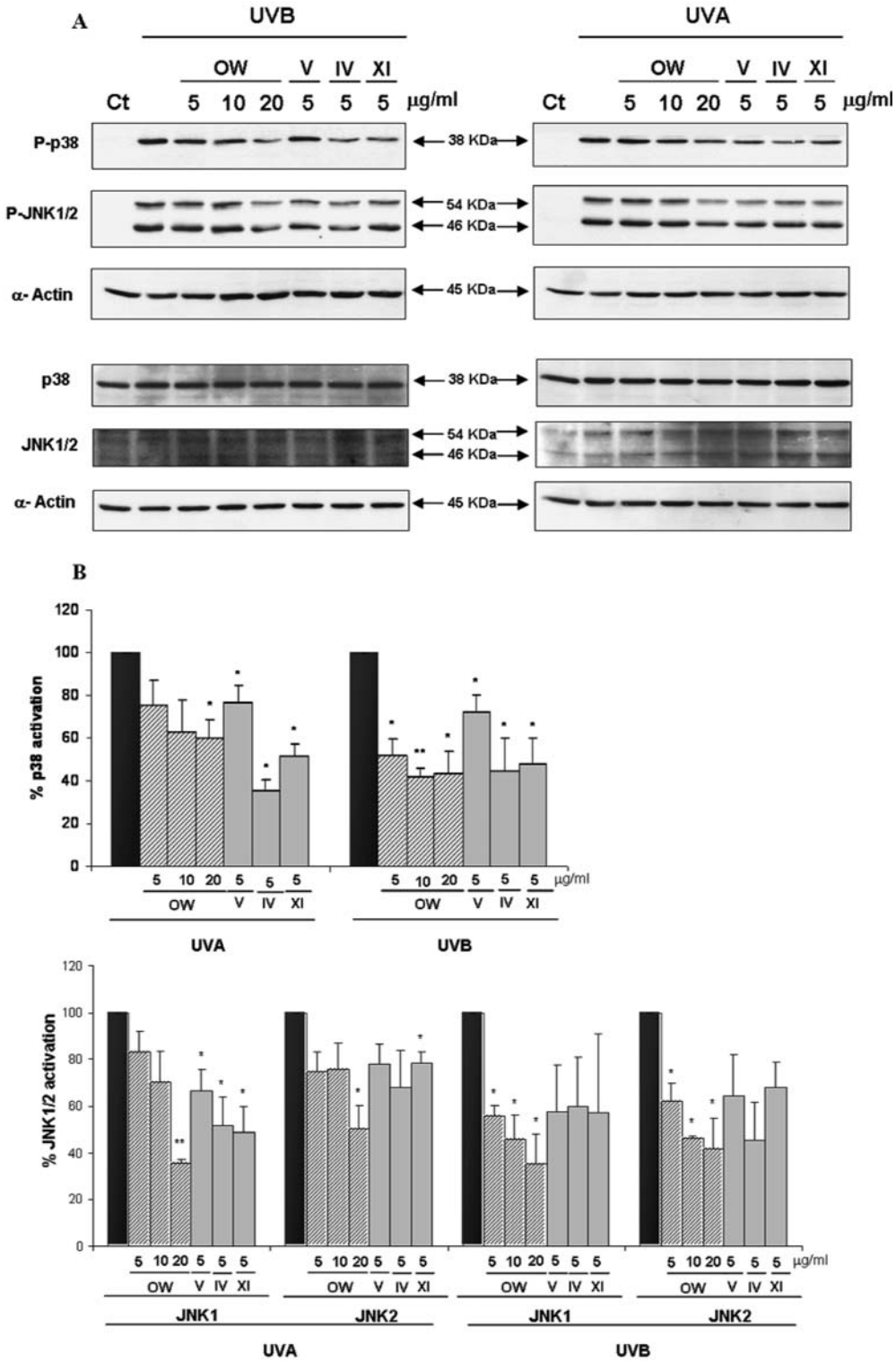

Figure 3. Effect of the polyphenolic fractions on UV-induced p38 and JNK1/2 activation. Serum-deprived HaCaT cells were pretreated with total or derived polyphenolic fractions (OW, IV, V and XI) at the indicated concentrations for 6 h before exposure to 20 J/cm^2 UVA or 0.05 J/cm^2 UVB. (A) To detect phosphorylated and total p38 and JNK1/2, Western blot analysis using phospho- and total-specific antibodies was performed, using actin expression as loading control. (B) The levels of phosphorylated and total p38 and JNK1/2 were quantified by densitometric scanning and percentage of activation was calculated by referring the density of phospho-p38 or -JNK1/2 to density of the corresponding actin bands and considering the density of UV-radiated nontreated cell bands as 100% activation.

reduction in the phosphorylation levels is specific (Figure 2). Once the stress-activated MAPKs act by triggering several transcription factors, which regulate the repair mechanisms and cell death, they are deactivated by a range of mechanisms. For instance, the

wild-type p53-induced phosphatase (Wip1) is induced by p53 in response to stress, which results in the dephosphorylation of proteins such as p38. Interestingly, Wip1 is activated via the JNK-c-Jun and p38-p53 signaling pathways.[41] A 6 h pretreatment of cells with the grape fractions caused a decrease in the active forms of p38 and JNK1/2 (Figure 3). The same concentration (5 μg/mL) of oligomeric grape procyanidins rich in gallate groups (fractions IV and XI) reduced the activation of these MAPKs more efficiently than the monomeric nongalloylated fraction V and the OW fraction, which had moderate polymerization and galloylation (Figure 3). In addition, dose-dependent inhibition was observed for the total fraction OW (Figure 3). The decrease in UV-induced ROS produced by the polyphenolic fractions inhibited p38 and JNK1/2 activation, which may in turn inhibit the activation of nuclear transcription factors downstream of these pathways, thus attenuating the transcription of proteins involved in proapoptotic responses and, thus, protecting skin from UV-induced cell damage and death.[42] It is important to emphasize that our data indicate that the grape fractions did not directly inhibit the stress-activated MAPKs, but the oxidative cell levels. Otherwise, lack of JNK and p38 activation in the presence of high ROS would prevent the activation of repair mechanisms or apoptosis and would be harmful for the organism.

In summary, our results provide evidence that galloylated procyanidin oligomers are more effective protective agents than nongalloylated monomers against oxidative damage induced by UVA and UVB radiation on human keratinocytes and epidermis. The total scavenging potential provided by the number of phenoxyl groups is directly related to the photoprotective capacity of grape polyphenols. In addition, small, flexible and amphiphilic procyanidin oligomers (mDP around 3) may contribute to the overall action of their hydroxyl moieties by facilitating interactions with biological membranes. Thus, our findings highlight the relevance of specific structural characteristics, such as polymerization and galloylation, for the photoprotective effects exerted by grape-derived polyphenols. These results support further research and should be taken into consideration into the clinical pharmacology of photoprotective plant-derived agents.

AUTHOR INFORMATION

Corresponding Author

*Tel: 0034 934021593. Fax: 0034 934021559. E-mail: martacascante@ub.edu.

Funding Sources

The authors would like to thankfully acknowledge the research project grants SAF2008-00164 and AGL2006-12210-C03-02/ALI from the Ministerio de Ciencia e Innovación, and from Red Temática de Investigación Cooperativa en Cáncer, Instituto de Salud Carlos III, Spanish Ministry of Science and Innovation & European Regional Development Fund (ERDF) "Una manera de hacer Europa" (ISCIII-RTICC Grants RD06/0020/0046 and RD06/0020/0010). It has also received financial support from the AGAUR-Generalitat de Catalunya (grant 2009SGR1308, 2009 CTP 00026 and Icrea Academia award 2010 granted to M. Cascante).

REFERENCES

(1) Jenkins, G. Molecular mechanisms of skin ageing. *Mech. Ageing Dev.* **2002**, *123*, 801–810.

(2) Matsumura, Y.; Ananthaswamy, H. N. Short-term and long-term cellular and molecular events following UV irradiation of skin: implications for molecular medicine. *Expert Rev. Mol. Med.* **2002**, *4*, 1–22.

(3) Rezvani, H. R.; Mazurier, F.; Cario-Andre, M.; Pain, C.; Ged, C.; Taieb, A.; de Verneuil, H. Protective effects of catalase overexpression on UVB-induced apoptosis in normal human keratinocytes. *J. Biol. Chem.* **2006**, *281*, 17999–18007.

(4) Kulms, D.; Schwarz, T. Molecular mechanisms involved in UV-induced apoptotic cell death. *Skin Pharmacol. Appl. Skin Physiol.* **2002**, *15*, 342–347.

(5) Pourzand, C.; Tyrrell, R. M. Apoptosis, the role of oxidative stress and the example of solar UV radiation. *Photochem. Photobiol.* **1999**, *70*, 380–390.

(6) Afanas'ev, I. B. Signaling by reactive oxygen and nitrogen species in skin diseases. *Curr. Drug Metab. 11*, 409−414.

(7) Yuan, H.; Zhang, X.; Huang, X.; Lu, Y.; Tang, W.; Man, Y.; Wang, S.; Xi, J.; Li, J. NADPH Oxidase 2-Derived Reactive Oxygen Species Mediate FFAs-Induced Dysfunction and Apoptosis of beta-Cells via JNK, p38 MAPK and p53 Pathways. *PLoS One 5*, e15726.

(8) Wu, W. B.; Chiang, H. S.; Fang, J. Y.; Chen, S. K.; Huang, C. C.; Hung, C. F. (+)-Catechin prevents ultraviolet B-induced human keratinocyte death via inhibition of JNK phosphorylation. *Life Sci.* **2006**, *79*, 801–807.

(9) Bachelor, M. A.; Bowden, G. T. UVA-mediated activation of signaling pathways involved in skin tumor promotion and progression. *Semin. Cancer Biol.* **2004**, *14*, 131–138.

(10) Le Panse, R.; Dubertret, L.; Coulomb, B. p38 mitogen-activated protein kinase activation by ultraviolet A radiation in human dermal fibroblasts. *Photochem. Photobiol.* **2003**, *78*, 168–174.

(11) Chiu, A.; Kimball, A. B. Topical vitamins, minerals and botanical ingredients as modulators of environmental and chronological skin damage. *Br. J. Dermatol.* **2003**, *149*, 681–691.

(12) Jeon, H. Y.; Kim, J. K.; Kim, W. G.; Lee, S. J. Effects of oral epigallocatechin gallate supplementation on the minimal erythema dose and UV-induced skin damage. *Skin Pharmacol. Physiol.* **2009**, *22*, 137–141.

(13) Kim, J.; Hwang, J. S.; Cho, Y. K.; Han, Y.; Jeon, Y. J.; Yang, K. H. Protective effects of (-)-epigallocatechin-3-gallate on UVA- and UVB-induced skin damage. *Skin Pharmacol. Appl. Skin Physiol.* **2001**, *14*, 11–19.

(14) Vostalova, J.; Zdarilova, A.; Svobodova, A. Prunella vulgaris extract and rosmarinic acid prevent UVB-induced DNA damage and oxidative stress in HaCaT keratinocytes. *Arch. Dermatol. Res. 302*, 171-181.

(15) Park, K.; Lee, J. H. Protective effects of resveratrol on UVB-irradiated HaCaT cells through attenuation of the caspase pathway. *Oncol. Rep.* **2008**, *19*, 413–417.

(16) Brand, R. M.; Jendrzejewski, J. L. Topical treatment with (-)-epigallocatechin-3-gallate and genistein after a single UV exposure can reduce skin damage. *J. Dermatol. Sci.* **2008**, *50*, 69–72.

(17) Sharma, S. D.; Meeran, S. M.; Katiyar, S. K. Dietary grape seed proanthocyanidins inhibit UVB-induced oxidative stress and activation of mitogen-activated protein kinases and nuclear factor-kappaB signaling in in vivo SKH-1 hairless mice. *Mol. Cancer Ther.* **2007**, *6*, 995–1005.

(18) Mittal, A.; Elmets, C. A.; Katiyar, S. K. Dietary feeding of proanthocyanidins from grape seeds prevents photocarcinogenesis in SKH-1 hairless mice: relationship to decreased fat and lipid peroxidation. *Carcinogenesis* **2003**, *24*, 1379–1388.

(19) Nichols, J. A.; Katiyar, S. K. Skin photoprotection by natural polyphenols: anti-inflammatory, antioxidant and DNA repair mechanisms. *Arch. Dermatol. Res. 302*, 71-83.

(20) Shi, J.; Yu, J.; Pohorly, J. E.; Kakuda, Y. Polyphenolics in grape seeds-biochemistry and functionality. *J. Med. Food* **2003**, *6*, 291–299.

(21) Lizarraga, D.; Lozano, C.; Briede, J. J.; van Delft, J. H.; Tourino, S.; Centelles, J. J.; Torres, J. L.; Cascante, M. The importance of polymerization and galloylation for the antiproliferative properties of procyanidin-rich natural extracts. *FEBS J.* **2007**, *274*, 4802–4811.

(22) Plumb, G. W.; De Pascual-Teresa, S.; Santos-Buelga, C.; Cheynier, V.; Williamson, G. Antioxidant properties of catechins and proanthocyanidins: effect of polymerisation, galloylation and glycosylation. *Free Radical Res.* **1998**, *29*, 351–358.

(23) Tourino, S.; Selga, A.; Jimenez, A.; Julia, L.; Lozano, C.; Lizarraga, D.; Cascante, M.; Torres, J. L. Procyanidin fractions from pine (Pinus pinaster) bark: radical scavenging power in solution, antioxidant activity in emulsion, and antiproliferative effect in melanoma cells. *J. Agric. Food Chem.* **2005**, *53*, 4728–4735.

(24) Matito, C.; Mastorakou, F.; Centelles, J. J.; Torres, J. L.; Cascante, M. Antiproliferative effect of antioxidant polyphenols from grape in murine Hepa-1c1c7. *Eur. J. Nutr.* **2003**, *42*, 43–49.

(25) Comin-Anduix, B.; Boros, L. G.; Marin, S.; Boren, J.; Callol-Massot, C.; Centelles, J. J.; Torres, J. L.; Agell, N.; Bassilian, S.; Cascante, M. Fermented wheat germ extract inhibits glycolysis/pentose cycle enzymes and induces apoptosis through poly(ADP-ribose) polymerase activation in Jurkat T-cell leukemia tumor cells. *J. Biol. Chem.* **2002**, *277*, 46408–46414.

(26) Boukamp, P.; Petrussevska, R. T.; Breitkreutz, D.; Hornung, J.; Markham, A.; Fusenig, N. E. Normal keratinization in a spontaneously immortalized aneuploid human keratinocyte cell line. *J. Cell Biol.* **1988**, *106*, 761–771.

(27) Torres, J. L.; Varela, B.; Garcia, M. T.; Carilla, J.; Matito, C.; Centelles, J. J.; Cascante, M.; Sort, X.; Bobet, R. Valorization of grape (Vitis vinifera) byproducts. Antioxidant and biological properties of polyphenolic fractions differing in procyanidin composition and flavonol content. *J. Agric. Food Chem.* **2002**, *50*, 7548–7555.

(28) Larsson, P.; Andersson, E.; Johansson, U.; Ollinger, K.; Rosdahl, I. Ultraviolet A and B affect human melanocytes and keratinocytes differently. A study of oxidative alterations and apoptosis. *Exp. Dermatol.* **2005**, *14*, 117–123.

(29) Pi, J.; He, Y.; Bortner, C.; Huang, J.; Liu, J.; Zhou, T.; Qu, W.; North, S. L.; Kasprzak, K. S.; Diwan, B. A.; Chignell, C. F.; Waalkes, M. P. Low level, long-term inorganic arsenite exposure causes generalized resistance to apoptosis in cultured human keratinocytes: potential role in skin co-carcinogenesis. *Int. J. Cancer* **2005**, *116*, 20–26.

(30) Royall, J. A.; Ischiropoulos, H. Evaluation of 2′,7′-dichlorofluorescin and dihydrorhodamine 123 as fluorescent probes for intracellular H2O2 in cultured endothelial cells. *Arch. Biochem. Biophys.* **1993**, *302*, 348–355.

(31) Henderson, L. M.; Chappell, J. B. Dihydrorhodamine 123: a fluorescent probe for superoxide generation? *Eur. J. Biochem.* **1993**, *217*, 973–980.

(32) Qin, Y.; Lu, M.; Gong, X. Dihydrorhodamine 123 is superior to 2,7-dichlorodihydrofluorescein diacetate and dihydrorhodamine 6G in detecting intracellular hydrogen peroxide in tumor cells. *Cell Biol. Int.* **2008**, *32*, 224–228.

(33) Lowry, O. H.; Rosebrough, N. J.; Farr, A. L.; Randall, R. J. Protein measurement with the Folin phenol reagent. *J. Biol. Chem.* **1951**, *193*, 265–275.

(34) Cimino, F.; Cristani, M.; Saija, A.; Bonina, F. P.; Virgili, F. Protective effects of a red orange extract on UVB-induced damage in human keratinocytes. *Biofactors* **2007**, *30*, 129–138.

(35) Kimura, S.; Warabi, E.; Yanagawa, T.; Ma, D.; Itoh, K.; Ishii, Y.; Kawachi, Y.; Ishii, T. Essential role of Nrf2 in keratinocyte protection from UVA by quercetin. *Biochem. Biophys. Res. Commun.* **2009**, *387*, 109–114.

(36) Alonso, C.; Ramon, E.; Lozano, C.; Parra, J. L.; Torres, J. L.; Coderch, L. Percutaneous absorption of flavan-3-ol conjugates from plant procyanidins. *Drugs Exp. Clin. Res.* **2004**, *30*, 1–10.

(37) Verstraeten, S. V.; Keen, C. L.; Schmitz, H. H.; Fraga, C. G.; Oteiza, P. I. Flavan-3-ols and procyanidins protect liposomes against lipid oxidation and disruption of the bilayer structure. *Free Radical Biol. Med.* **2003**, *34*, 84–92.

(38) Krutmann, J. The interaction of UVA and UVB wavebands with particular emphasis on signalling. *Prog. Biophys. Mol. Biol.* **2006**, *92*, 105–107.

(39) Bae, J. Y.; Lim, S. S.; Kim, S. J.; Choi, J. S.; Park, J.; Ju, S. M.; Han, S. J.; Kang, I. J.; Kang, Y. H. Bog blueberry anthocyanins alleviate photoaging in ultraviolet-B irradiation-induced human dermal fibroblasts. *Mol. Nutr. Food Res.* **2009**, *53*, 726–738.

(40) Rittie, L.; Fisher, G. J. UV-light-induced signal cascades and skin aging. *Ageing Res. Rev.* **2002**, *1*, 705–720.

(41) Song, J. Y.; Han, H. S.; Sabapathy, K.; Lee, B. M.; Yu, E.; Choi, J. Expression of a homeostatic regulator, Wip1 (wild-type p53-induced phosphatase), is temporally induced by c-Jun and p53 in response to UV irradiation. *J. Biol. Chem. 285*, 9067-9076.

(42) Roduit, R.; Schorderet, D. F. MAP kinase pathways in UV-induced apoptosis of retinal pigment epithelium ARPE19 cells. *Apoptosis* **2008**, *13*, 343–353.

ANNEX 4

El punicalagin i les catequines contenen subestructures polifenòliques que afecten la viabilitat cel·lular i que poden ser monitoritzades per radicals quimiosensors sensibles a la transferència d'electrons

Publicació a la revista *Journal of Agricultural and Food Chemistry* amb un factor d'impacte 2,816.

Anna Carreras[1], María Luisa Mateos-Martín[1], Amado Velázquez-Palenzuela[2], Enric Brillas[2], Susana Sánchez-Tena[3], Marta Cascante[3], Luis Juliá[1] i Josep Lluís Torres[1]

[1]Institut de Química Avançada de Catalunya (IQAC-CSIC), 08034 Barcelona, Espanya

[2]Departament de Química Física, Universitat de Barcelona, 08028 Barcelona, Espanya

[3]Facultat de Biologia, Universitat de Barcelona i IBUB, unitat associada al CSIC, 08028 Barcelona, Espanya

RESUM

Els polifenols derivats de plantes poden actuar com neutralitzadors o bé com generadors de radicals lliures depenent de la seva naturalesa i concentració. Aquest efecte dual, mediat per reaccions de transferència d'electrons, pot contribuir a la seva influència en la viabilitat cel·lular. Aquest estudi va utilitzar dos radicals estables (tris(2,3,5,6 tetracloro-4-nitrofenil)metil (TNPTM) i tris(2,4,6-tricloro-3,5-dinitrofenil)metil (HNTTM)) sensibles únicament a reaccions de reducció per transferència d'electrons, per monitoritzar les propietats redox dels polifenols (punicalagin i catequines) que contenen hidroxils fenòlics amb diferent capacitats de reducció. L'ús d'aquests dos radicals va revelar que subestructures del punicalagin que consisteixen en esters de gal·lat units per unions carboni-carboni (C−C) són més reactives que gal·lats senzills i menys reactives que el grup pirogal·lol de les catequines del té verd. Els hidroxils més reactius, detectats per TNPTM, son presents en els compostos que afecten de manera més important la viabilitat de cèl·lules HT29 de càncer de còlon. El TNPTM reacciona amb gal·lats units per enllaços C−C i amb el pirogal·lol i proporciona una mètode eficaç per detectar polifenols naturals potencialment beneficiosos.

JOURNAL OF AGRICULTURAL AND FOOD CHEMISTRY

Addition/Correction

pubs.acs.org/JAFC

Correction to Punicalagin and Catechins Contain Polyphenolic Substructures That Influence Cell Viability and Can Be Monitored by Radical Chemosensors Sensitive to Electron Transfer

Anna Carreras, María Luisa Mateos-Martín, Amado Velázquez-Palenzuela, Enric Brillas, Susana Sánchez-Tena, Marta Cascante, Luis Juliá, and Josep Lluís Torres*

J. Agric. Food Chem. **2012**, *60*, 1659. DOI: 10.1021/jf204059x

Author Susana Sánchez-Tena (Department of Biochemistry and Molecular Biology, Unit Associated with CSIC, University of Barcelona, Avinguda Diagonal 645, 08028 Barcelona, Spain) was inadvertently omitted from the original publication.

Published: April 26, 2012

JOURNAL OF AGRICULTURAL AND FOOD CHEMISTRY

Article

pubs.acs.org/JAFC

Punicalagin and Catechins Contain Polyphenolic Substructures That Influence Cell Viability and Can Be Monitored by Radical Chemosensors Sensitive to Electron Transfer

Anna Carreras,[†] María Luisa Mateos-Martín,[†] Amado Velázquez-Palenzuela,[§] Enric Brillas,[§] Marta Cascante,[⊗] Luis Juliá,[†] and Josep Lluís Torres*[,†]

[†]Department of Biological Chemistry and Molecular Modelling, Institute for Advanced Chemistry of Catalonia, IQAC-CSIC, Jordi Girona 18-26, 08034 Barcelona, Spain

[§]Department of Physical Chemistry, University of Barcelona, Martí i Franquès 1-11, 08028 Barcelona, Spain

[⊗]Department of Biochemistry and Molecular Biology, Unit Associated with CSIC, University of Barcelona, Avinguda Diagonal 645, 08028 Barcelona, Spain

Supporting Information

ABSTRACT: Plant polyphenols may be free radical scavengers or generators, depending on their nature and concentration. This dual effect, mediated by electron transfer reactions, may contribute to their influence on cell viability. This study used two stable radicals (tris(2,3,5,6-tetrachloro-4-nitrophenyl)methyl (TNPTM) and tris(2,4,6-trichloro-3,5-dinitrophenyl)methyl (HNTTM)) sensitive only to electron transfer reduction reactions to monitor the redox properties of polyphenols (punicalagin and catechins) that contain phenolic hydroxyls with different reducing capacities. The use of the two radicals reveals that punicalagin's substructures consisting of gallate esters linked together by carbon−carbon (C−C) bonds are more reactive than simple gallates and less reactive than the pyrogallol moiety of green tea catechins. The most reactive hydroxyls, detected by TNPTM, are present in the compounds that affect HT-29 cell viability the most. TNPTM reacts with C−C-linked gallates and pyrogallol and provides a convenient way to detect potentially beneficial polyphenols from natural sources.

KEYWORDS: *punicalagin, catechins, pyrogallol, TNPTM chemosensor, cell viability*

INTRODUCTION

The question of whether natural polyphenols provide benefits in terms of human health is a controversial one among scientists. Ever since Harman published his paper on free radicals and aging,[1] it has been assumed that polyphenols prevent disease and delay aging because they scavenge toxic free radicals, which progressively damage biomolecules in live tissues mainly by oxidation.[2] Because they scavenge potentially oxidizing free radicals, polyphenols are referred to as antioxidants. Nevertheless, although it is true that polyphenols scavenge radicals in solution, their intracellular effectiveness is less obvious, and many authors consider them to be virtually inactive in vivo after oral intake.[3] The reason is that the live organism prevents polyphenols from greatly altering the redox homeostasis by rapidly metabolizing and excreting them, as well as by activating regulatory enzymatic systems. Polyphenols are conjugated into glucuronides, methyl esters, and sulfates mainly in the intestine and liver.[4,5] Most of these conjugates are no longer free radical scavengers, and the very small amounts of remaining intact polyphenolic moieties are very unlikely to modify the redox homeostasis significantly.[3] The skin and intestinal tract may be exceptions to this because local concentrations of intact phenolics may be present in significant amounts in these tissues.[6] Moreover, not only may polyphenols be effective free radical scavengers, they may actually generate free radicals depending on the nature and concentration of the specific polyphenols.[3] This so-called pro-oxidant activity may be behind the moderate toxicity of green tea extracts at very high concentrations[7] and the reason why polyphenols are rapidly transformed and excreted after ingestion. Interestingly, at concentrations that are not so high, this mild pro-oxidant activity may result in an overall antioxidant effect via a mechanism known as hormesis, which can be defined as a low-dose stimulation of defense systems with a subsequent beneficial effect.[8] In the case of foodstuffs in which the redox regulation systems progressively lose their efficiency during the shelf life of the product (e.g., fish rich in PUFA), polyphenols have proven to effectively prevent lipid oxidation.[9] Whatever the case, if polyphenols exert an influence over the redox status of any system, whether it is antioxidant, toxic pro-oxidant, or hormetic pro-oxidant, it is somehow related to the reactivity of the constitutive hydroxyl groups in the polyphenols, the functional groups that first react with oxidants.

Different chemical mechanisms may be involved in the free radical-scavenging and/or free radical-generating effects of polyphenols. To better characterize the scavenging activity of polyphenols, several assays focused on different possible mechanisms of their overall action should be considered.[10] The mechanisms that have been proposed are hydrogen atom transfer (HAT), proton-coupled electron transfer (PCET), and sequential proton loss electron transfer (SPLET), with the generation of a

Received: March 1, 2011
Revised: January 5, 2012
Accepted: January 27, 2012
Published: January 27, 2012

dx.doi.org/10.1021/jf204059x | J. Agric. Food Chem. 2012, 60, 1659−1665

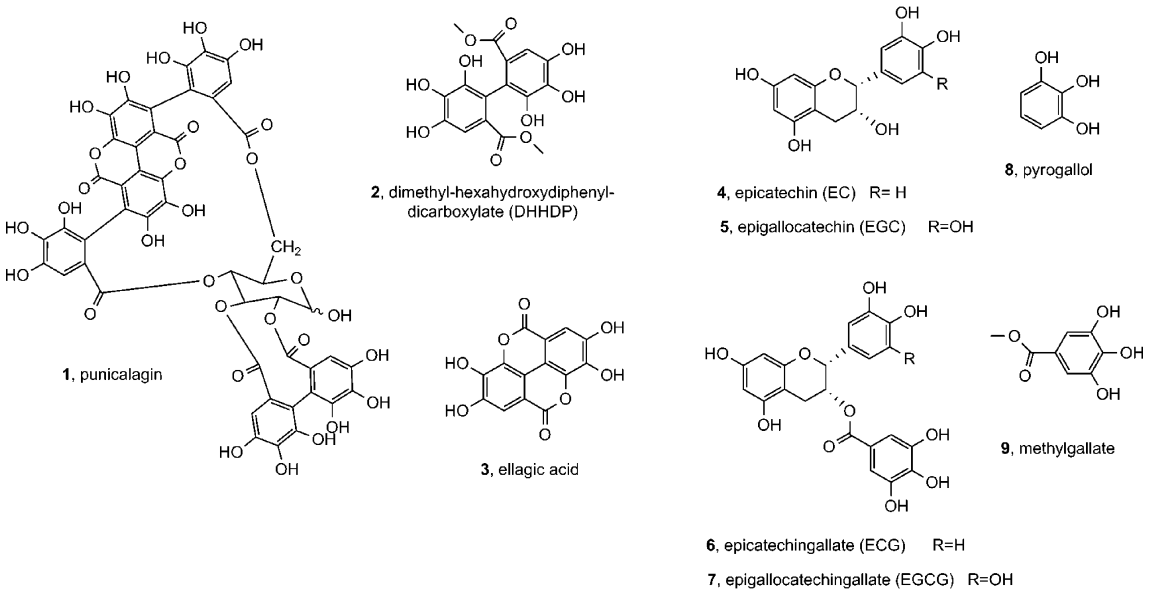

Figure 1. Structures of punicalagin (**1**), related compounds (**2** and **3**), green tea catechins (**4**–**7**), and simple phenols (**8** and **9**).

more stable phenoxyl radical.[11−13] Electron transfer to oxygen generates the superoxide radical $O_2^{\bullet-}$, which is enzymatically converted into hydrogen peroxide[14,15] and ultimately into the deleterious hydroxyl radical in the presence of transition metal cations (e.g., Fe^{2+}).[16] Moreover, the superoxide radical seems to mediate apoptosis.[17,18] Electron transfer appears to be most relevant in the redox cascades involving polyphenols, whether they scavenge or generate reactive radicals. To evaluate the electron transfer capacity of polyphenols, we developed stable radicals of the (2,4,6-trichlorophenyl)methyl (TTM) and perchlorotriphenylmethyl (PTM) series, which react exclusively by electron transfer.[13,19,20] We and others have used these radicals to evaluate the electron transfer capacity of natural and synthetic phenolic scavengers.[21,22] As the activity of the stable radicals of the TTM and PTM series essentially depends on the electron-withdrawing or electron-donating character of the meta- and/or para- substituents introduced into the phenyl rings, radicals with different redox potentials can be designed. The advantage of devising assays using this combination of radicals is that they can discriminate between oxidizing agents by their oxidizing ability, in contrast to the ferric ion reduction method that also operates exclusively by electron transfer processes but measures only the reducing ability based upon the redox potential of the ferric ion. Moreover, the outcome of the ferric ion method is also influenced by binding of the polyphenol to the ion.

Polyphenols may contain more than one reactive polyphenolic substructure. Punicalagin (**1**) (Figure 1), the most abundant polyphenol in pomegranate (*Punica granatum* L.),[23] is a hydrolyzable tannin of the ellagitannin kind because it contains an ellagic acid substructure (**3**). Punicalagin (**1**) releases ellagic acid (**3**) in the small intestine via spontaneous lactonization with later conversion into urolithin A by the gut microbiota.[24] Punicalagin (**1**) also contains in its structure gallate (three geminal phenolic hydroxyls and a carboxylate function) esters linked by carbon−carbon (C−C) bonds either to themselves (hexahydroxy-2,2′-diphenyl, HHDP moiety) or to the ellagic acid substructure. This ensemble of substructures and their metabolites contributes to the bioactivity of the whole molecule. The C−C bond structures constitutive of ellagitannins appear to be important for their activity. Pedunculagin, another hydrolyzable tannin that contains the HHDP moiety, shows higher cytotoxic activity than pentagalloylglucose, a hydrolyzable tannin that contains only simple gallate esters in its structure.[25] Catechins (flavanols of the flavan-3-ol type) are another family of polyphenols that display different polyphenolic substructures and are relevant to dietary considerations. Green tea is a common source of catechins, mainly, in order of abundance, (−)-epigallocatechin gallate (EGCG) (**7**), (−)-epigallocatechin (EGC) (**5**), (−)-epicatechin (EC) (**4**), and (−)-epicatechin gallate (ECG) (**6**) (Figure 1).[26] Tea flavanols scavenge reactive oxygen and nitrogen species, interfere with pro-oxidant processes, or inhibit pro-oxidant enzymes.[27] Polyphenols appear to exert their biological activity through different mechanisms involving redox reactions and protein−ligand interactions. Because the present paper focuses on the redox reactivity of different phenolic moieties and its possible relationship to cell viability in vitro, we selected pomegranate punicalagin (**1**) and green tea flavanols **4**–**7** for our study; together they contain a broad range of polyphenolic substructures. Here, we examine the electron transfer capacity (reducing power) of punicalagin (**1**), and its metabolite ellagic acid (**3**), its related substructure **2**, and green tea flavanols **4**–**7** bearing the catechol, pyrogallol, and gallate moieties, and we evaluate the effect of all these molecules on the viability of colon carcinoma HT-29 cells.

MATERIALS AND METHODS

Tris(2,3,5,6-tetrachloro-4-nitrophenyl)methyl (TNPTM) and tris-(2,4,6-trichloro-3,5-dinitrophenyl)methyl (HNTTM) were synthesized in our laboratory as described previously.[19,20] 1,1-Diphenyl-2-picrylhydrazyl (DPPH) was purchased from Sigma-Aldrich (St. Louis, MO). Punicalagin (**1**) (≥98% (HPLC)) was obtained from Biopurify (Sichuan, China), ellagic acid (**3**) and the catechins **4**–**7** were from from Sigma-Aldrich, and dimethyl-hexahydroxydiphenyl dicarboxylate (DHHDP, **2**) was synthesized in our laboratory following procedures described elsewhere[28] (see the Supporting Information).

Radical-Scavenging Capacity. The scavenging capacity was determined from mixtures (1:1, v/v) of fresh solutions of stable radicals (TNPTM, HNTTM, DPPH; 120 μM) and fresh solutions of polyphenols **1**–**9** in $CHCl_3$/MeOH (2:1) at different concentrations (1−120 μM) at room temperature. All of the solutions were prepared

and deoxygenated in the darkness. The reactions were monitored by electron paramagnetic resonance (EPR) on an EMX-Plus 10/12 (Bruker BioSpin, Rheinstetten, Germany) after 48 h (TNPTM), 7 h (HNTTM), and 30 min (DPPH). Operating conditions were as follows: center field, 3615 G; scan range, 250 G; microwave power, 5.2 mW; microwave frequency, 9.86 GHz; modulation frequency, 100 kHz; receiver gain, 6×10^3; and time constant, 4.1 s. The scavenging capacity of polyphenols is given as EC_{50}, which corresponds to the amount (micrograms or micromoles) of polyphenol able to consume half the amount of free radical divided by micromoles of initial radical. The results in micrograms per micromole convey the idea of the scavenging capacity of a given amount of polyphenol, and the results in micromoles per micromole provide information about the number of equivalents per molecule. To facilitate the comparison between structures, the results were also expressed as antiradical capacity (ARC), which is the inverse of EC_{50} in micrograms per micromole and hydrogen atoms donated or electrons transferred per molecule of polyphenol (H/e), which is the inverse of $2 \times EC_{50}$ in micromoles per micromole.

Kinetic Measurements. The rate constants of the reactions between TNPTM and polyphenols **2** and **8** were estimated by EPR. Freshly prepared solutions of TNPTM in CH_3Cl/MeOH (2:1) (240 μM) and the polyphenol (48 μM in the same solvent) were mixed (1:1, v/v, molar ratio 5:1), and the decay of the TNTPM band was followed at room temperature. Operating conditions were as follows: center field, 3450 G; scan range, 250 G; microwave power, 1.0 mW; microwave frequency, 9.86 GHz; modulation frequency, 100 kHz; receiver gain, 8.9×10^3; and time constant, 40.96 s. The rate constants and the total number of electrons transferred per polyphenol (n_e) were estimated with a simple and general kinetic model reported by Dangles et al.[29] defined by eq 1. The values for the rate constant, k were calculated from the integrated eq 2.

$$-\mathrm{d[TNPTM]}/\mathrm{d}t = k \times n\mathrm{[(poly)phenol][TNPTM]} = k_1\mathrm{[(poly)phenol][TNPTM]} \quad (1)$$

$$\ln \frac{1 - I_f/I_x}{1 - I_f/I_0} = -\frac{k_1 c}{I_0/I_f - 1} t \quad (2)$$

In eqs 1 and 2, n represents the number of reduced moles of TNPTM per mole of polyphenol; I_0 is the initial intensity of the TNPTM signal in the EPR spectra; I_f is the final visible intensity; and c is the initial concentration of polyphenol. The n_e values of the stoichiometry of the polyphenol were calculated using eq 3; ε is the molar absorptivity characteristic of the stable free radical.

$$n_e = \frac{I_0 - I_f}{\epsilon \times C} \quad (3)$$

Cyclic Voltammetry. Cyclic voltammetries were carried out in a standard thermostated cylindrical, one-compartment, three-electrode cell. A platinum (Pt) disk of 0.093 cm^2 area was used as the working electrode and a Pt wire as the counter electrode. The reference electrode was a saturated calomel electrode (SCE), submerged in a salt bridge of the same electrolyte, which was separated from the test solution by a Vycor membrane. Solutions of polyphenols ($\sim 10^{-3}$ M) in DMF containing tetrabutylammonium perchlorate (0.1 M) as the background electrolyte were studied. The volume of all test solutions was 50 mL. Electrochemical measurements were performed under an argon atmosphere at 25 °C using an Eco Chemie Autolab PGSTA-T100 potentiostat-galvanostat (Autolab, Utrecht, The Netherlands) controlled by a computer with Nova 1.5 software (Autolab). Cyclic voltammograms of all the solutions were recorded at scan rates ranging from 20 to 200 mV s^{-1}.

Cell Culture and Viability Assay. HT-29 human colon adenocarcinoma cells were obtained from the American Type Culture Collection. HT-29 cells were cultured in Dulbeco Modified Eagle's Medium (DMEM with 4500 mg L^{-1} glucose, L-glutamine, and sodium bicarbonate, without sodium pyruvate; Sigma-Aldrich), supplemented with 10% fetal bovine serum (PAA Laboratories, Pasching, Austria) and antibiotics, 100 U mL^{-1} penicillin and 100 mg L^{-1} streptomycin (Invitrogen, Paisley, U.K.), at 37 °C in a humidified atmosphere of CO_2 (5%). The effect of treatment with different polyphenols upon proliferation of HT-29 colon cancer cells was measured by the 3-(4,5-dimethylthiazol-2-yl)-2,5-diphenyl tetrazolium bromide (MTT) (Sigma-Aldrich) assay, which is based on the ability of live cells to cleave the tetrazolium ring, thus producing formazan, which absorbs at 570 nm. HT-29 cells (3000 cells/well) were grown on a 96-well plate for 24 h and then incubated with the different polyphenols at different concentrations (10−300 μM) in dimethyl sulfoxide (DMSO) (Sigma-Aldrich), except ellagic acid (**3**), which was dissolved in *N*-methylpyrrolidone because of its poor solubility in DMSO. After 72 h, 100 μL of MTT solution (0.5 mg mL^{-1}) was added to each well. After 1 h of incubation, the formazan salt was resuspended in 100 μL of DMSO. Cell viability was measured by absorbance at 550 nm on an ELISA plate reader (Tecan Sunrise MR20-301, TECAN, Austria). The experiments were also run in the presence of catalase (Sigma-Aldrich), 100 U mL^{-1} in DMEM.[30] The results were expressed as IC_{50}.

RESULTS

Radical-Scavenging Capacity of Polyphenols Measured by TNPTM, HNTTM, and DPPH. The scavenging capacity of punicalagin (**1**) and related compounds **2** and **3**, flavanols **4**−**7**, pyrogallol (**8**), and methylgallate (**9**) was measured by making them react with the stable radicals TNPTM, HNTTM, and DPPH in a mixture that includes a polar hydroxylated solvent ($CHCl_3$/MeOH (2:1) (v/v)) and monitoring the decrease of the EPR radical signal. TNPTM and HNTTM are reduced exclusively by accepting electrons, in contrast to DPPH, which reacts by HAT and/or ET depending on the solvent. Table 1 summarizes the results of the scavenging capacity of **1**−**9** against the three radicals.

Punicalagin (**1**), ECG (**6**), and EGCG (**7**) were the most active polyphenols against HNTTM and DPPH. The number of electrons transferred to HNTTM roughly corresponded to the number of putative reactive positions (geminal hydroxyls) of the flavanols except for ECG (**6**), which consumed a larger amount of radical. Surprisingly, DHHDP (**2**) transferred 4.3 electrons instead of 6, and punicalagin (**1**) transferred 14.2 electrons instead of 16. The scavenging capacities of the polyphenols against TNPTM radical were lower than those obtained with HNTTM and DPPH because TNPTM reacts only with the most reactive hydroxyls. One molecule each of EGC (**5**), EGCG (**7**), and pyrogallol (**8**) reacted with 3 molecules of TNPTM (roughly 1 electron transferred from each of the three geminal hydroxyls); 1 molecule of punicalagin (**1**) and its substructure DHHDP (**2**) reacted with 3.3 and 2 molecules of TNPTM, respectively (roughly 1 electron transferred from each C−C linked gallate). In contrast, ellagic acid (**3**), EC (**4**), ECG (**6**), and methylgallate (**9**) did not react at all with TNPTM. Figure 2 shows graphically the selective reactivity of characteristic phenolic moieties with TNPTM, monitored by the decrease of the TNPTM radical EPR signal upon reaction with DHHDP (**2**), pyrogallol (**8**), and methylgallate (**9**).

Kinetic Measurements. To further characterize the scavenging activity of the hexahydroxydiphenyl moiety within punicalagin (**1**) and pyrogallol (**8**), which are the only simple structures that react with TNTPM, we made kinetic measurements of the reactions of DHHDP (**2**) and pyrogallol (**8**) with TNPTM. The course of the reaction was monitored using EPR by recording the decay of the TNPTM signal as a result of the addition of the polyphenol in $CHCl_3$/MeOH (2:1) at a molar ratio TNPTM/polyphenol of 5:1. To calculate the stoichiometric factor, the reaction was monitored to completion over a period of 48 h.

Table 1. Scavenging Capacity of Ellagitannins and Flavanols against Stable Radicals[a]

radical	polyphenol	EC_{50} $\mu g\ \mu mol^{-1}$	EC_{50} $\mu mol\ \mu mol^{-1}$	ARP[b]	e/H[c]
TNPTM	ellagitannins				
	1	50.3 (2.6)	0.15 (0.01)	6.5 (0.3)	3.3 (0.2)
	2	51.2 (0.0)	0.26 (0.00)	3.9 (0.1)	1.9 (0.0)
	3	–[d]	–	–	–
	flavanols				
	4	–	–	–	–
	5	55.2 (6.5)	0.18 (0.02)	5.6 (0.6)	2.8 (0.3)
	6	–	–	–	–
	7	83.3 (5.9)	0.18 (0.01)	5.5 (0.3)	2.7 (0.1)
	simple phenols				
	8	21.7 (1.6)	0.17 (0.01)	5.8 (0.4)	2.9 (0.2)
	9	–	–	–	–
HNTTM	ellagitannins				
	1	38.1 (3.9)	0.04 (0.00)	28.4 (2.7)	14.2 (1.4)
	2	42.2 (5.0)	0.12 (0.02)	8.7 (1.1)	4.3 (0.5)
	3	30.4 (1.1)	0.10 (0.00)	9.9 (0.3)	5.0 (0.1)
	flavanols				
	4	54.0 (4.0)	0.19 (0.02)	5.3 (0.5)	2.7 (0.2)
	5	50.2 (2.2)	0.16 (0.01)	6.2 (0.0)	3.1 (0.1)
	6	24.0 (2.6)	0.05 (0.01)	18.5 (2.0)	9.3 (1.0)
	7	38.3 (3.2)	0.08 (0.01)	11.9 (0.9)	5.9 (0.4)
	simple phenols				
	8	19.7 (1.2)	0.16 (0.01)	6.4 (0.4)	3.2 (0.2)
	9	30.2 (2.5)	0.15 (0.01)	6.5 (0.5)	3.2 (0.3)
DPPH	ellagitannins				
	1	20.0 (1.6)	0.02 (0.00)	55.0 (3.3)	27.5 (1.7)
	2	31.2 (1.6)	0.08 (0.00)	12.2 (0.4)	6.1 (0.2)
	3	22.1 (0.2)	0.07 (0.00)	13.7 (0.3)	6.8 (0.1)
	flavanols				
	4	36.8 (1.6)	0.13 (0.01)	7.9 (0.3)	3.9 (0.2)
	5	31.5 (1.8)	0.11 (0.00)	9.1 (0.3)	4.6 (0.1)
	6	28.9 (3.1)	0.07 (0.01)	15.4 (1.6)	7.8 (0.8)
	7	31.4 (6.1)	0.06 (0.02)	17.3 (3.4)	8.7 (1.7)
	simple phenols				
	8	12.6 (1.2)	0.10 (0.01)	10.0 (0.8)	5.0 (0.4)
	9	31.7 (3.2)	0.17 (0.02)	5.8 (0.6)	2.9 (0.3)

[a]Values are means (standard deviation), $n = 3$. [b]Antiradical power ($1/EC_{50}$ ($\mu g\ \mu mol^{-1}$)). [c]Moles of reduced radical per mole of polyphenol ($1/(2 \times EC_{50})$) corresponding to the number of electrons or hydrogen atoms transferred per molecule of polyphenol. [d]EC_{50} ($\mu g\ \mu mol^{-1}$) $\geq$ 132).

The rate constants and stoichiometric factors for these reactions are given in Table 2. The reaction with pyrogallol (**8**) was faster than that with DHHDP (**2**), and the stoichiometric factors were consistent with those estimated from the concentration/activity curve and shown in Table 1, roughly corresponding to 2 and 3 electrons from DHHDP (**2**) and pyrogallol (**8**), respectively. As commented before, methylgallate (**9**) did not reduce the TNPTM.

Anodic Onset Potentials. To explain why most of the phenolic hydroxyls reacted with HNTTM and only some of them with TNPTM, the anodic onset potentials for the oxidation of DHHDP (**2**), ellagic acid (**3**), pyrogallol (**8**), and methylgallate (**9**) were measured by cyclic voltammetry in DMF solutions. The comparative results obtained at 100 mV s^{-1} are summarized in Table 3. The lower the anodic onset potential, the more reactive the phenolic hydroxyl is. Results in Table 3 show that the compounds reactive against TNPTM (**2** and **8**) possess the lowest anodic onset potentials.

Cell Viability of HT-29 Colon Adenocarcinoma Cells. The influence of polyphenols **1**–**9** on the viability of HT-29 colon cells was measured in regular DMEM and also in the presence of catalase[30] to account for artifactual results due to the formation of H_2O_2 from the superoxide radical generated in the medium by electron transfer to oxygen.[3] The results are presented in Table 4.

The active compounds were those that contained pyrogallol, hexahydroxydiphenyl, or gallate moieties (ellagitannins **1** and **2**; flavanols **5** and **7**; and simple pyrogallol **8**). Polyphenols bearing only two geminal hydroxyls (compounds **3** and **4**) were inactive. The effect on cell viability recorded for pyrogallol and structures containing pyrogallol (compounds **5** and **7**) was, at least in part, artifactual because catalase diminished or eliminated the activity. In contrast, catalase did not influence the activity of ellagitannins **1** and **3**, as well as the related compound **2**, which means that this activity was not due to extracellular hydrogen peroxide.[31]

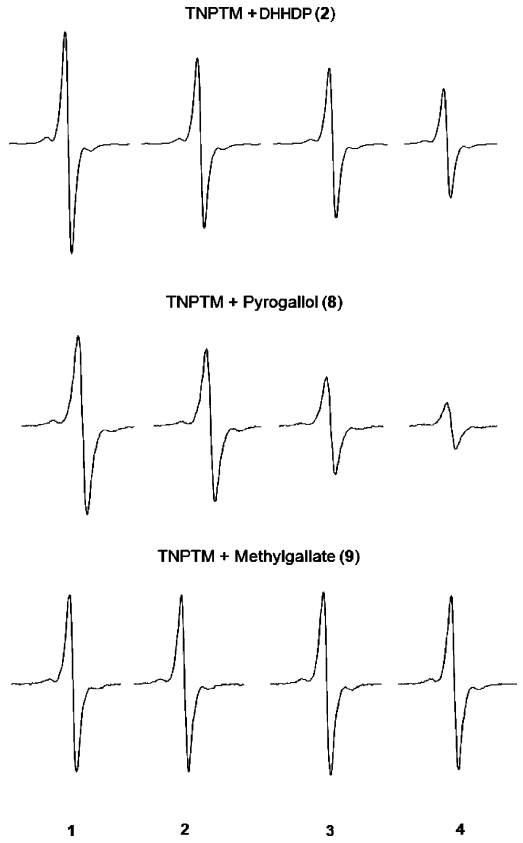

Figure 2. EPR spectra of TNPTM, initial concentration ~120 μM, upon reaction with DHHDP (**2**), pyrogallol (**8**), and methylgallate (**9**) at different initial concentrations: 0 μM (1), 5.7 μM (2), 18.1 μM (3), and 55.1 μM (4) for 48 h. Lande's factor for the TNPTM, g = 2.0026.

Table 2. Rate Constants and Stoichiometric Factors for the Reaction of TNPTM with DHHBD (2), Pyrogallol (8), and Methylgallate (9) in $CHCl_3$/MeOH (2:1)

polyphenol	TNPTM/polyphenol molar ratio[a]	k^b (M^{-1} s^{-1})	n^c
2	4.9–4.9	0.115 (0.010)	1.9
8	4.6–4.6	0.338 (0.070)	3.6
9	4.3–4.0	–	–

[a]Range of ratios for a number of experiments between 2 and 5. Initial concentrations around 120 and 24 μM (molar ratio, 5:1) for TNPTM and polyphenol, respectively. [b]Values are means (standard deviation), n = 2–5. [c]Moles of reduced radical per mole of polyphenol corresponding to the number of electrons transferred per molecule of polyphenol.

DISCUSSION

The biological relevance of polyphenols is still a matter of debate, even after decades of intense research. Particularly, the significant structural features behind polyphenol activities have not been satisfactorily established, probably because they interact with live systems in complex ways at different levels including redox reactions and protein–ligand interactions. Polyphenols may modify redox homeostasis by scavenging reactive radicals, by generating reactive radicals, or by a combination of the two. The electron transfer capacity of different phenolic hydroxyl groups determines the kind of effect elicited, if any. Pyrogallol (**8**) (three geminal hydroxyls) and polyphenols such as EGC (**5**) and EGCG (**7**) (gallocatechins), which contain this substructure, may be both

Table 3. Anodic Onset Potential (AOP) of Polyphenolic Moieties

polyphenol	AOP[a] (V vs SCE)
DHHDP (**2**)	0.50
ellagic acid (**3**)	0.64
pyrogallol (**8**)	0.45
methylgallate (**9**)	0.65

[a]10^{-3} M in DMF solutions with 0.1 M Bu_4NClO_4 on Pt at 100 mV s^{-1} and 25 °C.

Table 4. Viability of HT-29 Cells in the Presence of Polyphenols

	IC_{50}[a]	
polyphenol	μg mL^{-1} in DMEM	μg mL^{-1} in DMEM with catalase
ellagitannins and related compounds		
1	21.5 (3.5)	14.4 (0.4)
2	32.5 (3.9)	34.1 (0.5)
3	≥100	≥100
flavanols		
4	≥100	≥100
5	24.1 (2.7)	≥100
6	53.7 (12.0)	58.9 (8.0)
7	17.5 (3.2)	47.9 (8.0)
simple phenols		
8	5.6 (0.5)	71.4 (7.5)
9	24.6 (8.3)	31.6 (1.8)

[a]Cells were treated with the compounds for 72 h, and viability was monitored with MTT. Values are means (standard deviation), n = 2–3

scavengers and generators of free radicals and are among the most biologically active polyphenols. The gallate moiety (pyrogallol with an esterified carboxylate function) is another important structural feature. It has been widely reported that polyphenols that contain pyrogallols and/or gallates lower cell viability either by disrupting the cell cycle and triggering apoptosis or by other effects that involve redox reactions and/or protein–ligand interactions.[32−34] We focus our attention here on the redox reactions of polyphenols by using chemosensors that are able to discriminate between different phenolic hydroxyls according to their redox potentials. The results are compared with the influence on cell viability in vitro. Polyphenols **1**–**9** reacted with HNTTM, whereas only some of them (**1**, **2**, **5**, **7**, **8**) were able to reduce the TNPTM radical. This was expected for the structures containing pyrogallol (**5**, **7**, **8**)[20] and not for the ellagitanin punicalagin (**1**) because ellagic acid (**3**) was inactive against TNPTM. As expected, TNPTM did not react with catechols (two geminal hydroxyls) (**4**) or gallates (**6**, **9**). Punicalagin (**1**) contains an ellagic acid conjugated substructure and other substructures composed of gallate moieties linked by C–C bonds to each other (hexahydroxydiphenyl) or to an ellagic acid moiety. The stable radical TNPTM is reactive against these C–C-linked gallates as proven by the redox behavior of synthetic DHHDP (**2**). This dimeric gallate transferred two electrons to TNPTM, whereas methylgallate (**9**) was unreactive (Tables 1 and 2, last columns). The C–C bond appears to have activated two hydroxyl positions. Inspection of the structure of punicalagin (**1**) and the number of electrons (3.3) transferred to TNPTM (Table 1, last column) leads us to hypothesize that the C–C bond between the gallate moiety and the ellagic acid moiety produces the same hydroxyl activation that we detected for the

dx.doi.org/10.1021/jf204059x | J. Agric. Food Chem. 2012, 60, 1659–1665

hexahydroxydiphenyl substructure. The formation of hydrogen bonds between hydroxyls ortho to the C−C bond may be behind the reactivity of these diphenyl structures.[35] This result was corroborated by measuring the anionic onset potential (AOP) of the gallate conjugates **2**, **3**, and **9** and pyrogallol **8**. The reactivity of polyphenols given by the AOP followed the order **8** > **2** > **3** = **9** (Table 3). These results are also in agreement with the kinetic measurements (Table 2).

The outcome of the cell viability assay cannot be related to the redox behavior of the polyphenolic structures in a straightforward way because polyphenols influence cell functions by more than one mechanism. Whatever the case, our results (Table 3) corroborate that pyrogallols and gallates are active against colon adenocarcinoma cells and suggest that the hydroxydiphenyl substructure of punicalagin may play a role involving a particularly reactive redox position. As some of the effects ascribed to pyrogallols in vitro may be due to the artifactual generation of H_2O_2 in the culture medium,[3,15] we ran the in vitro experiments in the presence of catalase. This resulted in a significant decrease in the activity of the polyphenols that contained pyrogallols in their structure. This does not alter the fact that pyrogallols are the most reactive species, because they must be able to generate the superoxide radical as the first step in the formation of H_2O_2; it just shows that the experimental setup does not adequately mimic the situation in vivo, where the extracellular oxygen concentration is much lower.[3] Punicalagin (**1**) affected cell viability as effectively as gallocatechins. In this case, the effect was not artifactual because it was not affected by the addition of catalase to the medium, which suggests that punicalagin (**1**) did not generate the superoxide radical extracellularly, at least not to a sufficient extent to affect cell viability.

By combining the outcome of HNTTM and TNPTM assays, we may generate a picture of both the total electron transfer capacity of polyphenols and the presence of highly reactive hydroxyls. TNPTM detects the most redox reactive phenolics (e.g., pyrogallols and C−C-linked gallates) and may anticipate their influence on cell viability. Independent of whether these highly reactive positions directly scavenge radicals or trigger antioxidant defense responses, TNPTM is a useful chemical probe that easily detects the presence of some of the most biologically significant phenolic structures. This will be useful when the antioxidant potential of extracts and functional foods as well as new synthetic polyphenolic molecules is examined.

In conclusion, we show here that substructures of punicalagin that contain gallate moieties, linked either to each other (hexahydroxydiphenyl moieties) or to the ellagic acid moiety by C−C bonds, present phenolic hydroxyls that are more redox reactive than those in simple gallates and that these structures can be detected by the stable radical TNPTM. The most reactive polyphenolic structures are also those that have the greatest effect on cell viability in vitro. The chemosensor TNPTM may be a useful tool for detecting other potentially beneficial highly reactive polyphenols from natural sources.

■ ASSOCIATED CONTENT

Supporting Information

IR spectrum of TNPTM; plots of scavenging activity against TNPTM, HNTTM and DPPH; kinetics of the reaction between TNPTM and HDDP/pyrogallol; plots of cell viability on HT-29 cells. This material is available free of charge via the Internet at http://pubs.acs.org.

■ AUTHOR INFORMATION

Corresponding Author

*Phone: +34 93 400 61 12. Fax: +34 93 204 59 04. E-mail: joseplluis.torres@iqac.csic.es.

Funding

This work was supported by the Spanish Ministry of Education and Science (research grants AGL2006-12210-C03-02/ALI; SAF2008-00164; AGL2009-12374-C03-03/ALI), the Instituto de Salud Carlos III and European Regional Development Fund (ISCIII-RTICC, RD06/0020/0046), the Generalitat de Catalunya (2009SGR1308, 2009CTP 00026, and Icrea Academia award 2010 granted to M.C.), and the European Commission (Etherpaths Project KBBE-Grant Agreement 222639).

■ ACKNOWLEDGMENTS

We are grateful to the EPR facility at the Institut de Química Avançada de Catalunya (CSIC) for recording the EPR spectra. We appreciate language revision by Christopher Evans.

■ ABBREVIATIONS USED

DMEM, Dulbecco Modified Eagle's Medium; EGCG, epigallocatechin gallate; EGC, epigallocatechin; EC, epicatechin; ECG, epicatechin gallate; DHHDP, dimethylhexahydroxydiphenyl dicarboxylate; HHDP, hexahydroxy-2,2′-diphenyl; HNTTM, tris(2,4,6-trichloro-3,5-dinitrophenyl)methyl; TNPTM, tris(2,3,5,6-tetrachloro-4-nitrophenyl)methyl; DPPH, 1,1-diphenyl-2-picrylhydrazyl.

■ REFERENCES

(1) Harman, D. Aging: a theory based on free radical and radiation chemistry. *J. Gerontol.* **1956**, *11*, 298−300.

(2) Harman, D. The aging process. *Proc. Natl. Acad. Sci. U.S.A.* **1981**, *78*, 7124−7128.

(3) Halliwell, B. Are polyphenols antioxidants or pro-oxidants? What do we learn from cell culture and in vivo studies? *Arch. Biochem. Biophys.* **2008**, *476*, 107−112.

(4) Kuhnle, G.; Spencer, J. P. E; Schroeter, H.; Shenoy, B.; Debnam, E. S.; Srai, S. K. S.; Rice-Evans, C.; Hahn, U. Epicatechin and catechin are *O*-methylated and glucuronidated in the small intestine. *Biochem. Biophys. Res. Commun.* **2000**, *277*, 507−512.

(5) Gonthier, M. P.; Donovan, J. L.; Texier, O.; Felgines, C.; Rémésy, C.; Scalbert, A. Metabolism of dietary procyanidins in rats. *Free Radical Biol. Med.* **2003**, *35*, 837−844.

(6) Halliwell, B.; Zhao, K. C.; Whiteman, M. The gastrointestinal tract: a major site of antioxidant action? *Free Radical Res.* **2000**, *33*, 819−830.

(7) Lambert, J. D.; Sang, S. M.; Yang, C. S. Possible controversy over dietary polyphenols: benefits vs risks. *Chem. Res. Toxicol.* **2007**, *20*, 583−585.

(8) Mattson, M. P. Hormesis defined. *Ageing Res. Rev.* **2008**, *7*, 1−7.

(9) Pazos, M.; Gallardo, J. M.; Torres, J. L.; Medina, I. Activity of grape polyphenols as inhibitors of the oxidation of fish lipids and frozen fish muscle. *Food Chem.* **2005**, *92*, 547−557.

(10) Liu, Z.-Q. Chemical methods to evaluate antioxidant ability. *Chem. Rev.* **2010**, *110*, 5675−5691.

(11) Foti, M.; Ingold, K. U.; Lusztyk, J. The surprisingly high reactivity of phenoxyl radicals. *J. Am. Chem. Soc.* **1994**, *116*, 9440−9447.

(12) Foti, M.; Ruberto, G. Kinetic solvent effects on phenolic antioxidants determined by spectrophotometric measurements. *J. Agric. Food Chem.* **2000**, *49*, 342−348.

(13) Carreras, A.; Esparbé, I.; Brillas, E.; Rius, J.; Torres, J. L.; Juliá, L. Oxidant activity of tris(2,4,6-trichloro-3,5-dinitrophenyl)methyl radical with catechol and pyrogallol. Mechanistic considerations. *J. Org. Chem.* **2009**, *74*, 2368−2373.

(14) Kondo, K.; Kurihara, M.; Miyata, N.; Suzuki, T.; Toyoda, M. Scavenging mechanisms of (−)-epigallocatechin gallate and (−)-epicatechin gallate on peroxyl radicals and formation of superoxide during the inhibitory action. *Free Radical Biol. Med.* **1999**, *27*, 855−863.

(15) Long, L. H.; Clement, M. V.; Halliwell, B. Artifacts in cell culture: rapid generation of hydrogen peroxide on addition of (−)-epigallocatechin, (−)-epigallocatechin gallate, (+)-catechin, and quercetin to commonly used cell culture media. *Biochem. Biophys. Res. Commun.* **2000**, *273*, 50−53.

(16) Azam, S.; Hadi, N.; Khan, N. U.; Hadi, S. M. Prooxidant property of green tea polyphenols epicatechin and epigallocatechin-3-gallate: implications for anticancer properties. *Toxicol. in Vitro* **2004**, *18*, 555−561.

(17) Alanko, J.; Riutta, A.; Holm, P.; Mucha, I.; Vapaatalo, H.; Metsä-Ketelä, T. Modulation of arachidonic acid metabolism by phenols: relation to their structure and antioxidant/prooxidant properties. *Free Radical Biol. Med.* **1999**, *26*, 193−201.

(18) Afanas'ev, I. Signaling functions of free radicals superoxide and nitric oxide under physiological and pathological conditions. *Mol. Biotechnol.* **2007**, *37*, 2−4.

(19) Jiménez, A.; Selga, A.; Torres, J. L.; Juliá, L. Reducing activity of polyphenols with stable radicals of the TTM series. Electron transfer versus H-abstraction reactions in flavan-3-ols. *Org. Lett.* **2004**, *6*, 4583−4586.

(20) Torres, J. L.; Carreras, A.; Jiménez, A.; Brillas, E.; Torrelles, X.; Rius, J.; Juliá, L. Reducing power of simple polyphenols by electron-transfer reactions using a new stable radical of the PTM series, tris(2,3,5,6-tetrachloro-4-nitrophenyl)methyl radical. *J. Org. Chem.* **2007**, *72*, 3750−3756.

(21) Touriño, S.; Lizárraga, D.; Carreras, A.; Lorenzo, S.; Ugartondo, V.; Mitjans, M.; Vinardell, M. P.; Juliá, L.; Cascante, M.; Torres, J. L. Highly galloylated tannin fractions from witch hazel (*Hamamelis virginiana*) bark: electron transfer capacity, in vitro antioxidant activity, and effects on skin-related cells. *Chem. Res. Toxicol.* **2008**, *21*, 696−704.

(22) Yang, J.; Liu, G.-Y.; Lu, D.-L.; Dai, F.; Qian, Y.-P.; Jin, X.-L.; Zhou, B. Hybrid-increased radical-scavenging activity of resveratrol derivatives by incorporating a chroman moiety of vitamin E. *Chem.—Eur. J.* **2010**, *16*, 12808−12813.

(23) Gil, M. I.; Tomás-Barberán, F. A.; Hess-Pierce, B.; Holcroft, D. M.; Kader, A. A. Antioxidant activity of pomegranate juice and its relationship with phenolic composition and processing. *J. Agric. Food Chem.* **2000**, *48*, 4581−4589.

(24) Cerdá, B.; Tomás-Barberán, F. A.; Espín, J. C. Metabolism of antioxidant and chemopreventive ellagitannins from strawberries, raspberries, walnuts, and oak-aged wine in humans: Identification of biomarkers and individual variability. *J. Agric. Food Chem.* **2005**, *53*, 227−235.

(25) Fernandes, A.; Fernandes, I.; Cruz, L.; Mateus, N.; Cabral, M.; de Freitas, V. Antioxidant and biological properties of bioactive phenolic compounds from *Quercus suber* L. *J. Agric. Food Chem.* **2009**, *57*, 11154−11160.

(26) Wang, H. F.; Helliwell, K.; You, X. Q. Isocratic elution system for the determination of catechins, caffeine and gallic acid in green tea using HPLC. *Food Chem.* **2000**, *68*, 115−121.

(27) Aron, P. M.; Kennedy, J. A. Flavan-3-ols: nature, occurrence and biological activity. *Mol. Nutr. Food Res.* **2008**, *52*, 79−104.

(28) Quideau, S.; Feldman, K. S. Ellagitannin chemistry. The first synthesis of dehydrohexahydroxydiphenoate esters from oxidative coupling of unetherified methyl gallate. *J. Org. Chem.* **1997**, *62*, 8809−8813.

(29) Goupy, P.; Dufour, C.; Loonis, M.; Dangles, O. Quantitative kinetic analysis of hydrogen transfer reactions from dietary polyphenols to the DPPH radical. *J. Agric. Food Chem.* **2003**, *51*, 615−622.

(30) Bellion, P.; Hofmann, T.; Pool-Zobel, B. L.; Will, F.; Dietrich, H.; Knaup, B.; Richling, E.; Baum, M.; Eisenbrand, G.; Janzowski, C. Antioxidant effectiveness of phenolic apple juice extracts and their gut fermentation products in the human colon carcinoma cell line Caco-2. *J. Agric. Food Chem.* **2008**, *56*, 6310−6317.

(31) Sakagami, H.; Jiang, Y.; Kusama, K.; Atsumi, T.; Ueha, T.; Toguchi, M.; Iwakura, I.; Satoh, K.; Ito, H.; Hatano, T.; Yoshida, T. Cytotoxic activity of hydrolyzable tannins against human oral tumor cell lines − a possible mechanism. *Phytomedicine* **2000**, *7*, 39−47.

(32) Lizárraga, D.; Lozano, C.; Briedé, J. J.; van Delft, J. H.; Touriño, S.; Centelles, J. J.; Torres, J. L.; Cascante, M. The importance of polymerization and galloylation for the antiproliferative properties of procyanidin-rich natural extracts. *FEBS J.* **2007**, *274*, 4802−4811.

(33) Galati, G.; Lin, A.; Sultan, A. M.; O'Brien, P. J. Cellular and in vivo hepatotoxicity caused by green tea phenolic acids and catechins. *Free Radical Biol. Med.* **2006**, *40*, 570−580.

(34) Fernandes, I.; Faria, A.; Azevedo, J.; Soares, S.; Calhau, C. A.; De Freitas, V.; Mateus, N. Influence of anthocyanins, derivative pigments and other catechol and pyrogallol-type phenolics on breast cancer cell proliferation. *J. Agric. Food Chem.* **2010**, *58*, 3785−3792.

(35) Amorati, R.; Lucarini, M.; Mugnaini, V.; Pedulli, G. F. Antioxidant activity of o-bisphenols: the role of intramolecular hydrogen bonding. *J. Org. Chem.* **2003**, *68*, 5198−5204.